

Application and Review on Interim Guidelines for Alternative Assessment of the Weather Criterion

Hyeon Kyu, Yoon³, *Maritime & Ocean Engineering Research Institute / KORDI*

Sun Young, Kim, *Maritime & Ocean Engineering Research Institute / KORDI*

Sa Young, Hong, *Maritime & Ocean Engineering Research Institute / KORDI*

Young Shik, Kim, *Maritime & Ocean Engineering Research Institute / KORDI*

Jin Ha, Kim, *Maritime & Ocean Engineering Research Institute / KORDI*

Sung Jun, Lee, *Daewoo Shipbuilding & Marine Engineering Co., Ltd.*

ABSTRACT

International Maritime Organization (IMO) is planning to include the Alternative Assessment of the Weather Criterion in new revised Intact Stability (IS) Code. In this study, the procedure of the model test in the Interim Guidelines was reviewed by carrying out the model test and analyzing the test results. To do this, RO/RO passenger ship whose ratios of breadth to draft and the height of weight to draft were more than 3.5 and 0.5 respectively was selected as a test ship. Drifting test and motion test in regular waves were performed to estimate hydrodynamic heeling lever and roll-back angle. As the drifting test results, hydrodynamic heeling lever was changed in terms of heel angles, while it was not influenced by the small change of drifting speed. Motion tests in waves were carried out in the three wave steepness conditions to measure roll-back angle and examine the feasibility of so called, the Three-step method. Using the test data, the Weather Criterion was assessed for the test ship by using alternative method and compared with the current method.

Keywords: *Weather Criterion, Hydrodynamic heeling lever, Roll-back angle*

1. INTRODUCTION

A ship which moves in a seaway is usually influenced by waves. Especially in case of large passenger and cargo ships, the assessment of the influences of waves on those ships has to be carried out before and after the construction. For this reason, International Maritime Organization (IMO) defined a severe wind and rolling criterion, so called the Weather Criterion (IMO, 2002), and recommends for passenger or cargo ships of 24m in length and over to satisfy the criterion.

While a ship's seakeeping performance has

to be assessed in the condition of multi-directional irregular waves (Bhattacharyya, 1978, and Lloyd, 1978), the Weather Criterion is the simplified version of ultimate safety in the severe wind and wave conditions. Simplified severe environmental condition means that wind and wave direction is perpendicular to the ship length direction. The Weather Criterion can be assessed by determining the wind heeling lever and roll-back angle (Table 1) due to beam wave. Those parameters are calculated by the empirical formulae and look-up tables enclosed in Code on Intact Stability (IMO, 2002). However, such formulae and tables were made on the basis of the results in old researches (USSR, 1961, and Japan, 1982). For this reason, new formulae or

alternative assessment methods such as direct model test (Italy, 2004-2005) are under discussion because the old formulae might not be adequate to current ships. IMO Sub-Committee on Stability and Load Lines and on Fishing Vessels Safety suggests interim guidelines for alternative assessment of the Weather Criterion.

In this study, we performed the model test in the Ocean Engineering Basin (MOERI/KORDI, 1999) according to the interim guidelines in order to cope with the code's revision trend. If wind heeling lever and roll-back angle are determined, the Weather Criterion can be assessed. Wind heeling lever is the sum of the levers due to wind force and water drifting force with respect to the reference point. The levers due to wind force and water drifting force are measured by wind tunnel test and drifting test respectively. In this study, drifting test was performed to measure the hydrodynamic lever. In addition, motion tests in regular waves were carried out to obtain roll-back angles. To do this, we selected RO/RO passenger whose ratios of breadth to draft and height of weight center to draft are more 3.5 and 0.5 respectively as a test ship. Also, motion tests in small steepness waves were performed to apply the Three-step method to the test results and investigate its availability for estimating roll-back angle. Finally, the Weather Criterion was assessed by using alternative method and compared with the current method.

2. WEATHER CRITERION

The Weather Criterion, as recommended by the IMO, implies that passenger or cargo ships of 24 m more in length must withstand the combined effects of severe wind and beam wave induced rolling.

In order to describe the definition of the Weather Criterion, the general hydrostatic curve is displayed in Figure 1. Also, the symbols in Figure 1 are listed in Table 1.

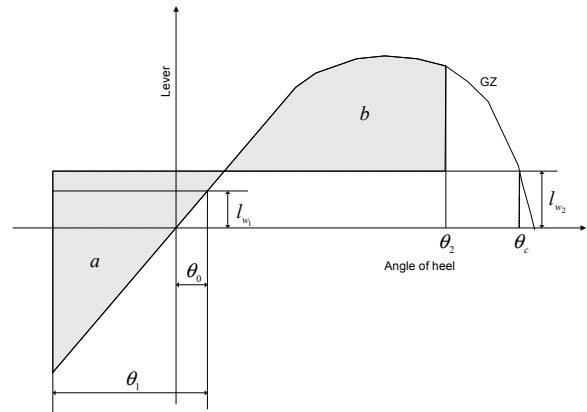


Figure 1 Definition of symbols for describing the Weather Criterion

Table 1 Description of symbols in Figure 1

Symbol	Description
θ_0	Angle of heel under action of steady wind
θ_1	Angle of roll to windward due to wave action
θ_2	Angle of downflooding or 50° or θ_c , whichever is less
θ_c	Angle of second intercept between wind heeling lever (l_{w_2}) and GZ curves
l_{w_1}	Steady wind heeling lever
l_{w_2}	Gust wind heeling lever

According to the Weather Criterion, area b should be equal to or greater than area a under the steady wind and beam wave action (Figure 1). Area a and b can be calculated if l_{w_1} , l_{w_2} , θ_1 , and θ_2 are known. l_{w_1} and θ_1 are determined by empirical formulae (IMO, 2002) which are the functions of the projected lateral area (A), vertical distance from the center of A to the center of the underwater lateral area, ship's principal particulars, geometrical parameters of bilge keels, etc. Since θ_2 is obtained by l_{w_2} and GZ curve, and l_{w_2} is one and half times of l_{w_1} , the Weather Criterion can be assessed if l_{w_1} and θ_1 are determined.

3. MODEL TEST

3.1 Test Ship

As a test ship, RO/RO passenger ship was selected. The scale ratio of model should be determined not to violate the minimum of the ship's length of 2.5m. Also shallow water effect has to be avoided in the maximum wave length condition of the test matrix. The scale ratio was decided to be 1/70. In Table 2, real and model ship's principal parameters in full loading condition are listed. Figure 2 depicts the model ship.

Longitudinal and lateral radii of gyrations are $0.40B$ and $0.26L$, respectively. B and L are the ship's breadth and length between perpendiculars. Longitudinal radius of gyration includes the added mass moment of inertia because it was measured by free roll decay test in the basin.

Table 2 Principal particulars of real and model ships

Item	Real	Model
Length over all (m)	175.0	2.500
Length between perpendiculars (m)	162.1	2.316
Breadth (m)	27.6	0.394
Mean draft (m)	6.976	0.100
Displacement (m^3)	18,322	0.0534
Metacentric height (m)	2.47	0.0353
Roll natural period (s)	13.849	1.6552



Figure 2 The object model ship

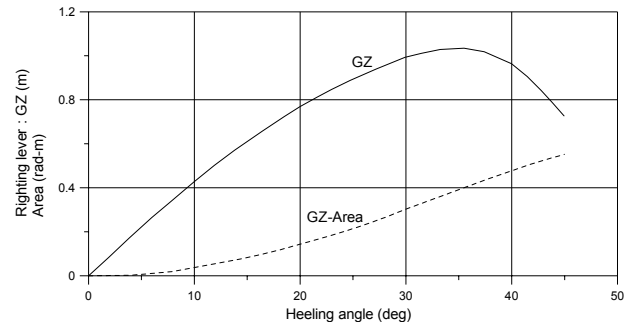


Figure 3 GZ curve of the object real ship

The parameters in the empirical formulae (IMO, 2002) to calculate roll-back angle are the functions of ship's geometrical dimensions. If an input dimension is over a certain value, resulting parameter is fixed to a constant value. However, the value may be changed following the variation of input parameters. Therefore, it will be more adequate to apply direct model test to measure roll-back angle than to use current empirical formulae. The ratios of breadth to draft and height of weight to draft (OG/d) of the object ship of which principal dimensions are listed in Table 2 are 3.96 and 0.84, respectively. Those values exceed the maximum values of 3.5 and 0.5. Therefore, the object ship is regarded to be suitable for application of the alternative method. Figure 3 depicts hydrostatic curves of the object ship.

3.2 Drifting Test

The objective to perform drifting test is to obtain the heeling lever due to hydrodynamic force acting on a ship when it is moving sideways with constant speed generated by steady wind. The hydrodynamic heeling lever (l_{water}) is defined in terms of reference origin located in the waterline. And then, if steady wind heeling lever (l_{wind}) with respect to the reference origin is estimated by empirical formula or wind tunnel test, l_{w_1} can be calculated by following equation,

$$l_{w_1} = l_{wind} - l_{water} \quad (1)$$

where, the upper lever from the waterline is positive.

Drifting speed of a ship which is the same as the towing speed in the model test is determined under the assumption that the steady wind blows with the speed of 26 m/s (Japan, 2005) in real scale and appropriate wind force acts on the ship. Since wind tunnel test was not carried out in this study, towing force was calculated by the following formula (IMO, 2002),

$$F_{wind} = PA_L, \quad (2)$$

where, P is 504 Pa and A_L is the lateral projected area of a ship above the waterline. In this study, wind forces or towing forces of the object real and model ships are 2,284 kN and 6.66N, respectively.

The configuration of drifting test in our basin is depicted in Figure 4. As shown in Figure 4, sway force and roll moment acting on a model ship are measured during towing with constant speed. In this case, longitudinal motions such as heave and pitch should be free.

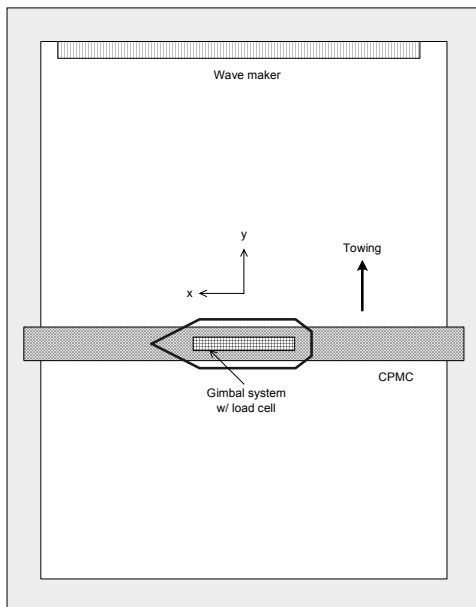


Figure 4 Configuration of drifting test

To do this, we used the gimbal system with two legs which one end is attached to the towing carriage and the other end to the model

ship. The maximum towing speed of our carriage is 3 m/s, and its resolution is controlled to 0.01 m/s

The roll angle range of drifting test should be covered from the roll-back angle to θ_2 . So, in this study, roll angle range was $-20 \sim 30^\circ$ and its interval was 5° . Also, in case that roll angle was 0° , 11 speed conditions were selected in order to measure the towing force of 6.66N. As the result, towing speed was 0.28 m/s. In order to investigate the effect of the small variation of drifting speed on the hydrodynamic lever, tests were performed at 3 different speed conditions which were 0.25, 0.28, and 0.31 m/s per each roll angle.

3.3 Motion Test in Waves

Before carrying out the motion test in waves, wave calibration test has to be performed. As shown in Figure 5, #2 wave probe was put into position where a model would be set in the motion test. #1 and #3 wave probes were arranged parallel to wave direction.

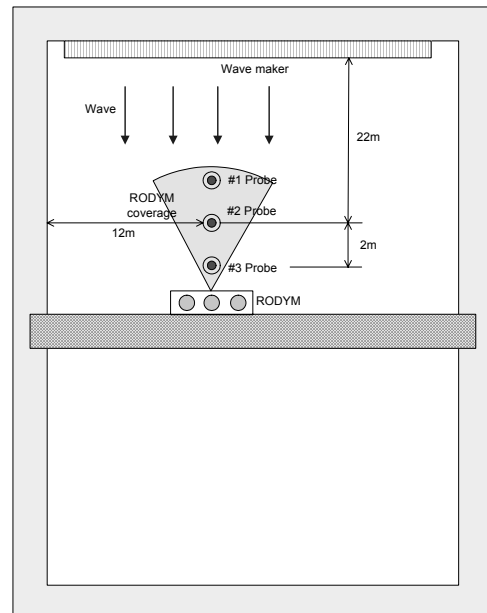


Figure 5 Configuration of wave calibration test

The distance between the wave maker and #1 wave probe was the three times of wave length of the longest wave among the test wave

conditions. The space between adjacent probes was 2m since the sway coverage of six-degree of freedom motion measuring device (RODYM) is within 5m.

When motion test in waves was performed, the model ship was put into position at #2 wave probe in Figure 5. The sway and yaw motion in waves were constrained until the roll motion was more or less generated. Wave probes depicted in Figure 5 were moved 5 m to the right hand side in motion test in waves.

Wave steepness appropriate to the roll natural period is $1/18.55$. In this study, in addition to the $1/18.55$, two small conditions of wave steepness which were $1/25$ and $1/30$ were added in order to check the validity of the Three-step method (Italy, 2004-2005). Ratios of wave frequencies to roll natural frequency were 0.8, 0.9, 0.95, 0.975, 1.0, 1.05, and 1.2. Those values are suggested in the Interim Guidelines (Italy, 2004-2005). Also, the ratios of 0.85 and 1.1 were added. In order to apply the Three-step method, the free roll decay tests have to be performed for obtaining damping coefficients. The initial heel angles were $25 \sim 40^\circ$ and the interval was 5° in the free roll decay tests.

4. RESULTS AND DISCUSSION

4.1 Drifting Test

As mentioned before in 3.2, the towing force of 6.66N corresponds to the towing speed of 0.28 m/s. In Figure 6, measured non-dimensionalized hydrodynamic levers in terms of heeling angles are displayed together with the results in case that the towing speeds were 0.25 and 0.31 m/s. The reference of lever is the origin located at the waterline. As shown in Figure 6, the end point of the lever is located above the waterline when initial heeling angles are large. This is because asymmetric vertical

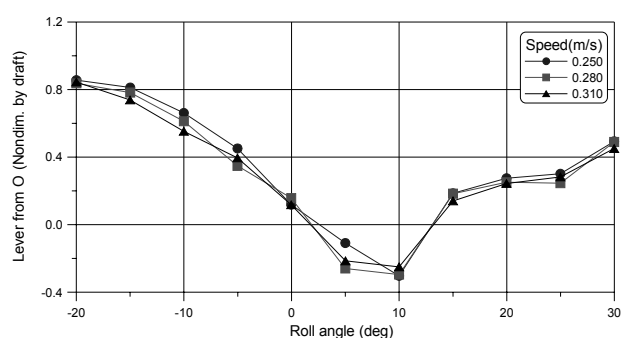


Figure 6 Nondimensional hydrodynamic levers from waterline with respect to roll angle

hydrodynamic pressure acting on the ship is distributed due to broad flat bottom shape and bilge keels. In the current method for assessment of the Weather Criterion, the hydrodynamic lever is half draft and the direction is below the waterline. Also it is assumed that the lever is constant with respect to heeling angles. However, these model tests demonstrate that current method should be revised.

Figure 7 depicts the hydrodynamic levers with respect to the towing speed. In these cases, heeling angles were 0° . The nondimensional levers are changed within about 0.15, even though the speed changes from 0.2 to 0.475 m/s. These values are relatively small compared to the values resulting from the changes of heeling angles. In particular, the effect of speed change is little in the interesting range of 0.25~0.4 m/s.

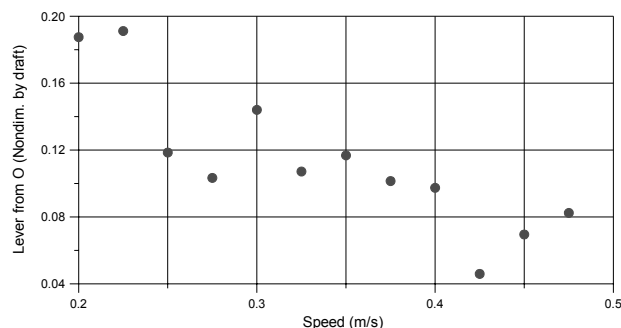


Figure 7 Nondimensional hydrodynamic levers from waterline with respect to towing speed

4.2 Motion Test in Waves

Wave Calibration Test. The results of wave calibration test in case that wave steepness was $1/18.55$ are displayed in Figure 8. Solid lines in Figure 8 mean the available upper and lower limits which are $\pm 5\%$ of the desired wave height. As shown in Figure 8, all measuring values are within the limits. Especially, the results sampled by #2 wave probe of which position the model ship would be put on were almost close to the desired heights.

Free Roll Decay Test. In Figure 9, the differences of adjacent peak roll angles measured in free roll decay tests when the initial roll angles were from 25 to 40° are depicted with respect to the mean angles of adjacent peaks. Solid line is the fitting results based on Bertin's expression (Himeno, 1981). When the parameter in the expression was identified, absolute peak values of half period were selected. The curve fitting formula is as follow,

$$\Delta\phi = 0.02092\phi_m^2 . \quad (3)$$

In (3), $\Delta\phi$ and ϕ_m are the difference and mean angle of adjacent peaks, respectively.

Motion Test. The amplitude of roll response in a regular wave was calculated by using the data which were sampled when yaw angle was within $\pm 15^\circ$. Since it was difficult to maintain the yaw angle within $\pm 15^\circ$, sway and yaw were constrained until the roll was generated more or less by mooring cable. And then the ship moved freely as soon as the cable was released. The peak roll amplitudes at specified wave conditions are displayed in Figure 10. The abscissa of Figure 10 is the ratio of wave frequency to the ship's natural roll frequency. The roll-back angle is the RMS value of peak roll amplitude in Figure 10.

As shown in Figure 10, maximum amplitudes appear between frequency ratio 0.9 and 0.95. The value is 25.84° in case of wave

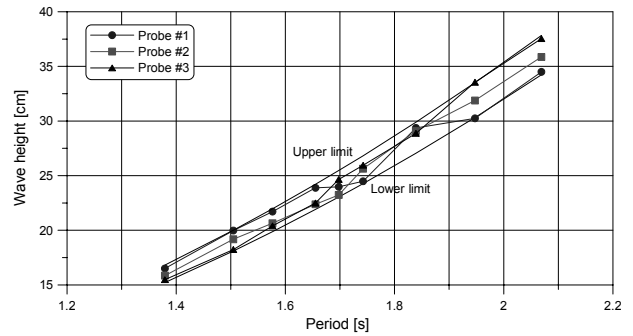


Figure 8 Wave height for wave steepness $1/18.55$

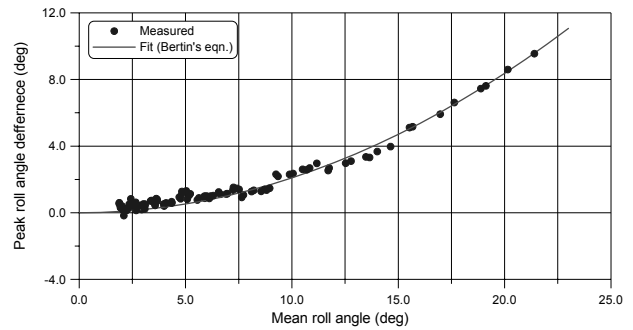


Figure 9 Free roll decay test results

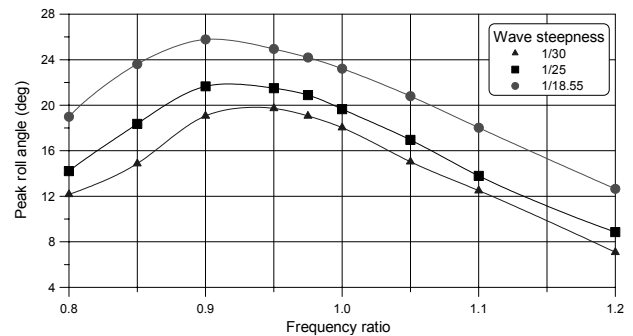


Figure 10 Peak roll amplitudes measured from motion test in waves

steepness $1/18.55$. The reason why the peak value arose near 0.9 not at 1.0 is that the larger the roll angle is, the smaller the steepness of GZ is, as shown in Figure 3. The effect of small steepness of GZ curve makes ship's natural roll frequency small.

Estimation of Roll-back Angle by Three-step Method. The Three-step method is the

one that estimates peak roll amplitude by using the test results in waves of small wave steepness because of limitation of wave maker or basin size. At the first step, roll damping coefficients

Table 3 Estimated peak roll amplitudes by using Three-step method

Wave steepness	Peak roll amplitude (°)	Estimated peak roll amplitude (°)
1/30	19.80	25.18
1/25	21.88	25.40
1/18.55	25.84	25.84

with respect to roll amplitude are identified by using free roll decay tests. And then effective wave slope coefficient at the peak roll amplitude obtained in the motion tests in waves of small wave steepness condition is identified under the assumption that the coefficient is constant. Finally, the peak roll amplitude against the wave of the desired steepness is estimated iteratively by the one dimensional roll equation.

Peak roll amplitudes measured in the motion test in waves of wave steepness 1/25 and 1/30 and estimated ones at the desired wave steepness 1/18.55 are summarized in Table 3. Since the differences between estimated and directly measured values are within 0.7°, the Three-step method is thought to be reasonable.

5. ASSESSMENT OF WEATHER CRITERION

In order to assess the Weather Criterion, areas a and b in Figure 1 have to be calculated. l_{w_2} is the gust heeling lever and its value is one and half of l_{w_1} which is obtained by wind tunnel test and drifting test. θ_1 is the roll-back angle which is the RMS value of peak roll angle measured by direct motion test in wave or estimated by the Three-step method. Since wind tunnel test was not carried out in this study, steady wind heeling lever is assumed to be the distance from the centroid of lateral

projected area above waterline to the reference point in the waterline.

The hydrostatic curve and l_{w_2} which were calculated by empirical formulae in Code (IMO, 2002) and estimated by the drifting test are depicted in Figure 11. Code and Test in Figure 11 denote l_{w_2} by empirical formulae and by the drifting test, respectively. When area a and b are calculated by the model test results, area a is composed of GZ curve, l_{w_2} : Test, and $\theta_1 - \theta_0$: Test. Also area b is composed of GZ curve, l_{w_2} : Test, and heeling angle of θ_2 . θ_2 of our object ship is above 40°. If the Weather Criterion might be satisfied in the lower θ_2 , it would be naturally satisfied in the larger θ_2 . For this reason, θ_2 which makes area b equal to area a was calculated. This θ_2 was denoted as $\theta_2|_{a=b}$. In Table 4, the parameters which are needed for assessment of the Weather Criterion in Figure 11 are listed. The parameters in the second and the third columns are the ones calculated by the empirical formulae and the model test results.

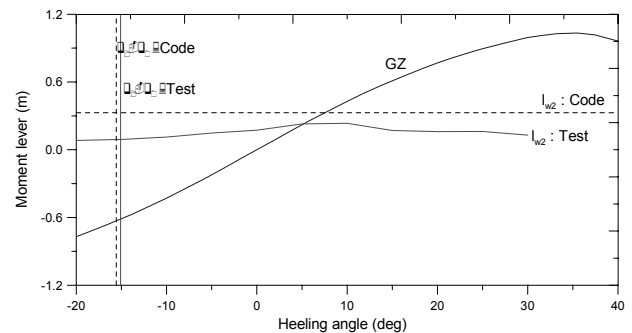


Figure 11 - GZ curve for assessment of the Weather Criterion

Table 4 - Calculated parameters for assessment of the Weather Criterion

Item	Formula	Model Test
θ_0 (°)	4.90	3.00
θ_1 (°)	-20.47	-18.09
$\theta_1 - \theta_0$ (°)	-15.57	-15.09
a (rad-m)	0.1994	0.1280
$\theta_2 _{a=b}$ (°)	33.61	23.91

Even though the values of $\theta_1 - \theta_0$ calculated by empirical formulae and estimated by the model test results are similar, the area a 's are considerably different. The reason is that the wind heeling lever calculated by the empirical formulae is larger than the case of the model test. Also following the same reason, $\theta_2|_{a=b}$ calculated by the empirical formulae is larger than the one by the model test. Anyway, since $\theta_2|_{a=b}$ is smaller than θ_2 of 40° in both cases, the Weather Criterion is satisfied for our object ship.

6. CONCLUSIONS

In this study, drifting test and motion test in waves of a RO/RO passenger model ship were carried out in the MOERI Ocean Engineering Basin according to the interim guidelines for alternative assessment of the Weather Criterion. As the result of the drifting test, the directions of the hydrodynamic heeling levers were above the waterline when the initial heel angles were large. Therefore the current assumption that the hydrodynamic heeling lever is half draft below the waterline and constant is unreasonable. The Three-step method which is used for obtaining roll-back angle in case that the model test cannot be performed at large steepness wave condition was proved to be effective. When the Weather Criteria were assessed by the current method and the alternative method for our test ship, the former was severer than the latter.

In the future, it is thought that the empirical formulae for assessment of the Weather Criterion for current ships have to be revised after a number of model tests.

7. ACKNOWLEDGMENTS

The work in this paper was supported by the project, "Development of Simulation Technology for Dynamic Stability of Ships".

8. REFERENCES

- Bhattacharyya, R, 1978, "Dynamics of Marine Vehicles", John Wiley & Sons, Inc., pp. 121-136.
- Himeno, Y., 1981, "Prediction of Ship Roll Damping – State of the Art", Report No. 239, Dept. of Naval Architecture and Marine Engineering, University of Michigan, pp. 8-10.
- International Maritime Organization, 2002, "Code on Intact Stability for All Types of Ships Covered by IMO Instruments, 2002 edition", IMO Publication, pp. 13-17.
- Italy, 2004-2005, "Review of the Intact Stability Code – Guidelines for alternative assessment of Weather Criterion", IMO, SLF Committee.
- Japan, 1982, "Weather Criteria, Results on Japanese Ships", SLF/7.
- Japan, 2005, "Proposal on draft explanatory notes to the severe wind and rolling criterion", IMO, SLF Committee.
- Maritime & Ocean Engineering Research Institute/ KORDI, 1999, "Guidebook for Ocean Engineering Basin". (in Korean)
- Lloyd, A.R.J.M., 1989, "SEAKEEPING: Ship Behaviour in Rough Weather", Ellis Horwood Limited, pp. 263-276.
- USSR, 1961, "Standards of Stability of Sea-Going Vessels and Coasters", Register of Shipping of the USSR, Mosrskoi Transport, Moscow.

Evaluation of the Weather Criterion by Experiments and its Effect to the Design of a RoPax Ferry

Shigesuke Ishida, *National Maritime Research Institute*

Harukuni Taguchi, *National Maritime Research Institute*

Hiroshi Sawada, *National Maritime Research Institute*

ABSTRACT

The guidelines of experiments for alternative assessment of the weather criterion in the intact stability code were established in IMO/SLF48, 2005. Following the guidelines, wind tunnel tests and drifting tests for evaluating wind heeling lever, l_{wl} , and roll tests in waves for evaluating the roll angle, ϕ_1 , were conducted. The results showed some difference from the current estimation, for example the wind heeling moment depended on heel angle and the centre of drift force existed higher than half draft. The weather criterion was assessed for allowable combinations of these results and the effect of experiment-supported assessment on the critical KG and so forth was discussed.

Keywords: *intact stability, weather criterion, safety standard, IMO*

1. INTRODUCTION

In 2005, the IMO Sub-Committee on Stability, Load Lines and Fishing Vessels Safety (SLF) restructured the Intact Stability Code (IS Code, IMO, 2002), and the weather criterion (Severe wind and rolling criterion), defined in section 3.2 of the code, was included in the Mandatory Criteria (Part A) of the revised code (IMO, 2006). The necessity of the criterion has been recognized to ensure ship stability safety in “dead ship condition”, in which the ability to control the ship is lost. However, the applicability of the criterion to some types of ships (e.g. modern large passenger ships), which did not exist at the time of development of the criterion, have been questioned. In order to solve the problem, the alternative assessment with model experiments is mentioned in the revised code.

To ensure uniform applicability of model experiments, which evaluate the wind heeling

lever and the resonant roll angle, the guidelines were developed and included as Annex 1 in the revised code. However, they were set as “interim guidelines” because the feasibility, reliability and so forth are not fully clarified and it is recognized that a considerable accumulation of the experimental experience is required to correctly evaluate the safety.

Some effects of this assessment were already discussed (Bulian et al., 2004, Francescutto et al., 2004). However, they were not based on full experiments included in the guidelines. With this background the authors conducted experiments with a Ro-Pax ferry model following the guidelines and examined the above mentioned items. The previous paper (Taguchi et al, 2005, hereafter just referred as “previous paper”) reported the results except the wind tunnel tests. In this paper, the effects of this experiment-supported assessment by full experiments are reported. In the following chapters the items explained in the previous paper are mentioned concisely.

2. THE WEATHER CRITERION AND ITS ALTERNATIVE ASSESSMENT

The weather criterion evaluates the ability of a ship to withstand the combined effects of beam wind and waves. The criterion requires that area “b” should be equal to or greater than area “a” (see Figure 1), where

l_{w1} : steady wind heeling lever at wind speed of 26 m/s

l_{w2} : gust wind heeling lever ($l_{w2} = 1.5 l_{w1}$)

ϕ_1 : roll amplitude in beam waves specified in the code

ϕ_2 : downflooding angle or 50 degrees or angle of second intercept between l_{w2} and GZ curves, whichever is less.

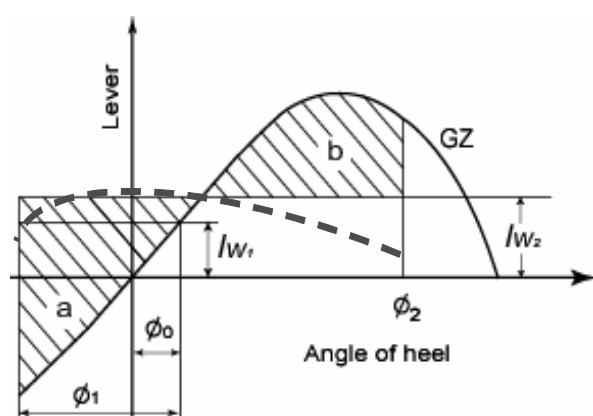


Figure 1 Weather criterion

In the revised code, l_{w1} and ϕ_1 can be evaluated by model experiments in the following conditions and it is allowed to consider the heeling lever as dependent on the heeling angle like the broken line in Figure 1,

l_{w1} : to the satisfaction of the Administration

ϕ_1 : when the parameters of the ship are out of the following limits or to the satisfaction of the Administration;

- B/d smaller 3.5
- $(KG/d-1)$ between -0.3 and 0.5
- T smaller than 20 seconds

where B , d and KG are the breadth, draft and the height of CG above keel of the ship respectively, and T is the natural rolling period.

3. THE SUBJECT SHIP

The subject ship is a Japanese Ro-Pax ferry. Table 1, Figures 2 and 3 show the principal particulars, the general arrangement and GZ curve respectively. Compared to general European Ro-Pax ferries this ship has finer shape. From Figure 3 it is found that up to about 40 degrees the GZ curve has a very small nonlinearity to heel angle.

Table 1 Principal particulars

Length between perpendiculars: L_{pp} [m]	170.0
Breadth: B [m]	25.0
Depth: D [m]	14.8
draft: d [m]	6.6
Displacement: W [ton]	14,983
Blockage coefficient: C_b [-]	0.521
B/d [-]	3.79
Area of Bilge Keels: A_{bk} [m ²]	61.32
Vertical center of gravity: KG [m]	10.63
Metacentric height: GoM [m]	1.41
Flooding angle: ϕ_f [deg]	39.5
Rolling Period: Tr [sec]	17.90
Lateral projected area: AL [m ²]	3433.0
Height to centre of AL above WL : H_c [m]	9.71

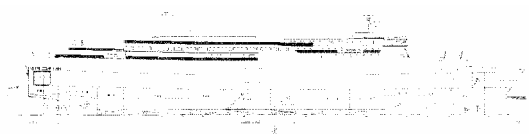


Figure 2 General arrangement

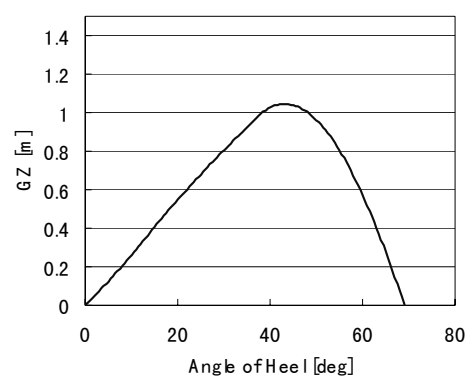


Figure 3 GZ curve

4. WIND HEELING LEVER l_{w1}

The wind heeling lever is estimated from the heeling moment when the ship is drifting

laterally by beam wind. Therefore, wind tunnel tests and drifting tests are necessary.

4.1 Wind Tunnel Tests

The wind tunnel tests were conducted at “pulsating wind tunnel with water channel” of NMRI (National Maritime Research Institute), with wind section of 3m in width and 2m in height. The test arrangement is shown in Figure 4. The connection between the model and load cell had a rotating device for testing the model in heeled conditions. In heeled conditions, the height of the model was adjusted by the adjusting plate to keep the displacement constant when floating freely. By using the model of 1.5m in length, the blockage ratio was kept less than 5%, which is requested by the guidelines. The gap between the model and the floor plate was kept within approximately 3mm and covered by soft sheets for avoiding the effect of downflow through the gap.

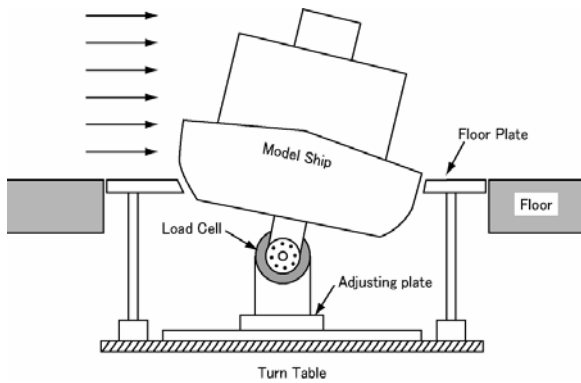


Figure 4 Arrangement for wind tunnel tests

The wind speed was varied from 5m/s to 15m/s in upright condition and confirmed that the drag coefficient is almost constant in this speed range. For the full tests a wind speed of 10m/s was used, corresponding to the Reynolds' number of 1.52×10^5 , as defined by the following equation:

$$Re = \frac{U_{\infty} B}{\nu} \quad (1)$$

where U_{∞} is the uniform wind speed outside the boundary layer, B is the breadth of the model and ν is the kinematic viscosity coefficient of air.

The horizontal force F_{wind} , the heeling moment M and the lift force L were measured by the load cell. The heeling moment M was converted to the one with respect to point O , defined as M_{wind} in the guidelines, by the following equation:

$$M_{wind} = M - F_{wind} l \cos \phi + L \cdot l \sin \phi \quad (2)$$

where l is the distance from the centre of the load cell to the point O , which is defined as the cross point of the centre line of the ship and waterline in upright condition.

4.2 Results of Wind Tunnel Tests

The measured drag coefficient C_D , lift coefficient C_L and heeling moment coefficient C_M are shown in Figure 5. They are nondimensionalized by the following equations:

$$\begin{pmatrix} C_D \\ C_L \end{pmatrix} = \begin{pmatrix} F_{wind} \\ L \end{pmatrix} / \left(\frac{1}{2} \rho_{air} U^2 A_L \right) \quad (3)$$

$$C_M = M_{wind} / \left(\frac{1}{2} \rho_{air} U^2 \frac{A_L^2}{L_{pp}} \right) \quad (4)$$

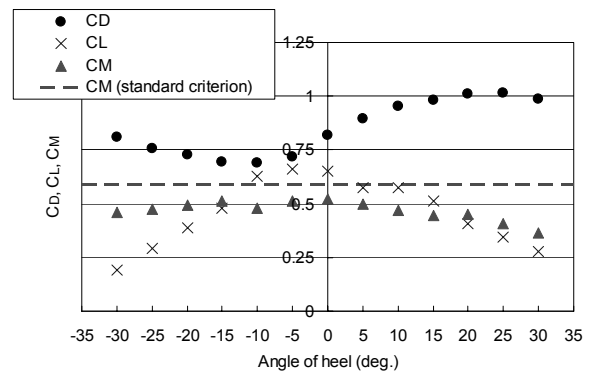


Figure 5 Results of wind tunnel tests

In the figure the angle of heel is defined as positive when the ship heels to lee side as shown in Figure 4. The broken line is the heeling moment coefficient calculated from the current weather criterion (IMO, 2002, called standard weather criterion hereafter).

It is characteristic in Figure 5 that at all the quantities (C_D , C_L and C_M) vary significantly with heel angle. As for the heeling moment, it is smaller than the standard criterion and further reduces when the ship heels, especially to lee side. The lift force is not so small and close to the drag force when the heeling angle is -5 degrees (weather side). However, the adjustment of the vertical position of the model is not necessary since the lift force is 0.7% of the displacement of the ship in the assumed wind speed of 26m/s.

The result is also shown in Figure 6 as the height of the centre of wind force above waterline, l_{wind} , by the following equation. It can be observed that the centre of wind force is also a function of heel angle.

$$l_{wind} = M_{wind} / F_{wind} \quad (5)$$

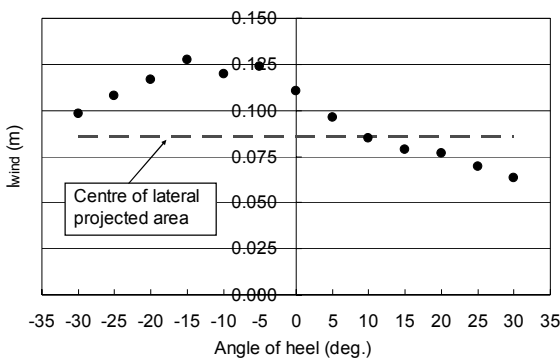


Figure 6 Height of the centre of wind force above waterline (model scale)

Although it is not requested in the guidelines, the effect of encounter angle, φ , was investigated. Figure 7 shows the wind heeling moment coefficient, C_M . Here $\varphi < 90$ means following wind. The figure shows that the wind heeling moment is almost at the

maximum in beam wind condition ($\varphi = 90$ degrees). This fact supports the assumption of existing regulations. However, for developing performance based, physics based criteria, the information on the effect of encounter angle to heeling moment might be necessary.

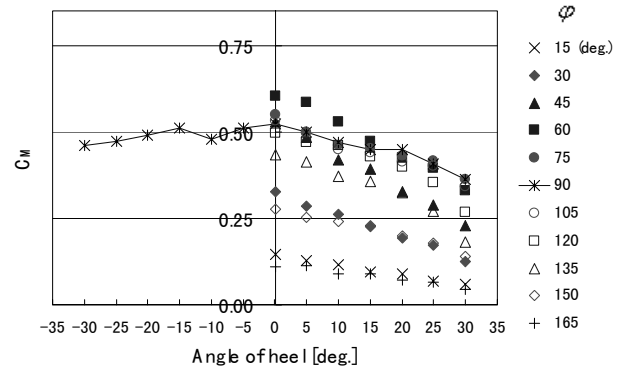


Figure 7 Wind heeling moment coefficient for various encounter angles

4.3 Drifting Tests

The detail of drifting tests was reported in the previous paper. Here, the height of the centre of drift force above waterline, l_{water} , is shown in Figure 8. l_{water} was calculated in the same manner as equation (5). The angle of heel is positive when the ship heels to the drift direction. The drift speed (towing speed) was decided, as requested in the guidelines, to make the measured drift force equal to the wind force at the wind speed of 26m/s in ship scale. Because drifting tests were conducted before wind tests, the wind drag coefficient, C_D , was assumed to be from 0.5 to 1.1. In upright condition and $C_D=0.8$ the drift speed was 0.195m/s (1.80m/s in ship scale).

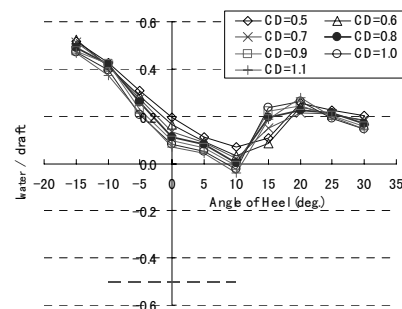


Figure 8 Height of the centre of drift force above waterline

Figure 8 shows that the centre of drift force is above half draft (which is assumed in the standard criterion) and is generally above the waterline for this ship. This phenomenon was reported by Hishida and Tomi (1960), Ishida (1993), Ishida and Fujiwara (2000) and referred in IMO/SLF (2003). This is due to the more dominant effect of the bottom pressure distribution than the side pressure when breadth/draft ratio is large. For the cross sections with this proportion, high position of the centre of sway force can be easily found in hydrodynamic tables of Lewis Form. This fact suggests that potential theory would explain this phenomenon. However, the effect of separated flow, e.g. from bilges, was also pointed out (Ishida and Fujiwara, 2000). It was confirmed experimentally in the previous paper that l_{water} reduces when the draft is enlarged.

4.4 Determination of l_{wl}

The heeling moments by wind, M_{wind} , and by drifting, M_{water} , both around point O , were divided the displacement, Δ , and the wind heeling lever, l_{wl} , was calculated as a function of heel angle (equation (6)). Figures 9 and 10 show the results.

$$l_{wl} = \frac{M_{wind} + M_{water}}{\Delta} \quad (6)$$

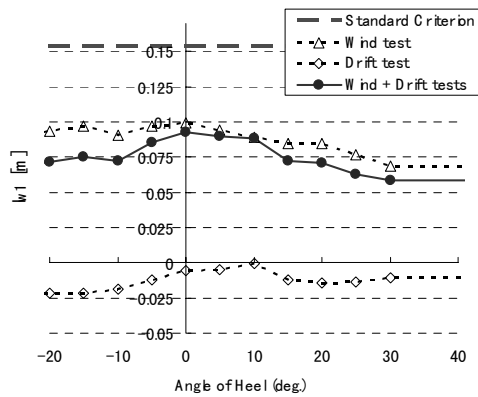


Figure 9 Wind heeling lever, l_{wl} , evaluated by the tests

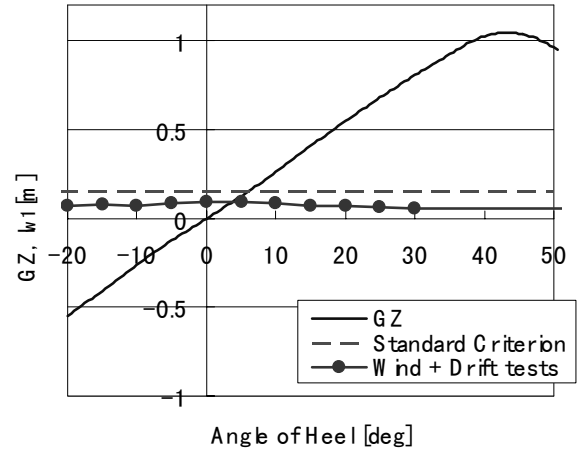


Figure 10 Wind heeling lever, l_{wl} , compared with the GZ curve

In Figure 9, the heeling levers due to wind (M_{wind}/Δ) and drift motion (M_{water}/Δ) are also included. In both figures, l_{wl} at angles greater than 30 degrees (tested range) is assumed to keep the same value as at 30 degrees as prescribed in the guidelines. Figure 9 and 10 show that, in the considered case, the wind heeling lever estimated by wind and drift tests is sensibly smaller than that required by the standard weather criterion.

5. ROLL ANGLE ϕ_l

The formula of roll angle ϕ_l in the weather criterion implies the maximum amplitude out of 20 to 50 roll cycles in beam irregular waves. And ϕ_l is related to the resonant roll amplitude, ϕ_r , in regular waves, whose height and period are equal to the significant wave height and mean wave period of the assumed irregular waves (IMO, 2006, Watanabe et al., 1956). The reduction factor is 0.7 (see equation (7)) and this alternative assessment estimates ϕ_r instead of ϕ_l by model experiments.

$$\phi_l = 0.7\phi_r \quad (7)$$

5.1 Direct Measurement Procedure

In the guidelines, this procedure is called “Direct measurement procedure” because the resonant roll angle, ϕ_r , is measured directly in waves with the steepness specified in the IS Code and the period equal to the natural roll period.

The results of experiments were mentioned in the previous paper. Here, Figure 11 is shown again. In the figure, “ s ” is the wave steepness, which is tabled in the Code as a function of the natural roll period. For this ship $s=0.0383$ (1/26.1), but lower steepnesses were also used. Due to the linearity of the GZ curve the amplitudes reach the maxima at the vicinity of the natural roll frequency in all steepnesses. From this result, ϕ_1 was decided as 19.3 degrees ($=0.7\phi_r$).

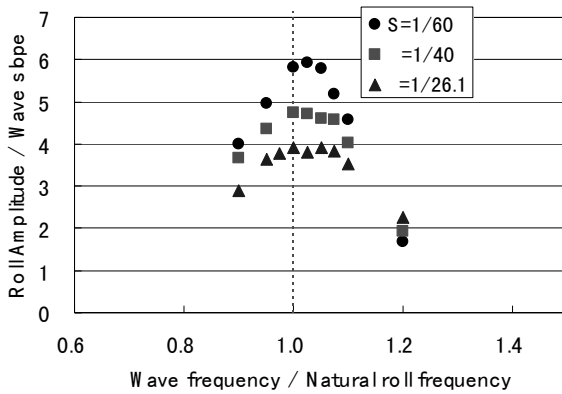


Figure 11 Roll amplitude in regular waves

5.2 Alternative Procedures

In the guidelines, alternatives procedures are included, i.e. “Three steps procedure” and “Parameter identification technique (PIT)”. In the “Three steps procedure”, the roll damping coefficient N is estimated by roll decay tests. And, the effective wave slope coefficient r is estimated by roll motion tests in waves with smaller value of s . Finally, ϕ_r (degrees) is calculated by the following equation:

$$\phi_r = \sqrt{\frac{90\pi rs}{N(\phi_r)}} \quad (8)$$

This method was adopted when the standard weather criterion was developed and is based on linear theory except roll damping. The previous paper showed that the estimated value of ϕ_1 is 19.5 degrees when the resonant roll amplitude at $s=1/60$ is used. This value of ϕ_1 is very close to that by the “Direct measurement procedure” due to the linear feature of GZ curve.

The PIT is a methodology to determine the parameters included in the equation of roll motion. Once all the parameters are decided by test data at small wave steepness, the roll amplitude at prescribed s can be extrapolated. In the guidelines, an equation with 9 parameters is presented, in which nonlinear features of roll damping, GZ curve and wave exciting moment are included. PIT analysis is not carried out in this paper. However, the difference of ϕ_1 by PIT from other 2 procedures is expected to be limited because of the linearity of GZ curve.

6. ALTERNATIVE ASSESSMENT OF THE WEATHER CRITERION

In the guidelines, simplified procedures on the wind heeling lever, l_{wl} , are also mentioned for making the assessment practically easier. For wind tunnel tests, the lateral horizontal force F_{wind} and the heeling moment M_{wind} can be obtained for the upright condition only and considered as constants (not depending on heeling angle). Instead of drifting tests, the heeling moment M_{water} due to drift can be considered as given by a force equal and opposite direction to F_{wind} acting at a depth of half draft in upright condition, as assumed in the standard criterion. And the combinations of complete procedures and simplified procedures are to the satisfaction of the Administration.

The comparison of the assessments of the weather criterion using experimental results is summarized in Table 2. In the table all the possible combinations of the wind tests and the drifting tests, complete procedures and simplified procedures are included. As for ϕ_1 , the standard criterion and the result of “Direct measurement procedure” are included. The results of “Three steps procedure” can be omitted here since the estimated ϕ_1 was almost equal to the one of “Direct measurement procedure” for this ship.

Table 2 Assessments of weather criterion by experiments

lwl	Standard Weather Criterion	Wind test + Drift test	Wind test + draft/2	Wind test (upright) + Drift test	Wind test (upright) + draft/2	Standard Weather Criterion	Wind test + Drift test	Wind test + draft/2	Wind test (upright) + Drift test	Wind test (upright) + draft/2
	Standard Weather Criterion					Direct Procedure (or Three Steps Procedure)				
ϕ_1	0.153	Function of heel angle			0.125	0.153	Function of heel angle			0.125
l_{wl} [m]	1.096									
r [-]	1.096									
T_r [sec]	16.3									
s [-]	0.0431									
ϕ_1 [deg]	15.4									
ϕ_0 [deg]	6.1	3.7	4.9	3.8	5.0	6.1	3.7	4.9	3.8	5.0
$\phi_0 - \phi_1$ [deg]	-9.3	-11.7	-10.4	-11.6	-10.4	-13.2	-15.7	-14.4	-15.5	-14.3
ϕ_r [deg]	39.5									
Area a [rad-m]	0.075	0.063	0.069	0.063	0.070	0.111	0.096	0.103	0.095	0.106
Area b [rad-m]	0.224	0.295	0.259	0.276	0.247	0.224	0.295	0.259	0.276	0.247
b/a [-]	2.99	4.71	3.76	4.41	3.51	2.02	3.09	2.51	2.90	2.34
Crit. KG [m]	11.48	11.88	11.68	11.79	11.62	11.35	11.82	11.59	11.73	11.52

The last line of Table 2 shows the critical values of the vertical centre of gravity (KG), in which the ratio of area b/a=1 (see Figure 1). These last results are to be taken with some caution, since the effects of changing the vertical centre of gravity on T_r (natural roll period) and on the other quantities related to roll motion, including ϕ_1 , have been neglected.

Table 2 shows that the alternative assessment by model experiments can change b/a significantly with respect to the standard criterion. For this ship, b/a's of the right side of the table are smaller than those of the left side. This tendency comes from the increased ϕ_1 obtained by experiments and it was suggested in the previous paper that ϕ_1 was enlarged by the small damping coefficient (N=0.011 at 20 degrees). On the other hand, the l_{wl} evaluated through all the combinations of the wind tests and drifting tests, complete procedures and simplified procedures, tends to make b/a larger than the standard criterion. It has to be noted that the leading cause of the fluctuations is the large variation in the vertical centre of

hydrodynamic pressure when evaluated through the drifting tests.

Figure 12 shows the critical values of KG. From Table 2 and Figure 12, it is recognized that the changes in the critical value of the vertical centre of gravity are more contained than b/a, but as much as 0.4m at the maximum from the standard criterion.

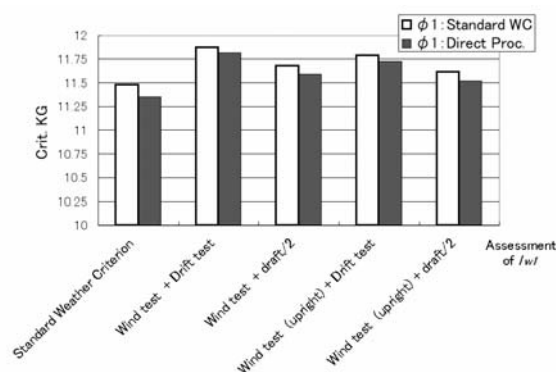


Figure 12 Variation of critical KG

7. CONCLUSIONS

In this paper, the results of the alternative assessment of the weather criterion by model experiments are reported. Almost full tests, included in the interim guidelines, were conducted. Considerable fluctuations of the assessment and their reasons are clarified. In order to make the assessment more uniform and to remove the word of “interim” from the guidelines, more extensive confirmation from the experience gained through the application of the guidelines is needed.

8. ACKNOWLEDGMENTS

Some parts of this investigation were carried out as a research activity of the SPL research panel of the Japan Ship Technology Research Association, funded by the Nippon Foundation. The authors express their sincere gratitude to the organizations.

9. REFERENCES

- Bulian, G., Francescutto, A., Serra, A. and Umeda, N., 2004, "The Development of a Standardized Experimental Approach to the Assessment of Ship Stability in the Frame of Weather Criterion", Proc. 7th International Ship Stability Workshop, pp. 118-126.
- Francescutto, A., Umeda, N., Serra, A., Bulian, G. and Paroka, D., 2004, "Experiment-Supported Weather Criterion and its Design Impact on Large Passenger Ships", Proc. 2nd International Maritime Conference on Design for Safety, pp.103-113.
- Hishida, T. and Tomi, T., 1960, "Wind Moment Acting on a Ship among Regular Waves", Journal of the Society of Naval Architects of Japan, Vol.108, pp.125-133 (in Japanese).
- IMO, 2002, "Code on Intact Stability for All Types of Ships Covered by Instruments", International Maritime Organization.
- IMO, 2003, SLF46/6/14, "Direct Estimation of Coefficients in the Weather Criterion", submitted by Japan.
- IMO, 2006, SLF49/5, "Revised Intact Stability Code prepared by the Intersessional Correspondence Group (Part of the Correspondence Group's report)", submitted by Germany.
- Ishida, S., 1993, "Model Experiment on the Mechanism of Capsizing of a Small Ship in Beam Seas (Part 2 On the Nonlinearity of Sway Damping and its Lever)", Journal of the Society of Naval Architects of Japan, Vol.174, pp.163-170 (in Japanese).
- Ishida, S. and Fujiwara, T., 2000, "On the Capsizing Mechanism of Small Craft in Beam Breaking Waves", Proc. 7th International Conference on Stability of Ships and Ocean Vehicles (STAB2000), Vol. B, pp.868-877.
- Taguchi, H., Ishida, S. and Sawada, H., 2005, "A trial experiment on the IMO draft guidelines for alternative assessment of the weather criterion", Proc. 8th International Ship Stability Workshop.
- Watanabe, Y., Kato, H., Inoue, S. et al., 1956, "A Proposed Standard of Stability for Passenger Ships (Part III: Ocean-going and Coasting Ships)", Journal of Society of Naval Architects of Japan, Vol. 99, pp. 29-46.

Estimating Probability of Capsize for Operator Guidance

Rubin Sheinberg, *U.S. Coast Guard ELC 023*

Karl Stambaugh, *U.S. Coast Guard ELC 023*

Andrew Eisele, *CDI Corporation*

Ross Leadbetter, *University of North Carolina*

ABSTRACT

Ships that are routinely called upon to perform demanding missions that often require operation in extreme weather environments will benefit from the development of Heavy Weather Guidance (HWG). This guidance is intended to assist vessel operators in the selection of safe speed and heading in severe weather conditions, thereby reducing the probability of dynamic instabilities and potentially disastrous capsize events. A simplified method of estimating the encounter-dependent capsize probability based on the results of time domain simulations is outlined along with procedures to extend these estimates to fully characterize the time-dependency of the probability. Additionally, an alternative method of calculating capsize probability involving integration of the Joint Probability Density Function (JPDF) of wave height and length over a region of predicted critical waves.

Keywords: *dynamic stability; operator guidance; heavy weather; risk assessment; mission planning; capsize; probability*

1. INTRODUCTION

A single analytical ship motion and dynamic stability simulation results in a single coherent dataset that represents the motion response and extreme motion behavior for one loading condition and one wave description over a range of operating speeds and headings; however, environmental conditions and ship loading are constantly changing and evolving during a realistic operational scenario, the practical utility of any single dataset or simulation is limited at best. For active operator guidance, therefore, it is necessary to produce predictions based on the actual loading condition of the ship, and the current “real-time” sea conditions.

This presents a significant challenge in the

design and development of an effective operational guidance strategy, particularly in the case of ships that are often called upon to operate in extreme environments for offshore patrol and search and rescue missions. Several potential solutions have been explored and found to possess significant limitations. Some of the more noteworthy approaches considered have included running time domain simulations onboard operational assets at sea, which gives highly accurate condition-specific results, but is too slow for timely guidance and therefore impractical. A second suggestion involved the development and maintenance of a catalog of previously generated polar plot bitmap images for a series of representative loading and seaway conditions, which could be referenced at sea to obtain approximate guidance on safe speed and heading based on the closest catalog condition. This approach eliminates the need for real-time simulation, but is both

cumbersome for the end-user, and of questionable accuracy as the deviation between actual conditions and catalog conditions increases.

The approach presented by the authors combines the individual advantages of each approach discarded above by 1) providing results for actual real-time seaway and loading conditions, and 2) relying on a pre-existing database to increase the analytical speed. Specifically, a prototype Heavy Weather Guidance (HWG) module for the Flooding Casualty Control Software (FCCS) program utilizes an electronic interpolation methodology to generate polar plots of potential capsizes based upon input of real-time significant wave height, wave period and ship loading conditions. Numerical simulations are carried out ashore to develop a comprehensive matrix of ship-class-specific, dynamic response polar plots that are stored in an electronic database. The actual at-sea and loading conditions are used to develop a reasonable polar plot for use in real-time operational guidance or mission planning and routing purposes.

2. NUMERICAL SIMULATION AND ANALYSIS

2.1 Dynamic Stability Simulation

During the development of the HWG module and methodology, numerical simulations were carried out utilizing the large amplitude ship motion and maneuvering prediction program FREDYN, developed by the Maritime Research Institute Netherlands (MARIN) in conjunction with the Cooperative Research Navies (CRNAV) consortium, which includes representation from navies of the U.S., U.K., France, Canada, Australia, and the Netherlands, as well as the USCG.

FREDYN automates the solution of the six degree-of-freedom (6-DOF) equations of

motion in the time-domain for a steered ship in regular or longcrested irregular waves, with or without wind contributions. The numerical models at the heart of the FREDYN program code have been extensively validated against both captive and free-running model tests for frigate type ships, which are in general reasonably similar in form, stability characteristics, and operational speed regimes as the ships considered in the present work.

2.2 Calculating Capsize Probability

The foundation of any operational guidance strategy ultimately lies in 1) the accurate characterization of the probability of capsizing, or any other undesirable dynamic behavior, and 2) the translation of these probabilities into a useful decision aid based on a specified level of acceptable risk.

This requires a statistical extrapolation of a relatively limited set of short-term simulation results into a robust and accurate long-term measure of capsizing probability. Although these calculations are transparent to the end-user, they form the basis of the polar plots at the heart of the HWG Module. Several new strategies for the calculation of capsizing probability have been explored during the HWG developmental effort, including a simplified estimation technique, and a modification of an alternative method first proposed by de Kat et al. (1994).

2.3 The Target Estimator Method.

The *Target Estimator Method* provides a simple direct-calculation procedure for the estimation of the *encounter-dependent probability of capsizing* based on a set of simulation results, and its subsequent extrapolation to fully characterize the *time-dependency* of the capsizing probability.

As a first step in this process, the capsizing probability per encountered wave, $p(c)$, is

estimated based on a simulation series where N_C represents the number of capsized occurrences in N_S simulations of constant duration, T . This calculation is shown in eq. 1,

$$p(c) = 1 - \left(\frac{N_s - N_C}{N_s} \right)^{\left(\frac{T_e}{T} \right)} \quad (1)$$

where T_e represents the encounter period for the specific condition being investigated. T_e can be estimated based on the relationship shown in eq. 2, in which T_z represents the average zero-upcrossing period of the seaway, $V_{m/s}$ is the ship speed in meters per second, g is the acceleration of gravity and γ is the vessel heading (0 deg = following seas).

$$T_e = \frac{T_z}{1 - \left[\frac{2\pi V_{m/s} \cos(\gamma)}{g T_z} \right]} \quad (2)$$

The calculation procedure defined in eq. 1 is readily extended to characterize the time-dependent probability of capsizing, $P_T(t)$ utilizing the simple relationship contained in eq. 3, where t represents the expected exposure duration.

$$P_T(t) = 1 - [1 - p(c)]^{\left(\frac{t}{T_e} \right)} \quad (3)$$

The *Average Return Period*, or *Mean Time-to-Capsize*, μ_t , for this process is easily calculated as shown in eq. 4, while the variance of the time-dependent probability, σ_t^2 , may be estimated as shown in eq. 5.

$$\mu_t = \frac{T_e}{p(c)} \quad (4)$$

$$\sigma_t^2 = \frac{P_T(1 - P_T)}{N_S} \quad (5)$$

The primary advantages of the *Target Estimator Method* are its relative ease of use,

and its ability to characterize the time-dependency of the capsizing probability based on known ship and seaway-related variables. Many other calculation techniques in use throughout the CRNAV community require fitted statistical distributions to characterize the time-dependent probability, which often rely on arbitrary shape, scale, and/or location parameters which have no real physical relationship to the ship or the seaway.

The *Target Estimator Method* has also been shown to provide generally excellent correlation with simulated capsizing data for a 378 ft. High Endurance Cutter utilized as the baseline test case during the present work. This is illustrated in Fig. 1, which provides a comparison of time-dependent capsizing probability estimates developed using the *Target Estimator Method* to actual simulated capsizing occurrences for the 378 ft. Cutter at 15 knots and a heading of 15 degrees (near following seas) for a variety of severe seaway conditions. In Fig. 1, the plotted data points represent the cumulative fraction of individual FREDYN simulations that have capsized by a given time-step in each seaway, and the plotted lines reflect the use of the *Target Estimator Method* (e.g. a continuous plot of eq. 3, with exposure duration, t , treated as an independent variable). Similar levels of agreement have been observed for other speeds, headings, and seaway conditions as well.

2.4 Limitations of the Target Estimator Method.

Although the *Target Estimator Method* is both accurate and simple to use, its range of practical application is restricted by the amount of simulation time required to produce reliable estimates in the operational range (e.g. speed-heading combinations) and seaway conditions for which capsizing probability is relatively low.

For the most extreme sea states, where capsizing probability is comparatively high, capsizes are encountered frequently during

simulations, and as such a reasonable statistical sample can be obtained quite readily for use in a direct calculation of the incident capsizing probability. On the other hand, when simulations take place in more mild environmental conditions, the amount of run-time required to achieve even a single capsizing occurrence may be quite substantial. The run-time requirements are then magnified by the need to collect multiple capsizing occurrences for a reasonable statistical sample. The complications presented by this issue become evident when typical levels of acceptable risk are considered.

2.5 Risk Assessment.

A proposed level of maximum acceptable annual risk, or annual probability of capsizing, is given by McTaggart et. al. (2002) and Dahle and Myrhaug (1995) as approximately 1×10^{-4} . However, the time dependency of capsizing risk is not addressed.

The author's contend that an evaluation of the climatology of extreme seas suggest that an exposure duration may be necessary to provide for an adequate level of safety. A possible source of exposure time frame may be determined from inspection of climatological data. A time-history of significant wave height and dominant (modal) period during Hurricane Katrina, measured at National Data Buoy Center (NDBC) station 42040 off the coast of Alabama in August 2005 is illustrated in Fig. 2. Very severe sea conditions, with significant wave heights above 10 meters, persisted for a duration of nearly 12 hours are clearly shown in Fig. 2. Likewise, conditions with significant wave heights greater than 8 meters persisted for more than 20 hours.

These trends are illustrated in more detail in Fig. 3 which shows the total duration of storm conditions as a function of significant wave height for Hurricanes Katrina and Ivan (also measured at NDBC station 42040 in September 2004).

Although a detailed treatment is not given in the present work, based on a review of historical archives available at NDBC, the seaway durations indicated by Figs. 2 and 3 are fairly typical of severe storm and hurricane conditions measured from a stationary reference (e.g. a tethered buoy).

Because an operational asset facing these types of conditions does not remain stationary, the correlation of historical seaway duration to operational exposure can not be performed on a one-to-one basis.

However, there is overwhelming evidence to suggest that operational exposures are likely to be substantially longer than one hour, should a vessel face this type of severe conditions.

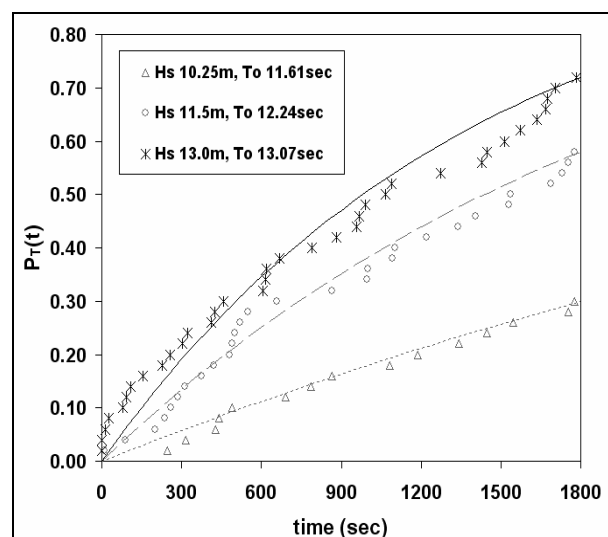


Figure 1. Correlation of Cumulative Time-to-Capsize Estimates made with the *Target Estimator Method* and Simulated Data

Based on the inspection of storm data, the author's would suggest that a cumulative probability of capsizing of 1×10^{-2} in a 12 hour exposure period is reasonable to form the basis for short-term operational guidance. This assumes the acceptable level of risk is inversely proportional to exposure time and an annual probability of capsizing is on the order of 1×10^{-4} . This is an area that requires further investigation.

2.6 Simulation Requirements.

Considering the fact that a typical time domain simulation series is composed of a unique, user-specified number of individual simulations, each of which is typically 30 minutes in duration, it is easy to develop an estimate of the simulation requirements to characterize a probability of capsize on the order of 1×10^{-2} for a 12 hour exposure period using the simple *Target Estimator Method* are substantial.

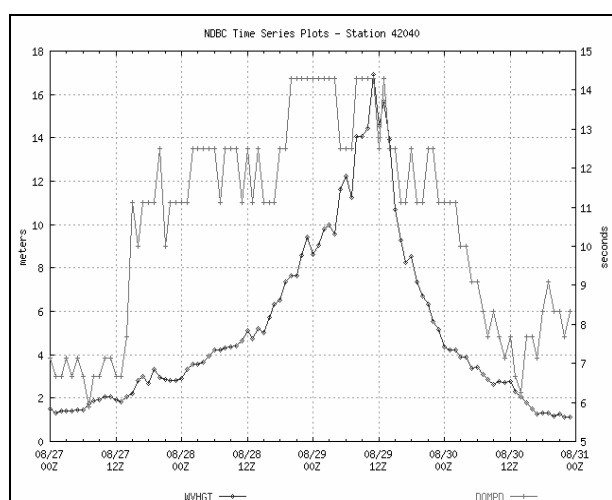


Figure 2. Hurricane Katrina Seaway Data

This fact is illustrated in Fig. 4, which shows the cumulative time-dependent probability levels calculated based on a single realized capsize occurrence for varying numbers of 30-minute simulations, assuming a constant encounter period slightly greater than 11 seconds. Although the assumption of constant encounter period in the development of Fig. 4 is not strictly valid, considering the variations shown in the number of simulations required to achieve a single capsize event, it is utilized to illustrate the basic order of magnitude of the problem only.

Inspection of Fig. 4 clearly demonstrates that more than 1,000 simulations would be required to provide the data necessary to characterize a cumulative capsize risk on the order of 1×10^{-2} for any appreciable exposure duration. Furthermore, since all time domain

data contained in the present work is based on multiples of discrete, 30 minute simulations, the number of simulations indicated by Fig. 4 is approximately twice the total simulation time required to capture one simulated capsize event, in hours.

For a complete statistical sample, there will need to be even more simulations run (10 to 100 times more). If 1×10^{-2} the number of time domain simulations is very large, but feasible given current processing capabilities.

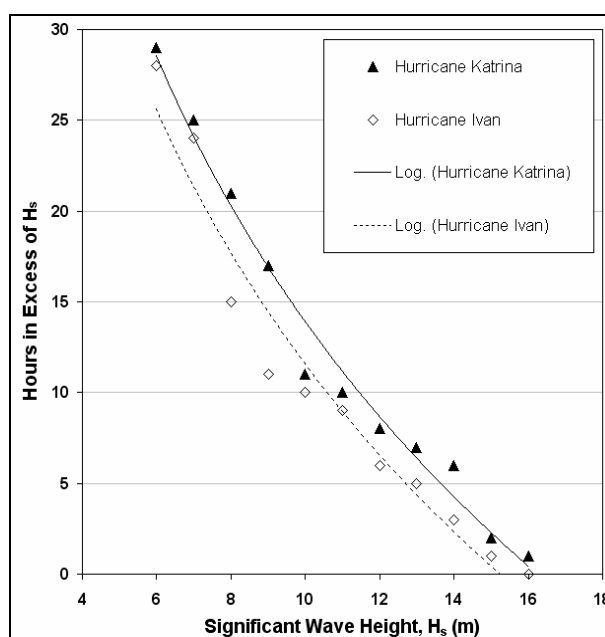


Figure 3. Duration of Extreme Sea Conditions for Recent Major Hurricanes

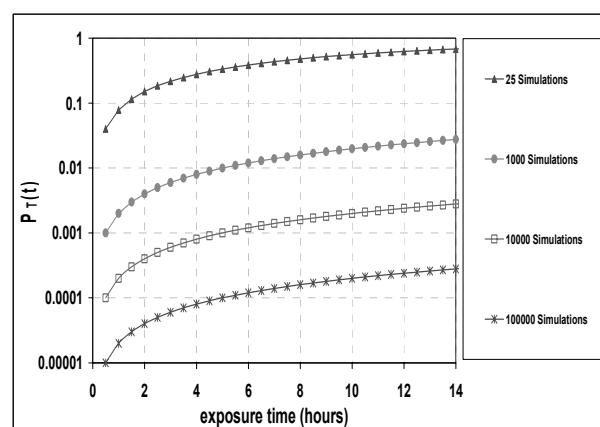


Figure 4. Time dependant probabilities for a single capsize occurrence in a varying number of simulations

2.7 The JPDF Integration Method.

As an alternative to direct-calculation method for the estimation of capsizing probability, the authors considered an approach proposed by de Kat et. al. (1994) that offers the potential for less simulation duration requirements. Briefly, this approach involves:

- a) running time domain simulations for a series of severe seaway conditions, and characterizing the localized wave height and length producing a capsizing event. This is accomplished through an evaluation of the time-dependent spatial wave conditions in the vicinity of the ship immediately prior to a capsizing event,
- b) cataloging the wave characteristics associated with each simulated capsizing event, such that, as many capsizing occurrences are collected, a deterministic region of “critical wave” parameters is defined within the generalized domain of wave height and length,
- c) estimating the probability of occurrence of individual waves in a target seaway using a Joint Probability Density Function (JPDF) of wave height and length, and,
- d) integrating the JPDF over the “critical wave” region to estimate the probability capsizing for the target seaway.

This approach is repeated for each specified set of ship conditions (loading, speed, heading, etc.) in order to provide a comprehensive database of capsizing probability calculations that form the basis of real-time operational guidance.

To facilitate these calculations, the JPDF may be approximated using the approach described in Longuet-Higgins (1983), or alternatively, an “exact distribution” may be computed for a Gaussian wave process as advocated by Rychlik et. al. (2004). Although the “exact” method of developing the JPDF is more accurate from a physical standpoint, the Longuet-Higgins approximation remains convenient for computational simplicity, given its reliance on a straightforward and easy to

use mathematical relationship, as shown in eq. 6,

$$p(R, \tau) = \left(\frac{2}{\pi^{1/2} \nu} \right) \left(\frac{R^2}{\tau^2} \right) e^{-R^2 \left[1 + \frac{(1-\tau)^2}{\nu^2} \right]} L(\nu) \quad (6)$$

in which R and τ are non-dimensional references to wave height and period, such that,

$$R = \frac{H}{2(2m_0)^{1/2}} \quad (7)$$

$$\tau = \frac{T}{T_1} \quad (8)$$

where H is the wave height, T is the wave period, and m_0 and T_1 are the variance (i.e. zeroth spectral moment) and average period of the seaway, respectively.

The JPDF calculation in eq. 6 is also dependent upon a spectral width parameter, ν and a normalization factor $L(\nu)$, in which,

$$\nu = \left(\frac{m_0 m_2}{m_1^2} - 1 \right)^{1/2} \quad (9)$$

$$L(\nu) = \frac{2}{1 + (1 + \nu^2)^{-1/2}} \quad (10)$$

where m_n is the n^{th} spectral moment of the seaway.

Because a spatial wave analysis is utilized in the definition of “critical wave” characteristics, the “critical” parameters are given in terms of wave height and length. Therefore, to allow for a one-to-one correlation, the calculated JPDF of wave height and period shown in eq. 6 is converted to the space domain according to the basic dispersion relationship, given in eq. 11.

$$L = T^2 \frac{g}{2\pi} \quad (11)$$

Although the application of the dispersion relationship is valid for simple harmonic (regular) waves, this relationship is generally not satisfied for an irregular seaway, except as an approximation for an extremely narrowband sea. However, use of this relationship remains relatively common for this type of analysis, mainly for convenience in the transformation of wave characteristics from time records to the space-domain, even if not strictly valid. In this case, the author's feel that the proposed method is sufficient to support a basic "engineering solution" to the estimation of capsizes probability, without requiring unrealistically extensive simulation requirements.

2.8 Limitations of the 1994 JPDP Integration Method.

A key component of the de Kat et. al. (1994) JPDP integration methodology involves the contention that the probability that "critical" conditions exists in any given seaway is equal to the encounter-dependent probability of capsizes. This is equivalent to a statistical assumption that any single wave occurrence falling within the range of "critical" parameters will result in a capsizes event.

Early evaluations supporting the present effort have indicated that estimates made utilizing this assumption result in an overestimation of capsizes probability by approximately an order-of-magnitude for a 378 ft. High Endurance Cutter, when compared to corresponding estimates developed with the previously described Target Estimator Method, for sea states in which adequate capsizes data is available. Similar findings have also been reported by Leadbetter and Rychlik (2005). This suggests that, at least for this particular ship class, many of the so-called "critical waves" can be encountered without resulting in a capsizes.

2.9 Current Innovation: The Capsizes Region Transfer Function.

In order to eliminate the order-of-

magnitude overestimates in the calculation of capsizes probability observed utilizing the original methodology proposed by de Kat et. al. (1994), Stambaugh and Eisele have developed a *Modified JPDP Integration Approach*. The primary innovation in the newly proposed methodology involves the definition of a *Capsizes Region Transfer Function* (CRTF), which modifies the calculated JPDP of wave height and length to account for "critical wave" encounters which do not result in capsizes. The author's liken this approach to the utilization of Response Amplitude Operators (RAO's) to translate sea spectra into derived responses in frequency domain seakeeping analysis, the only difference being that the CRTF is defined in three-dimensional space over the generalized domain of wave height and length.

For the purposes of mathematical simplicity, the first step in the modified approach involves the discretization of the JPDP of wave height and length into "bins" measuring 1 meter in wave height by $0.2 \times \text{LBP}$ in wave length, primarily to facilitate calculation in a simplified spreadsheet format, and to allow for subsequent modification by the empirical CRTF.

The CRTF itself is then generated concurrently with the definition of the "critical wave" region. Specifically, as capsizes are collected during a simulation series consisting of N_S simulations for a specific baseline seaway condition, the spatial wave analysis introduced in the original de Kat (1994) methodology is carried out as usual to identify the "critical" parameters associated with each capsizes wave. The capsizes wave occurrences are then organized in "bins" of wave height, H_j , and wave length, L_k , consistent with those utilized in the characterization of the discretized JPDP, such that as many capsizes are collected, a three dimensional histogram of capsizes occurrences, $N_C(H_j, L_k)$, is generated.

In addition to the collection of "critical wave" characteristics, the simulation time step

at capsizes is also recorded for each occurrence during the simulation series as t_1, t_2, \dots, t_{N_C} where N_C represents the total numbers of observed capsizes. Where a capsize does not occur for any particular simulation within the series, the total simulation duration, T_{sim} , is recorded, such that when eq. 12 is applied, the total simulated exposure duration for the baseline seaway, T_{exp} , is characterized.

$$T_{exp} = \sum_{i=1}^{N_C} t_i + (N_S - N_C)T_{sim} \quad (12)$$

Based on this exposure duration, the total number of waves encountered during the simulation series, N_e , follows as shown in eq. 13, where T_e represents the encounter period.

$$N_e = \frac{T_{exp}}{T_e} \quad (13)$$

The total number of wave encounters in the simulation series are then distributed into similar discrete “bins” in the generalized domain of wave height and period using eq. 14, such that a second three dimensional histogram, $N_W(H_j, L_k)$, is created,

$$N_W(H_j, L_k) = JPDF(H_j, L_k) \times N_e \quad (14)$$

for $j=1..N_{hb}$ and $k=1..N_{lb}$

where N_{hb} and N_{lb} represent the discrete number of wave height and wave length “bins”, respectively, and $JPDF(H_j, L_k)$ represents the joint distribution of wave height and length for the baseline seaway, calculated in accordance with eq. 6. Note that the parameters H_j and L_k in this relationship represent the individual wave height and wave length “bins”, respectively.

The process of time domain simulation, and subsequent characterization of capsize and wave occurrence histograms is repeated for several baseline seaway conditions, until a

reasonable set of capsize data has been obtained for the specific speed-heading combination under investigation. Current practice includes 50 individual runs of 30 minute duration, for a total of five to six steep seaway conditions located along the Buckley (1988) “envelope of extremes”, where capsizes generally occur more frequently. The three dimensional histograms of capsizes occurrences and total wave encounters developed for each individual baseline seaway are then summed to result in an aggregate characterization of capsizes and wave encounters for all simulations made at a specific speed and heading combination is repeated for several baseline seaway conditions, until a reasonable set of capsize data has been obtained for the specific speed-heading combination under investigation. Current practice includes 50 individual runs of 30 minute duration, for a total of five to six steep seaway conditions located along the Buckley (1988) “envelope of extremes”, where capsizes generally occur more frequently. The three dimensional histograms of capsizes occurrences and total wave encounters developed for each individual baseline seaway are then summed to result in an aggregate characterization of capsizes and wave encounters for all simulations made at a specific speed and heading combination.

The composite histograms are utilized to compute the CRTF for a specific speed and heading in accordance with eq. 15.

$$CRTF(H_j, L_k) = \frac{N_C(H_j, L_k)}{N_W(H_j, L_k)} \quad (15)$$

for $j=1..N_{hb}$ and $k=1..N_{lb}$

This process is illustrated graphically in Fig. 5. Note that for the sample shown in Fig. 5, the majority of capsizes resulted from wave conditions with heights ranging between 7 and 10 meters, and wave lengths between 0.8 and 1.0 times the ship length. However, the total number of wave encounters in this region is also relatively high, and in fact only a small

fraction (~10%) of these encounters actually resulted in a simulated capsizes event, therefore the computed CRTF is also relatively low in this area. On the other hand, only a handful of simulated capsizes events resulted from waves greater than or equal to 16 meters in height, but the total wave encounters exhibiting these characteristics was also very low, and therefore the CRTF is comparatively high in this region.

Once the CRTF has been developed for a particular speed and heading of interest, based on a relatively small sampling of baseline seaway conditions along the Buckley (1988) “envelope of extremes”, no additional simulation is required to characterize the *encounter-dependent* probability of capsizes, $p(c)$, for any other target seaway. This calculation is carried out strictly through mathematical variation of the JPDF of wave height and wave length for the target seaway, as shown in eq. 16.

$$p(c) = \sum_{j=1}^{N_{Hj}} \sum_{k=1}^{N_{Lk}} [JPDF_{target}(H_j, L_k) \times CRTF(H_j, L_k)] \cdot dH \cdot dL \quad (16)$$

where $JPDF_{target}(H_j, L_k)$ is the discretized joint probability density function of wave height and wave length for the target seaway condition, calculated using eq. 6, and dH and dL are the discrete “bin” dimensions for wave height and wave length, respectively. The time-dependency of the capsizes probability can then be characterized using eq. 3. The procedure for calculating probability of capsizes for a target seaway utilizing the CRTF in accordance with eq. 16 is illustrated graphically in Fig. 6.

Comparisons between the CRFT approach and the target estimator approach are presented in Table 1. There is a variability of results with wave height resulting from the statistical effects of the presence of multiple waves and ship dynamic memory effects. However, results are conservative for smaller seaways with low probability of capsizes or interest for operator guidance. Recent work with a slope based CRTF shows promise in minimizing the

variation with wave height. This should be the subject of additional investigation.

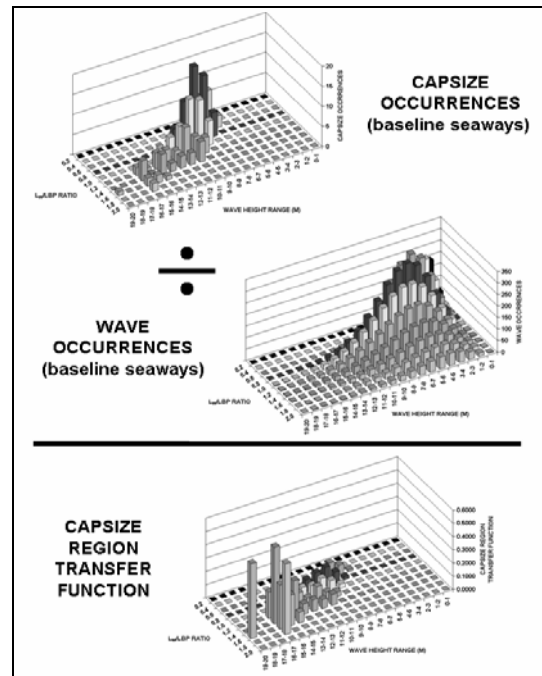


Figure 5. Capsizes Region Transfer Function (CRTF) Development

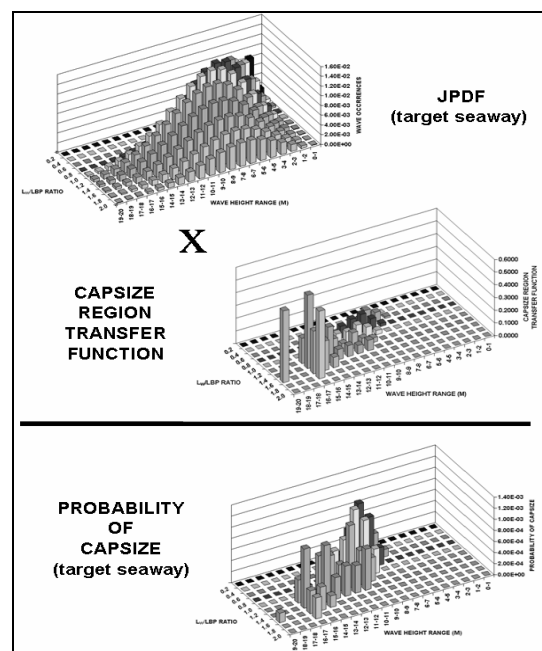


Figure 6. Use of the CRTF to calculate capsizes probability

Table 1 Comparison of Probability of Capsize Calculation

	Seaway and Simulation Parameters						Target Estimator Method		Modified JPDF Integration Method	
	H_s	T_o	T_z	T_e	N_c	N_s	$p(c)$	$P_T(t)$ for $t=1$ hr	$p(c)$	$P_T(t)$ for $t=1$ hr
	(m)	(sec)	(sec)	(sec)						
45 degrees	7.50	9.68	7.45	14.03	19	50	3.72E-03	6.16E-01	8.97E-03	9.01E-01
	9.00	10.87	8.12	14.25	34	50	8.98E-03	8.98E-01	1.35E-02	9.68E-01
	10.25	11.61	8.62	14.60	45	50	1.84E-02	9.90E-01	1.69E-02	9.85E-01
	11.50	12.24	9.05	14.74	49	50	3.15E-02	1.00E+00	2.01E-02	9.93E-01
	13.00	13.07	9.61	15.10	50	50	4.50E-02	1.00E+00	2.23E-02	9.95E-01
15 degrees	9.00	10.87	8.12	19.71	11	50	2.72E-03	3.92E-01	5.59E-03	6.41E-01
	10.25	11.61	8.61	19.32	15	50	3.82E-03	5.10E-01	7.49E-03	7.54E-01
	11.50	12.24	9.05	19.16	29	50	9.19E-03	8.24E-01	8.72E-03	8.07E-01
	13.00	13.07	9.61	19.10	36	50	1.34E-02	9.22E-01	8.93E-03	8.16E-01
	14.00	13.56	9.95	19.13	39	50	1.60E-02	9.52E-01	8.76E-03	8.09E-01

3. CONCLUSIONS

This paper has summarized an approach for the estimation of probability capsizes based on numerical simulation using a time-domain ship motion and maneuvering program for use with an operator Heavy Weather Guidance (HWG) system.

New approaches for the calculation and interpretation of the probability of capsizes have been presented, along with a strategy for the use of these probabilities as an operational decision aid based on recommendations for acceptable levels of short-term risk.

Based on the work presented herein, the following conclusions are presented:

- The time domain capsizes prediction technique proposed is suitable for predicting the general capsizes and dynamic stability behavior necessary for effective Heavy Weather Guidance.
- The estimation of capsizes probabilities are now possible based on the time domain simulations using estimated capsizes probabilities from a discrete number of time domain simulations and developing a capsizes transfer function for wave parameters in combination with a JPDF for a given seaway. Although refinements to the approach are

necessary, the general approach is certainly worth further investigation.

- Additional effort is required to evaluate the acceptable level of capsizes probability for short term operator guidance applications.

4. ACKNOWLEDGEMENTS

The authors would like to acknowledge the contributions of the CRNav group in review of the progress presented by the authors.

The opinions expressed herein are those of the authors and do not represent official policy of the U.S. Coast Guard.

5. REFERENCES

- Buckley, W.H., September 1988, "Extreme and Climatic Wave Spectra for use in Structural Design of Ships." *Naval Engineers Journal*.
- Dahle, E.A., and Myrhaug, D. October 1995. "Risk Analysis Applied to Capsizes of Fishing Vessels," *Marine Technology*.
- De Kat J.O., Brouwer, R., Mctaggart, K., and Thomas, W.L. 1994 "Intact Ship Survivability in Extreme Waves: Criteria from a Research Navy Perspective," STAB 94, *Fifth International Conference on Stability of Ships and Ocean Vehicle*, Melbourne, Florida.
- Leadbetter, M.R., and Rychlik, I. April 2005, "Capsizes Prediction Based on Wave Statistics," USCG Task Report.
- Longuet-Higgins, M.S. 1983, "On the Joint Distribution of Wave Periods and Amplitudes in a Random Wave Field," *Proceedings of the Royal Society of London*, A 389, pp 241-258.
- Mctaggart, K., Carnie, P., Witzke, D., and Maze, R. 2002, "Capsizes Probability Polar Plots for Ship Operator Guidance,"

Proceedings of the 2002 Stability Workshop,
Webb Institute.

Michel, W.H. Winter 1999, "Sea Spectra Revisited," *Marine Technology*, Vol. 36, No. 4, pp. 211-227.

Rychlik, I., et., al., 2004, "Wave Analysis for Fatigue and Oceanography: A toolbox of Matlab routines for statistical analysis and simulation of random waves and loads," Version 2.1.0, Mathematical Statistics Department, Lund University.

Analytical Study of the Effect of Drift Motion on the Capsizing Probability under Dead Ship Condition

Yoshitaka Ogawa, *National Maritime Research Institute*

J.O. de Kat, *Maritime Research Institute Netherlands*

Shigesuke Ishida, *National Maritime Research Institute*

ABSTRACT

The effect of drift motion on the capsizing probability under dead ship condition was examined in this paper. Drift speed in beam wind and waves was estimated by the combination of the manoeuvring model of the slow streaming condition, wind force and wave drift force. It is found that the estimated drift speed explains the drift speed measured by the model tests. The capsizing probability, which takes account of the effect of the drift motion, was evaluated. It is verified quantitatively that the drift motion has effect on the capsizing probability.

Keywords: *dead ship, drift motion owing to wind and waves, large passenger ship, cross flow model, capsizing probability*

1. INTRODUCTION

It is well known that a ship, which is almost longitudinally symmetric, suffers beam wind and waves when all her operational means such as propeller thrust and rudder control are lost. Therefore, it is important to assess the capsizing probability under dead ship condition properly and to provide the minimum requirements for an adequate stability. It is also known that a drift motion has effect on the capsizing probability. However, there is few study on the effect of it on the capsizing probability.

Based on the background, the analytical model for the estimation of the roll motion under dead ship condition is proposed. By means of the present method, the effect of the drift motion on the capsizing probability under dead ship is examined.

Firstly, model tests have been carried out by means of a large passenger ship, which has

a large windage area. The test comprised free drifting tests in beam wind and waves. The drift speed and roll motions of the passenger ship were discussed. It is found that wind has much effect on the drift speed. It is verified that roll motion of the large passenger ship in the severe sea state is not significant.

Secondly, the drift speed under dead ship condition was estimated by extending the manoeuvring model of the slow streaming condition, which is developed by Yoshimura (Yoshimura, 1988). Wind forces and wave induced lateral force are integrated with the drag owing to the drift motion in the present model.

In the present method, a lateral resistance, which is associated with the drift speed, was estimated under the assumption that the resistance due to water is mainly generated by the vortex-induced viscous forces. Wind force was estimated by means of the empirical formulas, which were developed by Blendermann and Fujiwara (Blendermann, 1996 and Fujiwara, 2001). With regard to the

wave drift motion, the wave-induced steady lateral force was estimated by means of the Kashiwagi's method (Kashiwagi, 1992). The only unknown in this method is the Kochin function, which is equivalent to the ship-generated progressive wave far from the ship. The Kochin function was estimated by means of the Enhanced Unified Theory (Kashiwagi, 1995), which incorporates the 3-D and forward-speed effects on the longitudinal source distribution representing ship disturbance in the far field.

By summarizing these estimated forces, the drift speed under dead ship condition was estimated. Having compared with the experimental data, it is confirmed that present method is useful for the qualitative estimation of the drift speed under dead ship condition.

Finally, the capsizing probability was evaluated by integrating a joint probability density function of Gaussian roll and roll rate in waves over the capsizing domain on the phase plane of the roll motion. Based on these findings, the effect of the drift motion on the capsizing probability under dead ship condition was discussed. It is confirmed that drift speed has effect on the capsizing probability under dead ship condition.

2. THE SUBJECT SHIP

The large passenger ship used in the present study has been designed at MARIN for the use in studies on parametric rolling in head and following seas, the results of which had been published at several international conferences (e.g., Luth, 1998). The principal dimensions of the large passenger ship are shown in Table 1. The profile of the large passenger ship is shown in Figure 1. The hull form is typical for a modern large passenger ship. It is equipped with bilge keels and anti-roll fins.

Concerning loading conditions of this ship, the limiting KG is governed by the weather

criterion in the IMO Intact Stability code. Figure 2 shows the righting lever (GZ) curves correspond to five KG values. In the calculation of the GZ curves, non-watertight superstructure and down-flooding openings were neglected. The steady and gust wind heeling levers, defined in the weather criterion, are also shown in Figure 2.

Table 1 Principle dimensions of the large passenger ship

Lpp(m)	240
B(m)	32.2
D(m)	22
d(m)	7.75
Displacement(m ³)	36895.58
Cb	0.616
B/d	4.15
Roll period(sec)	24.7
GM(m)	1.85
Logitudinal radius of gyration (κ_{yy}/L)	0.25
Transverse radius of gyration (κ_{xx}/L)	0.45

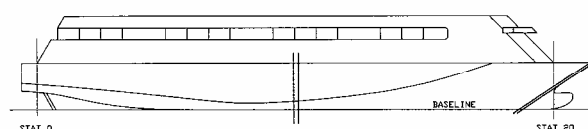


Figure 1 Profile of the large passenger ship

For three of these cases (KG=15 m, 15.6 m and 15.8 m; OG/d=0.935, 1.013 and 1.039), the ship complies with the current weather criterion. In particular, KG = 15.8 m represents the limiting KG case, so the other two KG cases (16 and 16.4 m) would result in failure of the weather criterion.

The present study was carried out for the case of KG=15.8m, which is a critical value against the weather criterion.

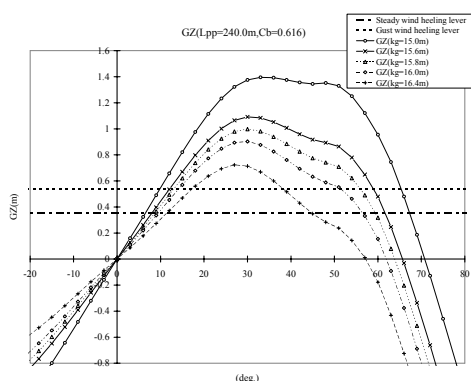


Figure 2 Righting lever (GZ) curve of the large passenger ship

3. EXPERIMENTS IN BEAM WIND AND WAVES

For the examination of the effect of wind and waves on the drift motion, model tests have been carried out at Seakeeping and Manoeuvring Basin of MARIN (dimensions 170m x 40m) in a severe sea states. The test program comprised free drifting tests in beam steady wind only (Wind speed U_T : 20 and 26 m/sec), irregular beam waves only ($H_s = 9.5$ m, $T_{01} = 10.4$ sec) and in combined beam waves and steady wind. The roll period was measured to be 24.7 sec. by a roll decay test.

Table 2 and 3 show the mean and the standard deviation of measured roll motion and yaw motion respectively. Even in such a severe sea state, the roll motion was very limited. It is clarified that the associated capsizing probability would be extremely low for such a sea state. It is found that the standard deviation of yaw motion in beam wind is small. This indicates that ship drifts with the small heading angle and with the steady heading angle generated at the initial stage of the drift motion.

Table 2 Mean and standard deviation of roll in beam wind and waves

U_T (m/sec)	$H_{1/3}$ (m)	T_{01} (sec)	Mean (deg.)	Standard Deviation (deg.)
20	----	----	2.96	0.17
26	----	----	4.90	0.27
----	9.5	10.4	0.40	1.13
20	9.5	10.4	2.89	1.06
26	9.5	10.4	5.22	1.32

Table 3 Mean and standard deviation of yaw in beam wind and waves

U_T (m/sec)	$H_{1/3}$ (m)	T_{01} (sec)	Mean (deg.)	Standard Deviation. (deg.)
20	----	----	14.7	1.59
26	----	----	21.25	0.79
----	9.5	10.4	1.38	9.56
20	9.5	10.4	10.75	1.15
26	9.5	10.4	16.31	1.45

Figure 3 and 4 show the trajectory where the ship drifts in beam wind only (wind speed U_T : 26m/sec) and in beam waves only ($H_s = 9.5$ m, $T_{01} = 10.4$ sec) respectively. In the present experiments, measurements were begun just in the beam wind and waves. The mean drift speed in beam wind only is 2.0m/sec. The mean drift speed in beam waves only is 0.8 m/sec. It is found that wind has much effect on the drift speed rather than waves.

Figure 5 shows the trajectory where the ship drifts in beam wind and waves. The mean drift speed in beam wind only (Wind speed $U_T = 26$ m/sec) is 2.2m/sec. It is clarified that the ship drifts at close to a beam sea heading angle. It is found that the trajectory in wind and waves looks very similar to the trajectory in beam wind only. It is verified that the wind has a dominant influence on the drift motion.

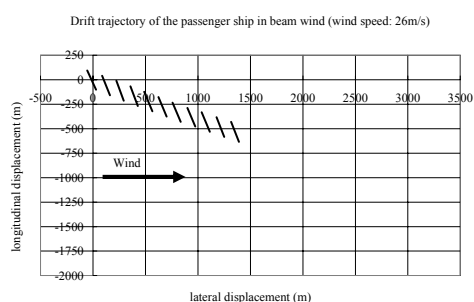


Figure 3 Drift trajectory of the passenger ship in beam wind (wind speed: 26m/s, time interval of trajectory: 70.7 sec)

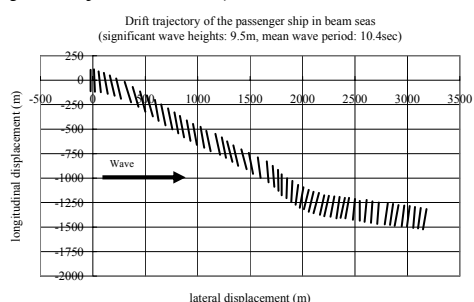


Figure 4 Drift trajectory of the passenger ship

in beam waves (significant wave heights: 9.5m, mean wave period: 10.4sec, time interval of trajectory: 70.7 sec)

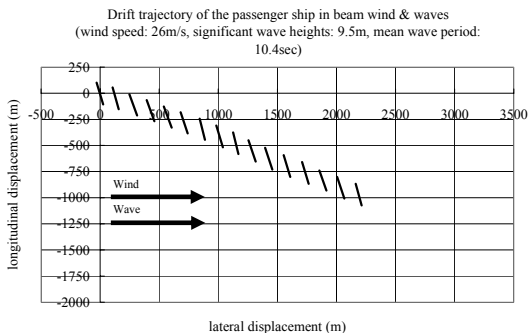


Figure 5 Drift trajectory of the passenger ship in beam wind and waves (wind speed: 26m/s, significant wave heights: 9.5m, mean wave period: 10.4sec, time interval of trajectory: 70.7 sec)

4. ESTIMATION METHOD OF DRIFT SPEED OWING TO WIND AND WAVES

4.1 Equation of Motion

The drift speed under dead ship condition was estimated by extending the cross flow model of the slow streaming condition, which was developed by Yoshimura (Yoshimura, 1988). Wind forces and wave induced lateral force are integrated with drag owing to the drift motion in the present model. The equation of the lateral motion of the drifting ship, which is almost longitudinally symmetric, can be described as follows:

$$(m + m_y)\dot{v} + (m + m_x)ur = Y_H + Y_A + Y_W. \quad (1)$$

Here m denotes ship's mass, m_x denotes longitudinal component of added mass, m_y denotes lateral component of added mass, u denotes the longitudinal component of ship speed, v denotes the lateral component of ship speed, r denotes angular velocity, Y_H denotes the resistance owing to drift motion, Y_A denotes the lateral component of wind force and Y_W denotes the lateral component of wave drift

force. However, the equation (1) can be expressed as follows because the results of the experiments show that the angular velocity is negligible.

$$(m + m_y)\dot{v} = Y_H + Y_A + Y_W \quad (2)$$

4.2 Resistance owing to drift motion

In accordance with Yoshimura's cross flow model, the resistance owing to a drift motion can be described as the cross flow drag of the slow streaming condition. In accordance with the similar procedure to the equation (2), the lateral component of the cross flow drag is approximated as follows:

$$Y_H = \frac{\rho}{2} L d V^2 C_{D0} \quad (3)$$

where ρ denotes the density of fluid, L denotes the ship length, d denotes the ship draught, V denotes the ship speed and C_{D0} denotes the cross flow drag coefficient. In this study, C_{D0} was assumed as 0.8.

Strictly, experimental results clarified that the longitudinal velocity of drift motion of the present large passenger ship can not be neglected. It means that not only the equation of the lateral motion but also the equation of the longitudinal motion should be solved.

However, in the present study, only the equation of the lateral motion was solved to estimate the lateral drift speed as the first step of the development of the rational estimation method of drift motions.

4.3 Wind Force

Wind force Y_A can be estimated by means of the experimental formulas by Blendermann (Blendermann, 1996) or Fujiwara (Fujiwara, 2001). In accordance with their methods, the lateral component of wind force is expressed as

follows:

$$Y_A = C_{YA} \frac{\rho_A}{2} U_T^2 A_L \quad (4)$$

where C_{YA} denotes the aerodynamic drag coefficient, ρ_A denotes the air density, U_T denotes the lateral wind velocity and A_L denotes the lateral projected area. The aerodynamic coefficients by means of the Blendermann's data for the passenger ship and the Fujiwara's empirical equation give almost the same value (0.895 and 0.883). In this study, C_{YA} was assumed as 0.895.

4.4 Wave Drift Force

According to Kashiwagi's theory (Kashiwagi, 1992) which is based on the momentum and energy conservation principles, the wave drift force was calculated. A Cartesian coordinate system was taken as shown in Figure 6. A ship is assumed to advance with a constant speed U and oscillate with a circular frequency ω in deep water. By means of the ship-generated progressive waves at far field, the wave induced sway force is expressed as

$$\begin{aligned} \frac{\bar{Y}}{\rho g \zeta_w^2} &\cong \frac{-1}{4\pi k_0} \left[-\int_{-\infty}^{k_1} + \int_{k_2}^{k_3} + \int_{k_4}^{\infty} \right] v \times \\ &\text{Im}[C(k) \cdot S^*(k)] dk \\ &+ \frac{1}{2} \sin \chi \cdot \text{Im}[C(k_0 \cos \chi) + iS(k_0 \cos \chi)], \end{aligned} \quad (5)$$

where

$$\left. \begin{aligned} \kappa(k) &= \frac{1}{g} (\omega + kU)^2 = K + 2k\tau + \frac{k^2}{K_0} \\ K &= \frac{\omega^2}{g}, \tau = \frac{U\omega}{g}, K_0 = \frac{g}{U^2} \end{aligned} \right\} \quad (6)$$

$$\left. \begin{aligned} k_1 \\ k_2 \end{aligned} \right\} = \frac{-K_0}{2} (1 + 2\tau \pm \sqrt{1 + 4\tau}) \quad (7)$$

$$\left. \begin{aligned} k_1 \\ k_2 \end{aligned} \right\} = \frac{K_0}{2} (1 - 2\tau \mp \sqrt{1 + 4\tau})$$

g is the gravitational acceleration, ζ_w is the wave amplitude and k_0 is the wave number of the incoming wave.

Here it should be understood that $k_3=k_4$ for $\tau > 1/4$ and the integration range from k_2 to ∞ in (5) becomes continuous.

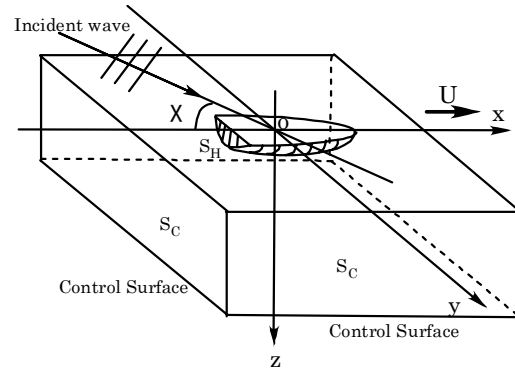


Figure 6 Coordinate system of Kashiwagi's theory

The wave-amplitude functions in (5), $C(k)$ and $S(k)$, are given by the following equations as the superposition of all components of ship-generated waves

$$\begin{aligned} C(k) &= H_{7C}(k) \\ &- \frac{\omega_0 \omega}{g} \sum_{j=1,3,5} \frac{X_j}{\zeta_w} \cdot H_j(k) \end{aligned} \quad (8)$$

$$\begin{aligned} S(k) &= H_{7S}(k) \\ &- \frac{\omega_0 \omega}{g} \sum_{j=2,4,6} \frac{X_j}{\zeta_w} \cdot H_j(k) \end{aligned} \quad (9)$$

where ω_0 is the circular frequency of the incoming wave, X_j is the complex amplitude of the ship motion of j -th mode and $H_j(k)$ is the Kochin function of the ship-generated progressive waves at far field. In the present method, the Kochin function was calculated by

means of the Kashiwagi's Enhanced Unified Theory (Kashiwagi, 1995).

Figure 7 shows the wave induced steady sway force in beam seas as a function of wave length ratio λ/L (λ :wave length, L :ship length). It is found that the wave induced steady sway force is not affected by the small difference of the heading angle.

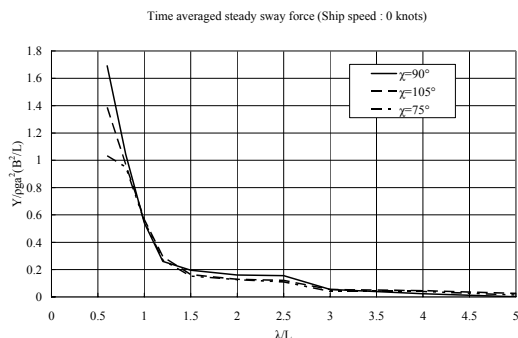


Figure 7 Wave induced steady sway force ($F_n=0.0$)

By means of the wave spectrum and the response amplitude operator shown in Figure 7, wave drift force in the irregular beam waves is calculated as follows:

$$Y_w = 2 \int_{-\pi}^{\pi} \int_0^{\infty} \frac{\bar{Y}}{2} S_{\zeta\zeta}(\omega) G(\theta) d\omega d\theta. \quad (10)$$

where $S_{\zeta\zeta}(\omega)$ denotes the wave spectrum, $G(\theta)$ denotes the angular distribution function and θ denotes the encounter angle of wave.

4.5 Comparison with Measured Drift Speed

By substituting of the equations (3), (4) and (10) into the equation (2), the lateral component of the drift speed was estimated. Figure 8 shows the lateral component of the drift speed in wind and waves as a function of wind speed. In this calculation, the significant wave height and mean wave period were given with the same condition of the present experiments ($H_s = 9.5$ m, $T_{01} = 10.4$ sec). Only wind speed was varied in the present calculation.

It is found that the estimated drift speed well explains the measured drift speed although the drift speed in the beam waves only (wind speed = 0 in Figure 8) is underestimated. It is clarified that the present method, which is the combination of the manoeuvring model of the slow streaming condition, wind force and wave drift force, gives a rational drift speed under dead ship condition.

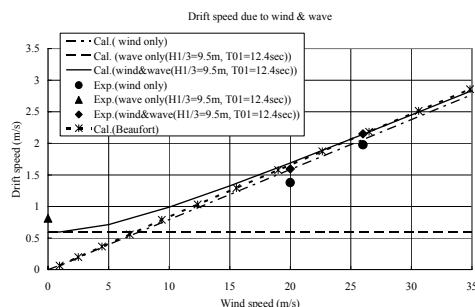


Figure 8 Relation between the wind speed and the drift speed owing to wind and waves.

5. EFFECT OF THE DRIFT MOTION ON THE CAPSIZING PROBABILITY

The capsizing probability is evaluated by integrating a joint probability density function of Gaussian roll and roll rate in waves over the capsizing domain on the phase plane of roll motion (Umeda, 1992). Although roll motion outside the safe region could be non-Gaussian in details, it is clarified that the difference between the present method and the more rigorous one, e.g. the piecewise linear method, could be minor for the present purpose (Belenky, 1995 and Iskandar et al., 2001).

In the present study, the wind velocity U_T is assumed to change with time around the average velocity with Davenport Spectrum. It is assumed that the wind generates long crested waves with the significant wave height $H_{1/3}$ and the mean wave period T_{01} given in Table 4. The ITTC spectrum is used for fully developed waves.

Firstly, the mean encounter frequency was calculated by means of the drift speed in accordance with the present method. Figure 9

shows the mean encounter frequency of the present large passenger ship with and without a drift motion. It is found that the encounter frequency with drift motions is closer to her natural roll frequency. It is clarified that the drift motion has effect on the encounter frequency.

Table 4 Sea states of the Beaufort chart

Beaufort	UT(m/sec)	H1/3(m)	T01(sec)
1	0.95	0.1	1.2
2	2.50	0.2	1.7
3	4.45	0.6	3.0
4	6.75	1.0	3.9
5	9.40	2.0	5.5
6	12.35	3.0	6.7
7	15.55	4.0	7.7
8	19.00	5.5	9.1
9	22.65	7.0	10.2
10	26.50	9.0	11.6
11	30.60	11.5	13.1
12	34.85	14.0	14.1

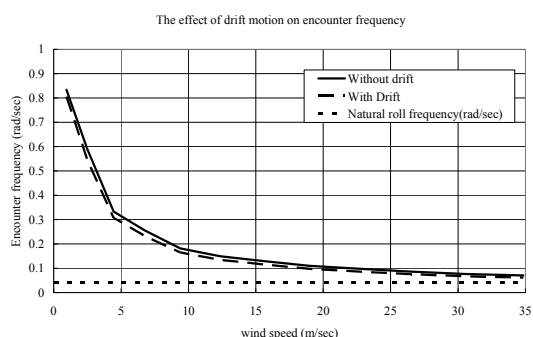


Figure 9 Relation between mean encounter frequency and the wind speed of the large passenger ship (without/with drift motion).

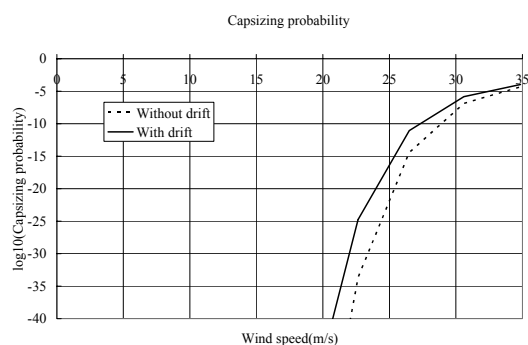


Figure 10 Capsizing probability of the large passenger ship (without/with the drift motion).

Figure 10 shows the capsizing probability of the present large passenger ship. The encounter wave spectrum transformed by the drift speed was used for the estimation of the capsizing probability. It is found that the capsizing probability of the present large passenger ship with drift motion is higher than that without drift motions owing to the difference of the encounter wave frequency. It is confirmed that the drift speed has effect on the capsizing probability under dead ship condition although the degree of the effect depends on the natural roll period.

6. CONCLUSIONS

In this study, model tests have been carried out by means of a large passenger ship in beam wind and waves. The effect of the drift motion on the capsizing probability under dead ship condition was discussed. It is concluded as follows

- (1) The wind has much effect on the drift motion under dead ship condition.
- (2) The present method, which is the combination of the manoeuvring model of the slow streaming condition, wind force and wave drift force, can estimate the drift speed under dead ship condition qualitatively.
- (3) The capsizing probability of the present large passenger ship is affected by the drift motion owing to the difference of the encounter wave frequency.

7. ACKNOWLEDGMENTS

This study was carried out as a part of a joint research between Maritime Research Institute Netherlands (MARIN) and National Maritime Research Institute (NMRI).

8. REFERENCES

- Belenky, V. L., 1995, "Analysis of probabilistic balance of IMO Stability regulation by Piece-wise linear method", Maritime Technology Transactions, Polosh Academy

of Science, vol.6, pp.5-55.

Blendermann, S W., 1996, “Wind Loading of Ships - Collected Data from Wind Tunnel Tests in Uniform Flow”, IFS Bericht 574, Institut fur Schi bau der Universitat Hamburg.

Fujiwara, T. et al., 2001, “An Estimation Method of Wind Forces and Moments Acting on Ships”, Mini Symposium on Prediction of Ship Manoeuvring Performance, Japan Marine Dynamics Research Sub-Committee.

Iskandar, B. H. and Umeda, N., 2001, “Capsizing probability of an Indonesian RoRo passenger ship in irregular beam seas (Third report)”, Journal of society of Naval Architects of Japan, vol.190, pp.211-216.

Kashiwagi, M., 1992, “Added resistance, wave-induced steady sway force and yaw moment on an advancing ship”, Ship Technology Research, vol. 39, No.1, pp. 3-16.

Kashiwagi, M., 1995, “Prediction of surge and its effect on added resistance by means of the enhanced unified theory”, Transaction of West-Japan Society of Naval Architects, vol. 89, pp. 77-89.

Luth, H.R., and Dallinga, R. P., 1998, “Prediction of excessive rolling of cruise vessels in head and following waves”, Proceedings of 7th International Symposium on Practical Design of Ships and Mobile Units, pp. 625-631.

Umeda, N., and et al., 1992, “Risk Analysis Applied to the Capsizing of High-Speed Craft in Beam Seas”, Proceedings of 5th International Symposium on the Practical Design of Ships and Mobile Units, pp. 1131-1145.

Yoshimura, Y., 1988, “Mathematical model for the manoeuvring ship motion in shallow

water (2nd report) –mathematical model at slow forward speed-”, Journal of the Kansai Society of naval architects, Japan, No.210, pp. 77-84.

Probabilistic Assessment of Resonant Instability

N. Themelis, *National Technical University of Athens*

K.J. Spyrou, *National Technical University of Athens*

ABSTRACT

Near regularity of excitation is conducive to large amplitude responses. Moreover, higher waves tend to appear in groups (Draper 1971). These observations are the drivers of our approach for the probabilistic assessment of intact stability. The intention is to maintain the rigour and breadth of the deterministic approach while taking fully into account the probabilistic character of the seaway. Critical wave groups are specified on the basis of deterministic analysis. A procedure is put forward for calculating the probability of encountering these wave groups. A Ro-Ro ship's tendency for instability due to resonant behaviour in beam seas is used as the showcase for demonstrating the feasibility of the approach.

Keywords: *ship stability, wave group, probabilistic assessment*

1. INTRODUCTION

The mechanics that govern extreme ship behaviour and could host loss of intact stability have been studied for several years in a primarily deterministic context. This analysis has improved our understanding of the various types of ship instability, some times supplying also simple criteria to guide design. However, none could disregard that potentially destabilizing environmental excitations are of a probabilistic nature.

A method to interface the deterministic analyses of ship dynamics with wind/wave models and statistics has been proposed recently, exploiting the groupiness characteristic of high waves and the idea that the probability of occurrence of a certain instability could be assumed as equal to the probability of encountering the critical (or "worse") wave groups that generate the instability (Spyrou, 2005, Spyrou & Themelis, 2005). The method builds upon certain ideas that have been around in the field of ship stability for a number of years: Tikka & Paulling (1990) for example, discussed the calculation of the probability of encountering a

high run of waves in astern seas and determined combinations of ship's speed and heading that could favour such an encounter. DeKat (1994) pointed out the importance of considering wave groups and he referred to the use of joint distributions of wave length and steepness in order to determine such wave groups, given a significant wave height and period. Along the same lines, Myrhaug et al. (1999) investigated synchronous rolling using joint distributions of successive wave periods, targeting essentially the encounter of a wave group with critical period.

In the current paper our objective is to demonstrate the feasibility of our method of stability assessment, through detailed application to a specific ship, of Ro-Ro ferry type. A popular route in the Mediterranean Sea is selected and probabilities of "instability" due to beam-sea resonance (in format of critical time as percentage of the duration of the voyage) are calculated. Two, conceptually different, cases of assessment are presented.

2. THE PROPOSED METHODOLOGY

Given a ship, the methodology can be deployed for "short" or "long-term"

assessments, depending on the intended period of exposure to the weather. In the current context, as “short-term” is meant an assessment gauging safety during a single trip. It is thus fed by the “few hours” forecast of weather parameters. Such an assessment could serve as a decision-making tool in connection with a system of departure control like the one used in Greece for passenger ships (Spyrou et al. 2004); or with other operational measures like weather routing. On the other hand, long-term assessments could be performed for a variety of reasons. Probabilities of instability on a seasonal or annual basis for reference routes can be determined with obvious utility at corporate and national administration levels. Moreover, by projecting the annual statistics to the ship’s life-span, a long-term assessment could be tied to ensuring a satisfactory safety level by design¹. In long-term assessments, the anticipated service profile should be specified beforehand. A restricted service, referring to specific routes, should lead to a different assessment result, compared to one of unrestricted service that sets no narrow limits to the navigational area (e.g. North Atlantic).

Different ship types are prone to instabilities of a different nature. In a general sense, an effective portfolio of criteria should cover against resonance phenomena (beam-sea resonance and parametric rolling in longitudinal seas); pure - loss of stability on a wave crest in following seas; instability due to breaking waves from abeam and “water-on-deck”; and finally broaching, including the so-called cumulative type. To become these criteria meaningful, norms of unsafe behaviour should be adhered to each one of them. The setting of warning and failure levels per criterion and ship type has been proposed, on the basis of threshold angular and linear displacements and accelerations, referring respectively to the safety of the ship and her cargo (Spyrou & Themelis 2005). The setting

of warning level should play a cautionary role and its exceedence could be allowed with a controlled probability.

The probability of occurrence of dangerous ship motion, loosely referred-to from here on as “instability”, could be assumed as equal to the probability of encounter of the critical (or worse) wave group that gives rise to this instability. Certain instabilities entail some regularity in the excitation, i.e. the amplitude is built up gradually; whereas others represent the outcome of the encounter of a single critical wave that can ‘kick’ the system out of its (safe) potential well. One might think therefore to disassemble the problem into two parts: one deterministic, for deducing the specification of the critical wave group (represented by the height, period and run-length) focused purely on ship motion dynamics; and one probabilistic centered upon seaway statistics, in order to determine the probability of encounter of such a wave group. For the specification of critical wave groups, advantage could be taken of the strengths of deterministic analyses: numerical simulation tools based on detailed models; and analytical techniques capturing key system dynamics (growth of amplitude per cycle, Melnikov’s method etc.) represent the two ends of the spectrum, each having particular strengths and weaknesses. However it should be remarked that, by disassembling (methodologically) the ship dynamics part from the probabilistic seaway, an informed decision based on more than one tools is allowed; i.e. results from different simulation codes or combinations of simulation with independent stability analysis techniques can be utilised. A flow-chart of the above described methodology is presented in Figure 1.

The groupiness characteristic of high waves coupled with the magnification of safety threats due to near regularity of the excitation, allow therefore the conceptual bridging of the deterministic and probabilistic viewpoints. Given a distribution of “weather nodes” (along the route of in a wider navigational area), individual probabilities per node are calculated.

¹ Some concern is necessary here for the observed slow drift of environmental parameters and the tendency for extremer seas as time progresses.

In summing up these probabilities, the duration of ship stay in the influence area of each node, as well as the principal direction of wave field encounter, are taken into account (Figure 2).

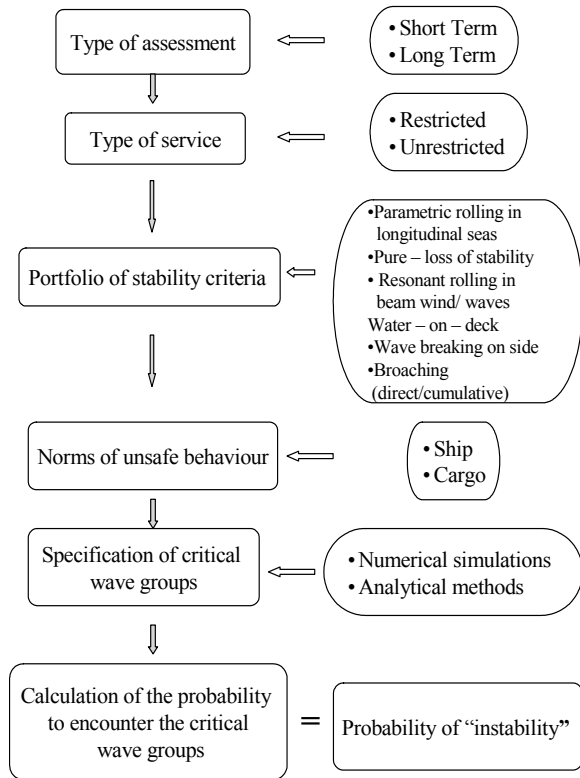


Figure 1 Flow chart of proposed methodology.

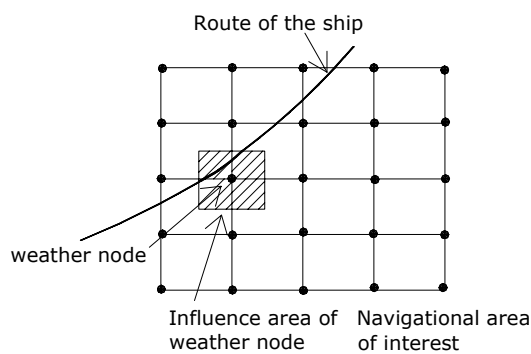


Figure 2 Weather nodes with their areas of influence.

To facilitate decision-making, the probabilistic treatment should be embedded upon a risk-based platform of assessment. In implementing this however, a scale for quantifying the consequences needs to be established.

3. PROBABILITY OF WAVE GROUPS

For a brief introduction to wave groups see for example Medina & Hudspeth (1990) and Masson & Chandler (1993). Application of the proposed methodology entails calculation of the probability of encounter of wave groups with successive periods in the critical range (related to the ship's roll natural period), given run length; and heights consistently above the critical height as determined from the deterministic analysis. A variety of parametric models might be useful in this respect. Bivariate distributions of wave height and period have been proposed by Longuet – Higgins (1975 & 1983); Cavanié et al. (1976); Tayfun 1993; and others. The probability density function (pdf) proposed by Tayfun (1993) is:

$$f(h, \tau) = C_T h \left(1 + \frac{1 - \kappa^2}{32 \kappa h^2} \right) e^{-\frac{1}{2} \left[\frac{4h^4}{1 + \kappa} + \left(\frac{\tau - \mu_{\tau/h}}{\sigma_{\tau/h}} \right)^2 \right]} \quad (1)$$

where:

$$\mu_{\tau/h} = 1 + \nu^2 (1 + \nu^2)^{-3/2} \quad (2)$$

$$\sigma_{\tau/h} = \frac{2\nu}{\sqrt{8h(1 + \nu^2)}} \quad (3)$$

$$C_T = \frac{2\sqrt{2}}{2\sqrt{4\pi\kappa(1 + \kappa)}\sigma_{\tau/h}} \quad (4)$$

$\mu_{\tau/h}$ and $\sigma_{\tau/h}$ are the conditional mean and standard deviation, C_T a normalizing factor, $h = \frac{H}{H_{ms}}$, $\tau = \frac{T}{T_m}$ the dimensionless wave height and period, $T_m = 2\pi \frac{m_0}{m_1}$ the mean spectral period, m_j the j th ordinary moment of wave spectrum. According to Longuet – Higgins (1975) the spectral bandwidth ν is given by:

$$v = \sqrt{\frac{m_2 m_0}{m_1^2} - 1} \quad (5)$$

The parameter κ depends on T_m and the frequency spectrum. According to (Stansell et al, 2002) is calculated:

$$\kappa^2 = \frac{1}{m_0} \left| \int_0^\infty S(\omega) e^{i\omega t} d\omega \right|, \quad t = T_m \quad (6)$$

Tayfun (1993) approximated the conditional distribution of successive wave periods given the wave height on the basis of the Gaussian distribution for one wave period. Wist et al. (2004) noted that, for three wave periods at least, the multivariate Gaussian distribution is a satisfactory model of the conditional distribution. Their conditional pdf of p successive wave periods $\mathbf{T} = [T_1, \dots, T_p]^T$, given that each wave height in the group exceeds the threshold H_{cr} , is given by equation (7). A general formula for variable threshold $H_{cr,i}$ per crest in the group could also be derived.

$$f_{\mathbf{T}/\mathbf{H}}(\mathbf{\tau}/h_i > h_{cr}) = \frac{e^{-\frac{1}{2}(\mathbf{\tau} - \boldsymbol{\mu}_{\tau/h_{cr}})^T \boldsymbol{\Sigma}_{\tau/h_{cr}}^{-1} (\mathbf{\tau} - \boldsymbol{\mu}_{\tau/h_{cr}})}}{(2\pi)^{p/2} |\boldsymbol{\Sigma}_{\tau/h_{cr}}|^{1/2}} \quad (7)$$

where the covariance matrix is given by:

$$\boldsymbol{\Sigma}_{\tau/h_{cr}} = \begin{bmatrix} \sigma_{\tau/h_{cr}}^2 & \text{Cov}[T_1, T_2/H_{cr}] & \text{Cov}[T_1, T_p/H_{cr}] \\ & \dots & \dots \\ \text{Cov}[T_1, T_p/H_{cr}] & \dots & \sigma_{\tau/h_{cr}}^2 \end{bmatrix} \quad (8)$$

and $\text{Cov}[T_i, T_j/H_{cr}] = \rho_{ij} \sigma_{\tau/h_{cr}}^2$. The mean values $\boldsymbol{\mu}_{\tau/h_{cr}}$ and the standard deviations $\sigma_{\tau/h_{cr}}$ are calculated from equations (2) and (3). Assuming the Markov chain property for the waves, the correlation coefficients ρ_{ij} is:

$$\rho_{1j} = \rho_{12}^{j-1} \quad (9)$$

The correlation coefficient ρ_{12} of two successive wave heights is calculated as follows (Stansell et al, 2002):

$$\rho_{12} = \frac{E(\kappa) - (1 - \kappa^2) \frac{K(\kappa)}{2} - \frac{\pi}{4}}{1 - \frac{\pi}{4}} \approx \frac{\pi}{16 - 4\pi} \left(\kappa^2 + \frac{\kappa^4}{16} + \frac{\kappa^6}{64} \right) \quad (10)$$

where $E(\cdot)$, $K(\cdot)$ are complete elliptic integrals of the first and second kind, respectively.

The above, rather lengthy, procedure is essential because for resonance phenomena, one needs to determine the probability, a specified number of successive wave periods to lie in some narrow interval $[\tau_1, \tau_2]$, given that the corresponding wave heights exceed the critical level h_{cr} .

4. MATHEMATICAL MODEL OF COUPLED ROLL IN BEAM SEAS

A mathematical model has been developed that could be used for analysing coupled rolling motion in beam seas. This model is outlined briefly in the following: For more details see Themelis & Spyrou (2005). From kinematics and in accordance to Fig. 3, the equations of motion in heave, sway and roll are written as follows:

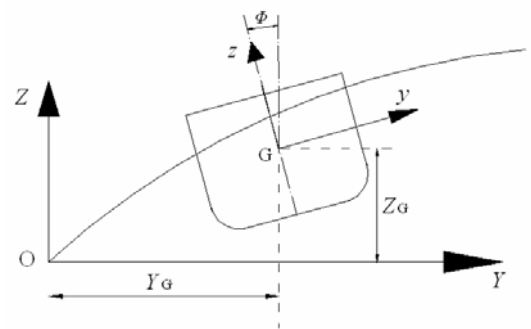


Figure 3 The inertial (OYZ) and body fixed (Gyz) coordinate systems.

$$m(\dot{v} - \dot{\phi}w) = \sum F_y \quad (11)$$

$$m(\dot{w} + \dot{\phi}v) = \sum F_z \quad (12)$$

$$I_G \ddot{\phi} = \sum M_G \quad (13)$$

where v , w are the sway and heave velocity of the ship's centre of gravity and $\dot{\phi}$ is the roll angular velocity, m and I_G are, mass and mass moment of inertia around x . The well-known transformation between the inertial and body fixed coordinate systems is applied.

The two forces and the moment that appear at the right-hand-side of (11)-(13) can be decomposed as follows:

$$\sum F = F_{Hs} + F_W^{FK} + F_R + F_V \quad (14)$$

F_{Hs} is hydrostatic, F_W^{FK} is Froude – Krylov, F_R is radiation and F_V is the viscous force.

Calculation of excitations In linear wave theory, the total wave velocity potential is the sum of the potentials of incident wave, diffraction and radiation. The hydrostatic and Froude – Krylov (hydrodynamic) forces are estimated by the integration of the incident wave pressure (static and dynamic respectively) over the wetted surface of the ship. For regular waves, the incident wave potential is calculated from:

$$\Phi_I = \frac{Ag}{\omega_w} e^{kZ^*} \sin(kY - \omega_w t) \quad (15)$$

$$Z^* = Z - A \cos(kY - \omega_w t) \quad (16)$$

The hydrostatic and Froude - Krylov forces are repetitively:

$$F_{HSi}(t) = -\rho g \iint_{S(t)} Z^* \bar{n}_i ds, \text{ for } i=2, 3, 4 \quad (17)$$

$$F_W^{FK}(t) = - \iint_{S(t)} \rho \frac{\partial \Phi_I}{\partial t} \bar{n}_i ds, \text{ for } i=2, 3, 4 \quad (18)$$

where $i = 2, 3, 4$ correspond to sway, heave and roll motion, ρ is seawater density and $S(t)$ is the instantaneous wetted surface. We should mention that the integration is performed over the instantaneous wetted surface and pressures are calculated from the exact wave elevation. As a matter of fact, the nonlinear part of the forces is taken into account, which is important for the accurate simulation of the large motions of the ship.

The radiation forces are frequency dependent. Using the impulse response function, obtained as the Fourier transform of the frequency dependent radiation transfer function, the radiation forces will be (Cummins, 1962):

$$F_{Rj}(t) = -a_{jk}(\infty) \ddot{s}_k - \int_0^{+\infty} K_{jk}(\tau) \dot{s}_k(t-\tau) d\tau \quad (19)$$

$$K_{jk}(\tau) = \frac{2}{\pi} \int_0^{\infty} b_{jk}(\omega_e) \cos(\omega_e \tau) d\omega \quad (20)$$

for $j, k=2, 3, 4$.

The convolution integral is the well-known memory effect. a_{jk}, b_{jk} are the added mass and damping coefficients. \dot{s}_k, \ddot{s}_k are velocity and acceleration of the ship in the k direction of motion and ω_e is the encounter frequency. In our model we use a state-space approximation of the radiation force in order to maintain the mathematical model in the form of a system of o.d.e.s which enables easier consideration of nonlinear dynamics.

Our model calculates also the sway drag force, roll damping, and cross coupling forces between sway, heave and roll. For example, the

(Figure 6). The adopted convention concerning the type of encounter is explained in Figure 7. The time has been scaled against the duration of the voyage (Table 4).

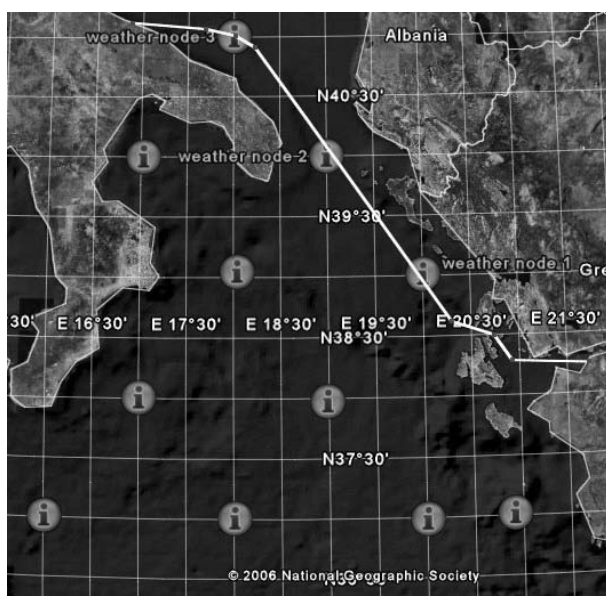


Figure 5 The examined Patra – Bari route superimposed on a map taken from Google Earth. Available nodes of wave data are also shown.

Table 2 Mean wave values for winter.

	$H_s(m)$	$T_p(sec)$	$\Theta_{wave}(deg)$
Weather node 1 (39°N, 20°E)	1.293	6.897	224.02
Weather node 2 (40°N, 19°E)	1.167	6.586	209.83
Weather node 3 (41°N, 18°E)	1.077	5.936	189.70

Table 3 Time spent in each grid sub area.

	Distance(nm)	Time(hr)	%
Weather node 1	138.77	6.03	46.2
Weather node 2	73.39	3.19	24.4
Weather node 3	87.48	3.80	29.1
Total	299.98	13.04	100.0

Table 4 Percentage of time spent in beam, head and following seas

	Beam seas	Head seas	Following seas
Weather node 1	19.70%	16.50%	10.27%
Weather node 2	5.58%	7.59%	11.28%
Weather node 3	9.37%	9.86%	9.85%
Average	34.66%	33.96%	31.42%

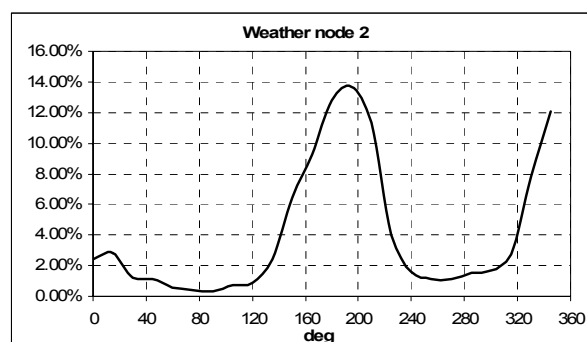


Figure 6 Wave direction characterization for operation near node 2.

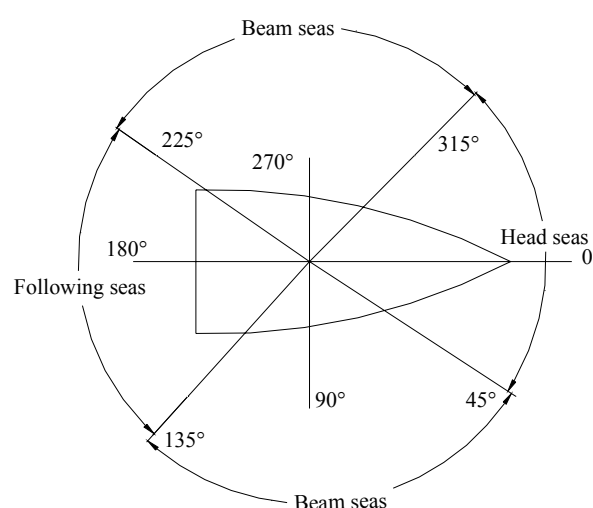


Figure 7 Convention for wave direction (0^0 waves coming from North, 90^0 East).

Norms of unsafe response for ship and cargo Norms of failure specific to the ship and her cargo were set. Concerning the ship, the principle of the weather criterion was adopted in order to determine the critical roll amplitude. For the investigated Ro-Ro ferry it meant that the critical roll angle should be the minor of: the angle of vanishing stability $\theta_c = 1.1$ rad; the down-flooding angle $\theta_f = 0.612$ rad; and $\theta_a = 0.8726$ rad (50 deg). Thus the critical roll angle should be $\phi_f = 0.612$ rad or 35 deg.

Turning to the cargo, the acceleration due to beam-sea rolling that could endanger the lashing of the remotest trailer was targeted as the critical response.

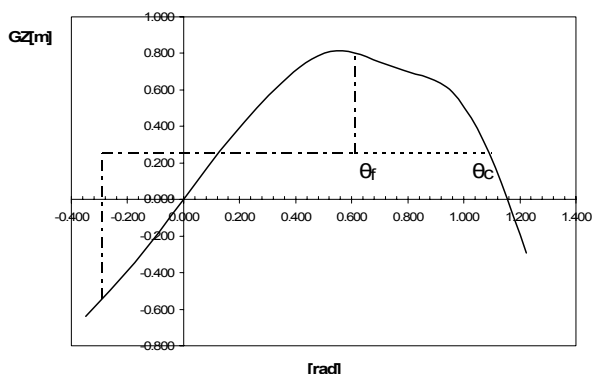


Figure 8 Application of the Weather Criterion.

The tendency of the trailer for transverse sliding and tipping was checked for three different lashing arrangements. Parameters and coefficients that are essential for the analysis are shown in Table 5. The Maximum Securing Load (MSL) is the least required strength of the lashings according to IMO. The most critical transverse acceleration was found corresponding to transverse sliding and a vertical securing angle of 60° (Figure 10). The critical acceleration is $a_y = 8 \text{ m/s}^2$.

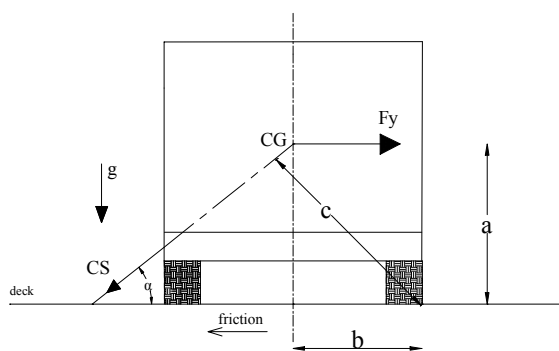


Figure 9 Forces acting on the trailer – lashing system (transverse section).

Table 5 Trailer and lashings characteristics.

cargo mass	$m = 40 \text{ t}$
Centre of gravity above deck	$a = 2.753 \text{ m}$
lever-arm of tipping	$b = 1.261 \text{ m}$
Coefficient of friction	Steel – rubber: $\mu = 0.3$
Lashing arrangement	4 chains with MSL = 100 kN on each side, symmetrical vertical securing angle: $\alpha = 30^\circ/45^\circ/60^\circ$

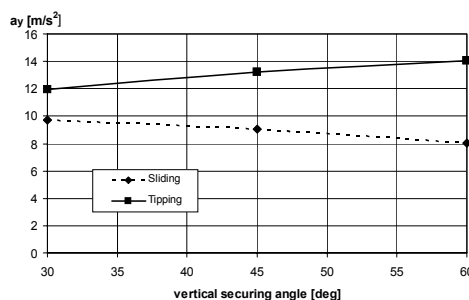


Figure 10 Critical transverse accelerations for sliding and tipping for the three lashing arrangements.

Critical wave groups The calculation of critical wave groups proceeds as follows: firstly, the range of wave periods (e.g. 4 – 19 sec) is discretised. Then, for each discrete period (representing however a narrow range around it) we set the desired number of successive waves (starting with $n = 2$) and we determine the minimum critical wave height H_{cr} that generates a response reaching the value of the severest norm (in this case roll angle, or acceleration at the remote trailer position). The calculation continues with $n = 3$ etc. Figures 11 and 12 summarise the key characteristics of the identified critical wave groups, respectively for ship and cargo.

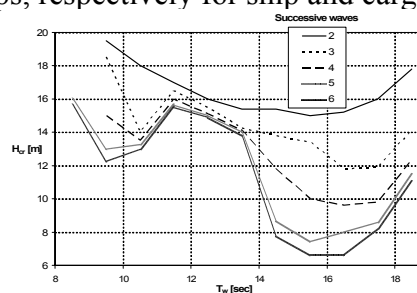


Figure 11 Critical wave groups with reference to the limiting roll angle (ship).

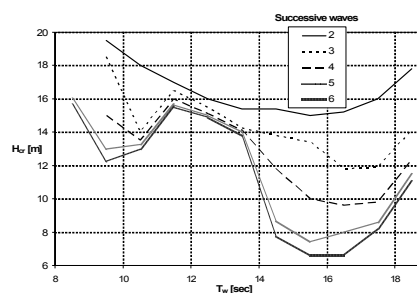


Figure 12 Critical wave groups for the limiting transverse acceleration (cargo).

Probability to encounter critical wave groups The JONSWAP frequency spectrum was used (Hasselmann, 1973). As is well-known, its spectral density function is:

$$S(\omega) = ag^2 \omega^{-5} \exp\left(-\frac{5}{4}\left(\frac{\omega}{\omega_p}\right)^4\right) \gamma \exp\left(-0.5\left(\frac{\omega - \omega_p}{\sigma\omega_p}\right)^2\right) \quad (25)$$

where

$$a = \frac{5}{16} \left(\frac{H_S^2 \omega_p^4}{g^2} \right) A_\gamma \quad (26)$$

$$A_\gamma \cong 1 - 0.287 \ln(\gamma) \quad (27)$$

$$\begin{aligned} \sigma &= 0.07 \text{ if } \omega \leq \omega_p \\ &= 0.09 \text{ if } \omega > \omega_p \end{aligned} \quad (28)$$

a is the generalized Philips' constant, A_γ a normalizing factor, γ the peakness parameter, σ the spectral width parameter and ω_p the angular spectral peak frequency. For the peakness parameter γ the following formulas can be used (DNV, 2002). For the calculation of probabilities P_i for each wave period partition around T_i , the values of H_S, T_p were taken from Table 2.

$$\begin{aligned} \gamma &= 5 \text{ for } \frac{T_p}{\sqrt{H_S}} \leq 3.6 \\ \gamma &= e^{5.75 - 1.15 \frac{T_p}{\sqrt{H_S}}} \text{ for } 3.6 \leq \frac{T_p}{\sqrt{H_S}} \leq 5 \end{aligned} \quad (29)$$

$$\gamma = 1 \text{ for } 5 \leq \frac{T_p}{\sqrt{H_S}}$$

It was preferred to express the probabilities as percentage of critical time scaled with regard to the duration of the voyage t_{tot} . This is done approximately with the following simple transformation:

$$\bar{t}_i = \frac{t_i}{t_{tot}} = P_i \frac{T_i}{T_m} \quad (30)$$

The contribution of each range of wave periods to the total probability can be deduced from Figures 14 and 15.

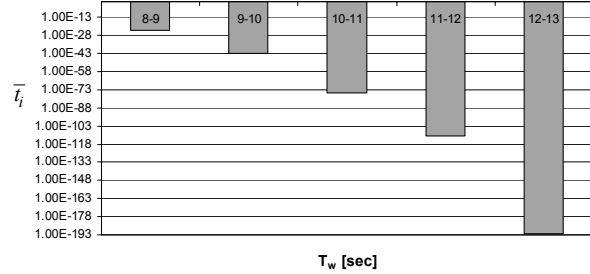


Figure 14 Critical time with reference to the roll angle (logarithmic scale).

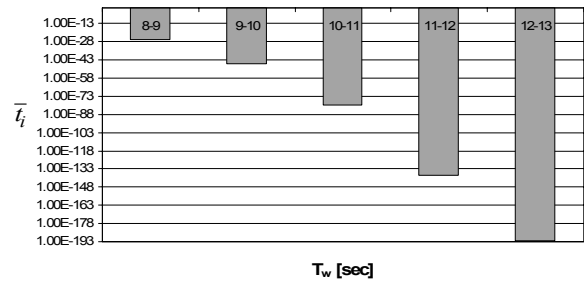


Figure 15 Critical time with reference to the transverse acceleration of trailer (logarithmic scale).

The probabilities are, in most cases, negligible, stemming of course from the fact that the range of wave periods which usually arise in the Ionian and Adriatic Sea are far below the Ro-Ro ferry's natural roll period. As a matter of fact, the probability of resonance should be extremely low. The critical time \bar{t}_i for the entire voyage is summarized below with reference to the two considered norms of beam-sea resonance:

Ship: ($\phi > 35^\circ$)	1.161E-22
Cargo: ($a_y > 8 \text{ m/s}^2$)	9.425E-25

In the above we have used H_S, T_p values that are the most probable for the winter season. The actual distribution of significant wave height H_S and peak period T_p for weather node 1 (winter season) is shown in figures 16 and 17 (extracted from the

Metadlas of the Mediterranean, see Athanassoulis et al 2004).

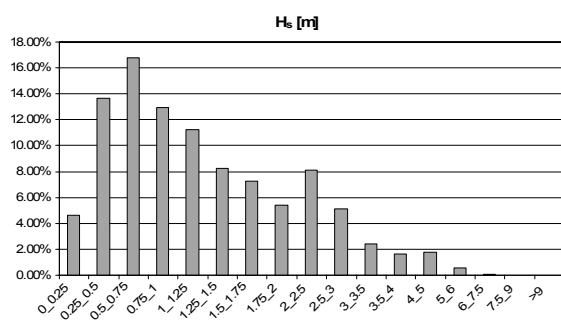


Figure 16 Distribution of significant wave height for winter (weather node 1).

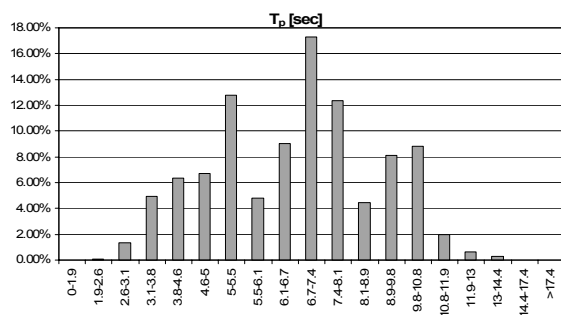


Figure 17 Distribution of peak period for winter (weather node 1).

As a next step, we examined the effect of combinations of H_s , T_p on the critical time \bar{t}_i , focusing on the requirement that the roll angle should not exceed 35° . Such thinking could be relevant in the context of a short-term assessment, e.g. for assessing whether the ship should be allowed to sail, given the weather forecast. For simplicity we assumed uniform weather conditions throughout the journey (i.e. the data of a single weather node characterize the entire journey). We derived the critical time \bar{t}_i as function of T_p for fixed H_s (Figure 18); and as function of H_s as function of T_p (Figures 19). For the rather extreme conditions that were deliberately examined, it is obvious that the exposure of the ship to critical weather is too high.

Figure 19 Critical times and probabilities as the period T_p is varied. H_s is fixed at a high value.

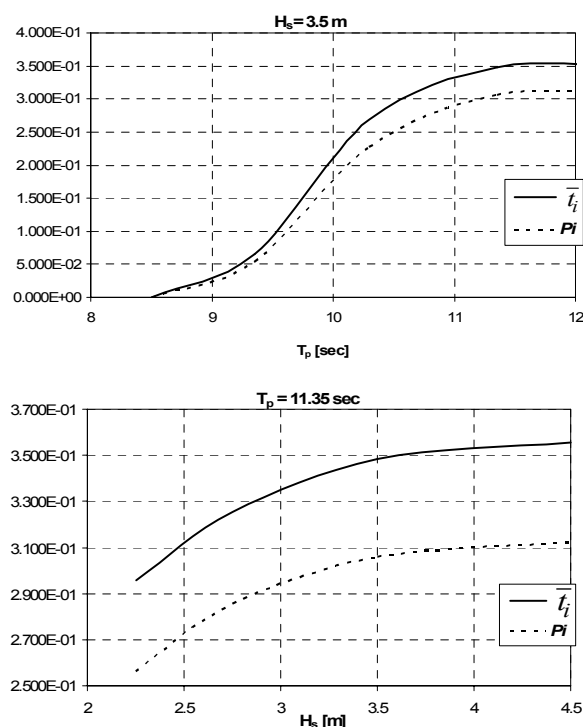


Figure 20 Critical times and probabilities as H_s is varied, for a fixed T_p .

6. CONCLUDING REMARKS

A survey of literature on probabilistic intact stability assessment would reveal that current methods are: either focusing narrowly on the problem (e.g. study of beam-sea resonance or parametric rolling only, with dubious assumptions regarding the nature of excitation and/or type of response); or, due to the rush for practicality, the widening of scope is accompanied by paying little attention to the true dynamical nature of the phenomena. Little confidence has been gained that stability standards could be based on the state-of-the-art of probabilistic approaches.

On the other hand, in the recent past, risk-based approaches have pervaded all facets of naval architecture and almost naturally, the question of a solid and yet practical probabilistic approach has been heard more loudly than ever.

An effort to fill this gap has been presented in the current paper. The developed method

was applied at a very practical level, selecting a Ro-Ro ferry and setting it to operate on a specific popular route. The assessment produced results that are logical, although further elaborations are needed in order to standardise the calculation methods that are suitable for each stage of the assessment.

7. ACKNOWLEDGEMENT

Part of this research work (related to short-term assessment) has been supported by the the General Secretariat for Research and Technology of Greece (project ESPEN). The part related to long-term assessment has been carried out for the needs of the project SAFEDOR funded by the European Commission.

8. REFERENCES

- Athanassoulis *et al*, 2004, “Metadlas: Wind and wave atlas of the Mediterranean Sea”, WEAU (consortium: CS, NTUA, CNR/ISMAR, THETIS, Semantic, MeteoFrance), ISBN 2-11-095674-7.
- Cavanié, A., Arhan, M. & Ezrtaty, R., 1976, “A statistical relationship between individual heights and periods of storm waves”. Proceedings, Conference on Behaviour of Offshore Structures, Trondheim, pp. 354-360.
- Cummins W. E., 1962, “The impulse response function and ship motions”, Schiffstechnik, Vol. 9, pp. 101-109.
- Det Norske Veritas, 2002, “DNV MaxWave”, Report No. 2001 – 1491.
- de Kat, J.O., 1994, “Irregular waves and their influence on extreme ship motions”, Report No. 208883-OP1 – ONR’94.
- Draper, L. 1971, “Severe wave conditions at sea”, Journal of the Institute of Navigation, Vol. 24, 3, pp. 273-277
- Hasselmann, K., 1973, “Measurements of wind - wave growth and swell decay during the Joint North Sea Wave Project (JONSWAP)”, Dt. Hydrogr. Z. Reihe A (8) 12.
- IMO, 1991, Code of safe practice for cargo stowage and securing and amendments thereto. Resolution A.714 (with 1994/95 amendments, Annex 1-13).
- Longuet-Higgins, M.S., 1975, “On the joint distribution of the periods and amplitudes of sea waves”, Journal of Geophysical Research, Vol. 80, pp. 6778-6789.
- Longuet-Higgins, M.S., 1983, “On the joint distribution of wave periods and amplitudes in a random wave field”, Proceedings of the Royal Society, A 389, pp. 241-258.
- Masson, D. & Chandler, P., 1993, “Wave groups: a closer look at spectral methods”, Coastal Engineering, Vol. 20, pp. 249-275.
- Medina, J.R. & Hudspeth, R.T., 1990, “A review of the analyses of ocean wave groups”, Coastal Engineering, Vol. 14, pp. 515 – 542.
- Myrhaug, D., Dahle, E.A., Rue, H. Slaattelid, O.H., 1999, “Statistics of successive wave periods with application to rolling of ships”, International Shipbuilding Progress, Vol. 47, pp. 253-266.
- Spyrou, K.J., 2005, “Design criteria for parametric rolling”, Oceanic Engineering International, Vol. 9, pp. 11-27.

Spyrou, K.J., Politis, K., Loukakis, T., Grigoropoulos, G., 2004, "Towards a risk – based system for the departure control of passengers ships in rough weather in Greece", Proceedings 2nd International Maritime Conference on Design for Safety, Sakai, Japan, Oct. 27 – 30, pp. 255 – 261.

Spyrou, K.J. & Themelis, N., 2005, "Probabilistic assessment of intact stability", Proceedings of 8th International Ship Stability Workshop, Istanbul, Oct. 6-7.

Stansell, P., Wolfram, J. & Linfoot, B., 2002, "Statistics of wave groups measured in the northern North Sea; comparisons between time series and spectral predictions", Applied Ocean Research, Vol. 24, pp. 91–106.

Tayfun, M.A., 1993, "Joint distributions of large wave heights and associated periods", Journal of Waterway, Port, Coastal and Ocean Engineering, Vol. 119, pp. 261–273.

Themelis, N. & Spyrou, K., 2005, " A coupled heave-sway-roll model for the analysis of large amplitude ship rolling and capsize of ships in beam seas on the basis of a nonlinear dynamics approach", Proceedings 16th International Conference on Hydrodynamics in Ship Design, Gdansk, Poland, Sept. 7 – 11.

Tikka, K.K & Paulling, J.R., 1990, "Prediction of critical wave conditions for extreme vessel response in random seas", Proceedings 4th International Conference on Stability of Ships and Ocean Vehicles STAB '90, Naples, Sept. 24 -28, pp. 386 – 394.

Wist, H. Myrhaug D. and Rue H., 2004, "Statistical properties of successive wave heights and successive wave periods", Applied Ocean Research, Vol. 26, pp. 114–13

A Sequential Linear Program for the Automatic Loading of Vessels

Sérgio Alvares R. de S. Maffra, *Tecgraf/PUC-Rio*

Luiz Cristovão Gomes Coelho, *Tecgraf/PUC-Rio*

Guilherme Tavares Malizia Alves, *Tecgraf/PUC-Rio*

Mauro Costa de Oliveira, *Petrobras/Cenpes*

Carlos Gomes Jordani, *Petrobras/Cenpes*

ABSTRACT

Large ships and platforms are kept in equilibrium by controlling the amount of mass in its tanks (ballast, oil, diesel, etc) as a way to compensate the disequilibrium caused by external forces, by its cargo or by its own weight. In this paper we present a sequential linear program that calculates the amount of liquid in each tank necessary to put the vessel at any desired position while minimizing the amount of liquid displacement, the structural stress or the free surface of all tanks selected for change.

Keywords: *linear programming, vessel stability, automatic loading*

1. INTRODUCTION

Sequential linear programs solve nonlinear problems by a sequence of linear approximations that are solved using linear programming (Bertsimas & Tsitsiklis, 1997). Generally speaking, these algorithms are iterative procedures that, at each step, try to guess the solution of the nonlinear problem using the solutions provided by the linear approximations until convergence is achieved. In this problem the nonlinearity arises in the computation of the center of gravity of the tanks, which are allowed to have an arbitrary geometric form, position and orientation. So, the longitudinal and transversal center of gravity values (LCG and TCG) may vary during the filling process. The linear approximations consist in considering each tank as a punctual load so that the equilibrium

of the vessel can be easily expressed as the constraints of a linear program, responsible for computing the concentrated mass in each tank. After computing these masses, the algorithm computes the actual position of the center of gravity of each tank, using the correct geometry. Convergence is achieved when the position of the punctual loads and the center of gravity of the tanks do not vary significantly. Using the minimization of the variation of mass at each punctual load as the objective function of the linear program, we guarantee that the solutions obtained correspond to the minimum displacement of liquids.

Our algorithm incorporates an optional heuristic to minimize the structural stress of the vessel, which consists in trying to achieve an even distribution of liquids among the cargo, ballast and oil tanks, assuming that the loading distribution can be similar to the buoyancy. This algorithm has been implemented in the

Sstab Program (Coelho et al., 2003) and has proved its efficiency in the design of ships and oil platforms (Campos Basin, Rio de Janeiro, Brasil) and also in the design of emergency plans performed by the Classification Societies ABS, DNV, LR, and BV.

Our algorithm also incorporates a second optional heuristic to minimize the free surface of the tanks vessel, which consists in trying to concentrate a maximum amount of liquids in the smaller number of tanks possible.

2. LINEAR PROGRAMMING

As mentioned in the Introduction, the algorithm proposed uses linear programming in order to compute an equilibrium configuration for a vessel. Generally speaking, linear programs (an instance of a linear programming problem) have two components: a set of linear constraints and a cost function that can be maximized or minimized. A general formulation for linear programs is shown in Equations 1 to 6.

$$\begin{array}{ll} \text{Minimize /} & C^t X \\ \text{Maximize} & \end{array} \quad (1)$$

$$\text{Subject to} \quad A_i^t X \geq b_i \quad i \in M_1 \quad (2)$$

$$A_i^t X \leq b_i \quad i \in M_2 \quad (3)$$

$$A_i^t X = b_i \quad i \in M_3 \quad (4)$$

$$x_j \geq 0 \quad j \in N_1 \quad (5)$$

$$x_j \leq 0 \quad j \in N_2 \quad (6)$$

In the figure, uppercase letters represent vectors and lowercase letters represent scalar values. X represents the vector containing all the variables that are being determined by the program and x represents a single variable. Different weights (C) can be assigned to each variable in the cost function (Equation 1). The different kinds of constraints are also shown (in light gray). Notice that equality and inequality constraints are acceptable. The first three sets of constraints (M_1 , M_2 and M_3) contain a vector A and a scalar value b, which represent the data associated with a constraint.

A feasible solution for a linear program is a solution that does not violate any of the constraints of the problem. An optimal solution is the feasible solution with the largest or smallest evaluation of the cost function, depending on whether the problem is a minimization or maximization problem.

In the next section the general linear programming problem is specialized for computing the equilibrium of a vessel.

2.1 Linear Program for the Equilibrium of a Vessel

A vessel is in equilibrium when the forces acting on it, and their derived moments, are balanced. That is, buoyancy, weight, external forces and the moments they generate must be balanced. Wind and current forces are examples of external forces that act on a vessel.

Among the forces mentioned above, the only ones that can be controlled are the weight forces resulting from the liquids stored in the tanks of the vessel. Therefore, the variables used in the automatic loading linear program must be related to the amount of liquids in the tanks of the vessel. For flexibility, the variation of volume in each tank was chosen. Given the variables of the problem, the equilibrium constraints and the constraints on the variables themselves can be easily written, as Equations 7 to 12 show.

$$\sum (V_i + \Delta V_i) \rho_i g = B - W \quad i \in T \quad (7)$$

$$\sum (V_i + \Delta V_i) \rho_i g x_i = -M_y \quad i \in T \quad (8)$$

$$\sum (V_i + \Delta V_i) \rho_i g y_i = -M_x \quad i \in T \quad (9)$$

$$V_i + \Delta V_i < V_i^{\max} \quad i \in T \quad (10)$$

$$V_i + \Delta V_i > 0 \quad i \in T \quad (11)$$

$$\sum (V_c + \Delta V_c) = V_k^{\text{total}} \quad c \in T_k \quad (12)$$

optional

V_i Initial volume at tank i

ΔV_i Variation of volume at tank i

V_i^{\max} Capacity of tank i

ρ_i	Density of the liquid in tank i
G	Gravity constant
x_i, y_i	Coordinates of the center of gravity of tank i
B	Buoyancy force
W	Weight of the vessel
M_x, M_y	Moments resulting from external forces
T	Set of tanks of the vessel
T_k	Set of tanks holding the same kind of liquid (k)
V_k^{total}	Total volume of liquids in tanks belonging to T_k

The first constraint assures a proper balance of forces. In order to be in equilibrium the weight of the liquids in the tanks and the weight of the platform must be equal to buoyancy. The second and third constraints assure the balance of the moments caused by the liquids and the ones caused by external forces. These first three constraints are responsible for maintaining the vessel in equilibrium.

Constraints ten and eleven are relative to the variables of the problem. The former guarantees that no tank receives more liquid than its maximum capacity while the latter guarantees that no tank will hold negative volumes.

The coordinate system to which Equation 2 refers is defined as having the X Axis pointing forward along the longitudinal axis of the model, the Y Axis defines a plane parallel to the sea surface and Z Axis always points upwards. Figure 1 shows a heeled ship and the global Cartesian coordinate system used.

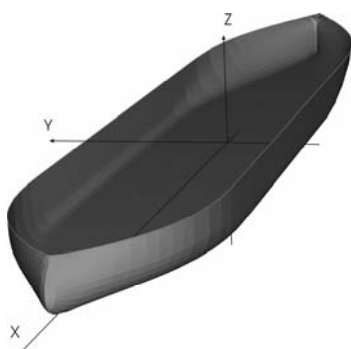


Figure 1- Coordinate System.

It is not uncommon for a vessel to contain tanks holding different kinds of liquids (fresh water, diesel, oil, sea water, etc). In these situations, it is important to guarantee that these different types of liquids are not mixed by the algorithm. That is accomplished by using the constraint expressed in Equation 12. This constraint forces indicates that the tanks belonging to the set T_k hold a determined amount of liquid. Therefore, by creating a set T_k for each type of liquid and using their total volume as the quantity of liquid that they must hold, the mixing of liquids can be easily avoided. This constraint, however, will rarely be used with ballast tanks, as sea water can be disposed of and collected by a vessel. The same is not true, for example, for oil tanks.

When creating an automatic loading program for a vessel, one must decide whether to use or not the sixth constraint. When used, one must also decide how many instances of this constraint will be used and for what types of tanks. Most of the times, this constraint is expected to be used with oil, fresh water and diesel tanks.

2.2 External Forces and Weight Forces

The constraints presented in the previous section account for the existence of external forces and their resulting moments. In our implementation these values are computed directly from a geometric model of the vessel. This model is constructed as a set of individual compartments that define its complete stability model. The compartments can be classified as external (hull body and deck elements) or internal (void spaces, elevators, access trunks, chain lockers, tanks, etc). Each individual compartment is composed of a set of planar faces, which are defined a set of three-dimensional coordinates (Coelho et al, 2003).

Wind forces and their resulting moments are computed, according to IMO's recommendation (IMO, 2001), as a function of the velocity of the wind and of the projected

area of the external compartments that are exposed to wind action. The same procedure is used for current forces.

The buoyancy is determined by computing the contribution of all submerged parts of the external compartment. Using the mesh intersection algorithms implemented in the MG library (Coelho et al., 2000), the external compartments are cut into two parts using a plane located at the sea surface position. The center of gravity and the volume of each submerged part are then used to compute the resulting buoyancy force and the center of buoyancy.

The same procedure is used to determine the center of gravity of each tank. Using a procedure similar to a binary search (Cormen, et al., 2001), the position of the free surface plane of each tank is determined based on the volume it is currently holding and also based on its current orientation. Then, after cutting the tanks in two parts (wet and dry surfaces), similar to what was done for the external compartments, the center of gravity can be determined by computing the geometric center of the faces containing liquids.

Figure 2 shows an example of the mesh operations performed on the external compartments and on tanks in order to compute the buoyancy or tank weights and the center of buoyancy or gravity of each compartment (hull or tank). The mesh of the hull is shown in green and the meshes corresponding to tanks, in yellow.

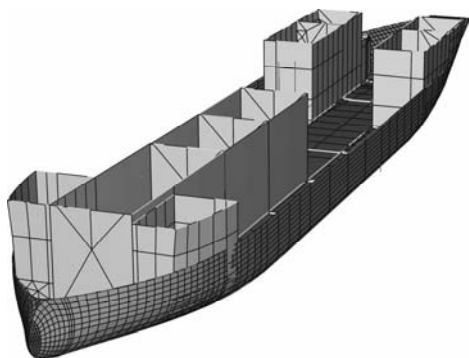


Figure 2- Cutting of compartments.

3. COST FUNCTION

The last component of the linear program created for the automatic loading algorithm that must be described is the cost function. As mentioned before, this function is used to select the best result from set of the feasible solutions of a problem instance. In the automatic loading, the cost function selected minimizes the variation of volume in each tank, as Equation 13 shows.

Another possible cost function is selecting the fastest pumping adjustment, that is, the fastest way of transferring liquids among the available tanks of the floating system. In order to create this cost function data about the pumping capacities of each tank are necessary.

$$\text{Minimize} \quad \sum \Delta V_i \quad i \in T \quad (13)$$

4. THE SEQUENTIAL LINEAR PROGRAM

Observing the tanks illustrated in Figure 2, it is easy to see the X and Y coordinates of its center of gravity are not constant, for many tanks at the stern and bow (all of them if the turn of bilge is significant). They are, actually a function of the volume contained in the tank. The linear program developed for the automatic ballast algorithm, however, considers them as constants. In order to consider the correct centers of gravity, the automatic ballast algorithm is implemented as a sequential linear program.

The algorithm proceeds as illustrated in Figure 3. The linear program, as described in Section 2.1 is used to estimate the first variations of volume. These are then used to compute the new centers of gravity of each tank, as described in Section 2.2. Finally, the new centers of gravity (CG) are compared with the previous ones. In case the distance between all of them is smaller than a predefined error tolerance, the algorithm stops and the desired

variation of volume in each tank is known. In case the distance between old and new CGs is larger than the error tolerance, the algorithm starts a new iteration, using the new CGs instead of the old ones.

The algorithm also stops after a maximum number of iterations is reached.

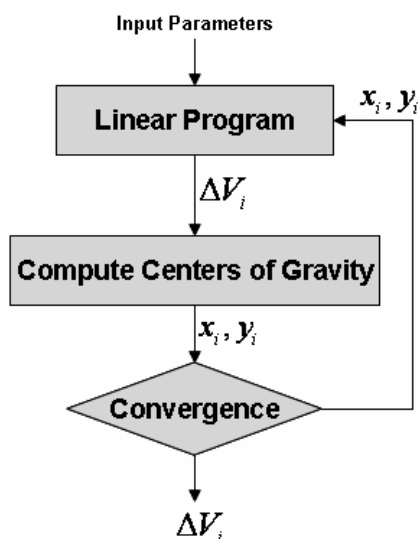


Figure 3- Chart Flow of the loading algorithm.

5. IMPROVING THE RESULTS

The equilibrium of a floating system is an essential requirement for the automatic ballast algorithm. In some cases, however, the consideration of other requirements is also important. Two additional requirements were included in the automatic ballast algorithm: the minimization of the structural stress of the vessel and the minimization of free surface effects of the tanks.

5.1 Minimization of Free Surface Effects

Free surface effects occur when a tank is partially filled with liquids. No free surface effect exists when a tank is empty or completely full. When dealing with semi-submersible platforms or self-elevating units, the minimization of this effect is important to

avoid variations in their center of gravity when the vessel heels for some reason.

The same strategy used to deal with the non-linearity of the center of gravity of the tanks can be applied to this problem. That is, the sequential linear program, as depicted in Figure 3 is used as a step of another iterative procedure. This new algorithm minimizes the effects of free surfaces by reducing the number of tanks used in the automatic ballast algorithm as shown in Figure 4. The algorithm begins with an empty set of tanks and at each iteration adds one tank to the set. The equilibrium of the vessel, using the updated set of tanks is then computed. Convergence is achieved when the equilibrium is computed successfully. Otherwise, the algorithm starts a new iteration, including an additional tank and then repeating the equilibrium computation.

Figure 7 shows an example of a ballast configuration computed using the algorithm presented in this section.

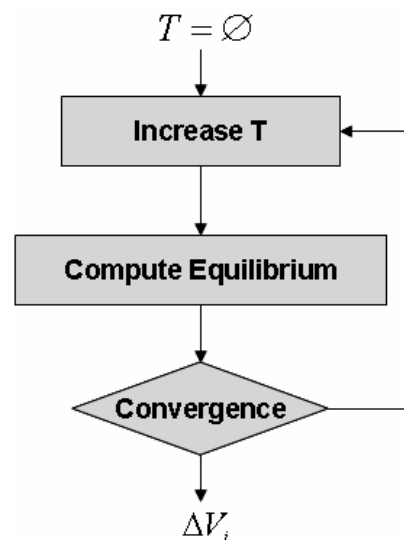


Figure 4- Minimization of free surfaces.

5.2 Minimization of Structural Stress

Some experiments performed with the automatic ballast algorithm have shown that some loading conditions proposed by the algorithm can result in violation of the envelopes of shear-forces or bending moments

of large ships. Irregular variations of the shear-forces have also been observed in many applications of the standard algorithm.

Both conditions were observed when the distribution of liquids among the tanks was uneven.

In order to reduce these effects, two more constraints have been introduced in the algorithm. The new constraints control the variation of volume among tanks, trying to create a regular longitudinal distribution of liquids. What, in most cases, will result in a reduction of stresses. Figure 5 shows the buoyancy curve (in blue) for a typical ship vessel. This curve is constant along the parallel body, so, theoretically, if the ship is loaded with a curve that exactly matches the buoyancy curve, the shear and bending effects will be zero.

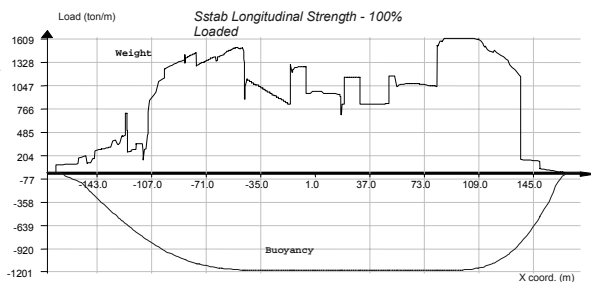


Figure 5- Buoyancy curve of a ship.

The new constraints can be seen in Equations 14 and 15. Two new parameters were introduced: a volume variation tolerance that is used among all tanks (TOL_g) and a volume variation tolerance for the neighbouring tanks (TOL_n). As Equations 4 and 5 show, the amount of liquid in the tanks will depend on the volume of its neighbouring tanks and of all other tanks.

The optimal value for both TOL_g and TOL_n is zero, which corresponds to a perfectly even distribution of liquids among the tanks. This value, however, is not acceptable for most cases. The determination of TOL_g and TOL_n is then performed by using an iterative procedure, as shown in Figure 6.

$$\left| \frac{v_i + \Delta v_i}{V_i^{\max}} - \frac{v_k + \Delta v_k}{V_k^{\max}} \right| < TOL \quad i \in T, k \in T \quad (14)$$

$$i \neq k$$

$$\left| \frac{v_i + \Delta v_i}{V_i^{\max}} - \frac{v_j + \Delta v_j}{V_j^{\max}} \right| < TOL \quad i \in T, j \in N \quad (15)$$

TOL_g	Global volume variation tolerance
TOL_n	Neighbor volume variation tolerance
N_i	Set of neighbor tanks of tank i

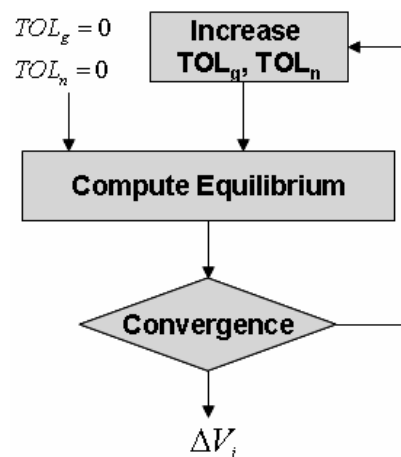


Figure 6- Determination of TOL_g and TOL_n.

6. RESULTS

We selected three examples to show the possibilities of the automatic loading algorithm. The first one shows a semi-submersible platform with 24.000 tons of ballast capacity with an operational draft of 23.10 meters. The total light weight is 25.600 tons and the CG of this light weight is 2.4 meters forward and 1.1 meters starboard. After selecting all ballast tanks (initially empty) to balance the model in even keel at the operational draft, the results obtained with the minimization with the free-surface parameter activated are shown by Table 1

Figure 7 shows the tank loading defined by

the algorithm. The compartments containing liquid are shown in solid blue. All other compartments are shown with transparency.

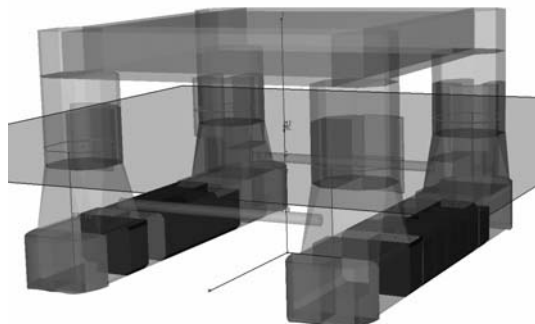


Figure 7- Ballast loading after algorithm.

Table 1- Tank loading after algorithm.

Name	Capacity (t)	Final Weight (t)	Final Filling (%)
BT_PS_FWD_09	441.67	441.67	100
BT_SB_FWD_21	441.67	441.67	100
BT_SB_FWD_22	427.14	427.14	100
BT_PS_FWD_11	438.71	438.71	100
BT_SB_FWD_19	438.71	438.71	100
BT_PS_FWD_13	438.71	438.71	100
BT_SB_FWD_17	438.71	438.71	100
BT_PS_FWD_14	622.88	622.88	100
BT_SB_FWD_18	622.88	622.88	100
BT_PS_MDS_15	438.71	438.71	100
BT_SB_MDS_15	438.71	438.71	100
BT_PS_MDS_16	819.31	646.82	79
BT_SB_MDS_16	819.31	819.31	100
BT_PS_AFT_09	441.67	352.32	80
BT_PS_AFT_11	438.71	438.71	100
BT_PS_AFT_11	438.71	438.71	100
BT_PS_MDS_15b	438.71	438.71	100
BT_SB_AFT_19	438.71	438.71	100
BT_SB_AFT_18	622.88	559.64	90
BT_PS_AFT_11	438.71	438.71	100
BT_PS_MDS_15b	438.71	438.71	100

It possible to see in Figure 7 that the most significant trim and heel tanks were not used. This is because of the sorting procedure applied to the selected set of tanks that was performed based on the heel and trim moment capacities and, with the minimization of free-surface parameter selected, those tanks are the last to be used.

The second example consists of a FPSO with the minimization of longitudinal stresses

parameter selected. In this example the idea is to maintain the total weight (light-weight + ballast + cargo + oil tanks) but to redistribute the cargo in order to minimize the shear and bending longitudinal forces.

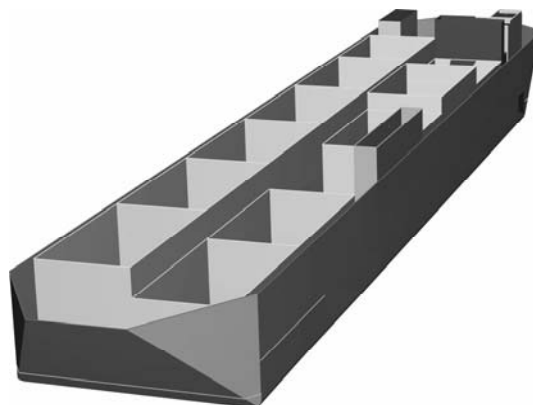


Figure 8 – Ship loaded with minimum shear.

Figure 8 shows the final loading of the tanks. As in the other images captured from Sstab, the meshes in green show the external hull. Ballast tanks are shown in solid blue and oil tanks in solid yellow.

Figures 9 and 10 show the graphs of shear forces and bending moments, respectively.

The last example shows an emergency situation where the automatic loading is used to restore the position of a platform after a damage occurrence. Figure 11 shows the model balanced after the damage. Damaged tanks are shown in solid red.

As shown in Figure 12, a new tank loading was defined by the algorithm to restore the platform to the even keel position before the recovering of the tanks.

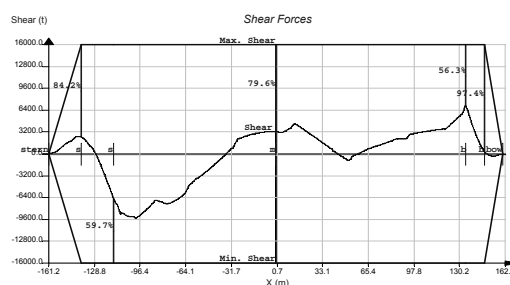


Figure 9- Shear forces of Figure 8.

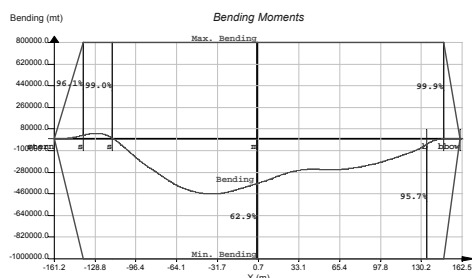


Figure 10- Bending forces of Figure 8.

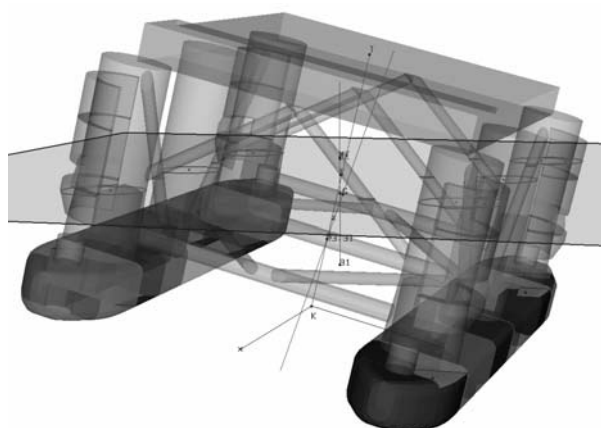


Figure 11- inclination due to damage.

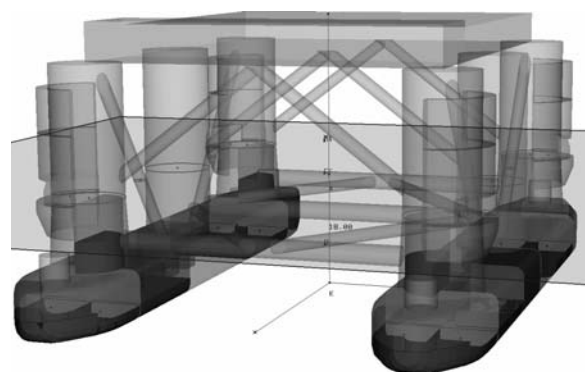


Figure 12- New loading restores even-keel.

7. CONCLUSIONS

An algorithm to balance the loading of tanks was successfully defined and implemented in Program Sstab. This algorithm is responsible for defining the operational conditions of semi-submersible oil platforms and FPSOs that are being designed by Petrobras.

The algorithm is fast enough to run in standard PCs. The tests were made in a Pentium IV with 2.8 GHz CPU capacity and 512 Mb of RAM and, in all three examples, Sstab took about a minute to complete the new loading definitions.

One of the major problems of using a linear programming library to solve this non linear problem is that there are no partial results for the loading condition. The user may want an answer like *how much could you do*. We are also working on this problem, using the same linear programming library. As an alternative, some non-linear library could be tested.

We are improving the data of the program to include the pumping properties and the costs of each operation, what will enable the implementation of the cost optimization.

8. ACKNOWLEDGMENTS

The authors would like to thank Petrobras, CENPES and Tecgraf/PUC-Rio for their support and for the opportunity of working in this project.

9. REFERENCES

- Bertsimas, D. and Tsitsiklis, J., 1997, "Introduction to Linear Optimization,," Athenas Scientific.
- Coelho, L.C.G., Figueiredo, L.H. and Gattass, M., 2000, "Intersecting and trimming parametric meshes on finite-element shells". International Journal for Numerical Methods in Engineering, Vol. 47, No. 4, pp. 777-800.
- Coelho, L.C.G., Jordani, C.G., Oliveira, M.C. and Masetti, I.Q., 2003, "Equilibrium, Ballast Control and Free-Surface Effect Computations Using the Sstab System", Proceedings of the 8th International Conference on the Stability of Ships and

Ocean Vehicles, pp. 377-389.

Cormen, T.H., Leiserson, C.E., Rivest, R.L.
and Stein, C., 2001, "Introduction to
Algorithms," MIT Press and McGraw-Hill.

IMO, 2001, "Code for the Construction and
Equipment of Mobile Offshore Drilling
Units."

Application of the Hull Turnover Afloat as a Shipbuilding Tool

Antônio Gil F. Bezerra, *CEO of INACE Group*

Antônio Paulo P. Bastos, *Former General Manager of INACE Shipyard*

Aurélio G. Girão, *Production Manager of INACE Shipyard*

Marcio F. Igreja, *Design Manager of INACE Shipyard, Member of SOBENA*

ABSTRACT

The upside down construction increases the assembly speed. However, the conventional turnover involves considerable difficulty. This paper describes a procedure to accomplish a turnover with the hull floating on the water. According to this procedure a relatively small force, applied by a crane, take the hull up to a given heel angle where the unbalanced weight and force of buoyancy rights the structure. A numeric method is introduced aimed at providing the designer with a tool to figure out the proper solutions for the turnover planning. Typical output obtained from ordinary stability software is used as data entry.

Keywords: *Hull turnover, Upside down hull construction, Ship stability.*

1. INTRODUCTION



Figure 1 Turnover afloat of a patrol vessel's hull at INACE Shipyard

The upside down position presents many advantages for building hulls that have too much shape, frequently without or with a short parallel middle body. This type of hull form is typical for military vessels, fast PSVs, crew boats, tugs, fishing boats, mega-yachts and the

like. The usage of the deck as a supporting base to assembly the framing or blocks is simpler than the erection in the normal position upon cradles. The upside down construction methodology increases the assembly speed and improves the shell distortion control. A better final product is obtained, with significant cost reduction.

Assuming that the upside down methodology gives several benefits to the hull construction, in the other hand the conventional turnover involves considerable difficulty. Normally the shipyards dedicated to the construction of small and medium sized vessels doesn't have cranes or grant cranes with sufficient capacity to turnover the entire hull in an only operation. One usual solution is to divide the hull, after the assembly, in two or more large blocks, noting that the joints between these units were not previously welded, but only aligned. However, an increasingly quantity of blocks implies in more re-alignment

problems, with the risk of loose the gains achieved before in the upside down phase. In the same way the adoption of big wheels, commonly used to turnover small boats, rolling them on the ground is not technically or economically feasible for larger vessels.

Additionally, in a turnover on land the interaction between the concentrated lifting forces and the distributed loading, associated to the hull own weight, may induce permanent deformations to the structure.

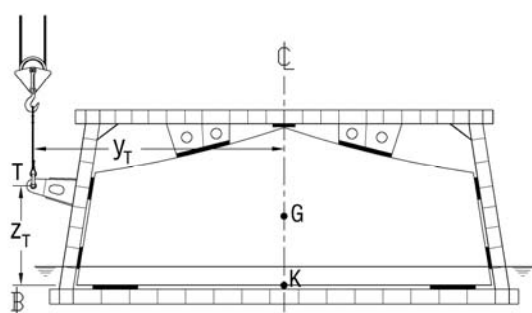


Figure 2 Typical turnover ring assembly

INACE Shipyard, located at Fortaleza, Brazil, introduced this procedure on 1996 for a Brazilian Navy patrol vessel. Until now three patrol vessels were successful turned according this technique. Figure 1 shows the last operation on October of 2005, for a 46 m patrol vessel under construction for the Namibian Navy

2. DEFINITIONS

2.1 Turnover Ring Assembly

Figure 2 is a hull transverse section showing a typical assembly for the turnover ring. It is a structural frame that surrounds the shell and the deck, in order to transfer the lifting force applied by the crane at the point T. In the figure the hull is floating in the upside down position.

Along this paper a hypothetical aluminium

hull for a fast PSV / crew boat was considered as a useful case study. In the condition shown in Figure 2 the hull structure is completely finished. All apertures on deck are closed or are not cut yet, providing a full watertight body.

Although in a heavy hull more than one ring can be necessary, in this study we considered only one attached to the hull. Indeed, the evaluations on Section 4 shows that the maximum force applied by the crane is relatively low, if compared with the hull weight.

The parameters indicated on Figure 2 are defined as the following:

- KG = Height of the center of gravity from the inverted base line (located over the flat main deck) = 1.53 m
- y_T = transversal position from center line (half beam) of the point T, where the crane lifting force is applied
- z_T = vertical position from base line (height) of the point T.

There are no previously defined values for y_T and z_T as the main goal of this paper is just to provide a criteria to determine a correct and safe position for the point T.

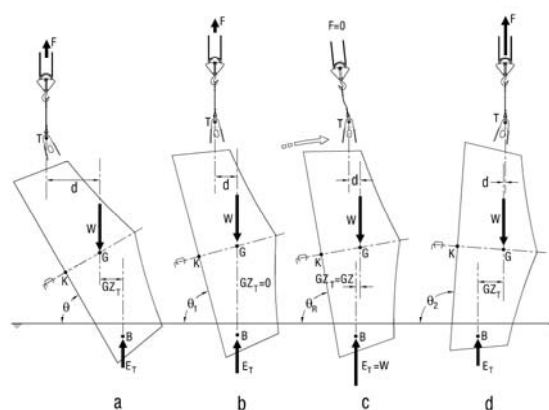


Figure 3 Turnover sequence, showing the interaction between the forces acting on the hull.

Figure 3 shows the turnover sequence. The ring structure was omitted for better visualization.

2.2 Parameters

Figure 3a represents the hull at a given heel angle θ . The parameters shown are defined as the following:

- W = Weight of the hull plus the ring, applied at the center of gravity G , equal to 42.06 metric tons for the present case study.
- F = Lifting force applied by the crane at the point T . The secondary goal of this paper is to determine the maximum lifting force demanded by the turnover, so the designer can figure out the safety for the cranes intended to use in the operation.
- E_T = Buoyancy force acting on the buoyancy center B . Note that differently of what occurs on an ordinary flotation condition, where the buoyancy force is always equal to W , in the turnover afloat process. E_T changes for each heel angle, following the variation of F .
- GZ_T = Distance between the vertical lines of W and E_T . Although similar, this distance is not equal to the righting arm GZ of an ordinary flotation condition.
- d = Distance between the vertical lines of W and F .

3. STATIC AND DYNAMIC CONSIDERATIONS

The correct determination of the turnover point (T) position on the ring is the main goal for the present paper. A wrong evaluation could introduce high risks to the operation or, on the other hand, the turnover may not occur.

3.1 Turnover Angle and Turnover Range

In Figure 3b the hull reached the beginning of the turnover. Then, from that point there will be only “capsizing” moments around point G , and the hull can even turnover itself without the help of F . We define θ_1 as the heel angle where the vertical line of B matches the vertical line of W , or the Turnover Angle.

Up to the Turnover Angle θ_1 there is equilibrium between the moments around G due to the forces E_T and F . This means that the crane has full control over the hull, and if something goes wrong the operator can lowering it back to the initial position (Fig.2). Near the Turnover Angle, F is very low and E_T is almost equal to W .

After the Turnover Angle θ_1 the position that corresponds to θ_R on Figure 3c could be anywhere in the range between θ_1 and θ_2 (Fig. 3d). In such condition the hull is turning free. Within this range the vertical line associated to F is yet placed “before” or very close to the vertical line of W . So, to restore the equilibrium F should act inverted, pointing to the water. This is impossible for the crane, and the hull remains accelerating itself “after” θ_1 .

The movement is relatively fast, and the crane has no mechanical conditions to follow it. The cable becomes loose for a while.

When the hull reach the position that corresponds to heel angle θ_2 the vertical line of F goes slightly “after” the vertical line of W , as shown in Figure 3d. Now, at least theoretically, F can balance E_T again

However, the distance d is yet very short at θ_2 . On the other side, at the same time, GZ_T is already larger than d . So F must be very intense to compensate the lack of lever arm.

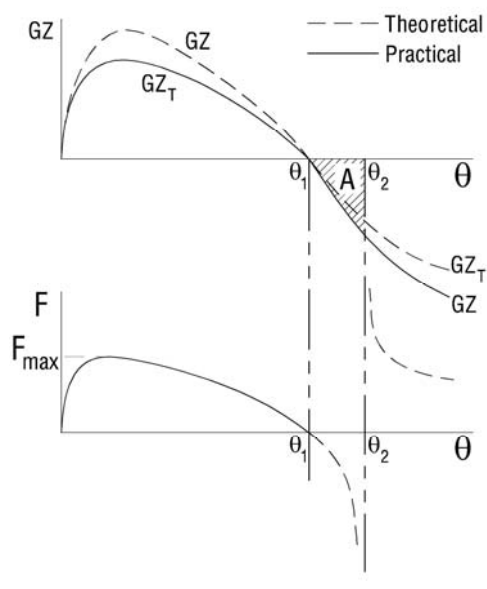
Additionally, the hull acquired considerable kinetics energy, accelerated by the moment generated by W and E_T , turning free between θ_1 and θ_2 . Therefore, the crane may be hit by a severe strike at θ_2 .

Figure 4 suggests that the way to avoid accidents in the turnover is to keep the heel angle range between θ_1 and θ_2 as short as possible.

As the force F “not exists” between θ_1 and θ_2 , only weight and displacement acts on the hull, in a conventional way. Thus the “capsiz-

ing” arm GZ_T works like the conventional GZ in an ordinary static stability curve.

Figure 4 Synchronism of GZ_T , GZ and F behaviours



It is known that the area below the GZ curve is directly proportional to the work generated by the “capsizing” moment. This work will be transformed in kinetics energy. Therefore, a good criteria to figure out if the heel angle range is too large is to compare the energy generated with the capacity of the crane system to absorb it.

We should note in Fig. 4 that the curve for F after θ_1 was considered theoretical due to the fact that after this point up to θ_2 it is impossible to the crane to control the movement, and after θ_2 it will be unnecessary try to keep the balance between forces F and E_T . The crane operator should release the cable, allowing the hull to “fall” towards the up right position, maybe only applying the breaks slightly to reduce the speed.

3.2 No Turnover

A short range between θ_1 and θ_2 means a more safety operation. But a very short range,

or even no range, can avoid the turnover. Secondary effects like the wind or water resistance and friction are difficult to figure out correctly in such situation, so the designer should take into account a margin to compensate them.

A wrong position for the point T could avoid the turnover too. Figure 5 shows the crane acting on point T' instead of point T . At that point the arm d becomes too short to compensate GZ_T . Although a well planned turnover occurs with very low values for force F when the hull is getting close to θ_1 , this force could reach values nearing W . This value is even greater than F_{max} , which should occur at low heel angles. This means that the hull is being lifted instead of turned.

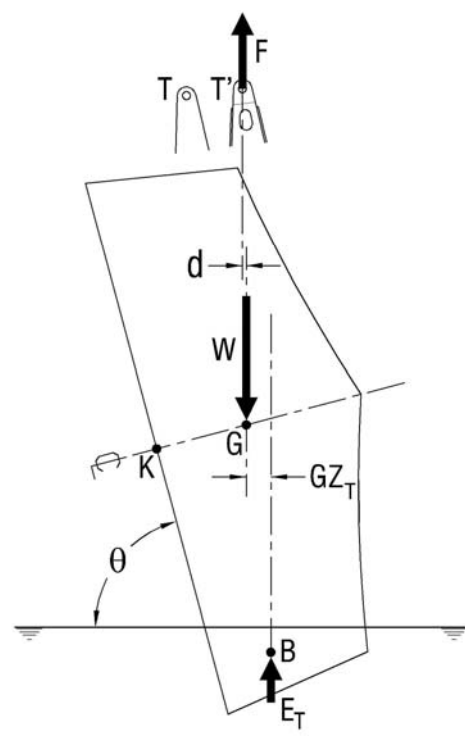


Figure 5 Applying F on point T' instead of T only lifts the hull

4. NUMERICAL METHOD

The methodology described in the present Section has the following objectives:

- Find the ideal position for the point T
- Figure out the maximum force that acts on the point T , and what is the related heel angle.

4.1 Equilibrium Equations

Considering that the process can be undertaken in an almost static way, we can state that the equilibrium equations are:

$$\sum M_G = 0 \quad (1)$$

$$\sum F_x = 0 \quad (2)$$

$$\sum F_y = 0 \quad (3)$$

$$\sum F_z = 0 \quad (4)$$

The forces acting along x and y directions (length and beam respectively) are not significant, and equations (2) and (3) will not be used.

In order to simplify the evaluations, the moments are considered around the point G. Taking into account all the moments based on the forces from the Figure 3a we can develop Eq.(1) as the following:

$$\begin{aligned} \sum M_G &= F \cdot d - E_T \cdot GZ_T \\ 0 &= F \cdot d - E_T \cdot GZ_T \\ F &= \frac{E_T \cdot GZ_T}{d} \end{aligned} \quad (5)$$

Considering all the vertical forces shown in Figure 3a we can develop (4) as the following:

$$\begin{aligned} \sum F_z &= E_T + F - W \\ 0 &= E_T + F - W \\ F &= W - E_T \end{aligned} \quad (6)$$

Thus to determine F there are two equations. According Eq. (5) F could be known if the moment balance becomes known too. To Eq. (6) the relation is about the vertical forces. So, only to best comprehension of the proposed method we can rewrite (5) and (6) as:

$$F_M = \frac{E_T \cdot GZ_T}{d} \quad (7)$$

$$F_V = W - E_T \quad (8)$$

If the results obtained by our method are consistent thus:

$$F = F_M = F_V \quad (9)$$

This means that the difference between the two forces should be:

$$\Delta F = F_M - F_V = 0 \quad (10)$$

4.2 Interpolation of the Cross Curves

An important characteristic of the present method is the capability of using conventional cross curves calculated by ordinary computer software. One recommendation is to choose a software that can run the curves for any desired angle. This property will allow the possibility to study the heel angle at steps as close as 1 degree, giving better precision to accurately find the heel angles θ_1 and θ_2 mentioned on Section 3.

Other recommendation is to run the curves using an inverted offsets table. For a sample, as in the present case study, a heel angle of 60 degrees in an upside down basis corresponds to 120 degrees from the up right position.

Table 1 is a typical output generated by an ordinary naval architecture computer software for the stability cross curves. It presents the curves in a numeric format, where for each listed heel angle:

- D = Displacement in salt water expressed in metric tons.
- GZ_0 = Righting arm considering the center of gravity hypothetically placed over the point K

Table 2 is a sample of how to determine F , E_T and GZ_T to a arbitrary chosen heel angle of 60 degrees,.

The corrected value of the conventional GZ , for the real z coordinate of G , was obtained using the well known equation:

$$GZ = GZ_0 - KG \cdot \sin \theta \quad (11)$$

The lever arm for the force F was obtained using the following equation:

$$d = (KG - z_T) \cdot \sin \theta + y_T \cdot \cos \theta \quad (12)$$

The value for KG was given in Section 2.1, and for merely checking how the method works we arbitrate $y_T = 5.5$ m and $z_T = 2.2$ m as the position of point T . Thus, substituting these values in (12) we found:

$$d = 2.17 \text{ m}$$

Note that the above value is constant for all displacements related to the current heel angle of 60 degrees.

Looking to the ΔF column in Table 2 we can note that with the increase of the displacement that difference is increasing too, positively. In the highlighted lines, between the displacements 26.01 t and 32.27 t, the signal of ΔF changes from negative to positive, meaning that the curve describing that parameter passed across a zero value in the range between -3.04 t and 6.50 t.

Therefore if ΔF is zero F_M and F_V matches each other and we can interpolate the values for E_T and GZ_T . In this study we use linear interpolation, observing that it not introduces significant imprecision to the results.

Table 1 Cross Curves of Stability for the hull related to the case study mentioned on 2.1.

10°		20°		30°		40°	
D	GZ ₀	D	GZ ₀	D	GZ ₀	D	GZ ₀
(t)	(m)	(t)	(m)	(t)	(m)	(t)	(m)
1.09	4.28	0.54	4.19	0.38	3.89	0.31	3.46
4.50	4.08	2.21	4.09	1.54	3.84	1.27	3.44
10.39	3.88	5.07	4.00	3.53	3.79	2.91	3.41
18.83	3.68	9.16	3.91	6.34	3.74	5.23	3.39
29.91	3.48	14.50	3.82	10.02	3.69	8.23	3.36
43.70	3.27	21.11	3.72	14.57	3.64	11.95	3.34
60.23	3.07	29.02	3.63	20.01	3.59	16.40	3.31
79.52	2.86	38.21	3.54	26.33	3.54	21.57	3.29
101.57	2.66	48.73	3.44	33.57	3.48	27.47	3.26
126.4	2.46	60.63	3.35	41.70	3.43	34.11	3.23
153.9	2.26	73.89	3.25	50.73	3.38	41.49	3.21
184.1	2.06	88.52	3.16	60.68	3.33	49.62	3.18
216.9	1.86	104.5	3.06	71.57	3.28	58.49	3.15
252.1	1.67	121.9	2.97	83.42	3.22	68.11	3.13
289.7	1.49	140.7	2.87	96.23	3.17	78.47	3.10

50°		60°		70°		80°	
D	GZ ₀						
(t)	(m)	(t)	(m)	(t)	(m)	(t)	(m)
0.29	2.92	0.30	2.29	0.34	1.60	0.46	0.87
1.18	2.92	1.22	2.31	1.41	1.63	1.89	0.94
2.70	2.91	2.78	2.32	3.20	1.67	4.29	1.01
4.85	2.91	4.99	2.34	5.75	1.71	7.68	1.09
7.63	2.90	7.86	2.35	9.04	1.75	12.06	1.16
11.06	2.90	11.38	2.37	13.08	1.79	17.45	1.23
15.16	2.89	15.57	2.38	17.88	1.83	23.83	1.31
19.92	2.89	20.45	2.40	23.46	1.86	31.24	1.38
25.36	2.88	26.01	2.41	29.83	1.90	39.64	1.45
31.48	2.88	32.27	2.42	36.99	1.94	48.70	1.51
38.26	2.87	39.22	2.44	44.93	1.98	58.21	1.55
45.74	2.87	46.85	2.45	53.66	2.01	68.08	1.59
53.91	2.86	55.19	2.47	63.14	2.05	78.22	1.61
62.76	2.85	64.23	2.48	73.16	2.08	88.61	1.63
72.31	2.85	73.98	2.49	83.57	2.10	99.22	1.65

The values interpolated on Table 2 for E_T and GZ_T were:

$$E_T = 28.00 \text{ t} \quad ; \quad GZ_T = 1.08 \text{ m}$$

In the same way the values interpolated on Table 2 for F_M and F_V were:

$$F_M = 14.06 \text{ t} \quad ; \quad F_V = 14.06 \text{ t}$$

It is important to note that they matched precisely, thus according (9):

$$F = F_M = F_V = 14.06 \text{ t}$$

Only for an additional check of the results coherence we can rearrange (6) to obtain exactly the same hull weight W defined in Section 2.2:

$$W = F + E_T$$

$$W = 14.06 + 28.00 = 42.06 \text{ t}$$

Table 2 Sample of interpolation from the Cross Curves, for a heel angle of 60° ($y_T = 5.5 \text{ m}$; $z_T = 2.2 \text{ m}$)

D From CC (t)	GZ ₀ From CC (m)	GZ Eq.(11) (m)	F _M Eq.(7) (t)	F _V Eq.(8) (t)	ΔF Eq.(10) (t)
0.30	2.29	0.96	0.13	41.76	-41.63
1.22	2.31	0.98	0.55	40.84	-40.29
2.78	2.32	0.99	1.27	39.28	-38.01
4.99	2.34	1.01	2.33	37.07	-34.74
7.86	2.35	1.02	3.71	34.20	-30.49
11.38	2.37	1.04	5.48	30.68	-25.20
15.57	2.38	1.05	7.57	26.49	-18.92
20.45	2.40	1.07	10.13	21.61	-11.48
26.01	2.41	1.08	13.01	16.05	-3.04
32.27	2.42	1.09	16.29	9.79	6.50
39.22	2.44	1.11	20.15	2.84	17.31
46.85	2.45	1.12	24.29	-4.79	29.08
55.19	2.47	1.14	29.12	-13.13	42.25
64.23	2.48	1.15	34.19	-22.17	56.36
73.98	2.49	1.16	39.72	-31.92	71.64

4.3 Analysis of the Turnover Force F

Repeating the process described in 4.2 for each desired heel angle generates the Table 3. Now we are looking in a first instance for the range where F becomes negative, i.e. the heel angles θ_1 and θ_2 defined in 3.1.

In Table 3 the normal step for the heel angle is 10 degrees. But near the Turnover Angle we refined the results lowering the interval to 1 degree. In the highlighted lines we see that F becomes negative from 80 to 83 degrees. These are the values for θ_1 and θ_2 respectively

Note as F falls to a low value at 79 degrees, close to the Turnover Angle, and how it jumps from a negative value to a high positive one after reaching θ_2 , as shown in Figure 4.

Other important result is the maximum value F_{\max} for the force F , and the heel angle θ_{\max} where it occurs. In the two last columns of Table 3 we obtained a maximum force equal to 16.34 t at a heel angle of 20 degrees.

Table 3 Turnover parameters as function of the heel angle ($y_T = 5.5 \text{ m}$; $z_T = 2.2 \text{ m}$)

θ (deg.)	E_T (t)	GZ _T (m)	d (m)	F (t)
0	0	0	5.50	0
10	26.03	3.28	5.30	16.03
20	25.72	3.14	4.94	16.34
30	25.85	2.78	4.43	16.21
40	26.23	2.28	3.78	15.83
50	26.87	1.71	3.02	15.19
60	28.00	1.08	2.17	14.06
70	30.62	0.47	1.25	11.44
75	33.97	0.18	0.78	8.09
79	41.03	0.01	0.39	1.03
80	44.92	-0.02	0.30	-2.86
81	44.51	-0.08	1.38	-2.45
82	46.47	-0.12	1.29	-4.41
83	48.70	-0.17	1.20	-6.64
84	4.50	-0.77	-0.09	37.56
85	8.72	-0.73	-0.19	33.34
90	18.42	-0.74	-0.57	23.64

The results given in Tables 2 and 3 were evaluated for a specific position of the turnover point, represented by the coordinates y_T and z_T . A slight change in the coordinate values can produce great modifications in the final results.

Table 4 shows an analysis where only the coordinate z_T changes, keeping the same value for y_T . We can see where the range $\Delta\theta$ is relatively large, and where the turnover shouldn't be accomplished properly.

Table 4 θ range and F_{\max} comparison for different Z_T values

Z_T (m)	θ_1 (deg.)	θ_2 (deg.)	$\Delta\theta$ (deg.)	F_{\max} (t)	θ_{\max} (deg.)
1.0	80	95	15	15.70	15
1.2	80	93	13	15.79	15
1.4	80	91	11	15.89	15
1.6	80	89	9	15.99	15
1.8	80	87	7	16.09	15
2.0	80	85	5	16.20	20
2.2	80	83	3	16.34	20
2.4	80	81	1	16.50	25
2.6	79	79	0	16.69	25
2.8	79	79	0	16.94	30
3.0	No Turnover			28.96	75
3.2	No Turnover			35.69	73

4.4 The Energy Criteria

Results similar as shown in Table 4 brings very important information about the turnover physics, and we can analyse what happens for each Turnover Point coordinates y_T and Z_T associated with a given combination of hull weight W and KG .

Despite we can figure out the value of $\Delta\theta$ for any situation, how to choose the most suitable one?

Normally a crane manufacturer states what is the maximum speed which his equipment can lower a given weight. For a sample a certain crane can lower 40 metric tons at 25 m / min. Expressing the weight in terms of mass, and converting the speed to m/s we obtain:

$$m = 40000 \text{ kg}$$

$$v = 0.42 \text{ m/s}$$

The classic equation for kinetics energy is:

$$K = \frac{1}{2} \cdot m \cdot v^2 \quad (13)$$

Substituting the values for m and v in (13) we found the kinetics energy absorption limit for the crane:

$$K_L = 3.5 \text{ kJ} \quad (14)$$

In the other hand, as shown in Figure 4, only the conventional GZ is effective between the heel angles θ_1 and θ_2 , describing a portion of a regular Static Stability Curve. In an ordinary flotation condition only the weight and displacement acts on the hull. As they are constant in such condition the Static Stability Curve can be plotted in terms of moment simple by multiplying the righting arm GZ by the constant weight value.

Expressing the heel angle in radians and the moment in N.m any area below the curve corresponds to the work necessary to change the hull from a given heel angle to another one. If the hull is coming back after heeling this is the work generated, transformed in kinetics energy achieved by the turning hull.

Therefore knowing the area A shown in Fig. 4 makes possible to determine the kinetics energy that arises between the heel angles θ_1 and θ_2 . Table 5 shows the integration (by trapeziums) of this area for the condition analyzed in Table 3:

Table 5 Integration of the kinetics energy below the static stability curve

θ (deg.)	GZ_0 m	GZ m	M kN.m	$\dot{A}A$ (kJ)
80	1.47	-0.04	-15	-
81	1.42	-0.09	-38	-0.46
82	1.37	-0.15	-60	-0.85
83	1.31	-0.21	-86	-1.27
Σ				2.6

Then the kinetics energy developed by the hull turning free up to θ_2 is equal to 2.6 kJ. This value corresponds to 74% of the crane limit, equal to 3.5 kJ, given by (14).

5. CONCLUSION AND DISCUSSION

Section 4.4 shows that for the case study analysed a $\Delta\theta = \theta_2 - \theta_1 = 3$ degrees is a suitable value to the turnover operation, with the hull kinetics energy corresponding to 74% of the crane limit,

Obviously is preferable to not exceed the crane limit, to avoid a strike against it. But we suggest, depending upon further investigation, that the $\Delta\theta$ should be adjusted to avoid kinetics energy values below 50% of the crane limit, as a margin can be necessary to compensate secondary effects due to wind, water resistance and water friction.

It is important to note that if we change, for a sample, only the value of z_T from 2.2 m to 1.6 m, keeping the same values for all the others parameters, we verified on Table 4 that $\Delta\theta$ is equal to 9 degrees.

Applying to this condition the same procedure used to create Table 5 reveals that when reach θ_2 the hull would have accumulated kinetics energy equal to 18 kJ, approximately 5 times the crane limit. This fact shows how a relatively small variation of the coordinate z_T (0.6m, corresponding to 17% of hull depth) can produce great risks for the operation.

Other interesting point, not covered in this paper, is the investigation about the influence of the trim variation along the heeling process.

6. ACKNOWLEDGMENTS

- To our families;
- To all employees and administrators of INACE Shipyard;
- To the Brazilian Navy, which was the first

organization to trust in the idea;

- To the Naval Architect Antônio Parente, for the help and valuable suggestions;
- To the trainees Sara Jorge (Naval Architecture-UFRJ), Fernando Prado (Naval Architecture-UFRJ) and Robson Cavalcante (Mechanical Engineering-UFC) for modeling the hull analyzed and
- To the team at the Centro Avançado de Retina e Catarata, at Fortaleza, Brazil. Without their care and orientation it would be impossible to the author M.F.Igreja to write this paper.

7. REFERENCE

- Lewis, E. V., Ed. 1988 Principles of Naval Architecture. Vol. I, Stability and Strength. The Society of Naval Architects and Marine Engineers, Jersey City, NJ.

Stability Characteristics of an Early XVII Century Portuguese *Nau*

Tiago A. Santos, *Technical University of Lisbon*

N. Fonseca, *Technical University of Lisbon*

F. Castro, *Texas A&M University,*

ABSTRACT

During the XVI and XVII centuries the India Route was the longest regular commercial route of its time and connected Lisbon, Portugal, with Goa or Cochin in the Indian subcontinent. However, there is presently very little technical knowledge about the technical characteristics of the different ship types employed in this trade. This paper starts by describing briefly the shipbuilding treatises, techniques and shipyard organization at this time. Then, a shipwreck discovered at the mouth of the Tagus River, which was identified as the Portuguese ship *Nossa Senhora dos Mártires*, of the *Nau* type, lost in this place in 1606, is described. Taking in consideration shipbuilding treatises and archaeological remains, a reconstruction of the ship's lines plan, structure and rigging is then presented. This information is used to investigate the floatability and stability of the ship in a number of different loading conditions, including overloading of the ship, which was a usual condition when these ships returned from India. Accidental conditions such as those arising from flooding are also discussed. The results are compared with modern stability criteria for large sailing vessels.

Keywords: *Intact stability, Damage stability, Nau, History, Archeology*

1. INTRODUCTION

The Portuguese ship *Nossa Senhora dos Mártires*, known to be of the *Nau* type, sunk at the entrance of river Tagus in Lisbon, on the 14th September 1606, therefore almost exactly 400 years ago. The ship was returning from India, after having travelled across the India Route (*Carreira da India*). This was the longest regular commercial route of its time and linked Lisbon, in Portugal, to Goa or Cochin in the Indian subcontinent. The route was sailed by Portuguese ships yearly between 1498, the year Vasco da Gama returned from his exploratory voyage, and the XVIII century.

It is known that *Nossa Senhora dos Mártires*, probably an almost new ship at the time, had left Lisbon on the 21st of March 1605 and arrived in Goa on the 28th September 1605.

After loading in Cochim, the ship departed from that harbour on 16th January 1606. The ship made a smooth voyage and scaled the Azores Islands in June, before arriving near Lisbon in the middle of a severe storm on the 13th September. The ship dropped anchors, but two days later the mooring cables broke and the ship's captain decided to attempt entering the river. On the morning of 15th September, the ship grounded on the coast at the entrance of river Tagus in very heavy following or stern quartering seas and, possibly, against a strong tidal current. The ship's hull was broken against the rocks in a matter of hours. On 19th September, about 200 bodies had already been washed ashore together with a large peppercorn black tide.

Although a substantial number of details relating to ship losses, life aboard, navigation techniques and events in India have been

studied extensively by historians, very little is known about the technical characteristics of the ships engaged in this trade. These ships were built in a pre-industrial era when technical design and documentation procedures almost did not exist and, in fact, their construction relied mostly on practical knowledge and tradition. For these reasons, modern investigators are left with little more than contemporary drawings such as those shown in Figure 1.

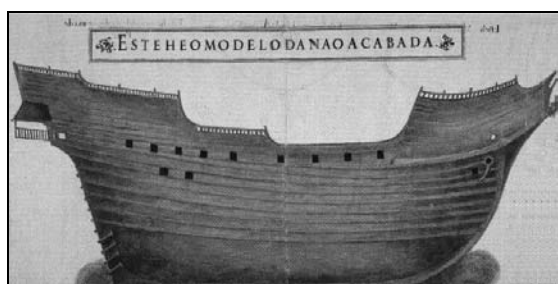


Figure 1 The India Nau from the *Livro de Traças de Carpintaria*, Manoel Fernandez (1616)

The current study is considered as the first stage of a larger and more comprehensive naval architecture investigation of the nautical characteristics of an early XVII century Portuguese *Nau*. The current paper attempts a step forward in the same line of classic studies in this field, such as those of Barata (1989), Branco (1994), Blot *et al.* (1994) and Domingues (2004). However, most works are still insufficiently integrated with naval architecture expertise and fail to explore many technical aspects of XVII century ship design and shipbuilding.

The methodology to investigate the technical characteristics of these ancient ships must be based on the analysis of archaeological remains and ancient shipbuilding treatises, which was in this case carried out by Castro (2001, 2003). Based on this work, Fonseca *et al.* (2005) present the analysis of the ship's stability at the departure from India and a comparison with modern stability criteria for large sailing vessels.

Compared to the former publication by the authors, this paper adds: a review of the ancient Portuguese shipbuilding treatises, a description

of the procedure to reconstruct the hull geometry, stability results for additional loading conditions including overloading, and stability results for various damage conditions. Additionally, the calculation of the weight distribution and position of the centre of gravity is slightly improved.

2 RECONSTRUCTION OF THE GEOMETRY OF *NOSSA SENHORA DOS MÁRTIRES*

2.1 Portuguese Documents on Shipbuilding

The Portuguese shipbuilding practices of the late XVI and early XVII centuries are relatively well known because of a number of texts comprising shipbuilding treatises and other documents. These documents are of fundamental value for the reconstruction of the characteristics of ships used in the India Route.

The first important text is Fernando Oliveira's *Livro da Fábrica das Naus* (Book on the Fabrication of Naus), dating from circa 1580. Oliveira was born around 1507 and published extensively on grammatics, navigation, naval warfare and shipbuilding. He travelled to Spain, Genoa, France and England, where he visited the shipyards. The *Livro da Fábrica das Naus* is one of the first European treatises on shipbuilding, the theoretical work of a scholar and not the practical work of a shipwright. It is comprised of a clear text, divided into nine chapters with few illustrations, covering timber characteristics and seasons; ship types; hull shape and structural details; hull erection sequence; rudder details. Oliveira illustrates his methods and practices with a 600 toneis *India Nau* but never completed his work.

The second important text to be considered is an anonymous list of the timbers necessary to build a three-decked, 600 toneis *Nau* for the India route included in the *Livro Nautico* (Nautical Book), a codex of Lisbon's National Library, dating from the 1590s, reproduced by Domingues (2004). This text is clear and detailed, explaining the hull erection sequence

and providing detailed lists of the timbers necessary for building each part of a ship. The building sequence is covered from keel laying up to rigging outfit, with examples given for the *Nau*, galleon and caravel types of ships.

The third important text is the manuscript entitled *Livro Primeiro da Arquitectura Naval* (First Book of Naval Architecture), by João Baptista Lavanha, written sometime around 1600. Lavanha was born in Lisbon in the middle of the XVI century, became cosmographer and published extensively on navigation matters but also on shipbuilding. The book contains general information on the nature of naval architecture, on timbers and on the dimensions and shapes of the hull structure up to the first deck. The book is incomplete and is clearly the work of a scholar, with a clear text which makes extensive use of geometry.

The fourth important text was Manoel Fernandez *Livro de Traças de Carpintaria* (Book of Shipwright Drawings) dated to 1616. Nothing is known for sure on the author, but certain documents refer Fernandez as a master shipwright at the Crown's Shipyard. The book comprises a large number of fine drawings, one of which is shown in Figure 2, illustrating a substantial number of ship types of this epoch, including a three-decked *Nau*. The drawings illustrate texts dedicated to individual ship types of different sizes, both sailing ships and rowing ships. The texts are frequently obscure and are clearly the work of a practical man, but most probably reflect contemporary practice in the shipyards. The book also contains details on the cranes, cradle and procedures used to launch the ships.

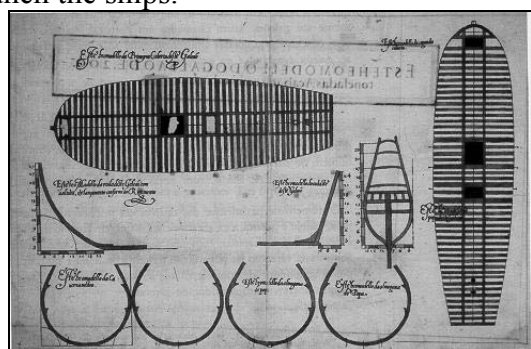


Figure 2 Plate from the *Livro de Traças de Carpintaria*, Fernandez (1616)

2.2 Lines and Rigging Plans

This section describes the method used to reconstruct the hull form, which is based on information included in contemporary documents and the archaeological remains recovered at the Pepper Wreck site. Written records show that Portuguese *nau* was conceived in the sixteenth and seventeenth centuries as a central box with two ends (Lowen, 1994). The frames that composed the central portion of the hull – the so-called box – were designed and built according to an old non-graphic system, developed in the Mediterranean sometime after the 11th century, probably for the building of galleys.

After mounting, leveling, and shoring the keel, stem and sternposts on the stocks, shipwrights would erect the stern panel, consisting on two fashion pieces and a number of transversal reinforcements of which the widest was placed at main deck level, and called *gio* (Figure 3).

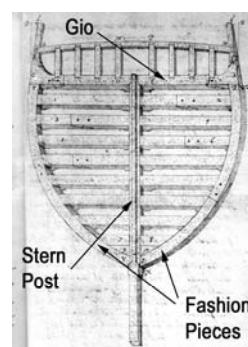


Figure 3 The stern panel

Traditionally the *gio* was half as wide as the ship's maximum breadth, which was measured, not necessarily at main deck, on the master frame.

With the keel and posts in place, including the stern panel arrangement, the next step was to erect the master frame, or midship frame. The master frame, or frames, for there were one, two, or three master frames in an *India nau*, depending on the keel length, was fully designed on the floor, somewhere in the shipyard. The master floor timber was assembled to the first futtocks with scarves and iron spikes, making sure that these connections

were solid on both sides, and would not move once erected on the keel.

The most important thing in the design of the master frame was the position of the turn of the bilge points. These symmetrical points marked the division between the ship's bottom and sides and were the control points for the design of all the frames that composed the central box. The last frames of this pre-designed and pre-assembled central box were appropriately called tail frames. The other two control points were located on the upper portion of the futtocks and marked the ship's width at main deck level, as shown in Figure 4.

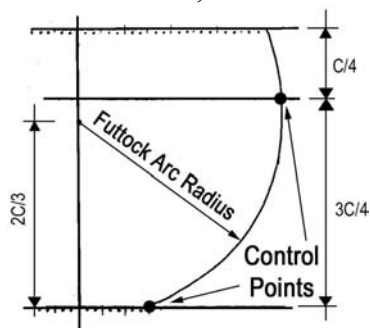


Figure 4 Position of control points

The section of the ship would change therefore incrementally, from the master frame's shape, to the tail frames, by narrowing and rising the positions of the turn of the bilge points, and by rising and widening the points of the deck breadth, as shown in Figure 5.

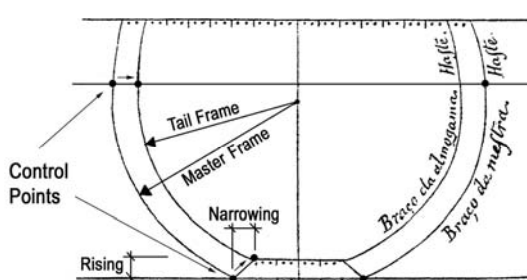


Figure 5 Narrowing and rising of the frames

A smooth rising and narrowing of the bottom was obtained with the help of one of a number of geometrical algorithms available to the shipwright at the time. One interesting particularity of this method is the fact that it is non-graphic. In other words, shipwrights did not need to make any drawings to obtain the shape of each one of the pre-designed frames.

All tasks were achieved with the help of two moulds and a variable number of gauges, as shown in Figure 6.

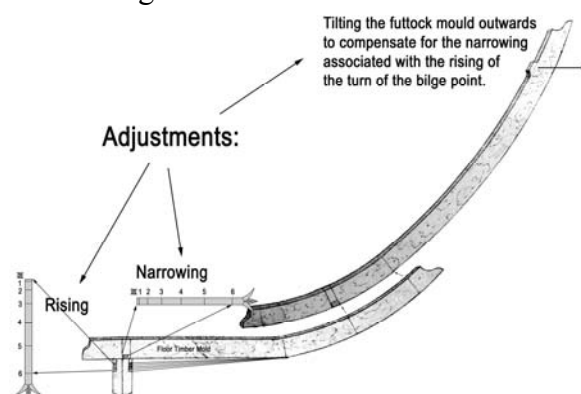


Figure 6 Adjustment of the mould

From the shape of the midship frame the shipwrights would deduce the shape of the tail frames by adding the total rising and subtracting the total narrowing of the turn of the bilge points. The length of the total rising or narrowing to be distributed along the pre-designed frames was called *compartida* in Portuguese. The gauge with the incremental values, to be added to or subtracted from each of the frames, was called *graminho*. The word *graminho* may lend itself to confusion because it designated both the gauge and the method, or algorithm, utilized to obtain the incremental values or coordinates of the curves.

Some of these geometric algorithms were described in sixteenth- and seventeenth-century Portuguese treatises and texts on shipbuilding, under designations like *meia lua*, *besta*, *saltarelha*, *brusca*, and *rabo de espada* (Barata 1989). These algorithms are very simple and well-understood. The one that seems to have been used in the design of the Pepper Wreck frames is the method known as *meia lua*.

The *meia lua* method, or *besta*, as Fernando Oliveira calls it, is referred in Italian texts from the fifteenth century onwards and consists of a quarter of a circle with a radius equal to the *compartida*. The quarter of a circle is divided into as many equal parts as the number of offsets required or, in other words, as many equal parts as the number of pre-designed frames to be placed from the midship frame to the tail frame in any particular vessel.

The offsets can be obtained by the expression: $x_i = 1 - \sin \alpha_i$ where α_i is the angle of the radius that touches point i on the quarter of the circle. However, the traditional way to obtain these values is graphic and quite simpler, consisting on adding another quarter of a circle, mirroring the first one, and on passing lines horizontally across, connecting the correspondent points. The resulting scale was directly engraved on a wooden gauge from the 1/1 scale drawing (see figure 7).

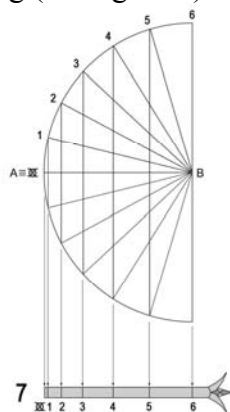


Figure 7 The *graminho*

Once the Nautical Archeologists started recording the remains of the ship's frames a number of turn of the bilge point's marks became apparent. These carpenter marks were

used to reconstruct the ship's hull form. The method used in the ship's reconstruction was fairly simple: the sets of values obtained from the archaeological remains were tested against the sets of theoretical values generated by all available algorithms (Castro 2005a). Several contemporary texts on shipbuilding offer a number of recipes to build an India *nau* and the sets of values generated with the algorithms above mentioned were adapted to the recipes.

As a result, the Pepper Wreck timbers seem to have been cut using *a meia lua* to distribute the incremental values of the bottom's rising and narrowing over 18 frames before the three central, master frames. According to the model of Fernando Oliveira (1580), another 18 pre-designed and pre-assembled frames were erected abaft the central frames, totaling 39 the number of pre-designed frames in this ship (Castro 2005a). Once the shape of the bottom was found, the remaining parts of the ship's hull were easy to reconstruct based on Oliveira's treatise. As in other shipbuilding texts and treatises of this time, most dimensions are simple fractions of the value of the keel length. Figure 8 presents the reconstructed lines plan and Table 1 the main particulars of the ship.

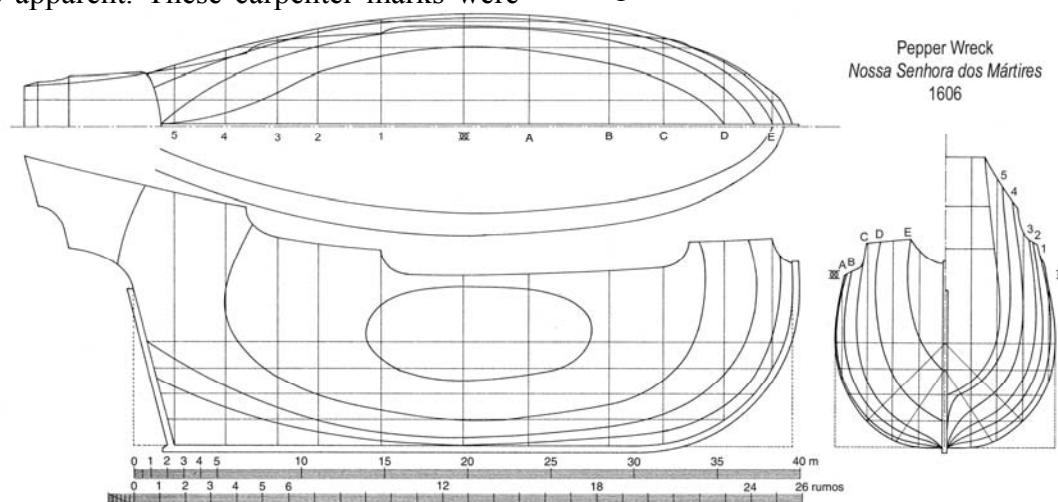


Figure 8 Lines plan of Nossa Senhora dos Mártires

Table 1 Main particulars of the ship

Length over all (m)	50.4
Length betw. perp. (m)	38.0
Breadth, extreme (m)	13.2
Depth to main deck (m)	8.21

Regarding the reconstruction of the internal space arrangement of an India *nau* is not a simple affair: firstly because contemporary data on this subject is scarce and fragmentary; secondly because these arrangements seem to have been changed by the ship's captains prior to every trip; and thirdly because the descriptions of cargoes, crews, passengers and victuals frequently pose more questions than they provide answers. Based on contemporary shipbuilding treatises Castro (2001), proposed a general arrangement with three decks, a poop deck at the stern and a forecastle (figure 9).

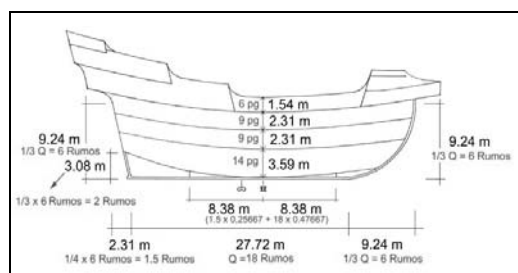


Figure 9 Reconstruction of the general arrangement of the *Pepper Wreck Nau*, Castro (2001)

The reconstruction of the ship's rigging arrangement was based upon the documents indicated above, that describe masts and spars for this type of ships, and give their dimensions as proportions of the keel length and maximum beam (Castro 2005b). According to these sources, which are fairly consistent, the lengths and diameters of the ship's masts and yards can be obtained from the ship's keel length and are simple fractions of the main mast. The sizes of the sails were easy to determine once the lengths of the masts and yards were known, with the exception of the spritsail, which in some documents seems to be much higher than the one designed for this study. Figure 10 show the reconstruction of the masts and yards and corresponding sail plan.

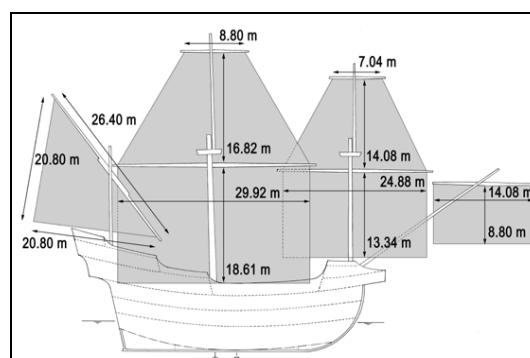


Figure 10 Reconstruction of the sail plan of the *Pepper Wreck Nau*, Castro (2005b)

Figures 11 and 12 show two three dimensional views of the ship, allowing an approximate understanding of how an India *Nau* might have looked like.

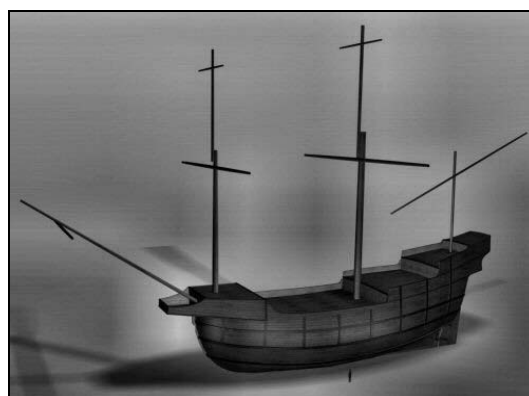


Figure 11 Three-dimensional view of the ship seen from the bow (courtesy of José Varela)



Figure 12 Three dimensional view of the ship seen from the stern (courtesy of José Varela)

3 RECONSTRUCTION OF THE LOADING CONDITIONS OF *NOSSA SENHORA DOS MÁRTIRES*

The analysis of the floatability and stability of any ship requires knowledge both on the ship's geometry and the ship's mass and centre of gravity. The estimation of these properties for an early XVII century ship, whose geometry and constructive details are not known accurately, represents a major task and one bound to yield a result with some uncertainty.

The loading condition at the departure from India for the return voyage was investigated in Fonseca et al. (2005). It is known that these ships tended to be severely overloaded and this appears to have caused a considerable number of losses around the turn of the 16th to the 17th centuries, especially in the area of the Cape of Good Hope. The former results are compared here with additional calculations for the arrival at Lisbon condition, since it is of interest to evaluate the ship's stability at the moment of the accident.

The weight of the ship has been subdivided in a number of components: hull, masts and yards, sails, rigging (shrouds, etc), anchors and ship's boats, artillery, ballast, cargo, crew, soldiers, passengers and supplies. Fonseca *et al.* (2005) describe the methodology to estimate all these weights and their positions onboard, as well as the related sources of information.

Figure 13 presents the weight distribution for the loading condition at the departure from India. For the arrival at Lisbon condition, it is assumed that weight of the water and wine, biscuit and other supplies is 10% of the corresponding weights when departing from India.

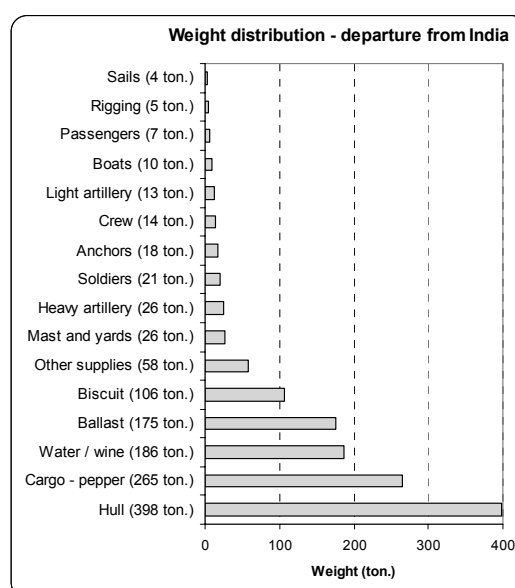


Figure 13 Weight distribution for the loading condition at the departure from India

When the ship is severely overloaded, as was common in those days, and the available literature clearly documents, the floatation characteristics of the ship change. On this subject, it is worth reading D'Intino (1998) or Malheiro do Vale (1988). In this case, it was assumed that the crew, soldiers and passengers were carrying in the return voyage twice the load they were legally allowed, apart from their personal belongings, which were included in the previous loading conditions. This load consisted of a number of boxes (called *liberdades* or *favores*) with spices or other items which the crew and soldiers were allowed by the Crown to carry from India and which they could then sell in Lisbon. Taking into account the estimate on the number of people on board and the different number of boxes which people of different categories were allowed to carry, it can be estimated that the ship could be carrying 1630 of these large boxes. If one assumes a standard weight of 59kg per box, the total extra weight is of over 96t. From contemporary texts, it is known that these boxes were mainly carried in the superstructures or in the main deck, therefore raising the centre of gravity to 5.36m at the departure from India and 5.25m at the arrival in Lisbon.

Table 2 presents the estimated total weight of the ship and position of the centre of gravity for these four conditions. Longitudinal position of the centre of gravity (Lcg) is with respect to the aft perpendicular and the vertical position (Vcg) is with respect to the baseline.

Table 2 Weight of the ship and position of the centre of gravity

	Weight (t)	Lcg (m)	Vcg (m)
Departure from India	1331.4	19.75	5.13
Arrival at Lisbon	1016.4	19.50	4.94
Depart from India (overloaded)	1427.6	19.77	5.36
Arrival at Lisbon (overloaded)	1112.6	19.55	5.25

4 ANALYSIS OF THE FLOATABILITY AND STABILITY OF AN INDIA NAU

4.1 Intact Floatability

Figure 14 shows the ship's hydrostatic properties. In these hydrostatic calculations the planking thickness (11cm) was taken into consideration when defining the hull sections and the forecastle and aft superstructure were not considered watertight. Table 3 shows the drafts, freeboard and metacentric height in the different conditions.

Regarding the issue of determining if these drafts are correct, it is worth mentioning that Oliveira (1580) points out that the first wale of the hull was layed at approximately the height of the beam shelves of the first deck amidships. He also indicates that below this level the hull had no wales because these would perturbate the flow of the water past the hull. So, it is possible to assume that this first wale was not too far below the waterline. Taking in consideration the drafts above and that the depth to the first deck was around 3.84m, the first wale would be between 0.37m and 1.41m below the waterline, depending on the loading condition. The second wale would be, for all the estimated loading conditions, above the waterline.

Table 3 Drafts of the ship in different loading conditions

	Draft Aft(m)	Draft Forw(m)	Trim (m)	Free-Board(m)	GM (m)
Departure from India	5.25	4.75	0.50	3.21	1.00
Arrival at Lisbon	4.68	3.74	0.94	4.0	1.13
Depart from India (overloaded)	5.48	5.03	0.45	2.96	0.77
Arrival at Lisbon (overloaded)	4.90	4.03	0.87	3.75	0.84

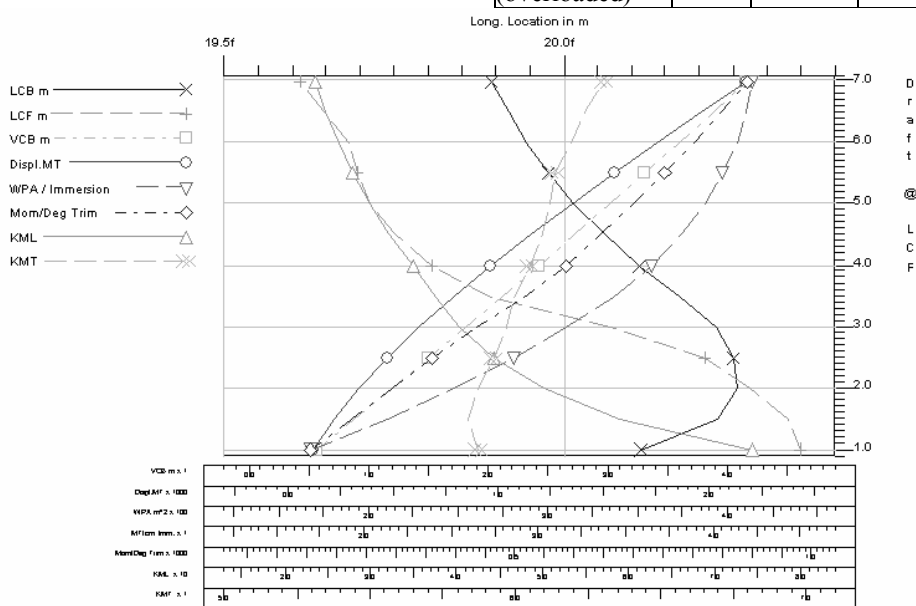


Figure 14 Hydrostatic properties of the *Pepper Wreck Nau*.

4.2 Intact Stability

The Portuguese shipbuilders of the late XVI century knew very little about ship stability, except that, for example, locating large weights high in the ship would degrade the ship's stability and that increasing the beam had good effects in the behavior and cargo carrying capacity of the ship, as mentioned by Oliveira (1580).

In what concerns the intact stability of this ship, Figure 15 shows the righting levers of the ship in the standard loading conditions. It is possible to see that the ranges of stability are 104° and 112° and the righting energies are 0.84m.rad and 1.19m.rad.

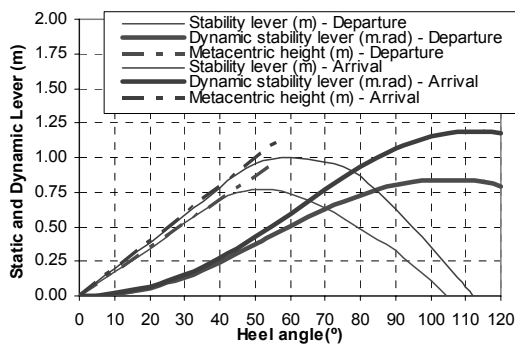


Figure 15 Righting lever curves for Pepper Wreck Nau (ship properly loaded).

Figure 16 shows the righting levers in the overloaded loading conditions. It may be seen that the ranges of stability have decreased to 93° and 100°, respectively. The maximum righting energies have also decreased to 0.55m.rad and 0.76m.rad.

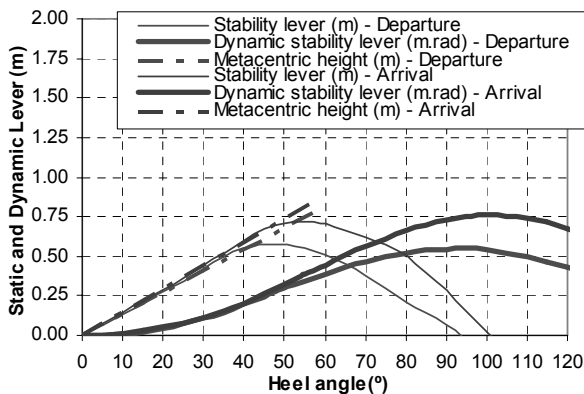


Figure 16 Righting lever curves for Pepper Wreck Nau (overloaded ship).

4.3 Evaluation of Intact Stability using a Large Sailing Vessel Criterion

It is interesting to investigate if a Portuguese *Nau* would comply with modern intact ship stability criteria. There are a number of such criteria available, some of which can be used in the stability evaluation of large sailing vessels. The International Maritime Organization generally advises the use of the classic cargo ship stability criterion and the weather criterion, both contained in IMO-Assembly (1990). However, it recognizes that both criteria are not suitable for ships fitted with extensive sail areas. For this purpose, the US Coast Guard (1983) established a criterion, contained in the Code of Federal Regulations which will be used in the present study.

According with this criterion, the ship shall have numerals X , Y and Z larger than given values. The X numeral expresses a measure of protection against water on deck. Numeral Y expresses the resistance against downflooding the interior of the ship and numeral Z indicates the capacity of the ship to resist a knockdown (leading to capsizing). The numerals are given by:

$$\frac{1000 \cdot \Delta \cdot HZ_a}{Ah} > X \frac{1000 \cdot \Delta \cdot HZ_b}{Ah} > Y \frac{1000 \cdot \Delta \cdot HZ_c}{Ah} > Z$$

where:

Δ = displacement (t),

A = projected lateral area of the hull and sails (m^2),

h = vertical distance between centre of pressure of the projected lateral area and center of the underwater lateral area (m).

HZ_a , HZ_b and HZ_c are calculated using:

$$HZ_a = \frac{GZ_c}{\cos^2 \theta_c}$$

$$HZ_b \text{ (or } HZ_c) = \frac{I}{((\theta_v / 2) + 14,3 \cdot \sin 2\theta_v)}$$

where:

θ_c = angle of deck immersion ($^\circ$),

GZ_c = righting arm (m) at the angle of deck immersion,

θ_v = angle of downflooding ($^\circ$) or 60° , whichever smaller, when calculating HZ_b ; 90° when calculating HZ_c ,

I = righting energy ($m.rad$) up to downflooding angle or 60° , whichever smaller, when calculating HZ_b ; righting energy up to 90° or the angle of extinction, whichever larger, but not more than 120° , when calculating HZ_c .

For a ship intended for navigation in exposed areas, the angle of extinction must be larger than 90° and the numerals must exceed the following values:

$$X = 16.4 \text{ t/m}^2 \quad Y = 18.6 \text{ t/m}^2 \quad Z = 20.8 \text{ t/m}^2$$

The calculations were made for the full sail plan and assuming that all sails act on the fore-and-aft plane and have the areas shown in Table 4. The ship has been assumed watertight up to the main deck level, that is, the gun holes could be secured watertight. Downflooding can occur only through the main deck hatches, located at the centreplane, near the mainmast, originating that the angle of downflooding is larger than 60° . The angles of deck edge immersion are approximately 28.3° and 39.9° . The angles of extinction are 104° and 112° , clearly above the minimum required angle of extinction of 90° .

The ship numerals can now be calculated and are given in Table 4. It may be concluded that the ship complies with the stability criterion in both loading conditions. It is worth noting that numeral X increases substantially from the departure condition to the arrival condition because of the large difference of the freeboards. This conclusion is valid in conjunction with the assumptions regarding watertightness and for the loading condition indicated above. In practice, watertightness was generally far from satisfactory and the overloading and overcrowding common practice. In fact, for instance, D'Intino (1998) indicates that the real distribution of cargo,

supplies and people onboard seldom followed the theoretical scheme of Falcão (1607).

If the criterion is applied to the loading conditions, which take in consideration the overloading, the results are as shown in Table 5. It may be concluded that the ship does not comply with the criterion in what concerns the X and Y numerals.

For numeral X the overloaded ship complies in the arrival condition but not in the departure condition. This is caused by the substantial increase in freeboard (0.8m) as the large amounts of provisions and water supplies are consumed. Regarding numeral Y, the ship does not comply in both conditions, especially in the arrival condition, because the ship is lighter and has an increased exposed area to the wind. Finally, for numeral Z, the ship still complies with the criterion, both the values have decreased substantially in relation to the previous conditions.

Table 4 Numerals and angles of extinction for standard loading conditions.

Parameter	Minimum value (criterion)	Departure	Arrival
X	16.4	19.4	31.1
Y	18.6	21.5	18.9
Z	20.8	31.9	31.7
Angle of extinction	90°	104°	112°

Table 5 Numerals and angles of extinction for overload loading conditions.

Parameter	Minimum value (criterion)	Departure	Arrival
X	16.4	14.7	23.1
Y	18.6	17.9	15.6
Z	20.8	23.5	24.0
Angle of	90°	93.4°	100.9°

4.4 Damage Stability

The India Route was sailed yearly by Portuguese ships between the beginning of the XVI century and the middle of the XVIII. The

circumstances of some of the shipwrecks that occurred during this period were registered by Gomes de Brito (1735) in his *História Trágico-Marítima* (Maritime and Tragic History).

Among the most frequent problems that beset the voyage of these ships when returning from India was the poor condition of ships regarding watertightness. This caused a steady inflow of water to the lower deck of ships, which had to be pumped out night and day while underway. There were pumps aboard for this purpose, linked by a pipe to the bottom of the lower hold. Aft of the main mast step was located a cofferdam (*arca da bomba*) where water collected and from where it was pumped.

As the ship continued voyage, often subject to heavy weather, especially while going round the Cape of Good Hope, the structure of the ship could gradually give way and the inflow of water increased. This had another negative consequence because it further reduced the freeboard and stability of the ship, a critical situation when sailing in the tempestuous seas of what is today South Africa.

An assessment of the effects of flooding of the lower hold will now be carried out. For this purpose account has to be taken that the lower hold is filled, first, by a layer of ballast with a height of 1.46m. On top of the ballast, the cargo of pepper is carried. Therefore, the lower hold is filled, with an estimated probable permeability of 0.1. For the analysis, the departure condition with overloading shall be considered. Table 6 shows the effects of various degrees of flooding in the lower hold. It may be seen that the metacentric height remains almost constant, the draft amidships increases by less than 0.15m and the trim by the stern remains largely constant.

Table 6 Effects of flooding the lower hold

Flooding	Water(t)	GM(m)	Draft(m)	Trim(m)
Intact	0.0	0.77	5.25	0.45
10%	7.3	0.76	5.26	0.43
30%	14.8	0.76	5.28	0.42
50%	36.9	0.75	5.33	0.41
70%	51.6	0.75	5.37	0.40
90%	66.4	0.82	5.41	0.40

5 CONCLUSIONS

This paper presents a study of the reconstruction of the hull form, weight distribution, loading conditions and floatation and stability characteristics of an early XVII century Portuguese *Nau*, the *Nossa Senhora dos Mártires*, which wrecked at the mouth of river Tagus in September 1606.

The ship's drafts in two standard loading conditions (departure and arrival) and two overloaded loading conditions (departure and arrival) were calculated and found to be in accordance with contemporary texts. The overloading was found to increase the draft by 0.25m.

The ship's stability in the two standard and two loading conditions was also calculated. The US Coast Guard intact stability criterion for large sailing vessels was then applied to the ship in these loading conditions. It was found that the ship complies with the criterion when not overloaded but fails to comply in case of overloading.

Finally, the effects of flooding of the lower hold when the ship was departing from India were also studied. It was found that, as the lower hold would probably be filled by ballast and cargo, the effects of flooding were a 0.15m increase of the draft, but almost no change in the metacentric height and trim by the stern.

6 REFERENCES

- Barata, J.G., 1989, "Estudos de Arqueologia Naval", Imprensa Nacional-Casa da Moeda, 2 Vols, Lisbon.
- Blot, J.Y., Ruiz, P., Ventura, M.F., Guedes Soares, C., 1994, "Aplicação de Métodos Automáticos ao Estudo de Formas de Cascos Antigos", Proceedings of 6^{as} Jornadas Técnicas de Engenharia Naval, pp. 5-1 a 5-35, Viana do Castelo.
- Branco, J.N.R., 1994, "A Caravela de Onze Rumos do Livro de Traças de Carpintaria", Proceedings of 6^{as} Jornadas Técnicas de

- Engenharia Naval, pp.1-1 a 1-35, Viana do Castelo.
- Castro, F., 2001, “The Pepper Wreck: a Portuguese Indiaman at the Mouth of the Tagus River”, PhD dissertation, Texas A&M University, USA.
- Castro, F., 2003, “The Pepper Wreck, and early 17th-century Portuguese Indiaman at the mouth of the Tagus River, Portugal”, *The International Journal of Nautical Archeology*, Vol. 32, 1, pp. 6-23.
- Castro, F., 2005a, “The Pepper Wreck”, College Station, Texas A&M University Press.
- Castro, F., 2005b, “Rigging the Pepper Wreck: Part I – Masts and Yards”, The International Journal of Nautical Archeology, Vol. 34, 1, pp. 112-124.
- D’Intino, R., 1998, “A Gente do Mar na Carreira da Índia”, Catálogo Oficial do Pavilhão de Portugal na Expo98, Lisboa.
- Domingues, F.C., 2004, “Os Navios do Mar Oceano – Teoria e Empiria na Arquitectura Naval Portuguesa dos Séculos XVI e XVII”, Centro de História da Universidade de Lisboa, Lisboa.
- Falcão, L.F., 1607, “Livro em que se Contem toda a Fazenda e Real Património dos Reinos de Portugal, Índia, e Ilhas Adjacentes e outras Particularidades, ordenado por Luiz de Figueiredo Falcao, Secretário de el Rei Filippe II”, Imprensa Nacional Casa da Moeda, Lisbon.
- Fernandez, M., 1616, “Livro de Traças de Carpintaria com todos os Modelos e Medidas para se Fazerem toda a Navegação, assim de Alto Bordo como de Remo Traçado”, Academia de Marinha, Lisbon.
- Fonseca, N., Santos, T.A., Castro, F., 2005, “Study of the Intact Stability of a Portuguese Nau from the Early XVII Century”, Proceedings of the IMAM2005 Conference, Lisbon, Portugal.
- Gomes, B., 1735, “História Trágico-Marítima em que se Escrevem Cronologicamente os Naufrágios que tiveram as Naus de Portugal, depois que se pôs em Exercício a Navegação da Índia”, Publicações Europa-América, Vols. 1 and 2, Lisboa.
- IMO, 1993, “Code on Intact Stability for All Types of Ships Covered by IMO Instruments”, Assembly Resolution A.749(18), International Maritime Organization, London, United Kingdom.
- Lavanha, J.B., 1608, “Livro Primeiro da Arquitectura Naval”, Academia de Marinha, Lisboa.
- Loewen, B., 1994, “Codo, Carvel, Mould and Ribband: the Archaeology of Ships, 1450-1620”, Mémoires-vives, 6-7: pp. 6-21.
- Malheiro do Vale, A.J., 1988, “Nau de Pedra”, Edição da Revista da Armada.
- Oliveira, F., 1580, “O Livro da Fábrica das Naus”, Academia de Marinha e Museu Marítimo de Macau, Macau.
- US Coast Guard, 1983, “Subdivision and Stability Regulations: Final Rules”, Code of Federal Regulations, US Government, Vol. 46, Ch. 1.

Parametric Roll Resonance of a Large Passenger Ship in Dead Ship Condition in All Heading Angles

Abdul Munif, *Institute of Technology (ITS) Surabaya-Indonesia*

Yoshiho Ikeda, *Graduate School of Engineering, Osaka Prefecture University*

Tomo Fujiwara, *Graduate School of Engineering, Osaka Prefecture University*

Toru Katayama, *Graduate School of Engineering, Osaka Prefecture University*

ABSTRACT

Although it has been widely believed that a ship in dead ship condition has the largest roll motion at resonance condition, the authors found that, because of parametric roll resonance, a kind of ships has significant heavy rolling in beam waves with slightly smaller period of the half value of its natural roll period if the roll damping is small. In the present paper, model experiments to measure ship motions of a large passenger ship in waves with various heading angle are carried out to confirm the region of heading angles where large parametric rolling appears. The results demonstrate that parametric rolling appears at wide region of heading angles and disappears in certain heading angles.

Keywords: *Parametric rolling, Head sea, Beam sea, Large passenger ship*

1. INTRODUCTION

As well known, occurrence of small parametric rolling of ships in beam seas has been pointed out by many researchers. In the previous paper proposed by Ikeda et. al. (2005), however, the authors found experimentally that heavy roll motion with much larger angle than that in resonance appears for a large passenger ship with flat stern and large bow flare in heavy beam seas due to parametric rolling. The measured results demonstrated that the large parametric rolling appears only when the ship has no bilge keel or smaller one. As wave height increases, the parametric rolling suddenly appears at higher wave height than a certain value. The authors also did a simulation of roll motion, and confirmed that similar parametric rolling appears for the ship in beam waves (Munif et.

al. 2005).

In the present study, some additional experimental works to clarify effects of wave height, size of bilge keels and heading angles of waves on occurrence of large parametric rolling are carried out to reveal the characteristics of the parametric rolling.

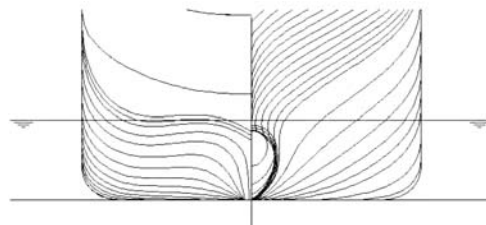


Figure 1 Body plan of the ship.

2. EXPERIMENTAL SETUP

The ship used in the experiments is the

110,000GT passenger ship designed by Fincantieri for an international cooperated research on damage stability of large passenger ships in IMO. The body plan and the principal particulars are shown in Figure 1 and Table 1, respectively. The bilge keels designed for the ship are divided into two parts, short forward one and long aft one. The roll damping can be changed by selecting these bilge keels.

Table 1 Principle particulars.

	Full Scale	Model
Scale	1/1	1/125.32
L_{OA}	290 m	2.200 m
L_{PP}	242.24 m	1.933 m
Breadth	36 m	0.287 m
Draft	8.4 m	0.067 m
Displacement	53,010 ton	26.98 kg
GM	1.579 m	0.0126 m
T_{roll}	23 sec	2.05 sec
Bilge keel : width	1.1 m	0.0088 m
Bilge keel : location	s.s.3.0–5.0, s.s.5.25–6.0	

In the previous study, a scale-model of the large passenger ship was located in transverse direction in the towing tank of Osaka Prefecture University, and the ship motions, roll, heave, pitch, sway and drift motions, were measured in regular beam waves. In the experiment, yaw and surge motions were fixed.

In the present study, the same model is located in regular waves for freely yawing conditions or various fixed heading angles for incident waves. Only transverse motion of the model is fixed by a guide. This means that drift motion in incident-wave direction is free but the motion perpendicular to it is fixed. The experimental conditions are shown in Table 2.

Table 2 Experimental conditions.

	Full scale	Model
Wave period	6.7–24.6 sec	0.6–2.2 sec
Wave length	70–944 m	0.56–7.55 m
Wave height	1.25–10 m	0.01–0.08 m
Bilge keel	without, full (front + aft), front, aft	

3. EXPERIMENTAL RESULTS

As mentioned before, in the previous paper, the authors experimentally showed that the effect of wave height on parametric rolling in regular beam waves. To confirm the results in wider wave height region, parametric rolling of the ship without bilge keels is measured for various wave heights. The maximum amplitude of the parametric rolling at each wave height is shown in Figure 2. The results demonstrate that the parametric rolling appears just over 30mm of wave height, rapidly increases with wave height, and reaches the maximum amplitude that is about 27 degree. It should be noted that the roll amplitude does not proportionately increase with increasing the wave height but seems to saturate to the maximum one.

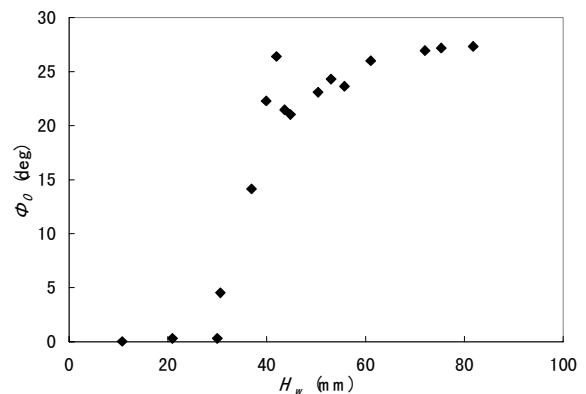


Figure 2 Effect of wave height on maximum amplitude of parametric rolling of the ship in regular beam seas

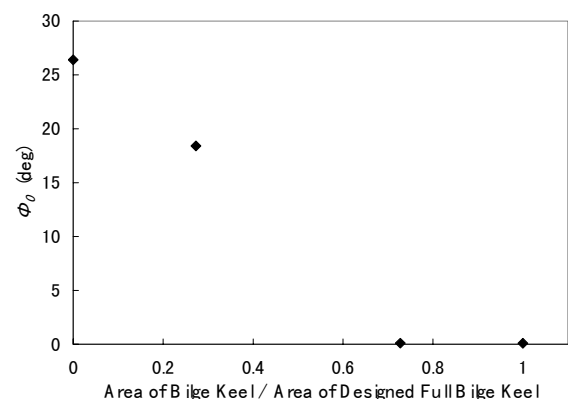


Figure 3 Effect of area of bilge keels on maximum amplitude of parametric rolling in regular beam seas.

In Figure 3, effect of area of bilge keels on maximum amplitude of parametric rolling is shown. This results demonstrate that the parametric rolling significantly depend on area of bilge keels. It is safely said that large bilge keels can completely erase parametric rolling in beam seas.

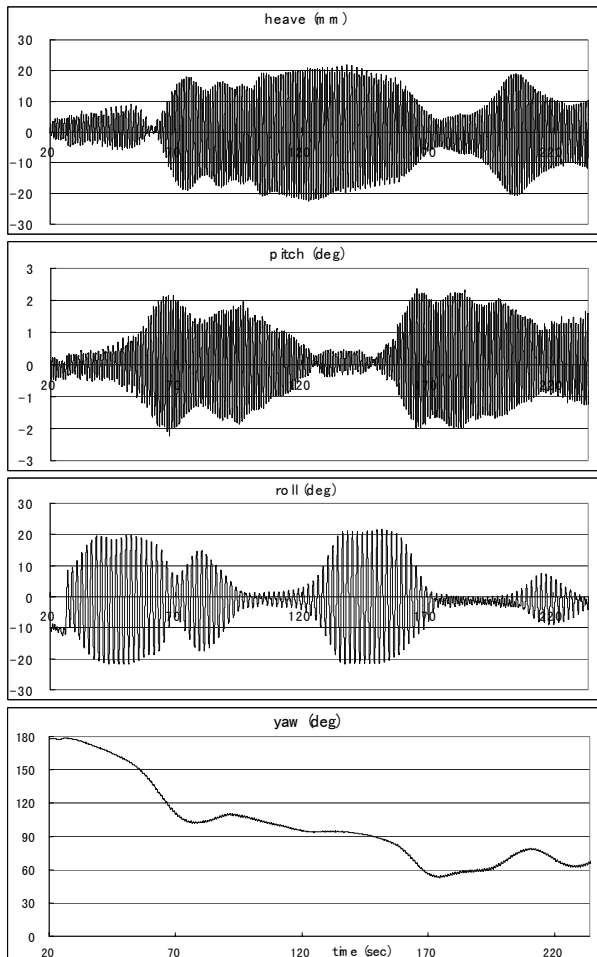


Figure 4 Time histories of motions of the ship without bilge keel released from head sea condition in regular waves at $T_w=0.95\text{sec}$ and $H_w=0.04\text{m}$.

To investigate the effect of heading angle on the parametric rolling of the dead ship, the model are released in head wave condition ($\chi=180^\circ$) or following wave condition ($\chi=0^\circ$) in regular waves with 0.04m of wave height and 0.95 second of wave period which is the period when the large parametric rolling in beam seas appears. The time histories of the heave, pitch, roll and yaw motions are measured and showed in Figures 4 and 5. The model has no bilge keel in these measurements. From the time histories

of the yaw angles, we can see that, in both cases, the heading angle of the ship slowly changes to beam sea condition. The time histories of roll motion in these figures show that the period of the roll motion is twice of the heave and pitch motions. The results demonstrate that the parametric rolling occurs in wide heading angles as well as in beam seas.

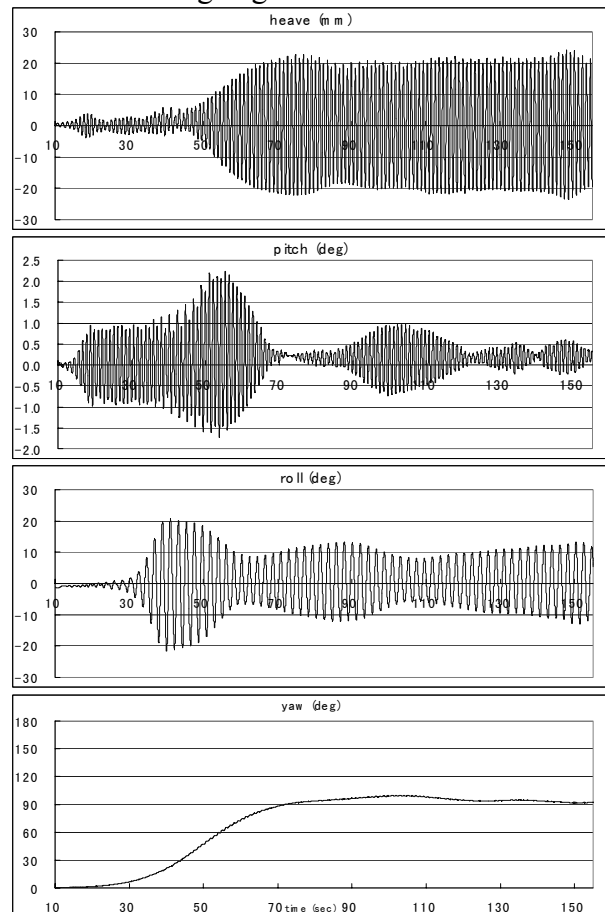


Figure 5 Time histories of motions of the ship without bilge keel released from following wave condition in regular waves at $T_w=0.95\text{sec}$ and $H_w=0.04\text{m}$.

Since it may take time to lead to the parametric rolling and reach its steady condition, a measurement of roll motion at some fixed heading angle; 0, 90, 180 degree are carried out. And using the results of above-mentioned measurement and of previous ones shown in Figures 4 and 5, the roll amplitude of the parametric rolling for each heading angle is plotted in a polar diagram as shown in Figure 6. The results show that amplitudes of the parametric rolling is significant in following

and head seas as well as beam seas when no bilge keel is attached.

Figures 7 and 8 show variation of GZ -curves of the ship on the basis of Froude-Krylov assumption in heading and beam seas, respectively. We can see the GZ -curves significantly vary between wave crest and wave trough in head and beam waves. These large variations of the GZ -curve create the large amplitude of parametric rolling.

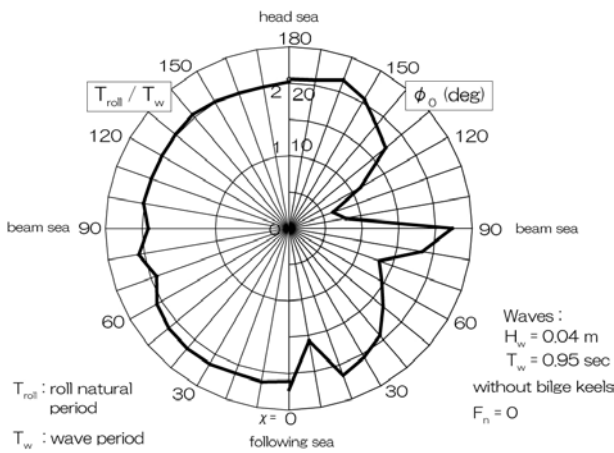


Figure 6 Effect of wave direction on amplitude of parametric rolling of the ship without bilge keel in regular waves.

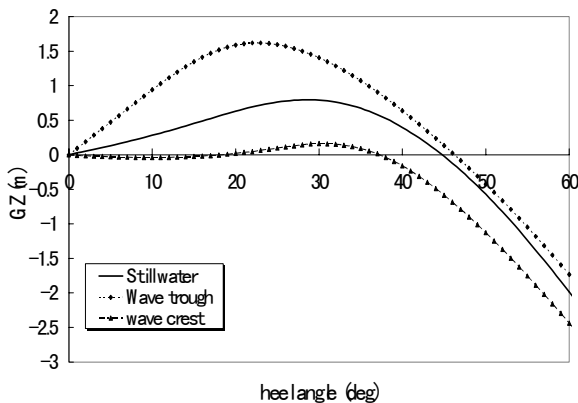


Figure 7 Variation of GZ curves in head waves of $\lambda/L=1.5$ and $H_w/\lambda=0.033$.

To investigate the effect of roll damping on occurrence of parametric rolling in various heading angles, motions of the model with bilge keels are measured in regular waves ($H_w = 0.08m$, $T_w = 0.95$ sec). In Figure 9 the time histories of motions of the ship with smaller

front bilge keels released from following wave condition in the regular waves are shown. Smaller parametric rolling occurs in all heading angles of waves. When larger aft bilge keels or full bilge keels are attached, no parametric rolling appears as shown in Figures 10 and 11.

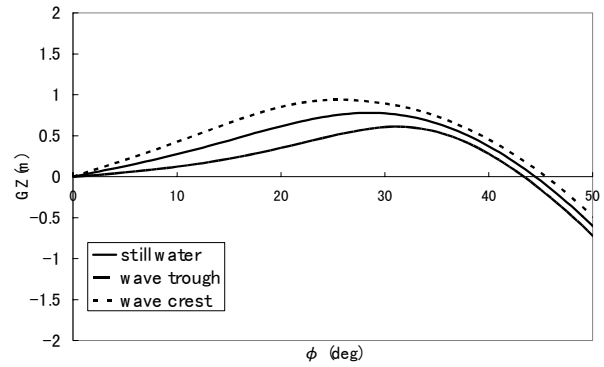


Figure 8 Variation of GZ curves in beam waves of $\lambda/L= 0.47$ and $H_w/\lambda=0.04$.

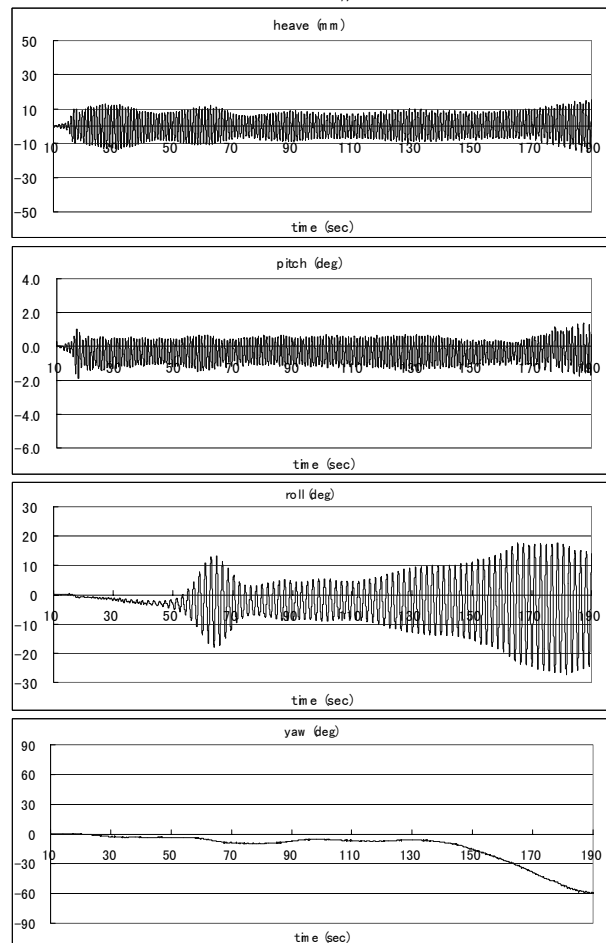


Figure 9 Time histories of motions of the ship with short (front) bilge keels released from following wave condition at $T_w=0.95$ sec and $H_w= 0.08m$.

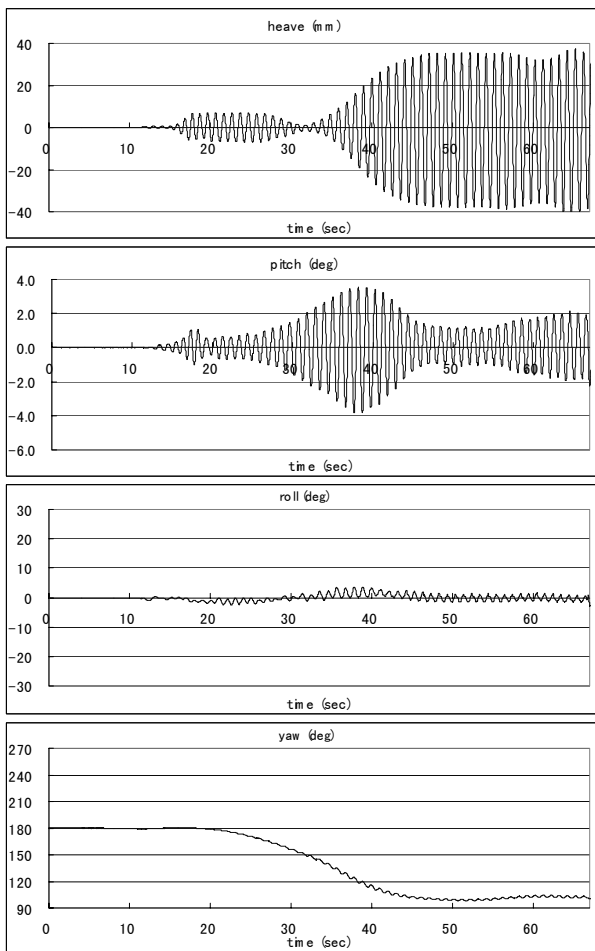


Figure 10 Time histories of motions of the ship with long (aft) bilge keels released from head wave condition at $T_w = 0.95\text{sec}$ and $H_w = 0.08\text{m}$.

To search the possibility of occurrence of parametric rolling of the ship with bilge keels in head waves, measurements of ship motions of the model with full bilge keels in fixed yaw condition are carried out in regular head waves with 0.08m of wave height and various wave periods. The results are shown in Figure 12. The results suggest that parametric rolling with about 10 degree can occur for the ship with full bilge keels in head waves at 1.2 second of wave period, which is longer by 26% than that when parametric rolling in beam seas occurs. In Figure 13, the time histories of motions of the case that the maximum parametric rolling occurs are shown. It should be noted it takes long time to develop parametric rolling. In Figure 14, the effect of heading angle on parametric rolling of the ship with full bilge keels in head waves is shown in a polar diagram. We can see that in heading angles of

± 20 degrees in head and following waves parametric rolling occurs even if size of bilge keels is enough to erase it in beam seas.

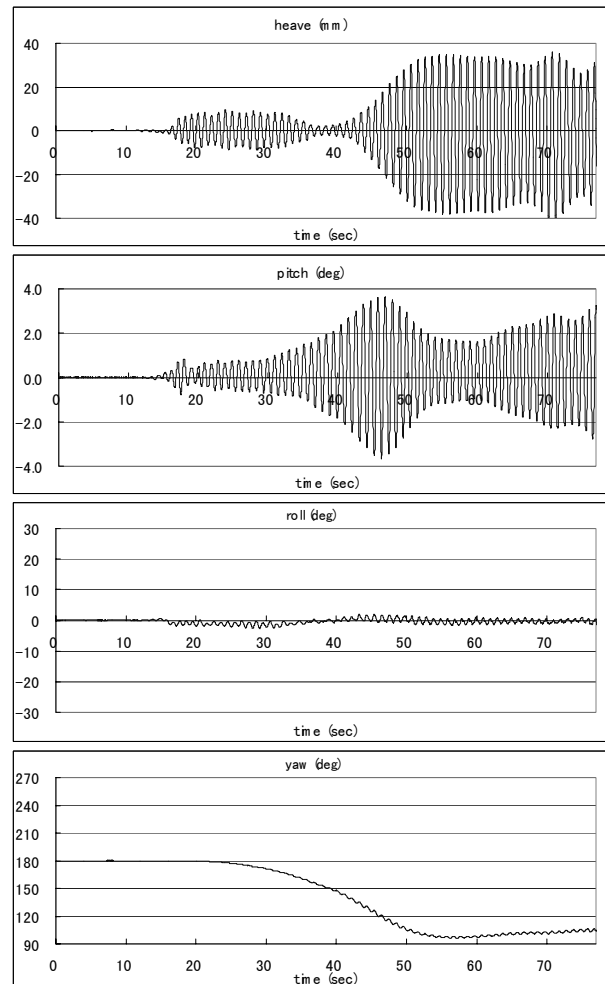


Figure 11 Time histories of motions of the ship with full (front and aft) bilge keels released from head wave condition at $T_w = 0.95\text{sec}$ and $H_w = 0.08\text{m}$.

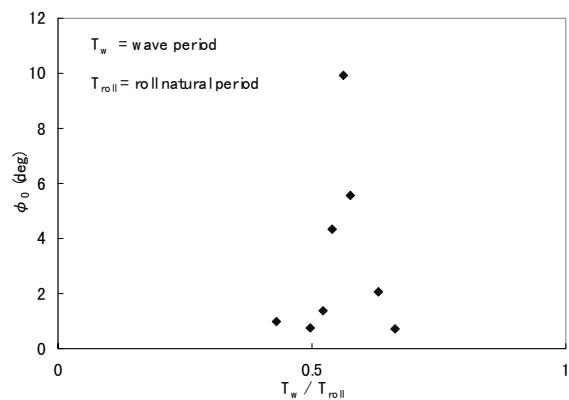


Figure 12 Parametric rolling of the ship with full bilge keels in regular head waves with $T_w = 1.2\text{sec}$ and $H_w = 0.08\text{m}$.

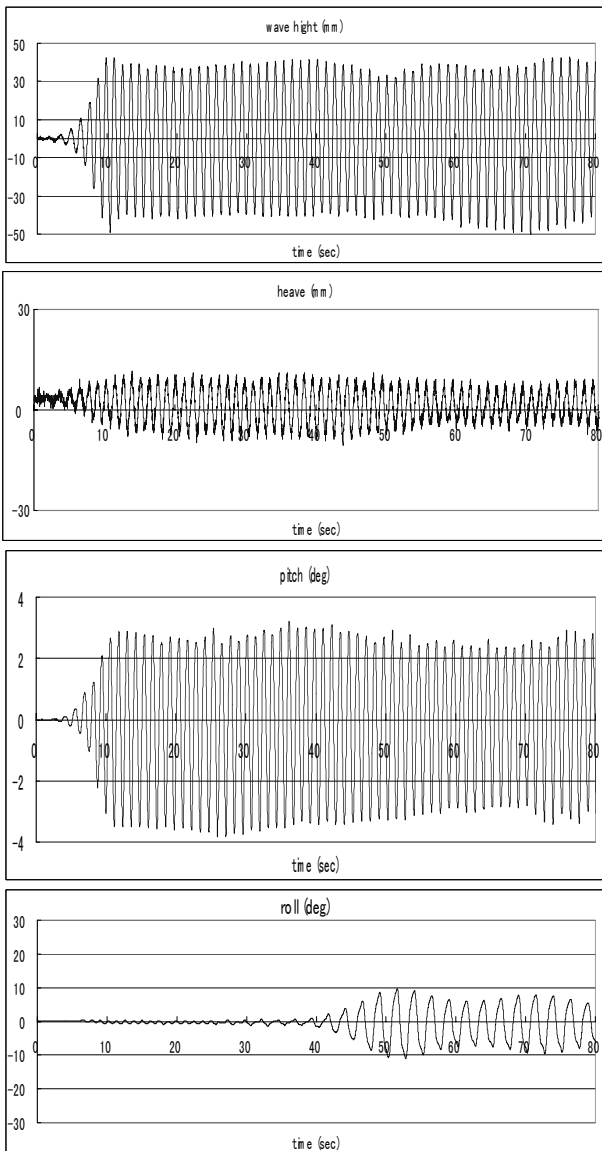


Figure 13 Time histories of motions of the ship with full bilge keels released from head wave condition in regular waves with $T_w=1.2$ sec and $H_w=0.08$ m.

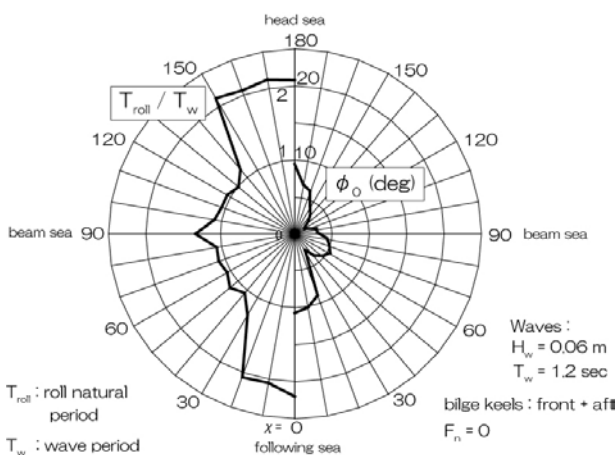


Figure 14 Effect of wave direction on amplitudes of rolling and its period of the ship with full bilge keels in regular waves.

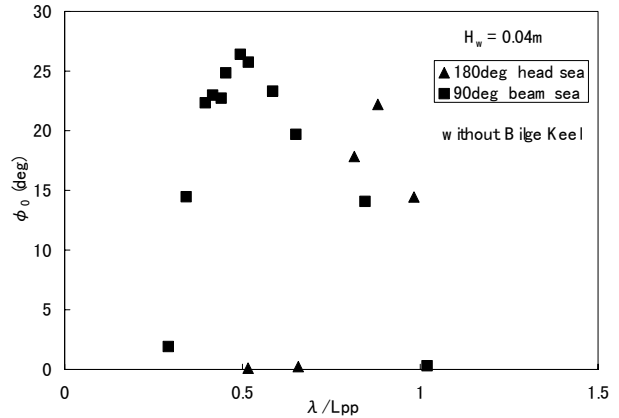


Figure 15 Difference of wave periods for which parametric rolling appears in beam and head waves.

In Figure 15, difference of wave periods for which parametric rolling appears in beam and head waves. The ship has no bilge keels and wave height is 0.04m. The results suggest that parametric rolling appears in different wave period in beam and head waves. This may be because of differences of drift speed and amplitude of stability variation in beam and head waves.

4. CONCLUSIONS

Following the previous paper of the authors in which large parametric rolling in beam seas is confirmed for a large passenger ship with a flat and shallow stern-bottom and large flare in bow in no bilge keel condition, parametric rolling in all heading angles of the same ship is experimentally investigated. Following conclusions are obtained.

When the ship has no bilge keels, parametric rolling occurs in wide heading angles including head and following seas as well as beam seas. Large variation of GZ value in waves due to a flat and shallow stern-bottom and large flare in bow induces the parametric rolling.

The effect of bilge keels on occurrence of large parametric rolling is significant. Large bilge keels can completely erase parametric rolling of the large passenger ship in dead ship condition in any heading angles of waves except head and following waves.

Parametric rolling of the ship in head seas can occur even if large bilge keels enough to erase it in beam seas are attached.

Wave periods when parametric rolling occurs in beam and head waves are different.

5. ACKNOWLEDGEMENT

This work was a part of the first author's post-doctoral research supported by Grand-in-Aid funded by the Japanese Society for the Promotion of Science (JSPS). Just after the present study, Dr. A. Munif was died on the 9th, February 2006 because of sickness. The other authors express their deepest regret for him and his family.

6. REFERENCES

Ikeda Y, Munif A, Katayama T, Fujiwara T, 2005, "Large Parametric Rolling of a Large Passenger Ship in Beam Seas and Role of Bilge Keel in Its Restraint", *Proc. of 8th International Ship Stability Workshop*.

Munif A, Katayama T, Ikeda Y., 2005, "Numerical Prediction of Parametric Rolling of a Large Passenger Ship in Beam Sea", *Conference Proc. of the Japan Society of Naval Architects and Ocean Engineers*, No.1.

Prediction of Parametric Roll Resonance in Longitudinal Regular Waves Using a Non-linear Method

T.M., Ahmed, *University of Southampton*

D.A Hudson, *University of Southampton*

P. Temarel, *University of Southampton*

E.J. Ballard, *Lloyds Register*

ABSTRACT

In this paper two non-linear, time-domain methods are proposed for the prediction of parametric roll resonance in longitudinal regular waves. Using a two-dimensional approach, periodic changes in the underwater hull geometry due to heave, pitch and wave passage are calculated as a first order function of the local breadth and flare at the still waterline in Method (I), and as a higher order function of the local instantaneous breadth in Method (II). The 1-DoF uncoupled equation of motion in roll -with parametric excitation terms- is then solved in the time-domain in the absence of an external roll excitation. Non-linearities in the roll damping and restoring terms are accounted for. The two methods have been applied to a post-Panamax C11 class containership, travelling in longitudinal regular waves. Obtained results demonstrate that the numerical methods succeeded in producing results similar to those available in the literature. Limitations of the methods used are discussed.

Keywords: *Parametric Roll Resonance, Non-linear, Time-domain.*

1. INTRODUCTION

The phenomenon of parametrically excited roll motion has been known to naval architects for almost half a century now (e.g. Paulling, 1961 and Blocki, 1980). In this phenomenon, transversely symmetrical ships may experience extreme roll motions in longitudinal waves i.e. head or following waves. This is explained by reasoning that in longitudinal waves, ships may experience variations in their transverse stability due to time-varying changes in the underwater hull geometry. In the past the concern with parametric roll was mostly for smaller ships in following seas (e.g. De Kat & Paulling, 1989 and Umeda & Hamamoto,

1995). Now the concern is for the vulnerability of large ships in head seas (Dallinga et al, 1998). The problem returned to prominence recently as a result of significant cargo loss and damage sustained by a C11 post-Panamax container carrier on a voyage from Taiwan to Seattle (France et al, 2003). A detailed investigation followed showing that the ship had experienced large roll motions accompanied by significant pitch and yaw motions, resulting from a periodic change of the transverse stability in head seas. The large change of stability was found to be a direct result of the hull form. A substantial bow flare and stern overhang -typical of large container carriers- caused a dramatic difference in the waterline form and, hence, in the transverse

stability of the ship (France et al, 2003).

For parametric roll to occur, however, certain conditions need to be satisfied, in particular (France et al, 2003): 1) the encounter frequency is equal or close to twice the natural frequency of roll. 2) The wavelength is of the same order as the ship length. 3) The wave height exceeds a critical level, or threshold value. 4) The roll damping is below a critical level, or threshold value.

Roll damping plays an important role in the development of parametric roll. If the “loss” of energy per cycle caused by damping is more than the energy “gain” caused by the change in stability, the roll angles will not increase and parametric roll will not develop. On the other hand, if the energy “gain” per cycle is more than the energy “loss” due to damping, the amplitude of parametric roll will start to grow (Shin et al, 2004).

Longitudinal waves i.e. head or following seas, cause the largest change in stability and therefore create maximum parametric excitation. While the physical basis for parametric roll is the same in head and following seas, parametric roll in head seas is more likely to be coupled with, or at least influenced by, heave and pitch motions of the ship, since these motions are typically more pronounced in head-seas (Shin et al, 2004).

Parametric roll should be limited to finite, though sometimes large, amplitudes of roll angle. This is where the role of non-linear terms comes into play since it is known that in the roll equation of motion non-linear terms tend to stabilize parametric roll. The two major non-linear terms in the roll equation of motion are the hydrostatic restoring and damping terms. Although the actions of both terms have similar consequences in limiting parametric roll, the physics of their actions are different. Non-linearity of the GZ curve at large angles of heel leads to a significant change in the effective restoring terms and, therefore, a significant change in the roll resonant period. Change of the roll resonant period may take the

system out of the instability zone. The input of additional energy ceases once the roll achieves a certain angle. As a result, an energy balance in motion is established and roll stabilizes at a certain amplitude, provided that capsizing does not occur. On the other hand, non-linear damping has the tendency to increase with roll velocity, thus, sooner or later it will grow above the damping threshold. The system then dissipates more energy than the input energy from parametric excitation, which also leads to stabilization of the roll amplitude (Shin et al, 2004). Non-linearity of the GZ curve is more important in the stabilization of parametric roll than non-linear damping (Bulian et al, 2003).

In this paper, Methods (I) and (II) have been applied to a post-Panamax C11 class containership, traveling in regular waves. Within the scope of the study special attention is focused on the influence of different operational aspects on parametric roll resonance, e.g. different wave heights, wave headings (head or following seas), encounter frequencies, forward speeds, loading conditions (different KG values), etc. Results obtained demonstrate that Method (II) has succeeded in producing results similar to those available in the open literature, whilst Method (I) has a more limited range of application.

2. NUMERICAL SIMULATION

In the literature many of the studies predicting parametric roll resonance are based on the assumption that the ship is a 3-DoF system in heave, pitch and roll. The heave and pitch motions are solved simultaneously and independently of the roll motion, an assumption that is justified experimentally (Oh et al, 2000). However, due to the heave-pitch-roll coupling, heave and pitch motions, together with the wave passage, are an effective amplitude and frequency of excitation in parametric roll. The uncoupled equation of motion in roll is then solved in the absence of an external roll excitation and with non-linearities accounted for in the roll damping and restoring moment (Neves et al, 1999). In

other words, the heave and pitch motions feed in the energy required for parametric roll to occur but no reverse influence is exerted by roll on heave and pitch since there is no direct excitation in roll.

In the study presented here and based on the assumptions mentioned previously, two non-linear time-domain methods are adopted and developed. Initially, the heave and pitch equations of motion are solved simultaneously and independently of the roll equation. This solution is obtained using a three-dimensional frequency-domain source distribution method (pulsating source method) which also provides the hydrodynamic data of the ship in roll (added inertia and linear damping). In Method (I), periodic changes in the underwater hull geometry due to heave, pitch and the wave passage are calculated as a first order function of the local breadth and flare at the still waterline, (Neves et al, 1999, and Neves et al, 2003). On the other hand, in Method (II), the periodic changes are calculated as a higher order function of the local instantaneous breadth, i.e. at every time step. In both cases these calculations are carried out using a two-dimensional approach for sections along the length of the ship. The formulation of Method (II) leads to a mathematical model with second order non-linearities defined in terms of the heave-pitch-wave passage couplings. Non-linearities in the roll restoring arm (Surendran et al, 2003) and roll damping (Himeno, 1981) are also accounted for. Finally, the 1-DoF uncoupled equation of motion in roll is solved in the time-domain, subjected to an initial roll angle, using a fourth-order-Runge-Kutta method in the absence of an external roll excitation.

2.1 Mathematical Formulation

For both aforementioned methods, the restoring coefficient in roll may be expressed as:

$$C_{44}(x,t) = \rho g \int_L A(x,t) GM_T(x,t) dx \quad (1)$$

where, x denotes the coordinate along the ship and $A(x,t)$ represents the immersed sectional area, such that:

$$A(x,t) GM_T(x,t) = I_T(x,t) + Z_b(x,t) A(x,t) - Z_g A(x,t) \quad (2)$$

where, $I_T(x,t)$ and $Z_b(x,t)$ represent the transverse second moment and the vertical coordinate of the immersed sectional areas, respectively, and $Z_g(x,t)$ represents the vertical coordinate of the ship's centre of gravity.

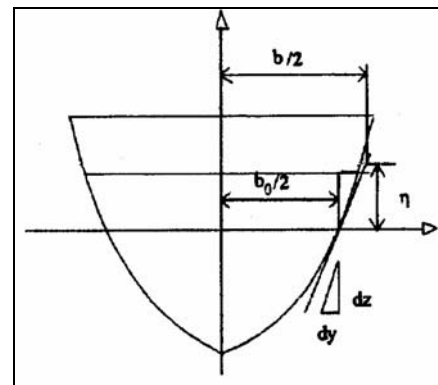


Figure (1) Variation of Sectional Beam with Relative Vertical Displacement

Therefore, for Method (I):

$$C_{44}(x,t) = \Delta g GZ + \rho g \int_L \left[\frac{1}{2} b_0^2 \frac{dy}{dz} \right]_{x,z=0} - Z_g b_0(x) \eta dx \quad (3)$$

and for Method (II):

$$C_{44}(x,t) = \Delta g GZ + \rho g \left\{ \int_L \alpha(x,t) \left[\frac{1}{2} b_0^2(x) + b_0(x) \alpha(x,t) + \frac{2}{3} \alpha^2(x,t) \right] dx - Z_g \int_L [b_0(x) + \alpha(x,t)] \eta(x,t) dx + \int_L \left[\frac{1}{2} b_0(x) + \frac{2}{3} \alpha(x,t) \right] \eta(x,t) |\eta(x,t)| dx \right\} \quad (4)$$

where, as shown in fig.(1) (Neves et al, 1999),

$$\alpha(x,t) = b(x,t) - b_0(x). \quad (5)$$

The relative vertical displacement η is expressed as:

$$\eta(x,t) = z_0 \cos(\omega_e t + \alpha_z) - x\theta_0 \cos(\omega_e t + \alpha_\theta) - \zeta \cos[kx \cos(\chi) - \omega_e t] \quad (6)$$

where, z_0 , θ_0 , α_z , α_θ are the heave and pitch magnitudes and phase angles, respectively, ζ is the wave amplitude ω_e is the encounter frequency, k is the wave number and χ is the wave heading.

The normalized 1-DoF uncoupled equation of motion in roll for a ship travelling in longitudinal regular waves takes the form:

$$\ddot{\phi} + (b_{44L} + b_{44N})\dot{\phi} + [c_{44L} + c_{(44N)3}]\phi^2 + c_{(44N)5}\phi^4 + e_0(t)]\phi = 0 \quad (7)$$

In equation (7), b_{44} and b_{44N} represent the linear and the equivalent linearized roll damping components, respectively. Based on the expression for (ΔgGZ) described in section (2.2), c_{44L} , $c_{(44N)3}$ and $c_{(44N)5}$ represent the linear, cubic polynomial and quintic polynomial roll restoring coefficients, respectively. $e_0(t)$ is the total parametric excitation term (1st and 2nd order) due to heave, pitch and wave passage and can be identified from equations (3) and (4). All coefficients in equation (7) are normalized with respect to the total roll moment of inertia ($I_{44} + A_{44}$), where I_{44} and A_{44} are the moment and added moment of inertia in roll, respectively.

2.2 Non-linear Roll Restoring Coefficients

As was mentioned before, the non-linear roll restoring coefficients representing the GZ curve have an important role in stabilizing the parametric roll motion of a ship. In the methods presented here, a quintic polynomial expression is used to account for the non-linearity in the GZ curve (Surendran et al, 2003). The righting arm curve is expressed as:

$$\Delta gGZ = C_{44L}\phi + C_{(44N)3}\phi^3 + C_{(44N)5}\phi^5 \quad (8)$$

Coefficients of the polynomial are determined by the static and dynamic characteristics of the GZ curve such as the metacentric height, GM_T ; the angle of vanishing stability, ϕ_v ; and the area under the GZ curve A_{ϕ_v} up to the angle of vanishing stability as follows ($C_{44L} = \Delta gGM_T$):

$$C_{(44N)3} = \Delta g \left[\frac{4}{\phi_v^4} (3A_{\phi_v} - GM_T \phi_v^2) \right] \quad (9)$$

$$C_{(44N)5} = -\Delta g \left[\frac{3}{\phi_v^6} (4A_{\phi_v} - GM_T \phi_v^2) \right]$$

2.3 Roll Damping

In the methods proposed in this paper, a semi-empirical model due to Ikeda and described by Himeno (1981) is used for the prediction of the total roll damping coefficient. This model assumes that the total roll damping coefficient can be calculated as the sum of five major components, namely: wave damping, frictional damping, eddy damping, lift damping and bilge keel damping.

Out of these five components the wave and lift damping coefficients are assumed linear, whereas the frictional and eddy damping coefficients, together with part of the bilge keel damping coefficient are taken as equivalent linearized damping coefficients, i.e. they are functions of the steady roll angle (through an iteration process for the roll angle and the value of a roll damping) but are proportional to the roll velocity in the roll equation of motion.

3. RESULTS

Methods (I) and (II) have been applied to a post-Panamax C11 class containership ($L=262$ m), travelling in longitudinal regular waves at two different loading conditions represented by: $KG=17.55$ m, figs.(2-11) and $KG=17.95$ m, figs.(12,13). The first loading condition results in a metacentric height $GM_T=1.615$ m and a

roll natural frequency $\omega_n=0.2673$ rad/s. The second loading condition results in a $GM_T=1.215$ m and $\omega_n=0.2314$ rad/s.

Most of the results have been obtained in two sea-states, namely, sea-state 6, SS(6), and sea-state 7, SS(7), where both are realistic sea-states occurring in the North Atlantic (Faltinsen, 1990). For SS(6) the mean significant wave height is $H_w=5$ m and the most probable modal wave period is $T_w=12.4$ s, for SS(7), $H_w=7.5$ m and $T_w=15$ s.

Special attention has been paid to the frequency tuning condition of $\omega_e = 2\omega_n$, since this is the first and most dangerous instability zone that arises from solving the damped Mathieu equation for parametric roll.

4. DISCUSSION OF RESULTS

Fig.(2) illustrates the case of the C11 containership advancing in regular head-waves of wave height $H_w=8.4$ m and wave period $T_w=14$ s, with a forward speed $V=10$ knots and an encounter frequency $\omega_e=0.5544$ rad/s. The simulation obtained using Method (I) fails to predict a steady parametric roll angle for this case since the resultant roll angles become very large after approximately $t=50$ s. This can be attributed to the fact that Method (I) is based on the assumption that the parametric excitation terms are linearized about the still waterline which is justified only for the case of small vertical motions due to small wave heights. On the other hand, Method (II) predicts parametric roll which steadies at a roll angle of 20° . This agrees with the results predicted for the same case by France et al. (2003) and Shin et al. (2004). On the other hand, fig.(3) represents parametric roll predicted using Methods (I) and (II) for a wave height of 1.5 m and a wave length of 262 m which is equal to the ship length. The ship is travelling in regular head-waves at a forward speed $V=4.025$ knots. The results predicted by both methods are quite close since at such a small wave height, the higher order terms in Method (II) are insignificant. The difference of 5° between the

steady roll angles predicted by the two methods is due to evaluating the instantaneous local breadth in Method (II) rather than the local breadth and flare at the still waterline in Method (I). In most of the remaining examples, Method (I) fails to simulate parametric roll.

The comparison between fig.(4) and fig.(5) illustrates the importance of the condition, "The wavelength is of the same order as the ship length" in the occurrence of parametric roll. Although SS(6) has a smaller wave height than SS(7), parametric roll is predicted, by Method (II), in fig.(4) but not in fig.(5). This is due to the fact that the wavelength of SS(6), $\lambda=240$ m (corresponding to $T_w=12.4$ s) is closer to the ship length, $L=262$ m, than that of SS(7), $\lambda=351$ m. It should be noted that in fig.(5), the value of the steady roll angle is almost equal to the value of the initial roll angle, hence this is interpreted as a case of non-occurrence of parametric roll.

The comparison between figs.(4), (6) and (7), all for SS(6), demonstrates that the frequency tuning condition of $\omega_e=2\omega_n$ is not always the worst case scenario in parametric roll. While in fig.(4) a steady roll angle of approximately 18° is predicted at $\omega_e=2\omega_n$, the steady roll angle increases to 28° and 43° in figs.(6) and (7) respectively, for different tuning conditions. This can be interpreted by reasoning that the roll natural frequency ω_n is assumed to be constant when it actually varies with time. One should also note that heave and pitch responses will change with changing forward speed.

Figs.(6-8) demonstrate the influence of varying the ship's forward speed on parametric roll, all for SS(6). While in figs.(6) and (7), parametric roll is predicted at forward speeds of $V=6$ and 12 knots respectively, parametric roll is not predicted in fig.(8) at a forward speed of $V=18$ knots. This can be attributed to the fact that forward speeds of 6 and 12 knots give encounter frequencies that are close to the encounter frequency of the first instability zone i.e. $\omega_e = 2\omega_n$. On the other hand, changing the forward speed to $V=18$ knots moves the system

out of the instability zone and its vicinity.

In fig.(7), for SS(6), extreme roll motions of 43° were obtained when using a predicted total roll damping coefficient b_{44} of 0.04. When b_{44} was increased by 33%, to be 10% of the critical roll damping (0.05346), parametric roll is no longer observed. This illustrates the importance of an accurate prediction of the non-potential flow roll damping especially for the “just on the edge” cases of parametric roll.

Fig.(9), for SS(7), shows another comparison between Methods (I) and (II). While Method (I) predicts parametric roll for the investigated case, Method (II) does not. This can be explained by reasoning that Method (I) tends to overestimate the parametric roll predictions as also demonstrated in fig.(3).

Figs.(10) and (11) compare results obtained for the same conditions (zero forward speed, $H_w=5$ m) in head and following seas using Method (II). They show that the behaviour is similar in both headings. While no parametric roll is seen in the predictions in fig.(10) for a frequency tuning condition of $\omega=\omega_e=\omega_n$, parametric roll of approximately 20° is detected at a frequency tuning condition of $\omega=\omega_e=2\omega_n$.

The comparison between figs.(5) and (12) demonstrates the influence of reducing the initial GM_T by 0.4 m on parametric roll. While in fig.(5) no parametric roll is predicted in SS(7) and at a frequency tuning condition of $\omega_e=2\omega_n$, parametric roll of up to 15° is predicted in fig.(12) for the same sea-state and tuning condition. This illustrates the influence of GM_T in the onset of parametric roll.

Finally, in fig.(13), parametric roll of 18° is again predicted for the lower initial GM_T , this time in following seas (SS(6)) and at a forward speed, $V=3.264$ knots giving a frequency tuning condition of $\omega_e=2\omega_n$.

5. CONCLUSIONS AND FUTURE WORK

In this paper, two methods have been presented for the prediction of parametric roll resonance in longitudinal regular waves. While Method (I) fails to obtain steady roll angles of parametric roll in the case of large wave heights, the results shown here demonstrate that Method (II) succeeds. Nevertheless, even in such large wave heights, Method (I) does provide an indication of the occurrence of parametric roll.

It is shown (e.g. fig.(2)) that Method (II) reproduces results that are available in the literature and are predicted by other numerical methods. Furthermore, Method (II) is capable of simulating and accurately predicting typical operational scenarios.

From an operational point of view, changing the forward speed of the ship can reduce the likelihood of parametric roll occurring if the change in speed moves the system out of the instability zone.

The frequency tuning condition of $\omega_e=2\omega_n$ is not always the worst case scenario in parametric roll resonance. One has to interpret this tuning condition over a wider range of encounter frequencies. Furthermore, metacentric height GM_T plays an important role, together with operational conditions, in influencing this tuning and, thus, the onset of parametric roll.

Accurate predictions of the total roll damping (linear and non-linear) are essential for any method that predicts parametric roll.

The few results presented in this paper on following seas demonstrate that parametric roll can occur in following seas, as in head seas, if the conditions for occurrence, i.e. wave height, wavelength, encounter frequency tuning are satisfied.

Further developments of this work will include:

- Extending Methods (I) and (II) to arbitrary

wave headings.

- Testing the capability of Method (II) to simulate the effects of changes in hull geometry.
- Applying Methods (I) and (II) to various hull forms, sea-states, operational conditions, etc and further verifying results against available published data.
- Extending an available partly non-linear three-dimensional method (hydrostatic and incident wave components) to simulate parametric roll resonance and comparing results with those of Methods (I) and (II).

6. REFERENCES

- Blocki, W., 1980, "Ship Safety in Connection with Parametric Resonance of Roll", International Shipbuilding Progress, Vol. 27, no. 306, pp. 36-53.
- Bulian, G., Francescutto, A., and Lugni, C., 2003, "On the Non-linear Modeling of Parametric Rolling in Regular and Irregular Waves", Proceedings of 8th International Conference on the Stability of Ships and Ocean Vehicles (STAB'03), Madrid, Spain, pp. 305-323.
- Dallinga, R.P., Blok, J.J., and Luth, H.R., 1998, "Excessive Rolling of Cruise ships in Head and Following Waves", RINA International Conference on Ship Motions and Manoeuvrability, Royal Institution of Naval Architects, London.
- De Kat, J.O. and Paulling, J.R., 1989, "The Simulation of Ship Motions and Capsizing in Severe Seas", Transactions of the Society of Naval Architects and Marine Engineers, Vol. 97.
- Faltinsen, O.M., 1990, Sea Loads on Ships and Offshore Structures, p.32, Cambridge University Press.
- France, W.N., Levadou, M., Treacle, T.W., Paulling, J.R., Michel, R.K. and Moore, C., 2003, "An Investigation of Head-sea Parametric Rolling and its Influence on Container Lashing Systems", Marine Technology, Vol. 40, no. 1, pp. 1-19.
- Himeno, Y., 1981, "Prediction of Ship Roll Damping –State of the Art", Dept. of Naval Architecture and Marine Engineering, The University of Michigan, Report no. 239.
- Neves, M.A.S., Perez, N. and Valerio, L., 1999, "Stability of Small Fishing Vessels in Longitudinal Waves", Ocean Engineering, Vol. 26, pp. 1389-1419.
- Neves, M.A.S., Perez, N. and Lorca, O., 2003, "Analysis of Roll Motion and Stability of a Fishing Vessel in Head-seas", Ocean Engineering, Vol. 30, pp. 921-935.
- Oh, I.G., Nayfeh, A.H. and Mook, D.T., 2000, "A Theoretical and Experimental Investigation of Indirectly Excited Roll Motions in Ships", Philosophical Transactions of the Royal Society, Vol. 358, pp. 1853-1881.
- Paulling, J.R., 1961, "The Transverse Stability of a Ship in a Longitudinal Seaway", Journal of Ship Research, Vol. 4, no. 4, pp. 37-49.
- Shin, Y.S., Belenky, V.L., Paulling, J.R., Weems, K.M. and Lin, W.M., 2004, "Criteria for Parametric Roll of Large Container Ships in Longitudinal Seas", SNAME Annual Meeting, Washington DC.
- Surendran, S. and Venkata Ramana Reddy, J., 2003, "Numerical Simulation of Ship Stability for Dynamic Environment", Ocean Engineering, Vol. 30, pp. 1305-1317.
- Umeda, N., and Hamamoto, M., 1995, "Model Experiments of Ship Capsizing in Astern Seas", Journal of the Society of Naval Architects of Japan, Vol. 177, pp. 207-21

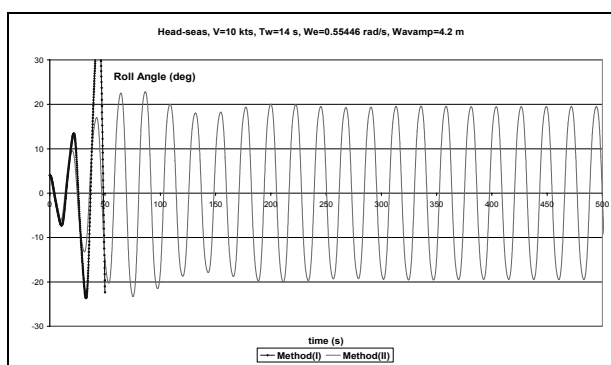


Figure (2) Illustration of parametric roll in regular head waves, predicted $b_{44}=0.025$

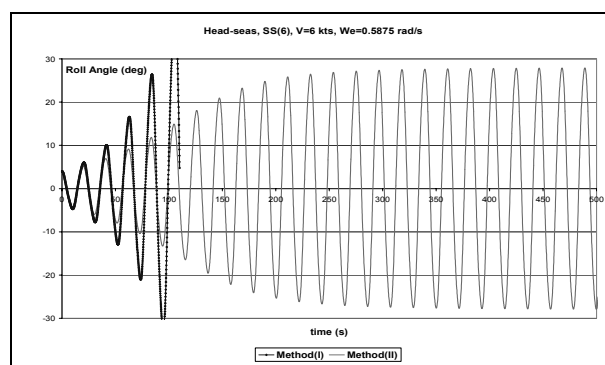


Figure (6) Illustration of parametric roll in regular head waves, predicted $b_{44}=0.06$

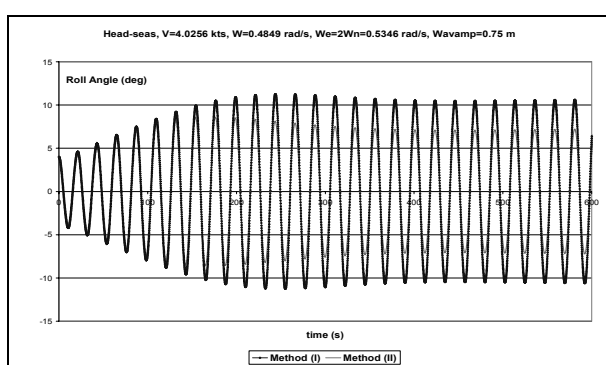


Figure (3) Illustration of parametric roll in regular head waves, predicted $b_{44}=0.0125$

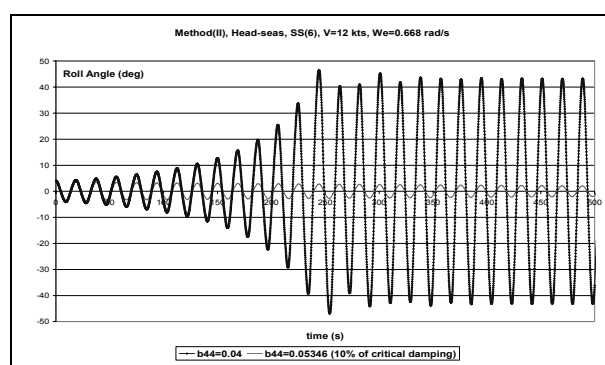


Figure (7) Illustration of parametric roll in regular head waves

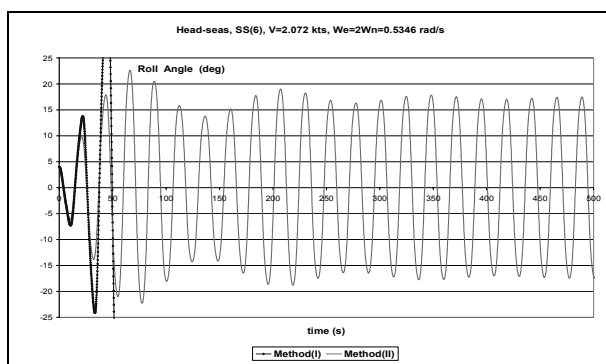


Figure (4) Illustration of parametric roll in regular head waves, predicted $b_{44}=0.015$

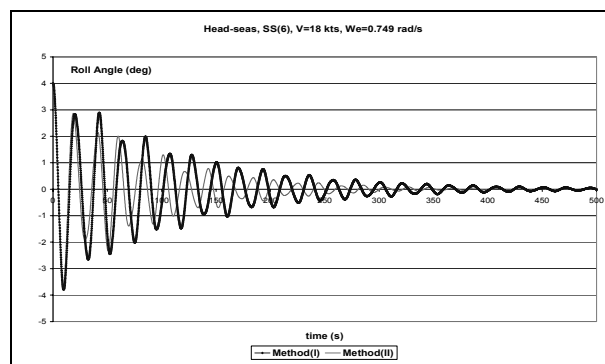


Figure (8) Illustration of parametric roll in regular head waves

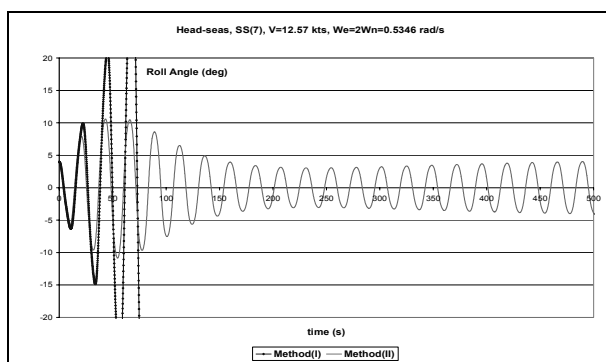


Figure (5) Illustration of parametric roll in regular head waves, predicted $b_{44}=0.02$

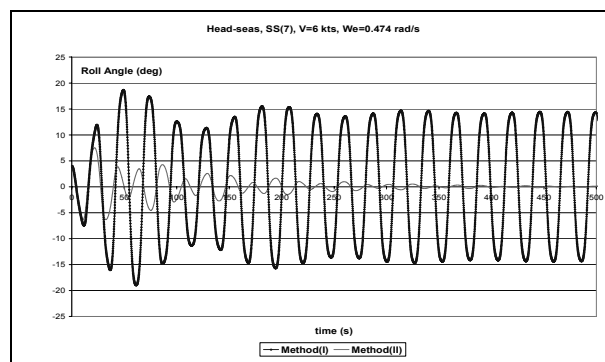


Figure (9) Illustration of parametric roll in regular head waves, predicted $b_{44}=0.017$

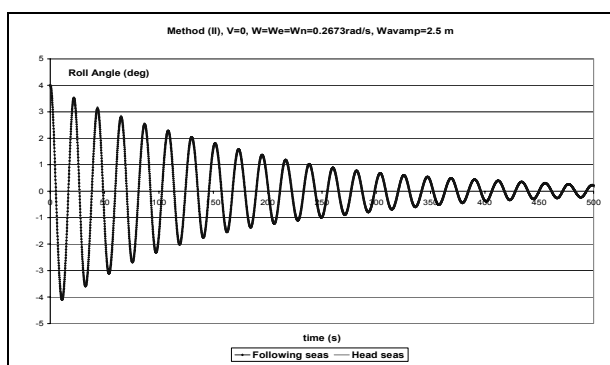


Figure (10) Illustration of parametric roll in regular following and head waves

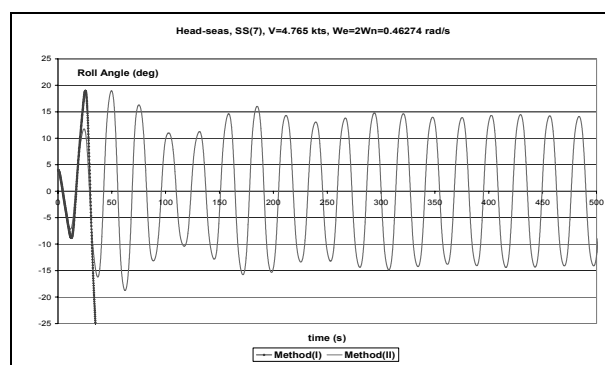


Figure (12) Illustration of parametric roll in regular head waves, $KG=17.95$ m, predicted $b_{44}=0.015$

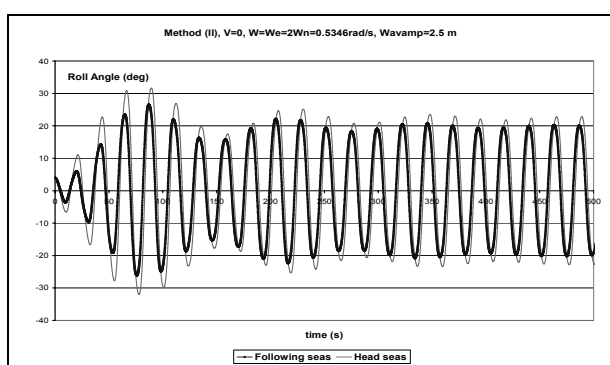


Figure (11) Illustration of parametric roll in regular following and head waves, predicted $b_{44}=0.013$

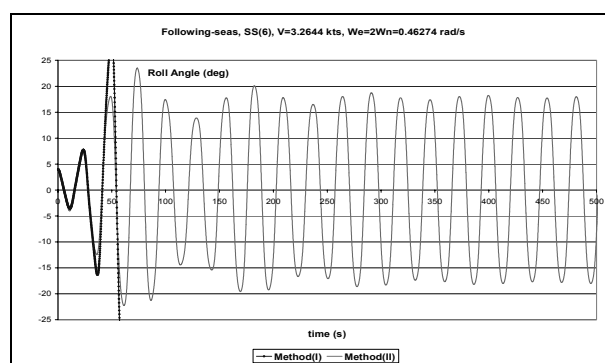


Figure (13) Illustration of parametric roll in regular following waves, $KG=17.95$ m, predicted $b_{44}=0.0156$

An Investigation on Roll Parametric Resonance in Regular Waves

Marcelo A. S. Neves, *Federal University of Rio de Janeiro*

Claudio A. Rodríguez, *Federal University of Rio de Janeiro*

ABSTRACT

Parametric resonance in regular waves is discussed. A set of non-linear equations is employed to describe the coupling between heave-roll-pitch modes. Limits of stability are the main area of interest of the paper. The present paper explores the influence of third order nonlinearities as well as the relevance of coupling between the vertical modes and the roll motion in the limits of stability.

The influence of initial conditions on the development of roll amplifications is investigated and the effect of coupled or uncoupled modelling of the roll motion is addressed.

Keywords: *parametric resonance, limits of stability, ship stability, nonlinear coupling*

1. INTRODUCTION

Lately, parametric resonance has become a source of great attention for the marine scientific community, classification societies and several other institutions involved in the development of ship's safety rules. Fishing, cruise and container vessels are known types of hulls that are often subjected to strong roll amplifications due to parametric instability (Neves et al., 2002, Luth & Dallinga, 1999, France et al., 2003). Experimental and numerical investigations have contributed to enlarge the knowledge of this phenomenon. However, there are not closed criteria that could let us measure or predict parametric roll motion with enough confidence for all kind of vessels, yet.

For many of these ships the simulation models available are capable of reproducing with confidence the amplification resulting from parametric resonance. But, unfortunately, there are some known cases of strong parametric excitation where the numerical

models based on Mathieu (or Mathieu-Duffing) equation tend to overpredict the resonant rolling motions observed in experiments (Umeda et al., 2003). Recent works (Neves & Rodríguez, 2004, 2005) have shown that a third order nonlinear analytical model equivalent to a kind of Hill equation can reproduce well such extreme situations. This new mathematical model may display some interesting dynamic features that are still open to investigation.

Neves & Rodríguez (2004) showed a comparison of the limits of stability for the second and third order models based on Hsu's approach for the roll variational equation. The present paper explores in depth the influence of third order nonlinearities as well as the relevance of coupling between the vertical modes and the roll motion in the limits of stability. The above effects are investigated through the analysis of the time domain numerical responses obtained by systematic variation of encounter frequency and wave amplitude. This new way of obtaining the limits of stability is a more realistic procedure of assessing parametric resonance and also has an additional feature: a color map that

identifies the magnitude of the steady roll parametric amplitude.

Other nonlinear characteristics of parametric roll behaviour, such as dependence on initial conditions are preliminarily investigated.

2. NONLINEAR MATHEMATICAL MODEL

As stated above, the mathematical model proposed by Neves & Rodríguez (2004, 2005) has demonstrated good capability in reproducing parametric resonance especially when strong roll amplifications take place. This mathematical model couples the equations of motions in heave, roll and pitch and contemplates nonlinearities up to the third order in the restoring actions as well as in the roll damping:

$$\begin{aligned}
& (m + Z_{zz})\ddot{z} + Z_{zz}\dot{z} + Z_{\theta\theta}\ddot{\theta} + Z_{\theta\theta}\dot{\theta} + Z_{zz}z + Z_{\theta}\theta + \\
& \frac{1}{2}Z_{zz}z^2 + \frac{1}{2}Z_{\phi\phi}\phi^2 + \frac{1}{2}Z_{\theta\theta}\theta^2 + Z_{z\theta}z\theta + \frac{1}{6}Z_{zzz}z^3 \\
& + \frac{1}{2}Z_{z\theta\theta}z^2\theta + \frac{1}{2}Z_{\phi\theta\theta}\phi^2z + \frac{1}{2}Z_{\phi\theta\theta}\phi^2\theta + \frac{1}{2}Z_{\theta\theta z}\theta^2z \\
& + \frac{1}{6}Z_{\theta\theta\theta}\theta^3 + Z_{\zeta z}(t)z + Z_{\zeta\theta}(t)\theta + Z_{\zeta\zeta z}(t)z + Z_{\zeta\zeta z}(t)z^2 \\
& + Z_{\zeta\zeta\theta}(t)\theta + Z_{\zeta z\theta}(t)z\theta + Z_{\phi\phi\zeta}(t)\phi^2 + Z_{\theta\theta\zeta}\theta^2 = Z_w(t)
\end{aligned} \quad (1)$$

$$\begin{aligned}
& (J_{xx} + K_{\phi})\ddot{\phi} + K_{\phi}\dot{\phi} + K_{\phi|\phi}|\dot{\phi}| + K_{\phi}\phi + K_{z\phi}z\phi + K_{\phi\theta}\phi\theta \\
& + \frac{1}{2}K_{z\phi}z^2\phi + \frac{1}{6}K_{\phi\phi\phi}\phi^3 + \frac{1}{2}K_{\theta\phi\theta}\theta^2\phi + K_{z\phi\theta}z\phi\theta \\
& + K_{\zeta\phi}(t)\phi + K_{\zeta\zeta\phi}(t)\phi + K_{\zeta z\phi}(t)z\phi + K_{\zeta\phi\theta}(t)\phi\theta = K_w(t)
\end{aligned}$$

$$\begin{aligned}
& (J_{yy} + M_{\theta})\ddot{\theta} + M_{\theta}\dot{\theta} + M_{zz}\ddot{z} + M_{zz}\dot{z} + M_{zz}z + M_{\theta}\theta + \frac{1}{2}M_{zz}z^2 \\
& + \frac{1}{2}M_{\phi\phi}\phi^2 + \frac{1}{2}M_{\theta\theta}\theta^2 + M_{z\theta}z\theta + \frac{1}{6}M_{zzz}z^3 + \frac{1}{2}M_{z\theta z}z^2\theta \\
& + \frac{1}{2}M_{\phi\theta z}\phi^2z + \frac{1}{2}M_{\phi\theta\theta}\phi^2\theta + \frac{1}{2}M_{\theta\theta z}\theta^2z + \frac{1}{6}M_{\theta\theta\theta}\theta^3 \\
& + M_{\zeta z}(t)z + M_{\zeta\theta}(t)\theta + M_{\zeta\zeta z}(t)z + M_{\zeta\zeta z}(t)z^2 + M_{\zeta\zeta\theta}(t)\theta \\
& + M_{\zeta z\theta}(t)z\theta + M_{\phi\phi\zeta}(t)\phi^2 + M_{\theta\theta\zeta}\theta^2 = M_w(t)
\end{aligned}$$

On the right hand side of these equations, $Z_w(t)$, $K_w(t)$, $M_w(t)$ describe wave external

excitations in the heave, roll and pitch modes, respectively. In the left hand side of the equations, nonlinear restoring terms include dependence on all body modes (z , ϕ , θ) and wave passage (ζ). Dots refer to velocities; double dots to accelerations. In all modes, coefficients with dotted and double dotted subscripts are damping and added masses coefficients, respectively.

In the numerical implementation of this mathematical model, added masses, vertical motion damping, and wave external excitations are assumed linear and are computed using the strip method theory. Roll damping is computed based on Ikeda's method as described by Himeno (1981); and restoring actions are taken into account considering couplings (up to the third order) among the heave, roll and pitch motions, and the wave profile passing along the ship. As demonstrated in previous works (Neves & Rodríguez, 2004, 2005) for certain hull forms and motions of moderate amplitude, nonlinear restoring actions of higher order play an important role in the dynamic behaviour.

Figure 1 illustrates the good agreement obtained in the comparisons between experimental results and numerical simulations for a typical transom stern fishing vessel (denominated TS), and also shows how a second order model fails to follow the trends.

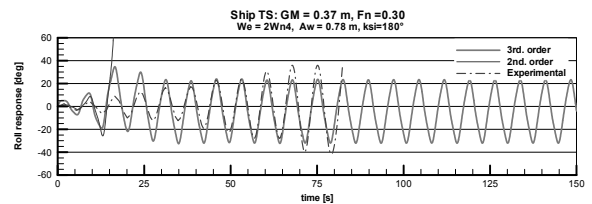


Figure 1 Roll response, $Fn=0.30$, $A_w=0.78$ m.

3. STABILITY ANALYSIS OF ROLL PARAMETRIC RESONANCE

3.1 Analytical Approach – Hsu's Limits

Stability of motion may be assessed by means of the variational system. In its linear

form it may be derived by assuming that the nonlinear motions can be expressed as the sum of steady oscillatory solutions plus some small perturbations:

$$\begin{aligned} z(t) &= \hat{z}(t) + \xi(t) = A_w \eta_3 \text{Cos}(\omega_e t + \alpha_z) + \xi(t) \\ \phi(t) &= \hat{\phi}(t) + \varphi(t) = A_w \eta_4 \text{Cos}(\omega_e t + \alpha_\phi) + \varphi(t) \\ \theta(t) &= \hat{\theta}(t) + \vartheta(t) = A_w \eta_5 \text{Cos}(\omega_e t + \alpha_\theta) + \vartheta(t) \end{aligned}$$

where $\hat{z}(t)$, $\hat{\phi}(t)$, and $\hat{\theta}(t)$ correspond to the heave, roll and pitch well known linear solutions (steady), and η_3, η_4, η_5 are the corresponding transfer functions. Perturbations in the heave, roll and pitch modes are defined as $\xi(t)$, $\varphi(t)$, and $\vartheta(t)$, respectively.

The linear variational equation in roll is then derived as:

$$\begin{aligned} (J_{xx} + K_{\ddot{\phi}})\ddot{\phi} + B_e \dot{\phi} + K_\phi \phi + (K_{z\phi} \hat{\phi} + K_{z\phi} \hat{z} \hat{\phi} \\ + K_{z\phi\theta} \hat{\phi} \hat{\theta}) \xi + \left(K_{z\phi} \hat{z} + K_{\phi\theta} \hat{\theta} + \frac{1}{2} K_{\phi\phi\phi} \hat{\phi}^2 + \frac{1}{2} K_{z\phi} \hat{z}^2 \right. \\ \left. + \frac{1}{2} K_{\theta\theta\phi} \hat{\theta}^2 + K_{z\phi\theta} \hat{z} \hat{\theta} \right) \varphi + (K_{\phi\theta} \hat{\phi} + K_{\theta\theta\phi} \hat{\theta} \hat{\phi} \\ + K_{z\phi\theta} \hat{z} \hat{\theta}) \vartheta + K_{\zeta\phi}(t) \varphi + K_{\zeta\phi}(t) \hat{\phi} \xi + K_{\zeta\phi}(t) \hat{z} \varphi \\ + K_{\zeta\phi\theta}(t) \hat{\theta} \varphi + K_{\zeta\phi\theta}(t) \hat{\phi} \vartheta + K_{\zeta\zeta\phi}(t) \varphi = 0 \end{aligned} \quad (2)$$

where, for simplicity, B_e is adopted as an equivalent damping moment. In the particular case of longitudinal waves, the roll linear solution is zero. That is, $\hat{\phi} \equiv 0$. Hence:

$$\begin{aligned} (J_{xx} + K_{\ddot{\phi}})\ddot{\phi} + B_e \dot{\phi} + [K_\phi + K_{z\phi} \hat{z} + K_{\phi\theta} \hat{\theta} \\ + \frac{1}{2} K_{z\phi} \hat{z}^2 + \frac{1}{2} K_{\theta\theta\phi} \hat{\theta}^2 + K_{z\phi\theta} \hat{z} \hat{\theta} + K_{\zeta\phi}(t) \\ + K_{\zeta\phi\theta}(t) \hat{z} + K_{\zeta\phi\theta}(t) \hat{\theta} + K_{\zeta\zeta\phi}(t)] \varphi = 0 \end{aligned} \quad (3)$$

Substituting: $\hat{z}(t) = A_w \eta_3 \text{Cos}(\omega_e t + \alpha_z)$ and $\hat{\theta}(t) = A_w \eta_5 \text{Cos}(\omega_e t + \alpha_\theta)$ and decomposing the wave coefficients in their sine and cosine terms, we arrive to an expression of the following type for the roll variational equation (see Neves & Rodríguez, 2004):

$$\begin{aligned} (J_{xx} + K_{\ddot{\phi}})\ddot{\phi} + B_e \dot{\phi} + [K_\phi + R_0 \\ + R_1 \text{Cos}(\omega_e t + \tau_1) + R_2 \text{Cos}(2\omega_e t + \tau_2)] \varphi = 0 \end{aligned} \quad (4)$$

where R_0 , R_1 , and R_2 are time-independent restoring coefficients, and τ_1 and τ_2 , are the phases of the periodic restoring moments relative to the wave. In contrast to the second order model, where the resultant roll variational equation is a Mathieu type, in the third order model we obtain a Hill type equation. As can be seen from eq. (4), in addition to the Mathieu terms two additional contributions appear. These new terms, as explained in Authors' previous works, rise interesting nonlinear features in the stability analysis of roll variational equation: nonlinear stiffness and biharmonic parametric excitation.

The stability analysis of Hill equation is presented by Hsu (1963), and when applied to equation (4), two instability regions appear defined by:

- First Region of Stability ($s = 1$):

$$2\omega_4 + \frac{A_w}{2\omega_4} [(d_{44}^{(1)})^2 + (e_{44}^{(1)})^2] > \omega_e \quad (5)$$

$$-4\omega_4^2 (f_{44}^{(0)})^2 \Big]^{1/2} > \omega_e$$

$$> 2\omega_4 - \frac{A_w}{2\omega_4} [(d_{44}^{(1)})^2 + (e_{44}^{(1)})^2]$$

$$-4\omega_4^2 (f_{44}^{(0)})^2 \Big]^{1/2}$$

- Second Region of Stability ($s = 2$):

$$\omega_4 + \frac{A_w}{4\omega_4} [(d_{44}^{(1)})^2 + (e_{44}^{(1)})^2] > \omega_e \quad (6)$$

$$-4\omega_4^2 (f_{44}^{(0)})^2 \Big]^{1/2} > \omega_e$$

$$> \omega_4 - \frac{A_w}{4\omega_4} [(d_{44}^{(1)})^2 + (e_{44}^{(1)})^2]$$

$$-4\omega_4^2 (f_{44}^{(0)})^2 \Big]^{1/2}$$

where:

$$d_{44}^{(1)} = \frac{[K_{z\phi}\eta_3\cos(\alpha_z) + K_{\phi\theta}\eta_5\cos(\alpha_\theta) + K_{\zeta\phi c}]}{(J_{xx} + K_{\ddot{\phi}})}$$

$$e_{44}^{(1)} = \frac{[-K_{z\phi}\eta_3\sin(\alpha_z) - K_{\phi\theta}\eta_5\sin(\alpha_\theta) + K_{\zeta\phi s}]}{(J_{xx} + K_{\ddot{\phi}})}$$

$$d_{44}^{(2)} = \left(\frac{A_w}{J_{xx} + K_{\ddot{\phi}}}\right) \left[\frac{1}{4} K_{z\phi}\eta_3^2 \cos(2\alpha_z) + \frac{1}{4} K_{\theta\theta\phi}\eta_5^2 \cos(2\alpha_\theta) + \frac{1}{2} K_{z\phi\theta}\eta_3\eta_5 \cos(\alpha_z + \alpha_\theta) + \frac{\eta_3}{2} [K_{\zeta\phi c} \cos(\alpha_z) + K_{\zeta\phi s} \sin(\alpha_z)] + \frac{\eta_5}{2} [K_{\zeta\theta\phi c} \cos(\alpha_\theta) + K_{\zeta\theta\phi s} \sin(\alpha_\theta)] + K_{\zeta\zeta\phi c} \right]$$

$$e_{44}^{(2)} = \left(\frac{A_w}{J_{xx} + K_{\ddot{\phi}}}\right) \left[-\frac{1}{4} K_{z\phi}\eta_3^2 \sin(2\alpha_z) - \frac{1}{4} K_{\theta\theta\phi}\eta_5^2 \sin(2\alpha_\theta) - \frac{1}{2} K_{z\phi\theta}\eta_3\eta_5 \sin(\alpha_z + \alpha_\theta) + \frac{\eta_3}{2} [-K_{\zeta\phi c} \sin(\alpha_z) + K_{\zeta\phi s} \cos(\alpha_z)] + \frac{\eta_5}{2} [-K_{\zeta\theta\phi c} \sin(\alpha_\theta) + K_{\zeta\theta\phi s} \cos(\alpha_\theta)] + K_{\zeta\zeta\phi s} \right]$$

$$f_{44}^{(0)} = \frac{B_e}{A_w (J_{xx} + K_{\ddot{\phi}})}$$

$$\omega_4 = [\omega_{n4}^2 + \omega_{m4}^2]^{1/2}$$

$$\omega_{n4}^2 = \frac{K_{\phi}}{(J_{xx} + K_{\ddot{\phi}})}$$

$$\omega_{m4}^2 = \left(\frac{A_w^2}{J_{xx} + K_{\ddot{\phi}}}\right) \left[\frac{1}{4} K_{z\phi}\eta_3^2 + \frac{1}{4} K_{\theta\theta\phi}\eta_5^2 + \frac{1}{2} K_{z\phi\theta}\eta_3\eta_5 \cos(\alpha_z - \alpha_\theta) \right]$$

$$+ \frac{\eta_3}{2} [K_{\zeta\phi c} \cos(\alpha_z) - K_{\zeta\phi s} \sin(\alpha_z)] + \frac{\eta_5}{2} [K_{\zeta\theta\phi c} \cos(\alpha_\theta) - K_{\zeta\theta\phi s} \sin(\alpha_\theta)] + K_{\zeta\zeta\phi 0}$$

The numerical implementation of Hsu's analytical approach for the TS ship in head seas under different speeds and for a metacentric height (GM) of 0.37 m gives the following stability limits (see Figures 2 to 5). Different from past Authors' works, in these cases damping is considered, although for simplicity only the linear damping was taken into account.

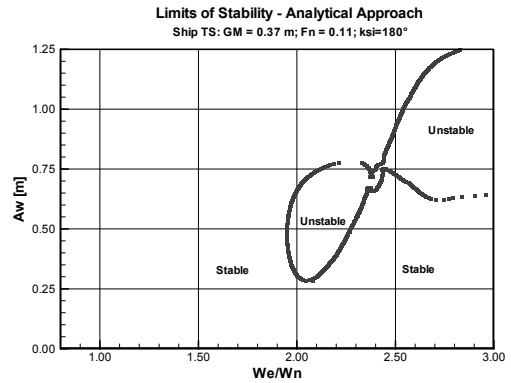


Figure 2 Analytical approach, $Fn=0.11$

As stated in Neves & Rodríguez (2004) and in Rodríguez (2004), the introduction of damping shortens the instability regions and displaces to the right the tuning frequency of the minimum threshold wave amplitude. Other main features of the Hsu's instability regions have already been discussed in Neves & Rodríguez (2004).

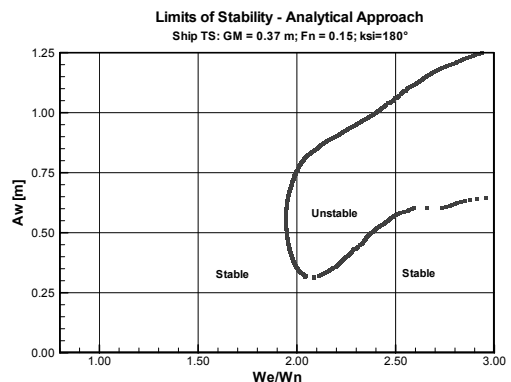


Figure 3 Analytical approach, $Fn=0.15$

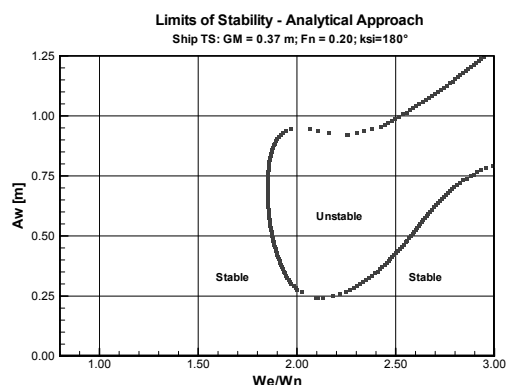


Figure 4 Analytical approach, $F_n=0.20$

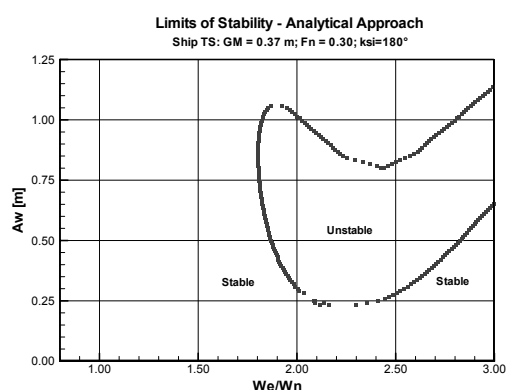


Figure 5 Analytical approach, $F_n=0.30$

Although the limits of stability using the analytical approach is a valuable and easy tool in the ship design stage as a rough indicator of the extension and location of the instability regions, they do NOT provide quantitative information, i.e., the steady amplitude of parametric rolling.

An alternative way of computing the instability regions is obtained by solving the motion equations for a large set of waves amplitudes and tuning factors (encounter frequency/natural roll frequency), which will be varied systematically. Then, each time instabilization takes place (roll amplification), a point will be plotted in the corresponding plane (A_w vs. tuning factor). Depending on the magnitude of the steady roll amplitude, these points will have an identifying color.

Yet this procedure is much more time consuming for computation, it has the advantage of letting us know the instability regions not only qualitative, but also

quantitatively.

Under this alternative method, two different numerical approaches could be used: one assuming an uncoupled nonlinear roll motion equation, and the other using the 3 DOF motion equations coupling the heave, roll and pitch modes.

3.2 Numerical Approach – Uncoupled Roll Motion

Here, the vertical modes are assumed linear while the rolling motion keeps all its nonlinear terms, resulting in an uncoupled roll equation. When the analytical approach was used, we analyzed the behaviour of the roll variational equation, which, as seen above, is linear. So, by comparing the analytical and the numerical uncoupled roll approach is possible to identify the effects of pure roll nonlinearities, which in the case of the former approach cancel due to the null linear roll response. Figures 6 to 9 show the instability regions obtained integrating the nonlinear roll equation of motion in the time-domain for an initial condition in roll of 2° .

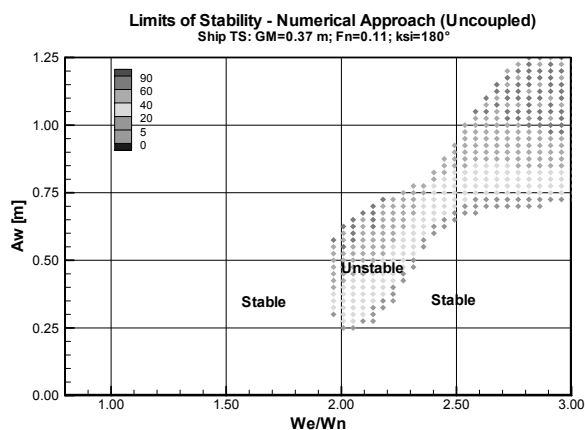
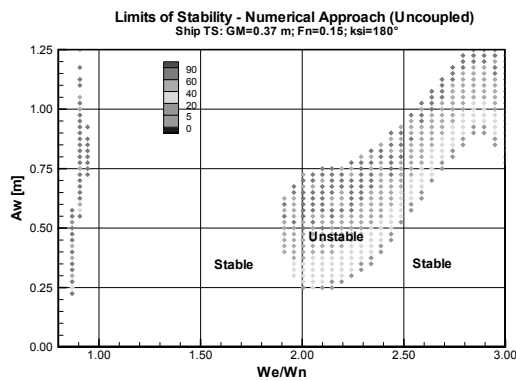
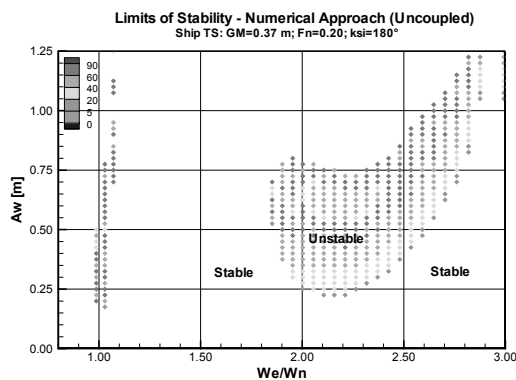
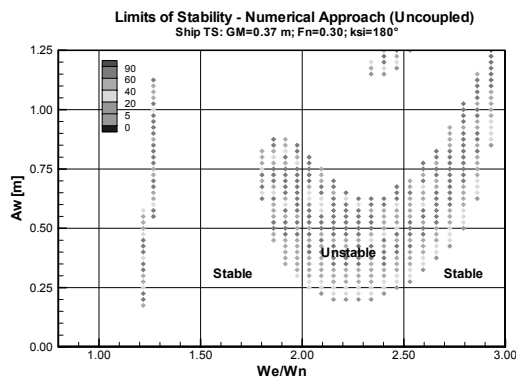


Figure 6 Num. uncoupled approach, $F_n=0.11$

As can be noted from figures 6 to 9, the shape and location of the regions of stability agree well with the analytical approach. This would indicate that pure roll nonlinearities have little or NO influence on these characteristics of the limits.

Figure 7 Num. uncoupled approach, $F_n=0.15$ Figure 8 Num. uncoupled approach, $F_n=0.20$ Figure 9 Num. uncoupled approach, $F_n=0.30$

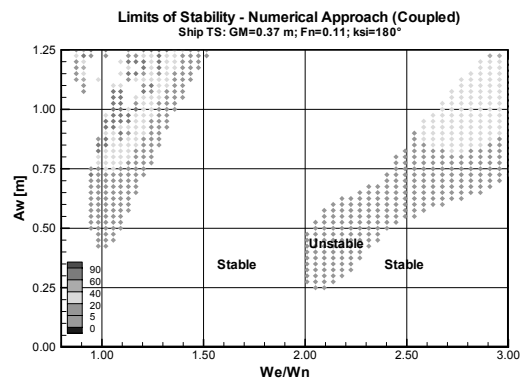
Concerning the amplitudes of parametric rolling, as expected, the greater the wave amplitudes the greater the responses within the instability regions. At low speeds parametric roll amplitudes grow gradually as wave amplitude increases (up the top limit), however, at high speeds ($F_n = 0.20$ and $F_n = 0.30$), parametric rolling is violent starting at angles of 20° and rapidly reaching capsizing angles for little increases in wave amplitudes (see fig. 9). Another characteristic observed at

high speeds is the appearance and accentuation of a concavity in the top limit, to the right of the Mathieu *exact* tuning ($\omega_e/\omega_{n4} = 2.0$).

3.3 Numerical Approach – 3 DOF Motion

A more refined and reliable way of getting the limits of stability for parametric resonance is to solve numerically the three-degrees-of-freedom (DOF) ship motion equations shown in section 2 of the present work, and plot the responses, as explained in the previous section. This more complete approach when applied to the same conditions tested above for TS ship resulted in the limits of stability shown in figures 10 to 13.

In general, the shape and location of first instability regions ($\omega_e = 2.0\omega_{n4}$) obtained with the 3 DOF numerical approach agrees well with the previous approaches. However, when comparing the limits of figures 10 to 13 with its corresponding ones of figures 6 to 9, relevant differences can be observed in the amplitudes of parametric rolling for all speeds cases. Such differences reflect the influence of nonlinearities of heave and pitch, which in general tend to control the magnitude of roll amplifications.

Figure 10 Num. 3 DOF approach, $F_n=0.11$ ($\phi = 2^\circ$)

Another significant and surprising feature is the notoriety that the second region of instability ($\omega_e = \omega_{n4}$) gain in comparison to the other approaches: not only the wider area, but also the trend and the magnitude of unstable

roll. Concerning the concavity of the instability regions at high speeds pointed out in the previous section, we confirm here its existence and also call the attention of the readers for the risk of getting more critical responses at frequencies higher than the Mathieu tunings, even for quite low wave amplitudes.

4. OTHER NONLINEAR CHARACTERISTICS OF PARAMETRIC ROLL BEHAVIOUR

Based on the procedure outlined in the previous sub-section, it is possible to compute the limits of stability for different initial conditions, and identify the conditions that bring different steady parametric roll amplitudes. This phenomenon would indicate the possibility of occurrence of jump effect, bifurcation or even chaos. Figure 14 illustrates the limits of stability for the same conditions showed in figure 12, but considering an initial condition for roll of 20° .

It is obvious that the first influence of initial conditions is to modify the size of the instability regions. In the case illustrated in figure 14, the first region of instability became greater (growing upwards and to the left side). This additional instability region denotes a zone of initial condition susceptibility. Then, a good beginning for the study of typical nonlinear behaviour would be the exploration of this zone.

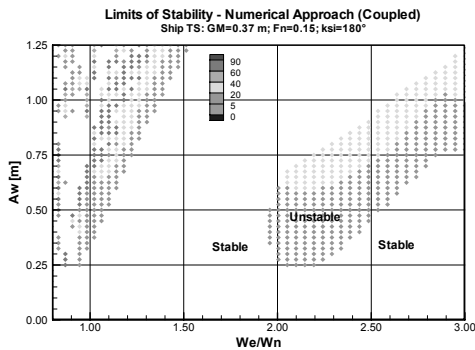


Figure 11 Num. 3 DOF approach, $F_n=0.15$ ($\phi_0 = 2^\circ$)

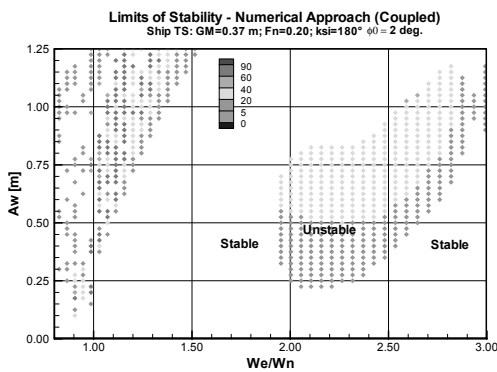


Figure 12 Num. 3 DOF approach, $F_n=0.20$ ($\phi_0 = 2^\circ$)

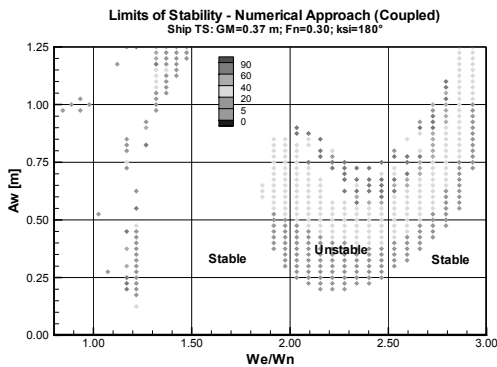


Figure 13 Num. 3 DOF approach, $F_n=0.30$ ($\phi_0 = 2^\circ$)

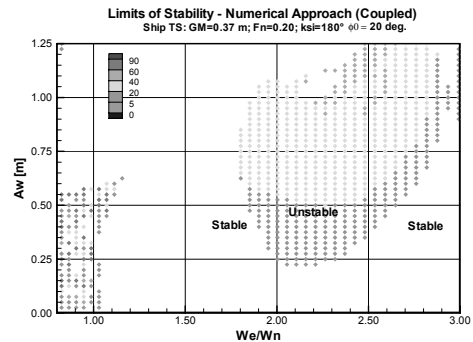


Figure 14 Num. 3 DOF approach, $F_n=0.20$ ($\phi_0 = 20^\circ$)

Time simulations are one of the most used tools for exploring such behaviour. Figures 15 to 17 show time series for three different initial conditions in roll for the case of TS ship at $F_n=0.20$, $A_w=0.95$ m and $\omega_e = 2.158 \omega_{n4}$.

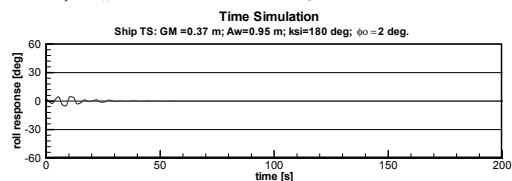
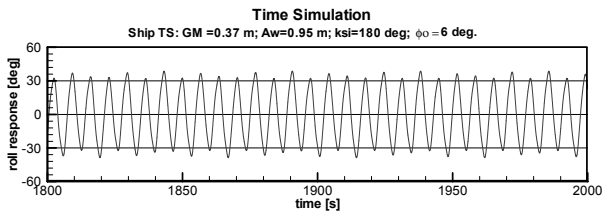
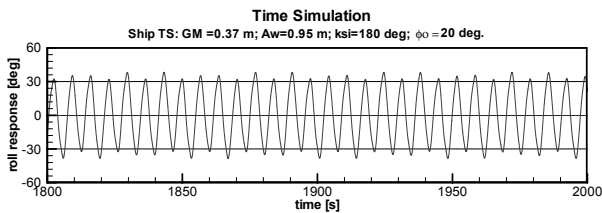
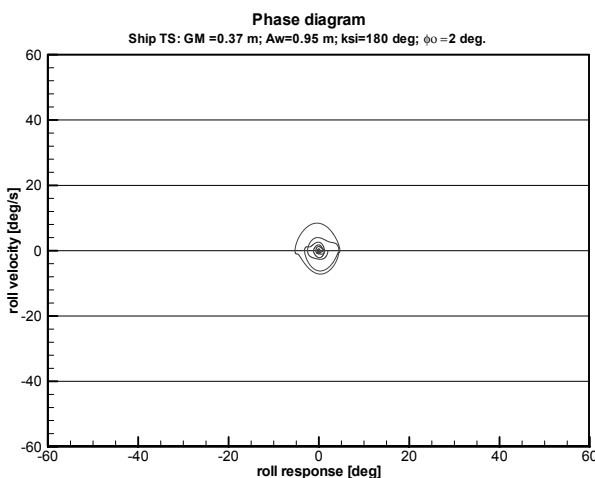
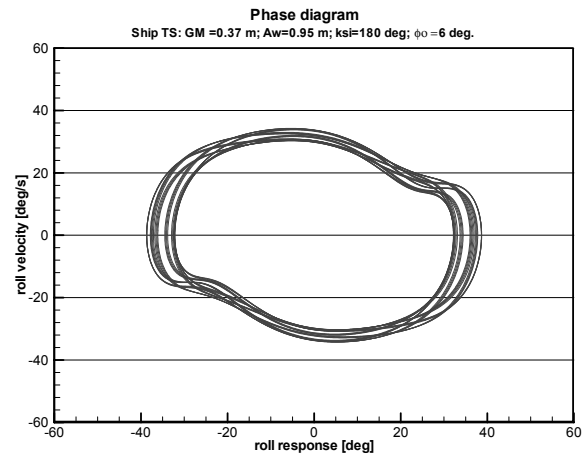
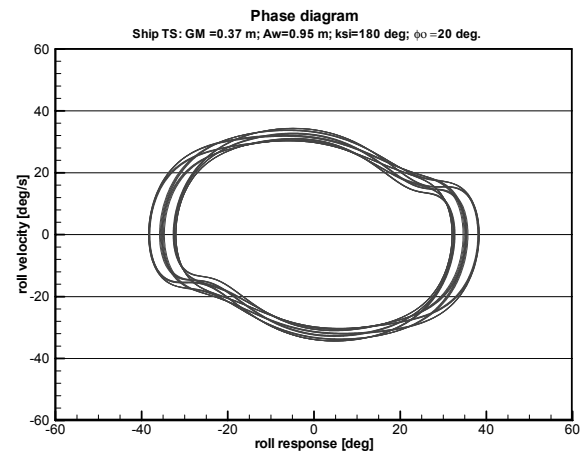


Figure 15 Time series, $F_n=0.20$; $\phi_0 = 2^\circ$

Figure 16 Time series, $F_n=0.20$; $\phi_0 = 6^\circ$ Figure 17 Time series, $F_n=0.20$; $\phi_0 = 20^\circ$

As expected, for these parameters different initial conditions resulted in different roll responses. For the smaller initial conditions no parametric resonance was developed, as had been noted in the stability map of figure 12 (2° of roll initial condition). For the initial condition larger than 6° , parametric rolling develops in an erratic way, no single amplitude is observed. Then, it becomes necessary to look at phase diagrams in order to identify if there is a multiperiod response or the possibility of occurrence of chaos. Figures 18 to 20 show the phase diagrams for the respective conditions shown in the time series, initial conditions $\phi_0 = 2^\circ$, $\phi_0 = 6^\circ$ and $\phi_0 = 20^\circ$.

Figure 18 Phase diagram, $F_n=0.20$; $\phi_0 = 2^\circ$ Figure 19 Phase diagram, $F_n=0.20$; $\phi_0 = 6^\circ$ Figure 20 Phase diagram, $F_n=0.20$; $\phi_0 = 20^\circ$

Clearly, it is noted that the small initial condition response is stable and does NOT develop parametric rolling. In other words, the response is attracted by a single attractor, which in this case corresponds to the null parametric rolling attractor.

For the larger initial conditions, the responses are attracted by a “not-easy-to-identify attractor”. We can just say that it is not a single point or a limit cycle attractor. Maybe a strange attractor or even a chaotic attractor, but a definite answer to this question should be given based on more specific nonlinear analysis tools such as bifurcation analysis, Poincaré mapping, Lyapunov exponents, etc. This kind of analysis is out of the scope of the present work, but literature on this subject is ample (Guckenheimer & Holmes, 1983, Seydel, 1988, Liaw et al., 1993).

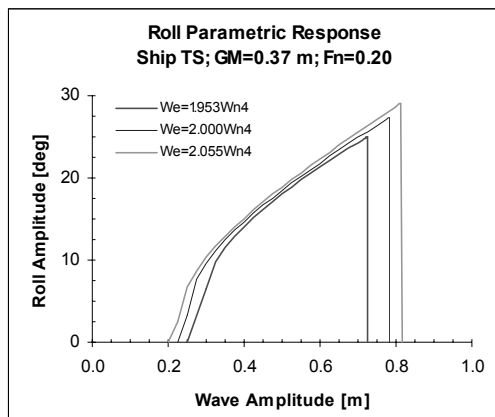


Figure 21 Jump in roll response at high wave amplitudes, $F_n=0.20$.

Figure 21 shows the roll amplitudes against wave amplitude for three tunings around the *exact* Mathieu tuning $\omega_e = 2.0 \omega_{n4}$. Again, for high amplitudes (extreme right of the graph) abrupt changes in roll response are observed, indicating the occurrence of a bifurcation for changing wave amplitudes.

5. CONCLUSIONS

Based on a third order mathematical model for parametric rolling, three approaches for computing the limits of stability have been presented.

The analytical approach has shown good agreement with the numerical responses, and due to its relatively easy implementation, should find good applicability in the ship preliminary design stage. One limitation of the analytical approach is that it does not provide information on the magnitude of parametric rolling. To overcome this inconvenience, two numerical approaches have been proposed. One using the uncoupled roll equation, and the other applying the full nonlinear equations coupling heave, roll and pitch. Comparing the two latter approaches, a relevant conclusion can be drawn, i.e., the extreme importance of nonlinear couplings between the vertical modes and roll in the determination of parametric roll amplitudes. As can be noted in the respective figures, the uncoupled numerical approach can

induce us to wrong predictions of parametric amplitudes.

Another contribution of the present investigation is the identification of initial conditions susceptibility zones within the instability regions, so that the analysis of typical nonlinear phenomena can be focused on these zones. Preliminary analysis of these zones has shown great influence of initial conditions on the development of parametric rolling.

6. ACKNOWLEDGMENTS

The present investigation is supported by CNPq within the STAB project (Nonlinear Stability of Ships). The Authors also acknowledge financial support from LabOceano-COPPE/UFRJ and CAPES.

7. REFERENCES

- France, W.N., Levadou, M., Treacle, T.W., Paulling, J.R., Michel, R.K., and Moore, C., 2003, "An Investigation of Head-Sea Parametric Rolling and its Influence on Container Lashing Systems", *Marine Technology*, vol. 40, no. 1, pp. 1-19.
- Guckenheimer, J., and Holmes, P., 1983, *Nonlinear Oscillations, Dynamical Systems, and Bifurcations of Vector Fields*, *Applied Mathematical Sciences*, vol. 42, Springer-Verlag.
- Himeno, Y., 1981, "Prediction of Ship Roll Damping – State of the Art", Report No. 239, Dept. Naval Architecture and Marine Engineering, The University of Michigan.
- Hsu, C.S., 1963, "On the Parametric Excitation of a Dynamic System Having Multiple Degrees of Freedom", *Transactions of the ASME Journal of Applied Mechanics*, vol. 30, no. 3, pp. 367-372.
- Liaw, C.Y., Bishop, S.R., and Thompson, J.C., 1981, "Parametric Rolling of a Ship in Head-Sea", *Journal of Ship Research*, vol. 25, no. 3, pp. 171-181.

- J.M.T., 1993, "Heave-Excited Rolling Motion of a Rectangular Vessel in Head Seas", International Journal of Offshore and Polar Engineering, ISOPE, vol. 3, no. 1, pp. 26-31.
- Luth, H.R., and Dallinga, R.P., 1999, "Prediction of Excessive Rolling of Cruise Vessels in Head and Following Waves", PRADS Conference.
- Neves, M.A.S., Pérez, N., and Lorca, O., 2002, "Experimental Analysis on Parametric Resonance for Two Fishing Vessels in Head Seas", Proceedings of 6th International Ship Stability Workshop, Webb Institute, NY.
- Neves, M.A.S. and Rodríguez, C., 2004, "Limits of Stability of Ships Subjected to Strong Parametric Excitation in Longitudinal Waves", Proceedings of International Maritime Conference on Design for Safety, Osaka, pp. 139-145.
- Neves, M.A.S. and Rodríguez, C., 2005, "A non-Linear Mathematical Model of Higher Order for Strong Parametric Resonance of the Roll Motion of Ship in Waves", Marine Systems & Ocean Technology - Journal of SOBENA, Vol. 1 No. 2, pp. 69-81.
- Rodríguez, C. A., 2004, "Dynamic Stability of Ships: A Third Order Non-linear Model", M. Sc. Thesis, COPPE – Federal University of Rio de Janeiro, Brazil (in Portuguese).
- Seydel R., 1988, *From Equilibrium to Chaos: Practical Bifurcation and Stability Analysis*, Elsevier Science Publishing Co., Inc., NY.
- Umeda, N., Hashimoto, H., Vassalos, D., Urano, S., and Okou, K., 2003, "Non-Linear Dynamics on Parametric Roll Resonance with Realistic Numerical Modeling", Proceedings of 8th International Conf. on the Stability of Ships and Ocean Vehicles (STAB'2003), Madrid, pp. 281-290.

An Analysis of the Parametric Roll Events Measured Onboard the PCTC AIDA

Jianbo Hua, *SSPA Sweden AB*

Mikael Palmquist, *Seaware AB*

Georg Lindgren, *Lund University*

ABSTRACT

Between February 1 and 4, 2004, the PCTC AIDA experienced head sea parametric rolling at five different occasions, which was recorded by an onboard operational decision support system.

By applying the common wave spectrum theory together with the ship dynamics theory appropriate for the parametric roll, it could be shown that the parametric roll could not occur to the PCTC AIDA at the onboard evaluated and hind-cast sea conditions expressed in term of a PM-spectrum with 12.6s –13.5s peak period. However, the heave and pitch motions were shown to be quite regular under the time intervals, during which the recorded successively growing roll motions took place. It can then be deduced that the ship-encountered waves were quite regular during these times. Both wave amplitude and wave period could be estimated from the measured instance heave and pitch motions. By time-domain simulation, it has been shown that the parametric rolls can occur to the present ship in these regular waves and get the magnitudes quite near the recorded ones.

Keywords: *Parametric roll, simulation, full-scale measurements, wave groups*

1. INTRODUCTION

It is well known that ships based upon the RoRo-concept can be subjected to considerable variation of metacentric height due to the wave profile along the ship. This problem was addressed as early as in 1980s after some capsizing accidents. Huss (1988) conducted a systematic investigation on the influence of hull form of RoRo-ships on the GM-variation in waves. The conclusion was that the hull forms optimized for efficient cargo handling and low resistance are more sensitive to the GM-variation in waves than conventional hull forms.

One consequence is that ships with considerable GM-variation in heading or following

waves are vulnerable for an unstable roll phenomenon called for parametrically excited roll. The magnitude of the GM-variation, ratio of the roll natural frequency to the encounter frequency and the roll damping are the main parameters governing the occurrence of this kind of roll problem.

Under a series of seakeeping model test in MDL, the seakeeping wave basin at SSPA, for a RoRo-ship by Söderberg (1985), the parametrically excited roll motions were measured. The same RoRo-ship was later used by Hua (1992) in a time-domain simulation study based a nonlinear strip numeric model, taking the coupling between the roll, heave and pitch into account, the parametrically excited roll motions were re-constructed in heading and following waves, fairly in agreement with the

model measurements.

In February 2003, the Wallenius PCTC M/V Aida experienced a sudden violent rolling in rough head sea southwest of the Azores. Roll angles as large as 50 degrees were read off the bridge inclinometer. When this incident was post-analysed it was found that the conditions were such that parametric rolling was the most likely cause. Partly due to this incident, M/V Aida was equipped with a measurement system in December 2003 for trial during the winter. Between February 1 and 4, 2004, the PCTC AIDA experienced head sea parametric rolling at five different occasions, although not as critical as in 2003, which was recorded by the onboard system, for details see Palmquist and Nygren (2004).

To the authors' knowledge, this is the first time that parametric rolling is recorded in full scale during normal operation. Actually, the parametric rolling occurred in a rather moderate sea state with a significant wave height well below the threshold wave height for this ship according to IMO MSC/Circ.707. In this paper, an analysis is conducted in order to identify the underlying factors causing the parametric rolling.

The main particulars of AIDA and loading condition at the recording occasion are listed in table 1.

Table 1 Main particulars of AIDA and loading condition at the recording occasion.

Lpp	190 m
B	32.26 m
Draught	9.34 m
Trim	0.68 m
KG	13.6 m
Displacement	34091.4 ton
GM	1.38 m

2. DATA FROM ONBOARD RECORDING

Among other functions, the Seaware En-Route Live[®] system conducts 6 d.o.f. ship motion measurements, on site wave spectrum

evaluation based upon the measured motions. In addition to this it provides a recording functionality that continuously records parameters such as ship motions, wind speed and direction from anemometer, ship speed and course from GPS, evaluated seastate and more.

Figure 1 below shows the recorded data during the entire voyage. The first graph shows measured heave, pitch and roll in terms of significant values during 2 minutes blocks of motion samples with a sampling frequency of 10 Hz. As seen, sudden and relatively large rolling occurred 5 times during 2 and 3 Feb 2004. The second and third graphs show mean values of wind speed and relative wind direction during 2 minutes blocks (based on approximately 1 Hz sampling frequency). Relative wave direction is defined so that 0 degrees represents head wind (positive values means wind on starboard side, negative on port side). The fourth (lower) graph displays significant wave height and mean zero-crossing period as estimated by the measurement system. The wind wave direction used for wave estimations is assumed to equal a moving average of the wind direction. **Figure 2** shows the measured time series of heave, pitch and roll at 2004-02-02 14:55:48UTC, and **Figure 3** at 2004-02-03 16:06:44UTC.

Hindcast wave spectra at the times of parametric rolling were obtained from the Swedish Meteorological and Hydrological Institute (SMHI) and compared against evaluated wave spectra by the measurement system. The hindcast wave spectra represent analysis fields for the time of concern, computed at European Centre for Medium-Range Weather Forecasts (ECMWF). In Figure 4 and Table 2, hindcast and evaluated wave spectra for the position of M/V Aida at 1200 UTC 2004-02-02 shows fairly good agreement, having almost identical peak periods. Table 3 is a corresponding comparison for 2004-02-03 at the time of large rolling. These also compare fairly well, although the evaluated peak period is approximately 1.5 s larger than for the hindcasts.

As mentioned in the introduction of this pa-

per, M/V Aida experienced far more extreme rolling in head sea the year before, in February 2003. As the loading conditions were quite similar, it is interesting to compare hindcast wave spectra for the two occasions. In Figure 4 it can be seen that the hindcast wave spectra for 2003-02-17, i.e. last years incident, is very similar to the hindcast wave spectra for 2004-02-02. The severe rolling experienced at 2003-02-17 can then be deduced most probably as a parametric roll.

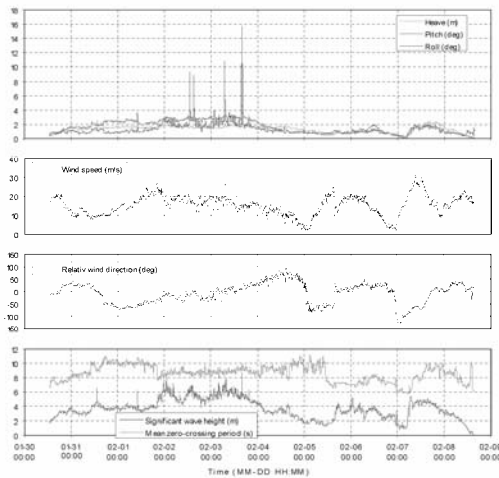


Figure 1 Overview of the voyage in terms of recorded motions, wind and wave conditions as estimated by the measurement system.

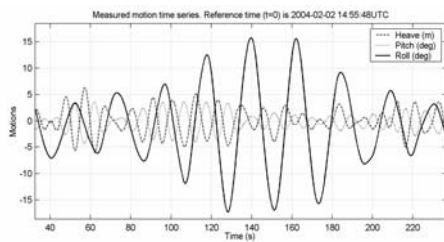


Figure 2 Measured time series of heave, pitch and roll at 2004-02-02 14:55:48UTC. Positive pitch is bow down, positive heave is upwards and positive roll is to starboard side.

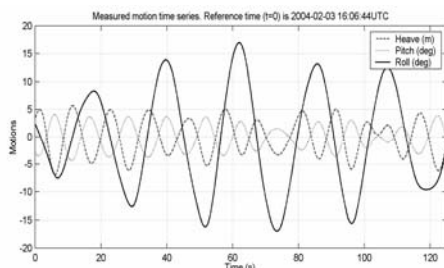


Figure 3 Measured time series of heave, pitch and roll at 2004-02-03 16:06:44UTC. Positive

pitch is bow down, positive heave is upwards and positive roll is to starboard side.

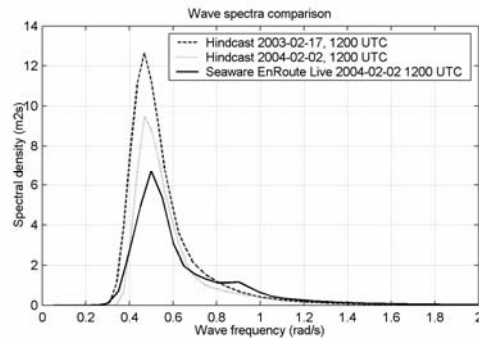


Figure 4 Comparison of wave spectra: Estimated wave spectra 2004-02-02, hindcast wave spectra 2004-02-02 and hindcast wave spectra for incident 2003-02-17. The peak periods were almost identical at the two occasions.

Table 2 Comparison of significant wave height and peak period 2004-02-2 – hindcast vs evaluated

	Sign. wave height, H_s (m)	Peak period, T_p (s)
Hindcast	5.6	13.4
EnRoute Live	~5.2-6.0	~12.7-13.2

Table 3 Comparison of significant wave height and peak period 2004-02-3 hindcast vs evaluated

	Sign. wave height, H_s (m)	Peak period, T_p (s)
Hindcast 12UTC	4.5	12.6
Hindcast 18UTC	4.3	12.6
EnRoute Live 16UTC	~5.1-6.0	~13.5-14.0

3. ANALYSIS OF THE ROLL EVENTS

3.1 Characteristics of the GM-Variation

So long as roll amplitude is limited, the parametric roll of a RoRo-ship can be expressed in the following single roll equation

$$\ddot{\phi} + D(\dot{\phi}) \cdot \dot{\phi} + \omega_0^2 \left\{ 1 + \frac{GM(t)}{GM_0} \right\} \cdot \phi = \omega_0^2 \cdot \phi_{bias} \quad (1)$$

In the above, $GM(t)$ is GM-variation as function of time when a wave passes through the ship. The contributing components to the GM-variation are the hydrostatic effect due to heave and pitch motion, effects of incident wave potential, radiation and diffraction potential. In Hua (1992), a nonlinear strip approach was applied for time domain simulation of parametric roll of a RoRo-ship in heading and following waves taking the coupled roll, heave and pitch into account while the radiation and diffraction effect on the GM-variation were calculated with a rough simplification. The numerical result shows that the radiation and diffraction effect were insignificant and the simulated parametric rolls were in fair agreement with the model measurements. Theoretically, the radiation and diffraction effect on the parametric excitation are in magnitude one order lower compared to the hydrostatic effect and the effect of incident wave potential respectively, and decrease with increasing wavelength. Thus, it is reasonable to take only the hydrostatic effect and the incident wave potential effect into consideration when analyzing the characteristics of the GM-variation of a ship in waves and for making quantitative study of the parametric roll.

The GM-variation of a ship in an irregular wave can be expressed as a Volterra system as the following, according to Hua (1995),

$$\partial GM(t) = \sum_i \partial GM_i(t) \quad (2)$$

where;

$$\begin{aligned} \partial GM_1(t) = & \sum_{n=1}^N a_n \cdot [f_1(\omega_n) \cdot e^{-i(\omega_n t + \beta_n)} + f_1^-(\omega_n) \cdot e^{i(\omega_n t + \beta_n)}] \\ \partial GM_2(t) = & \sum_{m=1}^M \sum_{n=1}^N a_m \cdot a_n \cdot \left[\begin{aligned} & u_2(\omega_m, \omega_n) \cdot e^{-i[(\omega_m + \omega_n)t + \beta_m + \beta_n]} + \\ & u_2^-(\omega_m, \omega_n) \cdot e^{-i[(\omega_m - \omega_n)t + \beta_m - \beta_n]} \end{aligned} \right] \\ & + \sum_{m=1}^M \sum_{n=1}^N a_m \cdot a_n \cdot \left[\begin{aligned} & v_2(\omega_m, \omega_n) \cdot e^{i[(\omega_m - \omega_n)t + \beta_m - \beta_n]} + \\ & v_2^-(\omega_m, \omega_n) \cdot e^{i[(\omega_m + \omega_n)t + \beta_m + \beta_n]} \end{aligned} \right] \end{aligned}$$

and so on for the higher order GM-variation.

In the above, a_m and a_n are the amplitudes of the regular wave components in an irregular wave. $f_1(\omega_n)$ and $f_1^-(\omega_n)$ are the complex first order transfer function of the GM-variation. $u_2(\omega_m, \omega_n)$ and $u_2^-(\omega_m, \omega_n)$ are the complex second order transfer function for the high frequency part, and $v_2(\omega_m, \omega_n)$ and $v_2^-(\omega_m, \omega_n)$ for the slow varying part, see Appendix for details.

Generally, the first order GM-variation is a governing factor to the parametric roll of a ship in heading waves. Figure 5 shows the first order transfer function for the GM-variation of the present ship in heading waves. The forward speed is 10 knots. As can be seen, the transfer function gets its maximum at wavelengths of near 0.6 times the ship length. However, the GM-variation becomes much lower than the half of the maximum when the wavelength becomes longer than the ship length.

The peak frequency of the wave spectrum is about 0.5 rad/s at the occasion when the parametric roll events were recorded, according to the hind cast. PM-spectrum is assumed in this study for approximate description of the wave spectrum. The wavelength corresponding to the peak frequency becomes 247.6m and its ratio to the ship length about 1.3. By Figure 5, the first transfer function can be estimated to be somewhat over 0.2 m/m at this frequency.

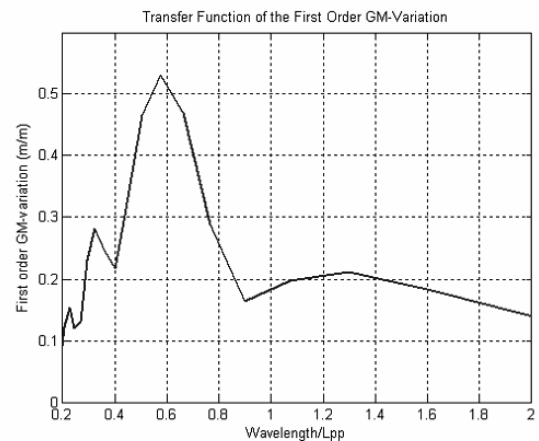


Figure 5 Transfer function of the first order GM-variation.

The spectrum of the GM-variation corresponding to the previous wave condition is shown in Figure 6. As can be seen, the highest spectrum peak is located at the wave frequency 0.7 rad/s, not the same as the corresponding wave spectrum, and the spectrum shape becomes wider. The major part of the spectrum area is located between 0.6-0.9 rad/s. That means that GM-variation in time domain is very irregular regarding the instance zero-cross period. A typical time series of the GM-variation is demonstrated in Figure 7, which shows that the zero-cross instance period changes from 5s to 8s from one cycle to another and its ratio to the natural roll period becomes between 0.215- 0.348. These ratios are relatively far below 0.5, which is required for parametric roll.

Figure 10 shows that this zero-cross mean period increases with increasing peak period of PM-spectrum. However, the maximal zero-cross mean period is still below 7s for the peak period up to 15s. This means that zero-cross period variation alone cannot explain parametric roll in the present ship in heading waves with peak period up to 15s, assuming a PM-spectrum is relevant for description of the wave condition.

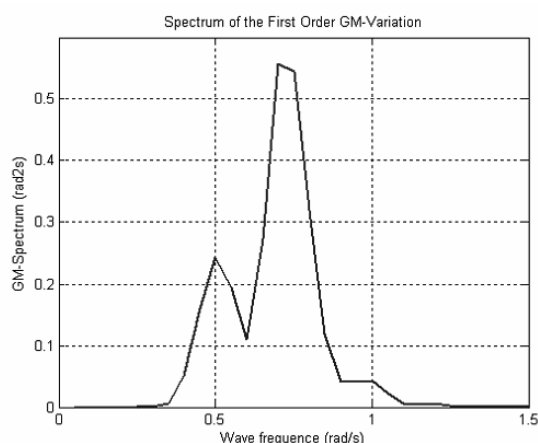


Figure 6 The energy spectrum of the first order GM-variation calculated from the wave energy spectrum (PM-spectrum with $H_s=5.5$ m and $T_p=12.6$ s) and the transfer function of the first order GM-variation in Figure 5.

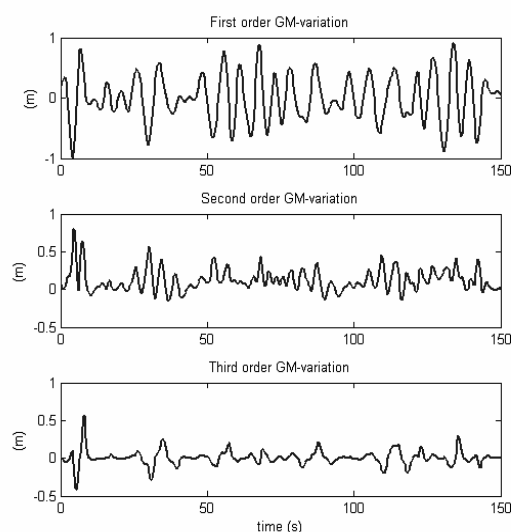


Figure 7 Time series of the first, second and third order GM-variation as function of time.

The zero-cross instance periods shown in Figure 7 are quite irregular and it could be argued that a more regular wave pattern is needed for parametric roll to occur. Such a regular pattern is in fact possible around GM-crests which are considerably higher than average. Figure 8 shows GM-variations with amplitudes higher than 1m. The figure shows 50 s of the variation around the peak instance. Figure 9 shows a histogram of the zero-cross periods close to the high peak, compared to a histogram of all zero-cross periods. The coefficient of variation is 10% with high amplitudes, much smaller than the 33% for all periods, indicating that wave groups become more regular with the presence of one high amplitude cycle. A more detailed study of the length of wave groups for high amplitude cycles is under way, and will be presented elsewhere.

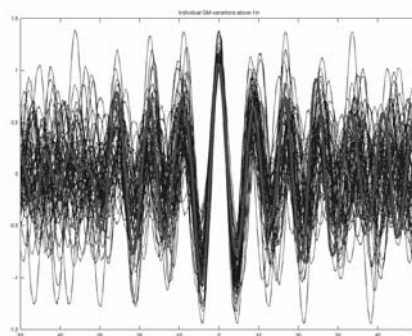


Figure 8 Individual GM-variation above 1m.

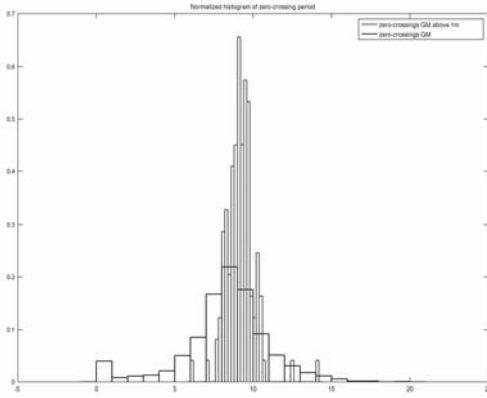


Figure 9 Normalized histogram of the zero-cross periods close to the high peak, compared to a histogram of all zero-cross periods.

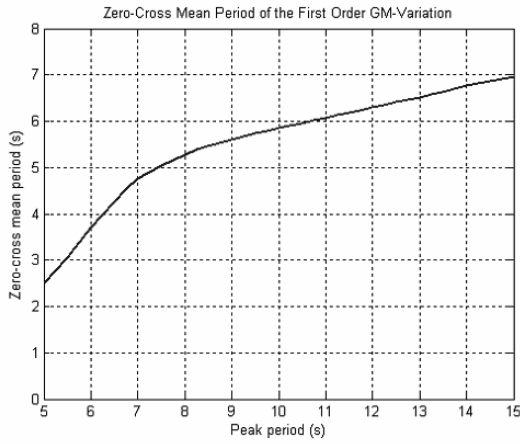


Figure 10 Zero-cross mean period of the first order GM-variation as function of wave peak period of PM-spectrum.

3.2 Roll Simulation

Since the measured maximal roll amplitude is below 20 degrees, it is relevant to apply the single roll equation in (1) for time domain simulation for analysis of the measured parametric rolls of the ship in the encountered wave conditions.

$D(\dot{\phi})$ in (1) is the non-linear roll damping coefficient as function of roll velocity, and expressed as the following

$$D(\dot{\phi}) = 2 \cdot \omega_0 \cdot \rho_0 + 2 \cdot \rho_1 \cdot |\dot{\phi}| \quad (3)$$

where ρ_0 is the coefficient for the linear part, and ρ_1 for the quadratic part. ω_0 the natural roll frequency in calm water,

Here, $\rho_0=0.03$ and $\rho_1=0.405$ are used so that the equivalent linear roll damping become 15% at 20 degrees roll amplitude according to the following definition

$$\rho_e(a_\phi) = \rho_0 + \frac{8}{3 \cdot \pi} \rho_1 \cdot a_\phi$$

so that

$$D(\dot{\phi}) = 2 \cdot \omega_0 \cdot \rho_e(a_\phi) \quad (4)$$

where a_ϕ is the expected roll amplitude. This roll damping is fair assumed according to our experience from model measurements for this kind of ship.

Time-domain simulations of the single roll equation in (1) have been conducted, using the time history of the GM-variation in the hind cast wave conditions as input and an initial roll angle of 3 degrees. Actually, no parametric roll could be observed in these simulations. This result could be expected since the zero-cross mean period of the GM-variation is about 6.5s, too low to approach 11.6s, which is required to meet the condition for the occurrence of parametric roll of the present ship. Besides, the instance zero-cross period of the GM-variation changes considerably from one period to another as shown in Figure 7.

However, the heave and pitch motion were quite regular in the time intervals during which the roll motions are successively growing, see Figure 2 and Figure 3. Both heave and pitch motion frequencies are almost twice the natural roll frequency. This can be deduced as that the instance wave encountered by the ship must be nearly regular regarding the wave period. The instance wave amplitude is estimated to be about 4m to 5m, by comparing the measured heave and pitch amplitude with the calculated transfer functions of heave and pitch respectively. The amplitude of the first order GM-

variation becomes then about 0.6m or more and its ratio to the initial GM becomes over 0.4.

Thus regular waves are assumed to cause the GM-variations in equation (1) and time domain simulations of parametric roll have been conducted. Figure 11 shows a time history of a simulated roll motion of the present ship in a regular wave. The wave frequency is 0.44 rad/s and the wave amplitude 4m. By increasing the wave amplitude from 4m to 5m, the highest roll angle becomes some degrees higher after 100s, comparing Figure 12 with Figure 11. Actually, the roll motions in Figure 11 and Figure 12 are very similar to the ones in Figure 2 and Figure 3 at the time intervals during which the parametric roll took place.

The pitch and heave motion are taken into account when calculating the GM-variations. Since the encounter frequency is relatively low, the radiation and diffraction effect on the GM-variation should be small and insignificant regarding the parametric roll. Thus, the roll motions in Figure 11 and Figure 12 from the time domain simulation of the single roll equation in (1) should be considered as good approximations of what occurred to the PCTC AIDA during Feb 2 to Feb 3 2004. Consequently, it can be concluded that close to regular waves might cause the recorded parametric roll events.

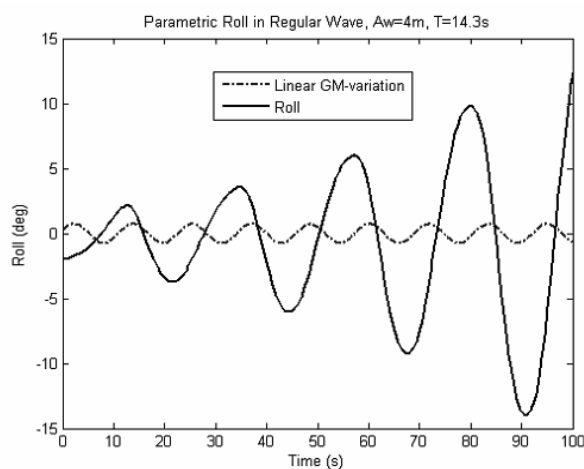


Figure 11 Parametric roll in a regular heading wave. The wave amplitude is 4m.

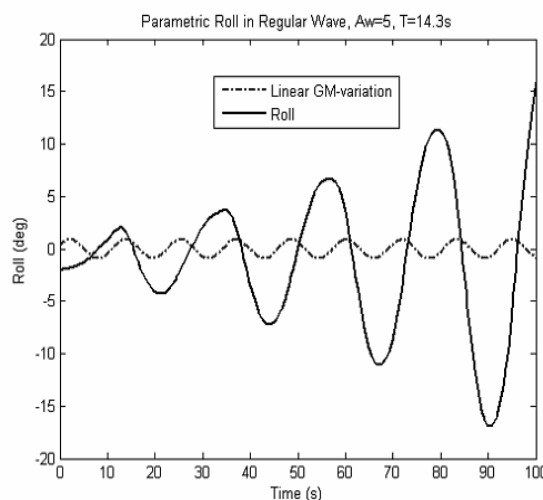


Figure 12 Parametric roll in a regular heading wave. The wave amplitude is 5m.

4. DISCUSSION AND CONCLUSION

By applying the common wave spectrum theory together and the ship dynamics theory appropriate for the parametric roll, it could be shown that the parametric roll could not occur to the PCTC AIDA at the onboard evaluated and hint-cast sea conditions expressed in term of a constant PM-spectrum with 12.6s peak period. That is because the zero-cross mean period of the GM-variation becomes about 6.5s, which is far below the required 11.6 s period half of the natural roll period. Besides, the GM-variation is too irregular in term of instance zero-cross period to be an excitation source required to cause the parametric roll motion of the ship.

However, the heave and pitch motions were shown to be quite regular under the time intervals, during which the recorded successively growing roll motions took place. It can be deduced as that the ship-encountered waves were quite regular during these times. The instance wave amplitude is estimated to be about 4m-5m under the roll events at 2004-02-02 14:55:48UTC and 2004-02-03 16:06:44UTC, and the instance wave period about 13s to 14.3s. By time-domain simulation of the single roll equation in (1), it has been shown that the parametric rolls can occur to the present ship in

these regular waves and get the magnitudes quite near the recorded ones.

The PCTC AIDA experienced similar wave condition in February 2003, and a sudden violent rolling up to 50 degrees was observed. According to the present analysis, it can also be deduced that that event could be caused by several almost regular waves of greater magnitude.

Normally, a wave spectrum provided by weather service is in general an average spectrum over at least 15 minutes up to 2 hours and over a large sea area. As matter of fact, an instance wave spectrum from two minutes wave record can be quite different from the average one. However, knowledge is lacking about the probability of the instance wave spectrum in term of instance peak period, which is required for the risk assessment of the parametric roll such ones as the PCTC AIDA has experienced.

5. REFERENCES

Hua, J., 1992" A Study of the Parametrically

Excited Roll Motion of a RoRo-Ship in Following and Heading Waves ", International Shipbuilding Progress, 39, no.420 pp.345-366

Hua, J., 1995, " On the Dynamic Stability Problems of RoRo-Ships , Doctoral thesis, Div. of Naval Architecture, Dept. of Vehicle Engineering, Royal Institute of Technology, S-100 44 Stockholm, Sweden.

Huss, M., 1988, "The Stability of Ships in Waves; a comparative study of modern hull forms with large B/T ratio", TRITA-SKP 1060, The Royal Institute of Technology, Sweden.

Palmquist, M. and Nygren, C. 2004, Recordings of head-sea parametric rolling on a PCTC, SLF 47/INF.5, IMO SUB-COMMITTEE ON STABILITY AND LOAD LINES AND ON FISHING VESSELS.

Söderberg, P. 1985, "Ro-Ro/Containerfartyg och färjor - rullning ", Transportforskningsdelegation, SSPA Report 3534-. In Swedish

6. APPENDIX

6.1 GM-variation Expressed as a Volterra system

Mathematically, the sectional beam of a ship as a function of draught can be expanded around the mean draught $T(x)$ as a Taylor Series;

$$B(x, T(x) + z) = B(x, T(x)) + \frac{\partial B}{\partial z} \cdot z + \frac{1}{2!} \frac{\partial^2 B}{\partial z^2} \cdot z^2 + \frac{1}{3!} \frac{\partial^3 B}{\partial z^3} \cdot z^3 + \dots \quad (5)$$

where z is a variable for the sectional draught change.

As well for the sectional moment with the keel line as reference;

$$M(x, T(x) + z) = M(x, T(x)) + \frac{\partial M}{\partial z} \cdot z + \frac{1}{2!} \frac{\partial^2 M}{\partial z^2} \cdot z^2 + \frac{1}{3!} \frac{\partial^3 M}{\partial z^3} \cdot z^3 + \dots \quad (6)$$

and the sectional area;

$$A(x, T(x) + z) = A(x, T(x)) + \frac{\partial A}{\partial z} \cdot z + \frac{1}{2!} \frac{\partial^2 A}{\partial z^2} \cdot z^2 + \frac{1}{3!} \frac{\partial^3 A}{\partial z^3} \cdot z^3 + \dots \quad (7)$$

For the sake of simplicity, we express (5), (6) and (7) as followed;

$$B(x, T(x) + z) = B(x, T(x)) + c_1(x) \cdot z + c_2(x) \cdot z^2 + c_3(x) \cdot z^3 + \dots \quad (8)$$

$$M(x, T(x) + z) = M(x, T(x)) + d_1(x) \cdot z + d_2(x) \cdot z^2 + d_3(x) \cdot z^3 + \dots \quad (9)$$

$$A(x, T(x) + z) = A(x, T(x)) + e_1(x) \cdot z + e_2(x) \cdot z^2 + e_3(x) \cdot z^3 + \dots \quad (10)$$

where;

$$\begin{aligned} c_1(x) &= \frac{\partial B}{\partial z}, & c_2(x) &= \frac{1}{2!} \frac{\partial^2 B}{\partial z^2}, & c_3(x) &= \frac{1}{3!} \frac{\partial^3 B}{\partial z^3} \dots \\ d_1(x) &= \frac{\partial M}{\partial z}, & d_2(x) &= \frac{1}{2!} \frac{\partial^2 M}{\partial z^2}, & d_3(x) &= \frac{1}{3!} \frac{\partial^3 M}{\partial z^3} \dots \\ e_1(x) &= \frac{\partial A}{\partial z}, & e_2(x) &= \frac{1}{2!} \frac{\partial^2 A}{\partial z^2}, & e_3(x) &= \frac{1}{3!} \frac{\partial^3 A}{\partial z^3} \dots \end{aligned}$$

$c_i(x)$, $d_i(x)$ and $e_i(x)$ can be obtained numerically by using piecewisely polynomial functions fitting the section form, moment and area along the ship.

The initial metacentric height GM_0 at the mean draught in still water is calculated as followed:

$$GM_0 = KB + BM - KG \quad (11)$$

where $KB = \frac{\int_L M(x, T(x)) \cdot dx}{\Delta}$ and $BM = \frac{\int_L B(x, T(x))^3 \cdot dx}{12 \cdot \Delta}$.

The initial GM-variation of a ship in a longitudinal regular or irregular wave can then be determined by integrating the sectional contribution over the ship length;

$$\begin{aligned} \partial GM &= \frac{1}{\Delta} \cdot \int_L \left(\frac{B(x, T(x) + r(x))^3}{12} + M(x, T(x) + r(x)) - A(x, T(x) + r(x)) \cdot KG(x) \right) \cdot dx \\ &\quad - GM_0 \end{aligned} \quad (12)$$

where the sectional mass center above the keel;

$$KG(x) = KG + x \cdot (\eta_5 - \alpha_{trim})$$

η_5 is pitch motion and α_{trim} trim. The Smith-effect is neglected in (12). First displacing the variable z in (8), (9) and (10) with $r(x,t)$, the relative motion of the wave surface against ship, and putting (8), (9) and (10) into (12). After having expanded it, we get the following expression;

$$\partial GM = \sum_i \partial GM_i \quad (13)$$

where

$$\partial GM_1(t) = \sum_{n=1}^N a_n \cdot \left[f_1(\omega_n) \cdot e^{-i \cdot (\omega_n \cdot t + \beta_n)} + f_1^-(\omega_n) \cdot e^{i \cdot (\omega_n \cdot t + \beta_n)} \right]$$

and

$$\begin{aligned} \partial GM_2(t) = & \sum_{m=1}^M \sum_{n=1}^N a_m \cdot a_n \cdot \left[u_2(\omega_m, \omega_n) \cdot e^{-i \cdot [(\omega_m + \omega_n) \cdot t + \beta_m + \beta_n]} + u_2^-(\omega_m, \omega_n) \cdot e^{-i \cdot [(\omega_m - \omega_n) \cdot t + \beta_m - \beta_n]} \right] \text{ etc.} \\ & + \sum_{m=1}^M \sum_{n=1}^N a_m \cdot a_n \cdot \left[v_2(\omega_m, \omega_n) \cdot e^{i \cdot [(\omega_m - \omega_n) \cdot t + \beta_m - \beta_n]} + v_2^-(\omega_m, \omega_n) \cdot e^{i \cdot [(\omega_m + \omega_n) \cdot t + \beta_m + \beta_n]} \right] \end{aligned}$$

$f_1(\omega_n)$ and $f_1^-(\omega_n)$ are the first order complex transfer functions for the GM-variation. $u_2(\omega_m, \omega_n)$, $u_2^-(\omega_m, \omega_n)$, $v_2(\omega_m, \omega_n)$ and $v_2^-(\omega_m, \omega_n)$ are the second order complex transfer functions. Detailed information about the calculation of the transfer functions can be found in Hua 1995.

Numerical Procedures and Practical Experience of Assessment of Parametric Roll of Container Carriers

Vadim Belenky, *American Bureau of Shipping*

Han-Chang Yu, *American Bureau of Shipping*

Kenneth Weems, *Science Application International Corporation*

Abstract

The paper examines several aspects related to practical assessment of parametric roll of container carriers. The numerical procedure is based on application of the Large Amplitude Motion Program (LAMP), the nonlinear potential flow code. Viscous roll damping is included from the roll decay test. The rational choice of the loading conditions is considered. Practical non-ergodicity of the response is taken into account.

The paper also examines the way to make the development of the polar diagram more efficient. Using an envelope presentation for the irregular wave may yield a way to work with parametric roll in probability rather than in time domain. A single wave group should then be considered as an elementary random event.

Keywords: *Parametric roll, Numerical simulation Polar diagram, Envelope presentation*

1. INTRODUCTION

The problem of large amplitude roll motions caused by parametric resonance, though known for quite some time, recently made its reappearance in relation to an accident with a large container carrier, (France *et al* 2003). This paper describes the development of on-board information required by the Guide on Parametric Roll (ABS, 2004).

Below is a brief literature review on the related subject.

The physical phenomenon of parametric roll was one of the focuses of the 8th International Ship Stability Workshop that was hosted by Istanbul Technical University on October 6th and 7th, 2005 in Istanbul, Turkey.

The paper by Neves and Rodríguez (2005) looking into a new mathematical model with nonlinearities defined up to the third order in

terms of the heave, roll and pitch couplings is introduced in order to simulate strong roll parametric amplifications in head seas. The influence of hull stern shape is discussed. A theoretical analysis discloses some essential dynamical characteristics associated with the proposed coupled third order mathematical model.

The paper by Umeda *et al* (2005) reviews the latest developments at Osaka University and, among others, includes theoretical prediction techniques for magnitude of parametric rolling. Poincaré mapping and averaging method were then used to obtain the magnitude of parametric roll.

A paper by Ikeda *et al* (2005) describes a model test carried out to evaluate the effect of bilge keels on parametric roll in beam seas. In the considered case, the amplitude of parametric roll decreased from 25 degrees to almost zero.

A number of papers related to parametric roll were considered at the 48th SLF. The paper SLF 48/4/12 considered parametric roll in relation to the new Intact Stability Code. Several important points were made: (1) regular wave case may be more complicated due to nonlinear behavior, (2) regular wave case appears to be more severe than irregular wave case, (3) for the irregular wave case, the probability distribution is not Gaussian. Other relevant papers at SLF-48 were focused on updating of the MSC Circular 707. The paper SLF 48/4/4 contains guidelines for all types of ships, while definition of parametric roll conditions are based on $T_R \approx 2T_E$ (T_R natural period of roll, T_E encounter period of waves) while wave length is between $0.8L$ and $1.2L$. The paper SLF 48/4/8 also suggests that the MSC Circ. 707 guidelines be made applicable to all types of ships as far as parametric roll is concerned. The paper addresses both wave pass effect and pitch coupling and recommends changing speed and heading in order to avoid the encounter period being twice the natural roll period. The papers SLF 48/4/16 and SLF 48/4/17 describe diagrams which are meant to be present on board a vessel. Parametric roll criterion is based on the frequency range $1.9 T_E < T_R < 2.1 T_R$.

Papers focused on parametric roll in head and following seas also were considered during the 7th International Ship Stability Workshop that was hosted by Shanghai Jiao Tong University on 13 November 2004 in Shanghai, China.

Spyrou (2004) examines an approximation of transient solution of a Mathieu equation to estimate how quickly parametric roll rises. The influence of restoring nonlinearity is studied and parametric roll response is found outside of the asymptotic instability zone. The probabilistic aspect includes an envelope presentation, which leads to a formula for joint probability of height of two consecutive waves above the given threshold. The Markov chain could be used to obtain the result for the entire wave group.

The paper by Bulian *et al* (2004) presents the preliminary results of an analytical, numerical and experimental study regarding the problem of non-ergodicity of parametric roll in longitudinal irregular long-crested waves. A series of numerical simulations is performed with 1.5-DOF model of parametrically excited roll motion. Qualitative indications given by the numerical simulations were then compared with experimental tests, showing good agreement

2. POLAR DIAGRAMS AS A FORM OF ON-BOARD INFORMATION

2.1 Format and Information Included

Polar diagrams in wave heading/speed coordinates are a convenient way to present any numerical information for on-board use (see e.g., MSC Circ. 707). Polar diagrams for parametric roll were discussed by Shin, et al, (2003, 2004) and were recommended by ABS (2004). A Generic Polar Diagram for Parametric Roll was proposed by SLF 48/4/4.

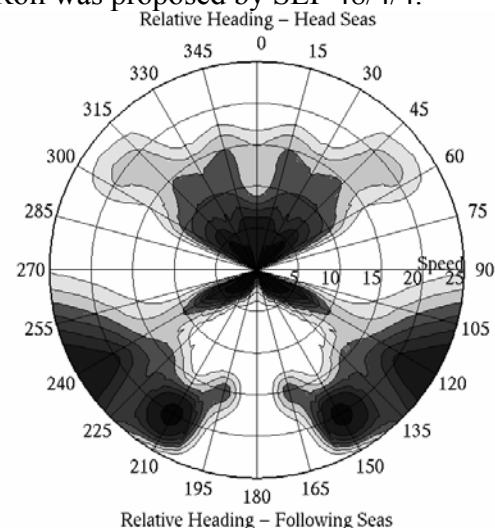


Figure 1 Sample polar diagram, Bretschneider spectrum, with significant wave height of 12.5 m and zero-crossing period of 11.5 seconds

Polar diagrams for parametric roll considered in this paper are a further development of format (ABS, 2004). They represent the maximum roll angle observed during a one-hour simulation limited by lashing

(ABS, 1988) and engine criteria (ABS, 2006). The area of the diagram where maximum roll angle did not exceed these criteria remains black. The area where these criteria were exceeded is color-coded in different types of yellow and red (from 22 to 40 degrees) in accordance with the value of observed angle. See Figure 1.

2.2 Intended Use of Polar Diagrams

These polar diagrams have been developed as a planning tool and are not intended for use when a vessel is already experiencing extreme roll motions. Real-time use of a polar diagram would be difficult. An experienced sailor is capable of evaluating significant wave height, but nearly no one could tell the exact wave heading with the naked eye. Decreased visibility and nighttime makes estimate of wave parameters even more difficult.

Most large container carriers nowadays use a weather routing service that usually includes a weather map that is updated every six hours. When a storm is on the route and a master is considering options, the polar diagrams are expected to be most useful. A weather map would include wave direction, so determining wave heading when the vessel encounters a storm will not be difficult. The speed will be also known as speed loss in waves is also known from operation experience. These two figures will determine the position of the point on the polar diagram corresponding most closely to current loading condition and expected significant wave height and zero-crossing periods of waves.

3. DEVELOPMENT OF POLAR DIAGRAMS

3.1 Principal Numerical Tools

Parametric roll resonance is a result of changing stability in waves, so a minimum requirement for any numerical simulation tool is

a capability to compute hydrostatic forces on instantaneous submerged surface. Such software would be capable of reproducing the phenomenon, but in order to achieve numerical accuracy sufficient for practical purposes, roll damping has to match experimental results (France, et al 2003).

With computational capability currently available for mass use, application of potential hydrodynamic methods seems to be a viable, practical solution. Viscous and vortex-induced forces could be added as external components to facilitate matching of roll damping to experimental results.

Two numerical tools which meet these requirements for evaluating parametric roll are the Large Amplitude Motions Program (LAMP) and NLOAD3D codes. Both of these codes are time-domain ship motions and loads prediction codes that are built on a 3-D potential flow solution of the wave-body hydrodynamic interaction problem. Both incorporate an approximate body-nonlinear approach (Weems, et al, 2000), which computes the incident wave forcing and hydrostatic restoring pressure on the actual wetted hull surface while solving for the hydrodynamic disturbance potential on the mean wetted surface using the instantaneous ship velocity and a combined body boundary condition. This approach is sophisticated enough to capture the critical hydrodynamic phenomena associated with parametric roll while remaining fast enough to run the large number of simulations required to build the polar diagrams.

Of the two, the LAMP code is the more general implementation of the approach and suitable for multi-hull and high-speed displacement ships as well as conventional monohulls. NLOAD3D has been specifically developed for large commercial ships. Key features of NLOAD3D include an automated procedure for calibrating roll damping based on experimental roll decay data and an integrated module for setting up and running dozens of simulations over a range of speeds, headings,

and wave realizations for the polar diagram.

3.2 Environmental and Loading Conditions

Parametric roll, as with any other resonance phenomenon, is quite sensitive to excitation frequency range as well as to natural frequency of the dynamical system. Excitation frequency range is defined by a geographical region of ocean, season and other meteorological and oceanographic factors. The most precise way to present such a range is to use measured or hindcasted wave spectrum in the region of interest. Although precise, such a method is quite expensive, as the set of diagrams then becomes route-specific and unusable for other routes.

The next best way is to use approximated spectra. Most of them have two parameters related to significant wave height and mean zero-crossing period. These figures could be obtained from wave statistics-based scatter diagrams. Here, an averaged scatter diagram from IACS Recommendation 34 was used.

In order to develop set route-independent diagrams, simulations have to be performed for a series of significant wave heights and zero-crossing periods. In lieu of any other data, the simulations are performed for three most probable mean zero-crossing periods for each significant wave height. The calculations start from survival condition with 14.5 m of significant wave height and are repeated for smaller significant wave height (2 meters as a step was used in this case) until large roll motions no longer present a practical problem.

The natural roll frequency is most sensitive to GM , therefore, the choice of loading conditions has to cover the entire range of operational values of GM . In lieu of sensitivity analysis, using a smaller step for GM , where the most frequent loading conditions are, seems to be a quite practical idea.

3.3 Roll Damping Calibration

Being potential flow time-domain simulation codes, LAMP and NLOAD3D calculate only the wave component of roll damping, so the rest of the roll damping moment (vortex and friction components) has to be added. At the same time, there are no reliable methods of extracting these contributions from the result of the roll decay test. Based on previous experience (France, *et al* 2003), the best way to get a realistic simulation with respect to roll damping is to calibrate the code to produce the same results as the roll decay test.

Non-potential roll damping moment is accepted in quadratic form

$$R(\dot{\phi}) = B_1 \dot{\phi} + B_2 |\dot{\phi}| \dot{\phi} \quad (1)$$

Here, B_1 is the linear damping coefficient and B_2 is the quadratic damping coefficient.

Following the standard procedure of processing of results of the roll decay test, a straight line is fitted, using points on the roll decrement chart

$$D = k \cdot Amp + f \quad (2)$$

Here, D is a relative decrement, Amp is roll amplitude (Amp), k is a slope and f is an intercept of the fitted line.

The calibration procedure for roll damping is essentially a numerical “roll decay test” being repeated for different values of damping coefficients B_1 and B_2 with the following standard roll decay processing until numerical slope and intercept would match those from the model test. This procedure could be expressed in the form of a system of two nonlinear algebraic equations and solved with any appropriate numerical method

$$(k, f) - \text{Damp}(B_1(f), B_2(k)) = 0 \quad (3)$$

Here, *Damp* is a symbolic expression for a run of numerical simulation followed by a standard procedure of roll decay processing. Symbols $B_1(f)$ and $B_2(k)$ express that the roll linear damping coefficient depends on intercept while the quadratic roll damping coefficient depends on the slope. Practical experience has shown that the calculations converge after 5-6 iterations, on average.

3.4 Consideration of Practical Non-ergodicity and Length of Record

Practical non-ergodicity of nonlinear rolling has been addressed by a number of authors since the late 1990s (Belenky *et al*, 1997, 1998, 2001, 2003, Shin, *et al*, 2004, Bulian, *et al* 2004) and was found to be especially strong in parametric roll (Belenky 2004). The reason is that waves capable of exciting parametric roll may appear in a different sequence, one after another in one wave record or separated by “harmless” waves in another one. In the last case, kinetic energy may be dispersed before the next portion of parametric excitation will come and, as a result, the roll variance may significantly differ between records.

The practical implication of the absence of ergodicity means that several statistically independent wave records have to be used for numerical simulations. Statistical independence of wave records is achieved by using different initial phases

Another aspect to be addressed is the length of a single record. As is well known (see, for example, Belenky and Sevastianov 2003), the length of a wave record modeled by the inverse Fourier Transform is related to the frequency step. If this length is exceeded, the record can no longer be considered as statistically representative. In the case of the constant frequency step, its autocorrelation function

experiences spikes that are not related to wave physics. See Figure 2.

If the frequencies are not evenly distributed, the error still exists, but it is speeded out instead of being concentrated in the form of spikes. See Figure 3.

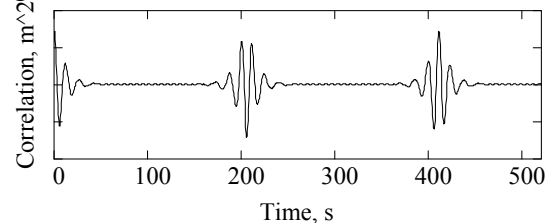


Figure 2 Wave autocorrelation function for constant frequency step.

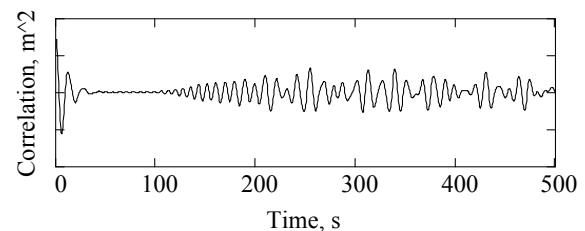


Figure 3 Wave autocorrelation function for unevenly divided frequency set.

The reason for the effect is an error in the numerical integration (Belenky 2005). The conventional inverse Fourier Transform is an equivalent of rectangular numerical integration. Respective Laplace transform allows the obtaining of the autocorrelation function directly from the spectrum:

$$R(\tau) = \int_0^{\infty} S(\omega) \cos(\omega\tau) d\omega \quad (4)$$

Here, S is spectral density, R is autocorrelation function, τ is time and ω is frequency.

It can be clearly seen that the integrand becomes quite oscillatory with time, and rectangular integration would not work well in such a case. There are integration methods that could handle oscillatory integrands¹, but their

¹ M. Pawlowski, 2005 Discussion at 8th International Ship Stability Workshop and private communication.

consideration is outside of the scope of this paper.

Practically, it means that the length of the wave record has to be chosen to avoid this error, and the constant frequency step has an advantage as the error-free length can be clearly defined with the following formula:

$$T = \frac{2\pi}{\Delta\omega} \quad (5)$$

Evidently, this length could be increased by decreasing the frequency step. However, it will lead to an increasing number of wave components necessary for correct presentation of the wave spectrum. Increasing the number of wave components may lead to a significant increase in the cost of the simulation as more components have to be added up at every time step. Based on the observation, an attempt to increase the length of the simulation twice leads to a four times increase in calculation time.

At the same time, several relatively short records do have an advantage in comparison with a fewer long ones. They not only save computation time but take care of the practical non-ergodicity problem. Obviously, statistical methods should be used to estimate the accuracy that could be achieved by different combinations of number and length of records.

3.5 Some Aspects of Topology of the Polar Diagram

As the polar diagram (such as shown in Figure 1) is a result of numerical simulation, all large amplitude roll motions are included (coming from both parametric and synchronous resonance). However, a simple analysis of frequencies could reveal motions apparently coming from synchronous resonance.

One polar diagram is generated for a specific sea state defined with significant wave height and mean zero-crossing period. Each of the two-

dimensional grid points of the polar diagram represent wave heading and ship speed. The encounter wave period can be determined using the mean zero-crossing period, wave heading and ship speed for each grid point. Large roll angles are often observed around the grid points where the encounter wave period is close to the roll natural period. This is typically due to the roll synchronous resonance rather than parametric roll response, which is mostly to occur near the grid points where the encounter period is one half of the roll natural period. For example, the large roll angle peaks around 20-25 knots speed near 60° and 300° headings in Figure 1 are typically due to roll synchronous resonance.

The most evident feature related to parametric roll is that, generally, the maximum angle is decreased with the increase of speed. This could be explained by the fact that roll damping increased with the speed raises the threshold of sensitivity to parametric excitation, so a lesser number of waves can transfer energy.

It is noticeable that for many such diagrams, the maximum of the parametric roll does not necessarily fall exactly in head seas. At the same time, head and following seas are expected to cause the most difference in stability between crest and trough of the wave. Shifting of maxima is also less noticeable for smaller speeds.

Such a shift of maximum can probably be explained by changes in encounter spectrum. As is well known, in head encounter, the spectrum becomes wider (see Figure 4, where four encountered spectra are shown, corresponding to 90, 120, 150, 180 degrees of wave heading).

As the encounter spectrum becomes broader, less energy is concentrated in the frequency range where the dynamical system is susceptible to parametric excitation. There are two competing factors; with 180 degrees of heading approaching, the dynamical system becomes more susceptible to parametric excitation due to increased wave influence on stability, and there

is less parametric excitation due to the form of the encounter wave spectrum.

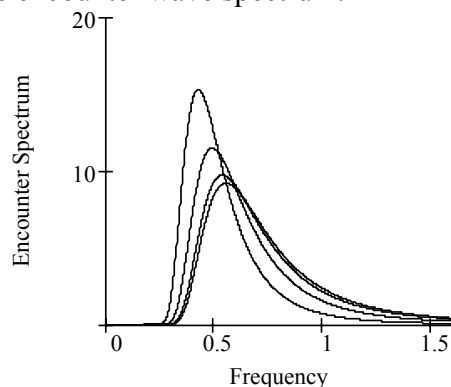


Figure 4 Transformation of encounter spectrum at 15 knots significant wave height 8.5 m

Wave direction has a smaller influence on encounter spectrum for smaller speeds; therefore, there is not as much of a shift of maximum for slower speeds.

A similar physical mechanism is responsible for topology in following seas. For the slower speeds and headings close to 90 degrees, the encounter spectrum becomes narrower, but the system already can take parametric excitation. As the concentration of energy is high (the encounter spectrum is narrow), severe parametric roll is observed. However, these conditions do not exist in the large area in the sample diagram in Figure 1 because decreasing heading and increasing speed leads to the appearance of negative encounter frequencies and even more narrow encounter spectrum. Apparently, the range of susceptible frequencies of the dynamical system is different from the frequency range of encounter spectrum, and the parametric roll mode very quickly ceases to exist.

For the cases of smaller GM , (see sample diagram in Figure 5), a significant area with parametric roll is also possible in following seas. Topology of such a diagram is generally similar to the one observed above and could be explained by the same physical reasons. Parametric roll in following seas is more likely because the low GM range of sensitivity to parametric excitation is shifted towards lower frequencies and following seas can match it.

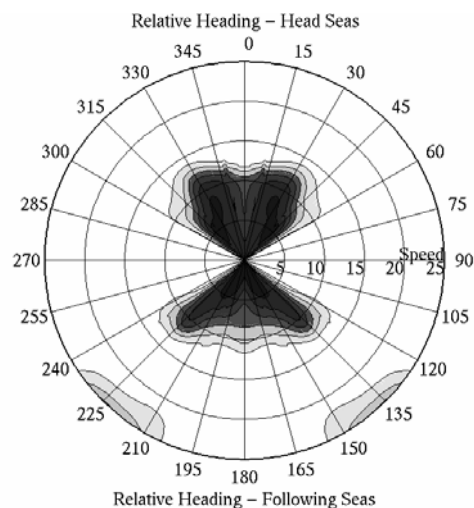


Figure 5 Polar diagram - relatively small GM Bretschneider spectrum, with significant wave height of 8.5 m and zero-crossing period of 11.5 seconds

4. RISK OF PARAMETRIC ROLL

4.1 General

The principal advantage of the polar diagrams is that they can be used as an instrument of risk assessment. The problem associated with these diagrams is that their development takes a long time (weeks) to develop. This motivates the search for more efficient ways to carry out this work.

One of the possible ways to achieve better efficiency is to search for the probability of an event that roll motions caused by parametric resonance would exceed a given value. This way is also preferable as probability of exceeding would be a more representative characteristic of risk rather than maximum roll angle during one hour.

4.2 Envelope Presentation and Wave Groups: Formulation of the Problem

The envelope presentation seems to provide the natural bridge between nonlinear dynamics with periodic excitation and realistic irregular seaway. The only evident limitation of the

envelope application is how it will work for head seas when the encounter spectrum actually becomes broader. At the same time, parametric roll could be excited in a relatively narrow band of frequencies. So, it is quite possible that the narrow-band envelope presentation still may work for parametric roll in head seas despite the fact that the encounter spectrum is no longer narrow-banded. The error in this case is done to the safe side as more regular excitation leads to faster development of parametric resonance and higher roll amplitude. So, using the envelope presentation is also a conservative approach.

The envelope presentation allows presenting the seaway as a flow of wave group encounters similar to the approach taken by Tikka and Paulling (1990). Each group is to be characterized by the length of the group and the highest wave in the group. Then, the problem is to be considered in two distinct time scales:

Small time scale is the period or time duration of several minutes. It is a roll response on the group with particular characteristics and initial conditions at the “entrance” to the group. Roll autocorrelation plays a significant roll in the small time scale problem.

Large time scale is the period of quasi-stationary waves, which is the time when statistical characteristics of waves could be assumed constant. For most of practical application, it is three or six hours (the time between weather updates). The large scale problem is a random flow of independent wave groups, each of which is associated with the roll response known from the small scale problem.

4.3 Source of Data for Envelope Presentation

The envelope presentation of a stochastic process substitutes the actual process with the combination of two other stochastic processes, amplitude $A(t)$ and phase $\Phi(t)$. For the narrow-band process, it is possible to use phase shift $\varphi(t)$ and mean frequency ω_m instead of the

phase.

$$\zeta(t) = A(t)\cos(\Phi(t)) = A(t)\cos(\omega_m t + \varphi(t)) \quad (6)$$

Stochastic processes $A(t)$ and $\cos(\varphi(t))$ are slow-change figures in comparison with $\zeta(t)$, if the latter is a narrow-band process. There are a number of theoretical results available for the elements of envelope presentation, including joint distribution for $A(t)$ and $\Phi(t)$ and their derivatives as well as autocorrelation functions for $A(t)$ and $\cos(\Phi(t))$ (see a collection of these formulae in Belenky and Sevastianov, 2003).

Using these formulae, it may be possible to generate processes $A(t)$ and $\varphi(t)$ but it seems to be more practical to obtain these data directly from time history of wave elevations calculated from given spectrum in a conventional way. Calculation of amplitudes is trivial, while calculation of phase shifts requires search of times of zero-crossing Tz_j . Linear interpolation of this figure against the times when the cosine function would cross the zero yields process $\Phi(t)$; linear interpolation was also used to convert a set of amplitude points into the process. Figure 6 shows the autocorrelation function calculated from the original process plotted along with the autocorrelation function calculated from the envelope presentation. Figure 7 shows spectra calculated from the autocorrelation function with Laplace Transform. Only positive peaks were used for the calculations shown in both figures. Using negative peaks leads to similar results.

As can be seen from these figures, the proposed scheme provides a quite adequate reproduction of the original process. A more “pointy” character of the envelope spectrum could be explained by neglecting of secondary peaks, which lead to more concentration of energy around the modal frequency.

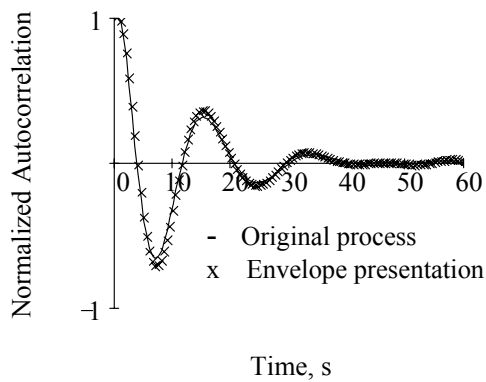


Figure 6 Autocorrelation functions for original process and envelope presentation

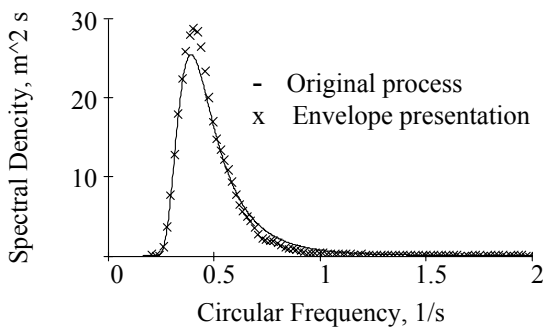


Figure 7 Spectra for original process and envelope presentation

4.4 Properties of Amplitudes and Phases

Amplitudes and phases (both Φ and φ) are stochastic processes themselves and could be characterized with respective autocorrelation functions (it is more convenient with cosine functions of phases), which are shown in Figures 8 and 9.

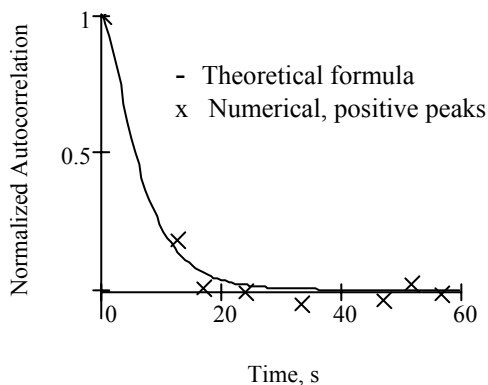


Figure 8 Autocorrelation function of amplitude

As can be seen from Figure 9, the autocorrelation function of $\cos(\Phi)$ is really close

to the autocorrelation function of the original process. It illustrates the role of phase in the envelope presentation – it keeps the memory. Autocorrelation functions of amplitude in Figure 8 and $\cos(\varphi)$ in Figure 9 show that these figures are slowly changing functions in comparison to the original process.

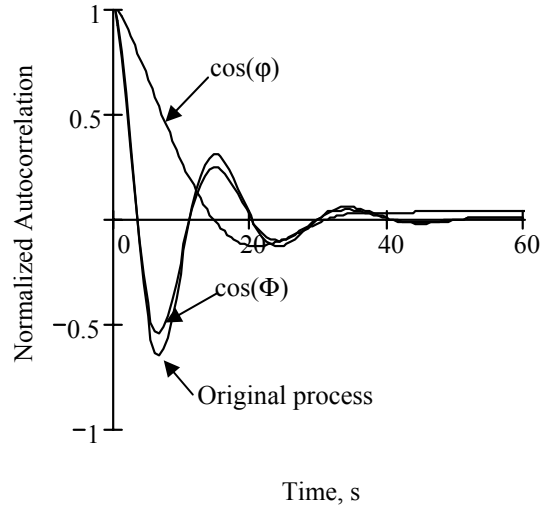


Figure 9 Autocorrelation functions original process, cosine of phase $\cos(\Phi)$ and phase shift $\cos(\varphi)$

4.5 Numerical Properties of Groups

The stochastic process of amplitudes does have its own maxima and minima. As the first expansion, the group of wave is defined as all the waves between two consecutive minima. This definition is, however, a subject for further revision, as it may lead to generation of groups that are too short.

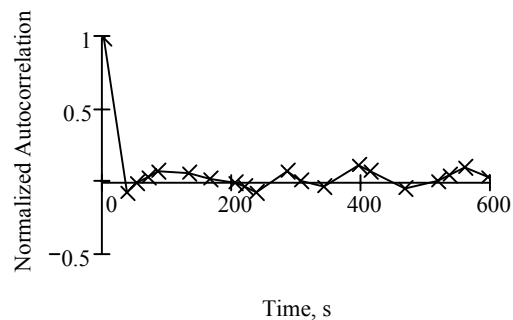


Figure 10 Autocorrelation function of group heights

Figures 10 and 11 show autocorrelation functions of group heights and lengths.

Consecutive groups could be assumed independent, as correlation drops to a small value on the second point.

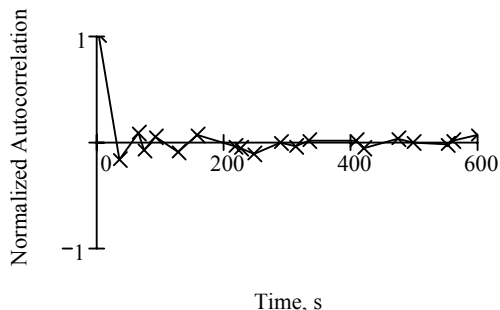


Figure 11 Autocorrelation function of group lengths

4.6 General Scheme of Numerical Assessment of Risk of Parametric Roll

Once the statistical characteristics of groups are determined by post-processing reconstructed time history of wave elevations, the entire seaway in large time scale (3-6 hours) can be presented as a flow of random events - encounters with a group.

Roll response on a group could be calculated with any appropriate numerical method, including potential codes described above. The only input to be determined for such a calculation is initial conditions, initial roll and roll rate. The initial conditions are random variables with unknown distribution (Belenky, et al 2003), so the calculations could be done for the range of initial conditions.

The values of roll angle and roll rate at the end of the group could also be called “exit conditions”. The initial conditions at the beginning of the next group are identical to the exit conditions of the previous group, therefore, their distribution should be the same.

Based on the above consideration, the distribution of initial conditions could be found by the iterations, excluding the responses from the set until the distribution of the initial and exit conditions match each other with the given

accuracy. Once the iterations converge, the response set will constitute the distribution that will yield the searched probability that parametric roll would exceed the given value.

An increase of calculation efficiency may come from the ability to pre-compute the response set for the wide range of groups. The iterations procedure that is based on the statistical characteristics of the groups from the given spectrum may be faster than direct calculations. If these time savings are significant enough, it may even be used for on-board calculations. However, the final conclusions could be made only after numerical implementation and testing of the algorithm discussed above.

5. CONCLUSIONS

The two-fold problem of parametric roll was considered here. The first part is a discussion of the polar diagram as a planning tool to prevent parametric roll.

The polar diagram is based on the maximum roll angle observed during a one-hour simulation. Criteria for polar diagrams are based on lashing strength and engine conditions. Exceeding of these criteria is color-coded, depending on the value of the roll angle. Simulations for polar diagrams are carried out using potential codes calibrated for roll damping with roll decay tests. Polar diagrams have complex topology, primarily influenced by encounter spectrum of waves and natural frequency. The choice of loading conditions should be determined by sufficient coverage of the range of natural frequency.

The second part of the paper considered application of an envelope presentation as a possible way to increase computational efficiency of the parametric roll analysis and facilitation of the application of risk evaluation methods. The proposed approach considers the problem in two-time scale, small (a wave group) and large (period while statistical characteristics

of wave are unchanged for 3-6 hrs.). Statistics for wave groups are calculated based on reconstructed seaway. Encounter with a wave group is considered as an elementary event and the problem is being solved in a probabilistic domain.

6. ACKNOWLEDGMENTS

The authors wish to express their appreciation and gratitude to the management of the American Bureau of Shipping and Science Application International Corporation.

The development of the LAMP System has been supported by the U.S. Navy, the Defence Advanced Research Projects Agency (DARPA), the U.S. Coast Guard, ABS, and SAIC. LAMP development has been supported by the Office of Naval Research (ONR) under Dr. Patrick Purtell. The development of NLOAD3D program has been supported by ABS.

7. REFERENCES

- American Bureau of Shipping, American Bureau of Shipping, 1988 "Guide for Certification of Container Securing Systems", New York
- American Bureau of Shipping, 2004 "Guide for the Assessment of Parametric Roll Resonance in the Design of Container Carriers", Houston, Texas
- American Bureau of Shipping, 2006 "Rules for Building and Classing Steel Vessels", Houston, Texas
- Belenky, V., 2004 "On Risk Evaluation at Extreme Seas" Proc. of 7th International Ship Stability Workshop, Shanghai, China, 1-3 Nov. 2004
- Belenky, V., 2005 "On Long Numerical Simulations at Extreme Seas" Proc. of 8th International Ship Stability Workshop, Istanbul, Turkey, 6-7 Oct. 2005
- Belenky, V.L., Degtyarev, A.B., and Boukhanovsky, A.V., 1998, "Probabilistic Qualities of Nonlinear Stochastic Rolling," Ocean Engineering, Vol. 25, No 1, pp. 1-25.
- Belenky, V.L., Suzuki, Sh. and Yamakoshi, Yu., 2001, "Preliminary Results of Experimental Validation of Practical Non-Ergodicity of Large Amplitude Rolling Motion", Proc. of 5th International Stability Workshop, Trieste, Italy, 12-13 Sept. 2001
- Belenky, V. L. and Sevastianov, N.B., 2003. "Stability and safety of ships", Vol. 2 "Risk of capsizing", Elsevier, Amsterdam.
- Belenky, V.L., Weems, K.M., W.M. Lin, and J.R. Paulling, 2003, "Probabilistic analysis of roll parametric resonance in head seas" Proc. of STAB'03 8th International Conference on Stability of Ships and Ocean Vehicles, Madrid, Spain
- Bulian, G., Lugni, C. and A. Francescutto 2004, "A contribution on the problem of practical ergodicity of parametric roll in longitudinal long crested irregular sea", Proceedings of 7th International Ship Stability Workshop, Shanghai, China, 1-3 November
- IACS Recommendation No. 34, "Standard Wave Data
- Ikeda, Y., Munif, A., Katayama, A. and T. Fujiwara 2005 "Large Parametric Rolling of a Large Passenger Ship in Beam Seas and Role of Bilge Keel in Its Restraint" Proceedings of 8th International Ship Stability Workshop, Istanbul, Turkey, 6-7 Oct. 2005
- France, W.M, Levadou, M, Treacle, T.W., Paulling, J. R., Michel, K. and Moore, C. 2003. "An Investigation of Head-Sea Parametric Rolling and its Influence on Container Lashing Systems," Marine Technology, Vol. 40, No. 1, pp. 1-19.

- Neves M. A. and C.A. Rodríguez 2005, "Stability Analysis of Ships Undergoing Strong Roll Amplifications in Head Seas" Proc. of 8th International Ship Stability Workshop, Istanbul, Turkey, 6-7 Oct. 2005
- Shin, Y.S, Belenky, V.L., Lin, W.M., Weems, K.M., Engle, A.H. 2003, "Nonlinear Time Domain Simulation Technology for Seakeeping and Wave-Load Analysis for Modern Ship Design" SNAME Transactions, Vol. 111
- Shin, Y.S, Belenky, V.L., Paulling, J.R., Weems, K.M., Lin, W.M., 2004, "Criteria for Parametric Roll of Large Containerships in Longitudinal Seas", SNAME Transactions Vol. 112
- SLF 48/4/4 Review of MSC/Circ.707 to include parametric rolling in head seas (Australia and Spain)
- SLF 48/4/8 Proposed Revision of MSC/Circ.707 (to include parametric rolling in head seas) (Germany)
- SLF 48/4/12 On the development of performance-based criteria for ship stability in longitudinal waves (Italy)
- SLF 48/4/16 Proposal on MSC/Circ.707 revision (Russian Federation)
- SLF 48/4/17 Proposal on MSC/Circ.707 revision (Russian Federation)
- Spyrou, K.J. 2004, "Criteria for parametric rolling?", Proceedings of 7th International Ship Stability Workshop, Shanghai, China, 1-3 Nov. 2004
- Tikka, K.K. and J.R. Paulling, 1990 "Prediction of Critical Wave Conditions for Extreme Vessel Response in Random Seas", Proc of. 4th International Conference on Stability of Ships and Ocean Vehicles (STAB'90), Naples, Italy
- Umeda, N., Hashimoto, H., Paroka, D. and M.Hori 2005 "Recent Developments of Theoretical Prediction on Capsizes of Intact Ships in Waves", Proceedings of 8th International Ship Stability Workshop, Istanbul, Turkey, 6-7 Oct. 2005
- Weems, K. M., Lin, W. M., Zhang, S., and Treakle, T., "Time Domain Prediction for Motions and Loads of Ships and Marine Structures in Large Seas Using a Mixed-Singularity Formulation," Proceedings of the Fourth Osaka Colloquium on Seakeeping Performance of Ships (OC2000), Osaka, Japan, 17-21 October, 2000.

On the Effect of Stochastic Variations of Restoring Moment in Long-crested Irregular Longitudinal Sea

Gabriele Bulian(*), *DINMA University of Trieste*

Alberto Francescutto, *DINMA University of Trieste*

(* Presently research fellow at the Dept. NAOE, Osaka University, Japan.

ABSTRACT

In this paper, the problem of dangerous conditions induced by variations of restoring in waves is addressed, with particular attention to parametric roll. An analytical model for the study of roll motion in irregular longitudinal long crested waves is presented. Stochastic stability boundaries in the first parametric resonance region are provided analytically. Nonlinear/non gaussian roll response above threshold is determined numerically and compared with experiments. A semi-empirical methodology is proposed to extend the classical deterministic static stability assessment to a rational probabilistic framework taking into account hydrostatic restoring variations in waves and different environmental conditions. Examples of application are provided.

Keywords: *irregular sea, parametric roll, nonlinear motions, stochastic stability, pure loss of stability, stability criteria, performance based criteria*

1. INTRODUCTION

Ships' restoring capabilities have, in the modern developments of Naval Architecture, been assessed by analysing the calm water curve of righting moment. This type of ship's characteristic is useful and physical with sufficient approximation when heeling moments are of concern in calm water or when excitation is mainly due to beam sea. It was however clear to several authors in the past (Kuo et al., 1986; Palmquist, 1996; Paulling, 1961) that large variations of the underwater geometry due to ship motions combined with geometrical/hydrodynamic waves' effect, could have detrimental effects on the safety of the ship, leading to large rolling motions and even capsizes. Due to the fact that dangerous phenomena in intact ship condition are mainly occurring in wavy sea, it is important to address the case where the restoring moment of the ship changes from an only angle-

dependent quantity, to a time/space-and-angle-dependent function. Variations of righting moment are often more evident in regular longitudinal waves and in the case of irregular long crested longitudinal sea. The latter case is a reasonable simplification of the actual short-crested sea surface, that is conservative when only static variations of righting moment are of concern.

This paper deals with the dynamic and static effects of such variations. Dynamic conditions are considered as those situations leading to the build-up of parametrically excited roll motions. Static aspects of the problem are relevant when dealing with the so called pure loss of stability. These two conditions occur, usually, in quite different ranges of speed, especially for those ships suffering of parametric roll in head sea. There is of course a range of frequency where the motion is neither purely quasi-static, nor parametrically excited in any of the instability regions.

To address the basic physics of the phenomenon, an analytical model is proposed, that has already been used in the past for analysing the problem of roll's ergodicity (Bulian et al., 2006) and to study the susceptibility of a small fishing vessel (Bulian & Francescutto, 2005) to suffer of parametric roll.

Starting from the Grim effective wave concept (Grim, 1961), and by making use of hydrostatic calculations, a simplified analytical 1.5-DOF model is developed that incorporates nonlinear stochastic fluctuations of the curve. From this modelling a series of analytical/numerical considerations are carried out.

The first, important characteristic of this modelling is that it shifts the usual concept of a deterministic curve, to a stochastic model for the righting lever (as was done in the past by Umeda and Yamakoshi (1986) for the case of pure loss of stability). The righting moment then becomes a stochastic process, whose characteristics depend on hull shape and sea spectrum. The classical deterministic curve turns out to be a particular case of this more general concept. By making use of this idea, several classical deterministic approaches (such as usual stability criteria) can be extended in a probabilistic framework to obtain probabilistic engineering measures of ship's restoring capabilities, taking into account the variations induced by waves.

The dynamic model can be employed to study dynamic aspects such as parametric roll in irregular sea. Although an extensive literature is available for the case of regular sea (see, e.g. the references in Bulian (2005)), a more limited number of analyses have been carried out in the case of irregular sea (among others, Belenky et al. 2003; Bulian et al., 2006; Dunwoody, 1989; Palmquist, 1996; France et al., 2003; Hua et al., 1999) especially concerning fundamental aspects of the phenomenon, such as stochastic stability boundaries (Bulian et al., 2004). The

availability of this analytical physically sound model allows to address, by using known results (Roberts, 1982), the problem of stochastic stability boundaries, after suitable linearisation procedures: such an analysis allows to give an indication of the critical speeds likely to lead to parametric stochastic instability for a given type of sea spectrum and significant wave height. When conditions are above threshold, numerical simulations can be carried out to analyse the non-gaussian behaviour of the motion (Bulian et al., 2006). A comparison between numerical simulations and experimental results will show, however, that for the ship under analysis, the model is too conservative, and a tuning coefficient must be introduced for the magnitude of the parametric excitation. After tuning the model, very good comparison is obtained with experiments.

The analysis of the modifications that the spectrum of the effective wave amplitude undergoes as the speed is changed, gives useful hints in determining critical conditions in terms of groupiness, by looking at the spectral bandwidth (Bulian et al., 2004). In addition, an analysis of the mean oscillation frequency of the process allows to find a region where a purely static model could be roughly applied (Umeda & Yamakoshi, 1986).

2. A SIMPLIFIED DYNAMIC 1.5-DOF MODEL

2.1 Development of the Model

Ship motions in irregular longitudinal sea have the peculiarity that the roll restoring capability of the ship is often quite strongly explicitly time and angle dependent. Such dependence (parametric excitation) is due to geometrical effects and coupling with longitudinal motions (heave and pitch) in a way that is similar to that known for the regular sea case. In the case of regular sea, parametric roll has been widely investigated in the past

experimentally, numerically, and theoretically (see, e.g., references in Bulian (2005 and 2006)). In the particular case of analytical approaches to parametric roll in longitudinal regular sea, basically two types of models can be found, namely 1-DOF and N-DOF models, where usually $N=3$, i.e., heave, pitch and roll. A single degree of freedom nonlinear model based on the quasi static assumption for heave and pitch and using hydrostatic calculations for the restoring has been developed and investigated in Bulian (2004,2005 and 2006). On the other hand, 3-DOF approaches can be found in Neves & Rodriguez (2004) and Tondl et al. (2000). In the case of 1-DOF models it is impossible to deal correctly with dynamic effects in heave and pitch, whereas such coupling is of course the key feature of 3-DOF models. On the other hand a 1-DOF model is more amenable to direct analytical approaches involving nonlinearities up to sufficiently high order (Bulian, 2004; Umeda et al., 2003; Spyrou, 2000). A fully analytical approach above threshold is more difficult to be applied to multi-DOF systems, and strong nonlinearities can hardly be tackled, but at the same time the threshold level can be predicted by multi-DOF analytical models without extremely cumbersome calculations. However, the increased accuracy of multi-DOF models is obtained at the cost of an increased number of parameters, while a 1-DOF model can be used with very few parameters. Despite the simplicity the 1-DOF modelling, comparisons with experimental results carried out in Bulian (2003) and Bulian et al. (2004), seem to indicate that it could be used as a practical first approach tool. On the basis of the outcomes for the 1-DOF model in regular wave, it has been decided to try to follow a similar way even in the case of irregular waves. Details of the derivation are reported in Bulian (2006). The basic assumptions on which the model is developed are:

- Long crested irregular longitudinal sea;
- Constant ship speed;
- Quasi static assumption for heave and pitch;
- The use of Grim's effective wave to

reduce the number of degrees of freedom of the forcing process (waves) from infinite to one;

- Hydrostatic pressure under the Grim effective wave;

On the basis of such assumptions, the models is (Bulian, 2006; Bulian et al., 2006):

$$\ddot{\phi} + d(\dot{\phi}) + \omega_0^2 \cdot \frac{\overline{GZ}(\phi, \eta_{eff}(t))}{GM} = 0 \quad (1)$$

where $d(\dot{\phi})$ is the damping term, and $\eta_{eff}(t)$ is the amplitude of the Grim effective wave. The spectrum S_η of the Grim effective wave amplitude η_{eff} (a zero mean gaussian process) is determined, in longitudinal sea, from the sea elevation spectrum S_z at the real frequencies as:

$$S_\eta(\omega) = 4 \left(\frac{Q \cdot \sin Q}{\pi^2 - Q^2} \right)^2 S_z(\omega); Q = \frac{\omega^2 \cdot L}{2g} \quad (2)$$

Doppler effect is applied to S_η to account for the effect of the assumed constant speed of advance. The final fully analytical model is obtained by combining (1) with the following 2D polynomial fitting of the surface $\overline{GZ}(\phi, \eta_{eff})$:

$$\begin{aligned} \overline{GZ}(\phi, \eta_{eff}) &= \sum_{n=0}^{N_G} K_n(\eta_{eff}) \cdot \phi^n \\ K_n(\eta_{eff}) &= \sum_{j=0}^{N_K} Q_{jn} \cdot \eta_{eff}^j \end{aligned} \quad (3)$$

2.2 Parametric Resonance: Stability Threshold

When the dominant frequency of the parametric excitation is close to of twice the roll natural frequency, the upright position can lose stability in a stochastic sense. Closed form results are available in Ibrahim (1985) and Roberts (1982) for the analytical determination

of stability boundaries for a parametrically excited 1-DOF system, based on a preliminary application of the stochastic averaging technique. In order to apply such known results, roll motion equation is firstly deterministically linearized with respect to the roll angle in the vicinity of $\phi = 0$, leading to:

$$\ddot{\phi} + 2\mu\dot{\phi} + \omega_0^2 \frac{K_1(\eta_{eff}(t))}{GM} \phi = 0 \quad (4)$$

Subsequently the parametric excitation term $K_1(\eta_{eff})$ is substituted by its “statistically equivalent linearization” according to Roberts & Spanos (1990):

$$\begin{aligned} K_1(\eta_{eff}) &= \sum_{j=0}^{N_K} Q_{j1} \cdot \eta_{eff}^j \rightarrow D_0 + D_1 \cdot \eta_{eff} \\ \underline{\underline{A}} \begin{pmatrix} D_0 \\ D_1 \end{pmatrix} &= \underline{\underline{B}}; \quad \underline{\underline{A}} = \begin{pmatrix} 1 & E\{\eta_{eff}\} \\ E\{\eta_{eff}\} & E\{\eta_{eff}^2\} \end{pmatrix} \\ \underline{\underline{B}} &= \begin{pmatrix} \sum_{j=0}^{N_K} Q_{j1} \cdot E\{\eta_{eff}^j\} \\ \sum_{j=0}^{N_K} Q_{j1} \cdot E\{\eta_{eff}^{j+1}\} \end{pmatrix} \\ \frac{E\{\eta_{eff}^k\}}{\sigma_\eta^k} &= \begin{cases} 0 & \text{for } k \text{ odd} \\ \left(\frac{2}{\pi}\right)^{\frac{k}{2}} \cdot \Gamma\left(\frac{k+1}{2}\right) & \text{for } k \text{ even} \end{cases} \end{aligned} \quad (5)$$

where $E\{\cdot\}$ is the expected value operator (often called “mean”). The “fully” linearized system is then:

$$\ddot{\phi} + 2\mu\dot{\phi} + \frac{\omega_0^2 \cdot D_0}{GM} \left(1 + \frac{D_1}{D_0} \cdot \eta_{eff}\right) \cdot \phi = 0 \quad (6)$$

The coefficients D_0 and D_1 depend on the actual standard deviation σ_η of the effective wave according to (5) and thus on the significant wave height. This meaning that the applied statistical linearization partially accounts for the non gaussian behaviour of the

parametric excitation term K_1 . If we let now C to be the roll amplitude, the asymptotic stochastic stability limit for $E\{C^n\}$ can be determined as:

$$\frac{\pi}{8} \left(1 + \frac{n}{2}\right) \frac{\omega_0^2 \cdot D_1^2}{GM \cdot D_0} S_\eta \left(2\omega_0 \sqrt{\frac{D_0}{GM}}\right) < \mu \quad (7)$$

In particular, a sufficiently practical condition could be assumed (arbitrarily) to be that associated to $n=1$, i.e., the condition for asymptotic stochastic stability of the mean of the roll envelope. When such condition is satisfied, the expected value of the roll envelope for the system (6) strictly decays to zero as the time is increased.

It is important to stress that, in the determination of the linear system (6), with the consequent application of the result (7), use has been made of the statistical linearization technique that is, basically, an “ensemble” (thus instantaneous) linearization technique not taking into account time domain effects. For this reason frequency mixing induced by the nonlinear transformation $K_1(\eta_{eff}(t))$ cannot be properly accounted for. If the majority of the energy spectrum of η_{eff} is concentrated close to twice the roll natural frequency, and if nonlinear effects in the transformation K_1 are not extremely significant, then the proposed approach can be considered suitable. On the other hand, when the energy of the parametric forcing η_{eff} is concentrated far from the sub-harmonic resonance condition and nonlinearities in K_1 are significant, then the direct Fourier transform of the autocorrelation function for the process $K_1(t)$ should be determined and used to obtain the magnitude of the parametric excitation in (7).

2.3 Response above Threshold

When the upright position loses stability, the ship starts rolling, and nonlinear effects become fundamental in bounding the motion's statistics. It can indeed be proved (Ibrahim,

1985) that, after performing stochastic averaging, the linearized model (6) cannot show a steady state probability density function for the roll motion, similarly to what happens in the case of regular deterministic excitation (Bulian, 2006; Francescutto, 2002). In order to obtain a steady state solution (i.e. steady state statistics for the roll motion, being it a stochastic process), nonlinear effects must be introduced. Linearization techniques (typical of the beam sea case) cannot be used for damping, due to the completely different role played by linear and nonlinear component. Boundedness of roll's statistics is obtained for $t \rightarrow \infty$ thanks to:

- Nonlinear damping (increased rate of energy dissipation at large rolling amplitudes/velocities);
- Nonlinear restoring (detuning effect);

In the case of regular sea, the deterministic averaging technique has been used to obtain an approximate nonlinear roll response curve in frequency domain (Bulian, 2004) in the region of the first parametric resonance. A similar approach could in principle be used for the stochastic case, by means of the stochastic averaging technique (Roberts & Spanos, 1984). In its original form, however, such technique is not able to account for the effects on roll amplitude statistics of constant terms in nonlinear restoring (Roberts & Spanos, 1984), and the only analytically detectable bounding effects are those given by the nonlinear damping. Although generalisations of the previous technique exist that are able to detect detuning effects (Ibrahim, 1985; Roberts & Spanos, 1984; To, 1998), the application of these latter techniques leads often to cumbersome calculations to arrive to an, in any case, approximate solution. This makes the Monte Carlo approach, at least for the time being, more appealing. In this work, roll response curves, when reported, have been determined by means of Monte Carlo approach.

2.4 Some Comments on other Regions Far from Subharmonic Resonance

In the previous sections we concentrated on the dangerous condition of 2:1 subharmonic resonance. The model (1) could, however, be used in different regions of encounter frequency. In particular it is interesting to discuss the case of so called "pure loss of stability". Such region is intended here as that zone of parameters (sea spectrum characteristics and ship speeds) where dynamic effects can be considered to be small, and the rolling motion has thus long characteristic period. Umeda and Yamakoshi (1986) used in the past the Grim simplification to address this phenomenon, that is typical in following sea in suitable speed ranges. In order to determine such speed range, it could be useful to analyse the characteristic frequencies (mean and zero-crossing) of the parametric excitation:

$$\begin{aligned} \text{mean: } \bar{\omega}_{e\eta} &= \bar{m}_1/m_0 \\ \text{zero-crossing: } \omega_{e\eta,z} &= \sqrt{m_2/m_0} \\ m_n &= \int_0^\infty \left| \omega + \frac{\omega^2 U}{g} \right|^n S_\eta(\omega) d\omega \end{aligned} \quad (8)$$

The ship speed U is considered as positive in head sea. Regions of minimum values for $\bar{\omega}_{e\eta}$ and $\omega_{e\eta,z}$ are those where the characteristic period of the variations of restoring is longest, and where, then, the quasi static approach is, hopefully, more likely to be in agreement with the reality.

Another important parameter in the qualitative analysis of dangerous conditions is the spectral bandwidth of the forcing process, i.e. a measure of the energy concentration (that can be proved to be related to the difference between the mean and zero crossing frequency of the forcing process). In particular, it was shown in Bulian et al. (2004); Bulian (2006); Panjaitan (1998) that conditions quite far from exact 2:1 resonance, but associated to small values of spectral bandwidth (i.e. narrow band forcing spectra) can be more dangerous than

conditions where the excitation frequency is closer to the 2:1 resonance, but where the bandwidth of the parametric excitation is large, and thus grouping is less marked.

2.5 Application

Some examples of application of the presented analytical model are reported in this section. Calculations are performed on a 132m long RoRo having the main particulars reported in Table 1.

Table 1: Main particulars of ship TR2.

Ship TR2	
Length: 132.22m	Volume: 7714m ³
Breadth: 19m	\overline{GM} : 0.865m
Draught: 5.875m	Roll period: 15.9s

Speed dependent roll damping coefficients have been obtained from experiments while righting arm calculations have been carried out using a free trim approach. Experimental data have been obtained from tests carried out in the INSEAN model basin (Bulian, 2006; Bulian et al., 2004 and 2006). Figure 1 compares experimental and numerical roll standard deviation (i.e. roll rms) for a Bretschneider sea spectrum having modal wave frequency corresponding to a wave length equal to the ship length.

It can be seen that the predictions with the proposed model (indicated as “Not tuned”) overestimate the experimental roll motion standard deviation (used here only as an indicator of roll motion amplitude, being the motion strongly non gaussian). Such overestimation can be due to an underestimation of the damping, or an overestimation of the parametric excitation. Since damping coefficients have been obtained from experiments, it is assumed here that the source of error is the modelled magnitude of the parametric excitation. For this reason, an empirical tuning coefficient k_c is introduced, and the effective wave amplitude process

$\eta_{eff}(t)$ is substituted by the tuned process $k_c \cdot \eta_{eff}(t)$ (this actually corresponds, for the Bretschneider sea spectrum, to a substitution, in the calculations, of the physical significant wave height $H_{1/3}$ with a “correct significant wave height” equal to $k_c \cdot H_{1/3}$).

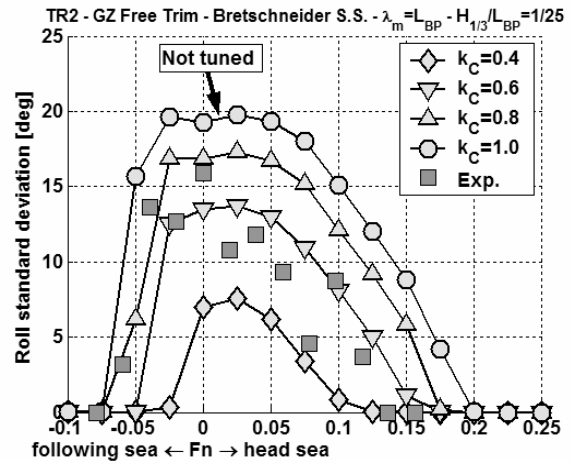


Figure 1: Comparison between predictions and experiments. Roll standard deviation.

Due to the original overestimation of roll, we tried different values of $k_c \leq 1$, in order to reduce the magnitude of the parametric excitation. It can be seen that the use of a suitable value for the tuning coefficients leads to a good correlation between prediction and experiments, and that a tuning coefficient of about 0.6 gives, in this case, a good mean correlation, apart from a relative shift between the experimental and the numerical response curves in terms of Froude number. Such good correlation is much more evident when we compare the numerically and experimentally determined cumulative distribution functions of the roll envelope, as in Figure 2. The tuning coefficient $k_c = 0.75$ in the figure has been selected by matching the numerical and the experimental roll standard deviation. It is to be said that the data used for the zero speed analysis and those used for the tests with forward speed come from different test campaigns (Bulian et al., 2004 and 2006) on the same model: differences in the wave generation, or other sources of errors could have influenced the outcomes, leading to experimental results at zero speed not

completely in line with those obtained with non-zero speed of advance.

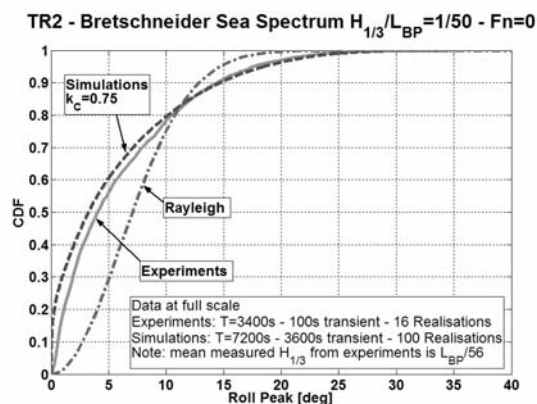


Figure 2: Comparison between tuned predictions and experiments. CDF of roll envelope.

In Figure 2 a Rayleigh distribution is superimposed in order to show that the usual narrow band gaussian approach is not suitable for parametric roll analysis (Belenky et al., 2003; Bulian et al, 2006; Hashimoto et al., 2005). On the other hand, the numerically predicted cumulative distribution function of roll envelope after tuning, very well agrees with the experimental results. It seems then that, although the magnitude of the parametric excitation as obtained by using the quasi static approach is too large for the ship under analysis, the general form of the mathematical model, in terms of nonlinear damping and restoring functions, is sufficiently suitable to reproduce the non gaussian roll motion statistics when the parametric excitation has the correct magnitude. However, such a large reduction in the magnitude of parametric excitation in irregular waves was not expected at the beginning of this study, having in mind the quite good average agreement obtained by a similar model in regular waves (Bulian, 2006). For this reason further research is worth on this point, in order to understand whether an “average” value for such tuning factor could be found, such to provide a first approach, fast tool for parametric roll analysis in irregular waves. It is however to be pointed out that, for the ship under analysis, the provided model is

conservative.

The developed analytical methodology allows to obtain in a quite fast way, indications regarding the limiting threshold significant wave height as function of ship speed and modal frequency of the wave spectrum. In Figure 3 such limiting surface is reported without any tuning on the parametric excitation. The presence of two local minima is related to the humps and hollows in the spectrum of the effective wave amplitude (see Figure 4). Such limiting surface can easily be linked with classical wave scatter diagrams and the (joint) probability density function of the ship speed (accounting for voluntary and/or involuntary speed reduction) in order to define an index of susceptibility I_S to parametric roll phenomenon, defined as the probability of sailing in a condition above the limiting surface (Bulian, 2006).

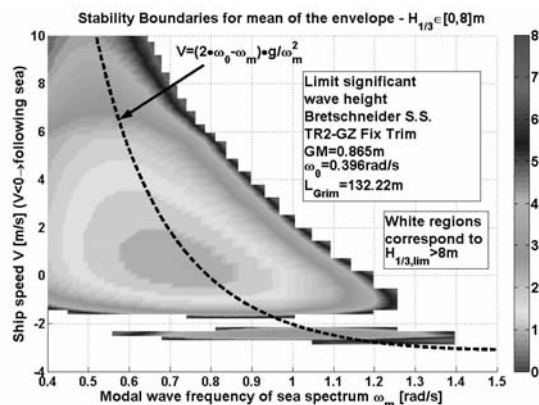


Figure 3: Estimated limit significant wave height for the inception of parametric roll.

As discussed in the previous section, the characteristic frequencies of the parametric excitation process, together with the analysis of the spectral bandwidth, could give useful information on the region where a quasi-static approach could be more successful. Figure 4 shows, on the left, a comparison between the wave spectrum and the effective wave spectrum when the modal wave length is equal to the ship length (the ship in this case is TR2), together with an analysis of the mean and zero crossing frequencies (upper right plot), and of

the spectral bandwidth of the effective wave process (lower right plot) as a function of Froude number. A definite minimum can be seen regarding frequencies around $Fn=0.35$ in following sea, while the minimum of the spectral bandwidth occurs close to $Fn=0.18$ in following sea. It is important to note that the region of minima for the effective wave frequencies is close to the region of maximum for the spectral bandwidth: it could then be guessed that the most dangerous conditions, with respect to the pure loss of stability, could occur between $Fn=0.18$ and $Fn=0.35$ in following sea with sufficiently large significant wave height, due to the occurrence of sufficiently strong grouping together with long characteristic periods for the excitation. In case of different ratios between ship length and modal wave length, results could differ. It is interesting to note that, for the ship under analysis, the second parametric resonance region occurs close to the region of maximum grouping, and this could endanger the ship. Although for the ship under analysis Froude numbers of 0.3 and above are unrealistic, the concept can be used for any ship, including high-speed vessels or small ships.

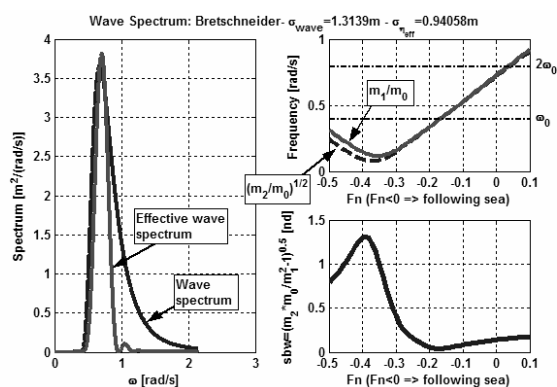


Figure 4: Analysis of characteristic frequencies and spectral bandwidth for the parametric excitation process.

3. A SEMI-EMPIRICAL PROBABILISTIC APPROACH TO STATIC STABILITY

The previous sections have dealt with a “first principles” dynamic analysis of roll

motion in irregular longitudinal waves. A direct physical approach, even if approximate, is for sure the most suitable, long lasting, easily upgradeable and elegant way of providing tools for the future generation of stability criteria. It is however important to have in mind that present stability criteria (IMO, 2002), and thus present design practice, are mainly based on static considerations for the righting arm curve in calm water dating back to the Rahola’s work (Rahola, 1939) or to the original developments of the Weather Criterion (IMO, 2005). At the same time there is considerable pressure towards the development of new criteria able to reduce the risk of large rolling angles that some ship typologies are presently facing when at sea, and Classification Societies have started facing the parametric roll matter by issuing some Guidelines (ABS, 2004): a global picture of the results and effects of their implementation is, however, not yet available to the public. In the meantime some evidence has been reported (Hinrichs & Krueger, 2004; Krueger, 2005) that statically determined stability variations in waves, could be roughly related to the probability of experiencing large rolling angles, or even capsize: the basic idea being that large restoring variations in waves together with small calm water righting arm, could identify dangerous designs.

An extension of the classical deterministic approach to static stability in order to rationally account for hydrostatic stability variations in irregular waves, in a sound probabilistic framework is thus presented. This allows, in principle, to address different environmental conditions in both long and short term. The idea is based on the nonlinear model (3) for \overline{GZ} as a function of the heeling angle and the effective wave. More details are available in Bulian (2006).

3.1 \overline{GZ} as a Random Quantity

Given a particular sea state, the effective wave spectrum can be obtained according to (2), and it is thus possible to determine the

variance σ_η^2 of the effective wave by integration. The effective wave process has a zero mean gaussian probability density function, i.e. $\eta_{eff} \in N(0, \sigma_\eta^2)$. We consider only ensemble averages, and we are not interested, in this section, in dynamic effects. The instantaneous probability density function of η_{eff} provides, thus, a full characterisation of the input random variable. The knowledge of the relationship $\overline{GZ}(\phi, \eta_{eff})$ in (3) allows to derive the metacentric height and the area under the righting arm as functions of the effective wave amplitude:

$$\begin{aligned} \overline{GM}(\eta_{eff}) &= \left. \frac{\partial \overline{GZ}(\phi, \eta_{eff})}{\partial \phi} \right|_{\phi=0} = \\ &= K_1(\eta_{eff}) \\ b(\phi, \eta_{eff}) &= \int_0^\phi \overline{GZ}(\xi, \eta_{eff}) d\xi = \\ &= \sum_{n=0}^{N_G} \frac{K_n(\eta_{eff})}{n+1} \cdot \phi^{n+1} \end{aligned} \quad (9)$$

Since η_{eff} is a random variable (actually it is a stochastic process, but, as said, we are here interested only in the ensemble domain), all the mentioned quantities, i.e., \overline{GZ} , \overline{GM} and b are to be considered as (correlated) random variables having non gaussian distributions. Thanks to their known polynomial relation with the effective wave amplitude, their probability density functions can be obtained numerically without necessarily using Monte Carlo simulations. However, even using a Monte Carlo approach is not very time consuming, and huge samples can fast be generated to obtain sufficiently reliable estimations.

3.2 The Definition of Compliance Level

We assume to have an arbitrary criterion $C\{\overline{GZ}\}$, i.e., a “rule” able to “judge” the geometrical \overline{GZ} curve properties. Such criterion is assumed to provide values in the interval $[0,1]$, where 0 means not compliance, whereas 1 mean full compliance. The criterion

$C\{\cdot\}$ could be binary (i.e. $C\{\cdot\} \rightarrow \{0,1\}$, pass/fail type) or fuzzy (i.e. $C\{\cdot\} \rightarrow [0,1]$, with different “levels” of compliance). Present IMO criteria (IMO, 2002) based on the analysis of \overline{GZ} are an example of binary criterion $C\{\cdot\}$, because they only provide a binary outcome: pass/fail. Often the criterion $C\{\cdot\}$ is based on the numerical values of the quantities \overline{GZ} , \overline{GM} and b . Given $C\{\cdot\}$ we can formally define the following function, that we call the “compliance level I_C ”:

$$\begin{aligned} I_C(\eta_{eff}) &= C\{\overline{GZ}(\phi, \eta_{eff})\} \\ I_C: \square &\rightarrow [0,1] \end{aligned} \quad (10)$$

Due to the random nature of η_{eff} , the compliance level is intended here as a random variable, and, in principle, its cumulative distribution function cdf_C can be found as:

$$\begin{aligned} cdf_C(I_C) &= \int_{\Omega(I_C)} pdf_\eta(\eta_{eff}) d\eta_{eff} \\ \Omega(x) &= \{\eta_{eff} : I_C(\eta_{eff}) \leq x\} \end{aligned} \quad (11)$$

Where pdf_η is the gaussian probability density function of the effective wave. Although cdf_C provides full information about the random nature of I_C , from a practical point of view it could be useful to rely, in performing comparisons, on a single quantity, such as the mean value of the compliance level, i.e.:

$$\begin{aligned} \mu_C = E\{I_C\} &= \int_0^1 I_C \cdot pdf_C(I_C) dI_C = \\ &= \int_{-\infty}^{\infty} I_C(\eta_{eff}) \cdot pdf_\eta(\eta_{eff}) d\eta_{eff} \end{aligned} \quad (12)$$

It is known that a wave crest amidship, for conventional ship types, can lead to a significant reduction of restoring. It is then not unlikely for a binary criterion $C\{\cdot\}$ to be fulfilled only up to a certain effective wave amplitude η_{crit} , i.e.,

$$\begin{cases} I_C(\eta_{eff}) = 1 & \text{for } \eta_{eff} \leq \eta_{crit} \\ I_C(\eta_{eff}) = 0 & \text{for } \eta_{eff} > \eta_{crit} \end{cases} \quad (13)$$

In this particular case (binary criterion with presence of critical effective wave amplitude) the following relations hold:

$$\begin{aligned} \mu_C &= \text{Prob}\{I_C = 1\} = \\ &= \text{cdf}_\eta(\eta_{crit}) = \Phi\left(\frac{\eta_{crit}}{\sigma_\eta}\right) \end{aligned} \quad (14)$$

where Φ is the cumulative distribution function of the standardized gaussian $N(0,1)$. It is to be stressed that all the previous relations refer to a short term approach, i.e., to a particular sea state. Given a two-parameters discrete wave scatter diagram with probability mass function $P_{SEA}(H_{1/3}, T_m)$, the long term expected value of the compliance level is obtained through the following weighted sum:

$$\mu_C = \sum_{T_m} \sum_{H_{1/3}} \mu_C(H_{1/3}, T_m) \cdot P_{SEA}(H_{1/3}, T_m) \quad (15)$$

Although the previous relation has been written for the long term expected value of the compliance level for a two-parameters wave spectrum, it can be generalised to the other quantities referred in this paragraph, and to a larger number of sea state parameters in continuous or discrete form (Bulian, 2006).

In the case of a ship marginally complying in calm water with a binary criterion $C\{\cdot\}$, under the assumptions of existence of η_{crit} , we always obtain $\mu_C = 0.5$ both in long and short term calculations, because of the fact that η_{eff} has a symmetric probability density function with zero mean. In this particular case, then, $\mu_C = 0.5$ allows to obtain the calm water marginal condition.

According to the considerations reported in (Hinrichs & Krueger, 2004; Krueger, 2005) it is (very) likely that $(\mu_C)_1 > (\mu_C)_2$ implies

{ship(or condition) "1"} to be safer than {ship(or condition) "2"} with respect to phenomena related to variations of stability in waves.

3.3 Direct Measures of Variation

In the previous paragraph, the magnitude of the hydrostatic variations of restoring in waves has basically been measured by means of an arbitrary criterion $C\{\cdot\}$. Although in any rule, by definition, there is a need to create a "criterion" (there cannot be any rule, i.e. a decision process, if a "criterion" is not specified), we could assume to apply this criterion to short or long term quantities directly related to (almost) physical variations of restoring in waves. In particular, it is important to note that absolute variations of restoring are often meaningless if they are not related to the corresponding mean or, as an approximation, to calm water values. In the case of short term analysis, an example of relevant measure of variation μ_M arising from the considerations reported in (Hinrichs & Krueger, 2004; Krueger, 2005) could be the coefficient of variation of the area under \overline{GZ} , defined as follows:

$$\mu_M = \sqrt{\frac{\text{Var}\{b(\phi, \eta_{eff})\}}{E^2\{b(\phi, \eta_{eff})\}}} \quad (16)$$

If we assume that, with sufficient practical accuracy, in the range of expected effective wave amplitudes the relation between b and η_{eff} is linear, then

$$\begin{aligned} b(\phi, \eta_{eff}) &\approx P_0(\phi) + P_1(\phi) \cdot \eta_{eff} \Rightarrow \\ \Rightarrow \mu_M &= \left| \frac{P_1(\phi)}{P_0(\phi)} \right| \sigma_\eta \end{aligned} \quad (17)$$

where it is important to note that, neglecting effects on trim induced by vertical shifting of the centre of gravity, $P_1(\phi)$ only depends on the hull form, whereas $P_0(\phi)$

depends on \overline{KG} : $P_0(\phi)$ is then under the control of the designer even if the hull form cannot be modified.

When long term nondimensional measures of variation are introduced, it is better to rely on the squared value of μ_M , in such a way to exploit the long term standard deviation of the effective wave amplitude. In linear approximation, indeed, we can obtain (Bulian, 2006):

$$\mu_{M, \text{long-term}} = \sqrt{E\{\mu_M^2\}} = \left| \frac{P_1(\phi)}{P_0(\phi)} \right| \sigma_{\eta, \text{long-term}} \quad (18)$$

where $\sigma_{\eta, \text{long-term}}$ is the standard deviation of η_{eff} determined by using the long term probability density function of η_{eff} .

In the general case of any quantity q defined by means of a nonlinear transformation $F(\eta_{\text{eff}})$ as in (9), the long term n-th statistical moment can be obtained starting from the short term probability density function of the effective wave amplitude $pdf_{\eta}(\eta_{\text{eff}} | \underline{p})$, and by using the joint probability of the sea state parameters vector \underline{p} (e.g. $\underline{p} = (H_{1/3}, T_m)$):

$$\begin{aligned} E\{q^n | \underline{p}\} &= \int_{-\infty}^{+\infty} F^n(\eta_{\text{eff}}) pdf_{\eta}(\eta_{\text{eff}} | \underline{p}) d\eta_{\text{eff}} \\ E\{q^n\} &= \int \dots \int_{P_1}^{P_n} E\{q^n | \underline{p}\} pdf_{SEA}(\underline{p}) dp_n \dots dp_1 \end{aligned} \quad (19)$$

Results in (17) and (18) are special cases of the previous relations.

The knowledge of a limited number of statistical moments is not sufficient, however, in general, to fully characterise the probability density function of a random variable, even if some asymptotic analytical approximations can be used (with caution), as the Gram-Charlier or Edgeworth expansions (Ibrahim, 1985; Ochi, 1990). It could then be useful to rely, instead, on intervals based on percentile levels, rather than on some statistical moment, in order to provide

uniformity even for different types of probability density function for the quantity of interest.

3.4 Application

As an example of application, in this section the estimated long term of the compliance level is determined for three ships in three different environmental conditions. The first ship is TR2, while the second ship is a 52m long RoRo named ITACA having the main particulars reported in Table 2.

Table 2: Main particulars of ship ITACA.

Ship ITACA	
Length: 52.55m	Draught: 2.1m
Breadth: 10m	Volume: 569m ³

The third ship is a scaled GEOSIM of ITACA, and it is called ITACA_{2.4}, where the 2.4 scale factor is used to obtain comparable dimensions between TR2 and ITACA_{2.4}. The used criterion is the set of statistical criteria provided by present Intact Stability Code (IMO, 2002), but the requirement for the position of the maximum of the \overline{GZ} curve has been neglected (Bulian, 2006). The situation satisfies with sufficient accuracy the case of binary criterion with presence of critical effective wave amplitude, as discussed above, and the dependence of the critical effective wave amplitude on the metacentric height for the three ships is reported in Figure 5. The condition $\eta_{\text{crit}} = 0$ for each ship identifies the usual marginal \overline{GM} in calm water. When \overline{GM} is reduced below the marginal value in calm water, the critical effective wave amplitude becomes negative: this is due to the fact that the static stability is, usually, increased in a wave trough ($\eta_{\text{crit}} < 0$). When \overline{GM} is below the marginal level, the selected criterion can only be satisfied when additional stability is provided by a wave trough amidship.

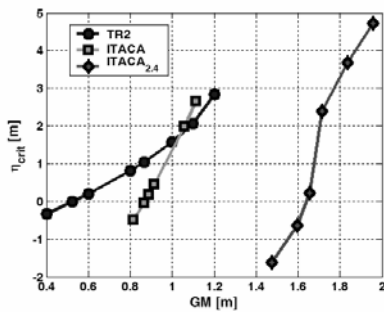


Figure 5: Dependence of critical effective wave amplitude η_{crit} on \overline{GM} according to the selected criterion.

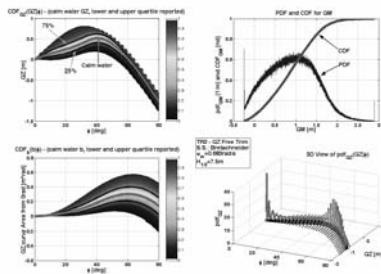


Figure 6: Example of short term representation of static stability in the proposed probabilistic approach. Ship TR2.

The used environmental conditions are obtained from the wave scatter diagrams for the North Atlantic region as recommended by IACS (2001) and for the East Mediterranean Sea (Area 27) as obtained from Hogben et al. (1986). The third considered environmental condition is the North Atlantic as above, with a maximum allowed operational significant wave height equal to 5.5m.

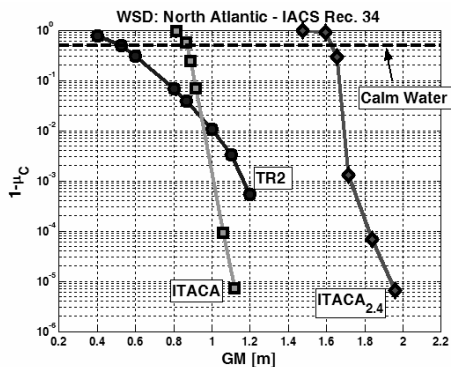


Figure 7: Mean long term compliance level in North Atlantic.

Figure 6 shows how the random quantities related to static stability can be visualised in a global way. \overline{GZ} , \overline{GM} and b in this case have been determined by Monte Carlo simulations, but an almost analytical approach can be used as well. The upper right plot shows the probability density function and the corresponding cumulative distribution of the metacentric height, highlighting the non gaussian shape. On the upper left plot the cumulative distribution of \overline{GZ} is reported: it is important to note that such plot is meaningful only when sections are considered at fixed values of the heeling angle (i.e. $cdf(\overline{GZ}|\phi)$), due to the geometrical correlation between \overline{GZ} at different heeling angles. Similarly, in the lower left plot the cumulative distribution of the area under the \overline{GZ} curve (dynamic stability) is reported, for which the same comments hold. The final lower right plot shows the probability density function of \overline{GZ} at different heeling angles. Calm water curves in the left plots are reported as magenta thick lines, together with the thick curves in black connecting the upper and lower interquartile points. A comparison between the obtained long term value of $1-\mu_C$ in the case of North Atlantic for the three ships is reported in Figure 7. If we select an arbitrary value of (required) $\mu_C \geq 0.5$, the corresponding increase in metacentric height with respect to the usual marginal calm water value can be obtained. Such increase is different for the three ships for any $\mu_C > 0.5$, due to the different hull form geometry and/or main dimensions.

The effect of different environmental conditions is assessed in Figure 8 for the ship TR2. Also in this case, given a particular value of $\mu_C \geq 0.5$, it is possible to obtain the corresponding metacentric height, and the increase in the metacentric height with respect to the marginal calm water value depends on both μ_C and the selected long term environmental condition.

As a final example, the linearized coefficient of variation of the area under \overline{GZ} up to 40deg according to (18) is reported in

Figure 9. In this case there is no marginal calm water value, since we are not basing the calculation on any arbitrary *a-priori* criterion. However, provided a limiting (arbitrary, but basically tuned on the present fleet) value for the coefficient of variation, the corresponding limiting metacentric height can be found for different ships and different environmental conditions. It is interesting to note that for the case of the two largest ships under analysis, TR2 and ITACA_{2,4}, the change of long term operational area from North Atlantic to East Mediterranean Sea has a large effect on the estimated long term coefficient of variation of $b(40\text{deg})$. On the other hand the effect is much more limited in the case of the original small RoRo ITACA. This is due to the combined effect of the reduction in the mean significant wave height from North Atlantic to East Mediterranean Sea, that would reduce the coefficient of variation of $b(40\text{deg})$, however, at the same time, the dominant wave length shortens from North Atlantic to East Mediterranean, leading to a sort of “static resonance” for ITACA, i.e., an increased matching between the effective wave transfer function (that only depends on the ship length) and the dominant sea spectra. For similar reasons, in the case of TR2 and ITACA_{2,4}, that have a length that is more than twice the length of ITACA, the modifications that the Wave Scatter Diagram undergoes between North Atlantic and East Mediterranean Sea lead to a global reduction in the coefficient of variations of $b(40\text{deg})$.

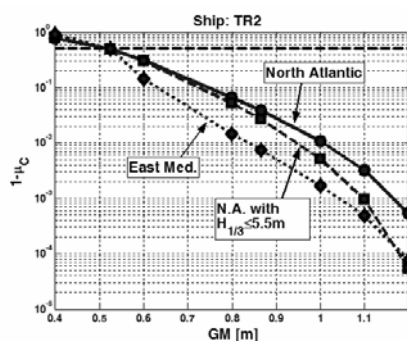


Figure 8: Effect of different assumed environmental conditions on the mean long term compliance level. Ship TR2.

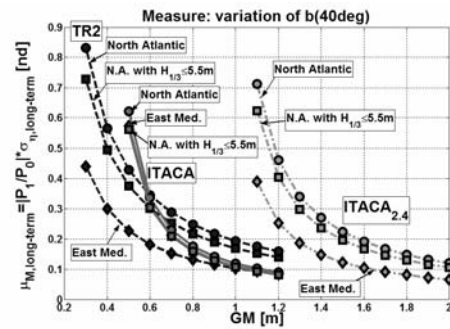


Figure 9: Effect of different assumed environmental conditions on the mean long term compliance level. Ship TR2.

4. FINAL REMARKS

The problem of the effects of variations of restoring moment in longitudinal long crested irregular waves has been dealt with both dynamically and statically by using a simplified nonlinear analytical model for roll motion exploiting the Grim effective wave concept.

In particular, subharmonic parametric roll resonance has been analysed, and a fully analytical approach has been proposed for the determination of the stochastic stability threshold from the original model. Roll motion above threshold, on the other hand, has been analysed by means of Monte Carlo simulations. From the comparison carried out with a series of available experimental data, we observed that the analytical model overestimates roll motion for the ship under analysis. However, after the introduction of a tuning factor on the basic parametric excitation (i.e. basically on the spectrum of the effective wave amplitude), good agreement has been achieved between the experimental data and the numerical predictions. In particular, the non-Rayleigh behaviour of the roll motion envelope seems to be quite well reproduced. The actual origin of the necessity of introducing the tuning factor still remain to be investigated. For the case of regions far from the subharmonic resonance, some considerations have been reported starting from the analysis of the characteristic

frequencies and of the spectral bandwidth of the parametric excitation: dangerous conditions related to the “pure loss of stability” are to be searched bearing in mind the grouping effect (roughly measured by the spectral bandwidth) induced by the Doppler effect.

The introduction, by means of the Grim effective wave, of non deterministic righting arm variations has allowed to propose a methodology for extending the classical deterministic concept of static stability in calm water, in a rational probabilistic framework where both the susceptibility of the ship to suffer hydrostatic restoring variations in waves and the sea state characteristics (short and long term) are taken into account. Present deterministic criteria can be then applied in this extended framework, and in addition, rational measures of restoring variations that are independent from any arbitrary a-priori criterion are introduced in a general way, with some particular examples. The developed ideas allows to introduce a ranking among different ships and/or loading/environmental conditions, taking approximately into account the danger inherent in the tendency for the ship to suffer large restoring variations in waves. The usual deterministic approach is a sub-case of the more general approach proposed here. Despite its semi-empirical nature (that needs of course some tuning), the proposed method could be a suitable interim procedure for highlighting ships likely to be endangered by too large hydrostatic restoring variations, waiting for the, hopefully fast, introduction of real first principles performance based approaches.

5. ACKNOWLEDGEMENTS

Part of this work has been carried out while Gabriele Bulian was at Osaka University as a research fellow, under the gratefully acknowledged financial support of the Scholarship PE05052 provided by the Japan Society for the Promotion of Science (JSPS).

6. REFERENCES

- American Bureau of Shipping (ABS), 2004, "Guide for the Assessment of Parametric Roll Resonance in the Design of Container Carriers".
- Belenky, V., Weems, K.M., Lin, W.M., Paulling, J.R., 2003, "Probabilistic Analysis of Roll Parametric Resonance in Head Sea", Proc. 8th International Conference on Stability of Ships and Ocean Vehicles (STAB2003), Madrid, pp. 325-340.
- Bulian, G., 2004, "Approximate Analytical Response Curve for a Parametrically Excited Highly Nonlinear 1-DOF System with an Application to Ship Roll Motion Prediction", Nonlinear Analysis: Real World Applications, Vol. 5, pp. 725-748. doi:10.1016/j.nonrwa.2004.03.002
- Bulian, G., 2005, "Nonlinear Parametric Rolling in Regular Waves - A General Procedure for the Analytical Approximation of the GZ Curve and Its Use in Time Domain Simulations", Ocean Engineering, Vol 32, No. 3-4, pp. 309-330, doi: 10.1016/j.oceaneng.2004.08.008.
- Bulian, G., 2006, "Development of analytical nonlinear models for parametric roll and hydrostatic restoring variations in regular and irregular waves", PhD Thesis, Department of Naval Architecture, Ocean and Environmental Engineering (DINMA), University of Trieste.
- Bulian, G., Francescutto, A., 2005, "Safety and Operability of Fishing Vessels in Beam and Longitudinal Waves", Proc. International RINA Conference on Fishing Vessels, Fishing Technology & Fisheries, Newcastle, pp. 47-60.
- Bulian, G., Francescutto, A., Lugni, C., 2004, "On the Nonlinear Modeling of Parametric Rolling in Regular and Irregular Waves", International Shipbuilding Progress, Vol.

51, pp. 173-203.

- Bulian, G., Francescutto, A., Lugni, C., 2006, "Theoretical, numerical and experimental study on the problem of ergodicity and 'practical ergodicity' with an application to parametric roll in longitudinal long crested irregular sea", Ocean Engineering, Vol. 33, pp. 1007-1043.
- Dunwoody, A. B., 1989, "Roll of a Ship in Astern Seas – Metacentric Height Spectra", Journal of Ship Research, Vol. 33, pp. 221-228.
- France, W. N., Levadou, M., Treakle, T. W., Paulling, J. R., Michel, R. K., Moore, C., 2003, "An Investigation of Head-Sea Parametric Rolling and Its Influence on Container Lashing Systems", Marine Technology, Vol. 40, pp. 1-19.
- Francescutto, A., 2002, "Theoretical Study of the Roll Motion in Longitudinal Waves", Technical Report (in Italian), Department of Naval Architecture, Ocean and Environmental Engineering (DINMA), University of Trieste.
- Grim, O., 1961, "Beitrag zu dem Problem der Sicherheit des Schiffes im Seegang", Schiff und Hafen 6, pp. 490-497.
- Hashimoto, H., Matsuda, A., Umeda, N., 2005, "Model Experiment on Parametric Roll of a Post-Panamax Container Ship in Short-Crested Irregular Seas", Conference Proc. Japan Society of Naval Architects and Ocean Engineers, Volume 1, pp. 71-74.
- Hinrichs, R., Krueger, S., 2004, "Towards the development of dynamic stability criteria", Submitted to the IMO Intersessional Correspondence Group on Intact Stability, Trieste.
- Hogben, N., Dacunha, N.M.C., Olliver, G.F., 1986, "Global wave statistics", British Maritime Technology Limited, Feltham, Middlesex.
- Hua, J., Wang, W.-H., Chang, J.R., 1999, "A Representation of GM-Variation in Waves by the Volterra System", Journal of Marine Science and Technology, Vol. 7, pp. 94-100.
- International Association of Classification Societies (IACS), Recommendation No.34, 2001, "Standard Wave Data".
- Ibrahim, R.A., 1985, "Parametric Random Vibration", Research Studies Press, John Wiley & Sons.
- International Maritime Organization (IMO), 2002, "Code on Intact Stability for All Types of Ships Covered by IMO Instruments – Resolution A.749(18) as amended by resolution MSC.75(69)", London.
- International Maritime Organization (IMO), Document SLF 48/4/5, 2005, "Proposal on draft explanatory notes to the severe wind and rolling criterion", Submitted by Japan, 10 June, London.
- Krueger, S., 2005, "Dynamic Intact Stability Criteria", Submitted to the IMO Intersessional Correspondence Group on Intact Stability, Szczecin.
- Kuo, C., Vassalos, D., Alexander, J.G., Barrie, D., 1986, "The Application of Ship Stability Criteria Based on Energy Balance", Proc. 3rd International Conference on Stability of ships and Ocean Vehicles (STAB86), Gdansk, pp. 133-143.
- Neves, M.A.S., Rodriguez, C.A., 2004, "Limits of Stability of Ships Subjected to Strong Parametric Excitation in Longitudinal Waves", Proc. 2nd International Maritime Conference on Design for Safety, Sakai, Japan, pp. 161-167.
- Ochi, M. K., 1990, "Applied Probability & Stochastic Processes in Engineering &

- Physical Sciences", John Wiley & Sons, New York.
- Palmquist, M., 1996, "Assessment of Dynamic Stability of Ships in Following Seas - Paper C: A Roll Motion Model for Ships in Quartering Waves", Licentiate Thesis, Naval Architecture – Dept. of Vehicle Engineering, KTH, Stockholm, Sweden.
- Panjaitan, J. P., 1998, "A Study on Ship Motions and Capsizing in Severe Astern Seas", Ph.D. Thesis, Department of Naval Architecture and Ocean Engineering (NAOE), Osaka University.
- Paulling, J. R., 1961, "The Transverse Stability of a Ship in a Longitudinal Seaway", Journal Ship Research, Vol 4., pp.37-49.
- Rahola, J., 1939, "The Judging of the Stability of Ships and the Determination of the Minimum Amount of Stability Especially Considering the Vessels Navigating Finnish Waters", Technical University of Finland, Helsinki.
- Roberts, J. B., 1982, "Effect of Parametric Excitation on Ship Rolling Motion in Random Waves", Journal of Ship Research, Vol. 26, pp. 246-253.
- Roberts, J.B., Spanos, P.D., 1984, "Stochastic Averaging: An Approximate Method of Solving Random Vibration Problems", International Journal of Non-linear Mechanics, Vol. 21, pp.111-134.
- Roberts, J.B., Spanos, P.D., 1990, "Random Vibration and Statistical Linearization", John Wiley & Sons, Chichester.
- Spyrou, K.J., 2000, "Designing Against Parametric Instability in Following Seas", Ocean Engineering, Vol. 27, pp. 625-653.
- To., C.W.S., 1998, "On the Stochastic Averaging Method of Energy Envelope", Journal of Sound and Vibration, Vol. 212, pp.165-172.
- Tondl, A., Ruijgrok, T., Verlhuust, F., Nabergoj, R., 2000, "Autoparametric Resonance in Mechanical Systems", Cambridge University Press.
- Umeda, N., Hashimoto, H., Vassalos, D., Urano, S., Okou, K., 2003, "Nonlinear Dynamics on Parametric Roll Resonance with Realistic Numerical Modelling", Proc. 8th International Conference on Stability of Ships and Ocean Vehicles (STAB2003), Madrid, pp. 281-290.
- Umeda, N., Yamakoshi, Y., 1986, "Experimental Study on Pure Loss of Stability in Regular and Irregular Following Sea", Proc. 3rd International Conference on Stability of ships and Ocean Vehicles (STAB86), Gdansk, pp. 93-100.

Model Experiment on Parametric Rolling of a Post-Panamax Containership in Head Waves

Harukuni Taguchi, *National Maritime Research Institute (NMRI)*

Shigesuke Ishida, *National Maritime Research Institute (NMRI)*

Hiroshi Sawada, *National Maritime Research Institute (NMRI)*

Makiko Minami, *National Maritime Research Institute (NMRI)*

ABSTRACT

Parametric rolling resonance in head waves was investigated experimentally. An experiment using a scale model of a post-Panamax containership was carried out in regular head waves at the 80 metres square basin of NMRI. In the experiment the wavelength, the wave height, the model speed and the encounter angle were widely varied to clarify overall property of parametric rolling resonance in head waves. As a result, conditions in which the head wave parametric rolling resonance is likely to occur and effects of the encounter period, the wave height and the encounter angle on parametric rolling amplitude were clarified. Moreover numerical simulations of roll motion of a ship in pure head waves were also carried out to investigate the property of parametric rolling resonance further.

Keywords: *parametric rolling in head waves, post-Panamax containership, International Maritime Organization, Intact Stability Code*

1. INTRODUCTION

A post-Panamax containership accident in the north Pacific Ocean, in which that ship suffered extensive loss and damage to onboard containers due to severe parametric rolling in head wave condition (France et al., 2003), led the International Maritime Organization (IMO) to start work to revise the Intact Stability Code (IS Code) in this aspect.

Regarding parametric rolling resonance, phenomenon in following waves is well known, while that in head waves has been less studied so far (e.g. Dallinga et al., 1998, Neves and Valerio, 2000, France et al., 2003, Neves et al., 2003, Bulian et al., 2003). Therefore the

property of behaviour of ships in parametric rolling resonance in head waves has not been clarified thoroughly.

In order to establish appropriate safety measures against severe parametric rolling in head wave condition, influence of hull forms, operating condition (ship speed and course in waves), and wave condition (wave length and wave height) on the occurrence of parametric rolling resonance and the resultant magnitude of roll motion should be clarified.

In this context an experiment with a scale model of a post-Panamax containership was carried out in regular head waves at the 80 metres square basin of NMRI. As a result, some property of the head wave parametric rolling resonance, e.g. conditions in which the

phenomenon is likely to occur, have been clarified. In order to examine the property of parametric rolling resonance, some numerical investigation was also carried out.

2. OUTLINE OF MODEL EXPERIMENT

The experiment was carried out with a free running model in regular waves of various length and height. Using an autopilot device and a motor controller, the encounter angle and the propeller revolution were kept constant for each run.

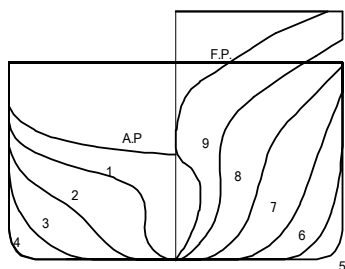


Figure 1 Body plan of model ship.

Table1. Principal particulars

	Ship	Model
L _{pp} (m)	283.8	3.700
B (m)	42.8	0.558
D (m)	24.4	0.318
d (m)	14.0	0.183
V (m ³)	106.970	0.237
C _b	0.629	0.629
GM (m)	1.08	0.014
T _φ (sec.)	30.26	3.460

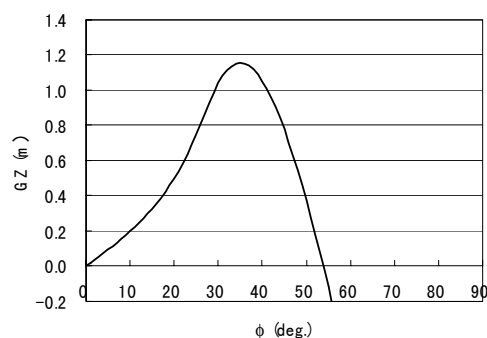


Figure 2 Stability curve (GM = 1.08 m).

The model ship is a 1/76.7 scale model of a 6600TEU containership. The main hull up to the upper deck and the forecastle were

reproduced in the model, but the deckhouse was ignored. Figure 1 shows the body plan of the model and its principal particulars are shown in Table 1. Figure 2 shows the stability curve in the test condition, which was calculated with only the main hull and the forecastle taken into account.

In the experiment six degrees of freedom motion, relative water heights at stem, S.S.5 (weather side) and A.E., lateral acceleration beneath the upper deck at S.S.8, rudder angle, number of propeller revolution and speed and trajectory of the model were measured.

In order to investigate the overall property of parametric rolling resonance, the wavelength λ , the wave height H_w , the model speed V_m , and the encounter angle χ were varied. Table 2 summaries the length and height of waves used in the experiment. The wave height of 11 cm in the model scale corresponds to that of 8.4 m in the actual scale. The encounter angle was varied at every 15 degrees from 135 degrees (bow wave) to 180 degrees (pure head wave). The model speed was varied in a wide range so that the critical condition for parametric rolling resonance could be clarified.

Table2. Waves used in the experiment

λ/L	H _w				
	5cm	8cm	11cm	15cm	20cm
0.9			○		
1.0			○	○	
1.2		○	○	○	○
1.4			○		
1.6	○	○	○		
1.8			○		
2.0			○		
2.2			○		
2.4			○		

3. EXPERIMENTAL RESULTS

3.1 Examples of Parametric Rolling

Typical time series of the ship motion and the lateral acceleration at bow in parametric

rolling resonance are shown in Figures 3

and 4.

Figure 3 shows the measured roll angle ϕ (top), pitch angle θ (middle) and lateral acceleration at bow $\ddot{\eta}$ (bottom) under the conditions of the wavelength to the ship length ratio $\lambda/L = 1.6$, the wave height $H_w = 11$ cm, the encounter angle $\chi = 180$ degrees, and the model speed $V_m = 0.48$ m/s (the corresponding Froude number $F_n = 0.08$). The ratio of the measured encounter period T_e to the natural rolling period T_ϕ , T_e/T_ϕ is about 0.48. Parametric rolling resonance, where there are two pitch cycles for each one roll cycle, occurs from the beginning. The roll motion immediately becomes in steady state where the amplitude of parametric rolling reaches 19 degrees. And the steady state amplitude of the lateral acceleration beneath the upper deck at S.S.8 is about 0.29 g (including the gravity component).

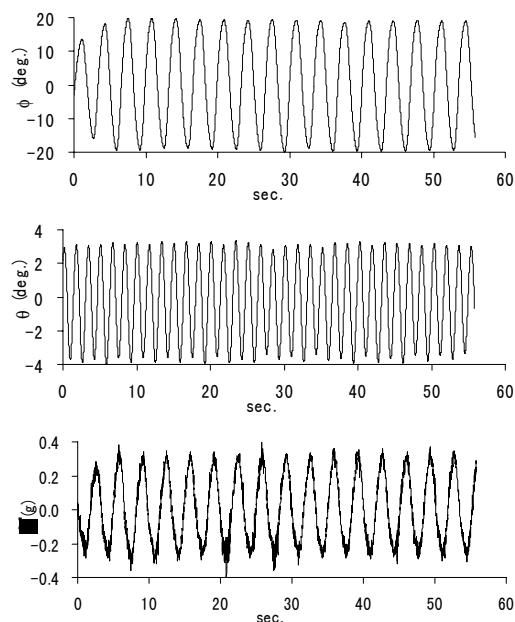


Figure 3 Measured roll angle (top), pitch angle (middle) and lateral acceleration at bow (bottom). $\lambda/L = 1.6$, $H_w = 11$ cm, $\chi = 180^\circ$, and $V_m = 0.48$ m/s ($F_n = 0.08$).

Time histories of the measured data under the conditions of $\lambda/L = 1.6$, $H_w = 8$ cm, $\chi = 135$ degrees, and $V_m = 0.63$ m/s ($F_n = 0.11$) are shown in Figure 4. In this case T_e/T_ϕ is about 0.49. At the beginning the model exhibits a large and small roll responses to every two

encounter waves and gradually transits to parametric rolling response. But even at the end of the run, the rolling amplitude seems not to reach steady state.

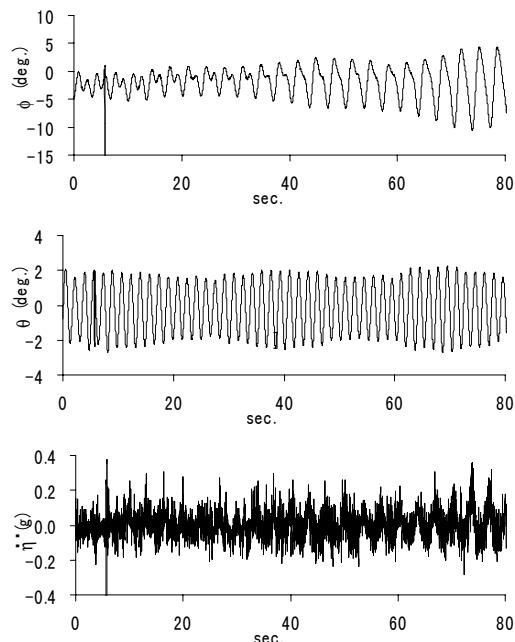


Figure 4 Measured roll angle (top), pitch angle (middle) and lateral acceleration at bow (bottom). $\lambda/L = 1.6$, $H_w = 8$ cm, $\chi = 135^\circ$, and $V_m = 0.63$ m/s ($F_n = 0.11$).

3.2 Occurrence of Parametric Rolling

Occurrence of parametric rolling resonance in waves of $H_w = 11$ cm are summarised in Figures 5 and 6.

Figure 5 shows the occurrence of parametric rolling resonance with the wavelength to the ship length ratio λ/L as parameter, where the encounter angle $\chi = 180$ degrees for the upper figure and $\chi = 150$ degrees for the lower one. The horizontal axis is the model speed in Froude number and the vertical axis is the ratio between the encounter period and the natural rolling period in each figure.

The experimental results are indicated on the lines that show the relation between the model ship speed and the encounter period. The symbol of black circle means condition

where the steady state parametric rolling resonance (see Figure 3) was observed, the cross means one where parametric rolling resonance was not observed, and the white triangle means one where parametric rolling resonance was observed but did not reach the steady state (see Figure 4).

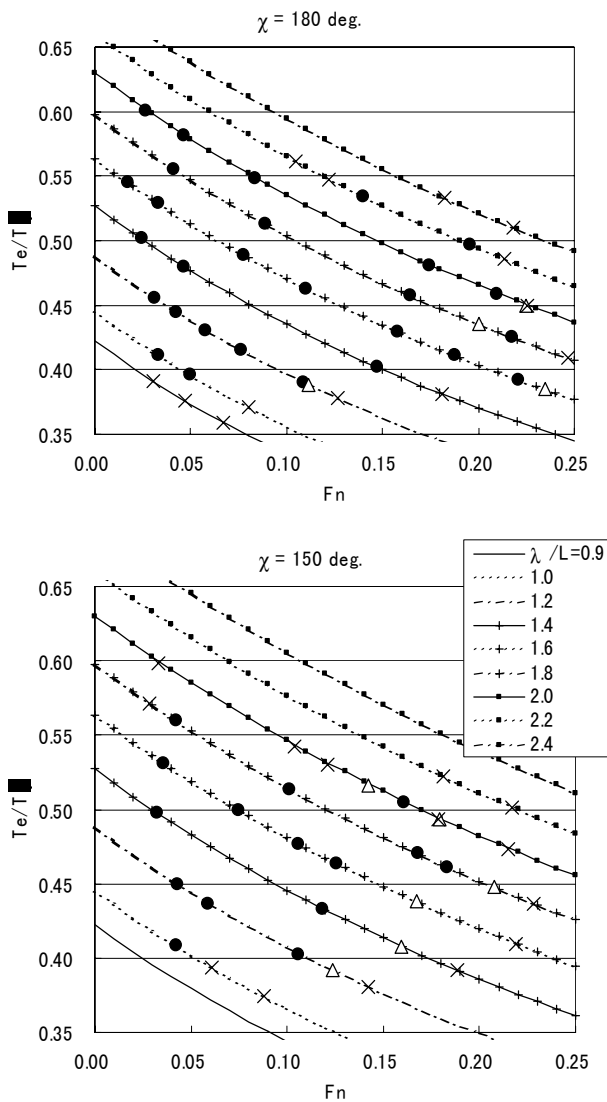


Figure 5 Occurrence of parametric rolling resonance. Hw = 11 cm and $\chi = 180^\circ$ (upper), $\chi = 150^\circ$ (lower).

Figure 6 summarizes the occurrence of parametric rolling resonance at various encounter angles ($\chi = 135^\circ$, 150° , 165° , and 180°), where $\lambda/L = 1.2$ in the upper figure and $\lambda/L = 1.6$ in the lower one. In each figure the horizontal axis is the encounter angle and the vertical axis is the model speed in Froude

number. Symbols mean as the same as in Figure 5.

From these figures we see the followings.

- (1) Parametric rolling resonance occurs in relatively wide range of the encounter period to the natural rolling period ratio, T_e/T_ϕ , namely $T_e/T_\phi = 0.4 \sim 0.6$.
- (2) In the same waves parametric rolling resonance is more likely to occur in pure head wave condition ($\chi = 180$ degrees) than in bow wave condition ($\chi = 135 \sim 165$ degrees).

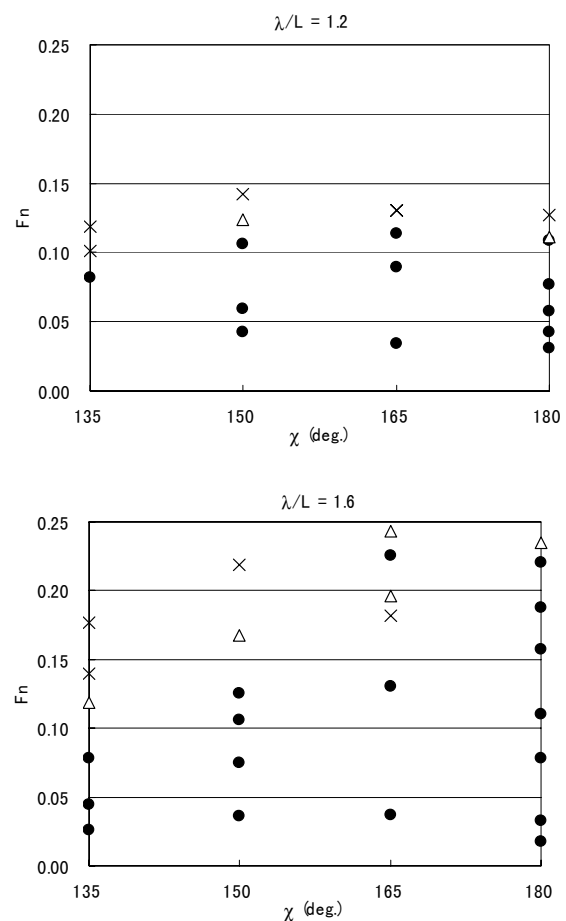


Figure 6 Occurrence of parametric rolling resonance. Hw = 11 cm and $\lambda/L = 1.2$ (upper), $\lambda/L = 1.6$ (lower).

3.3 Amplitude of Parametric Rolling

Influence of Encounter Period Figure 7 shows the steady state amplitude of parametric rolling for various encounter periods under the

condition of the wave height $H_w = 11\text{cm}$ and the encounter angle $\chi = 180$ degrees. The horizontal axis is the encounter period to the natural rolling period ratio and the vertical axis is the parametric rolling amplitude ϕ_s normalised by the wave slope, ϕ_s/kH_w (k is the wave number).

From this figure we see the followings.

- (1) The amplitude of parametric rolling changes largely with the variation of the encounter period.
- (2) For waves of the same length the parametric rolling amplitude becomes the maximum at about $T_e/T_\phi = 0.43 \sim 0.48$.
- (3) The normalised rolling amplitudes for the same encounter period are almost the same except for waves of $\lambda/L = 2.0$ and 2.2 .

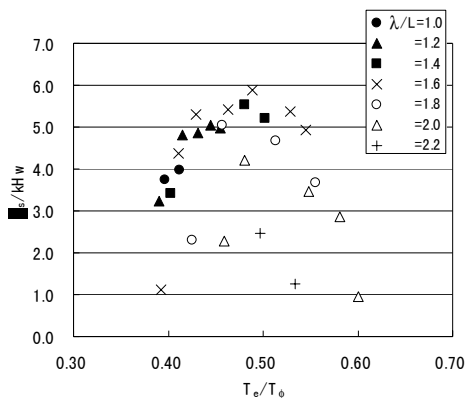


Figure 7 Influence of encounter period on parametric rolling amplitude. $H_w = 11\text{ cm}$ and $\chi = 180^\circ$.

Influence of Wave Height and Encounter Angle As indicated in Table 2, for waves of $\lambda/L = 1.0, 1.2,$ and 1.6 measurements with different wave heights were carried out.

Figure 8 shows the steady state parametric rolling amplitudes measured under the conditions of $\chi = 180$ degrees and $T_e/T_\phi = 0.40$ for $\lambda/L = 1.0,$ $T_e/T_\phi = 0.45$ for $\lambda/L = 1.2$ and 1.6 . The horizontal axis is the wave steepness $H_w/\lambda,$ and the vertical axis is the normalised rolling angle. In the experiment the rolling amplitude did not become larger as the wave height increased beyond 11 cm . Therefore as indicated in Figure 8 the normalised rolling

amplitude becomes smaller as the wave height increases.

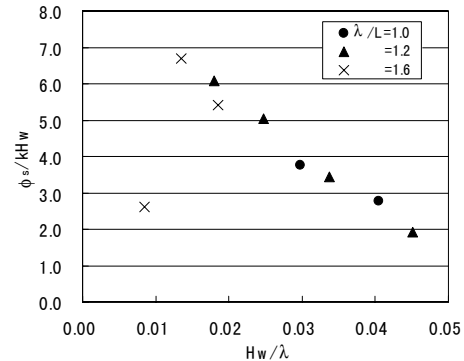


Figure 8 Influence of wave height on parametric rolling amplitude. $\chi = 180^\circ$ and $T_e/T_\phi = 0.40$ for $\lambda/L = 1.0,$ $T_e/T_\phi = 0.45$ for $\lambda/L = 1.2$ and 1.6 .

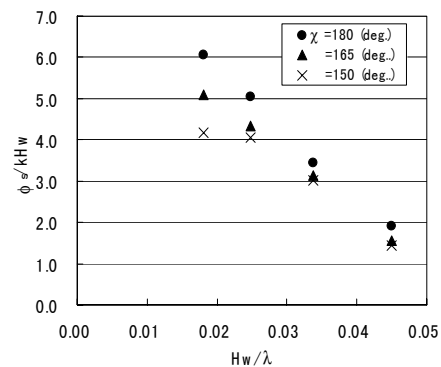


Figure 9 Influence of encounter angle on parametric rolling amplitude. $\lambda/L = 1.2$ and $T_e/T_\phi = 0.45$.

Figure 9 shows the influence of the encounter angle on the parametric rolling amplitudes under the conditions of $T_e/T_\phi = 0.45$ and $\lambda/L = 1.2$. The normalised rolling amplitudes for bow wave condition ($\chi = 150$ and 165 degrees) also become smaller as the wave height increases. And the rolling amplitudes for bow wave conditions are smaller than that for pure head wave condition ($\chi = 180$ degrees).

Investigation into the influence of the wave height on the parametric rolling amplitude is important for judging whether a parametric rolling resonance leads to capsizing in severe waves. In order to draw conclusion of this issue

it seems that more data in various condition (encounter period, wavelength wave height) is necessary.

4. NUMERICAL INVESTIGATION

In order to investigate the property of parametric rolling resonance further, we carried out numerical simulations with an equation of roll motion of a ship with stability variation in waves. In this paper, as the first step of the numerical investigation, we examine the parametric rolling resonance in pure head waves, where no roll exciting moment acts, and investigate effects of ship speed and wave height on the occurrence of parametric rolling resonance and the resultant rolling amplitude.

4.1 Equation of Roll Motion

Roll motion of a ship with stability variation in pure head wave can be generally expressed with equation (1).

$$(I_{xx} + J_{xx})\ddot{\phi} + A\dot{\phi} + B|\dot{\phi}|\dot{\phi} + W \cdot GZ(\phi; t) = 0 \quad (1)$$

where ϕ is the roll angle, I_{xx} is the moment of inertia, J_{xx} is the added moment of inertia, A and B are the linear and the quadratic damping coefficients, W is the displacement, $GZ(\phi; t)$ is the time dependent restoring arm in waves. The dots over the symbol represent differentiation with respect to time t . By dividing all terms in equation (1) by $(I_{xx} + J_{xx})$, this equation is rewritten to following form.

$$\ddot{\phi} + 2\alpha\dot{\phi} + \beta|\dot{\phi}|\dot{\phi} + \omega^2 \frac{GZ(\phi; t)}{GM} = 0 \quad (2)$$

where GM is the metacentric height in still water, $\alpha = A/2(I_{xx} + J_{xx})$, $\beta = B/(I_{xx} + J_{xx})$, and $\omega^2 = WGM/(I_{xx} + J_{xx})$. The stability variation in waves arises from the relative position of ship to wave $\xi_G(t)$, and the vertical ship motions, heave $\zeta(t)$ and pitch $\theta(t)$ in waves. Therefore

the time dependent restoring arm in waves can be expressed as equation (3).

$$GZ(\phi; t) = GZ\{\phi; \xi_G(t), \zeta(t), \theta(t)\} \quad (3)$$

GZ is calculated by integrating the hydrostatic pressure over the instantaneous submerged hull under the undisturbed wave profile, which is determined by the relative position of ship to wave and heave and pitch motions. With this calculation method the instantaneous variation of displacement due to the vertical motions is included. In this paper, the vertical motions are assumed to be linear to the wave height and computed with the strip theory.

In equation (2), the linear and the quadratic damping coefficients obtained from roll decay tests with forward velocity were used. Moreover we examine only steady state response of equation (2). Therefore numerical investigation was carried out with calculation method for obtaining bifurcation diagrams (Taguchi et al., 2003).

4.2 Occurrence of Parametric Rolling

Occurrence of parametric rolling resonance is directly detected with bifurcation diagram.

Influence of Encounter Period To draw bifurcation diagrams, numerical simulations were conducted for $\lambda/L = 1.2, 1.6,$ and 2.0 with the ship speed gradually changed from $Fn = 0$ to 0.25 (service speed) but the wave height kept constant as $H_w = 11$ cm. Figure 10 shows the obtained bifurcation diagrams expressed as the function of the resultant encounter period to the natural rolling period ratio, T_e/T_ϕ . In the diagrams the normalised steady state roll responses at Poincaré section, $\phi(nT)/kH_w$, are plotted as much as 20 cycles for every T_e/T_ϕ calculated. Two points at one T_e/T_ϕ means that parametric rolling resonance occurs at such

encounter period. In each diagram experimental results are also shown with symbols of the same meaning as in Figure 5.

From the top diagram, it is found that for $\lambda/L = 1.2$ the numerical simulation predicts that parametric rolling resonance occurs in wide range of the encounter period to the natural rolling period ratio, namely $T_e/T_\phi = 0.32$ ($Fn = 0.23$) \sim 0.49 ($Fn = 0$). However as indicated in the diagram, in the model experiment parametric rolling resonance was not observed at $T_e/T_\phi = 0.38$. So the numerical simulation with equation (2) overestimates occurrence of parametric rolling resonance in short encounter period range.

For $\lambda/L = 1.6$ (the middle diagram) it is found that parametric rolling resonance occurs in all the calculated range of parameter. In this case good agreement between the numerical simulation and the experimental results is found.

For $\lambda/L = 2.0$ (the bottom diagram) the parametric rolling resonance is predicted to occur in the range of $T_e/T_\phi = 0.45 \sim 0.57$. Compared with the experimental results, it is found that the numerical simulation well predicts the lower limit of the encounter periods for the occurrence of parametric rolling resonance, while it underestimates the upper limit.

The discrepancies between the numerical simulation and the experimental results in the range of encounter period which leads to parametric rolling resonance for $\lambda/L = 1.2$ and 2.0 seem to be mainly caused by the prediction of the stability variation in waves.

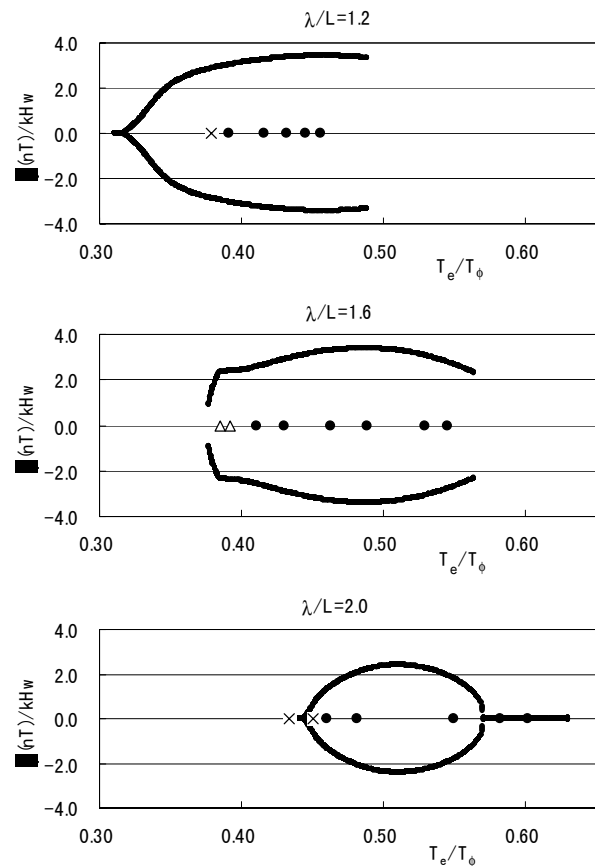


Figure 10 Bifurcation diagram with changing T_e/T_ϕ . $H_w = 11$ cm, $\chi = 180^\circ$, and $\lambda/L = 1.2$ (top); $\lambda/L = 1.6$ (middle); $\lambda/L = 2.0$ (bottom).

Influence of Wave Height Figure 11 shows bifurcation diagrams for $\lambda/L = 1.2, 1.6,$ and 2.0 with the wave height gradually changed but the ship speed kept constant as the resultant encounter period satisfies that $T_e/T_\phi = 0.45$. In each diagrams the horizontal axis is the wave steepness, while the vertical axis is the roll responses at Poincaré section normalised by the wave slope. The experimental results are also shown with the same manner as in Figure 10.

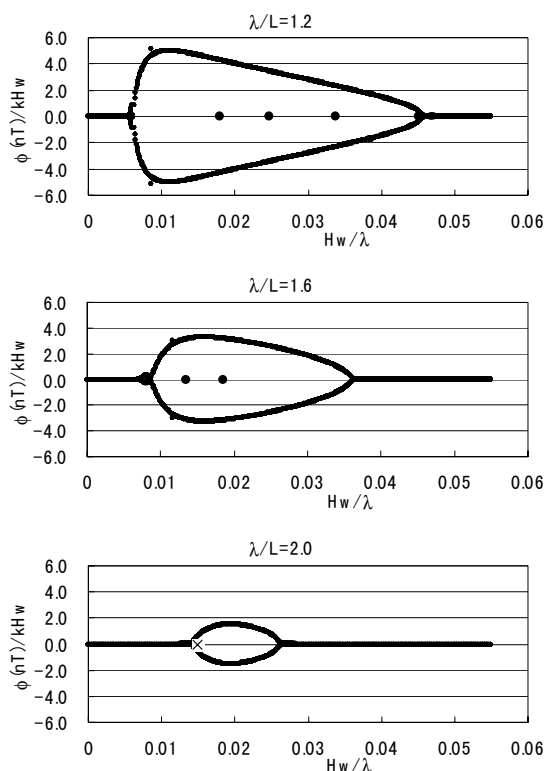


Figure 11 Bifurcation diagram with changing H_w/λ . $T_e/T_\phi = 0.45$, $\chi = 180^\circ$, and $\lambda/L = 1.2$ (top); $\lambda/L = 1.6$ (middle); $\lambda/L = 2.0$ (bottom).

From Figure 11 it is found that the numerical simulations are almost consistent with the experimental results for all the wavelengths examined. And it is also found by the numerical simulations that there are two threshold wave heights, the lower limit and the higher limit of wave heights, for occurrence of parametric rolling resonance. For $\lambda/L = 1.2$ (the upper diagram), the numerical simulation predicts that as the wave height increases from 0, the parametric rolling resonance appears at about $H_w/\lambda = 0.006$ and continue to exist up to about $H_w/\lambda = 0.045$. As the wave height increases further, the parametric rolling resonance disappears. As shown in Figure 8, for $\lambda/L = 1.2$ the model experiment was carried out in waves of up to 20 cm in height ($H_w/\lambda = 0.045$), and parametric rolling resonance was observed in all the wave height tested. In order to confirm the existence of the higher threshold of wave height for parametric rolling resonance, additional model experiment in higher waves seems necessary.

Figure 11 also shows that as the wavelength increases, the range of wave height, which leads to parametric rolling resonance, becomes smaller. As the occurrence of parametric rolling is directly related to the stability variation in waves, further investigation including quantitative examination of the stability variation seems necessary to confirm the effects of the wave height on the occurrence of parametric rolling resonance.

4.3 Amplitude of Parametric Rolling

In this sub section, steady state parametric rolling amplitudes obtained in the calculation of bifurcation diagrams are examined.

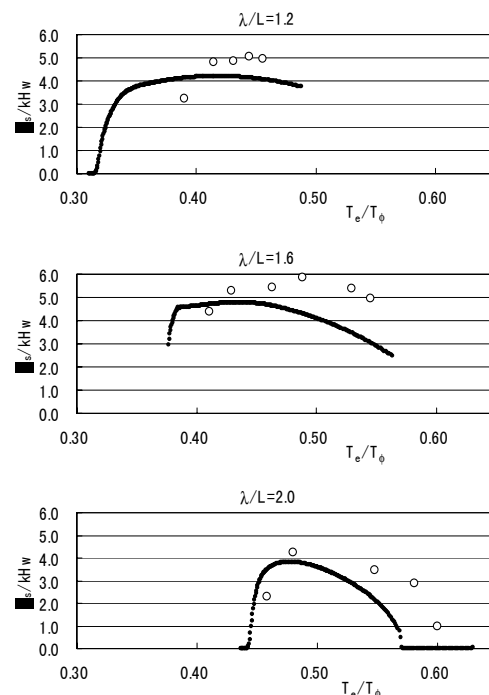


Figure 12 Influence of encounter period on parametric rolling amplitude. $H_w = 11$ cm, $\chi = 180^\circ$, and $\lambda/L = 1.2$ (top); $\lambda/L = 1.6$ (middle); $\lambda/L = 2.0$ (bottom).

Influence of Encounter Period Figure 12 shows the parametric rolling amplitude predicted by the numerical simulations with changing the ship speed as parameter. This figure corresponds to Figure 10. The horizontal axis is the encounter period to the natural rolling period ratio and the vertical axis is the steady state rolling amplitude normalised by

the wave slope. In the diagrams the experimental results are shown with the white circles.

From Figure 12 the numerical simulation seems to capture the tendency of parametric rolling amplitude found in the model experiment. But except for $\lambda/L = 2.0$, the numerical simulation underestimates the maximum amplitude of parametric rolling and there is also some discrepancy in the encounter period leading to the maximum response. As the stability curve of this ship is hard spring type (see Figure 2), the natural rolling period for large rolling amplitude tends to become shorter than that for small amplitude rolling. The numerical simulation may overestimate this effect and the resultant peak encounter period to the natural rolling period ratio becomes smaller than that in the model experiment.

Influence of Wave Height Figure 13 shows the predicted parametric rolling amplitude with changing the wave height as parameter. Compared to the experimental results, which are shown with white circles in the diagrams, the numerical simulation is found to predict the parametric rolling amplitude well. It is also found that the numerical simulation reproduces the tendency shown in the model experiment that the normalised parametric rolling amplitude becomes smaller as the wave height gets larger. In the numerical investigation, as shown in Figure 14, this tendency was observed at different encounter periods too.

5. CONCLUSIONS

The behaviour of a ship in parametric roll resonance in head waves was investigated experimentally with the free running model of a post-Panamax containership in regular waves. And some numerical investigation using an equation of roll motion of a ship with stability variation in waves was also carried out to examine the property of parametric rolling

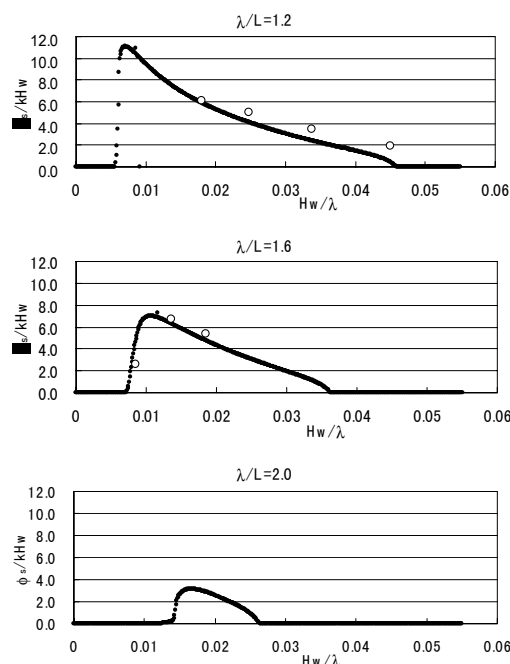


Figure 13 Influence of wave height on parametric rolling amplitude. $T_e/T_\phi = 0.45$, $\chi = 180^\circ$, and $\lambda/L = 1.2$ (top); $\lambda/L = 1.6$ (middle); $\lambda/L = 2.0$ (bottom).

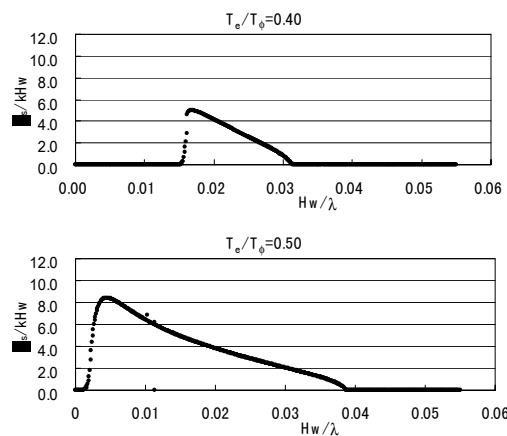


Figure 14 Influence of wave height on parametric rolling amplitude at $T_e/T_\phi = 0.40$ (upper) and 0.50 (lower). $\chi = 180^\circ$ and $\lambda/L = 1.6$.

resonance.

As a result the followings are clarified.

- (1) The parametric rolling resonance occurs in relatively wide range of the encounter period, where the ratio of it to the natural roll period, T_e/T_ϕ ranges from about 0.4 to

0.6.

- (2) In the same wave parametric rolling resonance is more likely to occur in head wave condition ($\chi = 180$ degrees) than in bow wave condition ($\chi = 135 \sim 165$ degrees).
- (3) The amplitude of parametric rolling changes largely with the variation of the encounter period and it becomes the maximum at about $T_e/T_\phi = 0.43 \sim 0.48$.
- (4) The parametric rolling amplitude normalised by the wave slope becomes smaller as the wave height increases.
- (5) The parametric rolling amplitudes for bow wave conditions become smaller than that for the head wave condition.
- (6) The numerical simulation using equation (2) can predict the property of parametric rolling resonance qualitatively.
- (7) Discrepancies found in both the occurrence range and the resultant amplitude of parametric rolling implies that some refinement for the stability variation model in waves, equation (3), is necessary to get more precise prediction.

6. ACKNOWLEDGMENTS

Some parts of this investigation were carried out as a research activity of the SPL research panel of the Japan Ship Technology Research Association, funded by the Nippon Foundation. The authors express their sincere gratitude to the both organizations.

7. REFERENCES

Bulian, G., Francescutto, A., and Lugni, C., 2003, "On the Nonlinear Modeling of Parametric Rolling in regular and Irregular Waves", Proceedings of the 8th

International Conference on the Stability of Ships and Ocean Vehicles, pp.305-323.

Dallinga, R.P., Blok, J.J., and Luth, H.R., 1998, "Excessive Rolling of Cruise Ships in Head and Following Waves", Proceedings of RINA International Conference on Ship Motions & Manoeuvrability, London, pp.1-16.

France, W.N., Levadou, M., and Treakle, T., 2003, "An Investigation of Head-Sea Parametric Rolling and Its Influence on Container Lashing Systems", Marine Technology, Vol. 40, No. 1, pp.1-19.

Neves, M.A.S. and Valerio, L., 2000, "Parametric Resonance in Waves of Arbitrary Heading", Proceedings of the 7th International Conference on the Stability of Ships and Ocean Vehicles, pp.680-687.

Neves, M.A.S., Perez, N., and Lorca, O., 2003, "Analysis of Roll Motion and Stability of a Fishing Vessel in Head Seas", Ocean Engineering, Vol.30, pp.921-935.

Taguchi, H., Sawada, H., and Tanizawa, K., 2003, "A Study on Complicated Roll Motion of a Ship Equipped with an Anti-Rolling Tank", Proceedings of the 8th International Conference on the Stability of Ships and Ocean Vehicles, pp.607-616.

Validation of Parametric Roll Motion Predictions for a Modern Containership Design

Jörg Brunswig, *Germanischer Lloyd*

Ricardo Pereira, *Germanischer Lloyd*

Daewoong, Kim, *Daewoo Shipbuilding & Marine Engineering Co., Ltd.*

ABSTRACT

This paper describes recent efforts to validate two nonlinear time domain programs for simulation of ship motions. The results of the methods ROLLSS and GL SIMBEL were compared with model test measurements of a modern post-Panmax containership model carried out at Hamburg Ship Model Basin (HSVA). This model was designed by Daewoo Shipbuilding & Marine Engineering Co., Ltd. (DSME). Furthermore, to obtain reliable roll damping coefficients, roll damping tests were performed prior to the calculations. For different load cases the occurrence of parametric roll in regular waves was investigated for a range of speeds, wave lengths and wave heights. The computed and measured roll motions revealed a significant nonlinear behaviour with respect to wave height.

Keywords: *Parametric Roll, Simulation, Roll Damping, Validation*

1. INTRODUCTION

The results of an internal research project DYNAS - Dynamic Stability - carried out at Germanischer Lloyd (GL) since 2003 are presented. The first phase of this project just finished. A systematic application of the nonlinear sea keeping methods GL SIMBEL (Pereira, 2003) and ROLLSS (Petey, 1988) to predict the motion behaviour of modern Panmax-, Post-Panmax containerships in severe sea ways was performed. The focus of the first phase was to validate the methods ROLLSS and GL SIMBEL with emphasis on parametric roll. The second phase of DYNAS aims to establish GL classification rules to avoid parametric roll, pure loss of stability, and broaching-to phenomena.

2. PARAMETRIC ROLL

Large modern containerships are susceptible to what is known as parametric rolling (SNAME 2003). Dangerous parametric roll motions with large amplitudes in waves are induced by the variation of transverse stability between the position on the wave crest and the position in the wave trough. Parametric roll primarily occurs under the following conditions:

- Slender hull
- The primary wave system's wavelength varies between half and twice the ship's length
- The wave height exceeds a threshold level
- Almost ahead or astern wave heading
- Low roll damping
- The natural roll frequency ω_r of the ship is about half the encounter frequency ω_e or almost equal to the encounter

frequency.

For frequency ratios of $\frac{\omega_r}{\omega_e} = \frac{1}{2}$ in head

waves or following waves, the stability varies with the encounter frequency ω_e which is approximately twice the roll frequency ω_r of the ship. The stability attains a minimum and maximum twice during each roll motion. The ship reaches the maximum roll angle in the wave trough, where the up-righting moment is large due to the increased stability. On the wave crest with low stability, the roll motion crosses zero. During one encounter period the ship gains energy twice and shows large amplitudes of symmetric rolling.

For frequency ratios of 1:1 in following waves, the stability attains a minimum and a maximum once during each roll motion. This situation is characterised by asymmetric rolling, i.e. the amplitude with the wave crest amidships is greater than the amplitude on the opposite side. In higher waves, parametric roll tends to occur within a bandwidth of frequency ratios between 0.9 and 1.1, see Figure 7.

3. SIMULATION METHODS

Because of two restrictions, linear sea keeping methods like GL PANEL (Papanikolaou/Schellin, 1991) or GL STRIP (Hachmann, 1991) are not suited to predict parametric roll. They do not account for stability changes caused by a passing wave, because the pressure forces are only integrated up to the undisturbed water surface. In addition, these methods are restricted to small amplitude ship motions. Therefore, they are incapable of predicting highly nonlinear phenomena such as parametric roll, which often leads to large roll angles.

The methods to be validated here remedy these problems by simulating in the time domain and treating the motions nonlinearly. We approach parametric roll investigations by the following two-step process:

ROLLSS (2 nonlinear degrees of freedom - surge and roll, very fast) is used to perform a large number of simulations to quickly identify regions of parametric roll occurrence.

GL SIMBEL (6 nonlinear degrees of freedom, slower) is used to yield more accurate results in these regions of interest.

3.1 ROLLSS

The method was first established by Söding (1982) and further developed by Kröger (1986) and Petey (1988). This time domain method uses response amplitude operators (RAO) computed with GL STRIP to determine the sway, heave, pitch, and yaw motions and simulates the surge and roll motions nonlinearly. The righting lever arm is calculated at each time step, using the concept of the equivalent wave (Söding 1982). The wave elevation at location x and time t is calculated by a superposition of all wave components in the chosen seaway spectrum:

$$\zeta(x, t) = \sum_{n=1}^{n_\omega} \Re \left[\hat{\zeta}_n \cdot e^{i(\omega_n t - k_n x \cos \mu_n)} \right] \quad (1)$$

where ω_n is the wave frequency, k_n the wave number and μ_n the wave direction. The equivalent wave is given by

$$\zeta(x, t) = \sum_{n=1}^{n_\omega} \Re \left[\hat{\zeta}_n \cdot e^{i(\omega_n t - k_n x \cos \mu_n)} \right] \quad (1)$$

$$\zeta_e(x, t) = \sum_{n=1}^{n_\omega} \Re \left[\left(\hat{a}_n + \hat{b}_n x + \hat{c}_n \cos \frac{2\pi x}{\lambda} \right) e^{i\omega_n t} \right] \quad (2)$$

where the coefficients \hat{a}_n , \hat{b}_n and \hat{c}_n are determined using the following minimisation problem:

$$\int_{-\frac{L}{2}}^{\frac{L}{2}} (\zeta(x, t) - \zeta_e(x, t))^2 dx = \min! \quad (3)$$

The wavelength of the equivalent wave is $\lambda = L_{pp}$, which is expected to yield the largest parametric roll excitation. The roll equation reads:

$$\ddot{\varphi} = \frac{M - d_L \dot{\varphi} - d_Q \varphi - (g - \ddot{z})mh(\varphi, T, \vartheta, t) - \ddot{\vartheta} \Theta_{xz} \sin \varphi}{\Theta_{xx}} \quad (4)$$

where M is the wave excitation moment obtained from GL STRIP, and d_L and d_Q are linear and quadratic damping coefficients, respectively. Gravity and ship mass are denoted by g and m , and \ddot{z} and $\ddot{\vartheta}$ are the heave and pitch accelerations calculated with GL STRIP. The righting lever arm h was pre-calculated as a function of roll angle φ , draught T and pitch angle ϑ using a hydrostatic method (user-coded NAPA Macros).

3.2 GL SIMBEL

The development of this method dates back to the eighties. It is primarily based on work of Söding (1982), Böttcher (1986) and Pereira (1988, 1989, and 2003). The method simulates large amplitude rigid body motions of mono- and multi hull vessels in six degrees of freedom. Shear forces and bending moments are also determined. In determining the external forces, several assumptions and simplifications were made. These forces comprise:

- forces and moments due to weight,
- Froude-Krylov wave pressures undisturbed by the ship,
- radiation and diffraction pressure, i.e. forces due to the influence of the ship on the pressure field,
- speed effects (resistance and manoeuvring forces),
- propeller and rudder forces (including a

proportional-integral-differential -PID-heading controller or a track-keeping controller),

- forces due to fins and bilge keel actions,
- wind forces,
- as well as forces due to fluid motion in tanks and damaged compartments.

Due to the nonlinearity of large ship motions, radiation and diffraction forces cannot be calculated separately. Radiation forces are generated by the ship motions. Radiation forces represent the difference between the forces of the non-moving ship in waves and the Froude-Krylov forces (undisturbed wave forces). If the ship partly emerges from the water, the diffraction component of the emerged part must be zero. Therefore, radiation and diffraction forces are determined using the relative-motion hypothesis. The force is assumed to depend on the motion of the ship minus the motion of the water at the different cross-sections. The orbital velocity of the wave components of the seaway is averaged over a ship cross section. The total force is obtained by integrating the contribution of the ship sections. Longitudinal interactions due to forward speed effects are treated in the same way as for linear strip methods. The pressure distribution not only depends on the instantaneous acceleration of the ship, but also on the preceding accelerations (memory effects). For linear computations in regular waves, these memory effects result in the frequency dependence of the complex added mass matrix, which contains the proportionality constant between the relative motion acceleration of a ship section and the force per length:

$$f = A\ddot{u} \quad (5)$$

where f and u are 3-component column vectors, while A is a complex 3 by 3 matrix.

For simulations of motions in a natural seaway, the frequency dependency of these

matrices constitutes a challenge, because many frequencies occur at the same time. A solution to this problem is the use of convolution integrals (impulse-response functions), which account for the dependency of these forces on the accelerations at different time steps. The state space model is a faster solution. It uses a relation between acceleration and force derivatives:

$$A_0\ddot{u} + A_1\frac{\partial}{\partial t}\ddot{u} + A_2\frac{\partial^2}{\partial t^2}\ddot{u} \dots = B_0 + B_1\dot{f} + B_2\ddot{f} + \dots \quad (6)$$

The 3×3 matrices A_k and B_k are frequency independent but depend on the actual submergence and roll motion. Implicitly, they are time dependent and are computed from the frequency dependent coefficients by regression analysis. During the simulation, the actual waterline inclination and immersion are considered on the interpolation of the matrices.

4. ROLL DAMPING

The damping moment model comprises a linear and a quadratic term:

$$d_D = -b_L \dot{\varphi} - b_Q \dot{\varphi} |\dot{\varphi}|. \quad (7)$$

The coefficient b_L contains a small speed independent part caused by wave generation of the rolling ship and another (in most cases larger) part that is proportional to the forward speed of the ship and is caused by lift forces generated by hull, propeller, and rudder. The coefficients are taken from Blume (1979). The coefficient b_Q includes bilge keel effects. Blume presents his model test results in diagrams for different breadth/depth ratios and different block coefficients. In his plots, the non-dimensional roll damping coefficient ϕ_{Stat}/ϕ_{Res} is used, which denotes the ratio between the heel angle due to a static moment and the roll amplitude for the equivalent

resonant roll moment. The ratio is dependent on Froude number. To check the accuracy of Blume's coefficients for a modern containership, model tests were carried out. The linear damping constant b_L was determined from forced roll motion model tests (motion excited by rotating masses), using the following equation:

$$b_L = \frac{m g G M_0}{\omega_r} \left(\frac{\phi_{Stat}}{\phi_{Res}} \right)_{5^\circ}, \quad (7)$$

where ω_r is the roll resonance frequency and $G M_0$ is the metacentric height.

The nonlinear roll damping coefficient b_Q was also determined from forced roll motion tests. For the resonance angle $\phi_{Res} = 20^\circ$ an effective linear roll damping coefficient b_{eff} was calculated:

$$b_{eff} = \frac{m g G M_0}{\omega_r} \left(\frac{\phi_{Stat}}{\phi_{Res}} \right)_{20^\circ}. \quad (7)$$

For a roll oscillation with frequency ω_r and amplitude $\varphi_A = 20^\circ$, it was assumed that the linear roll damping coefficient b_{eff} is equivalent to the quadratic damping constant b_Q (without bilge keels). To estimate b_Q , the linear component b_L was subtracted from b_{eff} :

$$b_Q = \frac{3\pi}{8 \omega_0 \varphi_A} (b_{eff} - b_L) \quad (7)$$

The results are shown in Figure 2 and compared with Blume's coefficients derived from experiments carried out in the seventies. The figure clearly shows that the results for zero speed are reasonable, but deviate significantly for higher Froude numbers. For the highest Froude numbers, twice the values compared to Blume's were determined. In all

subsequent calculations, the coefficients derived from our experiments were used. Roll damping coefficients could have been obtained also on the basis of other approaches, such as on the well-known concept documented by Ikeda et al. (1978). Their approach comprises friction damping, eddy damping, lift damping, and wave damping of the bare hull and normal force damping, hull pressure damping, and wave damping of bilge keels. As we had available experimental data obtained from model test measurements that already accounted for all hull damping components, we used these data to determine damping coefficients for the bare hull. To account for bilge keel damping, we added an equivalent bilge keel damping moment according to Gadd (1964).

5. PREPARATIVE CALCULATIONS

A large number of simulations in regular waves were carried out prior to the model tests to determine which situations regarding wave length and ship speed are relevant for validation purposes. The selected hull form from DSME is shown in Figure 1. The main particulars and investigated load cases of the ship were:

Length over all	332 [m]
Length b. perp.	317 [m]
Breadth	43.2 [m]
Design draught	14.4 [m]
r_{xx} / B	0.384 [-]
r_{yy} / L_{pp}	0.255 [-]
r_{zz} / L_{pp}	0.254 [-]
Load case 1	
GM0	1.26 [m]
Mass	140283
Draught aft	14.647
Draught fore	14.238
Load case 2	
GM0	3.8 [m]
Mass	122908
Draught aft	12.949
Draught fore	12.728

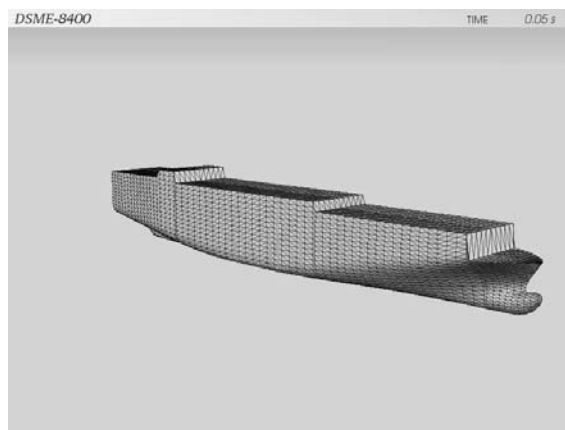


Figure 1: Containership Hull Form

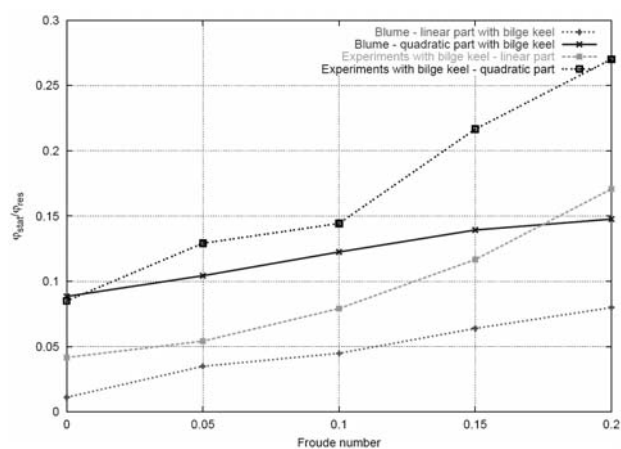


Figure 2: Comparison of the non-dimensional roll damping coefficient ϕ_{Stat} / ϕ_{Res} acc. to Blume with model tests

The first load case was chosen as the one with the smallest realistic GM_0 in the stability booklet. Load case 2 was chosen to represent the upper range of realistic transverse stability values. The purpose of this load case was to show the effect of a larger GM_0 on the frequency ratios and the maximum roll angles in parametric roll situations.

The range of wave lengths was set from 70 to 650 m, and Froude numbers from zero speed to $Fn = 0.25$ were investigated for wave heights ranging from 2 to 10 m. ROLLSS calculations were performed for 59 wave lengths, 26 speeds, and 5 wave heights. To reduce the computational effort, the number of wave lengths was decreased to 16 for the GL SIMBEL calculations.

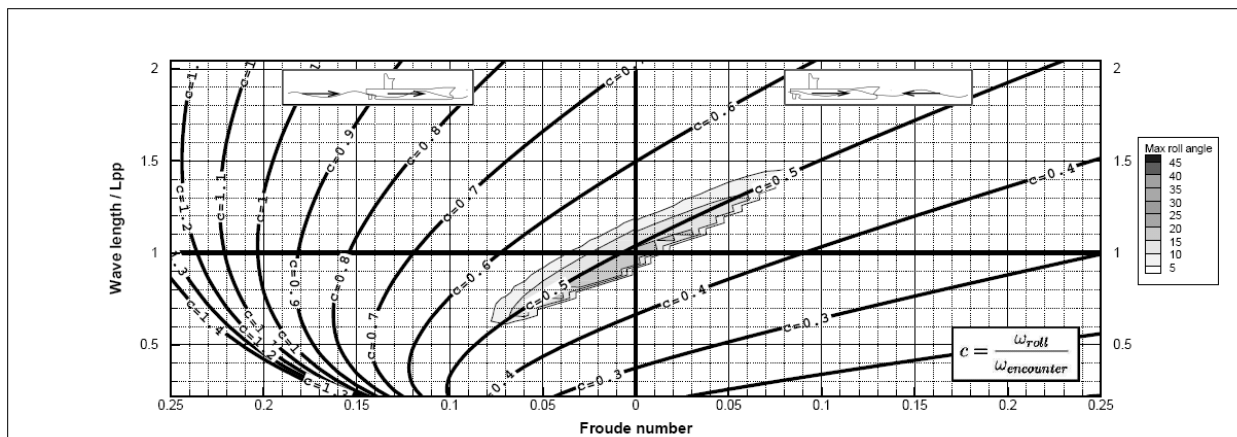


Figure 3: ROLLSS Results for Wave Height 2m

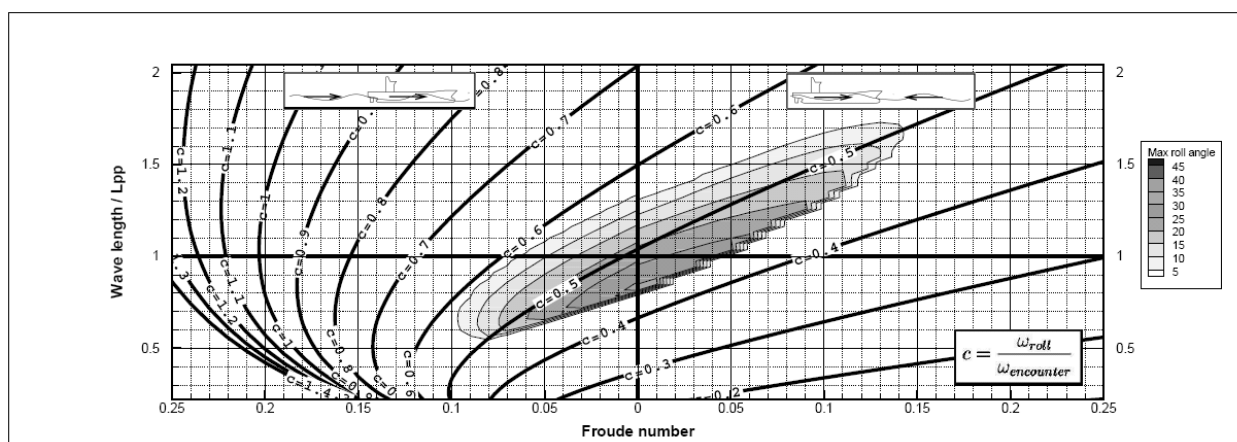


Figure 4: ROLLSS Results for Wave Height 4m

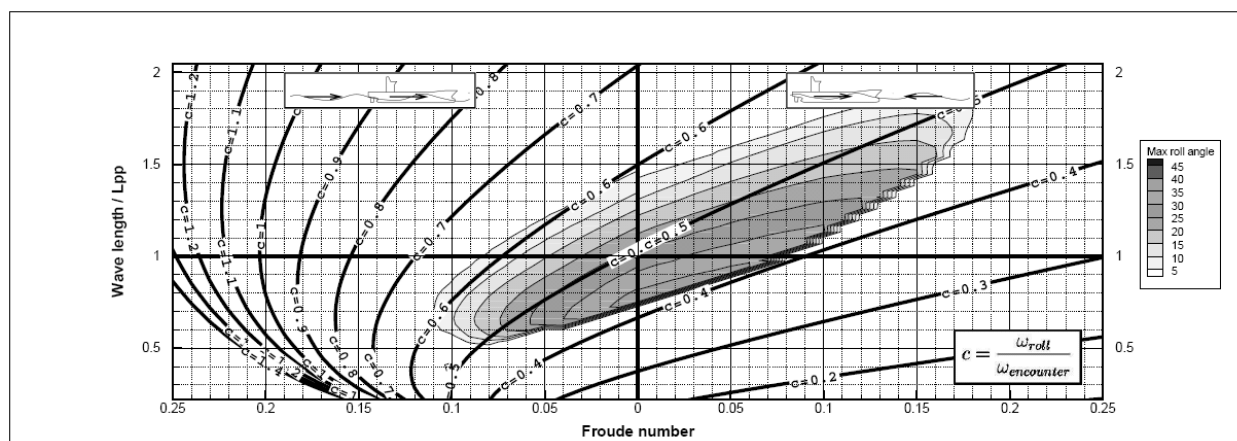


Figure 5: ROLLSS Results for Wave Height 6m

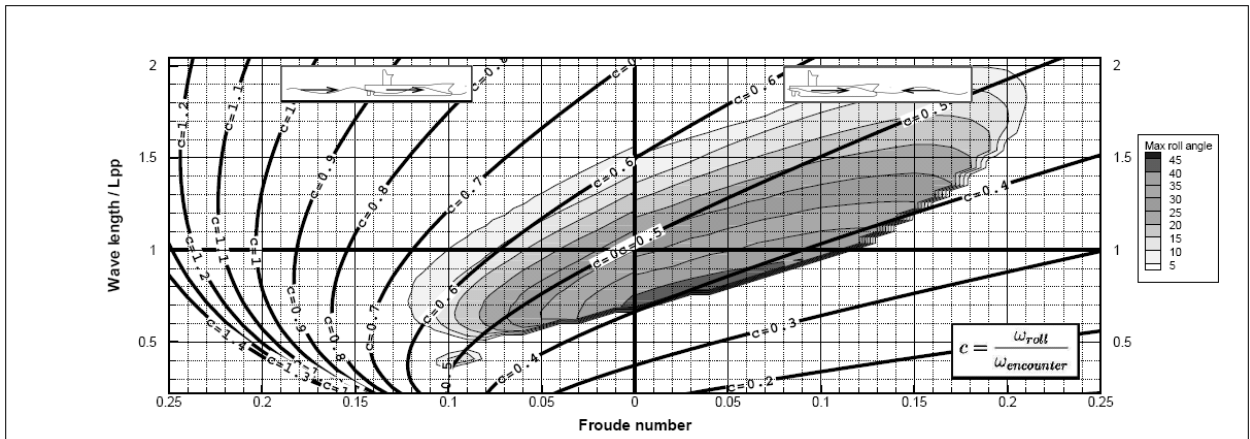


Figure 6: ROLLSS Results for Wave Height 8m

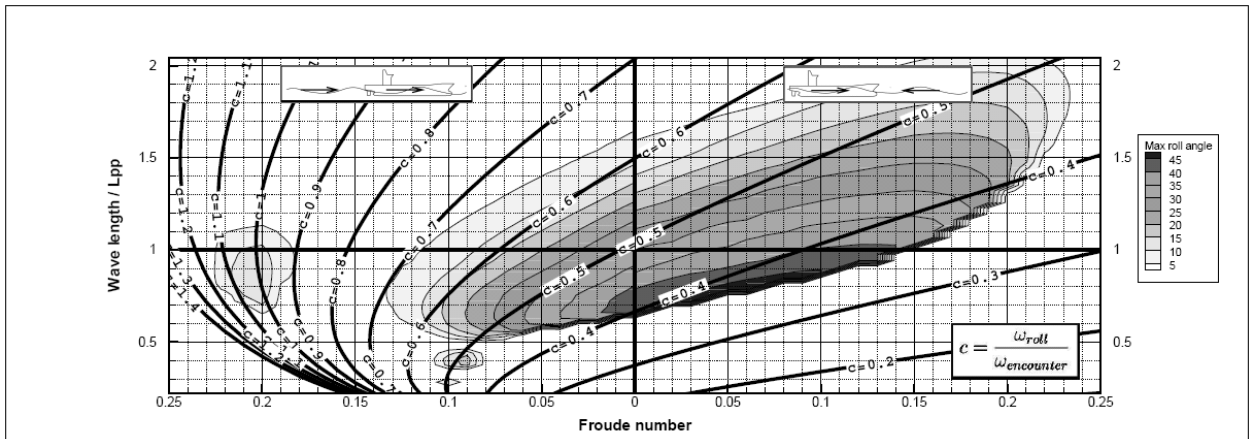


Figure 7: ROLLSS Results for Wave Height 10m

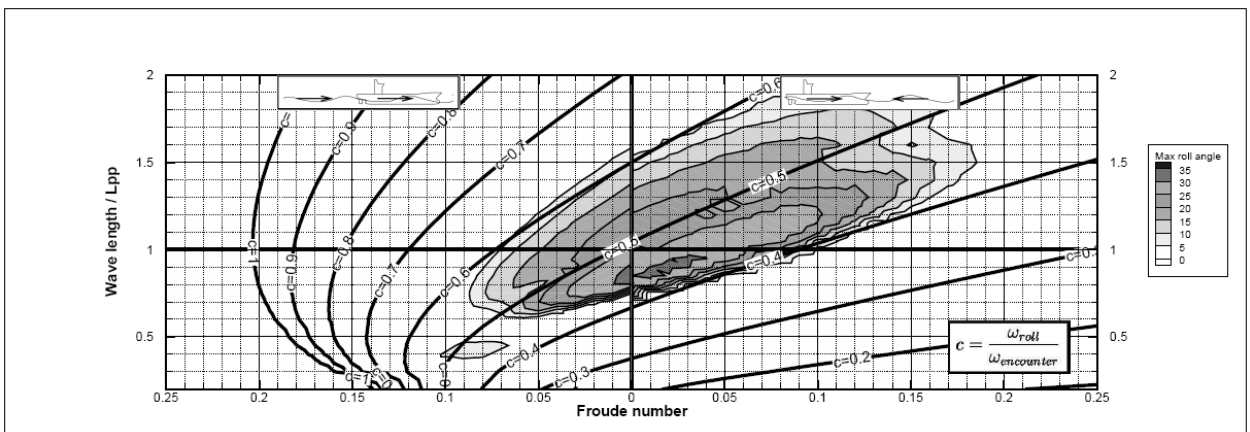


Figure 8: GL SIMBEL Results for Wave Height 8m

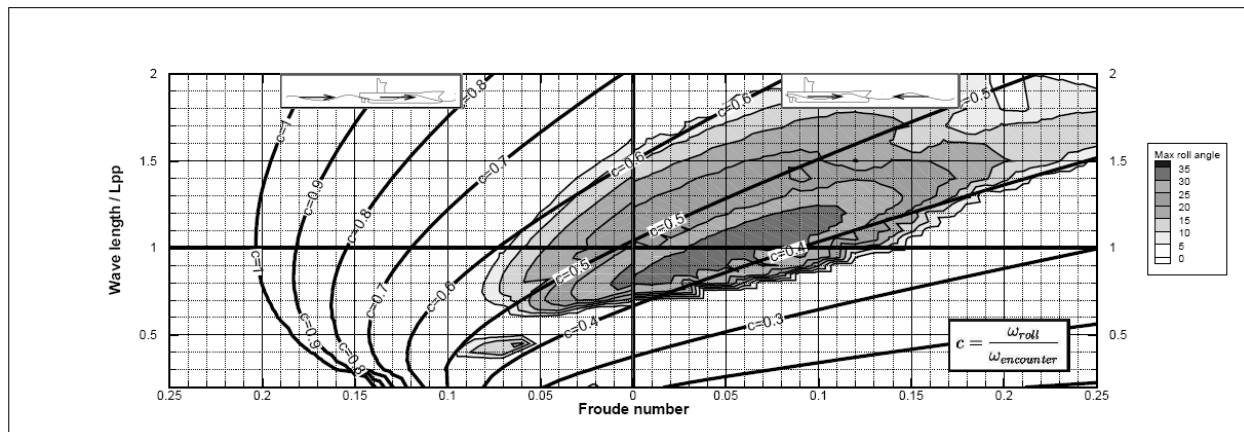


Figure 9: GL SIMBEL Results for Wave Height 10m

Table 1: Comparison of Maximum Roll Angles for Head Waves (Wave Height 10m)

Test Run No.	μ [°]	λ/L_{pp}	Fn [-]	φ_{max} [°]		
				Experiments	GL SIMBEL	ROLLSS
10	178	0.6	0.059	0.0	0.1	0.0
18	178	1.0	0.040	30.0	32.1	31.0
19	178	0.9	0.022	31.0	33.3	32.0
21 b	175	0.9	0.065	36.0	37.2	38.0
22	175	0.9	0.030	37.0	32.2	33.0
23	177	1.1	0.052	29.0	31.9	28.0
24	177	1.3	0.076	22.0	28.6	24.0
26	177	1.5	0.068	18.0	21.8	17.0
27	177	1.7	0.061	17.0	15.0	7.5
28	177	2.0	0.085	0.3	0.9	0.0
31	177	1.0	0.052	31.0	33.6	32.0
32	177	1.0	0.108	1.4	37.7	39.0
33 a	177	1.0	0.055	31.0	34.0	32.0
33 b	177	1.0	0.131	22.0	33.2	41.0
34 a	177	1.0	0.099	26.0	38.4	38.0
34 b	177	1.0	0.146	0.0	0.0	0.0

Table 2: Comparison of Maximum Roll Angles for Following Waves (Wave Height 10m)

Test Run No.	μ [°]	λ/L_{pp}	Fn [-]	φ_{max} [°]		
				Experiments	GL SIMBEL	ROLLSS
38	3	0.9	0.197	2.5	0.0	15.0
39	3	0.9	0.204	4.0	0.2	15.0
40	5	0.9	0.204	10.0	0.2	16.0
52	5	0.9	0.206	15.0	0.2	16.0
54	2	0.7	0.095	0.7	0.1	15.0
55	2	0.8	0.063	18.5	15.2	22.0
56	0	0.8	0.063	18.0	15.2	22.0
57	0	1.0	0.060	17.0	10.7	17.0

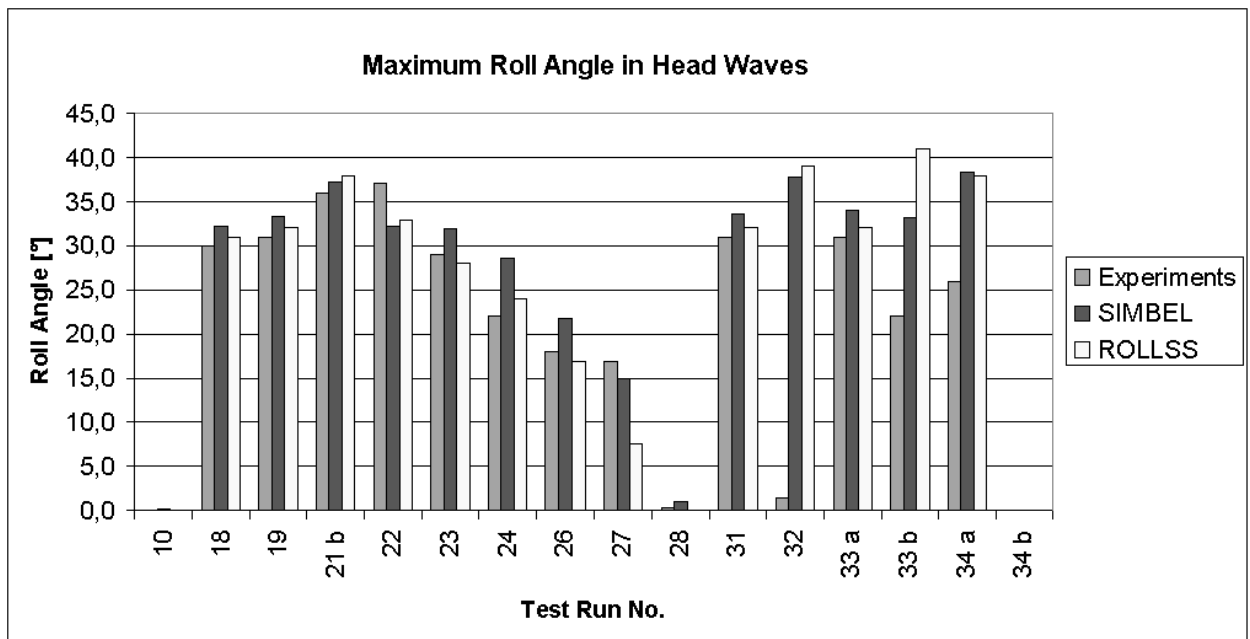


Figure 10: Comparison of Simulations and Tests in 10m Head Waves

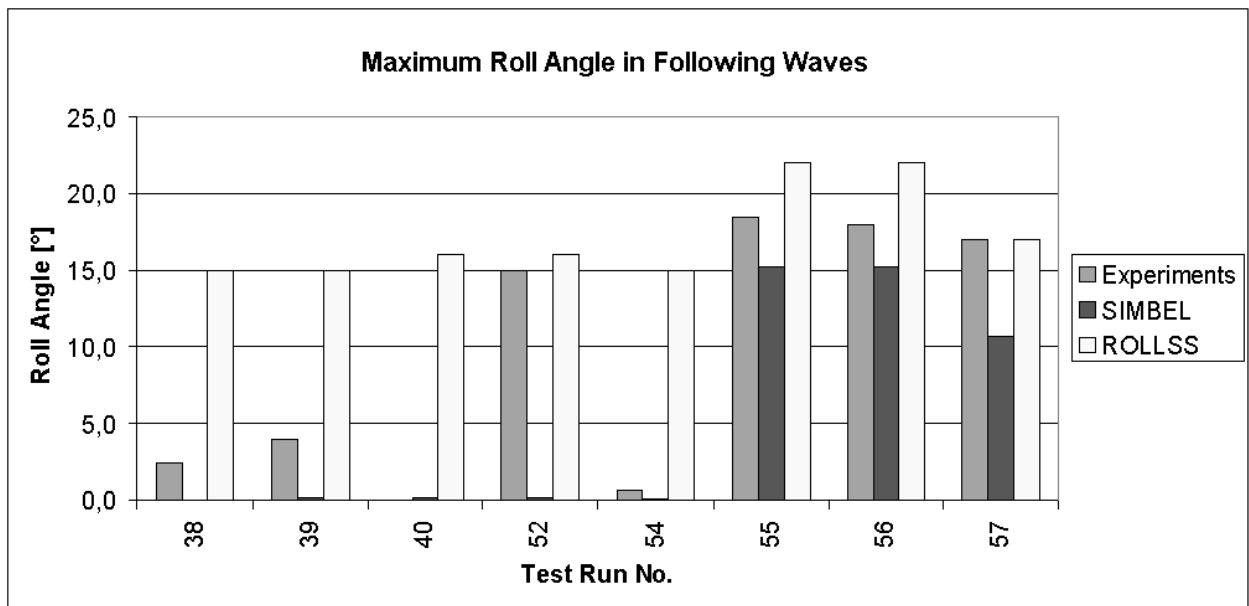


Figure 11: Comparison of Simulations and Tests in 10m Following Waves

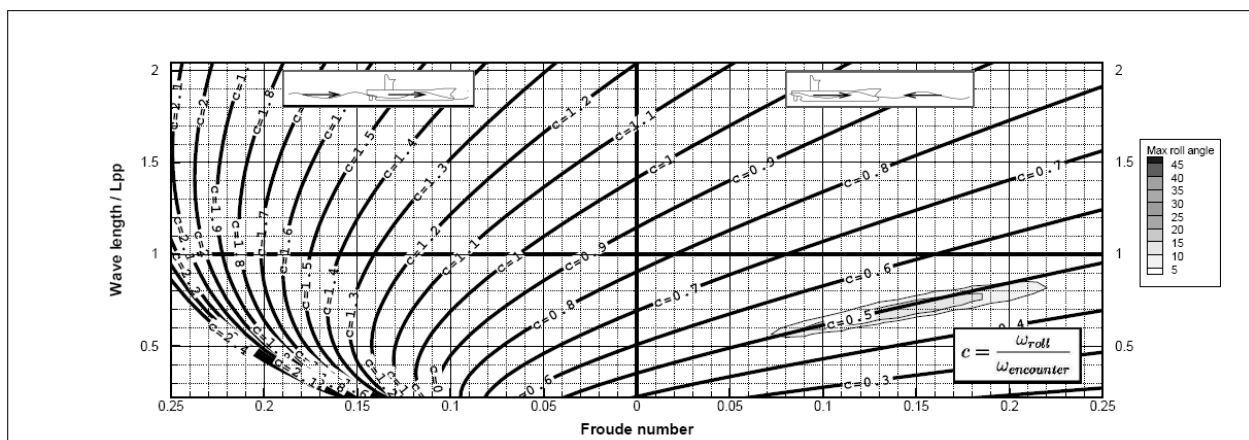


Figure 12: ROLLSS results for $GM_0=3.8\text{m}$, Wave Height 10m

Figures 3 to 9 show the results for load case 1. The left hand side of the figures depicts the results in following waves, whereas the right hand side shows the results in head waves. ROLLSS and GL SIMBEL yielded similar areas of parametric roll occurrence with small differences in the predicted maximum roll angles. As expected, these areas developed in the vicinity of the frequency ratio 0.5. They

become larger for higher wave amplitudes. The boundary towards smaller wavelengths shows a sudden transition from quiescence to large roll amplitudes. The decrease of roll angles towards longer waves is smoother. Only ROLLSS predicted parametric roll with the frequency ratio 1:1 at a wave height of 10 m, see Figure 7.

Figure 12 shows the results for load case 2. The curves of constant frequency ratio are shifted towards lower speeds in following waves and towards higher speeds in head waves. The area of occurrence of parametric roll is narrower than predicted for the smaller GM_0 , and maximum roll angles reach only 10° to 15° .

6. MODEL TESTS

In the German research project ROLL-S, a new sophisticated test procedure for a fully automated motion measurement of a free running ship model was developed (Kuehnlein et al. 2003). The ship's course was controlled by the master computer using telemetry. Ship motions in six degrees of freedom were accurately registered by computer controlled guidance of both towing and horizontal carriage. The speed of the propeller had to be fixed before starting the test. This resulted in a strong decrease of the model speed as soon as parametric rolling developed, making it difficult to hold a constant velocity during a test run or to reach a given Froude number.

The model tests were carried out in 10 m high regular waves for load case 1 only. The model scale was 1:53. The angle of encounter was close to 0° (following waves) or 180° (head waves). Because of the limited number of test runs, it was impossible to generate result plots as detailed as for the preparative simulations. Tables 1 and 2 summarise the obtained roll angles of the model tests and the simulations. Figures 10 and 11 show the same data as bar charts.

In following waves for the frequency ratio 1:1, GL SIMBEL simulations did not predict parametric roll for $\lambda/L_{pp} = 0.9$, compare Fig. 7 and 9. The extensive computer running times of GL SIMBEL set a limit to the number of cases investigated with this method. Consequently, significantly fewer cases were analyzed with GL SIMBEL than with ROLLSS. This situation, in conjunction with

the fact that the mathematical model of these two methods was not identical, possibly brought about the diverse predictions of GL SIMBEL and ROLLSS. Furthermore, for this frequency ratio (test runs no. 38, 39, 40, 52), it was difficult to determine the maximum roll angle in the experiments, because the roll motion still increased when reaching the end of the model basin. Therefore, the test runs for this condition were repeated several times, and the results did not show a clear trend for the maximum roll angles, see Table 2.

7. CONCLUSIONS

A large number of simulations were carried out using GL SIMBEL and ROLLSS. Model tests in regular waves were performed and the results were compared to the simulations. The results of simulations and experiments compared favourably for most test runs. The head sea experiments 32, 33b and 34a for situations close to the steep transition from quiescence to large roll angles showed bad correlation with the simulations.

For the frequency ratio 1:1 in following waves (test runs no. 38, 39, 40, 52) it was difficult to determine the maximum roll angle in the experiments because the roll motion still increased when reaching the end of the model basin.

Both methods demonstrated their ability to predict the occurrence of parametric roll in head and following seas. Although ROLLSS is based on a simpler mathematical model than GL SIMBEL, both methods predicted similar roll. This demonstrated that the chosen approaches were well suited for the phenomena investigated here. The main factor that causes the parametric roll, changes in the wetted surface of the ship, is captured in both methods. ROLLSS takes this into account with pre-calculated heeling arm curves and GL SIMBEL calculates the hydrostatic pressure at the actual position of

the ship at each time instant. For other headings, the accuracy of GL SIMBEL is expected to be better due to the nonlinear coupling of all ship motions. However, this was not yet experimentally validated.

The importance to re-evaluate the roll damping coefficients for modern ship designs was demonstrated. The next phase of DYNAS focuses on the validation of the numerical codes in irregular sea ways.

8. REFERENCES

- Blume, P., 1979, "Experimentelle Bestimmung der Koeffizienten der wirksamen Rolldämpfung und ihre Anwendung zur Abschätzung extremer Rollwinkel", Schiffstechnik, Vol. 26.
- Böttcher, H., 1986, "Ship motion simulation in a seaway using detailed hydrodynamic force coefficients", STAB 1986, 3rd International Conference on Stability of Ships and Ocean Vehicles, Gdansk.
- Gadd, G.E., 1964, "Bilge keels and bilge vanes", Report Nr. 64, National Physical Laboratory, Ship Division.
- Hachmann, D., 1991, "Calculation of Pressures on a Ship's Hull in Waves", Ship Technology Research, Vol. 38, No. 3.
- Ikedo, Y.; Himeno, Y.; Tanaka, N., 1978, "A Prediction Method for Ship Roll Damping", Department on Naval Architectural, University of Osaka Prefecture, Report Nr. 00405.
- Kröger, H.P., 1986, "Rollsimulation von Schiffen im Seegang", Schiffstechnik, Vol. 33.
- Kuehnlein, W.L.; Brink, Kay-Enno; Hennig, J., 2003, "Innovative deterministic seakeeping test procedures", STAB 2003, 8th International Conference on the Stability of Ships and Ocean Vehicles, Madrid.
- Papanikolaou, A.D.; Schellin, T.E., 1991, "A Three-Dimensional Panel Method for Motions and Loads of Ships with Forward Speed", Ship Technology Research, Vol. 39, No. 4.
- Pereira, R., 1988, "Simulation nichtlinearer Seegangslasten", Schiffstechnik, Vol. 35-4, pp. 173-193.
- Pereira, R., 1989, "Ermittlung der Belastungen von Schiffen in steilem Seegang durch Simulation", Jahrbuch der Schiffbautechnischen Gesellschaft, Summer Meeting, Berlin, Vol. 83, pp. 145-158.
- Pereira, R., 2003, "Numerical Simulation of Capsizing in Severe Seas", STAB 2003, 8th International Conference on the Stability of Ships and Ocean Vehicles, Madrid
- Petey, F., 1988, "Ermittlung der Kenersicherheit leerer Schiffe im Seegang aus Bewegungssimulationen", Report Nr. 487, Institut für Schiffbau der Universität Hamburg
- SNAME AD HOC PANEL #13, 2003, "Investigation of head-sea parametric rolling and resulting vessel and cargo securing loads", Marine Technology, 41.
- Söding, H., 1982, "Leckstabilität im Seegang", Report Nr. 429, Institut für Schiffbau der Universität Hamburg

Numerical Simulation of Parametric Roll in Head Seas

Dimitris Spanos, *National Technical University of Athens*

Apostolos Papanikolaou, *Ship Design Laboratory (NTUA-SDL)*

ABSTRACT

A time-domain numerical simulation method is applied for the investigation of parametric roll resonance in regular head waves for two different types of vessels, namely a fishing vessel and a RoRo ship. The employed mathematical model captures satisfactorily most of the parameters relevant to the problem hence enables an improved reproduction and understanding of the complicated non-linear parametric roll phenomenon. The coupling between the induced roll and pitch motions along with the nonlinear character of the restoring moment associated with large amplitude wave induced motions have been found to be the determinant factors of the observed roll resonance phenomenon. Furthermore, a strong dependence of the roll resonance on both the wave frequency of encounter and the incident wave height has been recorded. The obtained numerical results were compared with corresponding available experimental measurements and commented.

Keywords: *time-domain, numerical simulation, parametric resonance, roll motion, non-linear dynamics, dynamic stability, capsizing*

1. INTRODUCTION

The phenomenon of parametric roll has been extensively studied over the last decades, but it still remains of high interest because of the practical implications related to the induced large amplitude roll motions (e.g., France et al. 2003) and due to its complicated highly non-linear character that makes its prediction quite difficult in actual seaways.

Parametric roll is considered as the induced roll motion of a ship due to the periodic change of the restoring characteristics as the ship advances through the waves. Parametric roll is expected to occur when the wave frequency of encounter is close to the double of the natural roll frequency of the vessel. Given this condition, the other parameters of the problem eventually determine the occurrence as well as the intensity of the phenomenon. These parameters are particularly the hull form and the related hydrostatic characteristics, the vessel's loading condition and forward speed,

the roll damping effects and the wave characteristics like wave heights and frequencies.

Several approaches have been employed to analyze and understand the parametric roll phenomenon ranging from the uncoupled, one degree of freedom non-linear roll equation, adjusted with appropriate parameters, e.g. Francescutto (2002), Umeda et al. (2003), to models of multi degrees of freedom, where the roll motion is appropriately coupled with the other motions, Belenky (2003), Ribeiro et al. (2005), Neves, (2005), Krueger (2006). Parametric roll has been investigated for both regular and irregular seaways, as well as for following and head seas conditions. Despite the substantial progress for the regular waves, the resonance conditions in irregular waves have not yet been resolved. A recent review of the related literature has been carried out by ITTC (2005).

In subsequent sections, a nonlinear time-domain numerical simulation method is applied to investigate the behaviour of two different

types of vessels, namely a fishing vessel and a RoRo ship, with respect to parametric rolling in regular head waves. The same method has been applied earlier (Spanos & Papanikolaou, 2005) to systematically explore the physical parameter space of parametric rolling for the fishing vessel. There, a strong nonlinear dependence of the induced roll motion on the incoming wave heights has been observed. In the present paper this behaviour is further analyzed and interpreted in more depth in terms of motion couplings and nonlinear restoring. Having understood and verified numerically the performance of the fishing vessel, a different type of vessel, namely a modern RoRo, is herein additionally studied aiming at exploring the earlier identified basic characteristics of the nonlinear parametric roll phenomenon for a different type of hull form.

2. THE NUMERICAL SIMULATION METHOD

The numerical simulation method applied herein for the evaluation of extreme motions of ships in seaways is a nonlinear time domain numerical method which is based on linear potential theory with respect to the basic hydrodynamics of the problem and considers a variety of important non-linear terms of ship's equations of motions, like the excitation by large amplitude regular or irregular waves, the exact body geometry below and above the still waterline and its impact on ship's restoring, semiempirical nonlinear viscous damping, as well as possible sloshing effects due to moving fluids internally to the vessel or trapped on the deck, (Spanos, 2002).

The mathematical modelling of the method is herein implemented with the computer code CAPSIM. The method has been successfully applied in the past for the simulation of ship motions at zero forward speed in intact and damaged/flooded conditions as well as for the estimation of wave loads and particularly of drift forces on floating bodies, (Spanos & Papanikolaou, 2005b), and proved very

efficient and satisfactory in many practical cases.

The essential characteristics of the method are outlined in the following. The sailing ship is considered rigid and of arbitrary shape moving with six degrees of freedom in response to incident waves. The equations of motion of the body in the 3D space are derived by application of the momentum conservation theorem. The equations are expressed in the ship-fixed coordinated system and are given below

$$m(\dot{\vec{U}} + \vec{\omega} \wedge \vec{U}) = \vec{F} \quad (1)$$

$$[I]\dot{\vec{\omega}} + \vec{\omega} \wedge [I]\vec{\omega} = \vec{M} \quad (2)$$

where m and $[I]$ are the mass and the matrix of moments of inertia of the ship respectively, U and ω the linear and angular velocity and F, M are the external to the ship forces and moments. The velocity U is the relative velocity of the origin of the ship-fixed system to an inertia coordinate system that moves with a constant speed and course.

The external forces acting to the body comprise of gravity, hydrostatic and hydrodynamic components; others might be added in a straightforward way (wind & current forces, etc). Following the potential theory, the wave effects, as the dominant dynamic part, are further analyzed into Froude-Krylov or undisturbed incident wave, diffraction and radiation effects.

Incident wave forces together with the hydrostatic ones are calculated through direct integration of the dynamic and hydrostatic pressure over the instantaneous wetted part of the hull $S_w(t)$, which is defined by the undisturbed incoming wave and the instant position of the ship.

$$\vec{F}_1(t) = \iint_{S_w(t)} p \vec{n} ds \quad (3)$$

where \vec{n} is the unit normal vector and the pressure p comprises both hydrostatic and dynamic terms, according to Bernoulli's potential theory formula.

$$p = -\rho g z - \rho \frac{\partial \Phi}{\partial t} - \frac{1}{2} \rho |\nabla \Phi|^2 \quad (4)$$

where Φ is the velocity potential, ρ the water mass density, g the gravity acceleration, and z the vertical coordinate directing upwards.

The radiation forces are herein calculated by use of the added mass and damping coefficients calculated in the frequency domain and properly transformed into the time domain by application of the impulse response function concept introduced by Cummins (1962).

$$F_{R,i}(t) = -A_{ij}(\infty) \dot{U}_j - \int_0^{\infty} K_{ij}(\tau) U_j(t-\tau) d\tau \quad (5)$$

where $i, j=1 \div 6$, A_{ij} are the added masses at infinite frequency of oscillation and the kernel functions K_{ij} are the impulse response functions corresponding to the damping coefficients calculated in the frequency domain.

For irregular seaway excitation, the elementary diffraction forces, corresponding to the constituent wave frequencies of an assumed irregular sea spectrum, are taken directly proportional to the corresponding elementary diffraction forces calculated in the frequency domain.

Radiation (thus added-masses and damping coefficients) and diffraction forces in the frequency domain were herein calculated by application of the computer code NEWDRIFT, (Papanikolaou, 1989). This is a six-degrees of freedom (6 d.o.f.), three-dimensional (3D) panel code program for the calculation of motions and wave induced loads, including drift force effects acting on arbitrarily shaped bodies in regular waves. The code is based on the zero-speed Green function, pulsating source distribution method and accounts for the forward speed effects considering the slender body theory assumptions. The code employs triangular or quadrilateral panels for the modelling of the wetted ship surface.

Roll viscous effects are taken into account for the roll motion using a semi-empirical linear or quadratic roll velocity model.

The above formulated mathematical model for the present ship-wave (hydro-mechanical) system comprises of a set of six second-order nonlinear differential equations. Integrating this set of equations by a time integration method, the six degrees of freedom motions of the body are obtained in the time domain. Details of the simulation model can be found in (Spanos, 2002).

3. THE NUMERICAL EXPERIMENTS

The herein investigated vessels are, a fishing boat with a transom stern arrangement, and a single screw RoRo vessel with transom stern tunnelled stern sections and a bulbous bow. Despite the fundamental differences of the two hull forms they dispose some common features with respect to their waterplane area, likely to induce the parametric roll phenomenon under certain conditions: due to the intense change of their hull lines around the still waterline, particularly in the stern area, the hydrostatics of both hulls are sensitive to draught and pitch changes.

The details of the studied fishing vessel have been taken from Neves et al. (2002), who have tested the parametric roll of this ship in head waves in model tank. Its main particulars are listed in Table 1 and the geometric model developed for the present study in Figure 1.

Table 1 Main particulars of the fishing vessel

Length (m)	25.91
Length pp (m)	22.09
Beam (m)	6.86
Depth (m)	3.35
Draught (m)	2.48
Displacement (tons)	170.30
Roll radius of gyration (m)	2.215
Pitch radius of gyration (m)	5.522

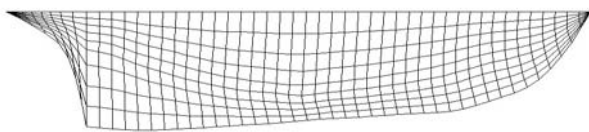


Figure 1 Modeling of wetted surface up to still water for the fishing vessel (2x365 panels)

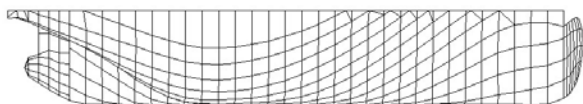


Figure 2 Modeling of the wetted surface up to still water for the RoRo ship (2x438 panels)

The hull characteristics and details of the studied RoRo ship have been disposed to the authors by the German shipyard, Flensburger Schiffbau Gesellschaft (FSG). The main particulars are presented in

Table 2 and the geometric model employed in numerical simulation in Figure 2 below. The radii of gyration assumed herein corresponding to $i_{xx} = 0.325B$ and $i_{yy} = 0.25L$.

Table 2 Main particulars of the RoRo ship

Length pp (m)	190.30
Beam (m)	26.50
Depth (m)	13.25
Draught (m)	7.65
Displacement (tons)	22341.6
Roll radius of gyration (m)	8.613
Pitch radius of gyration (m)	47.573

In the numerical simulation the vessels were free to move in heave, roll and pitch, whereas they were constrained in the other degrees of freedom. These captive numerical tests differ to a certain degree from the corresponding experimental tests in model tank for the fishing vessel, where the model was equipped with two towing lines at the bow and stern respectively as course keeping devices.

This arrangement permits some freedom to sway and yaw motions hence some effects of this on experimental measurements could be present.

In absence of refined roll damping data, the viscous roll damping was herein approximated with a linear model having a damping parameter varying as percentage of the critical roll damping. In Figure 3 the free roll decay of the fishing vessel for two values of damping at zero speed are depicted.

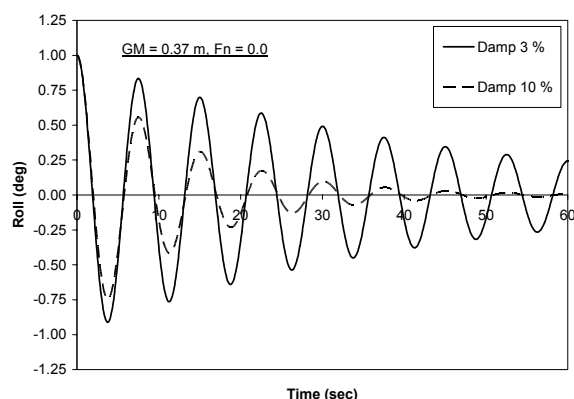


Figure 3 Free roll decay of the fishing vessel

4. SIMULATION RESULTS

The two vessels were tested in conditions of parametric roll resonance in head waves, namely for all the numerical tests the wave frequency of encounter was double the natural roll frequency of the vessel. Systematic variation of the basic parameters that of the vertical centre of gravity KG (correspondingly of the GM), forward speed, roll viscous damping and wave height was performed in order to investigate their effect on the vessels' motion.

The amplitude of the roll motion of the vessels as a function of the wave amplitude or wave height (double wave amplitude) was recorded and is presented in the followings. The recorded roll amplitude corresponds to the steady state response namely when the transients have died out.

The next Figure 4 samples two simulated cases for the studied fishing vessel, with different initial angles, where the steady state response is apparent after a time of 120 seconds. Numerical simulation tests proved that the steady state response was independent of the initial conditions. The next Figure 5 depicts the corresponding time series of the associated pitch motion. It shows that the pitch motion oscillates with the wave frequency of encounter and reaches quite a steady state within the first 20 sec after the start of the simulation.

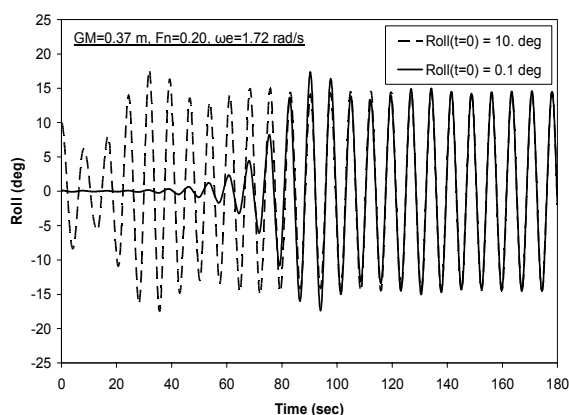


Figure 4 Simulated roll time series

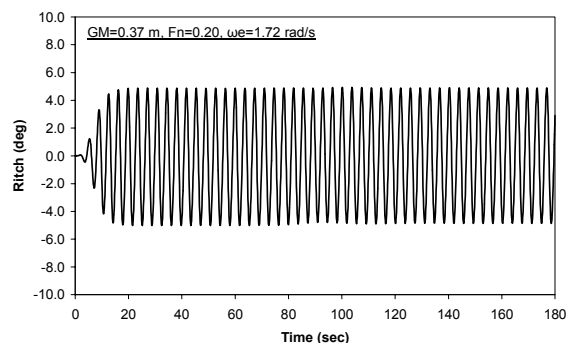


Figure 5 Simulated pitch time series

Figure 6 shows the roll-pitch diagram of the above example. The minimum pitch values (corresponding to trim by stern) occur at the higher roll angles, whereas for intermediate roll angles the maximum pitch (trim by bow) is observed.

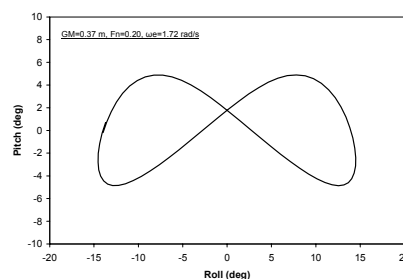


Figure 6 Roll-Pitch diagram

4.1 Fishing Vessel

Figure 7 to Figure 10 present the roll responses for the fishing vessel for two GM values (0.37 m and 0.50 m) and two Froude numbers F_n (0.20 and 0.30). Each curve in the diagrams corresponds to different assumed roll damping.

According to these results the parametric roll starts occurring for wave amplitudes greater than 0.20 m. Thereafter, roll motion increases with the wave amplitude in a complicated way. For the lower GM ($= 0.37$ m) capsizing occurs at wave amplitudes around 0.90 m and 0.70 m for F_n equal to 0.20 and 0.30 respectively. For the higher GM, despite the steeper increase of roll for the lower wave amplitudes, the vessel comes to finite maximum roll amplitude without capsizing. For even higher wave amplitudes, greater than those for which the maximum roll occurs, the roll motion amplitude gradually decreases until it diminishes completely.

These numerical results are plotted together with experimental measurements carried out in model tank by Neves et al., (2002). The tank measurements indicate that the numerical simulation captures the onset of the roll resonance, especially for the lower GM value ($= 0.37$ m). In the other case ($GM = 0.50$ m), there is only single experimental measurements for the higher wave amplitude ($= 1.0$ m) that resulted to zero roll amplitude. The numerical simulation indicates here also the absence of a rolling behaviour for the higher damping ($= 15\%$) whereas for the other damping values

non-rolling is observed at the range of even greater wave amplitudes. This very interesting nonlinear phenomenon, namely the reduction of roll amplitude at the region of larger waves, has also been recorded by Hashimoto et al., (2005) in similar experiments with a container ship in regular head waves. This behaviour has been also identified earlier in a basic theoretical nonlinear model of Umeda et al., (2003). Also, recent experimental measurements for a containership, carried out by Lee et. al. (2006), identify the same behavior, while green water on deck has been regarded as a possible explanatory reason at least for the range of the higher wave heights. In any case, such response needs further detailed investigation in order to clearly identify the causing conditions.

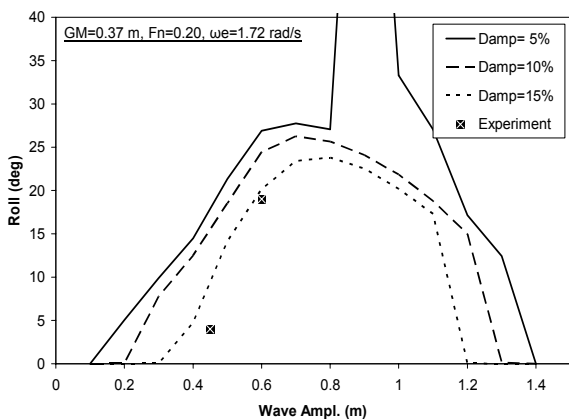


Figure 7 Roll vs. wave height for fishing vessel at $GM=0.37$ and $Fn=0.20$

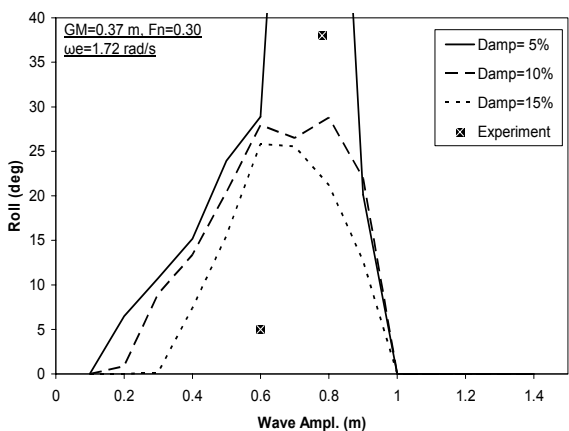


Figure 8 Roll vs. wave height for fishing vessel at $GM=0.37$ and $Fn=0.30$

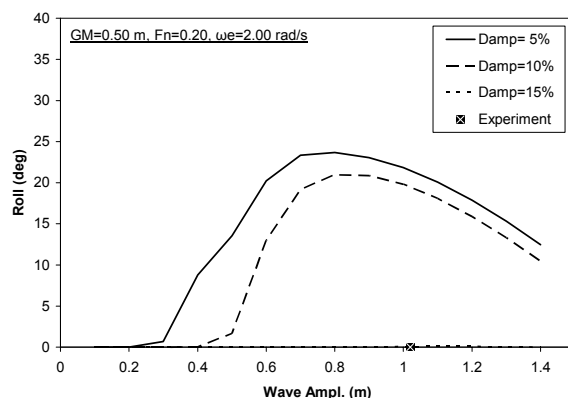


Figure 9 Roll vs. wave height for fishing vessel at $GM=0.50$ and $Fn=0.20$

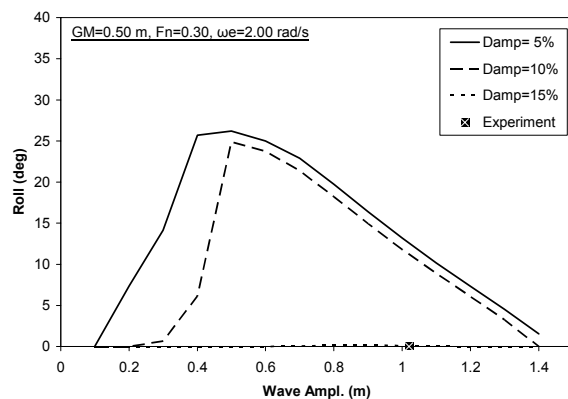


Figure 10 Roll vs. wave height for fishing vessel at $GM=0.50$ and $Fn=0.30$

The effect of viscous damping on the performance of the vessel is always to decrease the induced roll motion. In case of the higher GM value ($= 0.50$ m), a higher viscous damping seems sufficient to cancel the onset of the roll resonance throughout the range of investigated waves.

At the lower wave amplitudes range, up to the maximum roll occurrence, it is interesting to note that in the case of higher GM ($= 0.50$ m) the roll is strongly affected by the vessel's forward speed. In this region, the roll is getting larger with the increase of the speed. In the other case ($GM = 0.37$ m), there is not any notable effect of the forward speed on the roll motion.

4.2 RoRo Vessel

Figure 11 to Figure 14 present the simulated roll motion for the RoRo ship for two GM values (1.00 m and 1.50 m) and for two Froude numbers (0.15 and 0.25). Regular wave heights up to 6 m were investigated.

Roll resonance is observed for the RoRo ship in three out the four presented cases for wave heights greater than 4.0 m. In the case of the lower GM (= 1.00 m) and the higher Fn (= 0.25) no resonance occurred for any of the tested conditions, resulting a zero amplitude roll motion.

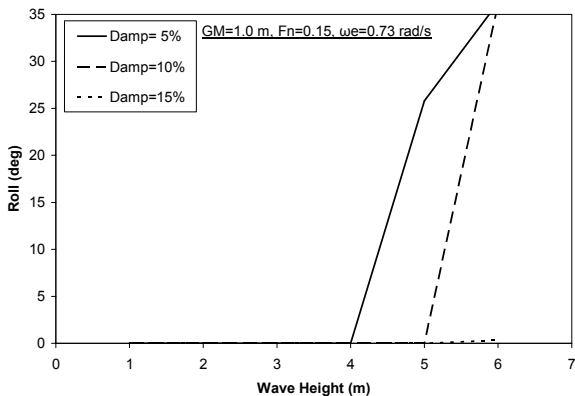


Figure 11 Roll vs. wave height for RoRo ship at GM=1.00m and Fn=0.15

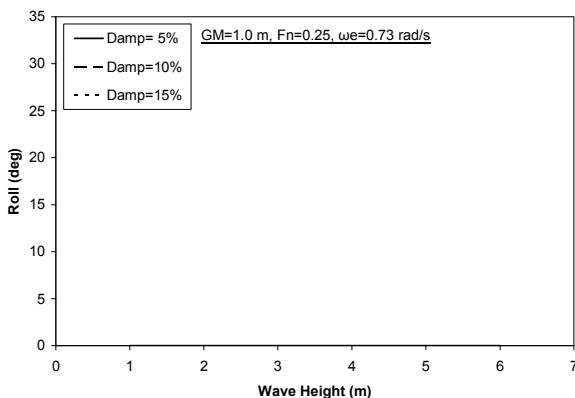


Figure 12 Roll vs. wave height for RoRo ship at GM=1.00m and Fn=0.25

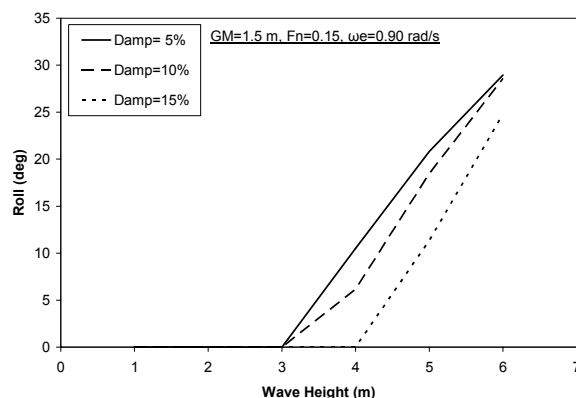


Figure 13 Roll vs. wave height for RoRo ship at GM=1.50m and Fn=0.15

The roll viscous damping seems to shift the occurrence of the roll resonance towards the higher wave amplitudes. Furthermore, the increase of roll stiffness (GM=1.50m) seems to favors resonance.

The tested range of wave heights for the RoRo ship practically corresponds to the left-side range of the numerical tests for the fishing vessels. The occurrence of resonance at a certain wave height and the increase of roll amplitude thereafter appear to be common features of both vessels.

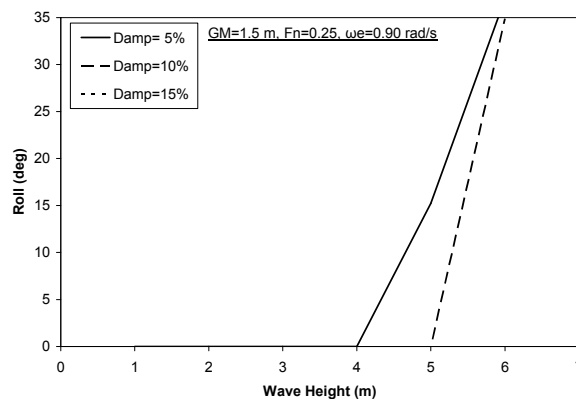


Figure 14 Roll vs. wave height for RoRo ship at GM=1.50m and Fn=0.25

5. DISCUSSION OF RESULTS

The roll resonance observed in the undertaken numerical tests for two different types of vessels is a typical head seas parametric roll resonance phenomenon. The

roll amplitude amplification is a direct consequence of the parametric variation of ship's restoring characteristics in view of the wave induced ship motions.

A detailed analysis of the motion and the forces has shown that, as GM is a non-linear function of the induced pitch motion as the ship advances in head waves, it varies in time inducing a periodic change of the restoring moments at a frequency equal the wave encounter frequency.

In Figure 15 and Figure 16 below, the metacentric height GM is depicted as function of trim (correspondingly pitch) for the fishing and RoRo vessel respectively, as calculated for the calm water conditions. These diagrams show the strong dependence of GM on the trim (pitch) and illustrate the expected variation of GM when pitch oscillates, at least for the hydrostatic term.

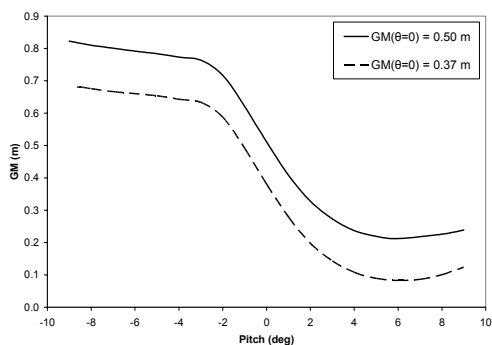


Figure 15 GM as function of pitch for the fishing vessel

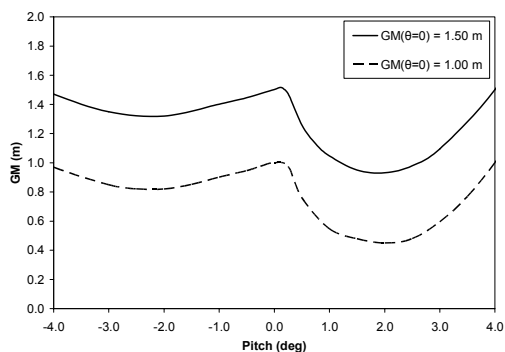


Figure 16 GM as function of pitch for the RoRo vessel

Figure 17 shows how the GM effectively changes in time in the presence of waves for the conditions corresponding to Figure 4. This GM differs to the one depicted in above figures, as it includes also hydrodynamic effects, namely it is the tangent of the actual restoring roll moment at the zero angle of heeling.

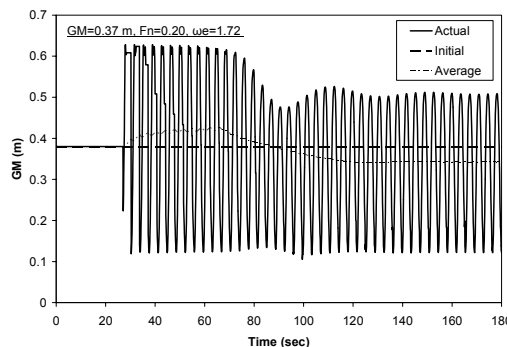


Figure 17 GM variation in time for the fishing vessel

It can be seen that the time averaged GM value remains quite constant at the beginning of the simulation where no roll motion occurs, namely it is equal to the hydrostatic value $GM = 0.37$ m, here denoted as initial GM. However, as vessel starts rolling the averaged GM changes and reaches in the steady state condition, after about 120 seconds, a value of about 0.33 m.

Similarly, in Figure 18 the GM variation is sampled for the steady state response of the RoRo ship where the roll amplitude has reached a value of 15 degrees after time 500 sec.

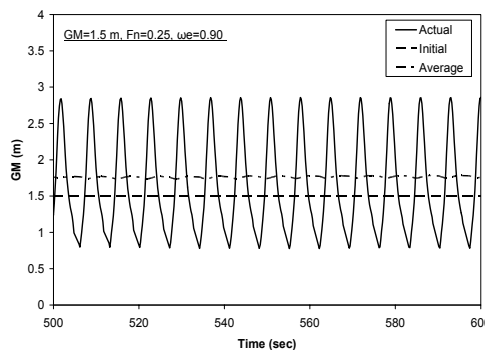


Figure 18 GM variation in time for the RoRo ship

In this case the average GM in the steady state response seems to be higher than the initial GM value. The observed changes of the average GM under the dynamic wave-induced conditions allow us the introduction of the notion of *effective GM in waves*, which is different to the initial GM in calm water.

Insight to the roll motion excitation mechanism is obtained by reviewing the hydrostatic GZ variation during a roll period, as illustrated with the Figure 19. In this diagram the righting arm GZ curves of constant pitch (trim) are plotted together with the actual hydrostatic GZ during a numerical test. The shape of the actual GZ-heel correlation is a symmetrical double-loop knot. The vessel while heeling from the upright position has a low GM value, which corresponds to the curve of constant pitch $\theta = +2.0$ deg (trim by bow). Then, as the vessel has heeled about +2 degrees it gradually changes its pitch to $\theta = -2.0$ deg (trim by stern) with a consequent increase of GZ and hence of the restoring moment. The vessel reaches its maximum heeling angle and then returns to the upright position under the excitation of higher restoring moment. This loop is repeated to the opposite side.

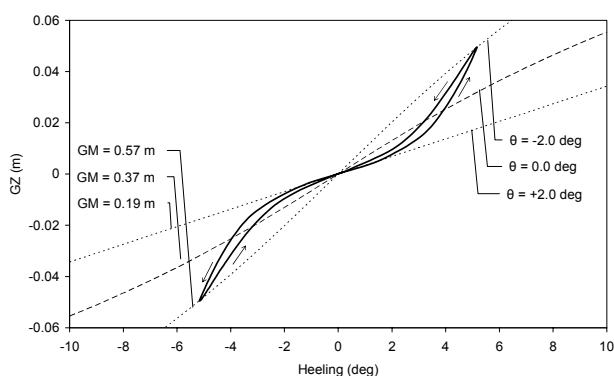


Figure 19 GZ variation in parametric rolling

Consequently the pitch motion, as a result of the wave excitation, changes the underwater part of the hull and subsequently the restoring moment, which in turn controls the roll motion. Hence, the coupling between roll and pitch motion is obviously a determinant factor for

the occurrence of the roll resonance in head waves.

The discussion on the background mechanism of the observed roll motion is herein complemented by an elaboration regarding finiteness of the roll amplitude recorded in roll resonance. For this purpose the diagram of Figure 20 is presented, where the roll amplitude is depicted for constant wave amplitudes and varying wave encounter frequency. Three response curves for different wave amplitudes are plotted. The double of the natural frequency is indicated with a vertical dashed line.

These results suggest the occurrence of a nonlinear roll resonance, similar to that depicted in the explanatory schematic Figure 21. The response curve is bended towards the lower frequencies indicating a jump phenomenon marked with dotted lines. The bending towards the lower frequencies is a direct consequence of the non-linear stiffness for the roll motion. It is specifically due to the convex character of the GZ curve versus roll angle.

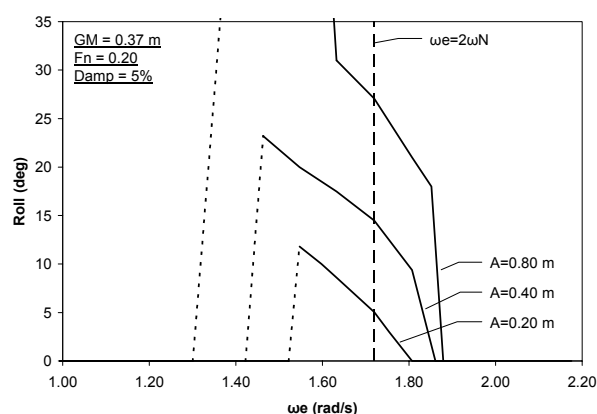


Figure 20 Non-linear roll resonance for the fishing vessel

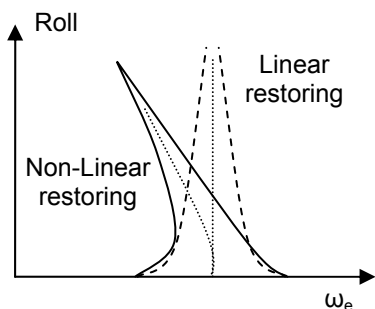


Figure 21 Basic behavior of roll resonance with linear and non-linear restoring

The presence of such non-linearity is the cause of the finiteness of the roll amplitude in parametric roll for the studied frequency ($\omega_e = 2 \omega_N$). In parametric resonance with linear restoring the amplitude would grow exponentially to infinity. The consideration of non-linear effects results to a saturation of the roll growth and thus finite roll amplitudes are recorded.

The roll amplification observed in Figure 20 occurs over a finite range of frequencies of considerable width. In case of irregular wave excitation, a strong interaction with the wave components around the double roll natural frequency can be expected, particularly if the wave energy density is high in the amplification bandwidth.

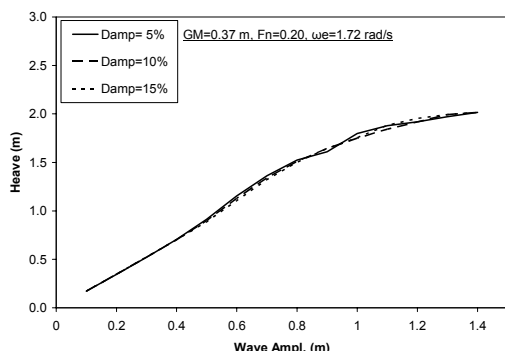


Figure 22 Heave response amplitudes for the fishing vessel

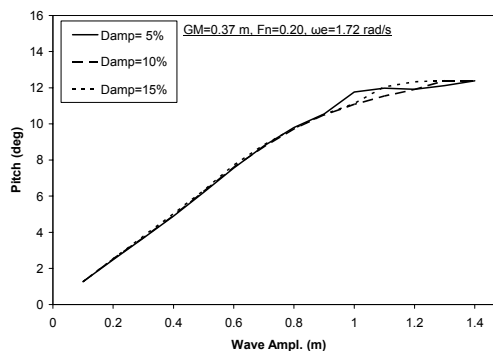


Figure 23 Pitch response amplitudes for the fishing vessel

While the roll motion strongly depends on the incoming wave amplitude, the other two motions, that of heave and pitch, are less affected by non-linear effects of wave amplitude, as demonstrated in Figure 22 and Figure 23 for the fishing vessel. Note that in case of the RoRo ship, these functions remain practically linear in the studied range of waves as demonstrated in Figure 24 for the pitch motion.

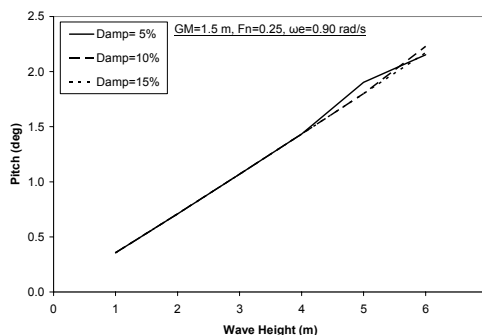


Figure 24 Pitch response amplitudes for the RoRo ship

6. CONCLUSIONS

The motion of two different types of vessels, namely a fishing boat and a RoRo ship, in parametric roll conditions in regular head waves has been studied with use of a nonlinear 6 DOF time domain numerical simulation method. The simulated results and subsequent analysis provide insight and improved understanding of the parametric roll resonance mechanism. Both vessels respond quite

likewise despite the fundamental differences of their hull forms.

The presented work revealed several aspects of the time domain simulation method, which are quite valuable for the validation of the method prior to its application for the assessment of the probability of the parametric roll in actual sea waves.

It proved that the non-linear character of the restoring moment and the coupling of the roll-pitch motion are the determinant factors for the induced roll resonance at wave encounter frequency close to the double roll natural frequency.

In terms of stability, it has been observed that capsizes due to intensive parametric roll can occur in presence of considerable wave amplitudes combined with low roll damping characteristics.

Findings at the range of even larger wave amplitude excitation, where the induced roll amplitude seems to decrease (and even completely diminish) with the increase of the wave amplitude, need further investigation in order to explain the observed phenomenon, identified also in relevant physical model experiments.

7. ACKNOWLEDGEMENTS

The present study was partly supported by the European Commission under the FP6 Sustainable Surface Transport Programme, namely the Integrated project SAFEDOR (Design, Operation and Regulation for Safety, task 2.3) Contract No. FP6-IP-516278 and the STREP project ADOPT (Advanced Decision Support System for Ship Design, Operation and Training), Contract No. FP6-TST4-CT-2005-516359. The European Community and the authors shall not in any way be liable or responsible for the use of any such knowledge, information or data, or of the consequences thereof.

8. REFERENCES

- Belenky, V.L., Weems, K.M., Lin, W.M., Paulling, J.R., 2003. "Probabilistic Analysis of Roll Parametric Resonance in Head Seas." Proc. of 8th Inter. Conf. on Stability of Ships and Ocean Vehicles, STAB2003, Madrid, Spain, pp.325-340.
- Cummins, W., 1962. "The impulse response function and ship motions," *Journal Schiffstechnik*, Vol. 9, no. 47, pp. 101-109, June
- France, W.M., Levadou, M., Treacle, T.W., Paulling, J.R., Michel, K. and Moore, C. 2003. "An Investigation of Head-Sea Parametric Rolling and its Influence on Container Lashing Systems", *Marine Technology*, Vol. 40, No. 1, pp 1-19.
- Francescutto, A., Bulian G., 2002. "Nonlinear and Stochastic Aspects of Parametric Rolling Modeling", *Proceedings of International Ship Stability Workshop*, Webb Institute, USA.
- Hashimoto, H., Matsuda, A., Umeda, N., 2005. "Model Experiment on Parametric Roll of a Post-Panamax Container Ship in Short-Crested Irregular Seas", *Conference Proceedings of the Japan society of naval architects and Ocean Engineers*, vol.1, pp.71-74, Nov. 2005
- ITTC, The specialist committee on Stability in Waves, 2005. "Final report and recommendations to the 24th ITTC"
- Krueger S., Kluwe, F., 2006. "Development of Dynamic Stability Criteria from Direct Seakeeping Simulations". Proc. of the 9th Inter. Marine Design Conference, Ann Arbor, MI, USA.
- Lee, H.-H., Lee I.-H., Lee Y.-W., Yoon, M.-T., 2006. "Experimental and Numerical Investigation into the Parametric Roll Resonance in Head Seas for an Ultra Large Containership", *Proceedings of the 9th Inter. Marine Design Conference*, Ann Arbor, MI, USA.

- Neves, M. A. S., Rodriguez, C.A., 2005. "Stability Analysis of Ship Undergoing Strong Roll Amplifications in Head Seas". Proceedings of the 8th International Ship Stability Workshop, Istanbul Technical University, Istanbul, Turkey.
- Neves, M., Perez, N., Lorca, O., 2002. "Experimental Analysis on Parametric Resonance for Two Fishing Vessels in Head Seas", Proceedings of the 6th International Ship Stability Workshop, Webb Institute, NY, USA
- Papanikolaou, A., 1989. "NEWDRIFT V.6: The six DOF three-dimensional diffraction theory program of NTUA-SDL for the calculation of motions and loads of arbitrarily shaped 3D bodies in regular waves", Internal Report, National Technical University of Athens, NTUA-SDL
- Ribeiro e Silva S., Santos T.A., Soares G., 2005. "Parametrically Excited Roll in Regular and Irregular Head Seas". Int. Shipbuilding Progress, Vol. 52, no. 1, pp.29-56.
- Spanos, D., 2002. "Time Domain Simulation of Motion and Flooding of Damaged Ships in Waves", Doctoral Thesis, Ship Design Laboratory, National Technical University of Athens
- Spanos, D., Papanikolaou, A., 2005." Numerical Simulation of a Fishing Vessel in Parametric Roll in Head Seas", Proc. of 8th Inter. Workshop on Stability and Operational Safety of Ships, Istanbul, Turkey, October 6-7, 2005
- Spanos, D., Papanikolaou, A., 2005b. "Yaw drift moment of a floating structure in waves, Proceedings of 24th Inter. conf. on Offshore Mechanics & Arctic Engineering", OMAE05, June 12-17, 2005, Halkidiki, Greece.
- Umeda, N., Hashimoto, H., Vassalos, D., Urano, S., Okou, K., 2003. "Nonlinear Dynamics on Parametric Roll Resonance with Realistic Numerical Modelling", Proc. of 8th Inter. Conference on the Stability of Ships and Ocean Vehicles STAB03, University of Madrid, Spain

Experimental and Numerical Studies on Parametric Roll of a Post-Panamax Container Ship in Irregular Waves

Hirotsuda Hashimoto, *Osaka University*

Naoya Umeda, *Osaka University*

Akihiko Matsuda, *NRIFE*

Shinya Nakamura, *Osaka University*

ABSTRACT

Firstly free running model experiments of a post-Panamax container ship were conducted in regular waves, long-crested and short-crested irregular waves. As a result, parametric roll in head and bow waves were clearly recorded even in long-crested and short-crested irregular waves. From the experimental results, effect of wave steepness, forward velocity, heading angle, irregularity of waves on parametric roll were systematically examined.

Secondly numerical prediction of parametric roll in long-crested irregular waves was carried out with an uncoupled roll model with restoring variation. The comparison between experimental and numerical results demonstrates that the uncoupled model can explain the experimental results qualitatively but not quantitatively.

Keywords: *Parametric Roll, Free Running Tests, Irregular Waves, Head Waves, Statistical Analysis, Numerical Prediction*

1. INTRODUCTION

Recent accidents of a post-Panamax container ship due to parametric roll in head waves (France et al, 2003) forced the International Maritime Organization (IMO) to start to revise the Intact Stability Code (2002) and the guidance for the master in following and quartering waves (MSC Circ.707, 1995). Although several experimental data were published for parametric roll even in irregular waves (Umeda et al, 1995), only limited outcomes are available for that in head and bow waves.

In this revision work at the IMO, the following questions were now raised to be urgently solved; does the parametric roll in head waves lead not only to cargo damage but

also ship capsize, does the danger of parametric roll decrease in irregular waves, especially in short-crested waves, in comparison with ideal regular waves, and how can we avoid and predict parametric roll in realistic head or bow waves? Responding to this situation, free running model experiments mainly focusing on irregular head and bow waves were conducted to directly obtain answers to the above questions. From the experimental results, effect of wave height on parametric roll in regular waves, effect of heading angle and forward velocity on parametric roll in regular waves, effect of irregularity of waves on parametric roll in head waves, effect of heading angle and forward velocity on parametric roll in short-crested irregular waves were systematically examined.

From a practical point of view, free running model experiment is obviously one of the most

reliable ways to examine occurrence condition and amplitude of parametric roll; however it is time-consuming and cost-wasting assessment to do model tests with all of the relevant conditions. Therefore we attempted to develop an uncoupled roll model for parametric roll prediction in irregular waves as an alternative option to assess parametric roll danger or to reduce total number of free running model experiment. Regarding parametric roll in irregular waves, how to take the restoring arm variation into account is problem. Because restoring arm and wave steepness has the nonlinear relationship, an ordinary seakeeping theory, that is linear theory, cannot be applied directly. Therefore we apply Grim's effective wave concept (Grim, 1961) to solve the restoring arm variation problem in irregular waves, and compared numerical results with the experimental results.

2. FREE RUNNING MODEL EXPERIMENTS

2.1 Outline of Model Experiment

Model experiments were conducted in the basin of National Research Institute of Fisheries Engineering (length: 60m, width: 25m, depth: 3.2m) with an 80-segmented wave maker. A scaled ship model of a post-Panamax container ship was used here, and her principal particulars and body plan are shown in Table.1 and Figure 1, respectively. The ship model had no deckhouse, but was watertight, and was propelled by an electric motor with a constant revolution control system. The onboard computer realises an autopilot system of the constant gain of 1.0 and stored data of roll, pitch and yaw motions obtained by a fiber-optic gyroscope. In addition, surge and sway velocity were obtained from the data of ship position recorded by an optical tracking sensor fixed to the basin.

In regular wave runs, several sets of propeller revolution number, n_c , wave height,

H , wave length, λ , autopilot course, χ_c , were used but the wave length to ship length ratio was fixed to be 1.6. Furthermore the vertical displacement of incident waves at the centre of ship gravity was obtained in consideration of wave phase velocity, ship position and wave height records. In long-crested irregular wave runs, significant wave height $H_{1/3}$ of 0.221m in model scale and mean period T_{01} of 1.3 seconds, which correspond to the wave height and period of regular waves, were used with the ITTC spectrum. In short-crested wave runs, $H_{1/3}$ and T_{01} were the same as the long-crested irregular wave runs, but with cosine to the 2nd or 4th power as the directional distributions function were used. By utilising the single summation method for generating wave signals, uniformity of short-crested waves in space is realised within $\pm 5\%$ error (Sera and Umeda, 2000). In case of irregular wave, model running were repeated so that number of encounter waves is about 150 in average. A photograph of the model runs in short-crested irregular waves is shown in Figure 2 as an example.

Table 1 Principal particulars of the post-Panamax container ship

Items	Ship	Model
Length between perpendiculars: L	283.8m	2.838m
breadth: B	42.8m	0.428m
depth: D	24.0m	0.24m
draught at FP: T_f	14.0m	0.14m
mean draught: T	14.0m	0.14m
draught at AP: T_a	14.0m	0.14m
block coefficient: C_b	0.630	0.630
pitch radius of gyration: K_{yy}/L_{pp}	0.239	0.258
longitudinal position of centre of gravity from amidships: X_{CG}	5.74m aft	0.0574m aft
metacentric height: GM	1.08m	0.0106m
natural roll period: T_ϕ	30.3s	3.20s
natural pitch period: T_θ		0.86s

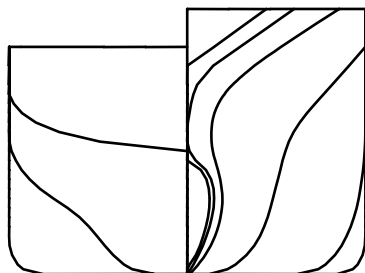


Figure 1 Body plan of the post-Panamax container ship

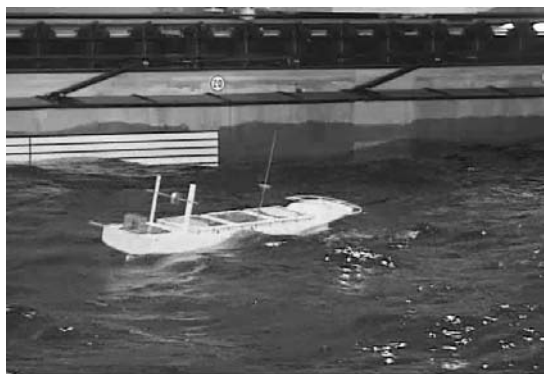


Figure 2 A photograph of free running model experiment in short-crested head waves

2.2 Experimental Results

Examples of measured time history of head sea parametric roll in regular waves, long-crested irregular waves and short-crested irregular waves are shown in Figures 3-5. Here propeller revolution number is the same and Froude numbers are obtained from measured average speed. $H_{1/3}$ and T_{01} are corresponding to the wave height and period of regular waves. In Figure 3, parametric roll with its steady amplitude of about 18 degrees can be clearly recorded after 10 seconds. In long-crested irregular waves, parametric roll was also observed with the maximum roll angle of about 20 degrees. Even in short-crested waves shown in Figure 5, parametric roll does not disappear and an amplitude of 22 degrees can be found. These demonstrate that wave irregularities or short-crestedness does not exclude danger of parametric roll in head waves.

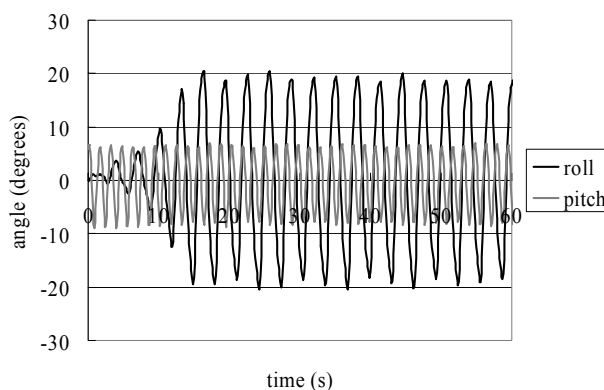


Figure 3 Time history of parametric roll in regular waves ($H/\lambda=1/20.6$, $\lambda/L=1.6$, $\chi_c=180$ degrees and $F_n=0.043$)

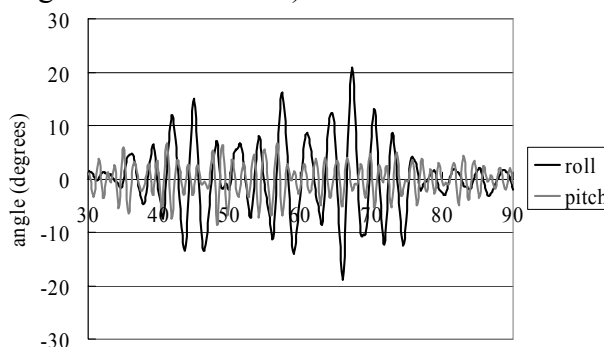


Figure 4 Time history of parametric roll in long-crested irregular waves ($H_{1/3}=0.221\text{m}$, $T_{01}=1.32\text{s}$, $\chi_c=180$ degrees and $F_n=0.021$)

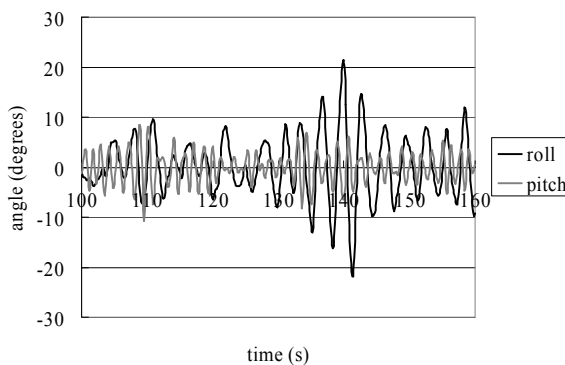


Figure 5 Time history of parametric roll in short-crested irregular waves ($H_{1/3}=0.221\text{m}$, $T_{01}=1.32\text{s}$, $\cos^2\theta$ distribution, $\chi_c=180$ degrees and $F_n=0.036$)

The effect of wave height on parametric roll in regular head waves is shown in Figure 6. Here, wave length to ship length ratio is 1.6 and propeller revolution number was set to realise ship forward velocity satisfying the ratio of 2.0 between encounter frequency and roll natural frequency. Parametric roll can be

found even in small wave steepness. With increase of wave steepness, parametric roll with its amplitude around 20 degrees was observed at $H/\lambda=0.0176$, and the amplitude does not significantly decrease up to $H/\lambda=0.0528$. Finally parametric roll disappears at $H/\lambda=0.0726$. This can be explained that ship condition deviates from a parametric roll condition with change in mean of restoring moment variation. Because H/λ of 0.072 corresponds to the wave height of 32 m in full scale and the maximum roll angle remains about 23 degrees, it is difficult to find direct relationship between the observed parametric roll and capsizing.

The effects of heading angle and forward velocity on parametric roll in regular waves are shown in Figure 7. Here, the heading angle of 180 degrees means pure head sea condition, and 270 degrees means beam sea condition. The Froude number in the Figure is estimated with the speed loss due to wave taken into account. In head waves, several runs of parametric roll with its maximum roll angle of about 20 degrees was found in smaller Froude number. At the Froude number of 0.1, parametric roll suddenly disappears. When the heading angle becomes larger, except for 270 degrees, the maximum roll angle is smaller than the case of 180 degrees of heading angle, but parametric roll itself does not disappear even in relatively high forward velocity while it does in head waves. This is because the area that satisfies the parametric roll condition shifts to higher forward velocity with increasing heading angle. However, if we focus on severe parametric roll for which the maximum angle is larger than 15 degrees, the danger decreases with increasing heading angle.

The effects of irregularity of incident waves on parametric roll in head waves are shown in Figure 8. Here the maximum amplitudes of parametric rolling in about 75 wave encounters are plotted. In case of smaller forward velocity, roll angles both in long-crested and short-crested irregular waves are slightly smaller than that in regular waves. Here some

statistical fluctuation due to non-ergodicity (Belenky, 2004) can be found. When the Froude number is larger than 0.1, however, parametric roll in irregular waves still occurs while no parametric roll occurs in regular waves. This tendency is more conspicuous in the case of short-crested irregular waves.

The effect of heading angle on the maximum roll angle of parametric roll in short-crested irregular waves is shown in Figure 9. Here cosine to the 2nd power was used as the directional distribution function. This figure shows that the ship cannot avoid parametric roll only by changing its course in short-crested irregular waves, and also shows that speed increase is effective in reducing danger of parametric roll at least in the heading angle ranging from 180 degrees to 240 degrees.

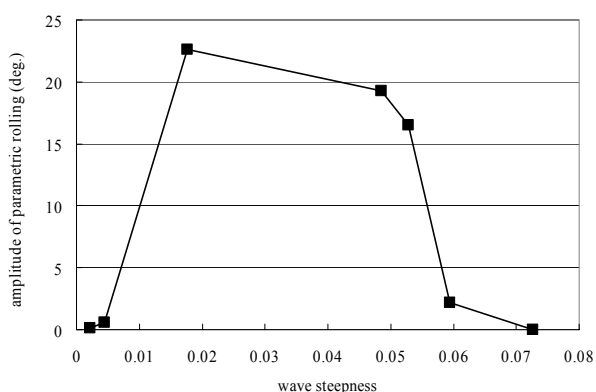


Figure 6 Effect of wave height on parametric roll in regular waves ($\lambda/L=1.6$ and $\chi_c=180$ degrees)

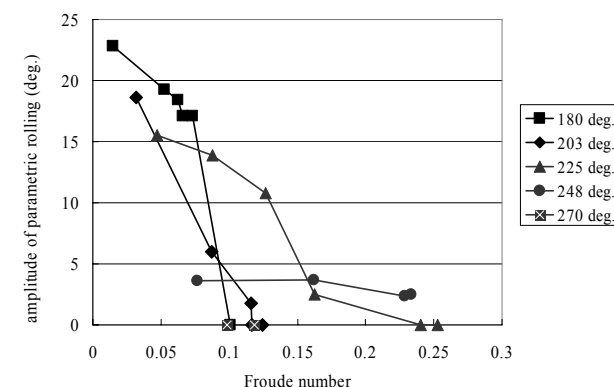


Figure 7 Effect of heading angle and forward velocity on parametric roll in regular waves ($H/\lambda=1/20.6$ and $\lambda/L=1.6$)

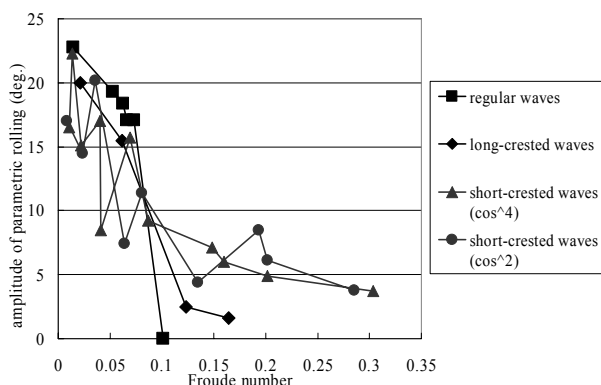


Figure 8 Effect of irregularity of waves on parametric roll in head waves ($H_{1/3}=0.221\text{m}$, $T_{01}=1.32\text{s}$ and $\chi_c=180$ degrees)

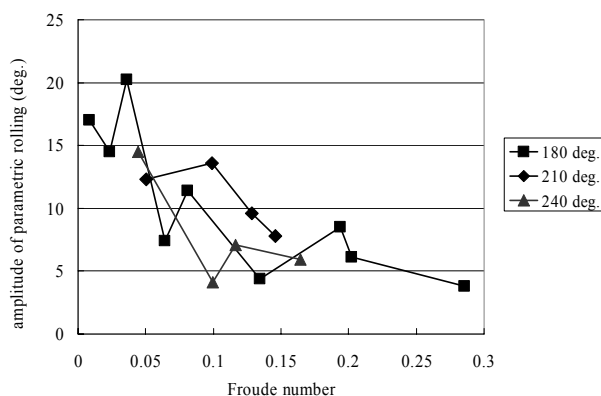


Figure 9 Effect of heading angle on parametric roll in short-crested irregular waves ($H_{1/3}=0.221\text{m}$, $T_{01}=1.32$ s and $\cos^2 \theta$ distribution)

2.3 Statistical Analysis

Statistical analysis focusing on instantaneous angle and amplitude of roll and pitch was carried out with recorded time histories. Probability density functions were obtained for both instantaneous angle and amplitude of roll and pitch, and compared with the Gaussian distribution and the Rayleigh distribution, respectively.

Examples of the results in long-crested irregular waves are shown in Figures 10-11. Here the experimental condition is $H_{1/3}=0.221\text{m}$, $T_{01}=1.32\text{s}$, autopilot course $\chi_c=180$ degrees. As shown in Figures 10-11, the instantaneous pitch angle agrees with the Gaussian distribution and

the pitch amplitude agrees with the Rayleigh distribution. Thus a linear theory can explain experimental results of the pitch motion even with quite high wave height of 22.1 m in full-scale. On the other hand, probability density functions of instantaneous angle and amplitude of roll around 0 degrees are conspicuously large, and do not follow the Gaussian and Rayleigh distributions at all. These results indicate that parametric roll is a strong nonlinear phenomenon. Pitch motion immediately starts whenever a ship meets incident waves while a ship starts to roll only when a ship meets the wave group that exceeds a parametric roll threshold. Therefore probability density around 0 degrees becomes large. For this reason, a conventional seakeeping theory based on a linear or weakly nonlinear assumption cannot be applied to parametric roll problems. Similar results have been reported by Belenky et al. (2003) and Ribeiro e Silva et al. (2005) based on their numerical simulations, however, no publication based on model experiments can be found so far.

Examples of the results in short-crested irregular waves are shown in Figures 12-13. Here the experimental condition is $H_{1/3}=0.221\text{m}$, $T_{01}=1.32\text{s}$, autopilot course $\chi_c=180$ degrees and $\cos^2 \theta$ distribution. The instantaneous pitch and the pitch amplitude agree well with the Gaussian and Rayleigh distributions, respectively. Instantaneous roll angle and roll amplitude do not agree with the relevant distribution as well as long-crested irregular wave runs; however, the difference becomes smaller to some extent.

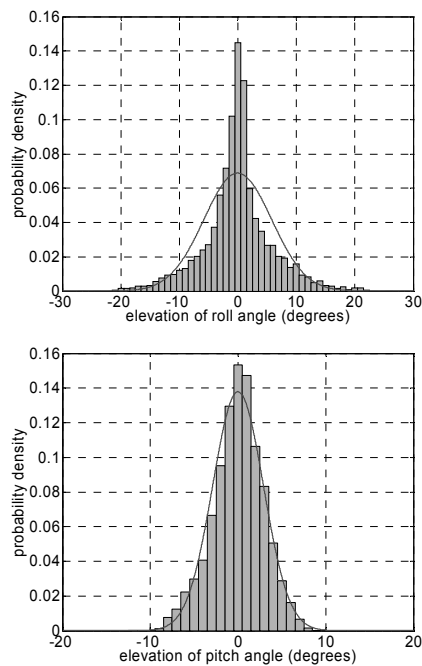


Figure 10 Probability density function of instantaneous roll and pitch angle in long-crested irregular waves for $F_n=0.021$ (histogram: experiment; dashed line: Gaussian distribution)

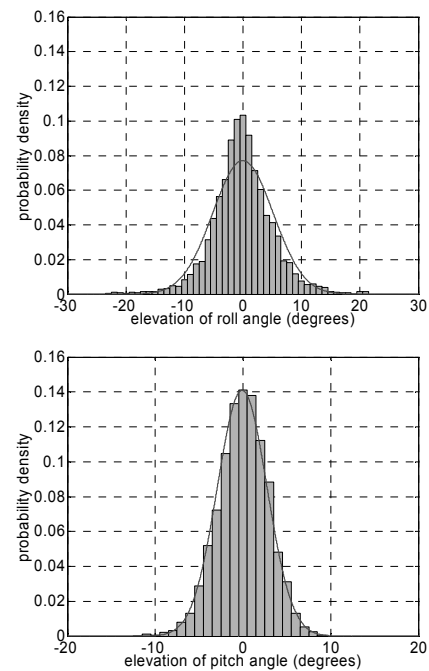


Figure 12 Probability density function of instantaneous roll and pitch angle in short-crested irregular waves for $F_n=0.029$ (histogram: experiment; dashed line: Gaussian distribution)

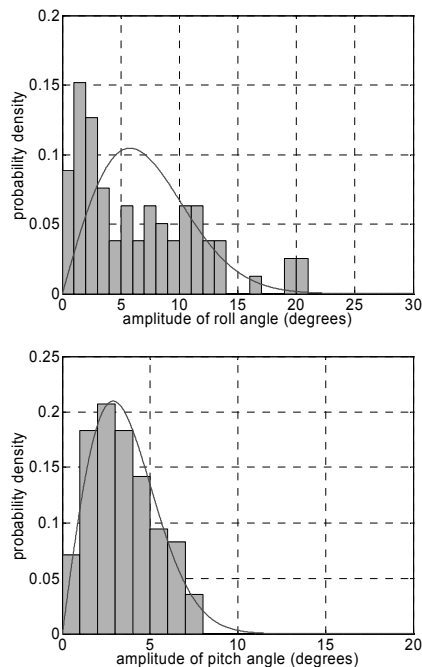


Figure 11 Probability density function of roll and pitch amplitude in long-crested irregular waves for $F_n=0.021$ (histogram: experiment; dashed line: Rayleigh distribution)

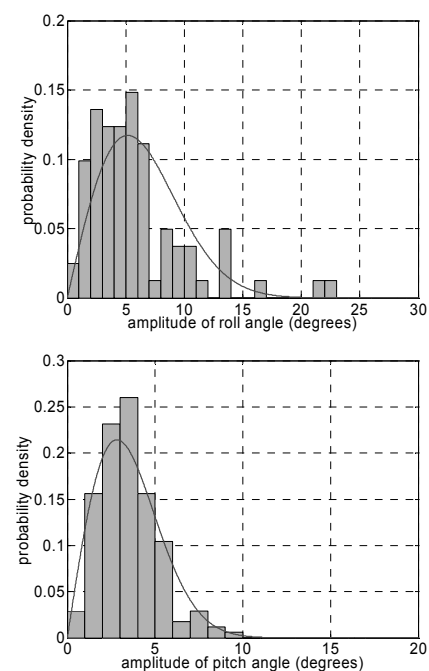


Figure 13 Probability density function of roll and pitch amplitude in short-crested irregular waves for $F_n=0.009$ (histogram: experiment; dashed line: Rayleigh distribution)

3. NUMERICAL SIMULATION

3.1 Mathematical Model

For simplicity, numerical simulations were carried out only for long-crested irregular waves, and it is assumed that a ship keeps constant forward velocity and constant heading angle of 180 degrees, that is pure head waves. This is because head wave is most dangerous situation for parametric roll occurrence both in regular and irregular waves as we confirmed in the experimental results. Under these assumptions, a mathematical model of ship roll motions can be described as follows:

$$(I_{xx} + J_{xx})\ddot{\phi} = -A\dot{\phi} - C\dot{\phi}^3 - WGZ(\phi) - WGZ_W \{ \zeta_{eff}(\xi_G, t), \phi \} + Mx_\phi(\zeta_{eff}(\xi_G, t))\phi \quad (1)$$

Here, I_{xx} : inertia moment in roll, J_{xx} : added inertia moment in roll, A, C : linear and cubic damping coefficients, W : ship weight, GZ : restoring arm, GZ_W : restoring arm variation due to wave, ζ_{eff} : effective wave amplitude, ξ_G : relative longitudinal position of the ship to a wave trough, t : time, Mx_ϕ : heel-induced hydrodynamic roll moment.

In the fourth terms of right hand side equation, Grim's effective wave concept is used to take restoring arm variation in irregular waves into account. Grim's effective wave concept is an approximation method of irregular wave profile along the ship to one regular wave called the effective wave. Here length of the effective wave is the same as the ship length between perpendiculars, and its trough or crest is assumed to be on amidships. The effective wave amplitude has linear relationship with the ocean wave elevation, but has nonlinear and non-memory effect on the restoring arm. The last term of the right-hand-side of the equation shows roll-dependent hydrodynamic roll moments that consist of diffraction, radiation and linear lift components, and are obtained by a strip theory with a heel

angle taken into account (Umeda et al, 2004). This is because the Froude-Krylov component on its own cannot deal with the speed dependence on the restoring variation, while it could be relatively large in head waves because of high encounter frequency. These hydrodynamic roll moments are assumed to have linear relationship with the wave steepness and are calculated as a function of frequency. Therefore those in irregular waves can be estimated with the linear superposition principle. The roll damping coefficients of A and C are obtained from roll decay model test with no forward velocity.

In numerical calculations, ocean waves are assumed to follow the ITTC spectrum same as in the free running model experiments, and are expressed as a sum of 1000 components of waves with non-uniformly different frequencies and random phases. To compare numerical results with the experimental ones, numerical calculations were carried out for $H_{1/3} = 22.1$ m, $T_{01} = 13.2$ s with several Froude numbers in long-crested irregular head waves.

3.2 Numerical Results

Numerical calculations in long-crested irregular waves with the same condition as Figure 4 were carried out and its results are shown in Figure 14. Here the wave elevation is obtained at the ship's center of gravity. In the numerical results, parametric roll with its roll period is twice as long as encounter period can be simulated. The calculated maximum roll angle is about 45 degrees while the measured result is 20 degrees.

Since this discrepancy is large, maximum roll angles of parametric roll are examined for several Froude numbers both in regular and irregular waves. Figures 15-16 show the comparison between experimental results and numerical results obtained with 1) Froude-Krylov component (FK only), 2) Froude-Krylov component and hydrodynamic

components (present), 3) experimentally obtained roll restoring moment (direct) (Hashimoto and Umeda, 2004). Here the Froude-Krylov components are calculated by integrating undisturbed wave pressure up to the wave surface with the Smith effect for a ship free in heave and pitch. All of the numerical results do not agree with experimental results except for the case at Froude number of 0.01 in regular waves. As mentioned before, experimentally obtained roll damping coefficients are used throughout. Therefore it is concluded that an uncoupled roll model could be insufficient for predicting parametric roll resonance not only in long-crested irregular waves but also in regular waves. This might be because that a ship tends to change her course from pure head waves to bow waves despite of her rudder effort while parametric roll occurs. Moreover ship surge motion might be not negligibly small because of severe wave steepness or long wave length in the experiment. From this point, a mathematical model taking surge and yaw motions into account could be recommended to predict parametric roll in relatively severe or long waves.

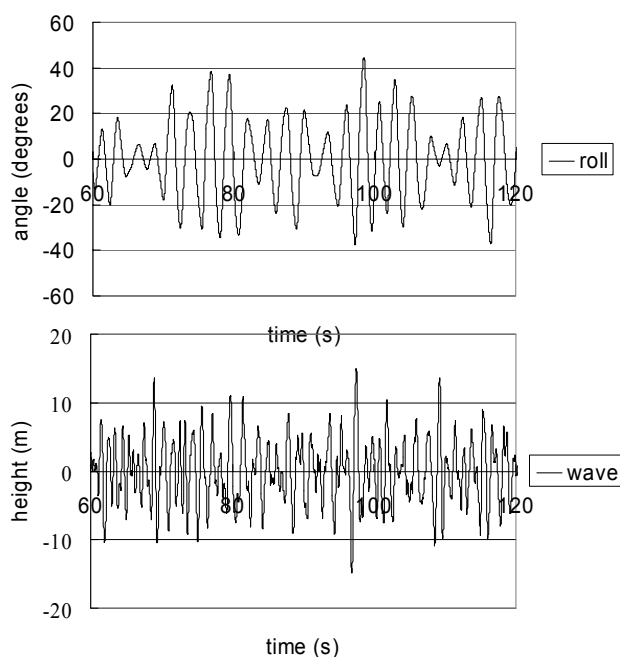


Figure 14 Calculated time series of roll angle and wave elevation in long-crested irregular waves ($H_{1/3}=0.221\text{m}$, $T_{01}=1.32\text{s}$, $\chi_c=180$ degrees and $Fn=0.02$)

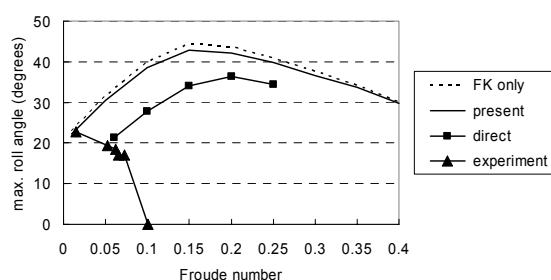


Figure 15 Comparison of maximum roll angle of parametric roll in regular waves with $H/\lambda=1/20.6$, $\lambda/L=1.6$ and $\chi_c=180$ degrees

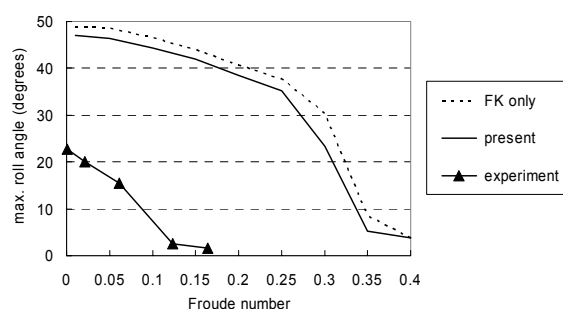


Figure 16 Comparison of maximum roll angle of parametric roll in long-crested irregular waves with $H_{1/3}=0.221\text{m}$, $T_{01}=1.32\text{s}$ and $\chi_c=180$ degrees

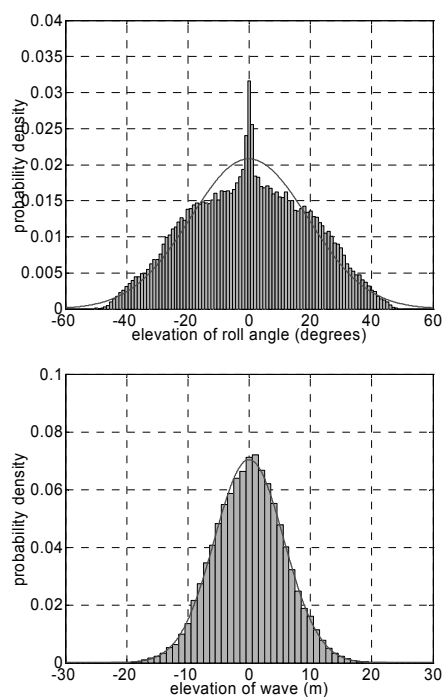


Figure 17 Probability density function of instantaneous elevation of roll angle and wave height in long-crested irregular waves (histogram: calculation; dashed line: Gaussian distribution)

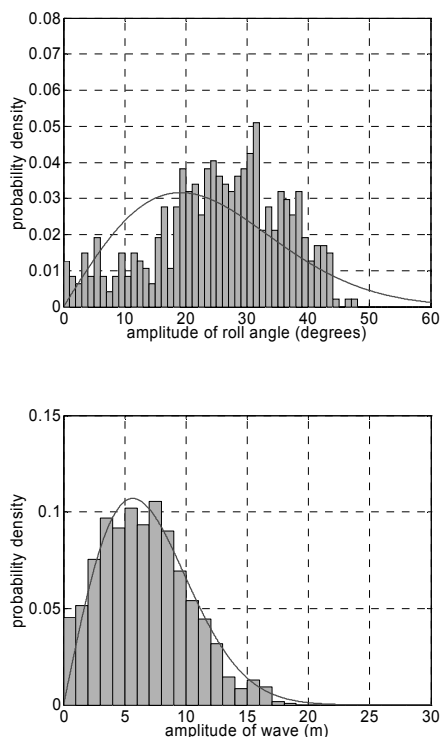


Figure 18 Probability density function of roll and wave amplitude in long-crested irregular waves (histogram: calculation; dashed line: Rayleigh distribution)

Figures 17-18 show the calculated probability density of instantaneous or amplitude of roll angle and wave elevation in long-crested irregular head waves. Although the numerical model reproduces the nonlinearity of parametric roll observed in the experiment, i.e. that the probability density of instantaneous and amplitude of roll angle does not follow the Gaussian and the Rayleigh distributions especially around 0 degrees, its quantitative accuracy is not sufficient and mathematical modelling technique should be improved for more practical purpose.

4. CONCLUSIONS

Capsizing due to parametric roll in head or bow waves was not observed in the experiment for the post-Panamax container ship model with the designed GM value.

The measured maximum roll amplitude of

parametric roll does not always increase with wave steepness in regular waves.

It is recommended to avoid ± 45 degrees of heading angle from head sea condition to prevent severe parametric roll exceeding 15 degrees of roll amplitude in regular waves.

The maximum angle of parametric roll in long-crested irregular waves or short-crested irregular waves is almost as large as the steady amplitude in regular waves.

Maximum roll angle of parametric roll does not depend on heading angle in short-crested irregular bow waves.

Increasing ship forward velocity can be recommended to decrease the parametric roll danger in irregular head and bow waves, as an alternative to decreasing it.

Instantaneous angle and amplitude of parametric roll cannot be explained using the Gaussian and Rayleigh distributions, respectively.

An uncoupled roll model with Grim's effective wave overestimates the occurrence area and its magnitude of parametric roll both in regular and long-crested irregular waves.

Roll-dependent hydrodynamic roll moments due to radiation and diffraction slightly improve the prediction accuracy of parametric roll.

The proposed mathematical model can reproduce the non-Gaussian statistical characteristic of parametric roll as observed in the experiment.

5. ACKNOWLEDGMENTS

This work was supported by a Grant-in Aid for Scientific Research of the Japan Society for Promotion of Science (No. 15360465). The work described here was partly carried out as a research activity of SPL project of Japan Ship

Technology Research Association in the fiscal year of 2005, funded by the Nippon Foundation, and was partly supported by the Shipbuilder' Association of Japan. The data of the subject ship were kindly supplied by National Maritime Research Institute. The authors express their sincere gratitude to the above organisations.

6. REFERENCES

- Belenky, V.L., 2004, "On Risk Evaluation at Extreme Waves", Proceedings of the 7th International Ship Stability Workshop, Shanghai, pp. 188-202.
- Belenky, V.L., Weems, K.M. and Paulling, J.R., 2003, "Probabilistic Analysis of Roll Parametric Resonance in Head waves", Proceedings of the 8th International Conference on Stability of Ships and Ocean Vehicles, Madrid, pp. 325-340.
- France, W.N., Levadou, M., Treacle, T.W., Paulling, J.R., Michel, R.K. and Moore, C., 2003, "An investigation of head-sea parametric roll and its influence on container lashing system", *Marine Technology*, 40(1), pp. 1-19.
- Grim, O., 1961, "Beitrag zu dem Problem der Sicherheit des Schiffes in Seegang", *Schiff und Hafen*, vol.6, pp. 490-497. (in German)
- Hashimoto, H. and Umeda, N., 2004, "Nonlinear Analysis of Parametric Rolling in Longitudinal and Quartering Seas with Realistic Modeling of Roll-Restoring Moment", *Journal of Marine Science and Technology*, vol. 9(3), pp. 117-126.
- IMO, 2002, "Code on Intact Stability for All Types of Ships Covered by IMO Instruments".
- IMO, 1995, "Guidance to the Master for Avoiding Dangerous Situations in Following and Quartering Waves", MSC Circular 707.
- Ribeiro, S., Santos, T. and Guedes, C., 2005, "Parametrically Excited Roll in Regular and Irregular Head waves", *International Shipbuilding Progress*, Vol. 52(1), pp. 27-54.
- Sera, W. and Umeda, N., 2000, "Homogeneity of Directional Irregular Waves with Side-Wall Reflections", *Journal of the Society of Naval Architects of Japan*, Vol. 188, pp. 251-256. (in Japanese).
- Umeda, N., Hamamoto, M., Takaishi, Y., Chiba, Y., Matsuda, A., Sera, W., Suzuki, S., Spyrou, K.J. and Watanave, K., 1995, "Model Experiments of Ship Capsize in Astern Waves", *Journal of the Society of Naval Architects of Japan*, Vol.177, pp. 207-217.
- Umeda, N., Ohkura, S., Urano, S., Hori, M. and Hashimoto, H., 2004, "Some Remarks on Theoretical Modelling of Intact Stability", Proceedings of the 7th International Ship Stability Workshop, Shanghai, pp. 85-91.

Parametric Roll and Ship Design

Marc Levadou, *Maritime Research Institute Netherlands (MARIN)*

Riaan van 't Veer, *Maritime Research Institute Netherlands (MARIN)*

ABSTRACT

The variety of vessels which can suffer from parametric roll is large. It has been observed on small fishing vessels sailing in following waves but also on large cruise and container vessels in head and following waves. The occurrence of parametric roll, with high roll angles, is governed by a complex combination of main dimensions, loading condition, hull form, appendage configuration, speed and encountered wave conditions. In this paper the influence of main dimension and of variations on the fore and aft body on the occurrence of parametric roll are investigated. A one degree of freedom motion method and a non-linear time domain simulation method were used. The results were validated with model tests on a C11 container ship. Also, the influence of different roll damping devices on the occurrence of parametric roll is evaluated.

Keywords: *Parametric roll, Ship design, Container vessels, Extreme motions, Roll damping, Transverse stability*

1. INTRODUCTION

In 1998 a post-Panamax, C11 class containership lost 1/3 of her deck containers and damaged another 1/3 in a severe storm. The incident was analysed by means of numerical simulations and model tests. The results confirmed that the vessel suffered from a severe case of parametric roll during the storm (France et al., 2003). Since the publication of these results, ship operators and ship designers have become more aware of the fact that this phenomenon can occur for larger vessels in confused seas and not only for small vessels in regular waves which was thought for many years.

New designs of large vessels, in particular container vessels, are since then more and more checked on their tendency for parametric roll behaviour. Class societies acknowledged the problem and have started incorporating parametric roll in their guides (Shin et al., 2004). Still, model tests are considered as the

way to assess the sensitivity for parametric roll and such tests are expensive in a design parameter space. Analytical tools which can predict the phenomenon are not easy to use, not always reliable or available. Therefore hull lines variations or optimisation with regard to parametric roll is seldom performed in an early stage of new designs.

In order to incorporate parametric roll in ship design an understanding of the phenomenon is required. A greater understanding is needed in how main dimensions, hull form changes and appendages configuration alter the probability of parametric roll.

In this paper results of a study on the effect of main dimension variations, hull form variations and different appendages configuration on the occurrence of parametric roll will be presented. In Chapter 2 the phenomenon is explained and a discussion of the minimal requirements for parametric roll to occur is given. In the third chapter a discussion will be given of how the main dimensions and the loading condition of a vessel can result in

conditions where parametric roll can occur. Different graphs are presented showing the “critical” combinations of vessel length and loading condition. In Chapter 4 results of the effect of hull form variations on a C11 post-panamax container vessel on the occurrence of parametric roll are presented. Variation of bow flare and stern configuration are investigated. In the last Chapter the effect of different roll reduction devices such as bilge keels and active fin stabilizers is discussed.

2. BACKGROUND

2.1 Theory

The theory behind parametric roll and its consequence has been studied and described by many investigators; see for example Kempf (1938), Graff & Heckscher (1941), Paulling & Rosenberg (1959), Paulling (1961), Oakley et al. (1974), Dunwoody (1989a), Dunwoody (1989b), Dallinga et al. (1998), Luth & Dallinga (1998) or Francescutto & Bulian (2002). Therefore, in this paper only the principles of parametric roll will be described.

In “normal” sailing conditions the ship motions of a vessel are caused by direct wave excitation. Resonant roll motion often occurs in beam waves and stern quartering waves when the combination of wave period, vessel speed and heading leads to a wave encounter period close to the natural roll period of the vessel.

In pure head seas condition, the first order roll wave excitation is zero. Nevertheless, under certain conditions of encounter period, roll motion can be excited in head seas, via a different phenomenon. This phenomenon is referred to as “auto parametrically excited motion” which is usually shortened to “parametric motion” or “parametric roll”. The term describes a state of motion that results not from direct excitation by a time-varying external force or moment but from the periodic variation of certain parameters of the oscillating system. The roll motion, once

started, may grow to large amplitude, limited by roll damping and, in extreme conditions, may result in danger to the ship or its contents.

For a ship in head or stern seas the uneven wave surface together with the pitch-heave motion of the ship results in a time-varying underwater hull geometry. This varying geometry, in turn, results in time-varying changes in the metacentric height, i.e., in the static roll stability. The variation of the static roll stability can cause instability if it occurs in the appropriate period.

From theory and as validated by model tests (Dallinga et al., 1998, Luth & Dallinga, 1998 and France et al., 2003), parametric roll occurs when the following requirements are satisfied:

- (1) The natural period of roll is equal to approximately twice the wave encounter period.
- (2) The wavelength is in the order of the ship length (between 0.8 and 1.2 times LBP).
- (3) The wave height (thus the GM variations) exceeds a critical value.
- (4) The roll damping is low (lower threshold wave height).

2.2 Prediction of Parametric Roll

Nonlinear, time-domain seakeeping computer codes are able to predict the phenomenon of parametric roll (see below). These computations are however not easy to use or available for everyone. In a preliminary design stage a simple and fast method is desirable. For parametric roll Dunwoody (1989a and 1989b) proposed such a method, which is used in this paper. His method is based on a single degree of freedom motion equation for roll, using a time varying restoring coefficient. This motion equation is known as the Mathieu equation, which is presented first.

Modelling in one degree of freedom The equation for one degree of freedom roll motions is given below.

$$(I_{xx} + A_{xx}) \frac{d^2 \phi}{dt^2} + B_{xx} \frac{d\phi}{dt} + C_{xx} \phi = M_x \quad (1)$$

In head seas condition the roll moment excitation will be zero, similar as in a roll-decay test. The roll motion equation reduce in these situations to:

$$\frac{d^2 \phi}{dt^2} + 2v \frac{d\phi}{dt} + \omega_\phi^2 \phi = 0 \quad (2)$$

Where the roll period is defined by:

$$\omega_\phi = \sqrt{\frac{C_{xx}}{I_{xx} + A_{xx}(\omega_\phi)}} = \sqrt{\frac{\rho g \nabla GM}{I_{xx} + A_{xx}(\omega_\phi)}} \quad (3)$$

And where the damping ratio is defined as:

$$v = \frac{B_{xx}(\omega_\phi)}{2(I_{xx} + A_{xx}(\omega_\phi))} \quad (4)$$

The restoring moment or static stability GM of the ship when sailing in waves will vary in time and the variation is a function of the actual wetted surface contour and thus depends on the hull lines around the calm water line. The largest variations in restoring occurs when the ship has large pitch motions, so when it sails in a wave length equal to about the ship length. A formula for the time varying restoring force, for the upright ship, in regular waves is given by:

$$C_{xx}(t) = \rho g \nabla (GM_m + GM_a \cos(\omega t)) \quad (5)$$

Where GM_m is the mean GM, that is the GM in calm water GM_a is the amplitude of the GM variation and ω is the wave frequency. When equation (5) is used in equation (1) a one-dimensional Mathieu equation is obtained; a linear second order differential equation with periodic coefficients. The damped Mathieu equation is now written as:

$$\frac{d^2 \phi}{dt^2} + 2v \frac{d\phi}{dt} + (\omega_\phi^2 + a \cos(\omega t)) \phi = 0 \quad (6)$$

Parametric resonance conditions for this equation can be found when:

$$\frac{\omega_\phi}{2\pi} = \frac{\omega}{2\pi} \frac{1}{2} n \quad (7)$$

According to Francescutto (2002) the threshold value for parametric roll in regular waves is:

$$\frac{\delta GM}{GM} = \frac{4v}{\omega_n} \quad (8)$$

This threshold has been used and compared with simulations and model test. The results are presented in section 4.4. Furthermore in this paper a one degree of freedom based method proposed by Dunwoody (1989a and 1989b) will be used. The method is shortly described below.

Response to GM fluctuations (Dunwoody, 1989). The method proposed by Dunwoody is based on the following assumptions:

1. The roll motion can be expressed by the differential equation for a single degree of freedom motion method with parametric excitation of the stiffness.
2. That there is a linear relation between roll stiffness excitation (GM fluctuations) and wave height.
3. That a relation can be made between the spectrum of the stiffness fluctuations with the incident wave height spectrum and the speed of the ship.
4. That GM fluctuations produce an effect analogous to a reduction in the roll damping.
5. If the reduction in roll damping is larger than the roll damping from the hull and appendages an unstable situation occurs and the vessel is subject to parametric roll.

Furthermore, Dunwoody demonstrates that for a wide band random process the spectral

density can be estimated for a frequency of twice the natural roll frequency.

Given the assumptions above the spectral density of the GM fluctuations can be expressed as the product of the spectral density of the wave encounter spectrum (at twice the natural roll frequency) and the square of the transfer function of the GM fluctuations (at twice the natural roll frequency). The equation is given below.

$$S_{GM} = \left(\frac{GM_a(\omega_\phi)}{\zeta_a} \right)^2 S_{e\zeta}(\omega_\phi) \quad (9)$$

According to Dunwoody the non dimensional damping reduction follows from:

$$\Delta\xi = \frac{\pi g^2 S_{GM}}{4 \omega_\phi^3 k_{xx}^4} \quad (10)$$

Parametric roll will occur if the non dimensional roll damping reduction exceeds the total roll damping B_{total} (made dimensionless by dividing with the critical roll damping B_{crit}). See equation (11).

$$\frac{B_{total}}{B_{crit}} - \Delta\xi \leq 0 \quad (11)$$

$$B_{crit} = 2\sqrt{(A_{xx} + I_{xx})\rho g \nabla GM}$$

The threshold wave height (the wave height for which parametric roll will start) can be determined by varying the wave spectrum in equation (9) and determining when equation (11) becomes zero.

Nonlinear, time domain seakeeping code PRETTI The development of a 3D panel code for seakeeping motion prediction has been a point of interest for the Co-operative Research Ships (CRS) since many years. In this joint-industry project a large group of different companies, such as class societies, ship-yards, ship operators, navies, and research/engineering companies are actively involved in research

related to many aspects in the design and operation of ships.

In recent years the CRS has developed a time-domain seakeeping code (Pretti) based on the hydrodynamics as calculated in the frequency domain by a 3D panel code (Precal). The current time-domain code incorporates non-linear excitation by pressure integration over the actual wetted surface. Diffraction forces are considered linear. Hydrodynamic coefficients and oscillatory (manoeuvring) derivatives are specific to sinusoidal motions and in a general theoretical model of a ship manoeuvring in a seaway, the ship motion cannot be considered simply sinusoidal. The motion equation must account for transient and random motions. This problem was initially discussed by Cummins (1962) and this approach of impulse response functions is adopted in Pretti.

The behaviour of a ship travelling in a seaway 'integrates' in practice two areas which are traditionally studied as separate problems and have led to two different mathematical approaches: a seakeeping theory assuming small motion amplitudes and the theory of manoeuvring assuming calm water and thus frequency independent hydrodynamics. In Pretti the two theories are combined as discussed by Bailey et al. (1997) or Fossen & Smogeli (2004). This is a challenging area of research since there is an overlap between the two models which require a careful implementation of manoeuvring coefficients. Ideally the aim is that with vanishing wave height the manoeuvring capabilities of the ship are found, and that the seakeeping hydrodynamics are captured in moderate wave conditions.

In large wave conditions with large amplitude motions the assumptions behind both the seakeeping and manoeuvring theory are violated since large variations in wetted surface are not accounted for when the basic coefficients in the models are calculated. Model tests are an essential guidance for the user of non-linear time domain simulation tools

to gain experience in the use of a unified model.

The current non-linear time domain code of CRS focuses on course-keeping of the ship in 6 degrees of freedom (6 DOF), in which the interaction with the manoeuvring model is already essential. Especially the sway hydrodynamics will influence roll motions and this means that seakeeping (roll damping) and manoeuvring is to be combined. Yaw manoeuvring forces and a PID controlled rudder are furthermore essential to keep the ship on track and course.

3. INFLUENCE OF MAIN DIMENSIONS ON PARAMETRIC ROLL

In the theoretical background four criteria for parametric roll to occur were given. The first two (the natural period of roll is equal to approximately twice the wave encounter period and the wavelength is on the order of the ship length) can be described with the following equations:

$$T_{\phi} \approx 2T_{pe} \quad (12)$$

$$\lambda \approx L_{pp} \quad (13)$$

Equation (14) gives an approximation for the natural roll period (assuming 10 % added mass). Equation (15) gives a relation between wave length (λ) and wave period for deep water.

$$T_{\phi} = \frac{2.2 \pi k_{xx}}{\sqrt{g GM}} \quad (14)$$

$$T_p = \sqrt{\frac{2\pi \lambda}{g}} \quad (15)$$

For zero speed equations (14) and (15) can be substituted in (12). GM can then be expressed in the following way (for zero speed).

$$GM = 0.605\pi \frac{k_{xx}^2}{\lambda} \quad (16)$$

For non zero speed the following relation between peak wave period and peak encounter wave period should be used (V_s being the ship speed and μ the wave direction, 180 being head waves).

$$T_{pe} = \frac{T_p}{1 - \frac{2\pi V_s \cos \mu}{T_p g}} \quad (17)$$

Equation (16) gives a relation between GM, radius of gyration and wave length. By substituting also the second criterion for parametric roll (see equation (13)) the relation becomes purely dependent of geometry and main dimensions.

When the radius of gyration is not known, standard values for k_{xx}/B can be used. By also using standard values for L/B , equation (16) can be rewritten in the following way.

$$GM = 0.605\pi \frac{L^2}{\lambda} \left(\frac{k_{xx}}{L} \right)^2 \quad (18)$$

In the table below some values for k_{xx}/L are given for a range of L/B and k_{xx}/B values.

k_{xx}/L for a range of L/B and k_{xx}/B values					
	L/B				
k_{xx}/B	5.6	5.8	6	6.2	6.4
0.38	0.0679	0.0655	0.0633	0.0613	0.0594
0.39	0.0696	0.0672	0.0650	0.0629	0.0609
0.40	0.0714	0.0690	0.0667	0.0645	0.0625
0.41	0.0732	0.0707	0.0683	0.0661	0.0641
0.42	0.0750	0.0724	0.0700	0.0677	0.0656

Using equation (18) and the above table the two graphs (one for zero speed and one for 10 knots) given below can be made. They show the combinations of GM and L_{pp} for which parametric roll instability might occur. In other words where the first two criteria for parametric roll to occur are met.

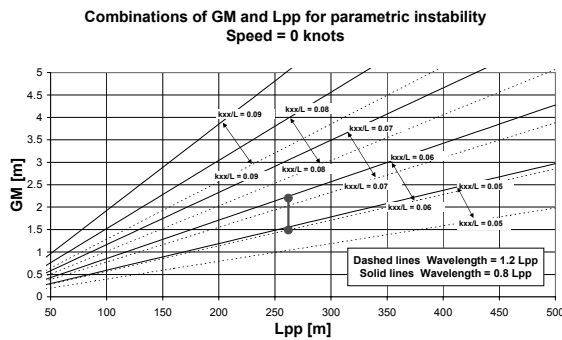


Figure 1 Combinations of GM and vessel length resulting in parametric instability (0 knots)

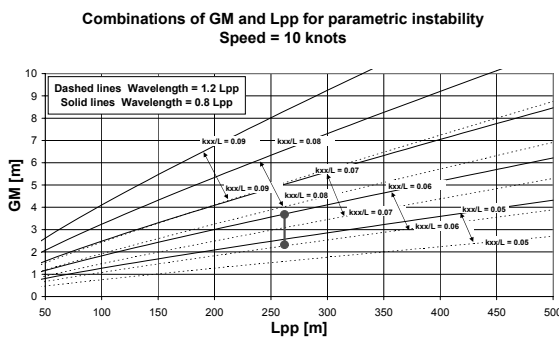


Figure 2 Combinations of GM and vessel length resulting in parametric instability (10 knots)

The figures show the relation between GM and Lpp for an upper limit of wavelength/Lpp = 1.2 (dashed lines) and a low limit of wavelength/Lpp = 0.8 (solid lines). For a given k_{xx}/Lpp ratio the area between the dashed and solid lines give the GM range for a certain Lpp for which the criteria are met.

With these graphs it is easy to investigate in an early stage if the vessel can be subject to parametric roll. To further illustrate how to use these graphs an example is given below.

C11 class container vessel:

$$\begin{aligned}
 L_{pp} &= 262 \text{ m} \\
 B &= 40 \text{ m} \\
 k_{xx}/B &= 0.40
 \end{aligned}$$

$$\text{Thus: } k_{xx}/L = 0.061$$

In the figures the range of GM's which will give parametric instability is indicated. At zero

speed the range will be between GM = 1.5 m and GM = 2.2 m and at 10 knots speed between GM = 2.2 m and GM = 3.8 m. This doesn't mean the vessel will actually be subject to parametric roll. This depends on other factors like the amount of parametric excitation (GM fluctuations in waves) and the amount of roll damping. These factors depend on the hull form and the appendages.

4. HULL FORM VARIATIONS

4.1 Selected Case

In order to investigate the influence of the hull form on the occurrence of parametric roll a hull form needed to be selected. As a case the post-Panamax, C11 containership which encountered the storm, as described in the introduction, is used. It is a logical starting point since model tests were previously performed on the same vessel at MARIN.



Figure 3 C11 Hull Form

A rendering of the C11 hull form is presented in Figure 3. Typical of post-PANAMAX containerships, the C11 has extensive bow and stern flare. The ship's natural roll period as used in this study was 25.7 seconds. This corresponds to the estimated roll period of the ship at the time of the incident. The GM in calm water was about 2 m.

The original hull form and variations at the bow and aft of the hull form were investigated. In the aft a Pram type hull form and a hull form with higher dead rise were taken. At the bow hull lines with a less pronounced bow flare (55 deg) and a more pronounced bow flare (45 deg) were used. This resulted in four variations of

the original hull form.

In order to have a fair comparison between the different variations it is necessary to keep the draft, GM and natural roll period the same. Because of the different under water hull forms it means that the displacement and KG will change slightly.

4.2 Model Tests

In order to have validation material model tests were performed. These were performed in the Seakeeping and Manoeuvring Basin (SMB) at MARIN. The basin measures 170 x 40 x 5 m in length, width and depth respectively. Not all hull form variations were tested. The original hull form (model 8004-1) and the pram aft body (model 8004-2) variation were tested.

The models were self propelled during the tests and completely free sailing. The only connection between the model and the carriage consisted of an umbilical for power and data transmission.

The model tests were performed for an average speed in waves of 5 knots. The tests were done for head sea conditions and a variation of wave heights and wave periods were tested. For each model the tests started with a test in high waves ($H_s = 7.5$ m) for which several wave periods were tested. This was done to determine the most critical wave period. For this critical wave period a series of tests with increasing wave heights were done. For all these tests the realisation of the encountered waves was kept the same. Only the height of the waves was increased. The same realisation of the waves was used for both the models. This means that wave group effect do not influence the comparison of the two vessels. From the model test results it is possible to determine the wave heights for which parametric roll will start (threshold wave height).



Figure 4 Original C11 (upper) and Pram type (lower) aft ship

4.3 Model Tests Results

In Figure 5 the roll damping of the two hull forms (determined from roll decay tests) is compared. One can see that the roll damping of the pram aft shape is slightly higher, which is according to expectations. Both models were equipped with 40 cm high 76.54 m long bilge keels.

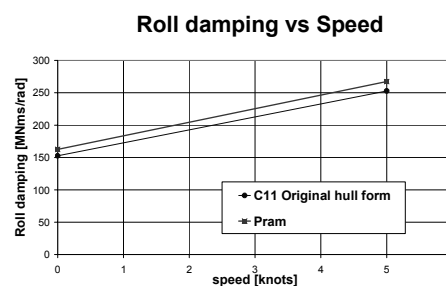


Figure 5 Roll damping comparison

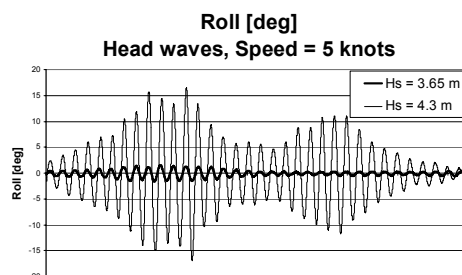


Figure 6 Time trace roll motion of C11 Original hull form

In Figure 6 a sample of the roll motion time traces are shown for the C11 original hull form in head seas at 5 knots speed. Results for two wave heights are given. They show the roll time trace for the vessel within the same wave realisation (same wave but only different amplitude). As can be seen the difference in wave height is small ($H_s = 4.3$ m versus $H_s = 3.65$ m) the difference in roll response is however big. The figure illustrates quite well the threshold behaviour of parametric roll.

The model tests results are summarized in Figure 7. The figure shows the mean of the 1/10 highest roll motions ($A1/10+$) as function of the wave height. Each dot in the figure represents a test in irregular head seas.

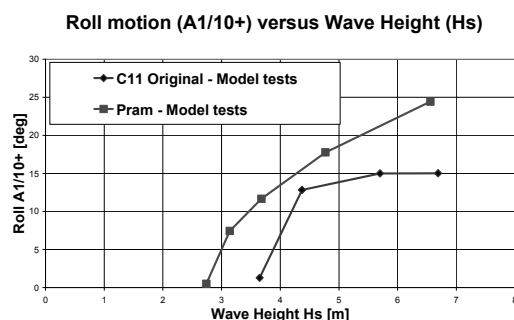


Figure 7 Model tests results

The model tests results show that the pram hull form results in higher roll angles. It also shows that the roll motions due to parametric roll start earlier meaning that the threshold wave height is lower.

From Figure 5 it could be seen that the damping of the pram is slightly higher than the original v-shape. The results presented in Figure 7 however show that the roll response is higher. It means that the excitation (GM variations) of the pram hull form is higher which is also according to expectations. The difference in GM variations will be discussed in the next section.

Using a criterion for parametric roll of 10 deg $A1/10$ one can determine the threshold wave height from Figure 7. For the C11 original hull form the threshold wave height becomes $H_s = 4.3$ m and for the pram $H_s = 3.5$ m.

4.4 Approximation Methods

The first step of the calculations was to validate the different approximation methods. If a good enough agreement was found with the model test the second step was to perform calculations for the other hull form variations which were not tested. Calculations were performed using a simplified one degree of freedom method (Dunwoody, 1989a and 1989b) and a non linear time domain program PRETTI (see also section 2.2).

GM variations As discussed earlier (see section 2.2) the GM variations in head waves represent the excitation for parametric roll. The static stability in “frozen” longitudinal waves is a good indication of the GM variations of a vessel sailing in waves. These were calculated for the original C11 hull form and the different hull form variations. For this purpose the program SHCP (NSSC, 2003) was used. The input for the program are the hull form, loading condition, wave height, wave length and the longitudinal position of the wave crest with respect to the hull. A range of wave conditions and roll angles can be entered. For each condition the pitch-heave static equilibrium is solved (thus preserving equilibrium of weight, buoyancy and trim moments). The righting arms calculated for each condition can be used to determine GM and thus the GM difference between the sagging and hogging conditions. Using this method one assumes that the dynamic pitch and heave motion do not influence the GM variations. Sample results are given in the figure below.

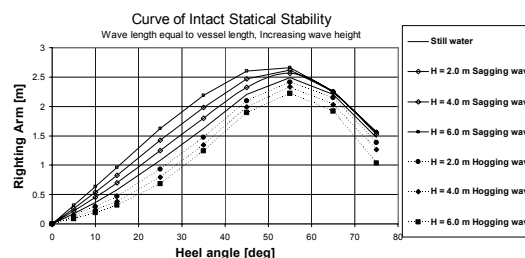


Figure 8 Curve of static stability C11 class container vessel

From Figure 8 the difference in GM between the sagging in hogging conditions can

be determined. This can be done for different wave lengths. In Figure 9 the GM variations for a range of wave lengths are given for a wave height of $H = 5.0$ m. The figure shows the GM in sagging condition, hogging condition, the difference between the two (Delta GM) and the difference divided by the wave height (Delta GM/H) which is plotted on the second y-axis (right).

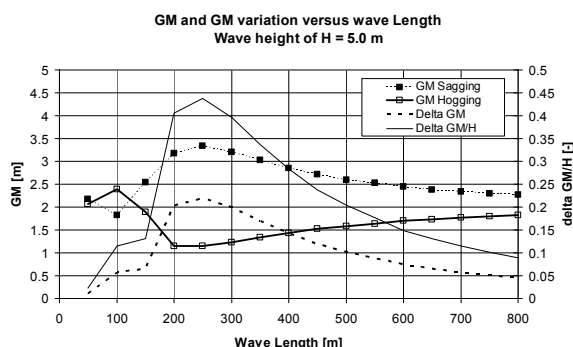


Figure 9 GM and GM variations versus wave length for C11 class container vessel

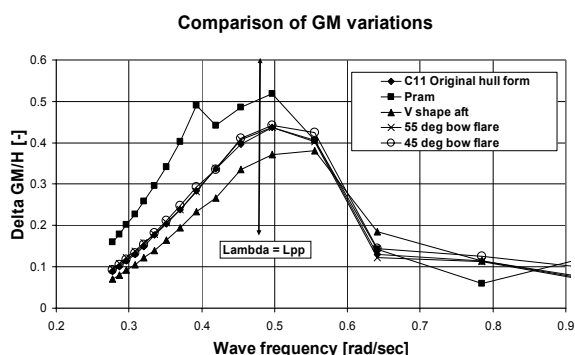


Figure 10 Influence of hull shape on GM variations

In Figure 10 the linearised GM variations (DeltaGM/H) are given as function of wave frequency for the C11 hull form and the four hull form variations. The frequency corresponding to a wave length equal to the length of the vessel is indicated in the figure.

The following observation can be made from the results presented in Figure10. First it can be observed that the changes to the bow flare do not seem to influence the GM variations. Secondly, the V shape aft hull form shows smaller GM variations than the original C11 hull form and the pram aft shape shows larger GM variations as the C11 hull form. The

latter is in accordance with the model tests results presented in Section 4.3.

Threshold value for parametric roll in regular waves Using equation (8) an estimate of the required GM fluctuations in regular waves can be made. This was done using the following data at 5 knots forward speed: $GM = 2.0$ m; $B_{xx} = 2.5 \cdot 10^5$ Nms/rad, $I_{xx} = 2.12 \cdot 10^7$ kNms²; $A_{xx} = 3.0 \cdot 10^5$ kNms², which leads to $\delta GM = 0.16$ m in regular waves of 12.8 s. This is the threshold value at zero roll amplitude. Model tests in regular were not performed with the C11, so that these values can not be verified. However, compared to the observations in irregular seas, the GM fluctuations are about a factor 10 larger before the C11 shows a steep increase in roll.

Response to GM fluctuations (Dunwoody)

The results presented in Figure 10 were used in Dunwoody’s method (see formula 7, 8 and 9). For the damping the results from roll decay tests (see Figure 5) were used. It was assumed that the different hull form variations had the same roll damping as the original C11 hull form. For each hull form variation the threshold wave height was determined for a speed of 5 knots and a wave period of $T_p = 14$ s. The results are given in Table 1.

Table 1 Threshold wave height for different hull variations

	Threshold wave height	
	Dunwoody	Model tests
C11 original	4.3 m	4.3 m
Pram aft	3.2 m	3.5 m
V shape aft	5.3 m	-
Large bow flare (45 deg)	4.3 m	-
Small bow flare (55 deg)	4.3 m	-

The results using Dunwoody’s method show very good comparison with the model tests performed. Furthermore the results from Dunwoody’s method confirm the results found from the GM variation calculation. The bow flare does not seem to have any influence on the threshold wave height. The aft shape of the

vessel has some influence. A very pronounced V shape aft gives the best performance with regard to parametric roll.

It must be mentioned that although the bow flare does not directly influence the occurrence of parametric roll it can indirectly influence it. A more pronounced bow flare will result in more slamming events which in turn will make a vessel master decide to reduce the speed earlier than a vessel with a less pronounced bow flare. Because the roll damping at low speed is smaller it is generally more vulnerable to parametric roll than at high speed. So, indirectly the bow flare can have influence on the occurrence of parametric roll.

With Dunwoody's method it is very easy to perform variations in wave conditions. The threshold wave height can then be determined for a variation of wave periods. By combining these lines with a wave scatter diagram it is then possible to evaluate the effect of the hull form on the probability of occurrence of parametric roll. This is shown in Figure 11.

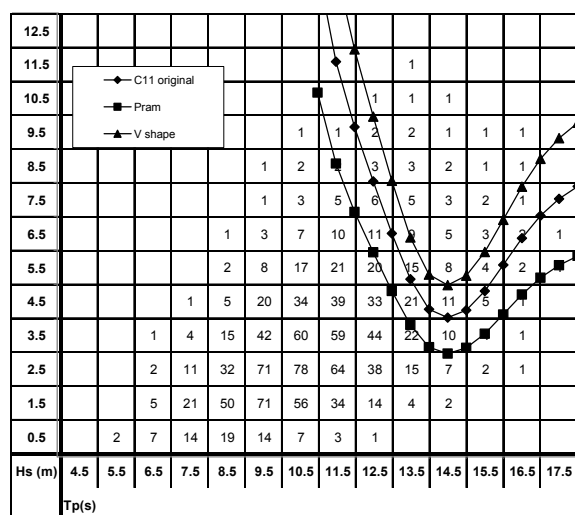


Figure 11 Threshold wave heights within North Atlantic scatter diagram

In Figure 11 the limiting wave height is shown for the original C11 hull form and the two aft shape variations (pram and sharp V). The probability of each combination of H_s and T_p is given in thousands. The wave scatter diagram used was area 9 (North Atlantic) all

directions from the Global Wave Statistics (Hogben et al., 1986).

From Figure 11 it can be determined that the V shape aft hull form has a 10% smaller number of occurrences of parametric roll (at 5 knots speed in head waves) in the North Atlantic. The results presented in the figure can not be used to estimate the exact number of occurrences of parametric roll for a given ship. In order to make that estimation the probability of the speed, wave heading and loading condition need to be incorporated. A method to determine this was presented by the author in 2003 (Levadou & Palazzi, 2003).

4.5 Simulation Methods

The non-linear time domain simulations have been performed in 5DOF (sway, heave, roll, pitch, yaw) for the lower sea states and in 3 DOF (heave, roll, pitch) for the more extreme sea states. It was verified that the results for intermediate sea states were comparable. The reason to limit the number of DOF in large sea states is a practical one: the Pretti code does not account for large yaw variations. Besides, in larger sea states the numerical model is more difficult to control, in particular due to the relative low forward speed which makes the rudder rather inefficient. Future enhancements are expected to overcome these limitations. Surge degree of freedom was neglected as well, for similar practical reason. The surge balance requires a dedicated implementation of added resistance, ship resistance and propulsion plant control, which is currently in development.

The viscous roll damping in Pretti is based on a time-domain implementation of Ikeda's method. For the bilge keel damping the water velocities at the bilge keel are assessed at each time instance and with a Keulegan-Carpenter number the drag on the bilge keels are calculated. Lift and eddy damping follows Ikeda's empirics.

All simulations were performed in the same 'relative' sea state realisation. This means that

the wave component phase and relative amplitudes were kept identical when the wave height was varied. To obtain reliable statistics the simulations were performed for a duration of 3 hours. The computer time required (CPU) is about half the simulation time. This means that a parametric study as presented in this paper is feasible in a design stage, although significant computer CPU is required for several days.

A mesh of the C11 container ship as used in the simulations is presented in Figure 12.

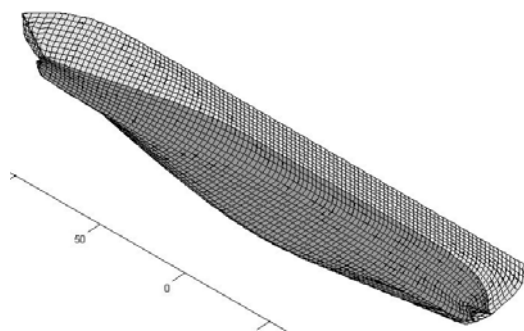


Figure 12 C11 container ship mesh for time-domain simulations

Model tests were carried out for two different hull shapes, the original C11 container ship and a modified one with the pram aft-body, denoted SIM Pram aft in Figure 13. The significant roll amplitude compares very well between simulations and model tests for the lower sea states. In the higher sea states the simulations predict larger parametric roll motions than the model tests show. The trend is however well predicted and the significant wave height at which parametric roll starts agrees well. The pram aft body might be beneficial for calm water resistance, but makes the design more sensitive for parametric roll. Striking is the fact that the original design shows less parametric roll in the higher sea states than the modified design, while this is opposite in the simulations. We consider this an effect of the not fully developed numerical models and the assumptions made in PRETTI. But, most likely non-linear hydrodynamics or more sophisticated non-linear (viscous) damping is required.

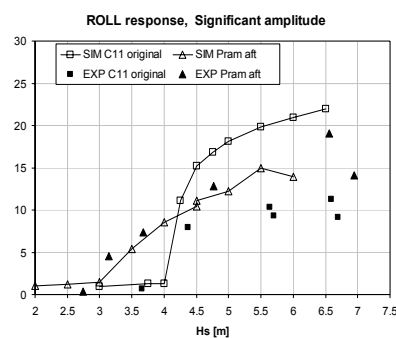


Figure 13 Significant roll amplitude from model experiments (EXP) and from non-linear simulations (SIM) for the C11 and Pram modified hull.

Following these results three other hull shape variations were investigated. The results are summarised in the figure below.

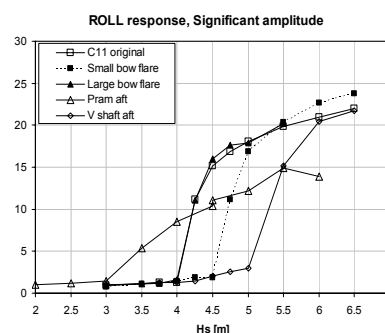


Figure 14 Significant roll amplitude in Jonswap wave spectra for the C11 and 4 modified hull shapes.

The numerical results are summarised in the following table 2, which compares the threshold value with Dunwoody. A threshold significant roll amplitude of about 5 degrees was used.

Table 2 Comparison Dunwoody and Pretti simulations

	Threshold wave height	
	Dunwoody	Simulations
C11 original	4.3 m	4.2 m
Pram aft	3.2 m	3.5 m
V shape aft	5.3 m	5.1 m
Large bow flare	4.3 m	4.2 m
Small bow flare	4.3 m	4.6 m

The comparison between Dunwoody and direct simulations is good, which is a striking conclusion. The dynamic GM variations in the simulations are comparable but too some extent different from the GM variations in an assumed static wave due to the fact that the equilibrium buoyancy condition in waves is not obtained; heave and pitch motions will change the buoyancy of the ship. The numerical simulations show a stronger influence of the bow flare than the static simulations, which could be due to the mentioned reason; the position of the ship in waves will be different in simulations than in a static approach.

5. ROLL STABILISATION

In the previous chapter the influence of the hull form on the parametric roll threshold wave height has been demonstrated. One other way to influence the threshold wave height is to change the roll damping of the vessel. Usually vessels have a small potential damping. Therefore, adding appendages (bilge keels, fin stabilizers) or anti roll tanks can increase the roll damping drastically. The influence of bilge keels and active fin stabilizers on the threshold wave height have been investigated by using Dunwoody's method.

5.1 Bilge Keel

The bilge keel damping is often associated with the energy dissipated by the drag forces of the bilge keel (Dallinga et al., 1998). Within this concept the damping is proportional with the roll velocity amplitude. Equation (17) gives the increase of roll damping per roll velocity amplitude change.

$$\frac{\partial B_{BK}}{\partial \dot{\phi}} = \frac{4}{3\pi} \rho 2 l_{BK} h_{BK} (C_{HF} r_{BK})^2 r_{BK} C_{Dbk} \quad (17)$$

According to Ridjanovic (1962) the effective drag coefficient depends on the amplitude of the transverse flow and the bilge keel height (see equation 18).

$$C_{Dbk} = 22.5 \frac{h_{BK}}{\pi r_{BK} C_{HF} \dot{\phi}} + 2.4 \quad (18)$$

Using these equations the bilge keel damping was calculated for several bilge keel heights. The contribution as a fraction of the total damping linearised for 10 deg roll amplitude is given in the first row of table 3 for 5 knot speed.

Table 3 Roll damping contribution of bilge keel

	Bilge keel height			
	0 cm	20 cm	40 cm	60 cm
Fraction	0	0.256	0.428	0.547
Total Damping [MNms/rad]	145	195	253	320

As can be seen the roll damping contribution of the bilge keel is very large. Using these fractions on the total roll damping determined from the roll decay tests the damping for a variation of bilge keels can be determined. These values are indicated in the second row of the table.

Using Dunwoody's method the threshold wave height was determined for the different bilge keel heights. The results are given in. As can be seen a 40 cm bilge keel raises the threshold wave height by $H_s = 1$ m. Adding 20 cm raises the threshold by about 0.6 m.

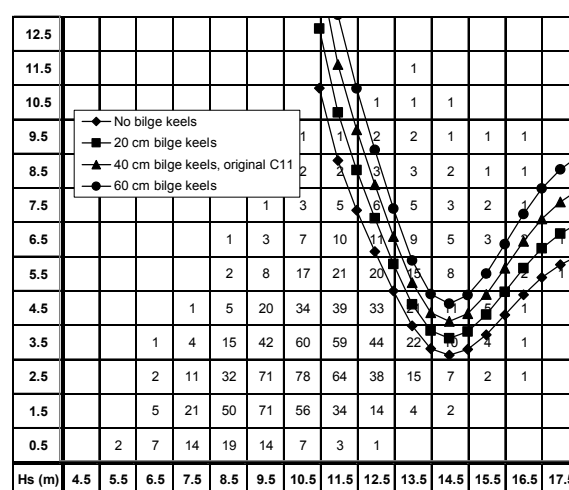


Figure 15 Influence of bilge keel height on threshold wave height

5.2 Active Fin Stabilizer

The influence of active fin stabilizers can be estimated using the same approach. The roll damping (passive and active part) was estimated using the following equation (Dallinga, 1993 and Dallinga et al., 1998).

$$B_{Fin} = 2r_{fin} \frac{1}{2} \rho V_s^2 A_{fin} C_{FH} \left[\frac{\partial C_{L_r}}{\partial \alpha_{pas}} \frac{r_{fin} C_{HF}}{V_s} + \frac{\partial C_{L_c}}{\partial \alpha_{act}} b_c \right] \quad (19)$$

Using this equations the damping of fin stabilizers was calculated for several fin stabilizers area. The damping linearised for a 10 deg roll amplitude is given in Table 4.

Table 4 Roll damping contribution of fin stabilizers

	Fin stabilizer damping		
	0 m ²	10 m ²	21 m ²
Fin Stab damping [MNms/rad]	0	87	173
Total Damping [MNms/rad]	253	340	426

Using Dunwoody's method the threshold wave height was determined for the different fin stabilizers area. The results are given in Table 4 for 5 knot speed.

As can be seen a 10 m² fin stabilizer raises the threshold wave height by H_s = 0.7 m. Adding a 21 m² fin stabilizer raises the threshold by about 1.0 m. The results show that the fin stabilizers give approximates the same increase in threshold wave height as bilge keels for 5 knot speed. However, for speeds higher the influence of the fin stabilizers will be higher. This is due to the fact that the fin stabilizer damping increasing with the square of the speed.

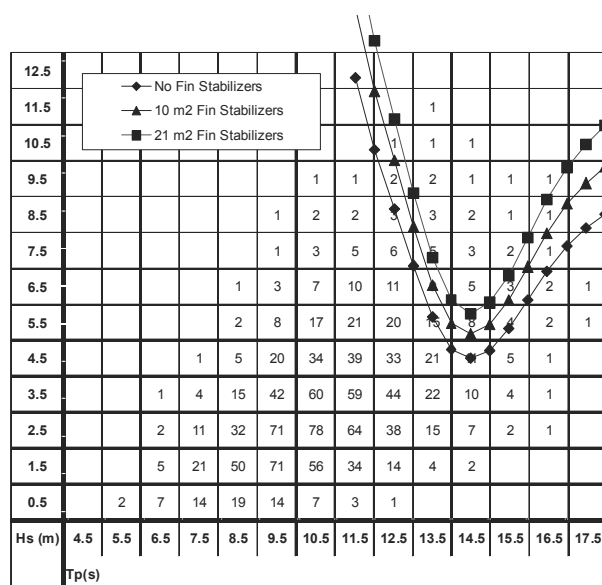


Figure 16 Influence of fin stabilizers on threshold wave height

5.3 Results summary

The results of the simulations and model tests have shown that the C11 original hull form results in a lesser probability of parametric roll to occur than the pram aft body. The pram aft body is however beneficial with respect to calm water resistance. Using the results presented in the previous chapters an estimation can be made of the bilge keel height or fin stabilizer area needed on the pram aft body in order to have a comparable threshold wave height as the C11 hull form. This estimation is given in Table 5.

Table 5 Bilge keel height or Fin stabilizer area needed for same threshold wave height

	BK height [cm]	Fin Stab [m ²]
C11 original	40	-
Pram aft body	80	-
Pram aft body	40	21

The results show that in order to achieve the same threshold wave height the bilge keel must be twice as big or the pram aft body must be equipped with a 21 m² fin stabilizer. These results are valid for 5 knots speed. For higher speeds the fin stabilizer will give more roll damping than the 80 cm bilge keel.

6. CONCLUSIONS

In the paper, the influence of main dimensions, hull form and roll stabilization on the occurrence of parametric roll is discussed. A one degree of freedom motion method and non linear time domain simulations were used and validated with model tests. Regarding the results the following conclusion may be drawn.

A relatively simple one degree of freedom motion method can be used in the preliminary stage of a design. An important factor on the results is the used roll damping. Empirical models for the roll damping, tuned with model tests, can be used in a preliminary stage. The method gives an idea of the threshold wave height for which parametric roll will start but not the actual roll angles associated with the rolling.

Non linear time domain simulations can be used to determine the threshold wave height and to determine the roll angles associated with the parametric roll. Here also tuning of the roll damping is needed in order to get reliable results.

The model tests and calculations on a C11 type container vessel have demonstrated that the aft body configuration has more influence on the occurrence of parametric roll than the bow flare. A V-shaped aft body is preferable to a pram type aft body.

Finally, the influence of bilge keel height on the occurrence of parametric roll has been shown. It has also been shown that active fin stabilizers can be used at low speed in order to increase the threshold wave height.

7. REFERENCES

- Bailey, P.A., Price, W.G. and Temarel, P., 1997, "A unified mathematical model describing the manoeuvring of a ship travelling in a seaway," RINA.
- Cummins, W.E. (1962), "The impulsive response function of ship motions", Schiffstechnik, Band 7.
- Dallinga, R.P., 1993. "Hydromechanic Aspects of the Design of Fin stabilizers", RINA Spring Meetings, London.
- Dallinga, R.P., Blok, J.J and Luth, H.R., 1998. "Excessive rolling of cruise ships in head and following waves, RINA International Conference on ship Motions & Maneuverability, London".
- Dunwoody, A.B., 1989a, "Roll of a ship in astern Seas – Metacentric height spectra", Journal of Ship Research vol 33, No. 3, pp 221-228.
- Dunwoody, A.B., 1989b, "Roll of a ship in astern Seas – Response to GM fluctuations", Journal of Ship Research vol 33, No. 4, pp 284-290.
- Fossen, T.I. and Smogeli, O.N., 2004, "Nonlinear Time-Domain Strip Theory Formulation for Low-Speed Manoeuvring and Station-Keeping", Modeling, identification and Control, Vol 25, No. 4.
- France, W. N., Levadou, M., Treacle, T. W., Paulling, J. R., Michel, R. K., and Moore, C., 2003, "An Investigation of Head-Sea Parametric Rolling and its Influence on Container Lashing Systems", Marine Technology vol 40, No. 1.
- Francescutto, A. and Bulian, G. 2002, "Nonlinear and stochastic aspects of parametric rolling modelling", Proceedings of the 6th International Ship Stability Workshop.
- Graff, W. and E. Heckscher, 1941, "Widerstands und Stabilitäts versuche mit drei Fischdampfermodellen", Werft-Reederei-Hafen, vol. 22, (also DTMB Translation No.75, June 1942).
- Hogben, N., Dacuhna, N.M.C. and Olliver,

G.F., 1986, "Global Wave Statistics", BMT, London,.

Ikeda, Y., Himeno, Y., Tanaka, Y., 1978, "A prediction method for ship roll damping", Technical Report 00405, University of Osaka.

Kempf, G., 1938, "Die Stabilitätsbeanspruchung der Schiffe durch Wellen und Schwingungen", Werft-Reederei-Hafen, vol. 19.

Levadou, M. and Palazzi, L., 2003, "Assessment of Operational Risks of Parametric roll", World Maritime Technology Conference, San Francisco.

Luth, H.R. and Dallinga, R.P., 1998, "Prediction of excessive rolling of cruise vessels in head waves and following waves", PRADS. The Hague Netherlands.

Naval Sea Systems Command, 2003, "Ship Hull Characteristics Program User Manual version 4.3".

Oakley, O. H., Paulling, J. R. and Wood, P. D., "Ship Motions and Capsizing in Astern Seas, Proceedings", Tenth ONR Symposium on Naval Hydrodynamics, ONR, ACR 204, 1974.

Paulling, J. R. and Rosenberg, R. M., 1959, "On Unstable Ship Motions Resulting from Nonlinear Coupling", Journal of Ship Research, vol 3, no.1.

Paulling, J. R., 1961, "The Transverse Stability of a Ship in a Longitudinal Seaway", Journal of Ship Research, vol. 4, no. 4.

Ridjanovic, M., 1962, "Drag coefficients of Flat Plates Oscillating Normally to their Planes", Schifftechnik, Band 9, Heft 45.

Shin, Y. S., Belenky, V. L., Paulling, J. R., Weems, K. M., Lin, W. M., 2004, "Criteria

for Parametric Roll of Large Containerships in Longitudinal Seas", SNAME.

8. NOMENCLATURE

A_{xx}	: added mass
A_{fin}	: fin stabilizer area
b_c	: damping gain
B	: width of the ship
B_{xx}	: damping
B_{total}	: total damping
B_{crit}	: critical damping
C_{xx}	: restoring
C_{Dbk}	: effective drag coefficient
C_{HF}	: magnification of the flow over the bilge coefficient
C_{FH}	: fin to the hull coefficient
$\frac{\partial C_L}{\partial \alpha}$: lift slope
g	: gravity
GMT	: transverse metacentre height
h_{BK}	: bilge keel height
H, H_s	: wave height, significant wave height
I_{xx}	: ship inertia
k_{xx}	: radius of gyration of roll
L or L_{pp}	: length between perpendiculars
l_{BK}	: bilge keel length
M_x	: first order wave excitation
r_{BK}	: arm of bilge keel to centre of gravity
r_{fin}	: arm of fin stabilizer to centre of gravity
S_{GM}	: spectral density of GM fluctuations
$S_{e\zeta}$: spectral density of the wave encounter
T_ϕ	: roll natural period
T_p	: wave peak period
T_{pe}	: encounter wave peak period
V_s	: ship speed
$\phi, \dot{\phi}$: roll motion, roll velocity
ρ	: density of water
∇	: displacement
ω_ϕ	: natural roll frequency

- ζ_a : Wave amplitude
 $\Delta\xi$: Non dimensional damping reduction
 λ : wave length

Stability and Safety Analysis of the Air Lifted Catamaran

Dracos Vassalos, *Universities of Glasgow and Strathclyde*

Nan Xie, *Universities of Glasgow and Strathclyde*

Andrzej Jasionowski, *Universities of Glasgow and Strathclyde*

ABSTRACT

The Air Lifted Catamaran (ALC) is an innovative fast marine transportation concept, comprising the application and variation of a new, skirtless air cushion and air-lubrication, thus rendering it a hybrid between catamaran and SES (Surface Effect Ship). Its features and capabilities are beyond current conventional high-speed mono-hull and catamaran. The present paper presents pertinent studies on stability concerning this craft, including dynamic stability, stability in turning and directional stability. The stability analysis takes into account air compressibility in the cushion, and is carried out in time domain. Some simulated results are presented and discussed, and requirements for design and operation of the craft based on IMO HSC Code 2000 are briefly outlined.

Keywords: *stability; air lifted vehicle; numerical simulation;*

1. INTRODUCTION

Conventional fast catamarans and mono-hulls have in the last few years gradually increased their operational speed, but at the cost of larger installed engines, burning more fuel and costing considerably more, to install, maintain and operate. The design speed of the Air Lifted Catamaran (ALC) is based upon speed capability of 70 knots for the 40m-long/350 passenger – fast ferry application, and operational speed of 50 knots for a 150m express cargo ship. Model tests have shown that its high-speed power reduction is around 25% when compared with the best of catamaran and mono-hull vessels, Allenstrom et al (2001), Allenstrom et al (2003). The present paper intends to address stability and safety issues of the ALC.

Recent international regulatory developments pertaining to high-speed craft, particularly the 2000 HSC code, acknowledge the necessity of

improvements of maritime safety standards for HSC in order to maintain the highest practical level of safety (IMO, 2000). However, the continuous update of stability rules and regulations for advanced high speed vessels compared to conventional vessels is greatly influenced by the fact that there are many different types of high speed vehicles, and many different alternative design solutions within each category, so a meaningful way to set safety and operational standards is to use performance based criteria and safety levels to which any type of craft must comply with.

The dynamic instability of high-speed craft has been known to lead to such violent motions that would cause serious accidents. With increasing vessel speed, this is becoming more and more a problem to the designers and operators (Vassalos, 1995). Papaniklaou et al have carried out an investigation of adaptation of stability rules and tools to SES (Papanikolaou, Georgantzi and Karayannis, 2002). In the present paper, a mathematical model is presented for the dynamic stability

analysis based on the features of the vessel. The mathematic model takes into account the air compressibility in the cushion (with the adiabatic gas law), and hydrodynamic forces coupled with the vessel motions. The free surface elevation in time domain induced by air pressure inside the cushion and at the periphery is represented in the form of convolution integrals, whose impulse response functions are calculated by the transfer functions of the moving pressure distributions in the frequency domain. Hydrodynamic forces acting on the rigid side-hull are calculated by a strip theory approximation in which the memory effect is also taken into account. The resulting non-linear equations of motions are solved using a Runge-Kutta scheme in time domain.

A number of case studies have been carried out for various design configurations of the ALC with the present code. A porpoising type of unstable phenomena has been identified for this type of vessel, which coincides with model experiments. The stable/unstable boundaries can be found with the present tool for different hull designs (such as cushion configurations, separation of the demi-hull, etc.), characteristics of inflow fan system and loading conditions (position of centre of gravity of the vessel) at various vessel speeds. The method developed in the present paper can be expected to be one of the tools for design of this type of vessel.

2. STATIC STABILITY OF THE AIR LIFTED CATAMARAN

2.1 The Vessel

The design feature of the ALC is similar, in some sense, to that of an SES catamaran. There are two demi-hulls, each of which contains air cushion(s). A forward planing surface ahead of the step creates some limited dynamic lift. The step and the forward planing surface also create the forward sealing of the air cushion chamber, the step being located in a plane close to

horizontal (no part of the step is to ventilate before the other). The bow section is slender in order to reduce displacement forces in a seaway, and the bow incorporate a voluminous part above a built-in chine/spray rail to reduce water deflection and reserve buoyancy in pitching motion. The side keels of varying height extend from just ahead of the step to the transom. The height of the keels is adjusted to the observed/expected shape of the air cushion. The only purpose of the side keels is to fence in the air cushion. There are spray rails on the outside of the side keels, at a height partly to deflect the water without wetting the rails on the upper sides. The cushion ceiling is at a height to avoid the sea hitting it when the vessel is moving in a seaway. There is a slope of the ceiling aft end in order to deflect passing waves in a seaway. A flap or enclosure arrangement in line with the sloped portion of the ceiling is arranged to fence the air cushion chamber in the rear part and to create dynamic lift and motion damping. Figure 1 shows the ALC concept E40.



Figure 1 The E40 ALC concept (Allenstrom et al, 2001)

2.2 Static Stability

The vessel has basically two operational conditions: on-cushion (cushion-borne) mode and off-cushion (hull-borne) mode. Although the major operation of the ALC involves the cushion-borne mode, the hull-borne operation should also be considered. This is necessary as a result of safety and survivability requirements since it is possible that there may be times where a failure occurs in either the lift system or the seals, which would result in the vessel

operating in the hull-borne mode. In addition, during very severe sea conditions, it may be necessary for the ALC craft to operate only in the hull-borne mode for survival purposes. Also, there may be certain situations wherein purely hull-borne operation is considered for the vessel, dependent upon the degree of buoyancy initially designed for the sidewalls, for fuel conservation prior to a high-speed on-cushion mode in response to particular commands. In view of all these possibilities, it is therefore necessary to develop appropriate means of analysis and prediction of hull-borne motions in waves. The methods of analysis of hull-borne stability in this case follow the techniques applied to a displacement ship, using the software PROTEUS for this purpose; this will not be discussed in the present paper.

In the steady state condition, the balance of the vessel vertical force and moment about the transverse axis require:

$$\begin{cases} mg - 2A_c p_0 + \rho g \nabla + L_A + L_H = 0 \\ 2x_c A_c p_0 + x_B \rho g \nabla + x_{cA} L_A + x_{cH} L_H = 0 \end{cases} \quad (1)$$

where m is the mass of the vessel; L_A and L_H are hydrodynamic lift acting on the hull due to appendage and the craft hull itself; ∇ is buoyancy; A_c is cushion area of each demi-hull; p_0 is the cushion excess pressure and ρ is water density. x_c , x_B , x_{cA} and x_{cH} are the longitudinal position of the centre of cushion pressure, buoyancy, appendage lift and hull lift, respectively.

Model test measurements have shown that the cushion excess pressure decreases with increasing vessel speed, which means that the cushion excess pressure will be lower at higher speed, the dynamic lift force playing a more important role. The two-phase fluid flow around the vessel is very complicated, accurate prediction of all those terms are difficult at present. Ideally, captive model tests at forward speed should be carried out to measure dynamic forces and moment acting on the hull, however, this is beyond the scope of the present study. T this end, some empirical

formulae are used. The fore body part and the stern flap are assumed to be lifting surfaces with different aspect ratios. The slopes of the lift force coefficients are taken from an aerofoil with finite aspect ratio.

In order to gain some basic understanding of the stability of the ALC, the metacentric height of the ALC at zero speed is evaluated. The procedure follows that of SES. (Blyth 1993, Faltinsen, 2002). The contributions of restoring moment from hydrostatic buoyancy of side hull and excess cushion chamber pressure are taken into account. For an ALC with side hulls of approximately constant section and wall-sided body surface at the free surface, the initial metacentric height will be:

$$\overline{GM} = \frac{1}{mg} [-2A_c p_0 (0.5h_0 + z_g) + 2\rho g A_c b_0^2 + \rho g S_{yy} - \rho g \nabla \overline{BG}] \quad (2)$$

where h_0 is water head of the cushion excess pressure; b_0 is the beam of cushion of demi-hull; S_{yy} is the transverse moment of inertia of water plane area of the ALC at on-cushion condition. The last two terms in the right hand side of (2) represent the metacentric height of normal catamaran. It can be seen that the excess pressure p_0 in the cushion chamber gives a negative contribution to the metacentric height of the ALC. The second term in (2) is due to the catamaran configuration of the present ALC; for normal SES, this term vanishes. (Faltinsen, 2002).

Figure 2 shows an example of the static right lever of the ALC at zero speed. The displacement of the vessel is 170 tonnes and KG of 4m.

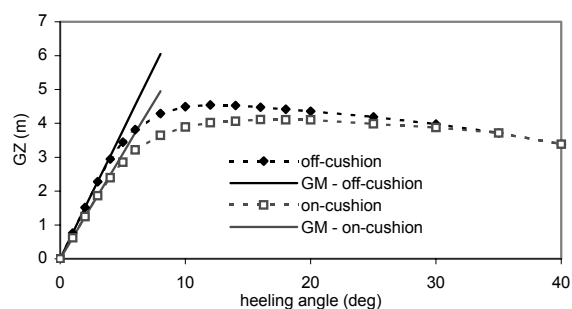


Figure 2 Static stability of an ALC at zero speed

3. DYNAMIC STABILITY ANALYSIS OF THE ALC

When the ALC is travelling at high speed, the analysis of the stability of the craft requires a dynamic model, which is presented in this section.

3.1 The Mathematical Model

The dynamic behaviour of the vessel can be described as

$$[\mathbf{M}][\ddot{\mathbf{x}}] = [\mathbf{F}_H] + [\mathbf{F}_R] + [\mathbf{F}_P] + [\mathbf{F}_A] + [\mathbf{F}_W] \quad (3)$$

where \mathbf{M} is the matrix of inertia of the craft; \mathbf{F}_H , \mathbf{F}_R , \mathbf{F}_P , \mathbf{F}_A and \mathbf{F}_W are hydrodynamic force, hydrostatic force, cushion pressure force, appendage force and wave force, respectively.

The hydrodynamic forces/moments and wave forces acting on the vessel are calculated by PROTEUS3 with a radiation/diffraction method (Jasionowski, 2001). Appendage forces are calculated by an empirical formula, in which a quasi-steady-state assumption has been utilised. In order to get the equation of the cushion pressure for port and starboard chambers, the adiabatic gas law and the continuity equation in each chamber will be used:

$$\begin{cases} \frac{p_i + p_a + p_0}{\rho_i^\gamma} = \frac{p_a + p_0}{\rho_0^\gamma} \\ \frac{d}{dt}(\rho_i V_i) = \rho_a (Q_{in,i} - Q_{out,i}) \end{cases} \quad (4)$$

where the subscript "1" and "2" stand for port and starboard cushion chamber, respectively; $Q_{in,i}$ is the inflow rate of the fan system, $Q_{out,i}$ is the outflow rate of the cushion chamber. V_i is the instantaneous cushion volume, which is a function of craft motion, and free surface elevation in side cushion. The inflow flux of each fan system is normally a function of the cushion pressure. The out flow rate is given by

$$Q_{out,i}(t) = c_n A_{L,i}(t) \sqrt{\frac{2(p_i(t) + p_0)}{\rho_a}} \quad i=1,2 \quad (5)$$

where the instantaneous escape area, $A_{L,i}(t)$, at the periphery is

$$A_{L,i}(t) = \oint_{L,i} [z_{r,i}(x, y, t) + z_{r,i}(x, y, t)] dl \quad i=1,2 \quad (6)$$

where z_r is the local relative vertical motion between hull and free surface given by

$$z_r = z_0 + z - x\theta + y\phi - \zeta_w - \zeta_p \quad (7)$$

The free surface elevation due to cushion pressure is expressed as

$$\begin{cases} \zeta_p(x, y, t) = \int_0^t h_\zeta(x, y, \tau) p(t - \tau) d\tau \\ h_\zeta(x, y, \tau) = \frac{2}{\pi} \int_0^\infty H_{\zeta,r}(x, y, \sigma) \cos(\sigma\tau) d\sigma \end{cases} \quad (8)$$

where $h_\zeta(x, y, \tau)$ is the impulse response function of the free surface elevation due to a unit cushion pressure. The free surface elevation transfer function, $H_\zeta(x, y, \sigma)$, is calculated by a pressure patch distribution method, in which the cushion area is represented by a number of rectangular pressure patches, see Figure 3. Full details of the formulation and numerical schemes can be found in Xie et al (Xie, Vassalos and Jasionowski, 2005a, 2005b),

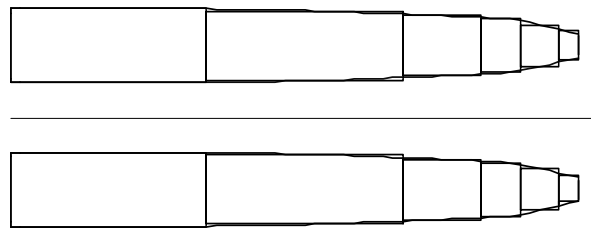


Figure 3 Representation of the cushion of the ALC

3.2 Numerical Simulations

Given all the terms in the equation of motions, (4), simulations can be carried out in time domain. A Runge-Kutta scheme is

employed for the integration of the differential equations.

Much of the simulation work is on the numerical calculation of the impulse/transfer response functions of the free surface elevation. Previous research work published is either for lower frequency range (Doctors, 1974) or for relatively lower speed (Kim et al, 1981). The present simulation requires the whole frequency range as well as relatively high Froude number. Figure 4 shows a comparison of the free surface elevation for a rectangular pressure patch. Figure 5 shows a sample of escape volume of the ALC. Figures 6 and 7 show samples of free surface elevation transfer function, and Figure 8 shows a sample of impulse response functions of free surface at the stern of the ALC.

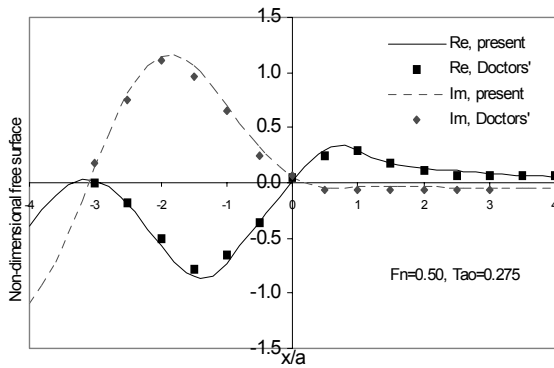


Figure 4 Wave-cut at $y=b$ for a rectangular pressure patch ($b/a=1, \tau=0.275, a$ = half length of pressure patch, b = half beam of the pressure patch)

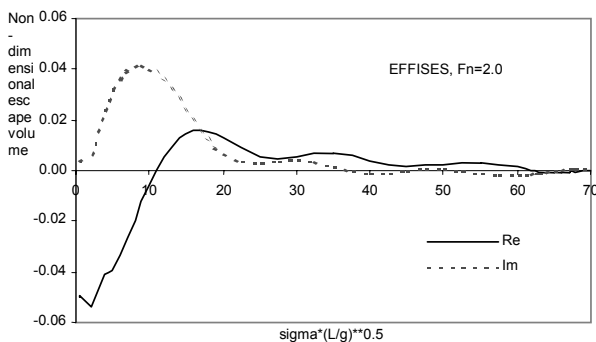


Figure 5 Samples of non-dimensional cushion escape volume

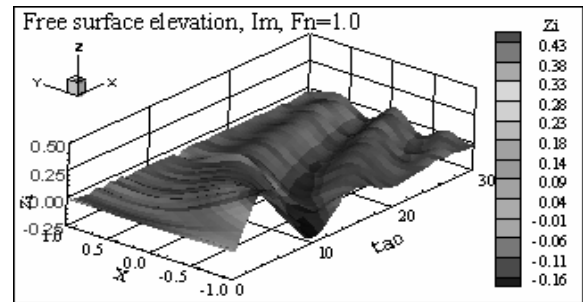


Figure 6 Transfer function of free surface elevation at $Fn=1.0$ (imaginary part)

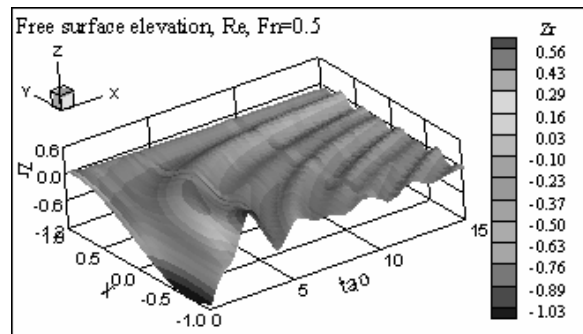


Figure 7 Transfer function of free surface elevation at $Fn=0.5$ (real part)

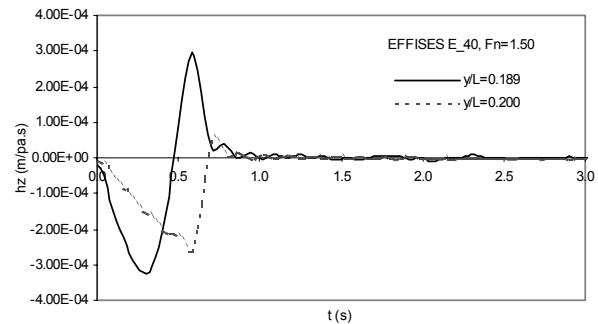


Figure 8 Impulse response function of free surface elevation of the ALC

Non-dimensional free surface elevation, ζ , is defined as:

$$\zeta = \frac{\rho g \zeta}{\Pi} \tag{9}$$

Non-dimensional escape area and escape volume are defined as:

$$\tilde{A} = \frac{1}{L} \int_{y_1}^{y_2} \tilde{\zeta}(x_a, y; \sigma) dy \tag{10}$$

$$\tilde{V} = \frac{1}{L^2} \iint_{S_c} \tilde{\zeta}(x, y; \sigma) dx dy \quad (11)$$

respectively, where L is cushion length, and S_c is cushion area.

The dynamic stability in still water is simulated with the vessel undergoing motions subject to an initial position. This will lead to its equilibrant position in case of a stable condition, but the vessel motions will not decay in case of unstable conditions. Figure 9 shows some of the simulated results for the ALC craft E40, in which combinations of the craft design parameters are shown for the stable/unstable conditions. In the unstable cases, the simulated cushion pressure is divergent. It is found from the simulated results that, in the case of a craft with instability, the pressure in the cushions accumulates, cushion volume and craft motions increase, the escape of the accumulated air requires a large escape area, the pitch angle increases suddenly, and the cushion collapses like a cavity breaking down. This has been observed during model testing where in some unstable conditions, in which the cushion pressure collapses, with the C.G., inflow rate, fan slope characterises, stern flap, cushion height, etc., all affecting the stability of the craft. Typically, the craft is stable for the longitudinal position of C.G. within a limited range. A small inflow rate will increase chance of instability. Also the stern flap angle should be set properly to ensure the craft has a correct trim altitude and restoring moment at speed.

The longitudinal stability in waves can be analysed in the similar way. Figures 12 and 13 show samples of the simulated craft motions in waves.

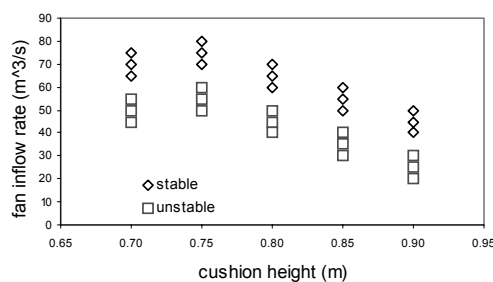


Figure 9 Sample of stable/unstable boundary of the ALC

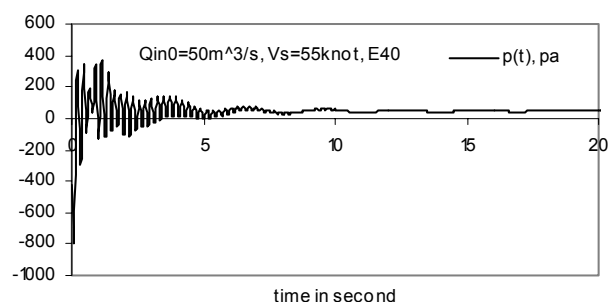


Figure 10 Sample of stable solution, cushion pressure

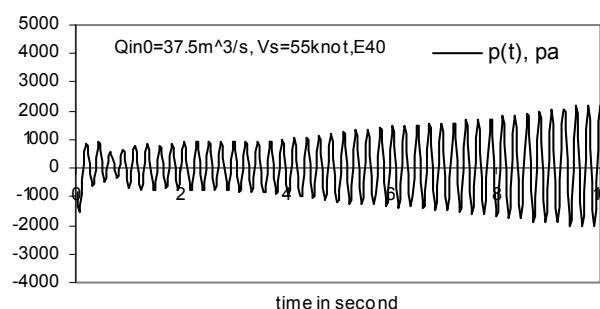


Figure 11 Sample of unstable solution, cushion pressure.

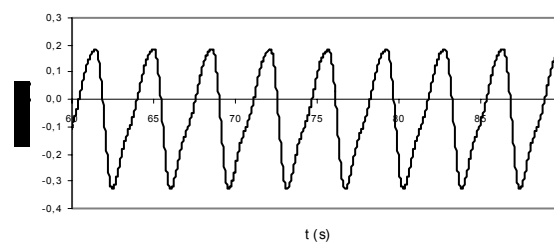


Figure 12 Simulated craft heave motion in waves

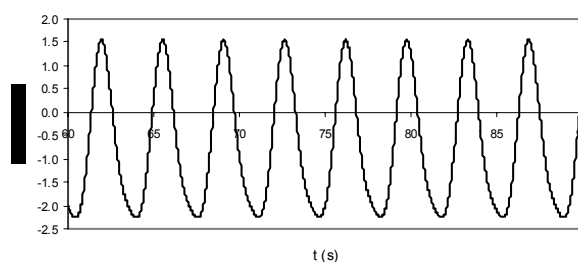


Figure 13 Simulated craft pitch motion in waves

4. STABILITY OF THE ALC IN MANEUVERING

The stability of the ALC in high speed turning is an important aspect of stability performance. In the Annex 7 of HSC Code

2000 (IMO, 2000), the stability criteria in the intact condition requires that a multi-hull craft should have sufficient stability in high speed turning. Heeling due to high speed turning is calculated as follows:

$$TL = \frac{1}{g} \frac{U_0^2}{R} \left(KG - \frac{d}{2} \right) \quad (12)$$

where TL =turning level (m), U_0 =speed of craft in turning (m/s), R =turning radius (m); KG =height of vertical centre of gravity above keel (m) and d =mean draught (m). In the present study, a mathematical model is presented for predicting the turning radius of the ALC.

4.1 The Mathematical Model

Extending the description of craft motions to horizontal plane with four degrees of freedom, attention is paid to two translatory motion components along x (surge) and y (sway) axes, and to two angular motions about x –(roll) and z –(yaw) axes. The equations of motion in the body-fixed coordinate system are expressed as (Wade and Wang, 1977; Kaplan, 1995):

$$\begin{cases} m(\dot{u} - ru) = X \\ m(\dot{v} + rv) = Y \\ I_x \dot{p} = K \\ I_z \dot{r} = N \end{cases} \quad (13)$$

where u and v are linear velocity components of the craft C.G. along the body-fixed system; p and r are the angular velocities about x – and z –axes, respectively; X, Y, K, N are external forces/moments applied to the craft. Each component of the force/moment is assumed to be expressible by a summation of five independent contributions: inviscid, cross flow drag, cushion pressure force, wind force and the resulting effect propulsion and control, (Wade and Wang, 1977; Kaplan, 1995), as shown next.

$$\begin{cases} X = X_{invis} + X_{drag} + X_p + X_w + X_\delta \\ Y = Y_{invis} + Y_{drag} + Y_p + Y_w + Y_\delta \\ K = K_{invis} + K_{drag} + K_p + K_w + K_{buoy} + K_\delta \\ N = N_{invis} + N_{drag} + N_p + N_w + N_\delta \end{cases} \quad (14)$$

The inviscid hydrodynamic force and moment are calculated as follows. The total apparent velocity at the cross flow plane of rigid side hull is given by

$$V_r = v + \xi r - f(\xi) p \quad (15)$$

where $f(\xi) = z_g - d(\xi)/2$ is the vertical distance of the centre of fluid pressure from the body C.G.; the 2-D added mass is $\mu(\xi)$, and the kinetic energy of a unit slice of the fluid

$$T(\xi, t) = \frac{1}{2} \mu(\xi) V_r^2(\xi) \quad (16)$$

The inviscid force/moment is then the change in the kinetic energy of the whole hull (integration along craft length). The cross-flow drag is:

$$Drag = -\frac{1}{2} \rho c_d s |V_r| V_r \quad (17)$$

where c_d = drag coefficient; s =project area. A water jet model is used (Wade and Wang, 1977). Wind force is calculated by formulae given by Aage (Aage, 1971).

Substituting all the external forces and moments into equations of motion, the linear and angular velocities can be obtained by solving the equation with a Runge-Kutta scheme, and the velocity components in the body fixed system are transformed to the earth fixed frame as shown next,

$$\begin{cases} \dot{x}_* = u \cos \psi - v \cos \varphi \sin \psi \\ \dot{y}_* = u \sin \psi + v \cos \varphi \cos \psi \\ \dot{\varphi} = p \\ \dot{\psi} = r / \cos \varphi \end{cases} \quad (18)$$

The solution of (15) give the trajectory of

the craft. In the case of steady turning, the deflecting angle of the nozzle of the water jet is

$$\delta(t) = \begin{cases} 0 & 0 < t < t_1 \\ \frac{t-t_1}{t_2-t_1} \delta_0 & t_1 < t < t_2 \\ \delta_0 & t_2 < t \end{cases} \quad (19)$$

4.2 Simulation Results

The ALC E40 is taken for numerical simulations. Since the water jet parameters are not available at the time of calculation, these parameters are derived from the literatures. The simulation starts with the craft in a straight course, with the deflecting angle of the nozzle of the water jet gradually increasing to the desired value, and then kept fixed, thus nozzles of the water jets generating a turning moment. Figures 14 to 17 show some of the simulated results of an ALC turning at about 50 knots of speed. From the simulated results, the turning lever can be obtained by (9). The heeling angle is also a part of the output of the simulations. In the HSC Code 2000, it is required that the total heel angle of the craft in the on-cushion mode due to beam wind and due to turning shall be less or equal to 12° . In the present case, the craft heel angle due to turning is about 1.7° , which is far less than the limited value.

Figure 18 shows the heeling angle of the craft in turning at different nozzle deflecting angles. It is found that the heeling angle will increase with increasing deflecting angles. This is not surprising, since larger a nozzle deflecting angle develops larger yaw turning moment and larger turning rate. It is expected that at large deflecting angles, the craft will experience significant heeling and resulting cushion pressure collapse and instability of the craft. Other simulated results (not shown here) indicate that larger nozzle deflecting angle also results higher turning levers that worsen stability. The dependency of turning diameters on craft speed and nozzle deflecting angle of

the water jet are shown in Figures 19 and 20. The turning levers at different speeds are shown in Figure 21. It seems that even through the present model provides reasonable results, it is realised that the above results are based on relatively simple external force models, the hydrodynamic forces are estimates and various parameters are assumed (e.g., water jet). It is expected that further refinement of the model should be made and verified when more accurate forces/parameters are available.

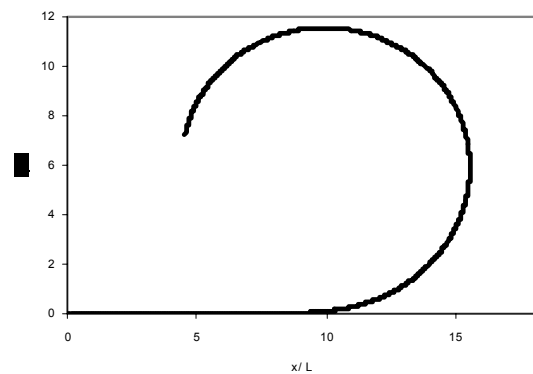


Figure 14 Simulated trajectory of the ALC at 50 knots

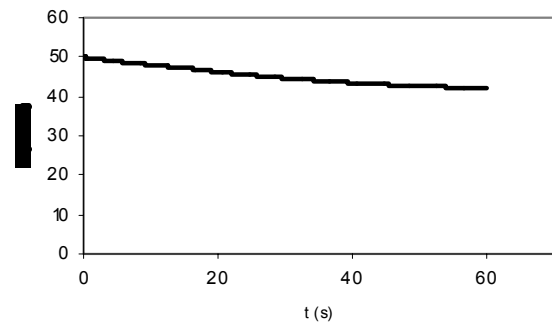


Figure 15 Simulated forward speed

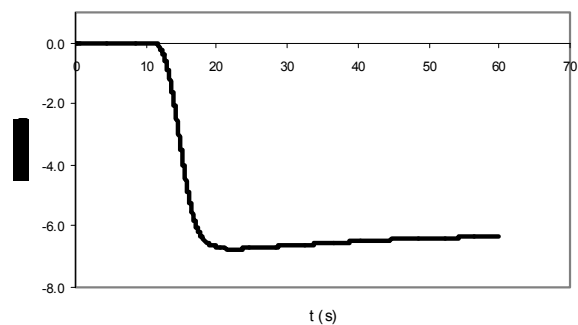


Figure 16 Simulated craft lateral speed

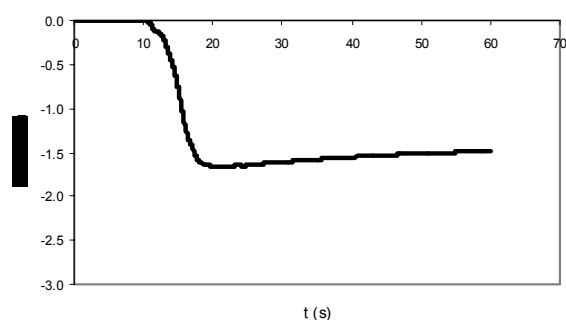


Figure 17 Simulated craft heel angle

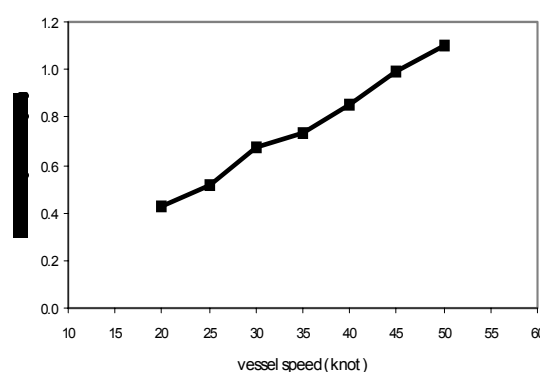
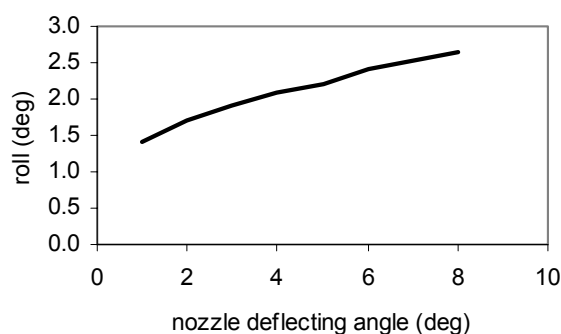
Figure 21 turning level of the ALC at deflecting angle $\delta_0 = 1.6^\circ$ 

Figure 18 Heel angle of the craft turning at 50knots

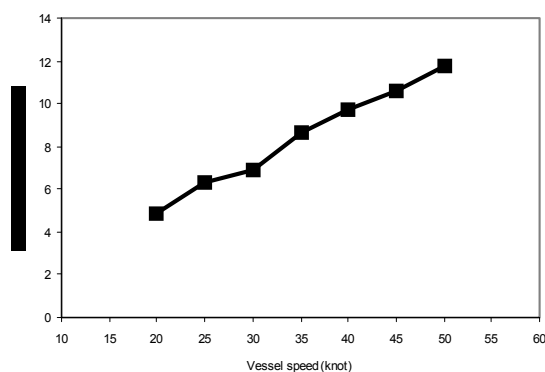
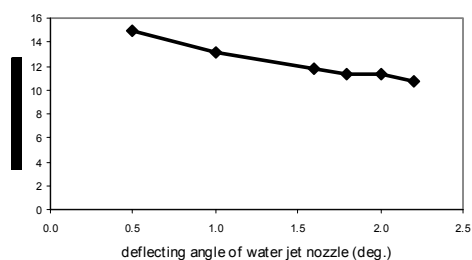
Figure 19 Turning diameter of the ALC at $\delta_0 = 1.6^\circ$ 

Figure 20 Turning diameter of the ALC at 50knts

4.3 Directional Stability

The ALC concept is sensible in directional stability due to its design characterises: relatively shallow draught, transom stern, the air chambers and high operational speed. The equations for analysis of directional stability are the same as for turning simulations. An autopilot control law is also incorporated in the form

$$\delta = k_1(\psi - \psi_d) + k_2\dot{\psi} \quad (20)$$

where k_1 and k_2 are the coefficients of the control law, and ψ_d is the desired vessel direction. Figures 22 ~ 24 show samples of the simulation. In this case, the initial yaw angle of the craft is $\psi_0 = 10^\circ$ and the desired orientation is $\psi_d = 0^\circ$; initial vessel speed is 50knots. The control parameters are taken to be $k_1 = 1$ and $k_2 = 2$. The simulated results indicate that the vessel can reach its desired orientation in about 20 seconds. Also in this process, the vessel undergoes roll motion due to the moment generated by the water jet. Numerical tests show that the control parameters k_1 and k_2 have a significant effect on the directional stability of the craft. In order to carry out more realistic simulation for the ALC, actual parameters should be used as the input of the simulator.

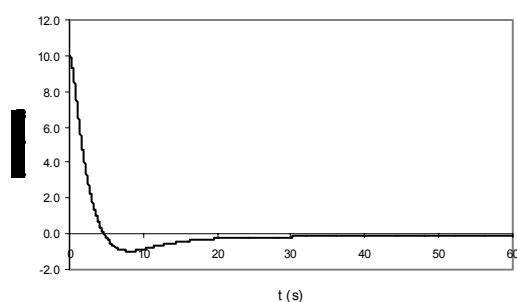


Figure 22 Simulated yaw time history

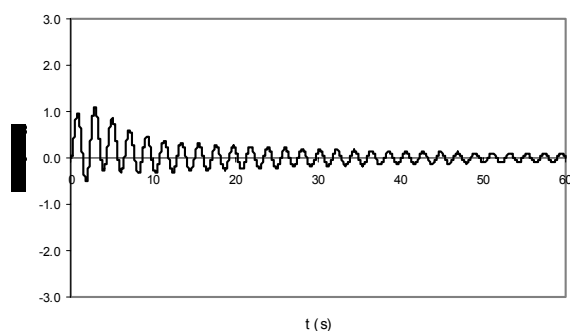


Figure 23 Simulated roll time history

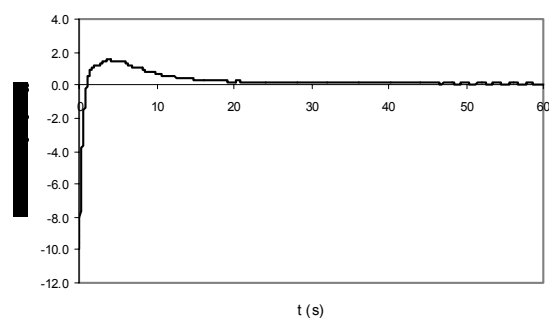


Figure 24 Simulated time history of nozzle deflecting angle

5. CONCLUSIONS

This paper presents some stability and safety studies for the Air Lifted Catamaran (ALC) carried out at the Ship Stability Research Centre (SSRC). Numerical prediction tools have been developed for stability analysis of the craft. Some sample results for the E40 concept are presented and discussed. Reasonable results are obtained. The effects of design parameters on the stability are discussed. Those tools could be helpful for the designer and operator of the craft. The stability analysis reported here is mainly for the craft at on-cushion mode. The stability and

survivability of the ALC craft at off-cushion mode (damage case) should be analysed with other methods. It is realized that some of the coefficients in the numerical simulations are empirical, or borrowed from other vessels, this may, in turn, partially affect the accuracy of the present prediction. It is certainly true that the prediction will be improved when more accurate data made available for the ALC.

6. ACKNOWLEDGMENTS

The present research was supported by the 5th framework EU project EFFISES, the EU funding is gratefully acknowledged.

7. REFERENCES

- Aage, C, 1971, "Wind Coefficients for Nine Ship Models", Hydro- or Aerodynamisk Laboratorium, Report No. A-3.
- Allenstrom, B., Liljenberg, H and Tuden, U., 2001, "An Air Lifted Catamaran – Hydrodynamic Aspects", Proceedings of FAST'01, Southampton, U.K. pp.29-40.
- Allenstrom, B., Liljenberg, H and Tuden, U., 2003, "Concept Development and Model Testing – New Generation Air Assisted Vessels (AAV) with Water Jet Propulsion", Proceedings of FAST'03, Italy. Pp.59-68.
- Blyth, A.G., 1993, "The Roll Stability of Surface Effect Ships", Transactions of The Royal Institution of Naval Architects, London, pp271-285.
- Doctors, L.J., 1974, "The Effect of Air Compressibility on the Non-linear Motions of An Air Cushion Vehicle over Waves", Proceedings of 11th Symposium on Naval Hydrodynamics, London, pp.373-388.
- Faltinsen, O.M., 2002, "Sea Loads on High Speed Marine Vehicles, NTNU, Trondheim.

IMO, 2000, HSC Code 2000, MSC 73/21/ADD.1, adopted Dec. 2000.

Jasionowski, A, 2001, "PROTEUS3 Users Manual", University of Strathclyde, Glasgow.

Kaplan, P., 1995, "Manoeuvring and Stability of SES and Catamaran Ships", Transactions of The Royal Institution Naval Architects. pp.17-36.

Kim, C.H. and Tsakonas, S., 1981, "An Analysis of Heave Added Mass and Damping of a Surface Effect Ship", Journal of Ship Research, Vol. 25, No.1. pp.44-61.

Papanikolaou, A.D., Georgantzi, N and Karayannis, T., 2002, "Adaptation of Stability Rules and Tools to SES", Report of National Technical University of Athens.

Vassalos, D., 1995, "Intact and Damage Stability and Survivability of Advanced Marine Vehicles", University of Strathclyde, Glasgow.

Wade, R. B. and Wang, S., 1977, "Some Aspects of Side-hull Hydrodynamics and Maneuvering in the Design of Surface Effect Ships", Proceedings of 11th Symposium on Naval Hydrodynamics, London. pp.355-371.

Xie, N., Vassalos, D. and Jasionowski, A., 2005a, "A Study of Hydrodynamics of Three-dimensional Planing Surface", Ocean Engineering, Vol. 32, pp. 1539-1555.

Xie, N., Vassalos, D. and Jasionowski, A., 2005b, "Seakeeping Analysis of the Air Lifted Vessel", Proceedings of The 4th International Workshop on Ship Hydrodynamics, Shanghai, pp. 113-120.

On the Stability of Air Cushion Supported Structures

Krish P Thiagarajan, *School of Oil & Gas Engineering, The University of Western Australia*

ABSTRACT

This paper presents a set of calculations to evaluate the restoring moment of structures supported by an air cushion. The air cushion is assumed to be enclosed within a number of compartments that are open to sea. The height of the water plug within the compartments is thus an important parameter. Calculations are verified against experimental data performed on three scaled model structures:

- a closed rectangular box barge
- a single chamber air cushion supported structure
- a nine-compartment air cushion supported structure.

It is found that the single chamber structure suffers from serious loss of stability, while the nine-compartment structure is more stable than the closed box barge itself. This is explained in terms of the additional stabilizing effect of the individual air cushions.

Keywords: *air cushion structures, metacentric height, static stability.*

1. INTRODUCTION

Air cushions are used in offshore applications to temporarily lighten a structure such as the case of a concrete gravity sub-structure while being towed in shallow waters. The base of the structure may have several skirted compartments open to the sea. The air cushions are located within the compartments, and sealed by a “water plug” so as to prevent air egress into the open water.

The effects of air-cushion support on the dynamics of Surface Effect Ships (SES) with and without forward speed were studied by Kaplan et al. (1975). A good literature review on this topic may be found in e.g. Graham and Sullivan (2002).

A three-dimensional numerical approach to evaluating the dynamics of an air cushion structure using the boundary integral equation

method is given by Lee and Newman (2000) and Pinkster (1997). Pinkster (1997) in particular, considered an air-cushion structure with various compartment configurations and concluded that compartmentalizing the air-cushion chamber reduces its effect on the hydrodynamic stability of the body. An air-cushion supported floating body has been studied experimentally in regular waves by both Thiagarajan et al. (2000) and Pinkster and Meevers-Scholte (2001).

Chenu et al. (2004) presented the results of a series of experiments on 1:100 scaled models of a box and air cushion supported structures. The authors conclude that the presence of air cushion in general reduces the stability of the structure. Increasing the water plug height and compartmentalization stabilize the vessel. In particular it was noted that a compartmented air cushion structure had better stability than the corresponding closed box structure. This was an interesting observation from the experiments.

On first intuition, one may be led to believe that the presence of internal free surfaces results in a significant loss of stability. However, it is shown through detailed calculations that loss of stability occurs only in the case of large air cushion chambers. Upon compartmentalization of the base structure, individual cushion chambers provide a pumping effect which restores stability. Our calculations are verified by comparison with the results from the inclining experiments of Chenu et al. (2004).

2. THEORETICAL DEVELOPMENT

We consider an air cushion structure and an equivalent box of same plan area and draft, Figure 1. It is acknowledged that these structures have different weight and centers of gravity. However, from a control volume approach, we can see that the air cushion structure + entrapped water may be statically and dynamically compared with the equivalent box. One can also contend that the restoring moments acting on the two control volumes must do work to restore the same displacement. We are interested in seeing if the restoring effects are different between the two cases. The control volume method (similar to added weight method of damaged stability, e.g. Lewis et al. 1988) is mathematically attractive because it enables us to develop a correction to the equivalent stability of a box.

For the case of the control volume in Fig. 1, the net external hydrostatic moment is balanced by the internal moment due to gravity. The hydrostatic and aerostatic pressures inside the compartments are internal forces cancelling one another in an inclined equilibrium state. Thus solving the problem reduces to finding the total mass and coordinates of center of gravity of the air cushion structure + entrained water in the compartments in the displaced condition (Fig. 2).

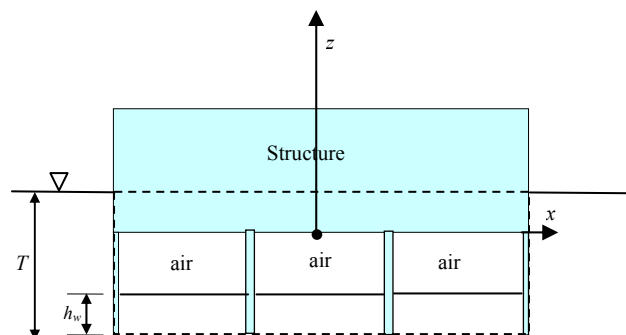


Figure 1. Structure geometry.

2.1 Preliminaries

We consider a compartmented structure similar to shown in Figure 1, with dimensions as shown in Table 1. The structure is given a set of static deflections $\zeta_k, k=1 \dots 6$, to obtain the configuration of Figure 2.

Table 1. Notations for dimensions

Length	L
Breadth	B
Still water draft	T
Compartment height	h_c
Compartment length	l
Compartment width	b
Number of compartments	$M \times N$
Initial height of water	h_w

Three coordinate systems are defined in Figure 2. These are:

- Global – (x, y, z)
- Body fixed – (x', y', z')
- Compartment fixed – (x^c, y^c, z^c)

As per convention, the global and body-fixed coordinate systems are coincident at the origin of time, and located at the intersection of the symmetry planes and the original water plane. The origin of the compartment fixed system is at the intersection of the symmetry

planes within each compartment and located at the top of the compartment (Figure 2).

The configuration considered here always has a compartment centered at the origin of the body fixed coordinate system. Then the compartment indices range from $(-m, -n)$ to (m, n) and

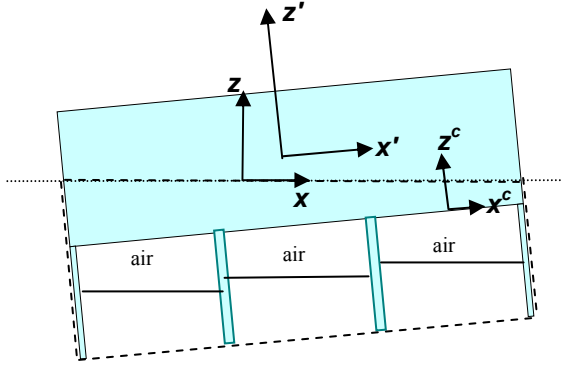


Figure 2. Coordinate systems definition

$$\begin{aligned} M &= (2m + 1); \\ N &= (2n + 1) \end{aligned} \quad (1)$$

Then the position vector may be written in the coordinate systems as

$$\mathbf{r} = \mathbf{r}_0 + \mathbf{r}' + \boldsymbol{\omega} \times \mathbf{r} \quad (2)$$

$$\mathbf{r}' = \mathbf{r}'_{ij} + \mathbf{r}^c \quad (3)$$

where subscripts (i, j) denote the indices of a compartment and

$$\begin{aligned} \mathbf{r}_0 &= (\zeta_1, \zeta_2, \zeta_3) \\ \boldsymbol{\omega} &= (\zeta_4, \zeta_5, \zeta_6) \end{aligned} \quad (4)$$

2.2 Air Cushion Volume and Pressure

The initial pressure and volume of air within a compartment is given by

$$\begin{aligned} p_0 &= p_a + \rho g (T - h_w) \\ v_0 &= lb (h_c - h_w) \end{aligned} \quad (5)$$

where p_a is the atmospheric pressure. When the structure is given a set of displacements ζ_k , the modified volume and pressure are given by

$$\begin{aligned} p &= p_a - \rho g z_0^c \\ v &= -lb z_0^c \end{aligned} \quad (6)$$

where z_0^c denotes the vertical coordinate of the internal water surface at the center point $(x_0^c, y_0^c) = (0, 0)$. As long as the displacements are small, one could reasonably assume that the position of the water surface z_0^c is incrementally different from the initial position of the water surface, i.e.,

$$z_0^c = -(h_c - h_w) + \Delta z_0^c \quad (7)$$

The change in pressure and volume is decided by the adiabatic gas law $p v^\gamma = \text{constant}$, where γ is the ratio of specific heats for air. Substituting for z_0^c into the adiabatic gas law and linearizing, we get

$$\frac{\Delta z_0^c}{h_c - h_w} = \frac{-\zeta_3 - y'_{ij} \zeta_4 + x'_{ij} \zeta_5}{\left(h_c - h_w + \frac{P_0 \gamma}{\rho g} \right)} \quad (8)$$

For practical purposes, the above equation results in a very small displacement of the internal surface, because of the relatively large magnitude of the denominator arising from the effect of atmospheric pressure. This in turn indicates that the air cushion performs like a stiff spring ensuring that the water plug behaves like entrapped water and is displaced along with the structure.

2.3 Moments Due to Weight

The total mass within the control volume of Fig. 2 is given by:

$$M = M_s + \sum_i \sum_j m_{ij} \quad (9)$$

where the mass of water within a compartment is given by

$$m_{ij} = \rho lb (h_w + \Delta z_0^c) \quad (10)$$

The coordinates of the center of gravity of the control volume in the global coordinate system is:

$$\mathbf{r}_G = \begin{pmatrix} x'_g + \zeta_5 z'_g - \zeta_6 y'_g \\ y'_g + \zeta_6 x'_g - \zeta_4 z'_g \\ z'_g + \zeta_4 y'_g - \zeta_5 x'_g \end{pmatrix} \quad (11)$$

The gravitational moment acting about the origin of the body fixed coordinate system is

$$\begin{aligned} \mathbf{M}_g &= \mathbf{r}_g \times (0, 0, Mg) \\ &= Mg \begin{pmatrix} -y'_g - \zeta_6 x'_g + \zeta_4 z'_g \\ x'_g + \zeta_5 z'_g - \zeta_6 y'_g \\ 0 \end{pmatrix} \end{aligned} \quad (12)$$

To find the coordinates of Eq. (11), we can use the fact that the gravitational moment in the body fixed system is made up of the component structure mass and the individual water plug masses. Denoting the centroids by the subscript g , we get

$$\begin{aligned} Mx'_g &= M_s x'_{gs} + \sum_i \sum_j m_{ij} (x'_{ij} + x_g^c) \\ My'_g &= M_s y'_{gs} + \sum_i \sum_j m_{ij} (y'_{ij} + y_g^c) \\ Mz'_g &= M_s z'_{gs} + \sum_i \sum_j m_{ij} (h_c - T + z_g^c) \end{aligned} \quad (13)$$

The first term on the right side of Eq. (13) denotes the structural mass component. The second term denotes the moment due to the

position of the water masses and their consequent moments about the origin of the compartment-fixed system. These moments are quite important, since the incompressibility of the air cushion results in the water plug moving with the structure. The last term denotes the moments due to the position of the center of gravity of the water masses with respect to the compartment coordinate system, and gives rise to the effects of the internal free surface. Upon evaluation of the centroid of the water plug in the displaced condition, we can find that

$$\begin{aligned} m_{ij} x_g^c &= -\rho \frac{l^3 b}{12} \zeta_5 \\ m_{ij} y_g^c &= \rho \frac{lb^3}{12} \zeta_4 \\ m_{ij} z_g^c &= \rho lb h_w \left(h_c - \frac{h_w}{2} \right) \end{aligned} \quad (14)$$

These are readily seen to be the terms due to internal free surface, and the last term is merely the linear term without any influence of the displacements.

Various terms may be substituted and the moments evaluated. The final results are shown in Eq. (15) and (16). Balance of forces between buoyancy and weight for the control volume provides the restoring moments in roll and pitch. Denoting the restoring coefficients as C_{44} and C_{55} , we get the expressions as shown in Eq. (17) and (18). D_r in the equations denotes the denominator of Eq. (8). S_{11} and S_{22} are the water plane moments about the x and y axes respectively.

$$M_{gx} = -M_s g y'_{gs} - \zeta_4 \left(\frac{\rho g L B b^2 (h_c - h_w) n(n+1)}{3D_r} + \rho g L B \frac{l^2}{12} + M_s g z'_{gs} - \rho g L B T h_w + \rho g L B \frac{h_w^2}{2} \right) - \zeta_6 M_s g x'_{gs} \quad (15)$$

$$M_{gy} = -M_s g x'_{gs} - \zeta_5 \left(\frac{\rho g L B l^2 (h_c - h_w) m(m+1)}{3D_r} - \rho g L B \frac{l^2}{12} - M_s g z'_{gs} + \rho g L B T h_w - \rho g L B \frac{h_w^2}{2} \right) - \zeta_6 M_s g y'_{gs} \quad (16)$$

$$C_{44} = \rho g S_{22} + \rho g V z'_B - M_s g z'_{gs} + \left(\frac{\rho g L B b^2 (h_c - h_w) n(n+1)}{3D_r} - \rho g L B \frac{l^2}{12} + \rho g L B T h_w - \rho g L B \frac{h_w^2}{2} \right) \quad (17)$$

$$C_{55} = \rho g S_{11} + \rho g V z'_B - M_s g z'_{gs} + \left(\frac{\rho g L B l^2 (h_c - h_w) m(m+1)}{3D_r} - \rho g L B \frac{b^2}{12} + \rho g L B T h_w - \rho g L B \frac{h_w^2}{2} \right) \quad (18)$$

3. COMPARISON WITH EXPERIMENTS

Chenu et al. (2004) reported a set of experiments on three models.

- Closed bottom box
- Box open to sea with one compartment
- Box open to sea with nine compartments.

All three models had common geometrical dimensions and draft, as shown in Table 2. Since the draft was kept constant, the structural weight was different. The ballast weight was altered to provide different water plug heights inside the compartments. Obtaining different water plug heights while maintaining a constant draft and even keel was a trial-and-error exercise requiring much caution. This was complicated for the one-compartment box because of its very marginal stability condition. For the nine-compartment box, the difficulty was in obtaining uniform air pressure in all the compartments. All these gave some element of uncertainty in the experiments.

Inclination tests were performed on the model to ascertain the restoring moments and from that the metacentric heights, as reported

by Chenu et al. (2004). In this paper, we consider the restoring moments and compare

them with the formulations derived in the previous section.

Table 2. Experimental particulars

Quantity	Symbol	Value
Length	L	0.5 m
Breadth	B	0.5 m
Draft	T	0.1 m
Box model		
Structure mass		24.25 kg
Vertical center of gravity		-0.01 m
One – compartment model		
Compartment height	h_c	0.085 m
Compartment length	l	0.47 m
Compartment width	b	0.47 m
9-compartment model		
Compartment height	h_c	0.085 m
Compartment length	l	0.154 m
Compartment width	b	0.154 m

Figures 3 and 4 show comparisons between experiments and theory for restoring moments in roll at four different values of water plug height. It is seen that the comparison is within 10% and the trends are captured by the theory. The margin of error in the figures is in line

with the level of uncertainty in the experiments. Further, the comparison is limited to four data points and firm conclusions need more data. This deficiency will be redressed in the future.

For comparison purposes, the restoring moment for the equivalent box was evaluated as 40.8 N-m. Both models clearly show a monotonic increase of the restoring moments with the height of the water inside the compartments. This increase is also captured by the theoretical formulation.

Apart from experimental uncertainty, one is left to wonder if nonlinear terms ignored in the formulations may be of importance to bridge the gap. This aspect will be clarified with more experimental data.

For the one-compartment model, the internal free surface destabilizes the model and almost cancels the effect of the external free surface. The remaining terms of the water plug contribute to a marginal stabilizing effect, which is seen in Figure 3.

Thiagarajan and Morris-Thomas (2006) have postulated that the air cushion structure may be likened to an equivalent shallow box whose draft is adjusted to incorporate the effect of the water plug. Their dynamic analysis shows good correlations between simple theoretical formulation and experiments in heave and pitch. We can evaluate the restoring forces for a shallow box whose draft is $(T-hw)$ and these are shown in Figure 5. The comparison is very interesting. The experimental data is encased between the two theoretical formulations. One could argue that the main difference in the theoretical formulations is the stiffness of the internal water surface. For the equivalent shallow box, the internal surfaces are solid, and hence provide maximum restoring moment.

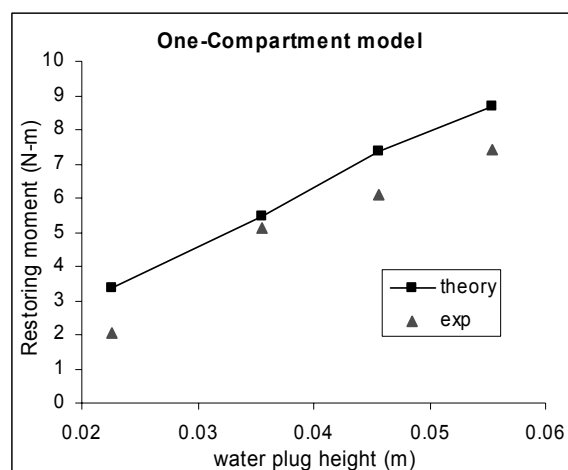


Figure 3. Restoring moment vs. water plug height for the one-compartment model

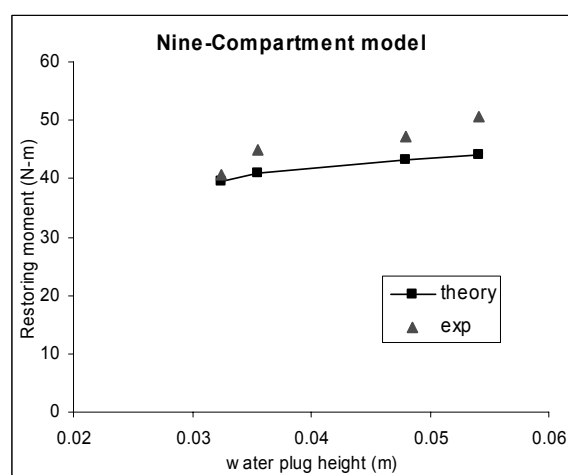


Figure 4. Restoring moment vs. water plug height for the nine-compartment model

The theoretical formulation that incorporates the internal effect shows that the destabilizing effect of the internal surface is offset by the physical displacement of the water plugs to balance the internal and external pressures. The actual experimental data seems to be somewhere in between. Further experimental data is needed to confirm the actual trends.

4. CONCLUSIONS

The theoretical formulations shown in the paper comprise the effect of various components that affect the stability of an air cushion platform. A control volume approach

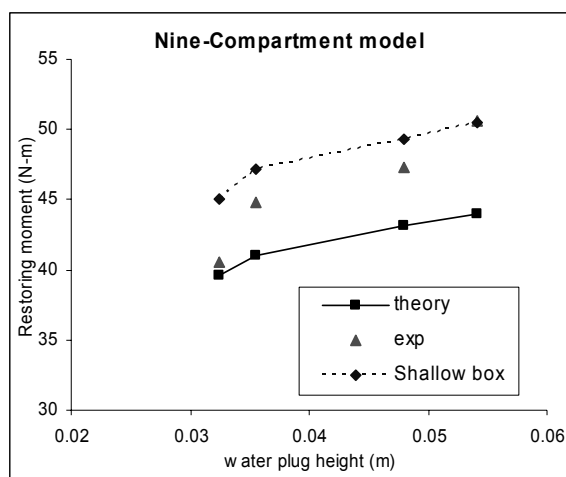


Figure 5. Comparison of stability of a nine-compartment model with a shallow box

is used where the water masses are treated as added weights. The resulting formulations are closed form expressions for the restoring moments in roll and pitch. The formulations are compared with experimental data and the comparisons are shown to be within 10%. It is shown that the destabilizing effect of the internal free surface is offset by the displacement of the water plugs with the structure. A nine-compartment structure thus has more stability than an equivalent box of the same draft. If the draft is altered to account for the height of the water plug, then the restoring moments are shown to be higher.

5. ACKNOWLEDGMENTS

The experimental data for this paper was developed in the course of a project on air cushion supported offshore structures, sponsored by Minerals and Energy Research Institute of Western Australia (MERIWA), with support from Woodside Energy Ltd., Concrete Institute of Australia and Ove Arup Ltd.

The theoretical development of this paper benefited from the discussions and background work done by the author during his sabbatical stay at the Department of Naval Architecture and Marine Engineering, The University of Michigan, in 2005.

6. REFERENCES

- Chenu, B., Morris-Thomas, M. T., Thiagarajan, K. P., 2004, "Some hydrodynamic characteristics of an air-cushion supported concrete gravity structure", Proceedings 15th Australasian Fluid Mechanics Conf, Sydney, Australia.
- Graham, T. A. and Sullivan, P. A., 2002, "Pitch heave dynamics of a segmented skirt air cushion", J. Ship Res., Vol. 46, pp 121-137.
- Kaplan, P., Schneider, J. and Goodman, T. R., 1975, "Motions of air cushion vehicles (ACV) in waves", Intl. Symp. Dynamics of Marine Vehicles and Structures in Waves, Ed. R. Bishop and W. Price, pp. 227-234.
- Lee, C. H. and Newman, J. N., 2000, "Wave effects on very large floating structures with air cushions", Marine Structures, Vol. 13, pp. 315-330.
- Lewis E. V. (Ed.) 1988, "Principles of Naval Architecture", Vol. 1, Ch. 3, Sec 4.7, pp. 166 - 170
- Pinkster, J. A., 1997, "The effect of air cushions under floating offshore structures", Proceedings BOSS' 97, pp. 1-17.
- Pinkster, J. A. and Meevers-Scholte, E. J. A., 2001, "Behaviour of a large air-supported MOB at sea", Marine Structures, Vol. 14, pp 163-179.
- Thiagarajan, K. P. and Morris-Thomas, M. T., 2006, "Wave-induced motions of an air cushion structure in shallow water", Ocean Engineering, Vol. 33, pp. 1143 - 1160.
- Thiagarajan, K. P., Sow, H. E., Ronalds, B. F. and Hill, A. B., 2000, "Vertical motions of a concrete gravity structure supported by air cushions in shallow water", in Proceedings Offshore Mech. and Arctic Eng., New Orleans, USA, paper 4191.

On the Stability and Safe Operation of Pod Driven Ships

Zafer Ayaz, *The Ship Stability Research Centre, Department of Naval Architecture and Marine Engineering, Universities of Glasgow and Strathclyde, UK*

Osman Turan, *The Ship Stability Research Centre, Department of Naval Architecture and Marine Engineering, Universities of Glasgow and Strathclyde, UK*

Mehmet Atlar, *School of Marine Science and Technology, University of Newcastle upon Tyne, UK*

ABSTRACT

The paper presents the enhancement of an existing 6 DOF non-linear numerical model to predict motion behaviour of a ship, which is driven by multitude of podded propulsors for high-speed, effectively combining manoeuvring and seakeeping equations in waves. The numerical model is then validated using a ROPAX and containership, for which are both driven by multi-pod propulsion systems and extensive manoeuvring and seakeeping model test data are available for both vessels. The effect of pod units on motions, including the instability and capsizing modes, are observed for these vessels, such as parametric rolling and surf-riding in extreme sea conditions, and these behaviours have been analysed. The link with design parameters and possible Risk Control Options (RCO) have been discussed and investigated. Finally dynamic intact stability characteristics of these ships are assessed and conclusions including some design alternatives in terms of safe operation of the vessels are drawn.

Keywords: Stability, azimuthing podded propulsion, safety, operation

1. INTRODUCTION

The stability characteristics of the ships are greatly influenced by the design approach to adopt their associated propulsion and steering units. This has been especially major concern by the introduction of powerful and multi-functional azimuthing podded propulsion and steering units within the last decade or so (FASTPOD, 2005, Ayaz et al., 2005). While, the sizes and power output of these propulsion/steering units are getting larger along with the speed and sizes of ships, the possible dangerous conditions related to stability and safe operations of these vessels have not been properly addressed in spite of some concerns reported in the open literature by some investigators (e.g. Van Terwisga et al.,

2001, Toxepus & Loeff, 2002) as well as by the last ITTC (ITTC, 2005b).

The azimuthing pod-propulsion systems have now been well proven in terms of their propulsion performance in slow to medium speed range whilst their low speed and harbour manoeuvring performance, especially for passenger ships and ice-breakers are their biggest advantages (ITTC, 2005b). The challenge in modern transport now appears to foster the application of this technology for very large and high-speed vessels, which are also growing in numbers, to meet the demands of fast ship operators and the competitive market conditions. However, during the design stage and operation of existing pod-driven ships, many interesting and important problems

and potential danger areas have been observed from control and stability point of view. These have not been thoroughly discussed even for relatively slow speed current applications and therefore further raise questions for the high-speed applications. From model tests and actual operational experiences some of these potential danger areas have been identified such as directional stability problems due to extreme pramming of the afterbody to accommodate the pod units, effect of large steering forces created by pod drives on roll motion in heavy seas and/or excessive steering actions imposed by autopilot in calm water and the wear and tear of the bearings and steering engine caused by these activities in heavy seas (ITTC, 2005, Van Terwisga et al., 2001, Toxepus & Loeff, 2002).

Amongst a number of research studies in this area, two large European wide research projects have been undertaken to address and produce solutions to aforementioned and many other design and operational problems of pod-driven ships (OPTIPOD, 2002, FASTPOD, 2005). As part of these research studies, an existing in-house 6 DOF non-linear numerical model has been enhanced with inclusion of propulsion and steering actions of the pod drives and used as an analysis tool to investigate some of the above mentioned stability problems of pod-driven ships (Ayaz et al., 2004, 2005).

Within the above framework this paper present the enhancement of an existing 6 DOF non-linear numerical model, which predicts the combined manoeuvring and seakeeping behaviour of a ship, to include the effect of multiple number of pod units in low and high speed operating conditions. The enhanced numerical model has been validated using the extensive manoeuvring and seakeeping model test data available for a high speed ROPAX and container vessel developed in FASTPOD project. The study on current paper has focus on the possible threats to stability in relation to the changes in design to accommodate pod-structure. The effect of pod units on motions

and the instability and capsizing modes observed for these vessels, such as parametric rolling and broaching-to associated with surf-riding in extreme sea conditions, have been analysed. The link with design parameters and possible RCOs (Risk Control Options) has been discussed. Finally dynamic intact stability characteristics of these ships are assessed and conclusions and design alternatives for safe operation of these vessels are identified.

2. NUMERICAL MODEL

2.1 Conventional mathematical model

The current numerical model, which was originally developed to identify the instability/capsizing limits of a ship driven by conventional propulsion system in astern seas, is a non-linear 6-DOF mathematical model and it allows a straightforward combination between the seakeeping and manoeuvring modes of vessel behaviour whilst accounting for extreme motions (Ayaz et al, 2006).

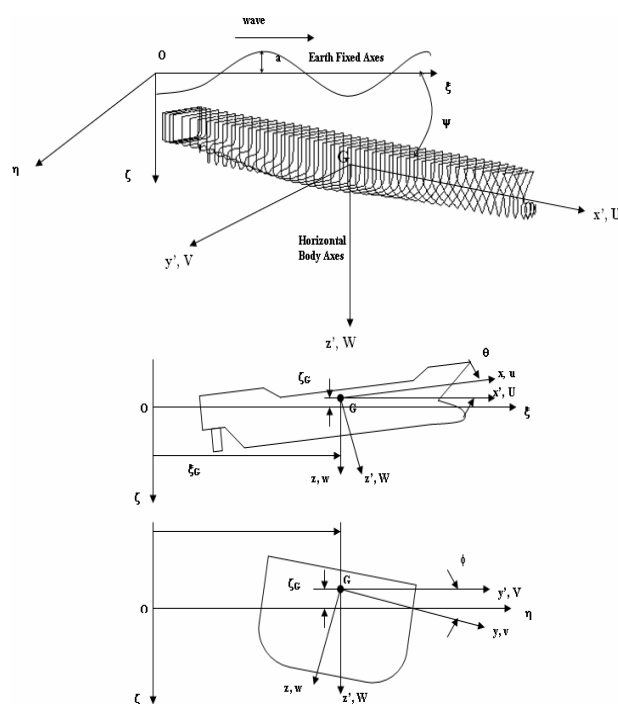


Figure 1 The axis system of numerical model.

The equations of motion have been derived using the relationship amongst three different co-ordinate axes system, namely: horizontal body axes, body axes and earth fixed axes systems represented by $G-x'y'z'$, $G-xyz$, $0-\xi\eta\zeta$, respectively. The relationship between them is illustrated in Fig. 1 where x, y, z represent linear motions, u, v, w are linear velocities, p, q, r are angular velocities and φ, θ, ψ are Euler angles of rotations. By applying Newton's 2nd. law the equation of motions are expressed in standard six degrees of freedom in terms of the linear (surge, sway, heave) motions in (1) and rotational (roll, pitch and yaw) motions in (2), respectively, along with the external forces as below:

$$\begin{aligned} m(\dot{U} - VR) &= -\iint_S p \mathbf{n}_x dS + X_H - F_N \sin \delta \\ &\quad + (1-t_p) \rho n^2 D^4 K_T \\ m(\dot{V} + UR) &= -\iint_S p \mathbf{n}_y dS + \rho U \int_{\Gamma_x} \Phi_D n_y ds \\ &\quad + Y_H - (1+a_H) F_N \cos \delta \\ m\dot{W} &= -\iint_S p n_z dS + \rho U \int_{\Gamma_x} \Phi_D n_z ds + Z_H \end{aligned} \quad (1)$$

$$\begin{aligned} (I_{xx} \cos^2 \theta + I_{yy} \sin^2 \theta) \dot{P} &= -\iint_S p (\mathbf{r} \times \mathbf{n}_{yz}) dS \\ &\quad + \rho U \int_{\Gamma_x} \Phi_D (\mathbf{r} \times \mathbf{n}_{yz}) ds + K_H + (1+a_H) z_R F_N \cos \delta \\ I_{yy} \dot{Q} &= -\iint_S p (\mathbf{r} \times \mathbf{n}_{zx}) dS + \rho U \int_{\Gamma_x} \Phi_D (r \times n_{zx}) ds \\ &\quad + M_H \\ (I_{xx} \sin^2 \theta + I_{zz} \cos^2 \theta) \dot{R} &= -\iint_S p (\mathbf{r} \times \mathbf{n}_{xy}) dS \\ &\quad + \rho U \int_{\Gamma_x} \Phi_D (\mathbf{r} \times \mathbf{n}_{xy}) ds + N_H - (1+a_H) x_R F_N \cos \delta \end{aligned} \quad (2)$$

where, U, V, W are surge, sway, heave linear velocities, Q, P, R are roll, pitch, yaw angular velocities in horizontal body axes system and I_{xx}, I_{yy}, I_{zz} are roll, pitch, yaw moments of inertias, respectively.

In (1) and (2), the first terms in the right-hand side of the equations in including pressure

term p , correspond to the incident (or Froude-Krylov) component of the wave-excitation forces/moments including hydrostatic forces. These are calculated on the hull by integrating pressure p up to the instantaneous wave surface together with the kinematic relations involving \mathbf{n} is normal vector and $\mathbf{r} \times \mathbf{n}$ is vector fixed with respect to centre of gravity. Here, the calculation of hydrostatic forces is of great importance to identify the dangerous conditions presented in §3. The hydrostatic forces and moments can be obtained by integrating the pressure, p over the entire wetted surface of the ship. The hydrostatic pressure p including that of a sinusoidal wave ζ_w at any time and position ξ in the earth fixed axes is given by:

$$p = (\zeta_G - x'\theta + z') - \rho g a e^{-kd} \cos(k(\zeta_G + x' \cos(\psi) - y' \sin(\psi) - ct)) \quad (3)$$

with

$$\begin{aligned} \zeta_w &= -\zeta_G + x'\theta \\ &\quad + a \cos(k(\zeta_G + x' \cos(\psi) - y' \sin(\psi) - ct)) \end{aligned} \quad (4)$$

where a the amplitude of wave, c the phase velocity of wave and d the draft of the ship. Using the above expressions in Gauss theorem, the Froude-Krylov forces can be described with respect to the horizontal body axes in the form of heave, roll and pitch motion which include restoring terms as follows:

$$\begin{aligned} Z'_{F.K}(\zeta_G, \theta, \psi, \varphi) &\equiv -\iiint_V \frac{\partial p(F.K)}{\partial z'} dV \\ K'_{F.K}(\zeta_G, \theta, \psi, \varphi) &\equiv -\iiint_V \left[y'_B \frac{\partial p(F.K)}{\partial z'} - z'_B \frac{\partial p(F.K)}{\partial y'} \right] dV \\ M'_{F.K}(\zeta_G, \theta, \psi, \varphi) &\equiv -\iiint_V \left[z' \frac{\partial p(F.K)}{\partial x'} - x' \frac{\partial p(F.K)}{\partial z'} \right] dV \end{aligned} \quad (5)$$

where Z', K' and M' are heave, roll and pitch Froude-Krylov forces including hydrostatic terms in horizontal body axes, respectively (F.K denotes Froude-Krylov), (y'_B, z'_B) the centre of buoyancy of the immersed section at each instant. As shown in (5), these forces are calculated as parameter of the Euler angles and

vertical position of centre of gravity of ship on wave (ζ_G) at each instant for instantaneous wave surface.

The second-term in (1) and (2) involving Φ_D corresponding to the diffraction forces and Γ_x denotes the contour of section under the still water free surface, which is obtained as disturbance forces using Ohkusu's low encounter frequency slender body theory where for motions in the astern seas conditions, while strip theory has been used for other conditions (Ayaz et. al, 2006). Since the assumption of relatively comparable wave length to ship length ratio in calculation of incident (Froude-Kyrlov) and diffraction forces, the current numerical model is more suited to long-crested waves than short-crested waves.

The third terms represented by subscript H indicate hull (manoeuvring) forces, moments, which are obtained using well-known MMG (acronym for Japanese Manoeuvring Group, Inoue et al, 1981) method. The fourth terms involving F_N and K_T denote conventional rudder forces and propulsion forces in surge motion, for the latter where: F_N , the rudder normal force; a_H , rudder-to-hull interaction coefficient, x_H , the longitudinal coordinate of the point of action of the rudder to hull interaction force, x_R , z_R , longitudinal and vertical coordinates of the rudder's centre of pressure, respectively; K_T , the thrust coefficient; D , the propeller diameter, n , the propeller rate of rotation; and δ , the steering or rudder angle. Although the above equations apply to a vessel to be driven by podded propulsors, here, the notations for the steering/propulsion used follows the similar notations for the conventional rudder/propulsor for the sake of convenience. The more detailed descriptions of equations of motions and other components of the mathematical model are given in (Ayaz et al, 2005, 2006).

The left hand sides of the non-linear equations (1) and (2) contain 12 variables. Those variables along with the helm (autopilot) and positions of ship on wave can be written

as:

\mathbf{X} : State Vector $x \in \mathbb{R}''$

$$\mathbf{X} : (\zeta_G, \dot{\zeta}_G, x, y, z, u, v, w, p, q, r, \varphi, \theta, \psi, \delta)^T \quad (6)$$

where ξ_g represent longitudinal position of centre of gravity of ship on wave, respectively and δ is the helm angle. Equations (1), (2), (3) yield to (4) in the matrix form of 2nd. Order classical motion equations as follows:

$$(\mathbf{M} + \mathbf{A})\ddot{\mathbf{X}}(t) + \mathbf{B}(X)\dot{\mathbf{X}}(t) + \mathbf{C}(X)\mathbf{X}(t) + \int_0^{\infty} K_{ij}(t)V_j(t-\tau)d\tau = \mathbf{F}(\zeta_w, X(t), \dot{X}(t), \ddot{X}(t)) \quad (7)$$

where, \mathbf{M} is inertia mass/moment inertia matrix, \mathbf{A} is added mass/moment inertia matrix, \mathbf{B} is damping coefficients matrix, \mathbf{C} is restoring coefficients matrix, \mathbf{F} is external force vector and ζ_w is wave amplitude. Here, the fourth term in the left-hand side of (4) represents "so-called" memory effect term incorporating the frequency-dependent vessel motion related terms (radiation forces/moments) into (4). The impulse response function (K_{ij}) will be solved from added mass and damping data and the convolution integral given in (7) then evaluated for each term in the equations of motion at each time step during the simulation. In this study, well-known 2-D strip theory is used for the calculation of radiation forces.

Finally, the control term introduced in (6) for helm angle is obtained by employing the PID (Proportional-Integral-Differential) control terms in equations of motions based on the following:

$$\delta_R + t_r \dot{\delta}_R = K_R(\psi - \psi_R) + K_P \dot{\psi} + K_I \int_0^t (\psi(\tau) - \psi_R) d\tau \quad (8)$$

where δ_R is the actual rudder angle; ψ_R is the desired heading angle; K_i the integral parameter; K_R yaw gain constant; K_P a yaw rate gain constant ($K_P > 0$, $K_d > 0$, $K_i > 0$); and t_r the time constant in rudder/pod activation.

2.2 Inclusion of pod effects in the mathematical model

An azimuthing podded drive is a highly attractive propulsion unit which combines the propulsion and steering actions of a ship, with a capability of 360° azimuthing, using an electric motor fitted inside the gondola part of the pod unit as shown in (Fig. 2). Thanks to electric motors being located outboard and power provided through either diesel or turbo generators inside ship's hull. This provides and improved onboard comfort, volume savings inside the hull and increased freedom in the general arrangement that can be obtained to enhance the design alongside the already well-established benefits in low speed manoeuvring. In order to illustrate the hydrodynamic characteristics of pod-driven ships, the afterbody arrangements of ships driven by a conventional twin-screw propeller system and a podded propulsor system are shown in Fig. 3.

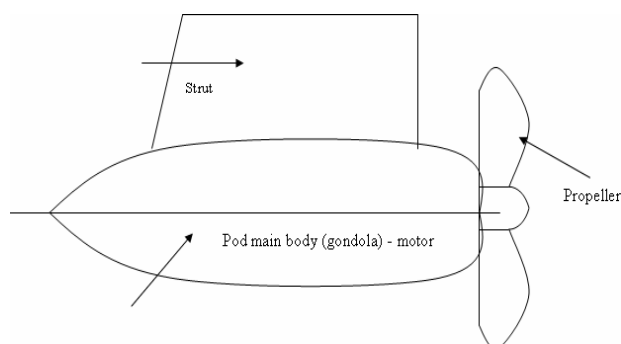


Figure 2 Sample body of a pod drive.

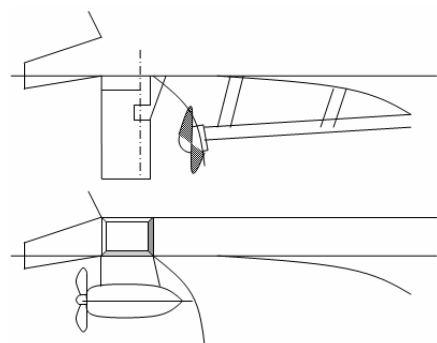


Figure 3 Conventional and azimuthing propulsion arrangements at aft part of a ship.

When a pod unit is slewed, unlike a conventional rudder which takes advantage of the accelerated propeller flow, the propeller slipstream is parallel to the pod for the most part and hence the pod remains at a zero angle of attack. As a result, although the pod propulsor has the superior advantage of vectoring the propeller thrust in any direction, the pod body (housing) without its propeller can only produce a lift proportional to the square of the ship forward speed, except the “straight ahead” condition. Within the same context although the pod housing should be considered as a single lifting surface subjected to the incoming flow, its two distinct components, which are the strut and gondola, suggest that the hydrodynamic characteristics of these parts can be developed separately and then combined by taking into account the interaction between them as precise as possible. Bearing in mind the fact that the interaction between the podded propulsors and the hull is relatively weak, particularly for high-speed applications as explored in this paper, there is a need to take into account this effect properly by taking into account the interaction amongst the pod housing, propeller and hull through properly selected interaction coefficients similar to the one for conventional rudders expressed in (1-2). Moreover, multitude number of the pods also requires taking this interaction effect between the pod units properly into account. In the following the motion equations given in (1) and (2) are modified to include the effect of the pod drives based upon the above background and concentrating on the 4 pods application (i.e. 2 steerable pod units), as shown in Fig 4. The following only states a brief summary of these modifications, the reader is referred to (Ayaz et al 2005) for the detailed derivations.

In Figure 4, T indicates thrust vector of pod induced forces and S indicates the side forces created by the propeller and the pod-housing unit. These terms can be obtained through lift and drag terms coefficients of the pod-unit.

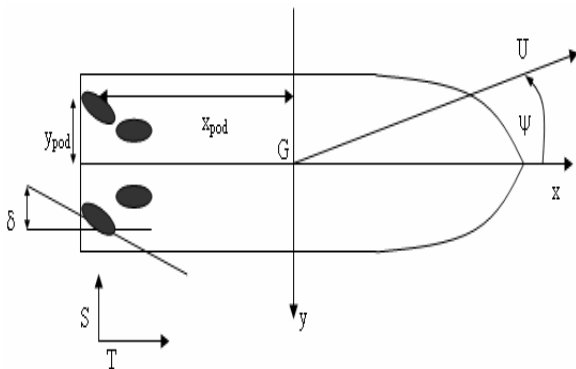


Figure 4 Locations and co-ordinate system for large high-speed pod-driven ship.

$$C_{D,L} = \frac{D, L}{0.5 \rho A_{POD} U^2_{POD}} \quad (9)$$

where A_{POD} is effective pod area and U_{POD} is flow speed over the effective pod area. The pod drag and lift terms are determined based on open water characteristics can be expressed as:

$$\begin{aligned} L &= f(\beta_{POD}, \delta_{POD}, J_{POD}) = f(\alpha_{POD}, J_{POD}) \\ D &= f(\beta_{POD}, \delta_{POD}, J_{POD}) = f(\alpha_{POD}, J_{POD}) \\ \alpha_{POD} &= \beta_{POD} - \delta_{POD} \end{aligned} \quad (10)$$

where lift, L , and drag, D , forces are determined with respect to local drift angle of pod unit, β_{POD} , pod's deflection δ_{POD} , angle of attack α_{POD} , and advance coefficient J_{POD} . The pod angle of attack depends on whether a pod unit is a lee-ward or wind-ward one. The advance coefficient and subsequent thrust coefficient should be obtained from the total pod and propeller thrust force by taking into account propeller blade drag and pod-house unit resistance which can be expressed as:

$$K_{Tpod} = K_{Tpod+prp} + \Delta K_{blade} + \Delta K_{pod-house} \quad (11)$$

By combining (9) and (10) and (11), lift and drag coefficients can be finally written in the polynomial forms as:

$$\begin{aligned} C_D(\alpha) &= A_1 \cos(B\alpha_{POD} - C) \\ &\quad + A_2 \cos(2(B\alpha_{POD} - C)) + D \\ C_L(\alpha) &= K(J_{POD})\alpha_{POD} \end{aligned} \quad (12)$$

where constants A_1, A_2, C, D are obtained for different angle of attack and drift angle based on regression analysis. From the expressions given in (10), (11), (12) with a given local pod inflow angle (angle of attack), α_{POD} , lift and drag forces described in flow-oriented coordinate system can be transformed into thrust, T , and side force, S , units described in a ship-fixed coordinate systems. The pod-unit side force, S , is written as:

$$S = 0.5 \rho A_{POD} U^2_{POD} f(A) \sin(\alpha_{POD}) \quad (13)$$

where $f(A)$ is the open water pod normal force coefficient, which is function of pod-strut aspect ratio, A , and it is described as:

$$f(A) = \frac{6.13 A}{A + 2.25} \quad (14)$$

Finally, the relationship between hull and pod unit is described through the interaction coefficient, a_{Hpod} which is dependent upon advance coefficient J_{POD} , as seen from the previous formulations, and it is a significant parameter to describe side force and moment induced on hull by the pod units. The term could be expressed as:

$$\begin{aligned} a_{Hpod} &= a J_{POD} + b \\ \text{where } J_{POD} &= \frac{U_{POD}}{nD_p} \end{aligned} \quad (15)$$

The terms a and b , here, were identified from a regression analysis similarly to the ones in (9). In the absence of such information these terms can be taken based on open-water test results. With incorporation of the aforementioned terms and considering vector representation of the pod-induced forces in the lateral and vertical planes, the conventional formulation in (1) and (2) becomes (16) and (17) as below. Here, subscript pod denotes forces and moments caused by pod drive. Here, the last terms in X', Y', K', N' (surge, sway, roll and yaw) are given in similar notation to the conventional MMG model in (1) and (2). In

case of the fixed pods, pod-induced forces will be modified for the local drift angle of pod, β_{POD} , instead of the pod deflection (or slewing) angle, δ_{POD} :

$$\begin{aligned} m(\dot{U} - VR) &= -\iint_S p \mathbf{n}_x dS + X_H - S \sin(\delta) \\ &+ (1 - t_p) T \cos(\delta) \\ m(\dot{V} + UR) &= -\iint_S p \mathbf{n}_y dS + \rho U \int_{\Gamma_x} \Phi_D n_y ds + Y_H \\ &- (1 + a_{Hpod}) S \cos(\delta) + X'_{pod} \sin(\delta) \\ m\dot{W} &= -\iint_S p \mathbf{n}_z dS + \rho U \int_{\Gamma_x} \Phi_D n_z ds + Z_H \end{aligned} \quad (16)$$

$$\begin{aligned} (I_{xx} \cos^2 \theta + I_{yy} \sin^2 \theta) \dot{P} &= -\iint_S p(\mathbf{r} \times \mathbf{n}_{yz}) dS \\ &+ \rho U \int_{\Gamma_x} \Phi_D(\mathbf{r} \times \mathbf{n}_{yz}) ds + K_H + z_{Rpod} Y'_{pod} \\ I_{yy} \dot{Q} &= -\iint_S p(\mathbf{r} \times \mathbf{n}_{zx}) dS + \rho U \int_{\Gamma_x} \Phi_D(\mathbf{r} \times \mathbf{n}_{zx}) ds \\ &+ M_H \\ (I_{xx} \sin^2 \theta + I_{zz} \cos^2 \theta) \dot{R} &= -\iint_S p(\mathbf{r} \times \mathbf{n}_{xy}) dS \\ &+ \rho U \int_{\Gamma_x} \Phi_D(\mathbf{r} \times \mathbf{n}_{xy}) ds + N_H - x_{pod} Y'_{pod} \end{aligned} \quad (17)$$

2.3 Risk Control Options

In order to mitigate or prevent the occurrence of instability/capsizing of pod-driven ships, both operational and design risk control options were considered. The risk control options have been introduced either through operational guidelines recommended by IMO (1994) or the design options with ride control systems (active fin stabilisers for roll and yaw). Initially, the operational measures have thought to be preventive while the design measures through ride-control system are assumed mitigating. However during the course of the project, it was seen that they can be both mitigating and preventing. Yet, definitive conclusion to describe them as “preventive” will require more detailed analysis. The expression for the lift force term

of a fin stabilizer is written, similar to pods and rudders, as:

$$L_{fin} = \frac{\partial C_L}{\partial \alpha} \cdot \alpha_{fin} \cdot \frac{l}{2} \cdot \rho \cdot U^2 \cdot A_{Fin} \quad (18)$$

where L_{fin} is lift force of fin, α_{fin} is the incidence angle and A_{fin} is the effective fin area. Here, the lift curve slope in free stream is described as (Whicker & Fehlner, 1958):

$$\frac{\partial C_{Lfin}}{\partial \alpha} = \frac{1.8 \cdot \pi \cdot A_{fin}}{1.8 + \sqrt{A_{fin}^2 + 4}} \quad (1/rad) \quad (19)$$

where, A_{fin} is the fin aspect ratio. The effect of activation on the fin characteristics is introduced through the control of the fin angle of attack. The method employs control parameter omitting fin servo and controller compensation coefficients to fin angle of attack, α_{fin} , as follows:

$$\alpha_{fin} = k_1 \phi + k_2 \dot{\phi} + k_3 \ddot{\phi} \quad (20)$$

where k_1 , k_2 , k_3 the roll angle, velocity, and acceleration gain values, respectively. Anti-yaw stabiliser induced forces will be measured with the similar control parameters used for the pod units.

3. NUMERICAL ANALYSIS

3.1 Validation Analysis

For the validation of the new mathematical model and further numerical analyses using the model, two ships; a high-speed ROPAX and a container ship, which are designed under FASTPOD project have been used (FASTPOD, 2005). The principal particulars of the vessels are given Table 1.

The FASTPOD ROPAX is propelled by four puller type pod units all equipped with 5.2

m propellers. Each pod absorbs approximately 27 MW power with the desired service speed approximately 38 knots. The forward pods are fixed and the aft pods are azimuthing for ship control.

FASTPOD Cargo is also propelled with four pod units all equipped with 6.5m propellers. Each pod absorbs approximately 36 MW power with the desired service speed approximately 35 knots.

Table 1. Principal particulars of FASTPOD ships

Parameter	FASTPOD ROPAX	FASTPOD Containership
L_{pp}	220 m	275 m
B (Beam)	30 m	30.0 m
D (Depth)	9.7 m	21.65 m
T (Draft)	6.8 m	10.30 m (design)
C_b	0.39	0.57
Δ	17600 t	49600 t (design)
LCG	-5.71 m (aft)	-7.2 m (aft)
VCG	14.60	13.60 (design)
V (speed)	38 knots	35 knots

For the validation analysis of the numerical model, free-running model test results for ROPAX vessel were used (Trägårdh et. al, 2004). These tests were conducted in the Marine Dynamics Laboratory facility at SSPA in Sweden. The four pod propellers were driven mechanically from inside the hull and assume a constant torque model. For the containership, a series of seakeeping model experiments, which were carried out at model basin facilities of CTO, Poland, are used since they were specifically focused on the occurrence of parametric resonance, of which this type of vessels are particularly vulnerable, in long-crested seas (Bednarek & Kanar, 2005).

For the ROPAX vessel, significant single amplitude, which has been measured as twice the standard deviation of each motion for time series in 6 DOF, was used for comparison with

model tests (Fig. 5). The comparison of the measurements with the predictions from the enhanced mathematical model displayed very good correlation as shown in (Fig. 5).

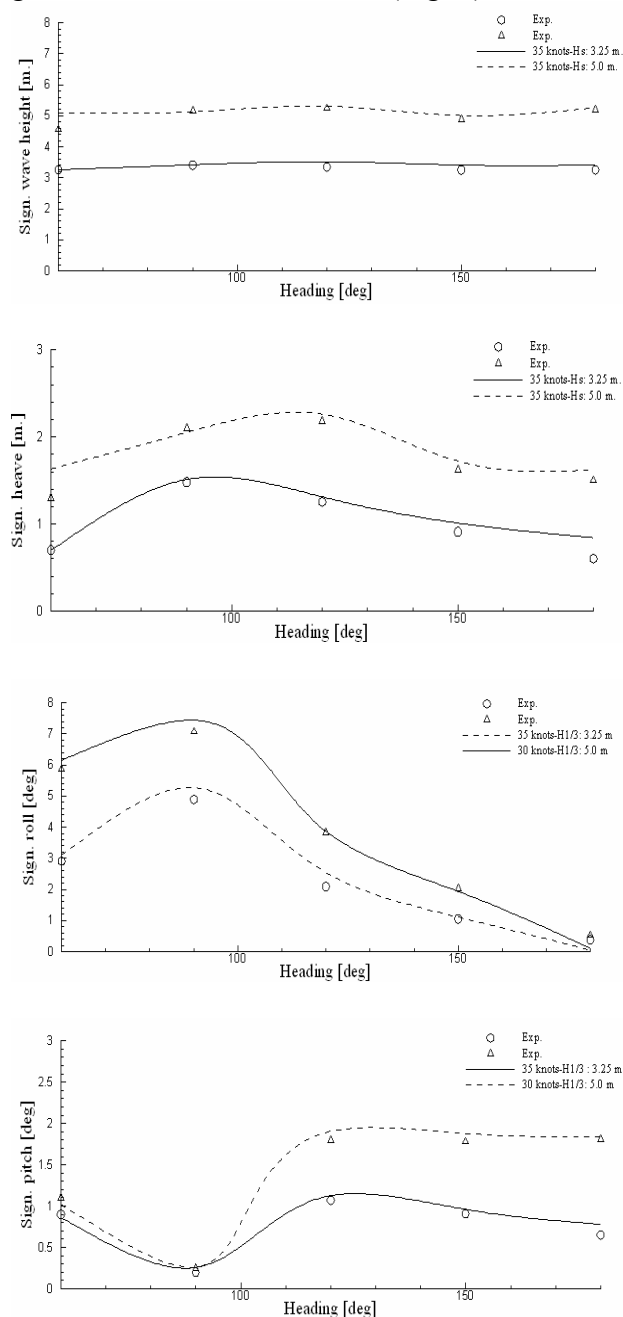


Figure 5 The significant single amplitude of the identified parameters for ROPAX.

The similar validation analysis has been also conducted for so-called “composed irregular” waves concept where, as the name indicates, a random wave is created with number of different frequency regular wave components. The numerical wave model has followed more “regular-like” cases where the

model was run to simulate relatively large wave amplitudes in beam seas. A test case for such simulation is illustrated in Figure 6.

In this analysis, although quantitative agreement seems to be obtained there is significant qualitative differences due to differences between numerical runs which was carried out with single wave period while experiments was conducted as two different regular wave runs.

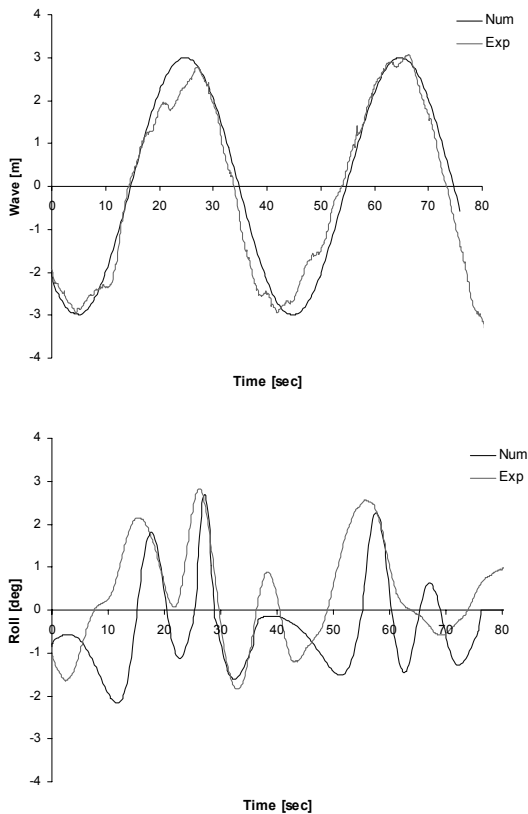


Figure 6 Composed irregular wave analysis.

The unique design and loading/stability characteristics of containership investigated required greater attention for the investigation of possible dangerous conditions that the ship may have faced to during the course of voyage. These were noted during the manoeuvring trials of ship model in open lake in which the large static heeling due to low GM enforced to abandon the turning circle tests for the maximum rudder angle (35 degrees) despite the superior turning and directional control abilities observed during the tests. Therefore, the dedicated seakeeping model tests were

carried out at the CTO model basin for the investigation of auto-parametric rolling of the containership in long-crested seas (Bednarek & Kanar, 2005). Parametric roll test matrix has been created in accordance with the assumption of following resonance condition:

$$\omega_\phi = \frac{1}{2} \omega_e n \quad (n = 1, 2, \dots) \quad (21)$$

where ω_e , is encounter frequency and ω_ϕ is natural roll frequency. The region of principal resonance has been shown from the solution of linear Mathieu equation for unforced roll motion which can be written as:

$$\ddot{\phi} + 2\left(\frac{2N}{T}\right)\dot{\phi} + \omega_0^2 \left[1 - \frac{\Delta GM}{GM_0} (\cos \omega_e t) \right] \phi = 0 \quad (22)$$

where the term $\Delta GM/GM$ (Θ_P) indicating fluctuating GM yields to:

$$\Theta_P = \frac{\Delta GM}{GM} = \frac{GM_{TROUGH} - GM_{crest}}{2GM_0} \quad (23)$$

Here, GM_0 represents the metacentric height in calm water while N in (22) is non-dimensional roll damping coefficient. In this study N term has been obtained using the roll decay tests. The relationship in (21)-(23) has been illustrated by the well-known Ince-Strutt stability diagram of the solutions of Mathieu's equation (Fig. 7).

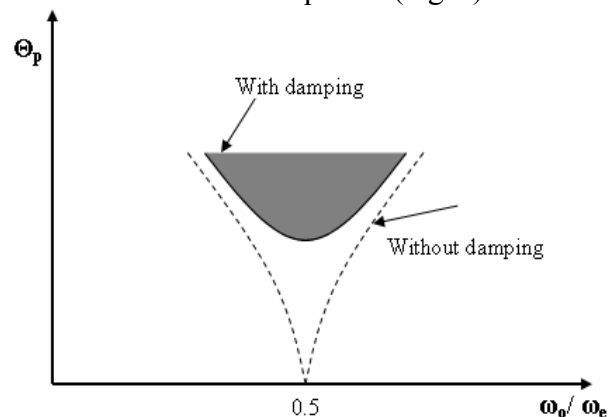


Figure 7 Ince-Strutt Diagram.

Moreover, the GZ (righting arm) curve of the vessel is plotted in Fig. 8 for wave trough

and wave crest as well as in the calm water for the resonance condition shown in Fig. 7.

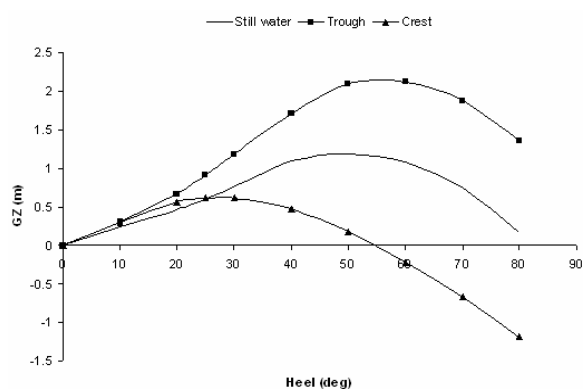


Figure 8 Containership GZ curve in calm water and waves for resonance condition.

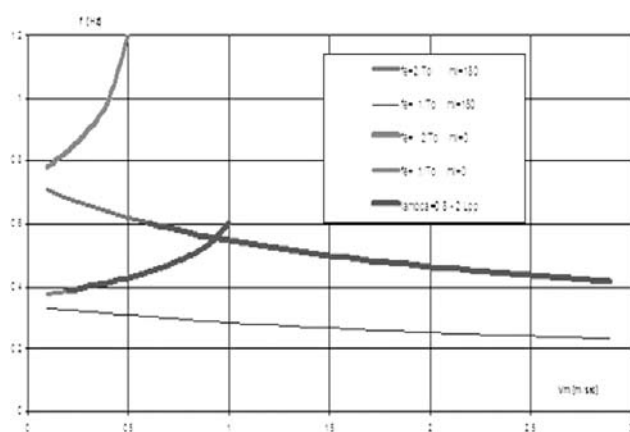


Figure 9 The diagram for speed (V) and wave frequency (f) in model basin where red line depicts parametric rolling zone (Bednarek & Kanar, 2005).

The boundary for occurrence of parametrical rolling in design condition of container ship is given in Figure 9.

The validation results of the enhanced mathematical model using all 6-DOF for the prediction of parametric roll behaviour of the container ship in steep regular waves are presented in Fig. 10 and 11.

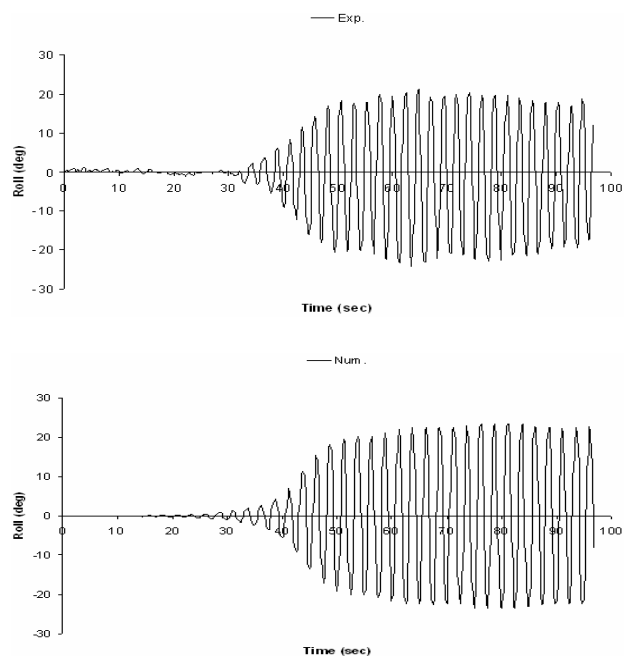


Figure 10 Parametric resonance for containership. Wave length/ L_{pp} =1.0, H =7.08 m., ψ =180°, V =14.9 knots (model scale)

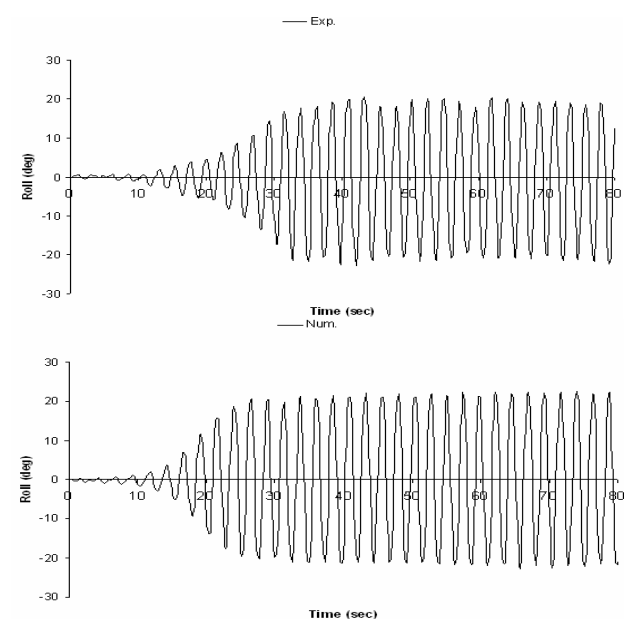


Figure 11 Parametric resonance for containership. Wave length/ L_{pp} =1.15, H =7.132 m., ψ =180°, V = 12.4 knots (model scale).

The prediction appears to be reasonable despite some initial differences leading up to parametrical build-up due to experimental set-up which aim to prevent capsizing during the trials.

3.2 Parametric Analysis

Following the validation analysis, parametrical investigation was carried out to identify susceptibility of pod-driven high speed ships that may lead to dangerous conditions in waves. This investigation was further extended to elaborate on the possible design or other operational risk control options. The latter option can be implemented either through operational guidelines recommended by IMO (1995) or the numerical simulation with ride control systems (active fin stabilisers for roll and yaw). In order to demonstrate the effectiveness of the fin stabilisation system, which has been opted for this investigation, the comparison of the roll motion amplitudes with and without the stabilisers is shown in Fig. 12.

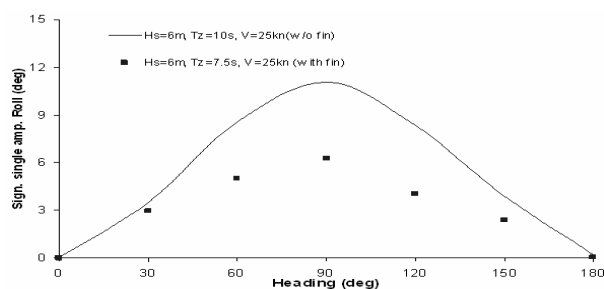


Figure 12 Comparison of roll motion of ROPAX with and without active roll fin stabilisers (rate $10^\circ/\text{sec}$).

Some of the instability and capsizing conditions identified by the numerical model are presented in Figs. 13-14. It is found that in the normal service speed conditions the ROPAX ship can be susceptible to some of dangerous conditions: surf-riding when captured by a single wave in following seas (Fig.13) the capsizing is also observed further towards to quartering seas.

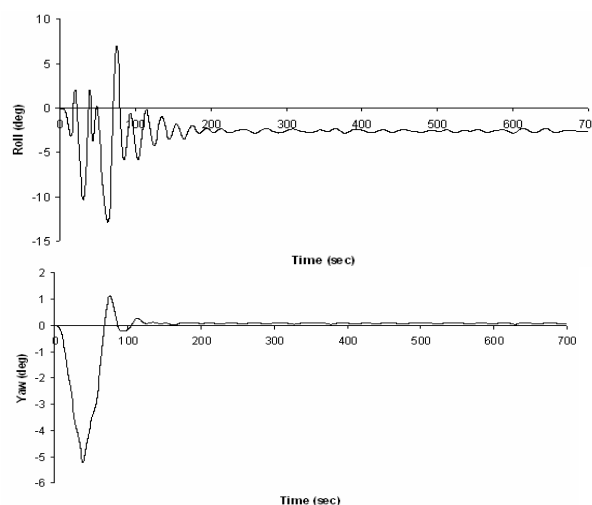


Figure 13 The occurrence of surf-riding for ROPAX in steep regular wave, $\lambda/L_{pp}=1.0$, $H=8$ m., $\psi=0^\circ$, $V=35$ knots.

Accordingly, the analysis in random waves, where more realistic sea conditions and less number of successive steep waves result in less likelihood of such dangerous conditions comparing to regular waves, have indicated yaw instability in some conditions. The anti-roll and yaw stabilisers were effective in this (Fig.14).

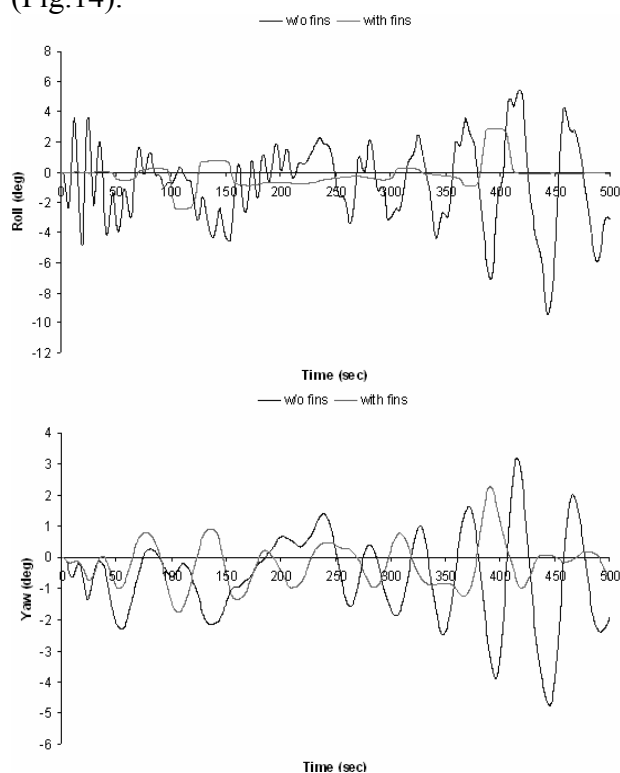


Figure 14 The occurrence of large build-up of yaw for ROPAX in random waves, $H_s=8$ m., $T_0=10.2$ sec., $\psi=30^\circ$, $V=30$ knots.

For further investigations of the containership critical motion behaviours, the conditions similar to model tests have been chosen from annual weather forecast of North Atlantic route where the vessel will be operating. The recommendations by IMO (1995) have been applied through changing course and speed.

It is seen that the ship is out-of-phase with resonance conditions which were observed in first condition (Fig. 15) and experienced the roll motions in lesser amplitudes in very high seas (Fig. 16). However, it should be noted that phasing-out of this motion should not be interpreted as the prevention since important coupled effects such as cargo shifting etc... are not taken into account. The steady wind speed of 40 knots has been assumed for all numerical

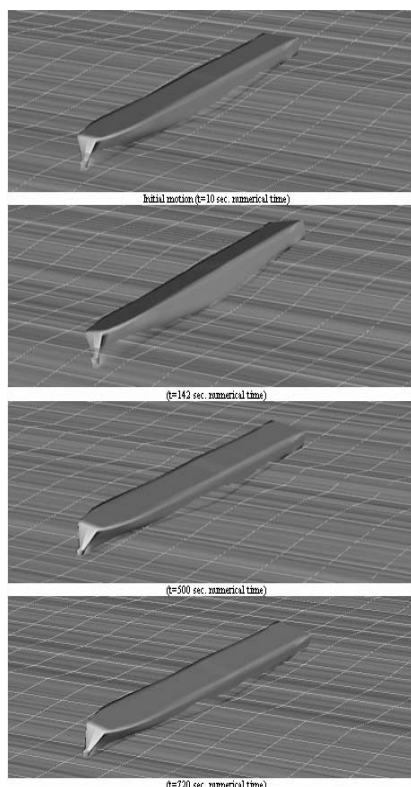


Figure 15 Numerical simulation of containership $V=15.14$ knots, $H_s=9.32$ m., $T_0=14.89$ sec., $\psi=0^\circ$.

Furthermore, as reported by Woodward et al (2005), the extreme steering can exert large manoeuvring induced side loads of spike nature

simulations. An operability diagram for the parametric rolling and slamming occurrence for containership is illustrated in Figure 17.

The stability of analysis pod-driven high speed craft has indicated some safety-critical conditions that could be observed although rather seldom, in the actual voyages. These conditions could be attributed to hull form which is shaped to accommodate pod units at the aft. In the design of pod system, the gondola and strut shapes have been chosen to be slender and rather long in order to achieve optimum propulsive efficiency and minimum cavitation danger. The selection process was also largely influenced by existing motor technology to accommodate such a large power per unit for the high-speed requirements of these ships (FASTPOD, 2005).

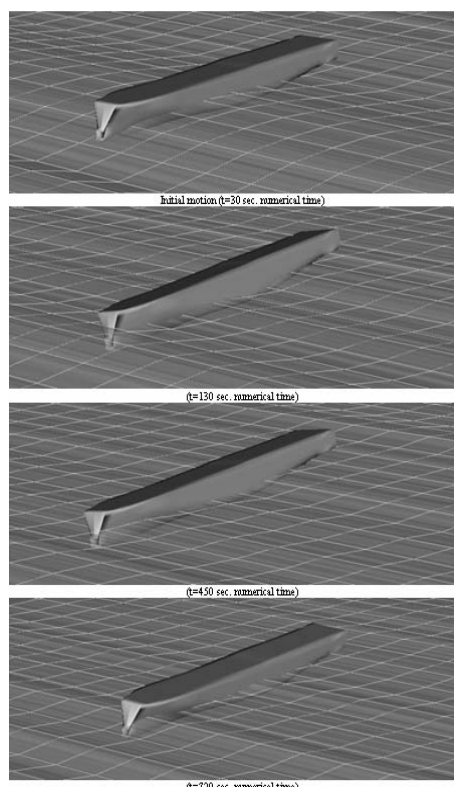


Figure 16 Numerical simulation of containership $V=16.155$ knots, $H_s=9.32$ m., $T_0=14.49$ sec., $\psi=15^\circ$.

on the entire pod units due to their high acceleration dependency. These loads do not only cause structural concern but can also induce large initial heeling which is further

safety-critical issue for pod driven ships. A detailed study discussing these effects is presented in an accompanying paper by the authors as reported in Ayaz et al (2006).

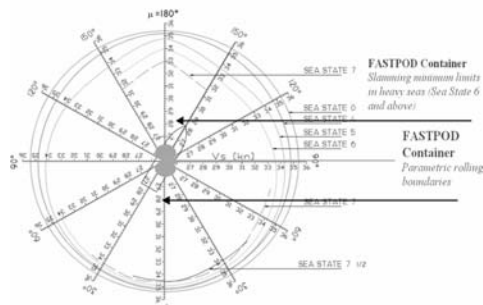


Figure 17 Parametric rolling (circles) and slamming boundaries (black arrows) on the attainable ship speed diagram under wave heading and wind direction for containership (Sea State 6 and above).

4. CONCLUSIONS

An existing 6 DOF non-linear numerical model has been enhanced for the simulation of motion control and stability analysis of pod-driven high-speed and large ships in waves. The enhancements have been accomplished by introducing the thrust and lateral force components of multitude of azimuthing and fixed pod drives in combination.

The numerical results have been verified against the experimental results for high-speed ROPAX and containership, which are designed under the EC funded collaborative project FASTPOD and displayed satisfactory agreement in overall.

It was observed from seakeeping analyses that large pod-driven vessels display favourable characteristics in high-speed and potentially dangerous operational conditions. However, large aft area to accommodate the multitude of large pod units could expose the ship to parametric build up of yaw-roll combination. This has been realised for extreme steep waves in low encounter frequency conditions which is suitable for the dangerous conditions like surf-riding and broaching. Many risk control options such as reducing the speed and

changing the course of vessel could be effective. Moreover, as design options, the effect of ride control systems has been investigated and it is shown that many dangerous conditions or instabilities can be mitigated by applying ride control systems. The shape of after body modification of the hull due to pod propulsion as well as bow flare requirement on a loading-critical ship type, such as container, the parametrical rolling or similar dangerous conditions have been observed near to pure following and head seas conditions although these are confined to very extreme cases.

It is thought that many of these problems associated with the container ship type could be caused due to very low GM to accommodate the targeted cargo as well as heavy pods in the aft. Anti-roll tanks can be proposed to tackle this problem as well as the aforementioned operational steps can be undertaken.

Based on the parametrical analysis undertaken during the course of this study, it could be argued that the improvement in motor technology and reduction in motor sizes and eventually pod sizes, will positively affect the viability of large pod-driven high-speed ships in terms of stability and control in waves.

Finally, it is believed the modified numerical model provides satisfactory results for the analysis of dynamic stability of high-speed, large podded ships by multiple large pod units in waves and it could be a useful tool during the preliminary design process for such vessels.

5. ACKNOWLEDGMENTS

This study was carried out under European Commission research project FASTPOD (GRD2-2001-50063). The authors wish to thank all 17 partners of FASTPOD project for the prompt collaboration during the whole development of the project.

6. REFERENCES

- Ayaz, Z., Turan, O., Vassalos, D., 2004, "Manoeuvring Aspects of Pod Driven Ships" Proceedings of First International Conference on Technological Advances in Podded Propulsion (T-POD), Newcastle upon Tyne, Atlar et al., University of Newcastle Publication, UK, pp. 135-152.
- Ayaz, Z., Turan, O., Vassalos, D., 2005, "Manoeuvring and Seakeeping Aspects of Pod Driven Ships" Journal of Engineering for the Maritime Environment-Proceedings of the Institution of Mechanical Engineers Part M, Vol. 219, pp. 77-91.
- Ayaz, Z., Vassalos D., Spyrou, K.J., 2006 (in press), "Manoeuvring Behaviour of Ships in Extreme Astern Seas", Ocean Engineering.
- Bednarek, A., Kanar, J., 2005 "Cargo Vessel-Results of Parametric Roll Model Tests" Project Report (FASTPOD-GRD2-2001-50063), *Commercial in confidence*, CTO, Poland.
- FASTPOD, "Fast Ship Application for Pod Drives", European Commission RTD Project, GRD2-2001-50063, 2002-2005.
- IMO, 1995 "Guidance to the Master for Avoiding Dangerous Situations in Following and Quartering Seas, MSC Circular 707, IMO Publication, London, UK.
- Inoue, S., Hirano, M., Kijima, K. and Takashina, J., 1981 "A Practical Calculation Method of Ship Manoeuvring" International Shipbuilding Progress, Vol. 28, No. 324, pp. 207-222.
- ITTC, 2005 "The Specialist Committee on Azimuthing Podded Propulsion. Final Report and Recommendations to the 24th. ITTC", Proceedings of 24th ITTC, University of Newcastle upon Tyne Publication, Vol. 2, pp. 543-600, Edinburgh, UK
- OPTIPOD "Optimal Design and Implementation of Azimuthing Pods for Safe and Efficient Propulsion of Ships" European Commission RTD Project, GRD1-1999-10294, 2000-2003
- Toxepus, S., Loeff, G., 2002, "Manoeuvring Aspects of Fast Ships with Pods" Proceedings of Euro conference on high-speed performance marine vehicles, Bergen, Norway, pp. 392-406.
- Tragardh, P., Hua, J., Lee-Andersen, M., 2004 "Development of Fast ROPAX, Seakeeping and Wave wash model tests, Free-running manoeuvring model tests" Project Report (FASTPOD-GRD2-2001-50063), *Commercial in confidence*, SSPA, Sweden AB.
- Van Terwisga, T., Quadvlieg, F., Valkhof, H., 2001, "Steerable Propulsion Units: Hydrodynamic Issues and Design Consequences" Paper written on the occasion of 80th anniversary of Schottel GmbH & Co, Germany.
- Whicker, L.F., Fehlner, L.F., 1958 "Free stream characteristics of a family of low aspect ratio all moveable control surfaces for application to ship design, David Taylor Model Basin Report, No:933, USA.
- Woodward, M.D., Atlar. M., Clarke, D., 2005, "Manoeuvring induced loads on fast pod drives" FAST 2005, St. Petersburg, Russia

The Effect of Pod-induced Heeling on the Stability of Large and High-speed Ships

Zafer Ayaz, *The Ship Stability Research Centre, Department of Naval Architecture and Marine Engineering, Universities of Glasgow and Strathclyde, UK*

Osman Turan, *The Ship Stability Research Centre, Department of Naval Architecture and Marine Engineering, Universities of Glasgow and Strathclyde, UK*

Michael D. Woodward, *School of Marine Science and Technology, University of Newcastle upon Tyne, UK*

Mehmet Atlar, *School of Marine Science and Technology, University of Newcastle upon Tyne, UK*

ABSTRACT

This paper presents a numerical and experimental investigation on the effect of pod propulsor induced heeling on the stability of large and high-speed ships. A six degrees of freedom numerical model to predict the coupled manoeuvring and seakeeping behaviour of a ship driven by pods has been developed and validated using the extensive captive and free-running model test data for a large and high-speed pod-driven Ropax and Cargo ship. The correlation between manoeuvring induced “spike” loads, heeling motion and turning has been investigated using the IMO turning motion tests for different speed ranges. The effect of static heeling on turning manoeuvre and dynamic heeling effects in combination with directional control have been investigated for these vessels. The implication of the effect of dynamic heeling on the stability of pod-driven large high-speed ships is highlighted with a view to improve the design of these vessels for their safe operations.

Keywords: *Azimuthing podded propulsion, steering-induced heeling, maneuvering induced spike loads*

1. INTRODUCTION

The azimuthing podded propulsion system has significant advantages over other conventional propulsion and steering systems during low speed manoeuvre and turning motions; providing large steering forces. However, the large pod induced steering angles could also seriously jeopardise stability and safety of pod-driven ships especially when considered in combination with the generally weak directional stability of pod-driven ships; as a result of prammed aft-shape to

accommodate pod-strut unit (Van Terwisga et al, 2001). Recent studies carried out under two large Europe wide research projects, on the design and operation of pod-driven ships, have also focused on this issue as part of the design for safe operation of pod-driven ships (OPTIPOD, 2002, FASTPOD, 2005). The studies indicated significantly high side forces, so-called “spike” loads, on the pod units of high-speed ships in the case of the turning manoeuvre; which is required by IMO in the ship design process. This is especially a pressing issue now as a growing number of

pod-driven high-speed Ropax and Cruise ships are being designed and entering into operation. While, the current IMO manoeuvring criteria (2002) does not reflect significant heel-induced effect on turning and directional stability, the IMO's Committee on revised intact stability code (IMO, 2004) and the 24th ITTC Specialists Committees on Stability in Waves and Azimuthing Podded Propulsion (ITTC, 2005a, b), have issued recommendations to include them as an essential measure of performance-based stability assessment as well as manoeuvring.

Based on the above background, this paper presents dedicated numerical tools to predict pod-induced forces and motions including the effect of waves when they exist. The numerical model has been validated using the extensive captive and free-running model test data for a large high-speed pod-driven Ropax and Cargo ship. The correlation between the "spike" loads, heeling motion and turning has been investigated using the IMO turning motion tests for different speed ranges. The effect of static heeling on the turning manoeuvre and dynamic heeling effects in combination with directional control have been investigated for pod-driven high-speed ships. Finally, the outcome of the effect of dynamic heeling on the stability of pod-driven large high-speed ships is highlighted and the possible solutions for regulatory design and operational issues are discussed.

2. POD-INDUCED HEELING

2.1 Effect of heeling during manoeuvring

The effect of heel, although overlooked in the manoeuvring criteria by IMO (2002), does have significant effect on manoeuvring; especially concerning directional stability and course-keeping. Furthermore, in combination with stability characteristics and inherent yaw-roll coupling, it could produce adverse effects for manoeuvring in waves as reported in (Ayaz

et. al, 2005). IMO IS (2002) recommends using the following approximate formula for passenger ships, while the angle of heel on account of turning should not exceed 10°:

$$M_R = 0.196 \frac{V_o^2}{L} \Delta (KG - \frac{d}{2}) \quad (1)$$

where M_R is heeling moment, V_o is service speed, L length of ship at waterline, Δ is displacement, d is mean draught and KG is height of centre of gravity above baseline.

A slightly modified form of the formulation is also recommended for high-speed multi-hull vessels in IMO HSC (2000) for the heeling moment and also for turning lever of the hull.

Over the years many researchers have investigated the effect of heel on the manoeuvring motions for conventional vessels; especially at high-speed e.g. Son & Nomoto (1981), Oltmann (1993) and Trägårdh (2003). They have emphasized the importance of inclusion of this mode of motion into the standard 3-DOF (surge, sway and yaw) preferred at conventional analysis. It is proven that expected factors such loading condition (GM), and stern shape as well as length-to-beam ratio and slenderness of the vessel do play a significant role in identifying the maximum heeling during manoeuvring. Trägårdh (2003) has carried out a regression analysis based on 20°/20° zig-zag manoeuvre model test results for 24 ships which included RoRo, LNG, cruise ships and container vessels. For most extreme cases, a maximum roll angle of 26° was recorded for a 60° overshoot angle. The study also reported a strange behaviour where in pull-out tests the yaw rate and roll angle is decreased, as expected, when the rudder was put amidships for pull-out however then increased as the speed picked up. The study concluded that the significant 'increases' and 'drops', respectively, in yaw-rate and speed during turnings would cause such behaviour along with the ship's geometrical characteristics and loading conditions.

Therefore, it is not surprising that current efforts towards performance-based stability analysis is required such analysis as prerequisite to the detailed stability analyses in waves or for limit-state conditions (ITTC, 2005a).

2.2 Effect of heeling during manoeuvring with pod-driven ships

A comprehensive up to date review of the impact of off-design conditions on loads and stability of pod-driven ships has been given by the 24th ITTC Specialist Committee on Azimuthing Podded Propulsion (2005b).

Within the context of steering related heel/roll behaviour, Toxopeus and Loeff (2002) investigated merits and drawbacks of pod-driven ships in operation. Toxopeus and Loeff (2002) identified that high turning rate can cause large gyration forces and thus large roll motions which adversely affect turning rate and the course stability. They also carried out analysis from the database of manoeuvring tests carried out for a number of pod-driven ships. The results showed maximum roll angles up to 28° with steady turning heel angles up to 17 degrees. The authors indicated, although IMO does not provide recommendations regarding roll angles, from practical experiences, angles above 13° are thought to be very large. The comparison analysis with conventionally-driven ships showed higher roll angles for pod-driven ships. Apart from the aforementioned differences, the authors also pointed out that the effect of steering rate of application; which differs between pods and rudders. The authors derived a broadly constant factor to present the trend of this phenomenon:

$$k = \frac{\sin(\phi)g\overline{GM}r_{tur}}{U^2} \quad (2)$$

where k an almost constant factor, GM is the metacentric height, ϕ is the heel angle, r_{tur} is

the turning diameter and U is the ship speed.

While Lepeix (2001), Hamalainen and Heered (2001) and Van Terwisga et al (2001) have emphasised on some safe limits on practical heel angles, more realistic observation of the heeling phenomenon in a pod driven ship has been given by Kurimo and Bystöm (2003) from full-scale trials. They also verified that the source of maximum heel angle is related to the magnitude of the maximum turning rate. The observed maximum heel angle was 13% smaller than that predicted from the model tests. The difference has been attributed to the possible differences in initial speed and initial metacentric heights in both runs. A simplified prediction has been proposed using assumptions that maximum heel angle is proportional to the square of the initial speed and inversely proportional to the metacentric height; as given in (1) and (2).

However, a comparative analysis conducted by Ayaz et al. (2005) for the pod-driven and conventional Ropax type ships, designed within the OPTIPOD project, has shown that successful hydrodynamic aft-hull optimisation could reduce the possible adverse affect of pod-induced heeling. In this analysis the two Ropax ships; a pod-driven and a conventional rudder-propeller steered, which have almost identical ship geometries and aft-body type (with a slightly lower GM value for the pod-driven ship), were investigated for the heeling effect during turning motion and results are shown in Fig. 1.

As shown in Figure 1, a pull-out test, where the ship's rudder is ordered to return to amidships or neutral position after completing a turning circle, was performed. The other major contributed factor for this outcome can be the greater speed loss for the pod-driven vessel as reported by the analysis of Trägårdh (2002) in calm water and waves.

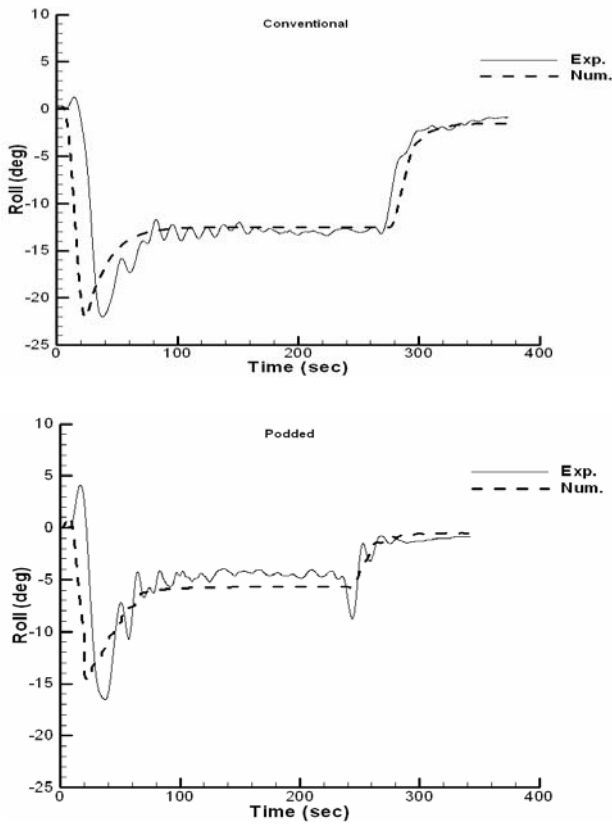


Figure 1 Rolling during pull-out manoeuvre at 28 knots for 172.2 m. conventional (top) and pod-driven (bottom) Ropax, (Ayaz et al., 2005).

In addition to the above, Woodward et al., (2005) were reported on the large magnitude of "spike" loads and associated "snap" rolling behaviour observed with the pod-driven ships which is discussed in Section 4.2 within more details..

3. NUMERICAL MODEL

The current numerical model consists of non-linear, 6-DOF motion equations allowing a straightforward combination between seakeeping and manoeuvring behaviour whilst accounting for extreme motions. The details of the mathematical model for pod-driven ship have been presented by Ayaz et al. (2005) and in an accompanying paper presented to this conference, Ayaz et al. (2006). The final equation of motion for pod-driven ships is given in (3) and (4);

$$m(\dot{U} - VR) = -\iint_S p \mathbf{n}_X dS + X_H - S \sin(\delta) + (1 - t_p) T \cos(\delta)$$

$$m(\dot{V} + UR) = -\iint_S p \mathbf{n}_Y dS + \rho U \int_{\Gamma_x} \Phi_D \mathbf{n}_Y ds + Y_H$$

$$-(1 + a_{Hpod}) S \cos(\delta) + X'_{pod} \sin(\delta)$$

$$m\dot{W} = -\iint_S p \mathbf{n}_Z dS + \rho U \int_{\Gamma_x} \Phi_D \mathbf{n}_Z ds + Z_H$$

where pod denotes pod-induced forces. The nomenclature for (3) and (4) including other details was presented in Ayaz et al (2006) and therefore will not be repeated here.

$$(I_{xx} \cos^2 \theta + I_{yy} \sin^2 \theta) \dot{P} = -\iint_S p (\mathbf{r} \times \mathbf{n}_{VZ}) dS + \rho U \int_{\Gamma_x} \Phi_D (\mathbf{r} \times \mathbf{n}_{VZ}) ds + K_H + (1 + a_H) z_R F_N \cos \delta$$

$$I_{yy} \dot{Q} = -\iint_S p (\mathbf{r} \times \mathbf{n}_{ZX}) dS + \rho U \int_{\Gamma_x} \Phi_D (\mathbf{r} \times \mathbf{n}_{ZX}) ds + M_H$$

$$(I_{xx} \sin^2 \theta + I_{zz} \cos^2 \theta) \dot{R} = -\iint_S p (\mathbf{r} \times \mathbf{n}_{XY}) dS + \rho U \int_{\Gamma_x} \Phi_D (\mathbf{r} \times \mathbf{n}_{XY}) ds + N_H - (1 + a_H) x_R F_N \cos \delta$$

In these equations, hull (manoeuvring) force terms are written based on MMG method (Inoue et al., 1981) as follows:

$$X_H = X_u \dot{u} - Y_v vr - \frac{u}{|u|} Y_r rr + X_{vr} vr - R_T(u)$$

$$Y_H = Y_v \dot{v} + Y_r \dot{r} + Y_v v + \frac{u}{|u|} Y_r r + Y_{|v|} |v| + Y_{|r|} |r|$$

$$Z_H = Z_w \dot{w} + Z_w w + Z_q \dot{q} + Z_q q$$

$$K_H = K_p \ddot{\phi} + C(\dot{\phi}) - z_y Y_H$$

$$M_H = M_q \dot{q} + M_q q + M_w \dot{w} + M_w w$$

$$N_H = N_r \dot{r} + N_v \dot{v} + N_r r + \frac{u}{|u|} N_v v + N_{|r|} |r| +$$

$$N_{|r|v} rrv + N_{|v|r} vvr$$

where, X_H , Y_H , Z_H , K_H , N_H , M_H are surge, sway, heave, roll, pitch, yaw hull forces, respectively. $R_T(u)$ is the total resistance force, $C(\dot{\phi})$ is the damping moment and z_y is the vertical coordinate of the centre of action of lateral force. Other terms represent the

acceleration and velocity coefficients. Furthermore, equation (5) does not include coupling between the vertical and horizontal motions. However, hydrodynamic terms which result from combined sinkage and rotation, that occur during heeling, are added to sway force and yaw moment in (5) if experimental values are available. These terms are represented in the first order on the basis of linear sway and yaw velocity coefficients as follows:

$$\begin{aligned} Y_H &= Y_\phi \phi + Y_{v|\phi} v|\phi| + Y_{r|\phi} r|\phi| \\ N_H &= N_\phi \phi + N_{v|\phi} v|\phi| + N_{r|\phi} r|\phi| \end{aligned} \quad (6)$$

It should be noted that this model is only valid for small heeling angles (up to $2^\circ \sim 3^\circ$). In the prediction of ship motions in seaway, the accurate representation of roll-damping characteristics becomes important. The non-linear damping motion could be described through linearized coefficients obtained from roll decay tests. However, the terms will be constantly changed based on the loading conditions and subsequent stability characteristics; such as non-linearity due to changes in geometry with the free-surface effects. Therefore, in the numerical model, Ikeda's (Himeno, 1981) pseudo-linearized terms which are obtained based on hull characteristics are used to calculate roll damping which could be expressed as follows:

$$K_\phi = (B_O + B_F + B_E + B_L + B_{BK}) \times (1 - e^{-10Fn}) \quad (7)$$

where the damping coefficient B is the superposition of potential, friction, eddy, lift and bilge keel damping terms, denoted by subscripts O, F, E, L, BK , respectively.

Here the mean roll-angle is obtained from the slope of the roll curve in the numerical model. The second term in (7) represents a correction for forward speed. Also, vertical coordinate of centre of action of lateral force can be estimated by applying practical calculation method based on the restoring arm lever (GZ),

which is calculated for each loading and wave condition, as follows:

$$z_y = \frac{g GZ(\phi)}{Ur} \quad (8)$$

where U is ship speed and r is yaw rate.

4. NUMERICAL ANALYSIS

For the validation and further numerical analyses, two ships; a Ropax and a Cargo ship (container), which were designed under the FASTPOD project, have been used (FASTPOD, 2005). The principal particulars of the two ships are given Table 1.

The FASTPOD Ropax is propelled by four puller-type pod units all equipped with 5.2 m propellers. Each pod absorbs approximately 27 MW power at the desired service speed; approximately 38 knots. The forward pods are fixed and the aft pods are azimuthing for ship control.

The FASTPOD Cargo (the design version used in this analysis) is propelled with two azimuthing pod units both equipped with 6.5m propellers and two tandem propellers (6.4 m. diameter each) positioned between them. Each pod absorbs approximately 36 MW power at the desired service speed of approximately 35 knots.

For the validation analysis of the numerical model, free-running model test results for the Ropax (Trägårdh et. al, 2004) and the Cargo ship (Bednarek & Kanar, 2005) were used.

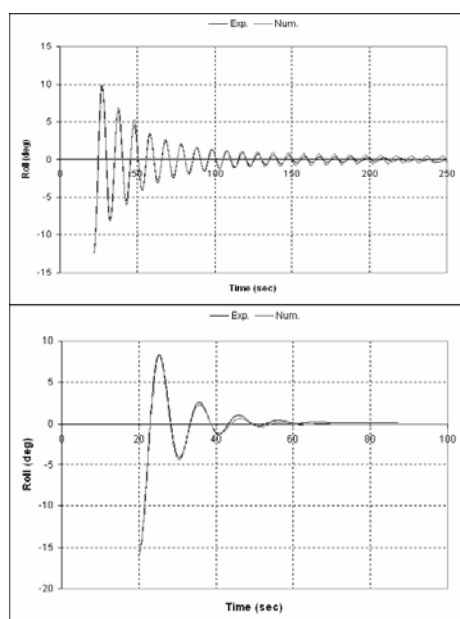
The comparison of the numerical model with the model tests on roll decay tests for each ship is shown in Figs. 2-3. The correlation between the predictions and model test results appears to be very good. Heeling moments obtained from the oblique towing tests of the Ropax for different speed are shown in Fig. 4 to be compared with the numerical predictions later in the paper.

Table1. Principal particulars of FASTPOD ship

Parameter	FASTPOD ROPAX	FASTPOD Cargo
L_{pp}	220.00 m	275.00 m
B (Beam)	30.00 m	30.00 m
D (Depth)	9.70 m	21.65 m
T (Draft)	6.80 m	10.30 m (design)
C_b	0.39	0.57
Δ	17600 t	49600 t (design)
LCG	-5.71 m (aft)	-7.20 m (aft)
VCG	14.60	13.60 (design)

4.1 Pod-Induced Heeling

It was mentioned that the effect of steering forces created by pod drives could be an important issue especially in case of large turning motions e.g. emergency manoeuvre or harbour manoeuvre.

Figure 2 Roll decay tests for Ropax at zero speed (top) and $V=35$ knots (bottom).

For the FASTPOD ships, the large size, high speed and high power make the effect of steering on heeling even more significant. During the course of the project, this issue has been highlighted considering manoeuvring loads on ships and their suitability to classification society rules. In the model

experiments, KG value of ship has been selected from a scantling analysis. In Figure 5, the model experiment result for heel angle has been compared against the numerical result for the turning circle manoeuvres at two different speeds. Furthermore, the turning manoeuvre motion for the IMO criteria has been carried out using design KG along with the scantling KG value chosen from IMO High Speed Craft rules (2000).

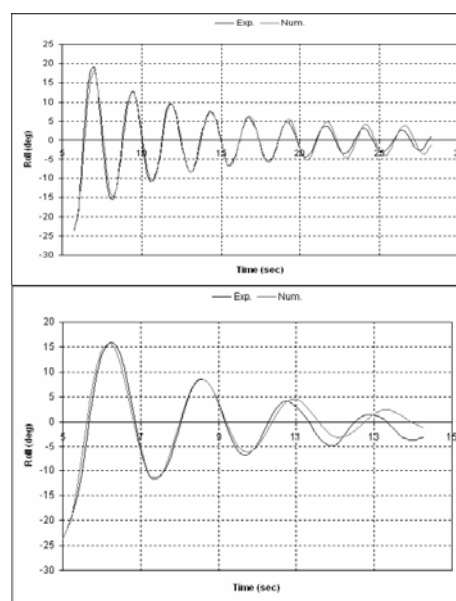
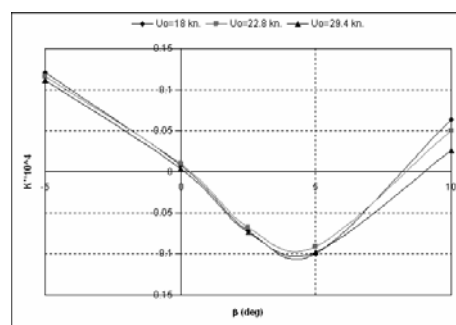
Figure 3 Roll decay tests for Cargo ship at zero speed (top) and $V=21$ knots (bottom), in model scale.

Figure 4 Heeling moments measured from oblique towing tests for three different speeds in non-dimensional form (Vogt, 2005).

Experimental (in full-scale) and design KG values are found as 14.60m and 12m respectively. The value of KG directly affects heeling motion, especially for maximum angle

as seen in Fig. 5. For the vessel tested, even in the case of limiting KG, the maximum heel angle of the ship during the turning motion at high-speed still is lower than many lower powered Ropax ships (Ayaz et. al., 2005). The numerical model displays satisfactory agreement with the model experiments at lower speed of 25 knots. While, a good quantitative agreement for maximum and steady heel angles was obtained at 38 knots (Fig. 5), the numerical model displays larger oscillation during the brief period when vessel restoring force applies to the ship to reach a steady heel. This oscillation can be attributed to some weakness in the modelling of the hull and pod induced damping as well as some inaccuracy in the exact position of the vertical centre of effort for the lateral forces given in (4) and (5).

However, for the zig-zag manoeuvre tests, although the model has agreement in terms of maximum amplitude, it is very rigid comparing to larger decaying in amplitude after changing the helm-angle (Fig. 6). The free-surface effects were included in the numerical simulation. This difference could indicate potential vortex-induced effects that occur between pods however which are not fully modelled numerically.

The significant outcome from the zig-zag test was concerning the inherent yaw-heel coupling observed during the tests (Fig. 6). The roll-amplitude increases rather largely with increasing helm angle.

This could be an indication for the effect of the roll-yaw coupling, which is observed during the simulations of ship motions in steep following waves, where similar hydrodynamic mechanism takes places in effect along with wave forces (Ayaz et. al., 2006).

For validation purposes, the maximum heeling moment occurring during the turning circle motion has been compared to the empirical value obtained from the IMO formula; expressed in (1) for the scantling design condition and comparative results are

given in Table 2.

Table 2 points out that although the maximum heeling angle did not exceed 10° , approximate formula given by IMO estimates the heeling moment as almost 1/3 of the maximum heeling moment calculated by numerical model and validated with model test.

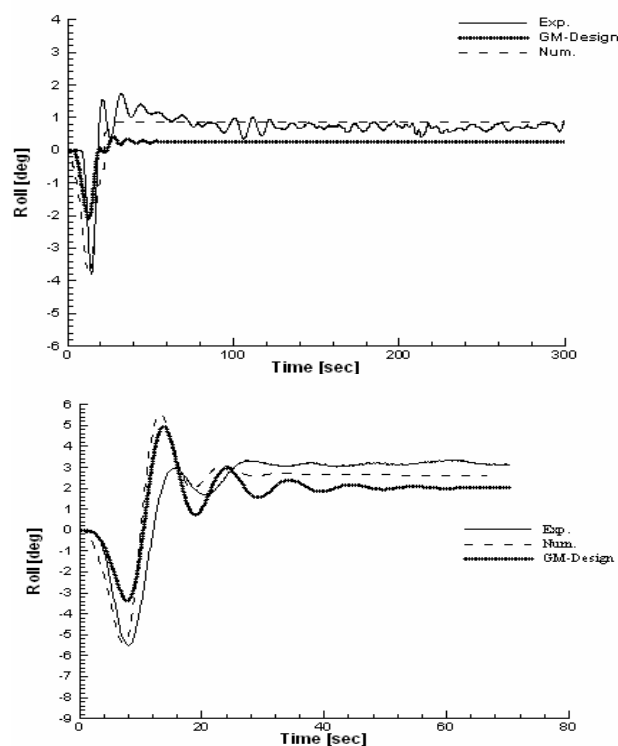


Figure 5 Comparison of roll motion of Ropax during turning circle motion at 25 knots (top) and 38 knots (bottom), for scantling condition (Exp) and design condition (GM-Design), respectively.

Furthermore, as will be presented in §4.2, the extreme steering can exert large manoeuvring induced side loads of spike nature on the entire pod units due to their high acceleration dependency. These loads do not only cause concern for inducing large initial heeling which is safety-critical issue for pod-driven ships but also for structural loads.

Finally, a similar exercise (i.e. turning circle manoeuvre) has been carried out for the Cargo ship in the design condition. Figure 7 illustrates the effects of speed in the design loading condition for this manoeuvre. Due to

lower righting arm moment (low GM) the vessel's maximum and steady heeling angle is considerably higher in comparison to the Ropax; even at lower Froude numbers. Also, the maximum heeling moment occurred during the turning circle motion of the Cargo ship, was compared to the empirical value obtained from the IMO formula and presented in Table 3.

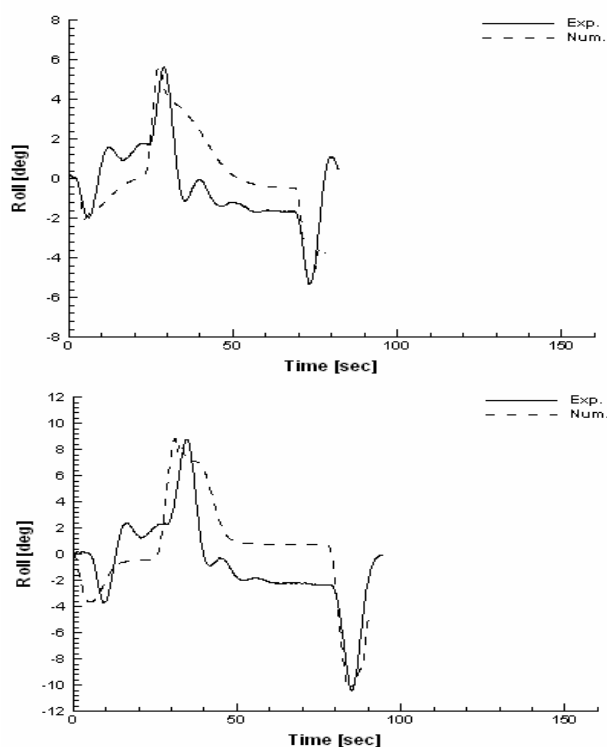


Figure 6 Comparison of roll motion of Ropax during 10°/10° (top) and 20°/20° (bottom) Zig-Zag tests at 38 knots.

The results indicate similar trend as with the Ropax, in which the IMO formula grossly underestimates the heeling moment in comparison to the numerical prediction; shown in Table 2.

Table 2. The comparison of maximum heeling moments obtained by the numerical model and the IMO formula (1) for Ropax.

V (knots)	Numerical (Kn.m)	IMO (Kn.m)
25	79850	29171
38	169321	67397

4.2 Pod-Induced Loads

The improved manoeuvring performance reported for ships fitted with azimuthing pod drives is most closely related to the enhanced slow speed capabilities. Conventional control arrangements can only produce a control force when there is a flow over the rudder; that is, when the ship is moving. Conversely, an

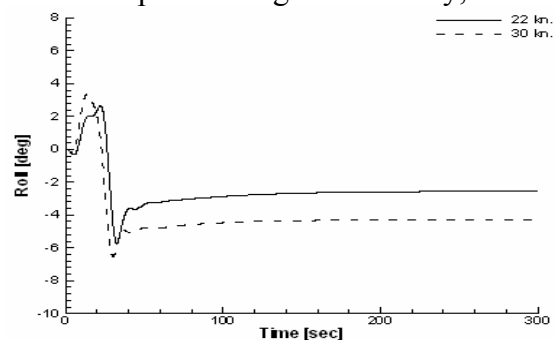


Figure 7 Comparison of roll motion of the Cargo ship during turning circle motion at 22 and 30 knots for design condition.

Table 3. The comparison of maximum heeling moments obtained by the numerical model and the IMO formula (1) for the Cargo ship.

V (knots)	Numerical (Kn.m)	IMO (Kn.m)
22	127888	37996
30	163186	70684

azimuthing pod drive can produce a control force in any direction; even when the ship is at a dead stop. Improved manoeuvring performance at sea-speed is less easy to define as improvements in turning ability are often accompanied by degraded course-keeping ability and vice-versa. Nevertheless, it services to say that most pod-driven applications demonstrate significant improvements in turning ability with equivalent or only slightly less course-keeping ability when compared with equivalent conventionally propelled ships.

This general improvement in control is achieved through the generation of significantly larger forces; coupled less desirably, with greater dynamic load variations.

While the steady state loading is relatively easy to both predict and measure, using scale model tests, the dynamic effect prove more difficult. Clearly, the acceleration related forces induced when slewing a 50t rudder are quite different from those for a 500t pod; especially when this mass has a gyroscopic component. When using predictions for only the steady state condition it is possible to seriously underestimate the total forces acting on the pod. Woodward et al (2005) presents evidence of spike loads associated with dynamic slewing which are shown to be more than double the steady state forces. This phenomenon is further elaborated by Woodward and Atlar (2006) where a relationship between the spike loads and snap rolling is established. Figure 8 shows the roll angle of the FASTPOD Ropax as a 35° helm angle is applied; clearly demonstrating snap rolling behaviour. Woodward and Atlar (2006) argue that the spike loading is highly acceleration dependant and that a more directionally course-stable design should present smaller spike loads. In turn, all things being equal, this should also help to reduce the maximum angle of snap rolling.

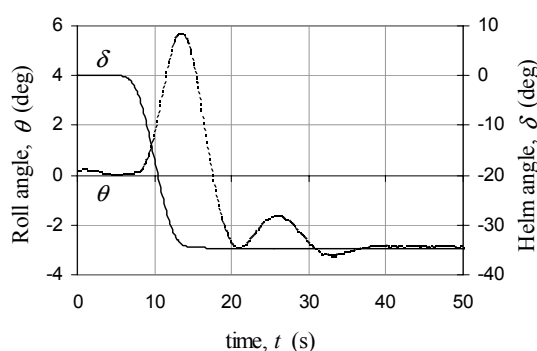


Figure 8 Snap roll motion of Ropax after initiating 35° helm angle.

4.3 Design implications

It is believed that the current approach in safety analysis could be modified in a way to identify potential pitfalls in static heeling and directional control for more detailed analysis in realistic seaways. This is especially vital for the new innovative ship designs fitted with multi-

purpose and powerful propulsion systems and operating at high speeds. This could indicate directional instability and steering-induced excessive forces that could be detrimental both static and structural safety. This approach will be in line with current performance-based approach advocated by regulatory bodies.

A good example will be the significant inherent yaw-heel coupling observed during the tests possibly due to pram aft shape to accommodate the pod structure. The roll amplitude increases rather largely with increasing helm angle. This could be precede for potentially dangerous roll-yaw coupling observed during the motions in simulations in steep following waves where similar hydrodynamic mechanism in calm-water manoeuvring tests in effect along with wave forces.

Dynamic manoeuvring induces acceleration dependant spike loads on pod drives that have important implications for snap rolling behaviour. Pod drives can produce a large control force to steer even the most course-stable ship however, poor course-stability can result in much greater, but less advantageous, dynamic forces. To minimise the magnitude of manoeuvring induced snap rolling it is recommended that designers of pod-driven ships care towards greater inherent course-stability.

5. CONCLUSIONS

The effect of pod propulsor induced heeling on the stability of large and high-speed ships has been investigated using an existing 6 DOF non-linear numerical model which was enhanced for the simulation of motion control and stability analysis of pod-driven ships. The key findings and conclusions from this study can be summarised as follows:

- The numerical predictions of heeling motion during manoeuvring compared with the experimental measurements displayed satisfactory correlations in

overall. However, the differences observed in some cases could be attributed to the less accurate modelling of hull damping and mainly vortex-induced effects that occur between the pods units.

- Although the steering induced heeling motion by pod drives is significant, it is found that the magnitude of KG more directly affects heeling motion, especially for the maximum amplitude. For the vessels tested in this study, the maximum heel angle of ship during the turning motion at high-speed is still lower than many conventionally driven similar type of ships of which results are available in open literature.
- A simple analysis in this study showed that although the maximum heeling angle did not exceed 10°, approximate formula given by IMO grossly underestimates the heeling moment (almost 1/3 of the maximum heeling moment) calculated by the numerical model and validated with the model tests.
- Dynamic manoeuvring induces acceleration dependant spike loads on pod drives that have important implications for snap rolling behaviour.

Overall, the current numerical model presented herein provides satisfactory results for the analysis of dynamic stability of large and high-speed ships driven by multiple, large pod units and it could be a useful tool for the conducting of the performance-based approach to safe design of such vessels.

6. ACKNOWLEDGMENTS

This study was carried out under European Commission research project FASTPOD (GRD2-2001-50063). The authors wish to thank all 17 partners (Newcastle University-School of Marine Science and Technology, Chantiers de L'Atlantique, CETENA S.p.A Centro per gli Studi di Tecnica Navale, CTO Ship Design Research Centre, Deltamarin, Fincantieri Cantieri Navali Italiani S.p.A.,

Stocznia Gdynia S.A., Hamburgische Schiffbau Versuchsanstalt GmbH, Lloyd's Register, Principia Marin, SSPA Sweden AB, The Ship Stability Research Centre, Universities of Glasgow and Strathclyde, Stocznia Szczecinska Nowa Spolka z o. o., Stena Rederi AB, Technicatome SA, BAE Systems Marine Ltd., VTT Technical Research Centre of Finland) of FASTPOD project for the prompt collaboration during the whole development of the project.

7. REFERENCES

- Ayaz, Z., Turan, O., Vassalos, D., 2005, "Manoeuvring and Seakeeping Aspects of Pod Driven Ships" Journal of Engineering for the Maritime Environment-Proceedings of the Institution of Mechanical Engineers Part M, Vol. 219, pp. 77-91.
- Ayaz, Z., Turan, O., Atlar, M., 2006, "On the Stability and Safe Operation of Pod-Driven Ships" 9th International Conference on Stability of Ships and Ocean Vehicles, Rio de Janeiro, Brazil, pp. 25-29.
- Bednarek, A., Kanar, J., 2005 "Cargo Vessel-Results of Parametric Roll Model Tests" Project Report (FASTPOD-GRD2-2001-50063), *Commercial in confidence*, CTO, Poland.
- FASTPOD, "Fast Ship Application for Pod Drives", European Commission RTD Project, GRD2-2001-50063, 2002-2005.
- Hamalainen, R. and Van Heerd, J., 2001, "Triple pod propulsion in the world's largest ever cruise liner", PRADS 2001, pp. 757-766, Shanghai, China.
- Himeno, Y., 1981 "Prediction of Ship Roll Damping- State of Art" Report No. 239, Department of Naval Architecture and Marine Engineering, University of Michigan, USA

- Hirano, M., Takashina, J., 1980 "A Calculation of Ship Turning Motion Taking Coupling Effect Due to Heel Into Consideration" Transactions of West Japan Society of Naval Architects, Vol. 59
- IMO, 2000 "International Code of Safety of High-Speed Craft", IMO Publication, London, UK.
- IMO, 2002 "Code on Intact Stability", IMO Publication, London, UK.
- IMO, 2004 "The Report of Marine Safety Committee" IMO Publication (www.imo.org), London, UK.
- ITTC, 2005a "The Specialist Committee on Stability in Waves. Final Report and Recommendations to the 24th. ITTC", Proceedings of 24th ITTC, University of Newcastle upon Tyne Publication, Vol. 2, pp. 369-408, Edinburgh, UK.
- ITTC, 2005b "The Specialist Committee on Azimuthing Podded Propulsion. Final Report and Recommendations to the 24th. ITTC" Proceedings of 24th ITTC, University of Newcastle upon Tyne Publication, Vol. 2, pp. 543-600, Edinburgh, UK
- Lepeix, R., 2001, "Hydrodynamic Trends in Hull Lines of Podded Driven Large Cruise Vessels" PRADS 2001, Vol. 2, pp. 767-776, Shanghai, China.
- Oltmann, P., 1993 "Roll- An often neglected element of manoeuvring" Proceedings of International Conference on Marine Simulation and Ship Manoeuvrability, pp. 463-471, St. Johns', Canada.
- OPTIPOD "Optimal Design and Implementation of Azimuthing Pods for Safe and Efficient Propulsion of Ships" European Commission RTD Project, GRD1-1999-10294, 2000-2003
- Son, K., Nomoto, K., 1981 "On the Coupled Motion of Steering and Roll" Journal of the Society of Naval Architects of Japan, Vol. 150, pp. 73-83.
- Toxepus, S., Loeff, G., 2002 "Manoeuvring Aspects of Fast Ships with Pods" Proceedings of Euro conference on high-speed performance marine vehicles, Bergen, Norway, pp. 392-406.
- Trägårdh, P., Hua, J., Lee-Andersen, M., 2004 "Development of Fast Ropax, Seakeeping and Wave wash model tests, Free-running manoeuvring model tests" Project Report (FASTPOD-GRD2-2001-50063), *Commercial in confidence*, SSPA, Sweden.
- Trägårdh, P., 2003 "Roll Motion of Manoeuvring Ships" Proceedings of International Conference on Marine Simulation and Ship Manoeuvrability, Vol. 3, pp. RC-9, Kanazawa, Japan.
- Van Terwisga, T., Quadvlieg, F., Valkhof, H., 2001, "Steerable Propulsion Units: Hydrodynamic Issues and Design Consequences" Paper written on the occasion of 80th anniversary of Schottel GmbH & Co, Germany.
- Vogt, M., 2005 "Manoeuvring Model Test for ROPAX vessel" Project Report (FASTPOD-GRD2-2001-50063), *Commercial in confidence*, HSVA, Germany.
- Woodward, M.D., Atlar, M., Clarke, D., 2005, "Manoeuvring induced loads on fast pod drives" FAST 2005, St. Petersburg, Russia
- Woodward, M.D., Atlar, M., 2006 "Pods – Guidance for the practising Naval Architect", Journal of Marine Design and Operation, Proc. IMarEST, N^o B9 2005/6 ISSN 1476-1556, pp 49-56.

On the Stability Characteristics of Different High Speed Craft

C. Bertorello, *Department of Naval Architecture and Marine Engineering, University of Naples Federico II, Naples, Italy*

S.Caldarella, *Department of Naval Architecture and Marine Engineering, University of Naples Federico II, Naples, Italy*

P.Cassella, *Department of Naval Architecture and Marine Engineering, University of Naples Federico II, Naples, Italy*

ABSTRACT

The demand of fast marine transportation has been increasing more and more during the last years and the sea transportation for passengers could become an alternative to land or air transportation.

Therefore, during the last years, the research has been focused on the multihull vessels, which for its larger deck area, its easy machinery arrangement should be preferred to the monohull.

In previous works, the hydrodynamic characteristics of the different vessels with equivalent service capabilities have been examined, as regard powering performances.

In this paper the comparison is extended to the stability characteristics according to the present IMO regulations.

1. INTRODUCTION

The increasing demand of high speed vessels has led to search for new unconventional ship hull forms. The new multihull vessels, can be subdivided into catamarans, trimarans and, more recently also pentamarans. At the present, the catamarans due to their wide deck area, high stability and safety at sea are the leading commercial type for short distance coastal trade.

Fast marine transportation with larger craft

sizes is now considered an attractive solution also for medium lines, where suitable high speed vessels could be used in competition with land and/or air transportation. The importance of this segment in the whole picture of marine transportation has called for further investigations, which suggested the study and the development of new multihull forms with lowest overall resistance and best seakeeping characteristics than the catamarans.

For this aim the trimaran and the pentamaran, based on a long slender main hull plus additional side hulls, with a very relatively small displacement volume, could be

interesting possibilities for the medium range routes.

Nevertheless trimaran ships have had a very limited use till now and there is very little information about pentamaran hull form and configuration.

Therefore, it seems important a comparison of the hydrodynamic performances and of the stability characteristics among the catamaran and these new proposed high speed multihull ships.

Basic designs for the three different multihull vessels, catamaran trimaran and pentamaran, have been developed to achieve equivalent service capabilities for transportation of 800 passengers and 250-300 cars at a cruising speed of 35-40 knots.

In previous works the hydrodynamic characteristics of these different vessels have been examined.

Different configurations for each considered multihull have been studied by experimental model tests and by numerical code application as regard powering performances.

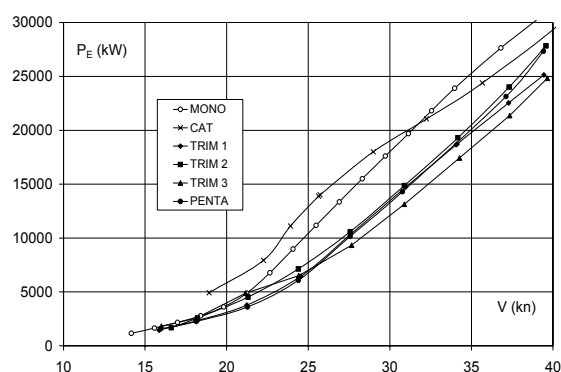


Fig 1. Effective horsepower for different multihulls and for equivalent monohull ship.

The prediction of trimaran and pentamaran resistance with a given main hull is substantially affected by dimension and location of the outriggers.

The hydrodynamic characteristics of trimaran and pentamaran configuration related to optimum outriggers location were compared in previous papers with those of equivalent catamaran.

Fig. 1 shows the comparison in the speed range $V=15-40$ knots among the effective horsepowers, evaluated by model tests with ITTC '57 methodology correlation and frictional line, for configurations of one catamaran, three trimarans, one pentamaran and for an equivalent monohull ship presently in service.

This figure highlights that, as regard powering performances in the range of medium high speeds the pentamaran and the trimaran seem interesting possibilities due to the benefits given by their very slender main hull form compared to the catamaran and the monohull ship.

In the considered speed 35-40 knots the trimaran indicated in the following with no. 3 presents the better performance. Anyway, to get a more complete picture about the potential of the different till now proposed multihulls intact and damaged stability must be considered.

Therefore, in this paper the comparison among the different multihulls is extended to the intact and damaged stability characteristics according to the present IMO regulations. Aim of this work is to verify if the catamaran and the considered hull configurations of the trimaran and pentamaran are suitable for a realistic ship to be used on medium range lines.

2. MULTIHULL FORMS FOR EQUIVALENT SHIP

First design requirements of multihull high speed ships to be used on medium routes for the transportation of 800 passengers and 250-300 cars are adequate deck area and displacement volume.

However, as the main dimensions of the passenger ships have constraints due to the port sizes, the maximum beam of all multihulls have been limited to 30 metres. So, hull designs of five different fast ships for equivalent service capabilities have been developed on the basis of a realistic general layout. They are:

- a hard chine catamaran (fig. 2);
- a first trimaran (fig. 3) having round bilge main hull derived from series 64 and outriggers having length 30% of the main hull length, and hull form derived also from series 64;
- a second trimaran (fig. 4) having the same main hull of the first trimaran and outriggers having length 30% of the main hull length, characterized by simple U section with a very small transom and a larger outrigger displaced volume in comparison with the first trimaran ;
- a third trimaran (fig. 5) having hard chine main hull form and the same outriggers of the second trimaran;
- a pentamaran (fig. 6) having the same main hull of the first trimaran with forward and after outriggers having length 20% of the main length, whose hull forms have been derived by geometrical affinity also from series 64

The principal characteristics of the five considered multihull ships in full scale are given in Table 1.

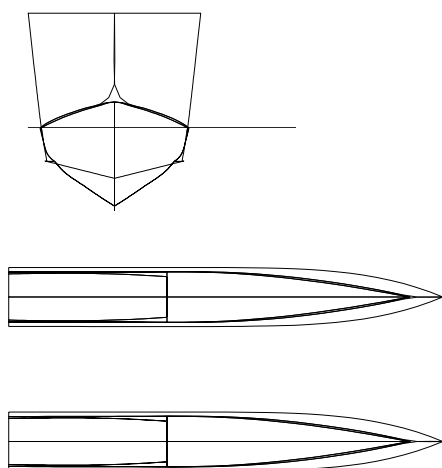


Fig 2. Catamaran hull form

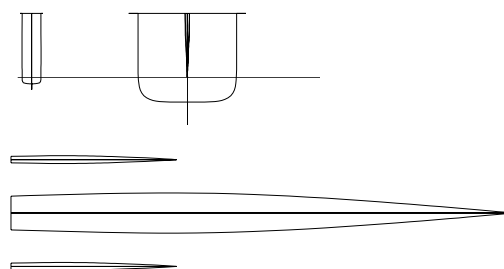


Fig 3. Hull forms and configuration of trim. 1

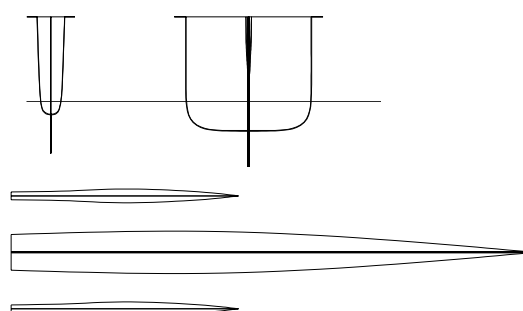


Fig 4. Hull forms and configuration of trim. 2

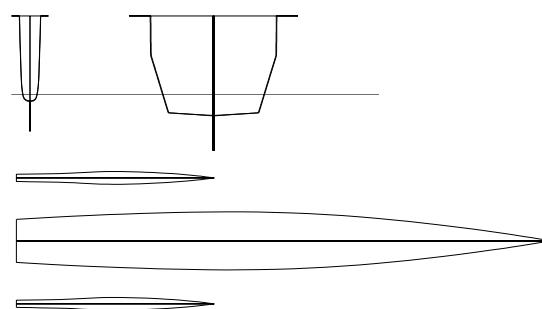


Fig 5. Hull forms and configuration of trim. 3

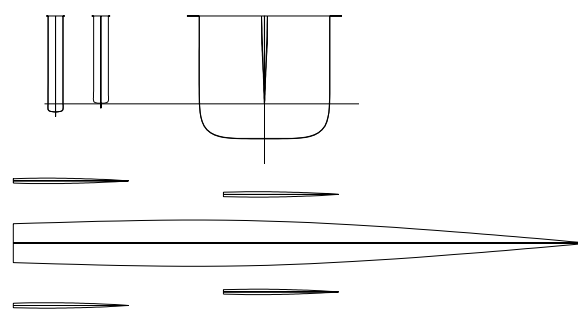


Fig 6. Hull forms and configuration of pentamaran

Tab.1 Main dimensions of the considered hullforms in full scale

	Trim.1	Trim. 2	Trim. 3	Pent.	Cat.
Δ [t]	2320	2320	2320	2320	2320
L_{wl} [m]	105.6	105.48	123.32	105.6	91.354
B [m]	25.137	25.699	30.477	24.796	28.016
T [m]	3.24	3.028	3.481	3.234	3.082
D [t]	9.4584	9.3798	10.4654	9.3872	9.6612

3. STABILITY CHARACTERISTICS

The considered ships with displacement volume of 2500 cubic metres and cruising speed of 35-40 knots have been treated as high speed craft, being this speed higher than

$$V(\text{m/sec}) > 3.7 \nabla^{0.1667} = 13.5 \text{ m/sec} = 26.2 \text{ knots}$$

Therefore, the stability characteristics have been examined according to the International Code of Safety for high-speed craft (IMO HSC Code 2000).

3.1 Intact Stability

Fig. 7 shows the curves of the stability arms GZ versus heel angles for the following conditions of the five considered multihull ships:

- Freeboard-Beam ratio $f/B = 0.20$
- Height of gravity centre - depth moulded ratio $KG/D = 0.60$ (as the stability criterion has not been satisfied for the pentamaran, only for this ship has been considered also the value $KG/D = 0.55$).

In order to verify the stability criteria, the quantities HL_1 , heeling lever due to wind and HTL , heeling lever due to wind+gusting + passengers crowding evaluated, as IMO Code, have been compared with the righting arm curves.

In applying both these criteria and those related to stability in damage condition, the total passengers weight $75 \text{ kg} \times 800 = 60 \text{ t}$, has been situated at 1.0 m of the ship's side.

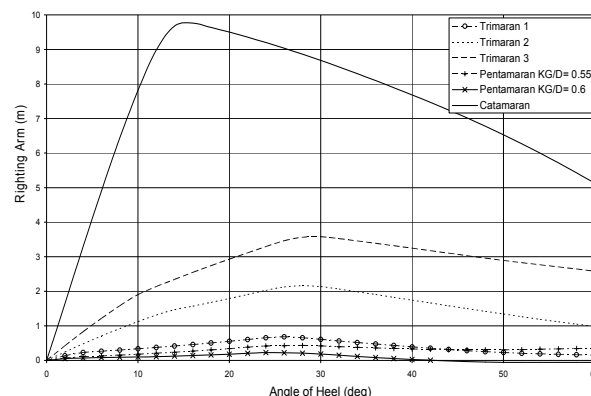


Fig 7. Intact stability curves for intact conditions of the hulls

Tables 2 report the obtained values for the required indexes of the intact stability related to the considered five ships:

- The area A_1 under the GZ curve which should be:

$$A_1 = 0.055x \quad 30^\circ/\theta \quad (\text{m.rad})$$
 (determined for the angle θ at which the maximum GZ occurs)
- The residual area under GZ curve A_2 ,
- which should be at least equal to 0.028 m.rad (determined for the angle of roll θ_r , taken as 15° in absence of model tests)
- The angle Θ_m at which the maximum GZ occurs, which should be at least 10°
- The angle of heel Θ_h due to heeling lever HL_1 , which should not exceed 16° .

Tab.2 Evaluated stability indices for intact conditions A_1 and A_2

Δ 2320	Trim.1	Trim. 2	Trim. 3	Pent.	Pent.2	Cat.
KG [m]	5.675	5.628	6.279	5.63	5.163	5.80
GM_t [m]	3.939	6.938	12.18	1.8	2.272	47.3
Θ_h [°]	3.64	1.82	1.376	22.5	0.244	12.2
Θ_m [°]	26	28.2	29.3	24.4	15.3	27.8
HL_1 [m]	0.133	0.134	0.182	0.13	0.131	0.12
HTL [m]	0.214	0.215	0.287	0.21	0.211	0.2
A_1 [m rad]	0.181	0.652	1.142	0.05	0.119	1.56
A_2 [m rad]	0.039	0.208	0.347	.0039	0.032	1.48

The analysis limited to intact stability highlights that in the case of $KG/D = 0.60$ we have stability excessive for the catamaran,

satisfactory for the three different trimarans, but unsatisfactory for the pentamaran. For this last ship the criteria have been satisfied only with the lower $KG/D=0.55$.

However, the operability of catamaran on medium routes is sensibly reduced because its excessive stability and consequently the lack of the comfort on board due to the high roll induced acceleration, the heave and pitch motions at sea in rough weather.

Fig.8-9 show the histograms of the obtained values A_1 and A_2 compared with the required values.

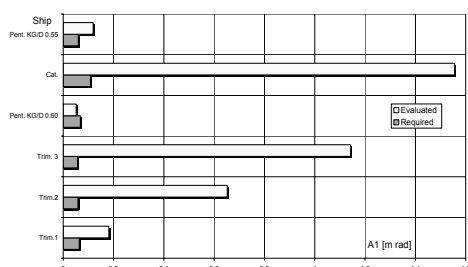


Fig. 8 Obtained values A_1 compared with the required values

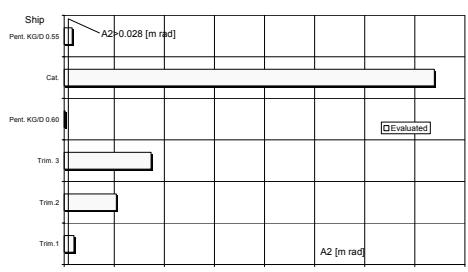


Fig. 9 Obtained values A_2 compared with the required value

3.2 Stability after damage

The following damages have been considered to occur separately on the surface of the hull from the most forward point of under water volume between the keel and the upper limit of the vulnerable area defined by IMO code (fig.10):

- For the single hull of the catamaran and for both the main hull of trimaran and

pentamaran two damages, one on the bottom and one on the side.

- For the side hull of the second and the third trimaran only one damage on the bottom.

As required by IMO Code related to multihull high sped craft, the following damage dimensions were considered:

- longitudinal extension equal to 0.55% of the length L ;
- penetration normal to the shell equal 0.5 m. (Fig.11);
- transversal extensions equal to 3.0 m being this dimension higher than the double of the required $0.1 \nabla^{1/3}$ girth along the shell.

One of the side hulls of the pentamaran and the side hull of the first trimaran, because of their limited dimension, were considered completely flooded up to upper limit of vulnerable area.

In order to verify the stability criteria for damage condition the quantities HL_3 , heeling lever due to steady wind and HL_4 , heeling lever due to wind + passengers crowding, evaluated as IMO Code have been compared with the righting arm curves in damage condition.

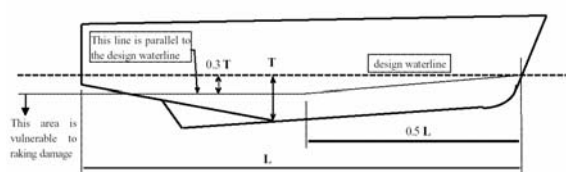


Fig 10. Vulnerable area

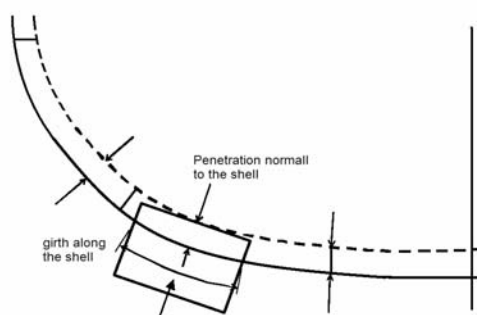


Fig 11. Transverse damage figure

Tables 3 and 4 give for the five examined multi-hull ships the obtained values HL_4 , θ_h and A_2 related respectively to the damage on the bottom and damage on the side of the single hull of the catamaran and of the main hull of trimarans and pentamaran.

Table 5 give the same indices related to the damage, as above considered, on the outrigger of the trimarans and of the pentamaran.

The angle of heel θ_h due to the wind heeling lever, after damage, should not exceed 20° .

In figg.12,13,14 the residual stability curves related to the above mentioned damages are given. In figg.15,16,17 the corresponding histograms of the obtained values A_2 compared with the required value $A_2 \geq 0,028$ m.rad. are presented.

The analysis of histograms relating to stability indices after damage highlights that the residual stability in any case is insufficient for the pentamaran and fully sufficient for the other examined multihulls, but very high again for the catamaran.

Tab.3 Evaluated stability index A_2 for damage on the bottom condition

Δ 2320	Trim.1	Trim2	Trim. 3	Pent.	Pent.2	Cat.
KG [m]	5.675	5.628	6.279	5.632	5.16	5.797
θ_h [°]	11.5	3.391	2.449	****	21.48	0.733
HL4 [m]	0.394	0.41	0.519	0.41	0.41	0.456
A_2 [m rad]	0.049	0.202	0.334	****	0.012	1.457

Tab.4 Evaluated stability index A_2 for damage on the side condition

Δ 2320	Trim.1	Trim2	Trim. 3	Pent.	Pent.2	Cat.
KG [m]	5.675	5.628	6.279	5.632	5.16	5.797
θ_h [°]	13.07	3.686	2.457	****	23.41	0.635
HL4 [m]	0.394	0.41	0.519	0.41	0.41	0.456
A_2 [m rad]	0.044	0.193	0.328	****	0.002	1.468

Tab.5 Evaluated stability index A_2 for damage on the outrigger condition

Δ 2320	Trim.1	Trim2	Trim. 3	Pent.	Pent.2
KG [m]	5.675	5.628	6.279	5.632	5.16
θ_h [°]	12.924	5.77	3.538	****	23.457
HL4 [m]	0.394	0.41	0.519	0.41	0.41
A_2 [m rad]	0.043	0.185	0.319	****	0.003

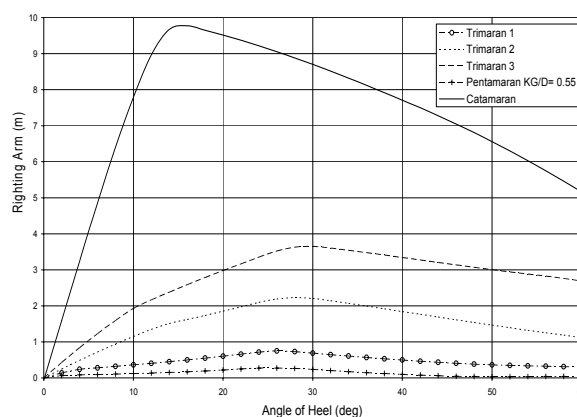


Fig 12 . residual stability curves for damage on the bottom

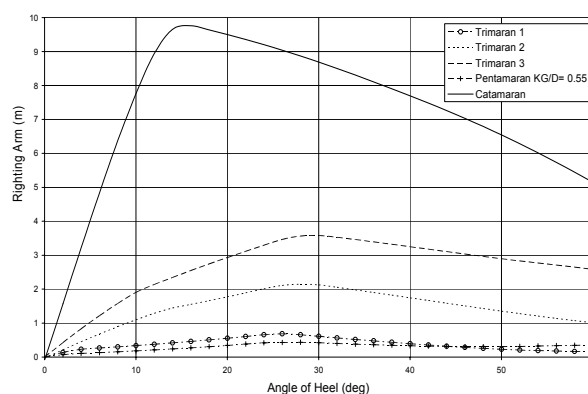


Fig 13. residual stability curves for damage on the side

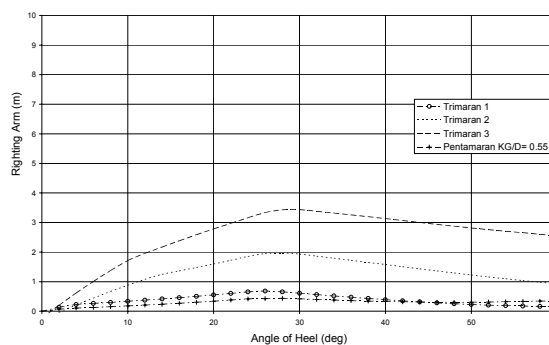


Fig14. residual stability curves for damage on the outriggers

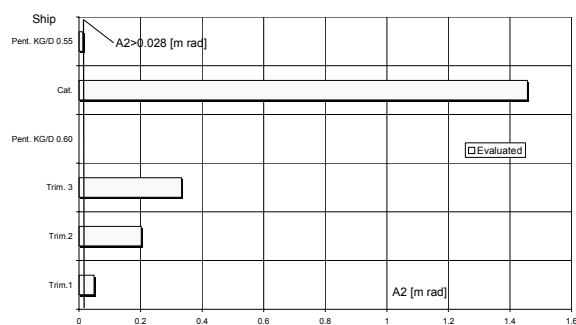


Fig 15. obtained values A_2 compared with the required values for damage on the bottom

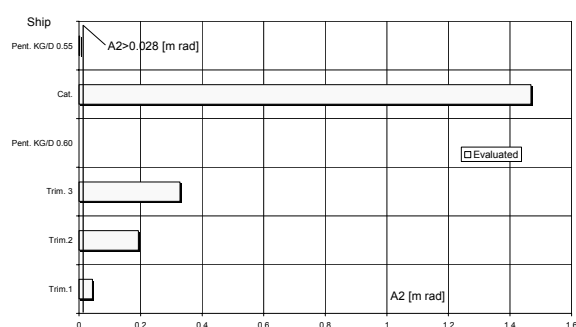


Fig16. obtained values A_2 compared with the required values curves for damage on the side

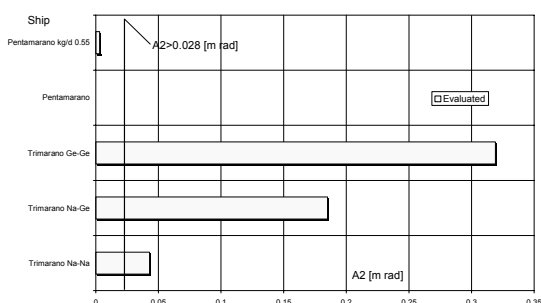


Fig 17. obtained values A_2 compared with the required values curves for damage on the outriggers

4. CONCLUSIONS

The speed of the marine vehicles has been increasing more and more during the last years.

Comparing the different high speed craft presently in service, it appears that the leading commercial types are:

- the catamaran for short routes ;
- the monohull for medium routes, being the

operability of the catamaran on medium routes sensibly reduced because its excessive stability.

New proposed high speed craft, trimaran and pentamaran, with a very slender unstable central hull stabilised by very small side hulls, for their powering performances, stability characteristics and comfort on board, large deck area and cargo capabilities seem definitely better than the equivalent monohull at medium and high F_n .

However, for minimum resistance, the side hulls should be very small to provide stability the side hulls should be large above the waterline and it is very important the choice of their hull form and dimensions.

At the present time, although the research in the field of these new proposed high speed vessels is grown significantly in the last years, there is still little information on the suitable multi-hull forms, dimensions, configuration and on the comparison of the performance and of the safety among the different vessels.

This paper has outlined an investigation relating to one pentamaran configuration, to three trimarans of various hull forms and configurations and to an equivalent catamaran.

The comparison among the considered vessels, carried out in the previous researches on the resistance in the Froude Number range 0.55-0.65, which is operative for the considered ships, has been based purely on static stability calculations, that do not take into account the dynamic effects of the marine environments.

From the results obtained the trimaran configuration no. 3 presents better powering and stability characteristics than the other examined multihull configurations.

Further studies should be necessary also for the performance of these craft in a realistic sea state. This will give a clearer picture of the multi-hull ships performance.

The results of this study are applicable only to the considered hull forms and configurations.

Other hullform and configurations of multihull vessels should be examined; however, from the obtained results, it seems that the trimaran has to be seen as a possible competitor to the high speed monohull ship for medium routes.

5. ACKNOWLEDGEMENTS

This work has been supported by the Italian Ministry of University and Scientific Research in the frame of the 2005-2006 research plan.

6. REFERENCES

- Begovic E., Bertorello C., Caldarella S., Cassella P., 2004, "Pentamaran Hull for Medium Size Fast Ferries" Proceedings of ICHD Conference, Perth, (Australia).
- Begovic E., Bove A., Bruzzone D., Caldarella S., Cassella P., Ferrando M., Tincani E., Zotti I., 2005, "Co-operative Investigation into Resistance of Different Trimaran Hull Forms and Configurations", Proceedings of the 8th International Conference on Fast Sea Transportation, St.Petersburg, (Russia).
- Bertorello C., Bruzzone D., Caldarella S., Cassella P., Zotti I., 2003, "On Hydrodynamic Performance of High Speed Crafts", Proceedings of the 7th International Conference on Fast Sea Transportation, Ischia (Italy).
- Bertorello C., Bruzzone D., Cassella P., Zotti I., 2001, "Experimental Performance Investigation on Different High Speed Crafts: Monohull Catamaran and Trimaran", Proceedings of 2nd HIPER 2001, Hamburg (Germany)
- Doctors L. J. and Scarce R. J., 2003 "The Optimisation of Trimaran Sidehull Position for Minimum Resistance", Proceedings of the 7th International Conference on Fast Sea Transportation, Ischia (Italy).
- Gee N., and Roy J., 2003 "The Effect of the Length on the Powering of Large Slender Hull Forms", Proceedings of the 7th International Conference on Fast Sea Transportation, Ischia (Italy).
- Yeh H.Y.H., 1965 "Series 64 Resistance Experiments on High Speed Displacement Forms", Marine Technology.
- IMO-International Code of Safety for High-Speed Craft – HSC CODE 2000

A Study on Transverse Stability Loss of Planing Craft at Super High Forward Speed

Toru Katayama, *Osaka Prefecture University*

Masashi Fujimoto, *Osaka Prefecture University*

Yoshiho Ikeda, *Osaka Prefecture University*

ABSTRACT

In this study, the mechanism of a transverse stability loss at super high forward speed is investigated. Towing tank test is carried out to observe the characteristics of the instability and it is confirmed that the instability has strong relationship to the change in running attitude and hydrodynamic roll moment due to high forward speed. Using some existing empirical formulas to estimate the dynamic normal force ($\rho V^2 S C_L$) on a planing surface, an estimation method of inception of the unstable phenomenon is proposed and its validity is confirmed through comparing with measured results.

Keywords: *Planing Craft, Transverse Stability Loss, Super High Forward speed, Lift*

1. INTRODUCTION

Following the demand of improvement in the speed of a planing craft which exists, if its thrust power is increased, the directional instability with transverse stability loss is often caused. Therefore, in order to secure safety, the elucidation of the cause of occurrence of this instability, the development of the estimation method in a design stage and the proposal of the evasion method are desired.

In this study, the transverse stability loss caused in connection with the directional stability loss is investigated. The transverse stability loss is simulated by a model test and its characteristics are indicated. Fundamental cause of the unstable phenomenon is revealed from the view point of the hydrodynamics. Moreover, an estimation method of occurrence of the unstable phenomenon is proposed.

2. OBSERVATION OF UNSTABLE PHENOMENON BY EXPERIMENT

2.1 Experimental Procedure

Schematic views of experimental setup are shown in Figure 1. A model, which is free in heaving, pitching and rolling, is attached to the high-speed towing carriage through a 3-components load-cell and it is towed horizontally at constant forward speed. Running attitude (θ ; rise, trim angle and heel angle) is measured. In the above-mentioned test, if the model heels over, that indicates the occurrences of the transverse stability loss. As additional test, the measurement of rise and trim angle at rolling fixed to upright condition is also carried out in the same experimental condition, when the model heels over.

In the experiment, two models with different features are used. The body plans are shown in Figure 2. The model M2025, upper side of the

figure, has constant deadrise angle and its form behind the square section number 5.0 is almost prismatic planing surface. On the other hand, another model TB-45 is a deep V monohedron type planing craft and its deadrise angle becomes gradually large ahead. The principle particulars are shown in Table 1.

2.2 Occurrence of Unstable Phenomenon

The measured results of the model M2025 are shown in Figures 3 to 5, and the measured results of the model TB-45 are shown in Figures 7 to 9, respectively. The square mark shows the result when the models are fixed in roll to upright, and the circle mark shows the results when the models are free in roll. Furthermore, the water plane areas for still water surface are obtained from the measured running attitude shown in these figures at roll fixed to upright, and they are shown in Figures 6 and 10.

For the model M2025, the heeling occurs at $Fn=4.9$, and its angle is 7 degrees. The running attitude (rise and trim angle) with the heeling is almost the same as the running attitude without heeling. And the running attitude is continuously changed according to increment of forward speed. Then the water plane area becomes gradually small and narrow triangle according to increment of forward speed.

On the other hand, for the model TB-45, at higher forward speed than $Fn=2.2$, the large heeling occurs and it reaches to 20 degrees. The running attitudes with and without heeling are shown in Figures 7 and 8. And they have large difference. The water plane areas shown in Figure 10 are drastically changed at higher forward speed than $Fn=2.2$ and it becomes narrow pentagon.

For both models, the heeling, which is a transverse instability, is observed at high forward speed range. And the water plane areas of both models become narrow when the instability occurs. From the results, it is

supposed that the point of action of the dynamic normal force on planing surface approaches the keel line according to decrement of the water plane breadth and the roll restoring moment is decreased.

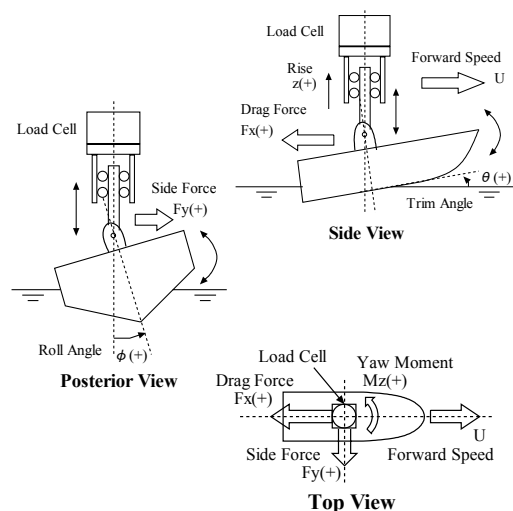


Figure 1 Schematic view of experiment and coordinate system.

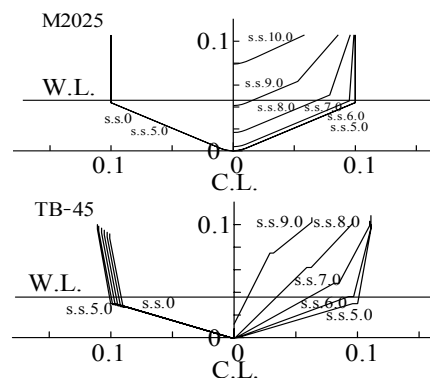


Figure 2 Body Plans of M2025 & TB45.

Table 1 Principal particulars & experimental conditions.

Model	M2025	TB-45
all over length: L_{OA} (m)	0.6	1.0
breadth: B (m)	0.20	0.22
depth: D (m)	0.106	0.102
draft at transom: d_a (m)	0.0403	0.0365
displacement: W (kgf)	2.8	3.1
initial trim angle (degree)	-2.258	0
height of the center of gravity: KG (m)	0.097	0.140
deadrise angle (degree)	25	18
longitudinal towing position from transom (m)	0.240	0.435
height of towing position from Base-Line (m)	0.149	0.075
towing speed (m/sec)	5 - 12	5 - 14

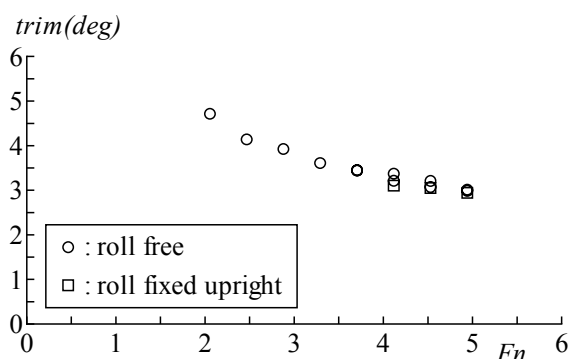


Figure 3 Measured pitching (trim angle) for M2025.

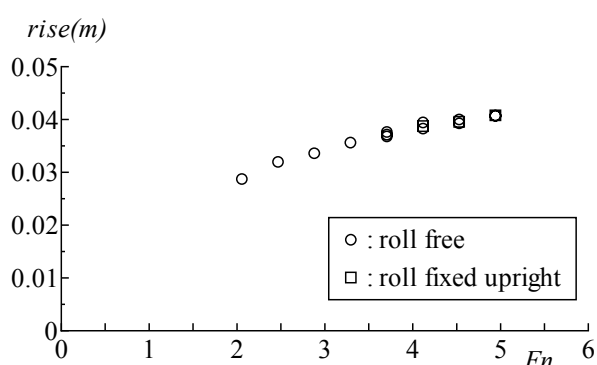


Figure 4 Measured heaving (rise) for M2025.

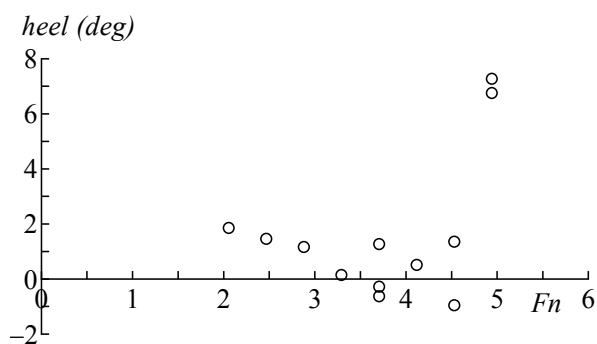


Figure 5 Measured rolling (heel angle) for M2025.

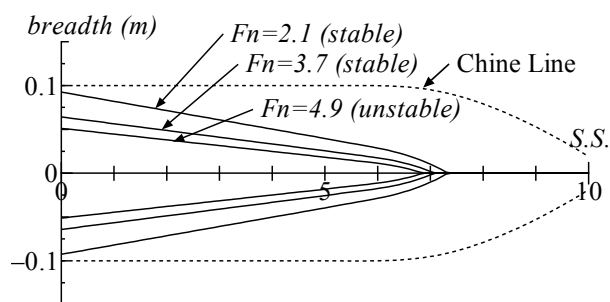


Figure 6 Water plane area for still water surface of M2025 at running condition.

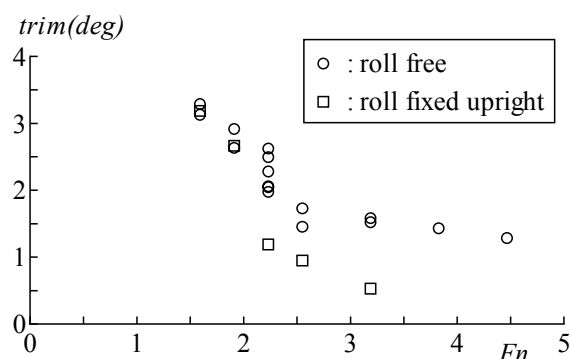


Figure 7 Measured pitching (trim angle) for TB-45.

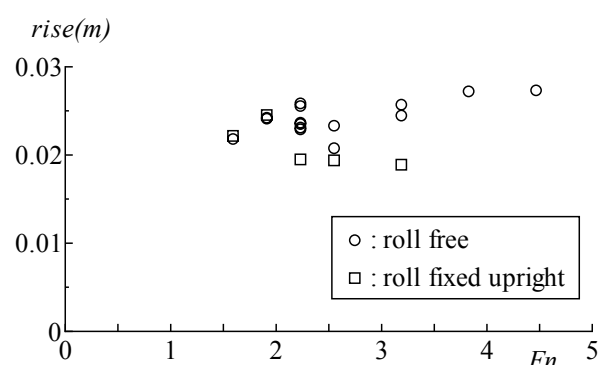


Figure 8 Measured heaving (rise) for TB-45.

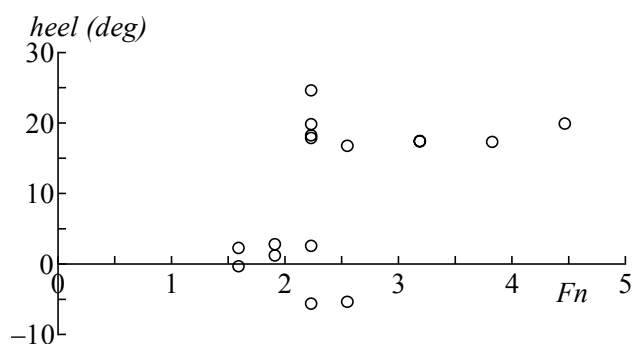


Figure 9 Measured rolling (heel angle) for TB-45.

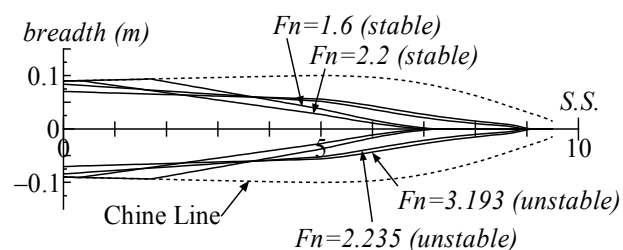


Figure 10 Water plane area for still water surface of TB-45 at running condition.

3. MECHANISM OF INSTABILITY

In the previous paper (Edward M. Lewandowski, 1996), an estimation method of roll restoring moment for planing hull is presented. However, it is difficult to apply the method to the hull shape which has the large difference from prismatic surface because some equations of the method are based on prismatic surfaces (Daniel Savitsky and P. Ward Brown, 1976). In order to ease the limitation, in this paper, based on a strip method, the total roll restoring moment of a 3D V-bottom planing hull is obtained. And the inspection method of transverse stability loss for 3D V-bottom hull is presented.

3.1 Roll Restoring Moment and Instability for 2D V-Bottom Planing Surface

As shown in Figure 11, if a craft has small heeling angle around the center of gravity, the relative deadrise angle to water surface decreases at the planing surface of the heeling side and the dynamic normal force on the side increases, moreover the point of action of the dynamic normal force moves outside. On the other hands, the relative deadrise angle increases at another side and the dynamic normal force on the side decreases, the point of action of the dynamic normal force moves inside. The roll moments caused by the dynamic normal forces on the each side of planing surface are written by the following formulas.

$$\{(cp + \Delta cp_+) - KG \sin \beta\}(N + \Delta N_+) \quad (1)$$

$$(-1)\{(cp - \Delta cp_-) - KG \sin \beta\}(N - \Delta N_-) \quad (2)$$

The next formula is obtained by adding Formulas (1) and (2) and the roll restoring moment caused by hydrostatic pressure.

$$(cp_{x+} - KG \sin \beta_x)N_{x+} - (cp_{x-} - KG \sin \beta_x)N_{x-} + M_{Bx} = M_x \quad (3)$$

where

$$\begin{cases} N_{x+} = N_x + \Delta N_{x+} \\ cp_{x+} = cp_x + \Delta cp_{x+} \end{cases} \begin{cases} N_{x-} = N_x - \Delta N_{x-} \\ cp_{x-} = cp_x - \Delta cp_{x-} \end{cases}$$

Equation (3) is the sectional roll restoring moment for 2D V-bottom planing surface.

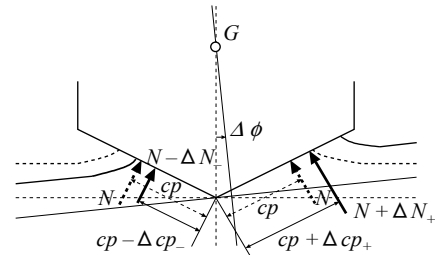


Figure 11 Dynamic normal force on a cross section of V-bottom planing surface with heeling and its point of action.

3.2 Estimation of Transverse Stability Loss for 3D-V Bottom Planing Hull

The roll restoring moment is obtained by integrating with the sectional roll restoring moment expressed by Equation (3).

$$M = \int_A^F M_x dx \quad (1)$$

Moreover, the following equation is obtained by dividing Equation (4) by ship weight W and small heeling angle $\Delta\phi$.

$$\frac{M}{W \cdot \Delta\phi} \quad (5)$$

Equation (5) is similar to the slope of GZ -curve around upright condition. If it is negative, the craft can not keep upright condition.

In the following part, the ways to calculation of the two terms (cp_x and N_x) in Equation (3) are explained. The position of action of the dynamic normal force on the one side of planing surface is expressed the following equation (Robert. F. Smiley, 1996).

$$cp = E_2 \frac{\pi}{4} c \quad (6)$$

In this equation, E_2 is equal to 0.8 for chines-wet condition, and E_2 is equal to 1.0 for chines-dry condition. And the variables in this equation are shown in Figure 12.

The position of action of the dynamic normal force on the one side of planing surface with small heeling $\Delta\phi$ around the center of gravity shown in Figure 11 is obtained by substituting c_{x+} or c_{x-} for Equation (6).

$$cp_{x+} = E_2 \frac{\pi}{4} c_{x+} = \frac{E_2 \pi^2 \{ \xi_x + (\cos \Delta\phi - 1) KG \}}{8 \cos \beta_x \cos \Delta\phi (\tan \beta_x - \tan \Delta\phi)} \quad (7)$$

$$cp_{x-} = E_2 \frac{\pi}{4} c_{x-} = \frac{E_2 \pi^2 \{ \xi_x + (\cos \Delta\phi - 1) KG \}}{8 \cos \beta_x \cos \Delta\phi (\tan \beta_x + \tan \Delta\phi)} \quad (8)$$

where ξ_x , β_x , KG are the variables shown in Figure 12.

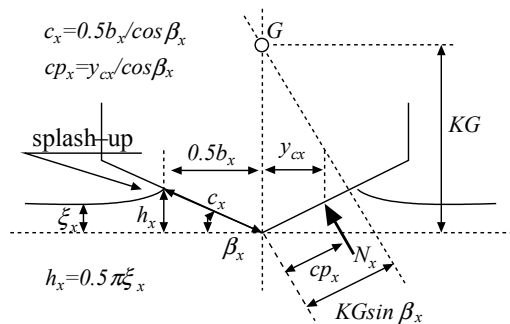


Figure 12 Symbols expressing geometric relations among the water surface, a cross section of planing surface and dynamic normal force on the cross section.

The sectional dynamic normal force on one side of a planing surface per unit length dN/dx is given by the following equation using the sectional dynamic normal force on the keel of a planing surface per unit length dR/dx .

$$\frac{dN}{dx} = \frac{1}{2 \cos \beta_x} \frac{dR}{dx} \quad (9)$$

A formula proposed by Peter R. Payne (1996) based on the momentum method is adopted as the sectional dynamic normal force on the keel of a planing surface per unit length.

$$\frac{dR}{dx} = u_0 \cos \tau \frac{d}{dx} [m'_x v] \quad (10)$$

where u_0 is forward speed, $v (=u_0 \sin \tau)$ is fluid velocity component normal to planing surface, τ is running trim angle. The m'_x is the sectional added mass of a cross-section per unit length, and it is expressed by the next equation.

$$m'_x = C_{m'_x} \frac{\pi}{2} \rho \left(\frac{b_x}{2} \right)^2 f(A) \quad (11)$$

$$f(A) = \frac{1}{\sqrt{1 + (KA)^2}}$$

$$K = \frac{1}{4} + \sqrt{\frac{2\beta_x}{\pi}}, A = \frac{b^2}{S}$$

where b is chine beam at transom, b_x is a local wetted beam including splash up effects, S is projection of the wetted surface area in the reference plane of a planing surface. $C_{m'_x}$ is added-mass coefficient, and it has two different values for chines-wet and chines-dry conditions as the following.

For chines-dry condition:

$$C_{m'_x} = \left(1 - \frac{\beta_{Ex}}{2\pi} \right)^2 \quad (12)$$

For chines-wet condition:

$$C_{m'_x} = \left(1 + k \frac{z_{cx}}{b_x} \right) \left(1 - \frac{\beta_{Ex}}{2\pi} \right)^2, k = 2 \quad (13)$$

where β_{Ex} in Equations (12) and (13) is called the effective deadrise angle, and it is expressed

as $\tan\beta_{Ex} = \tan\beta_x / \cos\tau$. z_{cx} is chine submergence below the level at which the “splash-up” first wets the chine shown in Figure 13.

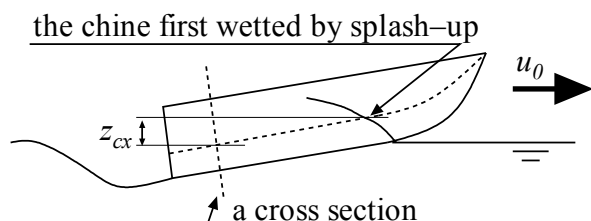


Figure 13 Local chine submergence below the level at which “splash-up” first wets the chine.

The sectional dynamic normal force on one side of a planing surface with small heeling shown in Figure 11 (N_{x+} and N_{x-}) is calculated by substituting b_{x+} , β_{x+} (or b_{x-} , β_{x-}) in Figure 14 and z_{cx+} (or z_{cx-}) with small heeling for Equations (7) to (11).

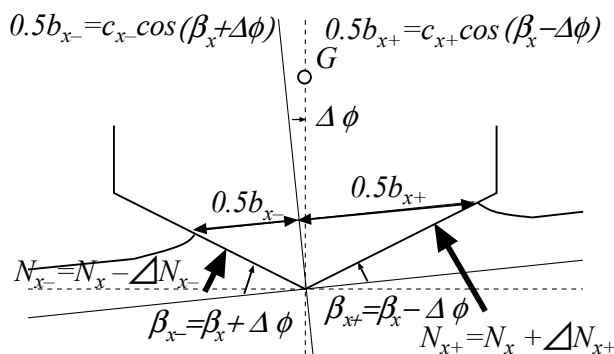


Figure 14 Symbols expressing geometric relations between the water surface and a cross section with small heel.

3.3 Fundamental Cause of Transverse Stability Loss

The estimation results of stability criteria for Model TB-45 and M2025 are shown in Figures 15 and 16, respectively. In Figure 15 for TB-45, two criteria are shown, on the other hand, in Figure 15 for M2025, one criterion is shown.

The longitudinal distribution of sectional roll restoring moment and the wetted surface area including splash up effects for TB-45 are shown in Figure 17. The figure shows the results at $d_a = 0.023$ m and $\tau = 1.0$ deg. In this case, the sectional roll restoring moment is negative at the front of the wetted surface and about square section number 2.0. From the investigation of calculation process, it is found that negative at the front is caused by decrement of sectional draft. On the other hand, negative about S.S.2.0 is caused by unsymmetrical wetted chine length according to heeling in the case which is chines-wet condition.

In Figure 18, the longitudinal distribution of sectional roll restoring moment and wetted surface area including splash up effects for TB-45 at $d_a = 0.011$ m and $\tau = 1.0$ deg are shown. And in Figure 19, those for M2025 at $\tau = 3.0$ deg on the stability limit line in Fig.16 are shown. In these figures, both results indicate the same tendency. From the investigation of calculation process of the sectional roll restoring moment, it is found that the negative value of the sectional roll moment is only caused by decrement of sectional draft in the case which is chines-dry condition.

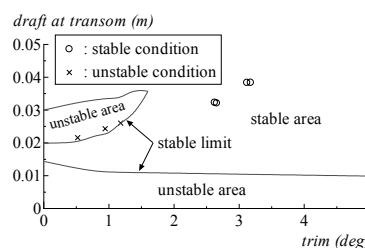


Figure 15 Stable limit for TB-45 shown on running attitude.

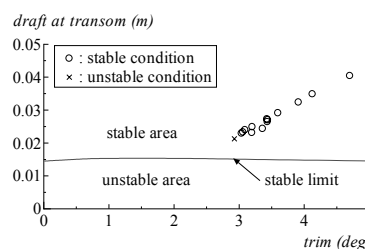


Figure 16 Stable limit for M2025 shown on running attitude.

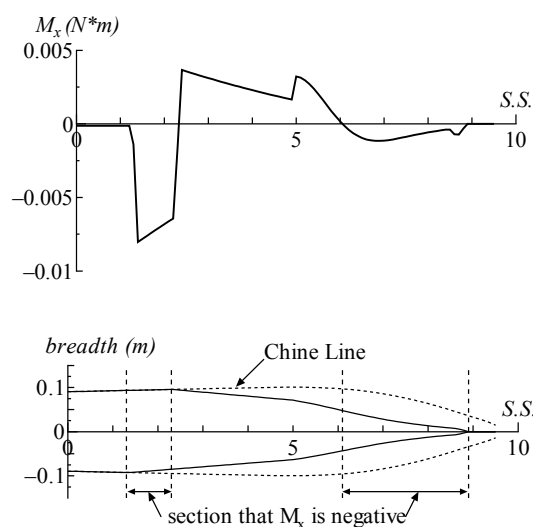


Figure 17 Longitudinal distribution of calculated roll restoring moment and wetted surface area including splash up effects for TB-45 at $d_a = 0.023$ m and $\tau = 1.0$ deg.

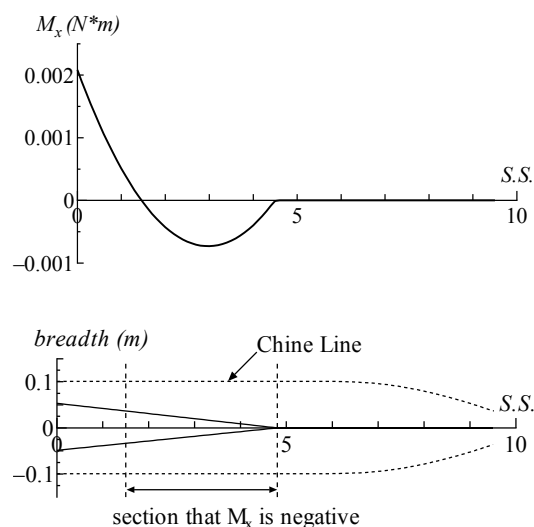


Figure 19 Longitudinal distribution of calculated roll restoring moment and wetted surface area including splash up effects for M2025 at $\tau = 3.0$ deg on the stability limit line in Fig.16.

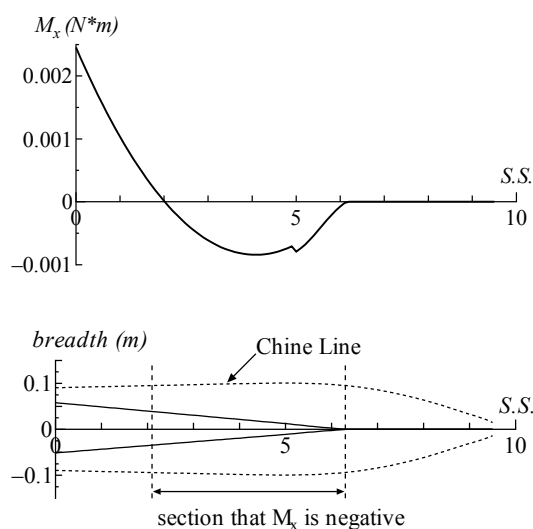


Figure 18 Longitudinal distribution of calculated roll restoring moment and wetted surface area including splash up effects for TB-45 at $d_a = 0.011$ m and $\tau = 1.0$ deg.

4. CONCLUSIONS

In this study, the fundamental cause of a transverse stability loss at super high forward speed is investigated and the following conclusions are obtained.

- 1) A transverse stability loss is simulated by

- 2) towing tank tests.
- 3) Using some existing empirical formulas proposed by Robert F. Smiley (1952) and P. R. Payne (1994), it is indicated that the transverse stability loss is caused by change in running attitude according to increment of forward speed.
- 4) An estimation method of its stability criteria is proposed.

Using the estimation method proposed in this study, it is found that there are two unstable regions, for a conventional deep V monohedron planing craft, depending hull form.

5. REFERENCES

- Robert F. Smiley, 1952, "A Theoretical and Experimental Investigation of the Effects of Yaw on Pressures, Forces, and Moments during Seaplane Landing and Planing", NACA Technical Note 2817.
- Edward M. Lewandowski, 1996, "Prediction of the Dynamic Roll Stability of Hard-Chine Planing Craft", Journal of Ship Research, Vol.40, No.2, pp.144-148.

P. R. Payne, 1994, "Recent Developments in "Added-Mass" Planing Theory", Ocean Engineering, Vol.21, No.3, pp.257-309.

Daniel Savitsky and P. Ward Brown, 1976, "Procedures for the Hydro Evaluation of Planing Hulls in Smooth and Rough Water", Marine Technology, Vol.13, No.4, pp.381-400.

Results Using Response-Tailored Design Waves in Simulations of Extreme Roll of Multi-Hull Ships

Laura K. Alford, *University of Michigan*

Armin W. Troesch, *University of Michigan*

Muhamed Saeed Khalid, *University of Michigan*

ABSTRACT

Random, response-tailored wave trains are created for use in numerical simulations. Random wave trains generated by a finite number of components are tailored to produce a specified, linear, large response by considering the statistical distribution of the response phases in the neighborhood of a typical maximum response. The statistical distribution is seen to be non-uniform. Using a non-uniform distribution for the random phases of the response, design wave elevations leading to extreme roll motion may be calculated using linear theory and used as input to nonlinear seakeeping codes. Examples of design wave predictions resulting in extreme roll are included for various multi-hull ships.

Keywords: *response-tailored waves, non-uniform phase distributions, extreme roll, multi-hull ships*

1. INTRODUCTION

To properly design a structure, the naval architect must know what said structure must withstand over the course of its lifetime. To determine this, the designer traditionally has inflicted certain extreme conditions on the structure and estimated its response to these conditions to be the design response. When using computer simulations, these extreme conditions are usually an extreme sea state characterized by statistical parameters such as significant wave height and peak period. In these randomly simulated storms, however, there is no guarantee that the storm will produce the most likely extreme response.

The need to generate a specific extreme response has led to simulations involving response-tailored design waves: waves formulated such that the extreme response in question occurs during the finite time of the simulation. Recent research into response-

tailored design waves includes work by Adegeest (1999), Clauss (2004), and Alford (2005).

Alford's work focuses on creating conditions that result in extreme roll for use in capsize investigations for a box barge and a high-speed containership. The method constructs a response time series using linear superposition of sinusoidal waves with a *non-uniform* phase distribution. The non-uniform response phase distribution produces a large linear response at a specified time. The incident wave phases are known from the linear seakeeping analysis and the response phases so the incident wave train may be calculated. This paper applies the above procedure to several concept models of high speed, multi-hull ships.

2. BACKGROUND

Even with modern computing power, nonlinear seakeeping analyses are expensive to

run. Simulating three hours of storm conditions may require days of real time computing resources. However, if the design conditions have been tailored to produce the design response it only becomes necessary to simulate a very short record as the design response is guaranteed to occur. In order to create the sea conditions that will produce a design response, consider the usual construction of a random wave train.

Assuming linearity, stationarity, and ergodicity of the ocean for a short period of time, one may represent the ocean surface at some

point (x,y) as the summation of many component waves:

$$\zeta(t) = \sum_{j=1}^N a_j \cos(\omega_j t + \beta_j) \quad (1)$$

- $\zeta(t)$ wave elevation
 N number of components
 a_j amplitude of j th component
 ω_j frequency of j th component
 β_j phase of j th component

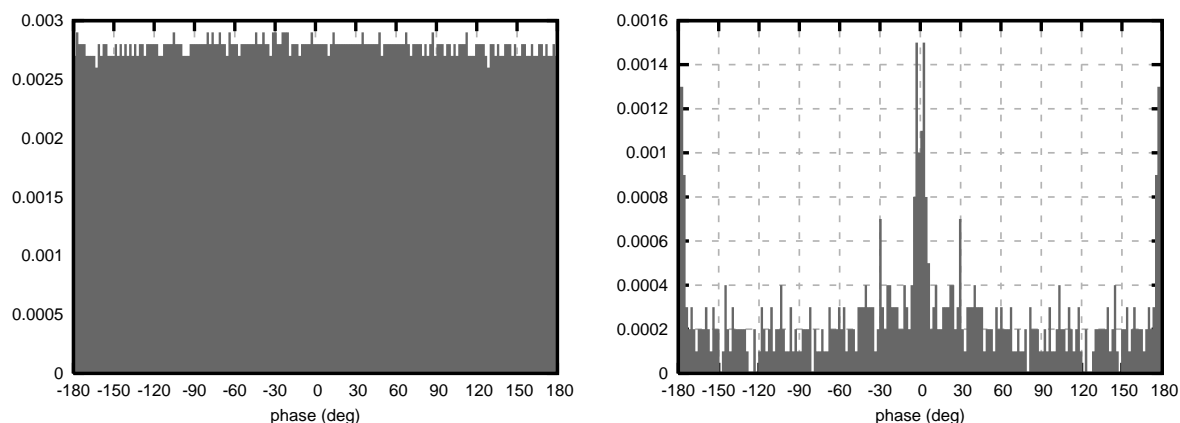


Figure 1 Phase distributions of two types of time series. *Left*: The combined phase distribution for 10 very long time series; $T = 104,857.6$ seconds, $\Delta t = 0.1$ seconds, $N = 1,048,576$ for each series. *Right*: The combined phase distribution for a short time series center about the maximum of each long time series; $T = 1638.4$ seconds, $\Delta t = 0.1$ seconds, $N = 16384$ for each time series.

The amplitudes and frequencies are determined by the spectrum (e.g. Pierson-Moskowitz, ITTC, Ochi 8-parameter, etc.) that will characterize the time series. The randomness enters through the phases, which are chosen from a uniform distribution between $-\pi$ and π . At each time step, the components are summed for the current t value and the wave elevation recorded. If this model is used to simulate many hours of exposure, eventually an extreme value will be recorded. Using the Fast Fourier Transform, any portion of the record may be broken down into its component amplitudes and phases. The number of compo-

nents is determined by the time step and the length of the resulting time series.

$$N = T_{record} / \Delta t \quad (2)$$

The shorter record, being a subset of the longer, has the same time step, Δt , as the long record. Therefore, it is clear that as the record length decreases, so too does the number of available components. Figure 1 shows the difference between the phase distribution resulting from the very long simulation and the phase distribution resulting from a very short portion ($\sim 1.5\%$) of the simulation that is centered around a large extreme value.

When the long time record is considered, the phases are approximately uniformly distributed; in the limit of an infinite number of wave phases and a finite extreme value, the distribution is uniform. However, for the short time series that includes the extreme value there are fewer components available (Equation 2), and the phases become focused in order to achieve the same maximum.

The resulting phase distribution of the short time series depends on many factors including:

- the crest height, especially as relates to the RMS of the process (a measure of how extreme the event is)
- the number of components and, by Equation 2, the length of the short record

The relationship between the extreme value and the phase distribution that produced it is currently unknown, but it is clear that a non-uniform distribution must be used if short simulations are to be considered the equal of full-length storm simulations. Indeed, it may even be considered superior to the storm simulations as the non-uniform distribution ensures that the extreme value will occur within the finite simulation time.

3. METHOD: SOLVING THE INVERSE PROBLEM

The procedure for creating a response-tailored design wave train assumes that the wave train that elicits a large linear response is similar to the wave train that produces a large nonlinear response. Based on the above analysis of the phase distribution associated with an extreme wave amplitude, an extreme response may be generated by using the response spectrum with a non-uniform phase distribution. Once the response is known, the incident wave may be back-computed according to linear systems theory, and the result will be response-tailored waves suitable for investigating anything from a design midship bending moment to extreme roll. Solving for the incident wave,

rather than the response, is known as the *inverse problem*.

The method used for this paper takes a simplified approach and assumes a zero-mean, Gaussian distribution with a given standard deviation for the response phases. In this paper, the response in question for all cases is roll.

The designer chooses a Target Extreme Value (TEV) of the response process to be produced. The TEV may be a function of many things, including: loading condition, heading angle, ship type, and sea state. Next, a linear seakeeping analysis is performed to calculate the 6 degrees of freedom (DOF) response amplitude operators (RAOs) of the ship and the RAO of the design response (if it is not one of the 6 DOF). The phases associated with the design response are then chosen according to a Gaussian distribution to ensure the extreme value chosen by the de-signer appears during the simulation, and the phases are then shifted so that the TEV occurs at the critical time. The phases for the incident wave are then back calculated via linear systems theory. Consider the representation of a linear system in Figure 2. Linear systems theory requires that the output have the same time dependence as the input, $e^{i\omega_j t}$, and due to the orthogonality property of Fourier Series the amplitude and phase of the output are:

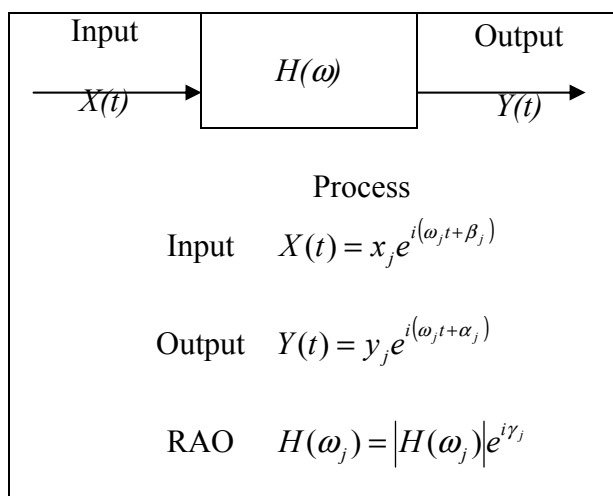


Figure 2 Definition of the Variables in a Linear System.

$$y_j = |H(\omega_j)|x_j \quad (3)$$

$$\alpha_j = \gamma_j + \beta_j \quad (4)$$

Conversely, if one knows the response, $Y(t)$, and the linear function, $H(\omega)$, the input may be calculated algebraically as:

$$x_j = \frac{y_j}{|H(\omega_j)|} \quad (5)$$

$$\beta_j = \alpha_j - \gamma_j \quad (6)$$

In this application, the input function is the incident wave, the linear function is the RAO of the response, and the output function is the design response. The relationships in Equations 5 and 6 hold for $j = 1, 2, \dots, N$ because of the properties of superposition and orthogonality in linear systems. With the incident wave now known to produce an extreme linear response, linear and nonlinear responses may be calculated and compared.

4. LINEAR ANALYSIS AND NONLINEAR TIME SIMULATION OF BLENDED NONLINEAR HYDRODYNAMIC FORCES ON MULTI-HULL SHIPS

The geometry of multi-hull ships increases the difficulty of not only nonlinear time simulations but even the linear, frequency domain calculations. Extensive modifications were made to an existing linear seakeeping code for monohulls in order to properly capture the geometry of a multi-hull ship and include the effects of forward speed.

For the nonlinear time domain simulation, the total dynamic and static pressure field acting on an arbitrary body floating in water is evaluated. The displacements and other kinematics such as the relative velocities, accelerations, etc., and the structural loads in terms of dynamic shear forces, bending and torsion moments, etc. are calculated using direct integra-

tion of the pressures resulting from large motions of a multi-hull ship in six degrees of freedom. The method employs quasi-nonlinear radiation and diffraction models, and body exact hydrostatic and Froude-Krylov pressures. Nonlinear time simulation of large motions with exact Euler angles, shear forces and moments for regular waves and random seas are calculated for six degrees of freedom. Corresponding to the instantaneous position of the body, the quasi-nonlinear radiation and diffraction pressures are obtained through two and three dimensional radial basis functions. The frequency dependent components of the pressures are then Fourier transformed into the time do-main to obtain blended time dependent nonlinear pressures conforming to the instantaneous position of the arbitrary shape of the body; the instantaneous position appropriately includes the partially or fully submerged top deck for calculating the blended nonlinear pressures and forces.

The nonlinearities come from Euler angles, large motions, and the exact instantaneous intersection of the body and free surface. The free surface is obtained by superimposing incident gravity waves and the radiated and diffracted waves. Forward speed end corrections are calculated by converting the two dimensional velocity potential into a three dimensional mathematical function via radial basis function then partial differentiation is performed with respect to the longitudinal direction. In order to restore the two dimensional characteristics of the boundary value solution, a backward conversion to two dimensions is done to obtain a two dimensional mathematical function for the combined quasi-nonlinear nodal radiation and diffracted pressures. For the given instantaneous position of the node, the established mathematical function will produce the quasi-nonlinear value of the combined radiation and diffraction pressure by keeping track of the relative position of the other nodes on the two dimensional segment/station. Comprehensive validation studies are currently underway for this nonlinear time simulator.

Table 1 Ship Particulars

Particulars	Catamaran		Compact Trimaran			Extended Length Trimaran		
	Overall Ship	Demi-hulls	Overall Ship	Side Hulls	Center Hull	Overall Ship	Side Hulls	Center Hull
LOA (m)	179	154	165.5	154	154	231	154	154
LWL (m)	154	154	154	154	154	231	154	154
B (molded, m)	32	11.2	55	10	10	55	10	10
Draft (m)	6.7	6.7	5	5	5	5	5	5
Displacement (t)	12,350	6175	12,350	4117	4115	12,350	4117	4115
Wet deck height (m)	11		9			9		
CL to CL (m)	20.8		22.5			22.5		
V_k (kts)	43		43			43		

5. RESULTS

The procedure described above has been used to create wave trains designed to induce extreme roll in three high speed, multi-hull ships: a catamaran, a compact trimaran, and an extended length trimaran. The hulls used to create all three ships are similar in length (see Table 1 for ship particulars) and differ in displacement such that each overall ship has the same displacement. The compact trimaran is essentially a catamaran hull in which a center hull has been added; in other words, the three hulls are placed “side-by-side-by-side”. For an interesting comparison, the extended length trimaran was created by moving the center hull of the compact trimaran forward by $L/2$.

The exercise presented in this paper compares wave trains that produce a TEV of $4.5\sigma_{\text{roll}}$ and $5.5\sigma_{\text{roll}}$ for each hull in ITTC Sea State 7 ($h_{1/3} = 7.5$ meters, $T_p = 15.0$ seconds). Here, σ_{roll} is the root-mean-square (RMS) of the roll process in Sea State 7. These TEVs have a probability of occurring of 1:25,000 and 1:3,700,000 respectively assuming a Rayleigh distribution for the peaks of the response. The

actual value of the TEVs depends upon the heading angle. To determine the most severe roll cases given the Sea State 7 conditions, polar plots of the roll RMS were constructed for each ship. The heading angle chosen for

the time simulations was that which produced the highest σ_{roll} . Therefore, while each extreme roll response that corresponds to a $4.5\sigma_{\text{roll}}$ or a $5.5\sigma_{\text{roll}}$ response has the same *probability*, it does not have the same *value*. This is just one choice of the Target Extreme Value needed in the procedure described above. The time simulations are 100 seconds long with the extreme response occurring at 50 seconds and use 201 non-zero wave components.

5.1 Catamaran

The roll polar plot for the catamaran is shown in Figure 3. The polar plot shows that the largest σ_{roll} occurs at a heading angle of 100° and has a value of 6.49° . Using this heading angle, the simulations in Figures 4 and 5 were created.

In both cases, the catamaran experiences a duration of enhanced roll both before and after the extreme roll event at $t = 50.0$. This duration seems to be about 25 seconds before and after the extreme event for the $4.5\sigma_{\text{roll}}$ case. For the $5.5\sigma_{\text{roll}}$ case, the duration before the extreme event is still around 25 seconds, but drops off to approximately 15 seconds afterwards. As for the wave train, it appears that a large roll angle for this catamaran is produced primarily by the slope of a single, large wave. Note that the wave height near the time of

maximum roll was $2.1h_{1/3}$ and $2.5h_{1/3}$ for the $4.5\sigma_{roll}$ and $5.5\sigma_{roll}$ responses, respectively.

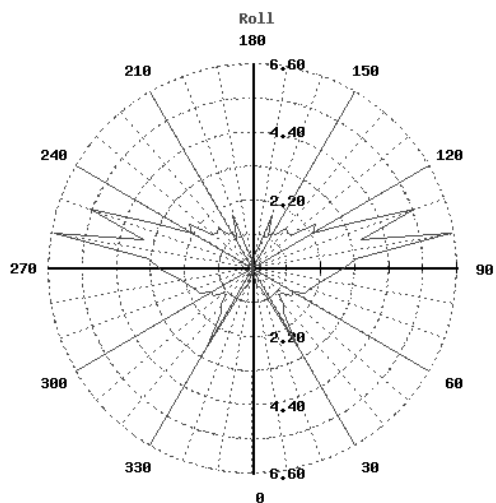


Figure 3 Symmetrical Catamaran: Polar plot - Roll RMS. ITTC Sea State 7. Forward speed = 43 kts.

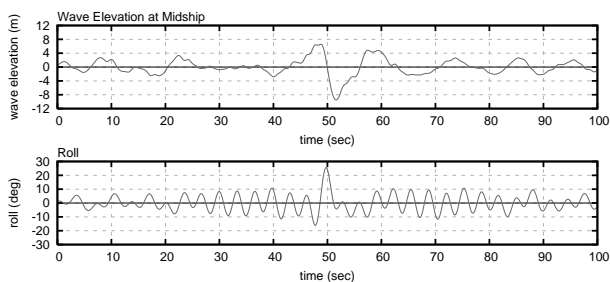


Figure 4 Symmetrical Catamaran: Design wave train leading to extreme roll of $4.5\sigma_{roll} = 29.2^\circ$. ITTC Sea State 7. Heading angle = 100° , forward speed = 43 kts.

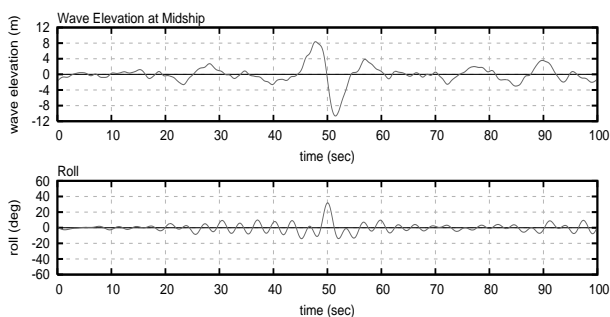


Figure 5 Symmetrical Catamaran: Design wave train leading to extreme roll of $5.5\sigma_{roll} = 35.7^\circ$. ITTC Sea State 7. Heading angle = 100° , forward speed = 43 kts

5.2 Compact Trimaran

The roll polar plot for the compact trimaran is shown in Figure 6. The polar plot shows that the largest σ_{roll} occurs at a heading angle of 95° and has a value of 1.46° . Using this heading angle, the simulations in Figures 7 and 8 were created.

There are several marked differences between the roll responses of the compact trimaran and of the catamaran. First, the compact trimaran does not experience any interval of enhanced roll. Rather, the extreme event, in both the $4.5\sigma_{roll}$ and $5.5\sigma_{roll}$ cases, appears rather alone with slightly deeper than average troughs preceding and following the event. The wave trains, however, do not show a particularly large wave to be the cause of extreme roll. Note that the wave height near the time of maximum roll was $1.3h_{1/3}$ and $2.1h_{1/3}$ for the $4.5\sigma_{roll}$ and $5.5\sigma_{roll}$ responses, respectively.

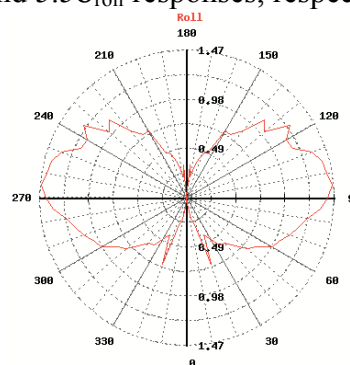


Figure 6 Compact Trimaran: Polar plot - Roll RMS. ITTC Sea State 7. Forward speed = 43 kts.

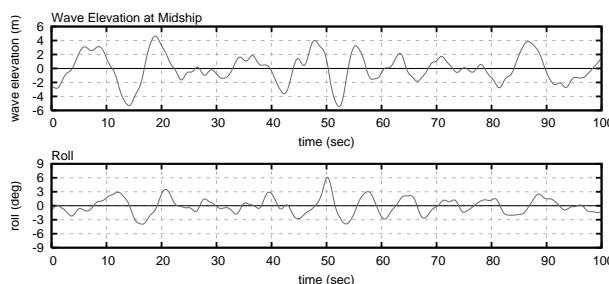


Figure 7 Compact Trimaran: Design wave train leading to extreme roll of $4.5\sigma_{roll} = 6.57^\circ$. ITTC Sea State 7. Heading angle = 95° , forward speed = 43 kts.

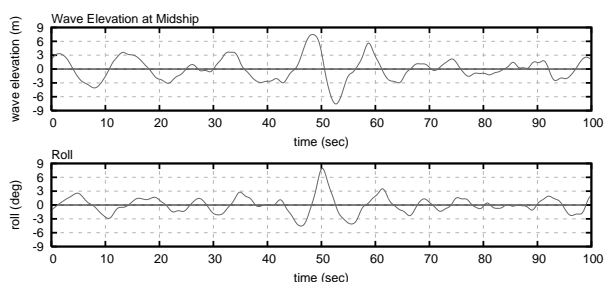


Figure 8 Compact Trimaran: Design wave train leading to extreme roll of $5.5\sigma_{roll} = 8.03^\circ$. ITTC Sea State 7. Heading angle = 95° , forward speed = 43 kts.

5.3 Extended Length Trimaran

The roll polar plot for the extended length trimaran is shown in Figure 9. The polar plot shows that the largest σ_{roll} occurs at a heading angle of 105° and has a value of 4.41° . Using this heading angle, the simulations in Figures 10 and 11 were created.

With the extended length trimaran, there is a return of the interval of enhanced rolling before and after the extreme events. This may be due to its resemblance in its aft sections to the catamaran. However, the duration of enhanced rolling after the extreme event appears much longer than seen above with the catamaran. The design wave trains include large, single waves, similar to those for the catamaran although not as large, suggesting that the extended length trimaran behaves similarly to the catamaran in roll. Note that the wave height near the time of maximum roll was $2.0h_{1/3}$ and $2.8h_{1/3}$ for the $4.5\sigma_{roll}$ and $5.5\sigma_{roll}$ responses, respectively.

6. CONCLUSIONS

The method just presented is a fast, efficient way to predict a design wave elevation leading to extreme responses from linear theory. As ship hulls become more and more complicated it becomes increasingly important to

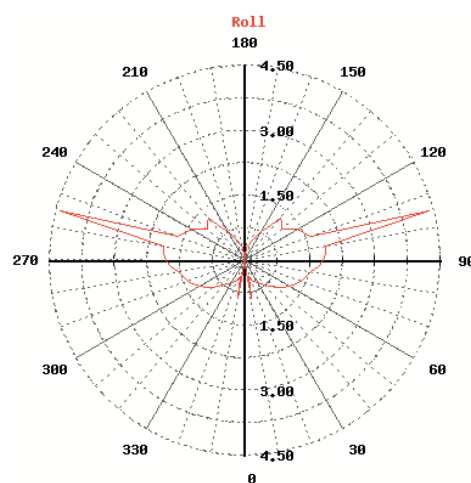


Figure 9 Extended Length Trimaran: Polar plot - Roll RMS. ITTC Sea State 7. Forward speed = 43 kts.

accurately predict extreme responses of these ships. Nonlinear seakeeping programs play a vital role in assessing the dynamic stability of these new hulls, but without a way to channel their resources the stability analyses are too expensive. The procedure and examples presented here show one way to efficiently use linear and nonlinear codes to evaluate new hulls. The procedure is especially helpful in the early design stages, where several hulls may be in contention. Potential instabilities may be exposed and efforts then concentrated on those designs showing more promise.

Ongoing research includes determining the relationship between the PDF of the phases around a maximum or minimum and possible input parameters. Also of interest is the probability of these design-tailored waves actually occurring in the real world. The designer needs to be able to assign a probability to each design wave or wave group that is calculated and assure it is physically realizable.

7. ACKNOWLEDGEMENTS

The work in this paper was partially supported by the National Defense Science and Engineering Graduate Fellowship; the Office

of Naval Research (ONR)-NNRNE Program for Design Loads Generators; the ONR Tools for Multi-Hull Design Optimization Program; the ONR High-Speed SeaLift Project; and the Department of Naval Architecture and Marine Engineering, University of Michigan.

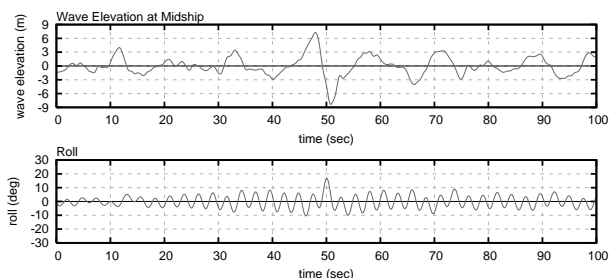


Figure 10 Extended Length Trimaran: Design wave train leading to extreme roll of $4.5\sigma_{roll} = 19.8^\circ$. ITTC Sea State 7. Heading angle = 105° , forward speed = 43 kts.

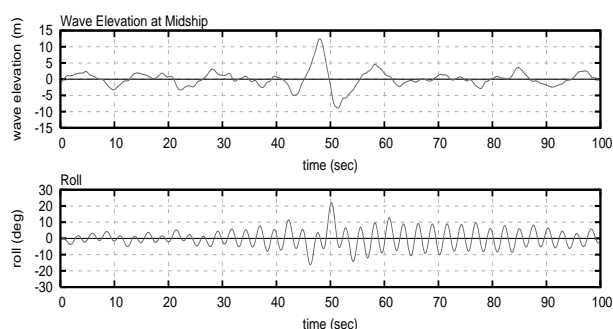


Figure 11 Extended Length Trimaran: Design wave train leading to extreme roll of $5.5\sigma_{roll} = 24.3^\circ$. ITTC Sea State 7. Heading angle = 105° , forward speed = 43 kts.

8. REFERENCES

- Adegeest, L., Braathen, A., and Løseth, R. M., 1998, "Use of non-linear sea-loads simulations in design of ships," Proc. Practical Design of Ships and Mobile Units (PRADS), pages 53-58.
- Adegeest, L., Braathen, A., and Vada, T., 1999, "Evaluation of methods for estimation of extreme nonlinear ship responses based on numerical simulations and model tests," Proc. Twenty-Second Symposium on Naval Hydrodynamics, pages 84-99.
- Beck, R. F., and Troesch, A. W., 1990, Students documentation and users manual for the computer program SHIPMO.BM. Department of Naval Architecture and Marine Engineering, University of Michigan, Ann Arbor.
- Chakrabarti, S., and Libby, A., 1988, "Further verification of gaussian wave packets," Applied Ocean Research, 10(2):106-108.
- Clauss, G. F., 2002, "Task-related rogue waves embedded in extreme seas," Proc. Twenty-First International Conference on Offshore Mechanics and Arctic Engineering.
- Clauss, G. F., and Bergmann, J., 1986, "Gaussian wave packets - a new approach to seakeeping tests of ocean structures," Applied Ocean Research, 10(2):190-206.
- Clauss, G. F., and Hennig, J., 2003, "Deterministic analysis of extreme roll motions using tailored wave sequences," Proc. Eighth International Conference on the Stability of Ships and Ocean Vehicles, pages 441-455.
- Clauss, G. F., and Hennig, J., and Schmittner, C. E., 2005, "Modelling extreme wave sequences for the hydrodynamic analysis of ships and offshore structures," Proc. Practical Design of Ships and Mobile Units (PRADS).
- Clauss, G. F., and Hennig, J., and Schmittner, C. E., and Kühnlein, W. L., 2004, "Non-linear calculation of tailored wave trains for experimental investigations of extreme structure behaviour," Proc. Twenty-Third International Conference on Offshore Mechanics and Arctic Engineering.
- Clauss, G. F., and Kühnlein, W. L., 1997, "Simulation of design storm wave conditions with tailored wave groups," Proc. First International Offshore and Polar Engineering Conference, pages 228-237.
- Clauss, G. F., and Steinhagen, U., 1999,

- “Numerical simulation of nonlinear transient waves and its validation by laboratory data,” Proc. First International Offshore and Polar Engineering Conference, pages 368-375.
- Davis, M., and Zarnick, E., 1964, “Testing ship models in transient waves,” Proc. Fifth Symposium on Naval Hydrodynamics, pages 507-543.
- Jensen, J. J., and Pedersen, P. T., 2006, “Critical wave episodes for assessment of parametric roll,” Proc. Ninth International Marine Design Conference, pages 399-411.
- Jensen, J. J., 2005, “Conditional second-order short-crested water waves applied to extreme wave episodes,” Proc. Ninth International Marine Design Conference, pages 399-411.
- Pastoor, L. W., 2002, *On the Assessment of Nonlinear ship motions and loads*. PhD thesis, Technische Universiteit Delft.
- Steinhagen, U., 2002, *Synthesizing Nonlinear Transient Gravity Waves in Random Seas*. PhD thesis, Technische Universität Berlin.
- Takezawa, S., and Hirayama, T., 1976, “Advanced experimental techniques for testing ship models in transient water waves. Part II: The controlled transient water waves for using in ship motion tests,” Proc. Eleventh Symposium on Naval Hydrodynamics, pages 37-54.
- Takezawa, S., and Takekawa, M., 1976, “Advanced experimental techniques for testing ship models in transient water waves. Part I: The transient test technique on ship motions in waves,” Proc. Eleventh Symposium on Naval Hydrodynamics, pages 23-35.
- Taylor, P. H., Jonathan, P., and Harland, L. A., 1995, “Time domain simulation of jack-up dynamics with the extremes of a gaussian process,” Offshore Technology, 1-A:53-58.
- Tromans, P. S., Anaturk, A. R., and Hagemeyer, P., 1991, “A new model for the kinematics of large ocean waves - application as a design wave,” Proc. First International Offshore and Polar Engineering Conference, pages 64-71.

Wave Weather Scenarios Modelling Using Grid Technology

Alexander V. Bogdanov, *Institute for High-Performance Computing and Information Systems*

Alexander B. Degtyarev, *Professor, Institute for High-Performance Computing and Information System,*

Elena N. Stankova, *Institute for High-Performance Computing and Information Systems*

Irina V. Shoshmina, *Researcher, Institute for High-Performance Computing and Information Systems*

ABSTRACT

The paper is focused on the description of the most effective approach to the wave climate modelling, based upon development of distributed hardware – software complexes. Such complexes should include a set of physical-mathematical models describing wave climate, including input meteorological data pre-processing and output data post-processing. The technology of distributed calculations, Grid technology, will provide simulation of the complex problems using remote heterogeneous computational resources, simultaneous visualization of the large amount of the scientific data. Distributed data processing and analyses will provide interconnection of the scientific tools with remote computers and data bases.

Keywords: *wave weather scenarios, Grid technology, mathematical modeling, regenerative paradigm, atmospheric parameters*

1. INTRODUCTION

Wave climate is considered as an ensemble of conditions of spatio-temporal wave fields characterized by frequency-directional spectra. Such approach with reference to shipbuilding is caused by expansion of the nomenclature of wave and wind characteristics, which are necessary for engineering offshore structures construction and operation, and ships operation. The use of expanded set of wave and wind characteristics makes it possible to introduce the term “scenario of wave weather” much more correctly and to use it for estimation of navigation safety. There are a lot of methodologies and approaches used for predicting wave and wind characteristics but it is impossible to use most of them for practical purposes in shipbuilding. Nowadays the most perspective approach from the authors point of

view is the development of the so-called wave weather scenario, assuming elaboration of the set of united probabilistic-hydrodynamic mathematical models for external forces acting on a ship. General theoretical solution of such approach was presented in the paper (Degtyarev A., 2005). In this paper we focus attention on presentation of some technical issues – specifically the computational component.

Introduction of “climatic spectrum” definition allows to create ensembles of wave weather scenarios and to use them for marine object behaviour simulation. The whole cycle of such simulation should represent hardware-software complex, or virtual testbed, capable to consider: analysis of big files of information coming from measurement systems; identification of extreme situations; determination of CFD characteristics of mathematical models; construction and

analysis of scripts of interaction dynamics between marine objects and environment described by a system of spatiotemporal random fields; analysis of alternatives and decision-making in uncertainty conditions. Realization of such complexes requires tremendous computational resources, powerful visualization tools, elaborated high-performance numerical algorithms. The best way to meet all the requirements is to create a distributed computational environment – Grid, capable to offer computational resources, adequate to problem being solved.

2. SCENARIOS OF WAVE WEATHER AS INITIAL DATA IN SEAWORTHINESS PROBLEMS.

Such approach to wave weather evolution presentation in considered water space permits to develop mathematical model of sea waves for long-term periods. The main characteristic of this model is multiscale, i.e. taking into account different time intervals: quasistationarity, synoptic variability, seasonal and year-to-year variability. As a result it is possible to obtain wind wave fields ensemble realizations for any time length.

Thus, introduction of “climatic wave spectrum” and “wave climate” definitions results in expansion of design conditions base of external action for ship’s dynamic problems solution. Now instead of traditional limited set of some integral parameters (significant wave height, spectrum approximation, etc.) we can introduce new concept – wave weather scenario. It can take into account the following items relevant to the problem reviewed (Degtyarev A., 2005):

- peculiarities of wave formation conditions – wind waves, swell, sea properties;
- geographical features of considered region;
- variability of hydrometeorological conditions – features and characteristics of storms evaluation and weather stability;
- scenarios of synoptic variability –

alternation of stormy and good weather states;

- characteristics of seasonal variability – features of summer, winter time and off-season for considered navigation regions, special missions carried out by ship, etc.;
- long-term presence of ship in given region or in known exploitation conditions comparable with considered object lifetime.

With the above parameters set, it is possible to propose the following scenarios of wave weather for use in problems of research design, seaworthiness safety estimation and risk assessment for both ships and offshore structures:

- **short-term scenario** – modeling of spatio-temporal wave fields realizations taking into account all the above parameters;
- **“storm” scenario** – wave actions modeling for typical storms in given region and season;
- **“mission” scenario** – variation of wind and wave conditions and external influences on a ship carrying out a specific mission: voyage, rescue operation, ship raising, survey operations, combat mission, etc.;
- **“navigation” scenario** – sequence of ordinary scenarios “mission” covering long period including some seasons such as fishery, long navigation;
- **“lifetime” scenario** - taking into account year-to-year and climatic variability of given region where ships and offshore structures operate. It is primarily related to risk estimation in complicated expansive open-sea objects insurance.

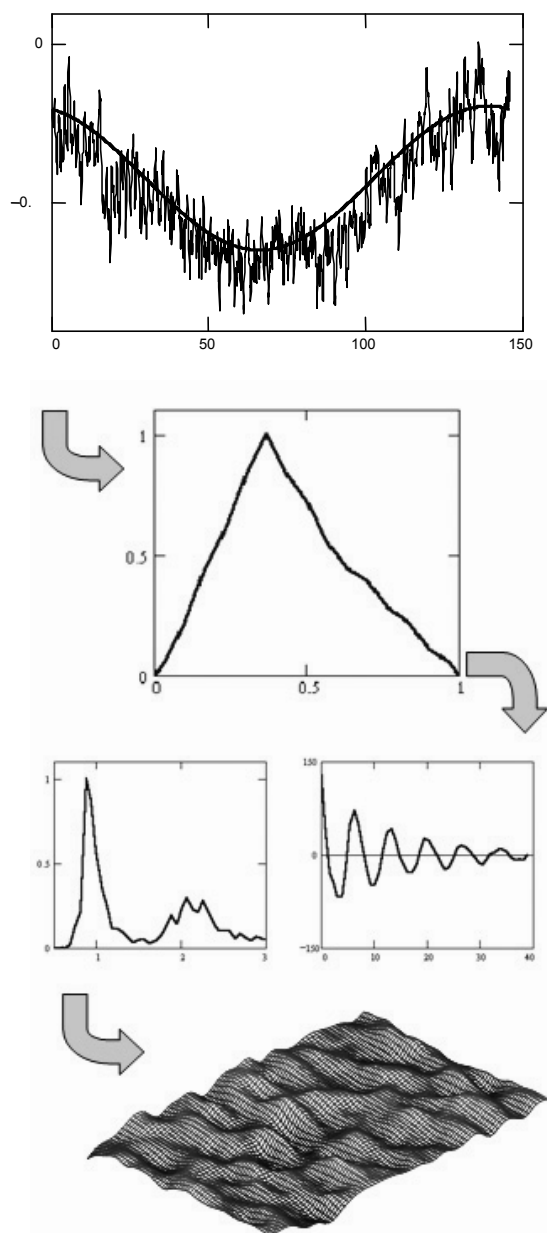


Figure 1. Scheme of wave weather scenario generation (annual variation of average wave height – form of storm – typical wave spectrum – sea surface) (Degtyarev A., 2005)

3. WAVE WEATHER SCENERIES MODELLING

Initial statistical information about wind and wave regime in given region is required for sceneries creation with the help of the methods described above. Obviously it is impossible to obtain such information from measured data

only. The most fundamental starting point for derivation of equations governing the wave spectrum evolution is the equation for the conservation of the wave action density N (see, e.g., (Komen, et al., 1994), (Lavrenov, 1998):

$$\frac{\partial N}{\partial t} + \frac{\partial N}{\partial \varphi} \dot{\varphi} + \frac{\partial N}{\partial \theta} \dot{\theta} + \frac{\partial N}{\partial k} \dot{k} + \frac{\partial N}{\partial \beta} \dot{\beta} + \frac{\partial N}{\partial \omega} \dot{\omega} = G \quad (1)$$

The action N is a function of latitude φ , longitude θ , wavenumber k , angle between the direction of wave propagation and the parallel β , angular frequency ω , and time t . G is net source function. It is represented as the sum of the input G_{in} by the wind, the nonlinear transfer G_{nl} by resonant wave-wave interaction, and the dissipation G_{ds} . There are some other terms of equation (interaction with slowly changing currents, etc.) which are normally small. They are not included in the propagation operator.

Equation (1) describes functional relation between fields of atmosphere pressure, wind and waves. There are many calculation models based on (1) devoted to obtaining time-spatial wave field. The only difference between them is in sources function presentation and computational layout. Present spectral wind wave models based on equation (1) are rather well developed. They incorporate a representation of all significant mechanisms affecting the wave spectrum evolution and are quite sophisticated numerically. Being determined by wind data (or atmospheric pressure), and data on boundary layer stability, the models compute two dimensional (with respect of frequency and direction) spectrum $S(\omega, \beta)$ at nodes r_i of numerical grid at times t_j .

The first wave model which was realized as world-renown software is WAM-model. The theory and methods of numerical simulation are continuously improving. Now we have new results and models WAVEWATCH (Tolman, 1991), PHIDIAS (Van Vledder, et.al, 1994), TOMAWAC (Benoit, 1996), INTERPOL (Lavrenov, 1998) for deep and SWAN (Ris, 1997) for shallow water.

Specifics of computer presentation of hydrometeorological fields information are vast amount of data used and long calculation time. Hence, the use of high performance computers is necessary.

Any hydrodynamic model devoted to wave fields calculation requires initial wind data in meshes of net domain with assigned discretization in time domain. Available information was heterogeneous, fragmentary and discrepant till recently. A significant advance in numerical wave hindcasts resulted from the NCEP/NCAR meteorological reanalysis project (Kalnay, et.al, 1996), which produced global data series of great interest to wave modelling. The use of the reanalysis products to drive the wave model removed many of the inhomogeneities present in earlier data sets.

At the same time it is necessary to note that such technology is rather rough as long as reanalysis information is presented with rough space resolution. It makes it possible to obtain general representation about atmosphere processes evolution. To improve atmosphere parameters it is possible to use special interpolation procedures (Russian Registry of Shipping Publisher, 2003) or to use regional models of atmosphere circulation. There are well-known such models as American model MM5 and European model HIRLAM. These models permit to calculate parameters of atmosphere boundary layer with high spatio-temporal resolution. These parameters include wind speed and direction, pressure, temperature, etc.

Codes of all the models mentioned are open source. It is also possible to obtain detailed manuals for these software.

All these models allow to obtain initial information for statistical generalization, spectra parameterisation, storms classification and scenario wave calculations.

Thus, the general algorithm for data preparation and realization of different

scenarios looks as follows (Degtyarev A., 2005):

1. Initial data of pressure fields processing using reanalysis data for considered region or with the help of regional models of atmosphere circulation. Input data are: bathymetrical map, coastline and variation edge of the ice.

2. Verification of prepared data on the basis of comparison with natural observations. If occurrence of interpolation is bad than change of model parameters for recalculation should be made and i.1 should be repeated.

3. Wave fields calculation on the basis of model (1). Computational grid has to cover the considered region entirely. It is necessary for taking influence of distant storms and incoming swell into account. Character of expansion of computational grid is defined by the expert evaluation taking into account geographical conditions of considered region. Time period of calculation depends on purpose of calculation. 20-25 years are necessary for reliable statistical data. For purposes of extremes statistics this period has to be prolonged up to 30-40 years.

4. Verification of wave fields with the help of waves measurements in considered region (if we have long buoy records). Correction of model parameters and recalculation at i.3 if big error of statistical characteristics exists (e.g. see (Russian Registry of Shipping Publisher, 2003)).

5. Assimilation of calculated data and measurements

6. Statistical processing of obtained spatio-temporal wave fields and measurement data

- calculation of trivial statistics;
- determination of statistical parameters characterizing stormy and good weather periods (weather window);
- storms and weather windows classification;
- parameters of storms and weather

- windows interchange;
- climatic wave spectra classification;
 - extreme statistics calculation;
 - calculation parameters related with extreme waves.
7. Data assimilation for models of wave scenarios operation.
8. Using year-to-year rhythmic model for climatic variation of reproducing wave weather in a given region.
9. Superposition of climatic variations and results of probabilistic modeling of annual rhythmic.
10. Superposition of obtained results and results of stochastic modeling of storms and weather windows interchange.
11. Stochastic modeling of climatic spectra sequence corresponding to classes of storms and weather windows.
12. Time variation of frequency-directional spectra reproduction on the basis of obtained realization of average wave height and climatic spectra consecution.
13. Spatio-temporal wave fields generation for each wave spectrum.
14. Subject to solving problem and considered time scale, either reiteration of i.i.8-13 or collecting wave scenario ensembles. The continuity and Navier-Stokes equations are needed

4. POSSIBLE STRUCTURE OF THE DISTRIBUTED HARD-SOFTWARE COMPLEX

The general algorithm for data preparation and realization of different scenarios presented above offers the natural structure of the distributed hard-software complex. The complex should consist of several blocks, the

first one should be responsible for the initial data of pressure fields preparation, the second – for wave fields calculation, the third – for the statistical treatment of obtained spatio-temporal wave fields and measurement data, the fourth – for wave scenario ensemble collection.

Each block realization requires large volume of calculation conducting with the help of complex mathematical models and tremendous amount of input and output data processing.

Consequently it appears to be very difficult to gather all necessary computational resources and data bases in one place. Very often all the required facilities are distributed over different universities and supercomputer centres. To join them together it is necessary to elaborate distributed calculation environment – calculation Grid.

To make Grid a reality requires new approaches, methods, tools for maintaining large amounts of data and/or computer-intensive calculations. Our approach is to gridify applications: not to develop a generic Grid solution but support specific types of applications by tuning and modifying Grid middleware to fulfil application needs and achieve the best performance.

The applications can be mapped on Grid architecture with the help of solutions for parallelization of specific application types. There are special mathematical techniques, that allow to present traditional numerical procedures in parallel, even if parallelization of sequential code is impossible, with the help of appropriate Grid middleware.

Special attention should be paid for parallel processing of extra-large datasets. During the analysis of the problem of processing extra-large multivariate datasets on parallel and distributed (Grid) systems we find that the formal approaches to parallelization fail because of the long-range correlations between data and their non-scalar nature. To overcome

those difficulties the new paradigm of the data processing is proposed, based on a statistical modelling of the datasets, which in its turn is realized for different types of data. This paradigm was described in (Bogdanov A., etc., 2004, 2005). The development of the parallel models for problems of considered classes is possible to represent as the next four stages.

Reduction of the dimensionality for the initial data $\Xi(\mathbf{r}, t) \in H$ in the linear space H . The goal of this stage is the construction of the set of most informative indexes, characterizing the sample variability.

Identification of the model. Previous stages takes possibility to express the dependence between non-scalar components of $\Xi(\mathbf{r}, t) \in H$ in terms of the system of scalar indexes $Z = \{z_k(t)\}$. For the quantitative description of the temporal (t) and intra-element (k) dependencies of these data the model of linear stochastic dynamic system has been considered (Adomian G., 1983)

$$LZ = RE + BH \quad (2)$$

Here L , R , B – are the linear differential operators, E – is the multivariate white noise (independent realizations of random value), and H is the set of driving stochastic factors (predictors). The equation (2) is the generalization for different models applied for wave weather scenarios.

Statistical synthesis. The equation (2) could be used as the algorithm for Monte-Carlo simulation of multivariate time series $Z = \{z_k(t)\}$. Hence it is considered as the milestone for the construction of the hierarchy of the stochastic operators of Monte-Carlo procedure

Verification, scenarios and forecast. The procedure of verification is proposed as the technique for qualitative control of the statistical model.

In view of parallel processing, the principal feature of models construction is the intrinsic formalization of the parallel algorithm, using the possibility of the elimination of the correlations between data in computational procedure

All these stages of regenerative paradigm were performed in process of wave weather scenarios construction (Degtyarev A., 2005). For example, reduction of dimensionality was used when random function of climatic wave spectrum was presented as deterministic function with random parameters.

Such basis is related with principles of intrinsic parallelization of proposed algorithms. These principles allow classifying the methods of statistical processing and Monte-Carlo simulation. There were proposed (Bogdanov A., 2004) three principles for such probabilistic models.

Decomposition of the statistical ensemble. This principle reflects the postulate of the independence of sample elements. It allows dividing the sample on the independent fragments and process these data in parallel. The resulting computational algorithm is rather homogenic. The main problem of the ensemble decomposition is the further integration of the estimates, obtained on the different processors.

Decomposition on the base of principle of mixing. This is the modification of statistical ensemble decomposition for the model of time series with local dependence between data. Realization could be divided into the set of non-overlapping fragments. Each fragment is simulated by equation (2) in parallel. After that, the matching of the parallel fragments may be organized as binary tree algorithm

Decomposition of the indexing variable. This principle corresponds to alternative way for dependence elimination in stochastic model. It is important for the multivariate data. The general approach is based on the specific construction of data transformation operators,

thus the values of the transformed data for different values of index variable could be computed independently.

This approach shows a very effective scaling and parallelization that allows applying it to Grid.

Special user-friendly interfaces should be developed providing user access to all heterogeneous resources and data bases, enabling the user to monitor application execution and moving the data at user's request.

5. PROTOTYPE OF THE GRID SEGMENT

As a prototype of the Grid segment for wave weather scenarios modelling let us consider Russian-Dutch High-Performance Grid segment (Bogdanov et.al, 2005), with one of its sites based in the Institute for High-Performance Computing and Information Systems.

Each Grid-site base configuration consists of 5 computer systems minimum: Configuration server, Computing Element (CE), Storage Element (SE), User Interface (UI) and Working Node (WN).

User Interface element provides access to the Grid segment resources. User logs into UI computer in order to choose Grid resources, install the task for execution, get output data and transfer data if necessary.

Configuration server provides semiautomatic installation and configuration (both initial and secondary) of all base control elements.

Computing Element is the main working point on the local site. CE provides common interface for computational resources involved. Among its functions are task launching and task scheduling.

Working nodes provide user task implementation. A site can contain several working nodes. Storage Element provides user universal access to the available databases.

6. CONCLUSIONS

The description of the most effective approach to the wave climate modeling based upon the elaboration of the distributed hardware – software complexes is presented. Possible structure of such complexes based upon Grid technology for distributed calculations is discussed.

7. ACKNOWLEDGMENTS

Russian-Dutch High-Performance Grid segment references in the paper was developed in the frame of the NWO-RFBR project N 047.016.007:: "High Performance simulation on the Grid"

8. REFERENCES

- Adomian G. 1983, "Stochastic systems." Academic Press, NY.
- Benoit M., Marcos F., 1996, Becq F. "Development of third-generation shallow water wave model with unstructured spatial meshing" //Proc. 25th Int.Conf.Coast.Eng. ASCE.
- Bogdanov A.V., Valuev I.A., Gorodnichev M.A., Evlampiev A.A., Korkhov V.V., Luzan, P.I., Malashonok D.Yu., Malyshkin V.E., Malyshkin N.V., Morozov I.V., Slood P.M.A., Stankova E.N., Shoshmina I.V., 2005, "Experience of the Experimental Grid Segment Elaboration for Heavy Engineering Applications" // Proceedings of the All-Russian Scientific Conference "Science in the Internet: Technologies of Distributed Computations", Novorossiysk, 19-24 September, p.33-35

- Bogdanov A., Boukhanovsky A., 2004, "Advanced high performance algorithms for data processing." LNCS 3036, Springer-Verlag, , pp.239-246
- Bogdanov A., Degtyarev A., Nechaev Yu., 2005, Parallel algorithms for virtual testbed. // Proceedings of International Conference "Computer Science & Informational Technologies", Yerevan, Armenia, September, pp.393-398
- Boukhanovsky A., Degtyarev A., Lopatoukhin L., Rozhkov V., 1998, "Probabilistic modelling of wave climate." //Izv. of RAS "Physics of atmosphere and ocean", v.34, N2, pp.261-266 (in Russian)
- Boukhanovsky A., Degtyarev A., Rozhkov V., 2001, "Peculiarities of computer simulation and statistical representation of time-spatial metocean fields." LNCS 2073, Springer-Verlag,, pp.463-472
- Degtyarev A., October, 2005, "New approach to wave weather scenarios modelling." //Proceedings of 8th International Ship Stability Workshop, Istambul, Turkey, paper 3.2, 15p.
- Kalnay E., Kanamitsu M., Kistler R., Collins W., Deaven D., Gandin L., Iredell M., Saha S., White G., Woollen J., Zhu Y., Leetmaa A., Reynolds R., Chelliah M., Ebisuzaki W., Higgins W., Janowiak J., Mo K. C., Ropelewski C., Wang J., Roy Jenne, Dennis Joseph, (1996) "The NCEP/NCAR 40-Year Reanalysis Project." Bulletin of the American Meteorological Society. March, 77, N3, pp.437-471.
- Komen G.L., Cavaleri L., Donelan M., Hasselmann K., Hasselmann S., Janssen P., 1994, "Dynamics and modelling of ocean waves." Cambridge University Press.
- Lavrenov, I.V., 1998 , "Mathematical modelling of wind waves in a spatially-non-uniform ocean." St. Petersburg, "Gidrometeoizdat" Publisher, (in Russian).
- Reference data., 2003, "Wind and wave conditions for Barents Sea," Okhotsk Sea and Caspian Sea. St.Petersburg, Russian Registry of Shipping Publisher, (in Russian)
- Ris R.C., 1997, "Spectral modelling of wind waves in coastal areas" //Communication on Hydraulic and Geotechnical Engineering, June – TUDelft, N97-4
- Tolman H.L., 1991, "A third-generation model for wind waves on slowly varying, unsteady and inhomogeneous depths and current" //J.Phys.Ocean., vol.21, N6, pp.782-797.
- Van Vledder G.Ph., de Ronde J.G. Stive M.J.F., 1994, "Performance of a spectral wind-wave model in shallow water" //Proc. 24th Int. Conf. Coast. Eng. ASCE, pp.753-762

Spatial Variability of the Wave Field Generated in an Offshore Basin

P. Petrova, *Unit of Marine Technology and Engineering, Technical University of Lisbon*

C. Guedes Soares, *Unit of Marine Technology and Engineering, Technical University of Lisbon*

ABSTRACT

Results of a study on the spatial variability of irregular wave fields generated in an offshore basin are presented. The available data set consists of approximately 3-hour deep and shallow water time series of the free surface elevation. Some of the shallow water wave fields include a simultaneous current. The spatial variability has been checked by means of nonparametric and parametric statistical significance tests. The nonparametric methods serve to validate the conclusions of the parametric ones, since they are considered more reliable when samples with non-Gaussian statistics are checked. The statistical tests were applied to various sets of data from two locations and also multivariate tests were performed for the whole set of 15 gauges deployed in the basin.

Keywords: *Wave spatial variability, Statistical tests, Model tests*

1. INTRODUCTION

The model tests in a tank are of importance for the study of the physical processes observed in the real sea and are currently used to determine the motions and loads of ships and offshore platforms. They are especially important to understand non-linear phenomena, such as ship stability in waves and capsizing. The offshore basins offer the possibility of testing self-propelled ship models and this is very useful for studying stability of ships in waves.

The problem of using the whole area of the basin for the model tests is to ensure that the wave field is properly generated and the wave properties are maintained spatially. The limited size of the basin generates effects that are not observed in the open ocean, as reflection of the incident waves from the end wall of the basin and interaction effects from the sidewalls among others. They can change the wave field,

such that it can have different statistical properties in the affected areas of the basin. It is therefore important to determine those regions where the wave characteristics can be considered identical from a statistical point of view.

The other problem concerns the duration of the generated time series, which are expected to be sufficiently long for analysis, but this raises the question of maintaining stationary conditions during the process of measurements. Moreover, the model tests are carried out assuming identical wave conditions not only in time (stationarity), but also in space (homogeneity). Thus, the wave field at different locations in the tank is expected to follow similar statistical representation.

In order to check the consistency between the wave statistics in space and time, two types of statistical tests can be used: parametric ones, based on a preliminary assumption of the form of the underlying distribution and nonparametric, which are distribution-free

(Conover, 1980; Hogg and Tanis, 1993; Sprent, 1989).

The parametric tests assume that the initial population has a Gaussian distribution or the distribution is slightly skewed. However, when the process is non-Gaussian the parametric tests are expected to yield non-reliable statistics. In case of highly skewed data sets, the sample mean and variance become more dependent and it makes the Student's distribution inappropriate for testing the means of two samples. Moreover, this test loses its power when applied to samples with observed outliers, since the distribution should be symmetric. When the distributions are almost Gaussian but differ in variances the T -statistics should also be avoided.

In these cases, nonparametric tests are applied as an alternative and better option. The reason is that they are based on weaker initial assumptions; they are more powerful, i.e. have increased potential to show significant result when the true value of the obtained test statistic is estimated towards the alternative hypothesis and refer to the robust methods, which are less affected by the presence of outliers in the samples.

The results of the tests also depend on the imposed level of significance, since it determines the size of the critical region for the tested null hypothesis. Usually, the level of significance is set at 0.05, which means that in no more than one in twenty statistical tests type I error can occur. However, in the case of multiple tests performed, the risk of making such an error increases, due to statistical variability in the total experiment.

A way to avoid this problem is to use the Bonferroni correction. The method reduces the level of significance of each individual test, in order to assure that the overall experiment-wise level of significance for the total number of performed tests is conserved.

The paper presents the results of a study of the spatial variability of waves in an ocean

basin laboratory by using statistical tests to determine if the statistical properties of the samples of waves measured at different locations of the tank are consistent, i.e. if they all belong to the same population.

The aim of the paper is not only the spatial analysis of the specific basin characteristics, but also to present an approach that can be adopted in other cases of studying the spatial variability of the data. Although the approach adopted uses well established statistical tests, the authors are not aware of any papers showing results from investigations of the spatial variability of waves in an offshore basin, using these methods.

The statistical significance tests are briefly reviewed in section 2. Description of the data sets and the samples used for the statistical tests is given in section 3. Analysis and discussion of the results is done in section 4. The general conclusions about the spatial variability of the wave field in an offshore basin are presented in section 5.

2. STATISTICAL TESTS

2.1 Parametric Statistical Tests

Location Test of the Equality of Two Independent Normal Distributions The null hypothesis of the test, $H_0 : \mu_X = \mu_Y$, states that two randomly chosen samples, X and Y , derived from normally distributed populations, $N(\mu_X, \sigma_X^2)$ and $N(\mu_Y, \sigma_Y^2)$, that have equal variances, $\sigma_X^2 = \sigma_Y^2$, have also equal means, $\mu_X = \mu_Y$. The test statistic, T , follows the Students' distribution with $r = n + m - 2$ degrees of freedom.

$$T = \frac{\bar{X} - \bar{Y}}{\sqrt{\left[\frac{(n-1)S_X^2 + (m-1)S_Y^2}{n+m-2} \right] \left(\frac{1}{n} + \frac{1}{m} \right)}} \quad (1)$$

where n and m are the sizes of X and Y ; \bar{X} and \bar{Y} are the sample means; S_X^2 and S_Y^2 are the sample variances. The alternative hypotheses

and the corresponding critical regions are shown in Table 7.4-1 in Hogg and Tanis (1993).

Two-sample variance test The test statistic has F -distribution with $r_1 = n - 1$ and $r_2 = m - 1$ degrees of freedom. The critical regions are given in Table 7.4-2 in Hogg and Tanis (1993).

$$F = \frac{(n-1)S_X^2 / [\sigma_X^2(n-1)]}{(m-1)S_Y^2 / [\sigma_Y^2(m-1)]} = \frac{S_X^2}{S_Y^2} \quad (2)$$

One-way ANOVA test The test checks the equality between several independent normal distributions, $N(\mu_i, \sigma_i^2)_{i=1, \dots, m}$, with unknown means and unknown, but equal variances. The test statistic is the ratio between two unbiased estimators of the populational standard deviation σ^2 , i.e. $SS(T)$ - the sum of squares among the treatments and $SS(E)$ - the sum of squares within the treatments

$$\frac{SS(T)/(m-1)}{SS(E)/(n-m)} = F \quad (3)$$

The statistic has F -distribution with $r_1 = m - 1$ and $r_2 = n - m$ degrees of freedom. The critical region for the null hypothesis, $H_0 : \mu_1 = \dots = \mu_{i=1, \dots, m}$, is $F \geq F_\alpha(m-1, n-m)$, where the reference value F_α is calculated from Table VII of the Appendix in Hogg and Tanis (1993).

2.2 Nonparametric Statistical Tests Based on Ranks

Wilcoxon-Mann-Whitney Test for Two Sample Means The assumptions are independence within and between the considered random samples and similar shapes of the populational distributions, which can be also asymmetrical. Each data in the ordered sample $X_{i1}, X_{i2}, \dots, X_{in_i}$, where $n_{i=1,2}$ denotes the sample size, has a rank from 1 to $n = n_1 + n_2$. The test statistic, T , equals the sum of the assigned ranks to one of the populations

The null hypothesis $H_0 : F(x) = G(x)$, where F and G correspond to the considered sample distributions, is accepted if there is no trend towards larger or smaller positions in the combined ordered sample. In the case of ties the correspondent T -statistic is given by Conover (1980).

Variance Test for Two Samples The absolute deviation from the mean of each data is ranked. The test statistic is defined as the sum of squares of the ranks assigned to one of the populations, e.g.

$$T = \sum_{i=1}^{n_1} [R(U_i)]^2 \quad (4)$$

In the case of ties, the rank is obtained as an average of the associated ranks.

Location Test of the Equality Between Several Samples – Kruskal-Wallis Test The test is an expansion of the two-sample Wilcoxon test to several independent samples, say m , of size $n_{i=1, \dots, m}$, $X_{i1}, X_{i2}, \dots, X_{in_i}$. The procedure is the same as in the Wilcoxon test: the samples are combined and set in ascending order and to each value is given a rank or mid-rank in case of tied observations. Let $R(X_{ij})$ be the rank of X_{ij} and R_i - the rank assigned to the i th sample

$$R_i = \sum_{j=1}^{n_i} R(X_{ij}), i = 1, \dots, m \quad (5)$$

The test statistic is given by

$$T = \frac{1}{S^2} \left(\sum_{i=1}^k \frac{R_i^2}{n_i} - \frac{n(n+1)^2}{4} \right) \quad (6)$$

with n designating the total number of observations and

$$S^2 = \frac{1}{n-1} \left(\sum_{all\ ranks} R(X_{ij})^2 - \frac{n(n+1)^2}{4} \right) \quad (7)$$

The decision about the test depends on the rules defined in Conover (1980).

Variance test for several samples The nonparametric variance test for two samples is

extended to the case of m samples. The test statistic is formulated as

$$T_2 = \frac{1}{D^2} \left[\sum_{i=1}^m \frac{S_i^2}{n_i} - n(\bar{S})^2 \right] \quad (8)$$

where n_i is the number of observations in sample i ; $n = n_1 + n_2 + \dots + n_m$; S_i is the sum of squared ranks in i th sample; $\bar{S} = \frac{1}{n} \sum_{i=1}^m S_i$ is the average of the squared ranks; $\sum R_i^4$ is the sum calculated after raising each rank to the power of four and $D^2 = \frac{1}{n-1} \left[\sum_{i=1}^n R_i^4 - n(\bar{S})^2 \right]$. The

full description of the test is given in Conover (1980).

Bonferroni Correction The Bonferroni correction is applied to the multiple tests - the level of significance of each individual test is decreased, in order to assure that the experiment-wise level of significance remains the same. Although this adjustment decreases the risk of making type I error, it has a disadvantage of increasing the chance of making type II error at the same time.

Considering that the number of gauges is $n=15$, the total number of performed tests will be $N_{total} = n(n-1)/2 = 105$. The correction is given as the ratio between the level of significance of the entire set of experiments, α , and the number of performed tests N_{total} .

2.3 Statistical Test for Stationarity

Nonparametric run test is applied to check the stationarity of the process (Bendat and Piersol, 1971). The test considers a sequence of N random observations, $X_{i=1 \dots N}$. If the sample mean is \bar{X} , then each observation obtains a sign (+) if $X_i \geq \bar{X}$, and sign (-), if $X_i < \bar{X}$. Subsequently, the run, r , is defined in the sequence of positive and negative signs as the sequence of identical observations, preceded by a different observation, or no observation at all. The region where the hypothesis should be accepted is determined as

$$\frac{r_N}{2} \cdot 1 - \frac{\alpha}{2} < r \leq \frac{r_N}{2} \cdot \frac{\alpha}{2} \quad (9)$$

The corresponding r values are calculated from Table A.6 in Bendat and Piersol (1971).

3. DESCRIPTION OF THE DATA SETS

The study uses time series of the surface elevation recorded in the offshore basin of MARINTEK. The measurements were performed by total of 23 gauges, but the set of data in the study is referred to 15 of them, deployed in the tank as shown in Figure 1.

Two wave generators were applied, BM2 and BM3 located at the beginning of the basin and at one of its side walls, respectively. The tank has a beach at the wall opposite to BM2, which serves to absorb the energy of the incident waves.

The basic characteristics of the generated deep and shallow water sea states are given in Table 1 and Table 2. The information includes the significant wave height, H_s ; the spectral peak period, T_p ; the type of the spectrum and the current velocity, U_c , when current has also been generated. The last column shows the associated wavemaker.

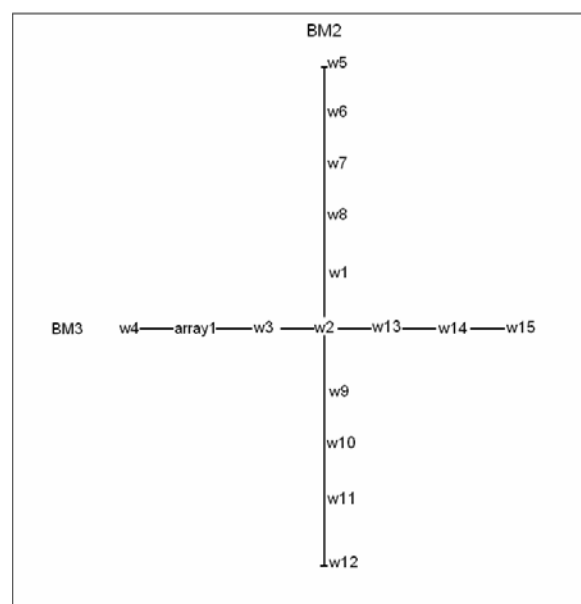


Figure 1. Location of the wave gauges and wave generators

In the deep water tests the water depth was maintained at 100m (in scale). The test runs 8201, 8202, 8219 and 8241 correspond to unidirectional irregular wave fields generated by BM2 and represented by a JONSWAP spectrum with a peak enhancement factor $\gamma = 3$. In the first three tests the peak period is constant, $T_p = 10$ s, while the significant wave height has values of 3.5m, 7m and 9m. In test 8241 the significant wave height is $H_s = 3.5$ m and the peak period is smaller, $T_p = 7$ s. The multidirectional tests are designated by 8233, 8234 and 8235 for angles of propagation of 60°, 120° and 90°, respectively. The waves were generated by both BM2 and BM3 wavemakers and correspond to a two-peaked spectrum (Guedes Soares, 1984) with individual components representing a JONSWAP spectrum with peak factor $\gamma = 3$.

Table 1. Deep water irregular waves, h=100m

Test	Hs [m]	Tp [s]	Spec	Wave dir θ [deg]	Wave maker
8201	3.5	10	J3	0	BM2
8202	7.0	10	J3	0	BM2
8219	9.0	10	J3	0	BM2
8241	3.5	7	J3	0	BM2
8233	3.6/3.6	7/20	2P J3/J3	0/60	BM2/BM3
8234	3.6/3.6	7/20	2P J3/J3	0/120	BM2/BM3
8235	3.6/3.6	7/20	2P J3/J3	0/90	BM2/BM3

Table 2. Shallow water irregular waves, h=20m

Test	Hs [m]	Tp [s]	Spec	Wave dir θ [deg]	Uc [m/s]	Wave maker
8001	3.5	10	J3	0	-	BM2
8002	7.0	10	J3	0	-	BM2
8051	3.5	10	J3	0	1.0	BM2
8052	7.0	10	J3	0	1.0	BM2
8101	3.5	10	J3	0	2.0	BM2
8102	7.0	10	J3	0	2.0	BM2
8151	3.5	10	J3	0	3.0	BM2
8152	7.0	10	J3	0	3.0	BM2

The shallow water data are described in Table 2. The water depth is constant, set at 20m (in scale). Two types of seas were generated: irregular waves without current and irregular waves with uniform collinear current in the direction of propagation of waves. The current mean velocity corresponds to three cases: $U_c=1$ m/s, $U_c=2$ m/s and $U_c=3$ m/s. As could be seen from the table, the tests are coupled, namely, each value of current velocity, U_c , is associated with two sea states with significant wave heights of 3.5m and 7m. The peak period is constant for all tests considered. The sea state is given by a one-peak JONSWAP spectrum. The applied generator in all shallow water tests is BM2.

All deep and shallow water tests correspond to total of 12088s (3.36h) of measurements with a sampling frequency $dt=0.1768$ s. Hence, the number of observations in the time series is 68371, on the average. The only exception is test 8001, where the record length is 12371s (3.44h), which corresponds to approximately 69972 measurements.

The time series of the free surface elevation were processed as follows. Each record was truncated at the beginning, in order to leave out the part with no recordings, due to the distance between the wavemaker and the gauges. Since the gauges are located at different distances from the wave generators, the resulting records will contain different number of observations. In order to avoid this problem, the longer series were further truncated at the end, such that eventually they have the same number of observations, as the shorter ones. Subsequently, the truncated records were split into ten approximately 20-minute records.

The linear trend in each segment record was removed and the mean level was adjusted to zero. The significant wave height was calculated by means of the spectral definition, $H_{m0} = 4\sqrt{m_0}$, where m_0 is the variance of the elevation process. Consequently, a sample of ten values of the significant wave height was associated with each gauge. These samples

were further used as an input for the statistical significance tests.

4. ANALYSIS OF THE RESULTS FROM THE STATISTICAL TESTS

Parametric and nonparametric significance tests were applied to the samples of significant wave heights at each gauge, in order to check the hypothesis of equality between the means and variances of the sample distributions. The nonparametric tests are useful, since they do not assume an exact form of the initial distribution which makes them suitable for testing non-normal and highly skewed data. This is exactly the present case, because the significant wave heights are not normally distributed. Furthermore, the nonparametric tests are preferred, because they are more powerful and are not largely influenced by the presence of outliers in the samples. Consequently, they can be used to validate the results from the parametric tests.

Due to space limitation, detailed numeric results from the statistical tests are not provided here. Only the basic results concerning the final conclusion on the variability in space of the wave field and the stationarity within the generated time series are presented in the following in two subsections for the deep and shallow water tests, respectively.

4.1 Deep Water Irregular Waves

The measured time series were first checked for stationarity. A run test, as described in Bendat and Piersol (1971), was used for the purpose. Different statistical parameters were calculated and the values were compared with the corresponding median values.

The number of runs for each considered statistics was found and the critical regions were defined according to Eq. (9). With r denoting the observed runs, the two critical regions are: $r \leq r_{\frac{N}{2}, 1-\frac{\alpha}{2}}$ and $r > r_{\frac{N}{2}, \frac{\alpha}{2}}$. The

lower bound of the critical interval for $N=10$

(since the time series are divided in 10 segments of equal length) and level of significance 5% is determined as $r_{5,0.975} = 2$ and the upper limit is determined as $r_{5,0.025} = 9$ (Table A.6; Bendat and Piersol, 1971). Hence, the hypothesis of stationarity will be rejected at the chosen level of significance, if the number of runs is less than 2, or more than 9.

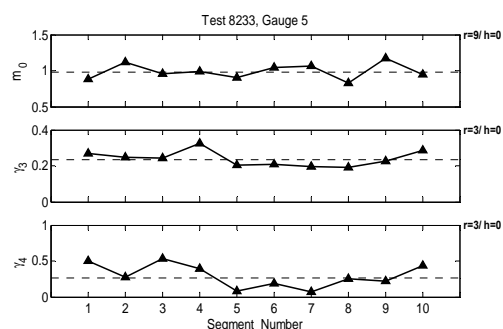


Figure 2. Test for stationarity of the deep water time series - test 8233, gauge 5

As an example of the run tests applied to the deep water records, the one based on the time series recorded by gauge 5 of test 8233 is illustrated in Figure 2. The plot represents the runs about the medians of three sample parameters: the coefficient of skewness, $\gamma_3 = \mu_3 / \sigma^3$, the excess of kurtosis, $\gamma_4 = \mu_4 / \sigma^4 - 3$ and the zero spectral moment, m_0 , where μ_3 and μ_4 are the third and fourth order central moments, respectively. The number of calculated runs is given to the right of the relevant figure along with the test significance denoted by h . The variable h can be either 0, in case of the null hypothesis being accepted, or 1, in case of significant result, i.e. the null hypothesis being rejected. The results are $r=9$ for the variation of m_0 and $r=3$ for γ_3 as well as for γ_4 . Consequently, since none of the runs fall in the defined critical regions, the hypothesis of stationarity is accepted. No significant results were reported by any of the run tests applied to the records in the considered deep water wave fields.

After the stationarity was validated for the generated time series, parametric and nonparametric tests checking the spatial variability in the wave field were performed.

The samples used in the tests constitute of ten significant wave height values calculated at each of the ten segments of approximately 20-minute duration in the truncated original records.

The results from the multivariate parametric ANOVA test and nonparametric Kruskal-Wallis test are presented in Table 3. The tests check the consistency between the distributions throughout the group of fifteen gauges in the tank. The null hypothesis states that the means of all distributions are equal, namely $H_0 : \mu_1 = \dots = \mu_{15}$, where $\mu_{i=1,\dots,15}$ represents the mean of the i th sample. The final conclusion, whether the null hypothesis is accepted or not, is based on the comparison of the output test statistic with the reference critical value. For the chosen level of significance $\alpha = 0.05$ the critical value, $F_{0.05}(14,135) = 1.6966$ is calculated from Table VII in Hogg and Tanis (1993). The corresponding critical value of the Kruskal-Wallis test is $\chi_{0.95}^2(14) = 23.68$ (Table A2; Conover, 1980). The hypothesis of equality between the sample means is rejected if the obtained test statistic is larger than the critical one. As can be seen from Table 3, the results from the ANOVA test and the Kruskal-Wallis test are in agreement.

Table 3. Statistical results from the performed ANOVA and Kruskal-Wallis tests – deep water sea states

Test	ANOVA test F	Kruskal-Wallis T_1	Variance test T_2
8201	5.0880	48.3305	5.5354
8202	1.4721	18.9866	10.7875
8219	1.5649	18.4318	6.6782
8241	5.1738	53.1378	8.8311
8233	36.4850	116.3381	8.8484
8234	67.2692	132.5520	15.8630
8235	27.0093	97.7612	14.6637

The equality between all sample means is accepted only for tests 8202 and 8219. The large values of the test statistics obtained for the directional deep water cases (8233, 8234 and 8235) clearly state rejection of H_0 . The

smallest found statistics in the directional sea states pertain to test 8235 - two wave systems, propagating perpendicularly to each other.

Analyzing the obtained results with respect to the properties of the performed tests given in Table 1, it is possible to conclude that the higher sea states correspond to smaller test statistics and consequently represent more consistent wave field. For example, tests 8202 and 8219 have the largest significant wave heights, 7m and 9m, respectively. In both cases the tests do not give significant difference between the considered samples for the chosen level of significance of 5%.

In case of significant results reported by the tests comparing more than two samples, multiple comparisons were further performed, in order to find the pairs of samples that tend to differ, i.e. such tests were run for all directional tests and for the unidirectional tests 8201 and 8241.

The two-sample tests include the parametric T -test and the nonparametric Wilcoxon and Kruskal-Wallis tests. The 5% initial level of significance was reduced for each test to approximately 0.0005 by the applied Bonferroni correction. As was expected, the significantly decreased critical region produced an increase in the number of gauges found to have the same distribution. Nevertheless, large number of gauges was still reported as significantly different in the directional sea states.

The probability value, p -value, is used as a representative statistic of the test significance. It is associated with the probability to have a statistic as large, or larger than the observed one in the direction of the alternative hypothesis, calculated when H_0 is true. Comparisons between the obtained p -values in the multiple comparison tests have shown that for the highest sea states, referred to tests 8202 and 8219, all p -values are larger than the Bonferroni corrected critical level 0.0005. Following the definition of the p -value, it can be concluded that the observed significant differences between the sample means are probably due to chance fluctuations and the

null hypothesis has to be accepted.

The other quantity of interest is the sample variance. Moreover, the parametric tests for equality between the means assume that the variances are unknown but equal. As in the case for checking the hypothesis of equal means, parametric and nonparametric tests were applied for the variances. The obtained results allow saying that the considered samples have distributions with equal variances. In all tests, the nonparametric variance test on several samples showed statistics that did not fall in the determined critical region for $\alpha = 0.05$ and for the total of fifteen gauges, which is defined as $T_2 > \chi_{0.05}^2(14) = 23.68$.

The results for the nonparametric variance tests are shown in the last column of Table 3. On the other hand, the parametric multiple variance χ^2 tests and the two-sample variance F test detected few or none significant differences in each considered test.

Finally, the regions of consistency deduced from the test results at a level of significance 0.05 and assuming the Bonferroni correction in the multiple comparisons are shown in Table 4. The first column represents the corresponding gauge number. Equal numbers are further used to designate the regions where the tests accept the hypothesis of equality between the distributions in the case of several regions of homogeneity defined. It is seen that the unidirectional wave fields numbered as 8202 and 8219 do not show significant variability in space. In the other two unidirectional tests, 8219 and 8241, where the ANOVA and Kruskal-Wallis tests reject the equality between the samples (Table 3), gauges 13 to 15 have been excluded since they are significantly different from the others. Gauge 5 of test 8241 was also excluded for the same reason.

The statistical test results are in agreement with the conclusion that the severer sea state reflects increased homogeneity in the wave field. Comparison between tests 8201 and 8241 having equal significant wave height of 3.5m

but different peak periods, 10s and 7s, respectively, shows that the test statistics of the waves with smaller peak period are larger. The most outstanding gauge in test 8241 is gauge 5.

Table 4. Regions of consistency in the deep water sea states

Test GNo	8201	8202	8219	8241	8233	8234	8235
1	1	1	1	1	2	-	2
2	1	1	1	1	2	2	2
3	1	1	1	1	2	2	2
4	1	1	1	2	-	-	2
5	1	1	1	-	1	-	-
6	1	1	1	1	1	1	1
7	1	1	1	1	1	1	1
8	1	1	1	1	1	4	4
9	1	1	1	1	2	-	2
10	1	1	1	1	3	3	3
11	1	1	1	1	3	3	3
12	1	1	1	1	3	3	3
13	2	1	1	2	2	2	2
14	2	1	1	2	4	2	2
15	2	1	1	2	4	-	2

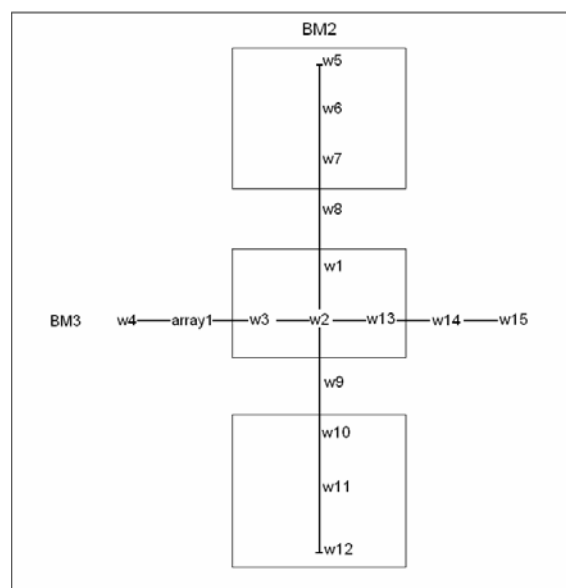


Figure 3. Regions of consistency in the deep water directional sea states

Significant differences were reported for all directional sea states, even for the highly decreased level of significance of 0.0005. The results from the tests of the directional waves show that special attention should be paid when such types of wave fields are generated. From the three directional cases shown in Table 3, 8235 was found to have the smallest

statistics. This tendency is seen also in the multiple comparisons tests. In all directional sea states, gauges 5 to 7 located at the beginning of the tank were found to form a separate region. Comparisons between the obtained results for the rest of the gauges in the three directional wave fields make it possible to define three regions of consistency, as shown in Figure 3.

4.2 Shallow Water Irregular Waves

The stationarity tests for the shallow water time series do not yield significant results either. The procedure is the same as for the deep water data. The calculated number of runs in the performed tests at different gauges and tests do not fall into the critical regions of the test. Consequently, the stationarity hypothesis can be considered to hold true for all tests run.

The shallow water run tests are illustrated in Figure 4 with the time series recorded by gauge 6 of test 8101 being considered. The runs in the three sample statistics were found to be equal to $r=7$. For rejecting the null hypothesis they have to be smaller than 2 or larger than 9. Hence, the result is not significant, $h=0$, and the stationarity hypothesis is accepted.

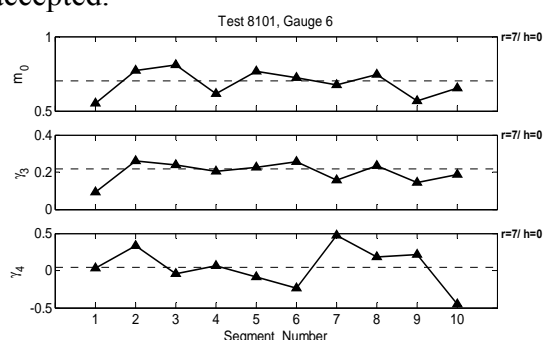


Figure 4. Test for stationarity of the shallow water time series - test 8101, gauge 6

Table 5 demonstrates the results from the ANOVA and the Kruskal-Wallis tests based on the shallow water sea states. The critical regions are the same as for the deep water cases. Significant differences are observed between the samples in all tests. The largest statistics correspond to test 8001 with the smallest significant wave height and no current effect. Considering the couples of tests with

equal current velocity but different significant wave heights, i.e. 8051-8052, 8101-8102, 8151-8152, a clear trend observed before in the deep water tests is found, i.e. the consistency of the wave field is increasing with increase in the significant wave height.

Table 5. Statistical results from the performed ANOVA and Kruskal-Wallis tests - shallow water sea states

Test	ANOVA test F	Kruskal-Wallis T_1	Variance test T_2
8001	24.8223	108.1555	4.8274
8002	12.6356	85.2492	10.2666
8051	24.5094	103.6681	11.6055
8052	16.5147	90.4016	20.3945
8101	18.4400	90.1558	11.0799
8102	12.6129	79.0603	11.0926
8151	19.0290	100.2808	8.5295
8152	12.4671	80.2289	8.3427

On the other hand, definite conclusion on how the current velocity affects the wave field statistics can not be made, due to the limited number of sea states considered. A decrease in the test statistics is observed between the cases corresponding to $U_c=1\text{m/s}$ and $U_c=2\text{m/s}$, but subsequently the statistic increases again for $U_c=3\text{m/s}$.

Considering the obtained p -values from the parametric and nonparametric tests, values much smaller than the reduced level of significance 0.0005 were found for all parametric and nonparametric shallow water tests. These cases correspond to clear rejection of the hypothesis of equal means.

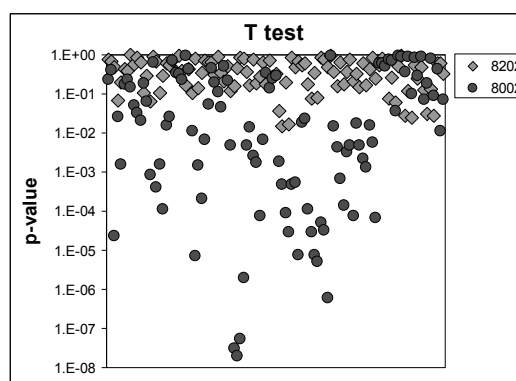


Figure 5. Comparison between the p -values of the model tests 8202 and 8002

Figure 5 compares the obtained p -values of the performed T -tests for the model tests 8202 and 8002. The two sea states have the same wave characteristics, i.e. significant wave height $H_s=7\text{m}$ and spectral peak period $T_p=10\text{s}$, but refer to deep and shallow water, respectively. It is seen that the shallow water waves have very small p -values, which are associated with significant differences between the samples.

Table 6. Regions of consistency in the shallow water sea states

Test GNo	8001	8002	8051	8052	8101	8102	8151	8152
1	-	1	-	1	1	1	1	1
2	3	2	2	2	2	2	3	2
3	3	2	2	2	2	2	3	2
4	4	-	-	2	-	-	-	-
5	1	1	1	1	1	1	1	1
6	1	1	1	1	1	1	1	1
7	1	1	1	1	1	1	1	1
8	1	1	1	1	1	1	1	1
9	2	2	2	2	2	2	3	2
10	2	2	2	2	2	2	2	2
11	2	2	2	2	2	2	2	2
12	2	2	2	2	2	2	2	2
13	3	2	2	2	2	2	3	2
14	4	2	2	3	2	2	3	2
15	4	-	2	3	2	2	3	2

The nonparametric variance tests performed on the total of 15 gauges for all shallow water data do not reject the null hypothesis of equality between the sample variances. They are shown in the last column of Table 5. However, the parametric variance χ^2 test and the F test show more cases with significant differences, than the deep water tests.

The regions of consistency, based on the obtained results from the location shallow water tests, are shown in Table 6. It is seen that the shallow water wave fields vary more, as compared to the generated deep water sea states. Nevertheless, gauges 5 to 8 can be considered to form a region where the wave statistics differ from the statistical representation of waves at the opposite side of the tank, i.e. at gauges 9 to 12.

Furthermore, it is seen that for all shallow water data there is a region where the tests

always yield consistency between the sample distributions. Consequently, for all shallow water time series two regions, as depicted in Figure 6, can be deduced.

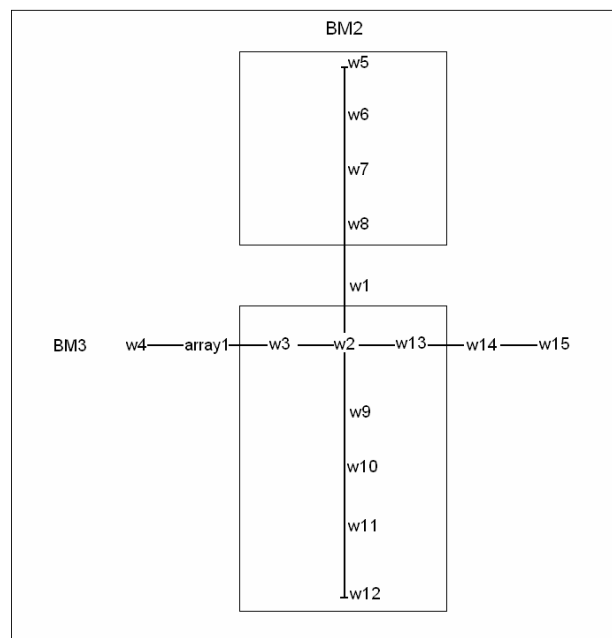


Figure 6. Regions of consistency in the shallow water sea states

5. CONCLUSIONS

A method has been described to study the spatial variability of waves in an offshore basin both in deep and shallow water. It is based on well-known statistical tests checking for significant differences between samples at various locations.

The stationarity of the generated 3-hour time series was validated by means of run tests.

The results of the statistical tests for the deep water unidirectional cases allow considering the sea states at the various locations as consistent, except for three gauges close to the wall opposite to BM3, which in some cases have different properties. It has been concluded that the higher sea states correspond to increased consistency between the gauges, which is reflected in the smaller test statistics obtained.

However, significant difference has been observed for all deep water cases in which two different spectra were generated from two

walls. The smallest variability pertains to the case of two wave systems propagating perpendicularly to each other.

The shallow water wave tests demonstrate pronounced variability in space. The tests detect significant differences between the samples in all tests. The trend observed in the deep water tests is also seen here, namely, the consistency of the wave field is increasing with increase of the significant wave height. In shallow water tests two regions of homogeneous conditions were found as shown in Figure 6.

The results from the variance tests performed over the group of all fifteen gauges in the tank, for both deep and shallow water data, showed that the samples can be considered as having the same variance.

6. ACKNOWLEDGMENTS

The data analysed in this paper has been obtained at MARINTEK in the scope of the project: Large Scale Facilities “Interactions Between Waves and Currents”, which has been partially funded by the European Union under contract № ERBFMGECT980135.

The first author has been financed by the Portuguese Foundation of Science and Technology (FCT) under the Pluriannual Funding to the Unit of Marine Technology and Engineering.

7. REFERENCES

- Bendat J.S. and Piersol, A.G., 1971, Random Data: Analysis and Measurement Procedures, John Wiley & Sons, New York.
- Conover, W.J., 1980, Practical Nonparametric Statistics, Second Edition, John Wiley & Sons, New York.
- Guedes Soares, C., 1984, Representation of Double-Peaked Sea Wave Spectra, *Ocean Engineering*, Vol. 11, p. 185-207.
- Hogg, R.V, Tanis, E.A., 1993, Probability and Statistical Inference, Macmillan Publishing House, New York.

Sprenst, P., 1989, Applied Nonparametric Statistical Methods, Chapman and Hall, London.

Influence of Current on the Probability Distribution of Wave Asymmetry and Steepness

Ewa M. Antão, *Unit of Marine Technology and Engineering, Technical University of Lisbon,
Instituto Superior Técnico, Av. Rovisco Pais, 1049-001 Lisboa, Portugal*

C. Guedes Soares, *Unit of Marine Technology and Engineering, Technical University of Lisbon,
Instituto Superior Técnico, Av. Rovisco Pais, 1049-001 Lisboa, Portugal*

ABSTRACT

The empirical distributions of wave asymmetry and steepness were analyzed in order to determine how the presence of a current influences the distributions. This investigation is based on the analysis of data generated on a wave basin. The data set was a large number of sea states that were available without current and with following or opposing current. Influence of current on wave asymmetry was also described as well as ratios of increase and decrease of wave steepness and nonlinearity of sea states analyzed. The empirical steepness and asymmetry distributions were fitted by theoretical distributions.

Keywords: *steepness, influence of current, deep water waves, wave statistics*

1. INTRODUCTION

Wave asymmetry and steepness are not as much studied as other wave parameters such as height, period and crest heights, which have been the ones that have attracted the attention of most researchers in the field.

However a recent study has shown that in general the larger density of bad weather accidents coincide with the ocean areas where the steepest sea states can be found (Guedes Soares et al, 2001). Steep waves can cause damages in ships and offshore structures (Kjeldsen, 1997, Guedes Soares et al, 2004) and they can also induce the capsizing of smaller vessels (Dahle et. al., 1988). In fact, Dahle et. al., (1988) also brought the attention to the fact that currents can increase the wave steepness and make them even more dangerous for small vessels.

The interaction of waves and current has

been much studied related to numerical approaches that describe the velocity fields in the fluid but less work has been done on how the wave elevation is modified by the presence of current, as discussed in the recent paper of Guedes Soares and Pablo (2006).

Myrhaug and Kjeldsen (1984) developed parametric model of joint probability distribution of vertical asymmetry factor and wave height, as well as model of joint probability distribution of wave steepness and height. These models however are valid for extreme waves on the Norwegian continental shelf. Another model presented in Myrhaug and Kjeldsen (1987) describes joint distribution of crest front steepness and wave height. The probability of occurrence of waves with different steepness is estimated with each parametric model for a family of JONSWAP spectra. These models do not describe influence of current on steepness and asymmetry of waves.

The main objective of this work is to study

the probability distribution of the asymmetry and steepness of individual waves, based on the analysis of wave data generated in an offshore wave basin without current and with following and opposing current.

The changes of the distributions of sea state parameters without current were analyzed for the sea states with following and opposing currents. In general a following current decreases wave steepness and an opposing one increases it.

In this work a short description of the changes of asymmetry of individual waves due to following and opposing current is also presented.

2. DATA DESCRIPTION

The data used in this study were recorded in January 2000 in a wave tank belonging to The Danish Hydraulic Institute in Hørsholm (DHI). There are all together 110 records of deep water waves sampled in intervals of $\Delta t = 0.217$ seconds. In the majority of files there are $N = 24001$ ordinates per record corresponding to a duration of 87 minutes. An example of one of the records is shown in figure 1.

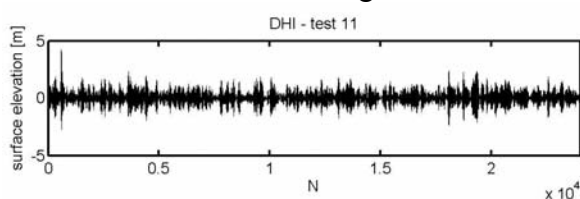


Figure 1. Example of time series recorded in the DHI basin.

The records contain sea states with 2D waves with and without current in different combinations. All sea states were generated from a JONSWAP spectrum with a peak enhancement factor of 3.0. A description of the characteristics of the 30 sea states studied here is given in table 1. In the table, in addition to significant wave heights and spectral peak period of the wave systems, there are also their

directions and the direction and velocity of the current.

Table 1. Description of sea states used in this study.

No Test	Hs [m]	Tp [s]	Wave Dir [deg]	Curr. Dir [deg]	Curr. Vel [m/s]
1	3,6	7	0	-	-
2	3,6	10	0	-	-
3	3,6	14	0	-	-
4	3,6	20	0	-	-
5	4,6	7	0	-	-
6	4,6	14	0	-	-
7	4,6	20	0	-	-
8	2,3	7	0	-	-
9	2,3	14	0	-	-
10	2,3	20	0	-	-
15	3,6	7	0	0	1,5
16	3,6	10	0	0	1,5
17	3,6	14	0	0	1,5
18	3,6	20	0	0	1,5
19	4,6	7	0	0	1,5
20	4,6	14	0	0	1,5
21	4,6	20	0	0	1,5
22	2,3	7	0	0	1,5
23	2,3	14	0	0	1,5
24	2,3	20	0	0	1,5
25	3,6	7	0	180	1,5
26	3,6	10	0	180	1,5
27	3,6	14	0	180	1,5
28	3,6	20	0	180	1,5
29	4,6	7	0	180	1,5
30	4,6	14	0	180	1,5
31	4,6	20	0	180	1,5
32	2,3	7	0	180	1,5
33	2,3	14	0	180	1,5
34	2,3	20	0	180	1,5

The first ten sea states have no current but they are different combinations of three significant heights with four spectral peak periods. The next group of 20 sea states are of repeated values of Hs and Tp however opposite or following current was added to them.

This variety of sea states with different characteristics allows a comprehensive investigation on the effect of current on the asymmetry and steepness distributions. Such distributions calculated and plotted for full field data are usually inconclusive because not

all sea state parameters are measured, as usually there is no simultaneous data on direction and velocity of current.

3. INFLUENCE OF CURRENT ON ASYMMETRY OF INDIVIDUAL WAVES

There are different definitions of horizontal and vertical asymmetry of an ocean wave. The magnitudes used in this study were defined as follows (Guedes Soares et al., 2004):

$$a_v = \frac{H_D}{cr} \quad (1)$$

$$a_h = \frac{T_b}{T_f} \quad (2)$$

where H_D is wave height from down-crossing definition, cr is wave crest height, T_b is wave back period and T_f is period of wave front. Wave back period is the time between maximum of the wave crest and the minimum of the wave trough following the crest. Wave front period is the time between maximum of the wave crest and the minimum of the wave trough before that crest.

On the basis of table 2 changes of horizontal and vertical asymmetry were investigated. The table shows mean values of vertical and horizontal asymmetry calculated from respective asymmetries of individual waves.

The presence of a current, regardless of its direction, increases the vertical asymmetry of waves in case of high sea states and decreases it in case of low sea states. Medium sea states can go either way when current is added. Horizontal asymmetry, on the other hand, increases more with following current.

It is difficult to be sure about the results of the vertical asymmetry, because it seems already very high with absence of the current. It is possible that with opposite current waves started to break and in this situation it would be

impossible to say precisely, how values of steepness changed.

Table 2. Mean asymmetry for sea states with and without current; $H_s=3.6\text{m}$: 1-4, $H_s=4.6\text{m}$: 5-7, $H_s=2.3\text{m}$: 8-10.

No Sea State	No Current		Following Current		Opposite Current	
	vertical asymmetry	horizontal asymmetry	vertical asymmetry	horizontal asymmetry	vertical asymmetry	horizontal asymmetry
1	2,15	1,10	2,39	1,10	2,48	1,07
2	2,65	1,09	2,29	1,10	2,30	1,11
3	3,16	1,18	4,47	1,10	2,70	1,11
4	3,54	1,14	3,37	1,26	3,12	1,14
5	2,16	1,06	3,28	1,08	2,37	1,06
6	2,87	1,16	2,88	1,14	3,05	1,14
7	2,65	1,14	3,93	1,33	3,81	1,20
8	2,32	1,07	2,29	1,07	2,22	1,08
9	3,11	1,16	2,63	1,16	4,55	1,16
10	5,31	1,22	2,95	1,29	4,83	1,21

4. INFLUENCE OF CURRENT ON INDIVIDUAL WAVE STEEPNESS

Several definitions of wave steepness have been proposed. Myrhaug and Kjeldsen (1986), Stansberg (1998), Stansell et al. (2003) and also Guedes Soares et al. (2004) presented different sets of definitions to investigate steepness of an irregular waves. In this study the classical steepness s given by equation (3) will be investigated, as it is most often used parameter.

The classical wave steepness s is calculated according to equation:

$$s = \frac{H}{L} \quad (3)$$

The wave length L for this formula can be calculated for each wave separately from the dispersion relation as:

$$L = \frac{gT^2}{2\pi} \quad (4)$$

where g is a gravity acceleration and T is the wave period [s]. After replacing L in equation of wave steepness (eq. 3) by equation 4 the wave steepness formula looks as follows:

$$s = \frac{2\pi H}{gT^2} \quad (5)$$

Wave steepness is directly proportional to the wave height and inversely proportional to the square of its period. Thus wave steepness is not statistically independent of period and height.

The subject of influence of uniform steady current on waves has been investigated for some time. The interaction theory of current on waves in a constant depth was first derived by Longuet-Higgins and Steward (1961). When waves propagate through a region with variable current, some of their characteristic parameters, such as their length, height, steepness, velocity and direction will suffer modifications. The presence of a current alters the velocity of the waves and affects the relation between the observed wave length and period. The current also produces changes in other properties of the waves, as happens with the velocity (and acceleration) of water particles.

Peregrine (1976) identified the “stopping current” velocity for finite amplitude waves, which is the velocity for which breaking of waves occurs.

Huang et al (1972) were probably the first who dealt with the effect of currents in an irregular sea state, showing how wave spectra were changed by the presence of currents, a theory that was the basis of several other developments which were compared with experimental data in Guedes Soares and Pablo (2006).

This study concerns the statistical aspects of individual wave steepness, as influenced by a simultaneous current.

Table 3. Individual wave mean steepnesses and their ratios.

No Sea State	Hs	Tp	Mean Wave Steepness for Test with		
			No Current	Following Current	Opposing Current
1	2,3	7	0,019	0,014	0,032
2	2,3	14	0,007	0,006	0,015
3	2,3	20	0,004	0,004	0,009
4	3,6	7	0,030	0,022	0,040
5	3,6	10	0,019	0,016	0,032
6	3,6	14	0,011	0,009	0,020
7	3,6	20	0,006	0,005	0,010
8	4,6	7	0,037	0,029	0,042
9	4,6	14	0,014	0,012	0,025
10	4,6	20	0,008	0,007	0,012

The presence of a current in a wave field always influences steepness of waves: an opposing current increases amplitudes of waves and decreases their wavelengths (increases steepness) and a following one decreases wave amplitudes and increases wavelengths (decreases steepness).

Table 4. Steepness changes due to current.

No Sea State	Hs	Tp	Ratio of Mean Steepnesses for Sea States	
			Foll. Current No Current [%]	Opp. Current No Current [%]
1	2,3	7	74,0	168,5
2	2,3	14	85,3	204,6
3	2,3	20	91,6	209,1
4	3,6	7	73,8	134,1
5	3,6	10	79,7	162,2
6	3,6	14	79,5	175,7
7	3,6	20	88,5	171,9
8	4,6	7	79,0	113,2
9	4,6	14	86,3	174,3
10	4,6	20	89,5	161,9

Tables 3 and 4 show the ratios of increased and decreased steepness caused by opposing and following currents for sea states 1-10,

where opposite and following currents have the same velocity equal to 1.5 m/s.

Looking at tables 3 and 4 it is visible that all ratios of increase and decrease of steepness grow with the growth of the spectral peak period value for given significant wave height.

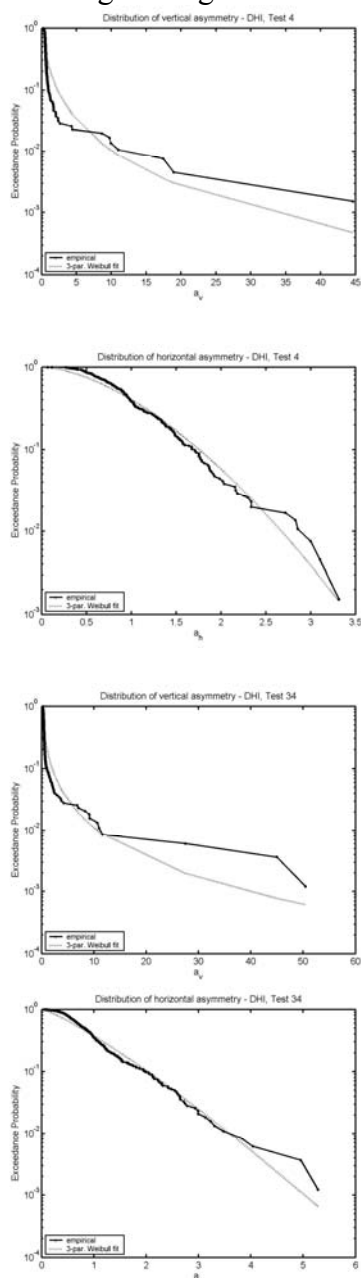


Figure 2. Distribution of vertical asymmetry (first column), distribution of horizontal asymmetry (second column). Asymmetry values were normalized.

The highest ratios of increase of wave steepness in the presence of an opposing

current appeared for the lowest sea states. The ratios grow with the growth of spectral peak period values. The highest decrease of wave steepness in the presence of a following current indicate ratios for sea states with lowest values of the spectral peak value.

5. PROBABILITY DISTRIBUTION OF ASYMMETRY OF INDIVIDUAL WAVES

The vertical and horizontal asymmetry have a very different range of values and statistical behaviour, in particular in the tail of the distributions. Because of a very long tail that most of vertical asymmetry distributions have, it is quite difficult to model values close to the median of the distribution.

Nevertheless, the tail of the vertical asymmetry distributions was fitted quite successfully with 3-parameter Weibull distribution. However the probability of the highest values of the vertical asymmetry is underestimated by the Weibull distribution – see figure 2.

The horizontal asymmetry does not reach so high values, thus the tail is not so long, and it was possible to model successfully the horizontal asymmetry with a 3-parameter Weibull distribution. The best fits were obtained for series without current and with opposing current.

A comparison of asymmetry distributions with current and without it is shown in figure 3. It is visible that current does not seem to have much influence on the extreme values of vertical asymmetry, as it is difficult to notice any pattern on plots from the first column of figure 3. The highest values of horizontal asymmetry were most often provoked by a following current.

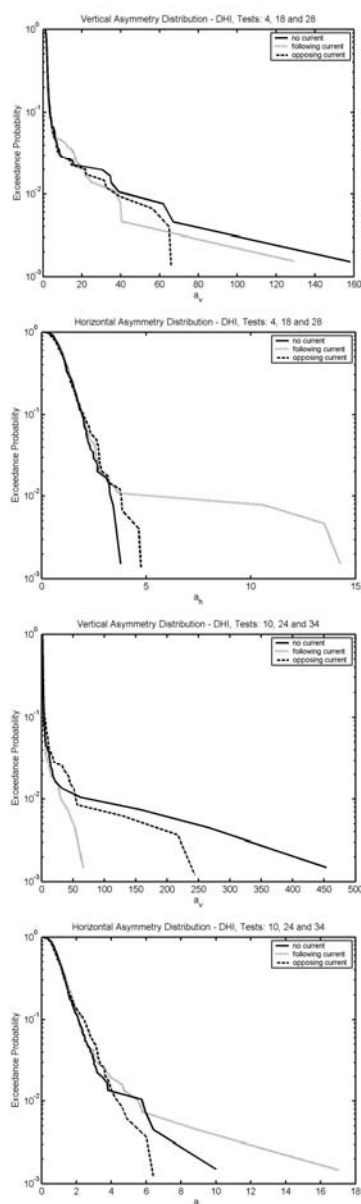


Figure 3. Comparison of distributions of asymmetry of sea states with following, opposing and no current. First column – vertical asymmetry, second column – horizontal asymmetry.

6. PROBABILITY DISTRIBUTION OF STEEPNESS OF INDIVIDUAL WAVES

Marginal distributions of non-normalized wave steepness were also analyzed. Some histograms are presented in figure 4. They are relatively smooth due to the large duration of the time series, which were equal to 87 minutes. This regular structure allowed

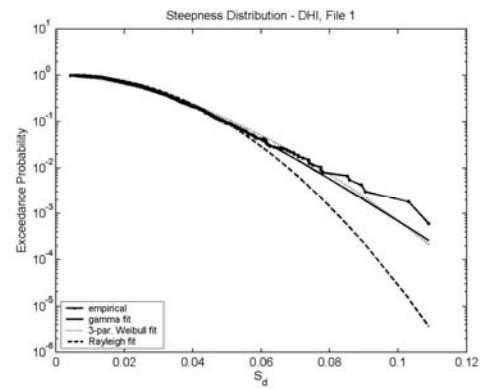
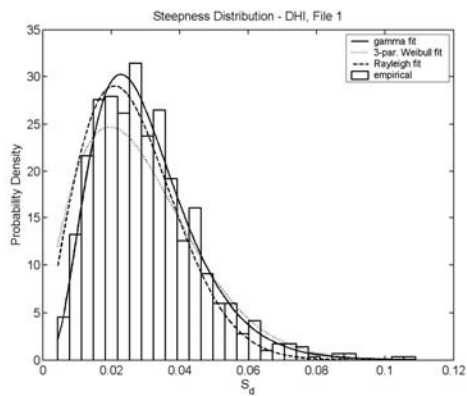
attempts of fitting theoretical distribution to the empirical one. Thus Rayleigh, Gamma and 3-parameter Weibull formulae were tried.

The best fits in the region close to the median of the distribution were obtained with the Gamma distribution as shown in figure 4. On the tail of the distribution the Gamma and Weibull distributions are very similar. They fit well in some cases, but usually they underpredict the probabilities of large wave steepness.

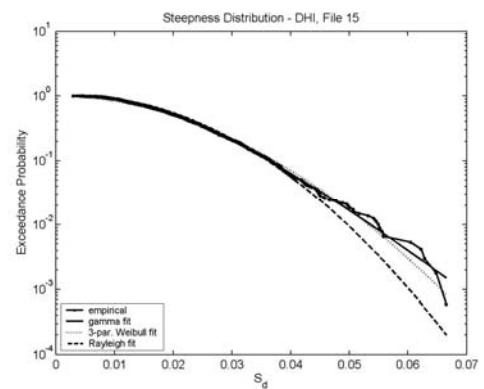
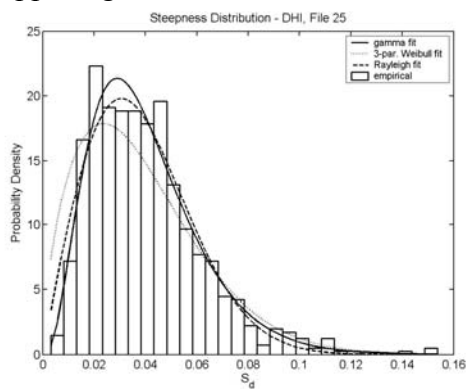
On the basis of all the plots of histograms of wave steepness it was also possible to state that the opposite current provokes a clear shift of the distribution peak towards higher values of steepness, while the shift of the distribution peak towards lower values of steepness with the presence of the following current is not very clear. Currents also influence the range of steepness values, which is increasing when an opposing current is added.

A different comparison of changes of steepness distribution under influence of a current is presented in figure 5. It is visible that values of wave steepness decrease with growth of spectral peak period value and sea states with opposing current have waves of highest values of steepness. More interesting though is that the difference between values of steepness of sea states with opposing current and values of steepness of sea states with following or no current grows with growth of spectral peak period of the sea state. The situation is the same for higher sea states ($H_s = 5$ m) and sea states with weaker current exhibit similar behaviour.

- No current



- Opposing Current



- Following Current

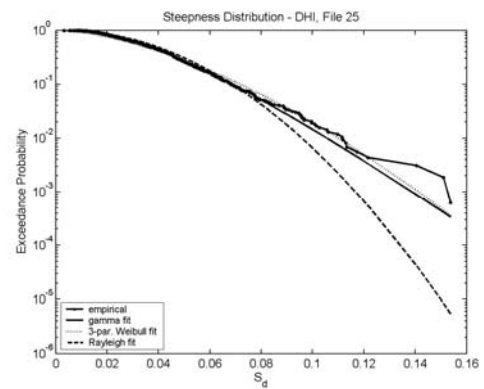
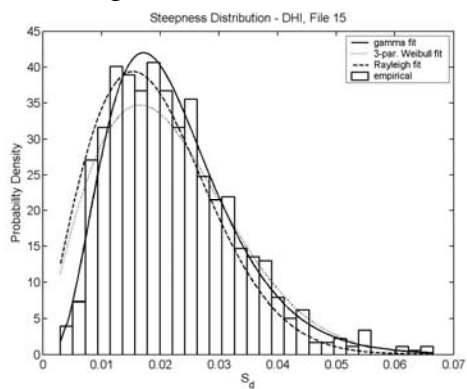


Figure 4. Marginal distribution of steepness for a sea state ($H_s = 3.6$ m, $T_p = 7$ s) – comparison of sea state with following, opposing and no current.

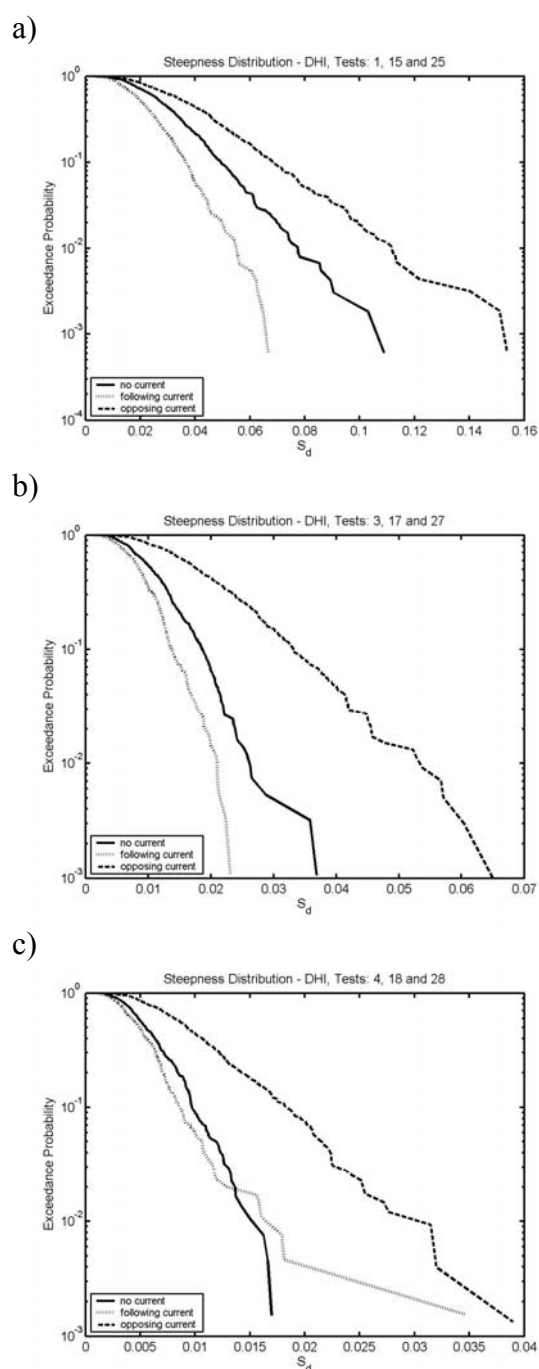


Figure 5. Comparison of steepness distributions without current and with following and opposing currents for sea states: a) $H_s = 3.6$ m and $T_p = 7$ s, b) $H_s = 3.6$ m and $T_p = 14$ s, c) $H_s = 3.6$ m and $T_p = 20$ s.

7. CONCLUSIONS

Vertical and horizontal asymmetry changes caused by following and opposing currents

were described. Vertical asymmetry changes appeared to be quite difficult to interpret. Nevertheless the presence of a current, regardless its direction, seems to increase vertical asymmetry of waves in case of high sea states and decrease it in case of low sea states. Horizontal asymmetry appears to increase more with following current.

Modelling vertical asymmetry with a theoretical distribution is difficult because of the presence of a very long tail in majority of distribution. The tail itself could be modelled by 3-parameter Weibull distribution; however the distribution underestimates the probabilities of the highest values of the vertical asymmetry.

The horizontal asymmetry distributions do not have equally long tail and they could be modelled by a theoretical distribution. The tail of this empirical distribution was fitted quite well with 3-parameter Weibull distribution. The highest values of horizontal asymmetry most often provoked a following current.

An analysis of the marginal steepness distribution was performed and quite successful fits of empirical steepness distribution with Gamma theoretical distributions were presented for sea states with or without current. The Weibull distribution also gave satisfying fits.

Comparisons of changes of cumulative distribution of wave steepness for sea states with and without current with growth of significant wave period were presented. It appeared that the difference between values of steepness of sea states with opposing current and values of steepness of sea states with following or no current grows with growth of spectral peak period of the sea state.

The highest ratios of increase of wave steepness in the presence of an opposing current appeared for the lowest sea states. The ratios grow with the growth of spectral peak period values. The highest decrease of wave steepness in the presence of a following current

indicate ratios for sea states with lowest values of the spectral peak value.

8. ACKNOWLEDGMENTS

The data analyzed here was collected in the project “Interaction of Wave Spectra with Currents”, funded by EU Large-Scale Facilities Programme at DHI Water and Environment.

The work has been performed in the scope of the project MARSTRUCT, Network of Excellence on Marine Structures, (www.mar.ist.utl.pt/marstruct/), which has been financed by the EU through the GROWTH Programme under contract TNE3-CT-2003-506141.

9. REFERENCES

- Guedes Soares, C.; Bitner-Gregersen, E., and Antão, P., 2001, “Analysis of the Frequency of Ship Accidents under Severe North Atlantic Weather Conditions.” *Proceedings of the Conference on Design and Operation for Abnormal Conditions II*, RINA; London, United Kingdom. London, pp. 221-230.
- Guedes Soares, C., Cherneva, Z. and Antão, E., 2004, “Steepness and asymmetry of the largest waves in storm sea states”, *Ocean Engineering*, N° 31, pp.1147-1167.
- Guedes Soares C. and de Pablo, H., 2006, “Experimental study of the transformation of wave spectra by a uniform current”, *Ocean Engineering*, Vol. 33, pp.293-310.
- Guedes Soares, C., Pascoal, R., Antão, E. M., Voogt, A., Buchner, B., 2004, “An Approach to Calculate the Probability of Impact on an FPSO Bow”, *Proceedings of the 23rd International Conference on Offshore Mechanics and Arctic Engineering (OMAE 2004)*, ASME, Paper OMAE 2004-51575
- Huang, N.E., Chen, D.T., Tung, C.C., Smith, J.R., 1972. Interactions between steady non-uniform currents and gravity waves with application for current instruments. *J. Phys. Oceanogr.* 2, 420–431.
- Kjeldsen, S.P., 1997, “Examples of Heavy Weather Damages caused by Giant Waves”, *SNAJ Bulletin of the Society of Naval Architects of Japan*, Vol. 828, pp 744-748.
- Longuet-Higgins, M., S. and Steward, R., W., 1961, “The changes of amplitude of short gravity waves on steady non-uniform currents”, *Journal of Fluid Mechanics*, Vol.10, No 4, pp. 529-549.
- Myrhaug, D. and Kjeldsen, S., P., 1984, “Parametric modelling of joint probability density distributions for steepness and asymmetry in deep water waves”, *Applied Ocean Research*, Vol. 6, pp. 207-220.
- Myrhaug, D. and Kjeldsen, S., P., 1986, “Steepness and asymmetry of extreme waves and the highest waves in deep water”, *Ocean Engineering*, Vol. 13, pp.
- Myrhaug, D. and Kjeldsen, S., P., 1987, “Prediction of Occurrences of Steep and High Waves in Deep Waters”, *Journal of Waterway, Port, Coastal and Ocean Engineering*, Vol. 113, pp 122-138.
- Peregrine, D., H., 1976, “Interaction of water waves and currents”, *Advances in Applied Mechanics*, Vol. 16, Academic Press, pp. 9-117.
- Stansberg, C., 1998, “Non-Gaussian extremes in numerically generated second-order random waves on deep water”, *Proceedings of Eighth ISOPE Conference*, Montreal, Canada, III, pp. 103-110.
- Stansell, P., Wolfram, J., Zachary, S., 2003, “Horizontal asymmetry and steepness distributions for wind-driven ocean waves from severe storms”, *Applied Ocean Research*, Vol. 25, pp. 137-155.

Wave Data Along Ship Routes in the Mediterranean Sea

G.A. Athanassoulis, *School of Naval Architecture & Marine Engineering*

K.A. Belibassakis, *School of Naval Architecture & Marine Engineering*

Th.P. Gerostathis, *School of Naval Architecture & Marine Engineering*

ABSTRACT

The calculation of reliable wave statistics for the probabilistic assessment of ship stability requires various data sets to be assembled, including temporal long term representative directional wave and wind data, for a set of geographical points distributed along the route. In the present paper we give a description of the above data available in the Mediterranean Sea, and their exploitation for the long-term probabilistic assessment of ship stability. We also discuss the problems and consequent limitations associated to each source of data.

Keywords: *wave data, ship routes, Mediterranean Sea*

1. INTRODUCTION

The calculation of reliable wave statistics for the probabilistic assessment of ship stability requires various data sets to be assembled, including temporal long term representative directional wave and wind data, for a set of geographical points distributed along the route. In general, there are four main sources of marine wind and wave data, which can be exploited for deriving long-term wave statistics: visual observations from ships, data measured from buoys or platforms, data measured by remote instruments on board of high altitude satellites, meteorological and wave models operational at the various meteoceanographic centres. The above data have different characteristics expressed as quality, accuracy, errors present in the data, geographical distribution, number of data and missing values. In the present paper we give a description of the above data available in the Mediterranean Sea. We also discuss the problems and consequent limitations associated

with each source of data. The above data can also be exploited for the short-term assessment of ship stability by reconstructing wave spectra from integrated parameters along ship routes in the Mediterranean Sea (using, e.g., simple mixture-type models for the directional wave spectrum), and applying the model spectrum to investigate critical events associated with the short-term ship stability.

2. WAVE AND WIND DATA SOURCES IN THE MEDITERRANEAN SEA

There are four main sources of marine wind and wave data available to the user: (a) visual observations from ships, (b) data measured from buoys or platforms, (c) data measured by remote instruments on board of high altitude flying satellites, and (d) meteorological and wave models operational at the various meteoceanographic centres. The above data have different characteristics expressed as quality, accuracy, errors present in the data, geographical distributions, quantity of data. In the following, we give a brief description of the

wave and wind data sources, and the data in the Mediterranean Sea that are available to NTUA. We also list the problems and consequent limitations associated to each source and/or instrument.

2.1 Visual Data

Many decades of visual data exist, and a full generation of atlases has been based on this kind of data. Apart from other drawbacks, a major limitation of the visual data is their preferential distribution along the most common maritime routes, and the tendency of ships to avoid the stormy areas, which leads to the derivation of biased statistics. The “Wind and Wave Atlas of the North-Eastern Mediterranean Sea”, Athanassoulis & Skarsoulis (1992), prepared by NTUA under the authority of Hellenic Navy General Staff, is based on visual data from the British Meteorological Office, the Greek National Meteorological Service and the U.S. National Climatic Data Center. The observations used for the considered area of North-Eastern Mediterranean Sea come from voluntary ships, collected in the period 1949-1988.

2.2 Buoy data

A substantial number of buoys, either non-directional or directional ones, are distributed along the coasts of the Mediterranean Sea. Extended buoy networks exist and operate along the Spanish, French, Italian and Greek coastline and are presented in brief below. Also, some buoys operate in other places along the coasts of Mediterranean Sea, as e.g. the buoy in Cape Arnaoutis, Cyprus ($35^{\circ}9.16'N$, $32^{\circ}15.88'E$), and various buoys along the coasts of Israel and Turkey.

The Spanish buoy network consists of the deep sea and the coastal networks, shown in Figures 1a and 1b, respectively. The deep sea

network is based on 11 Seawatch (Figure 1a, black circles) and 3 WaveScan (Figure 1a, white circles) buoy stations. The instruments are located at points with depths between 200 and 800 m and measure atmospheric and oceanographic parameters. Measurements are transmitted every hour via satellite to Puertos del Estado (PE) and directly posted to the web site of PE (<http://www.puertos.es>).

The Coastal Network, also belonging to Puertos del Estado, is providing real time data in some specific points located at shallow waters. The main objective of the measurements is to complement those of the Deep Sea Network at those locations of special interest for the port operations or wave modelling validation. The buoys employed are scalar Waverider (Figure 1b, black circles) and directional (Figure 1b, white circles). More details about the Spanish network can be found in the web page of PE (<http://www.puertos.es>)

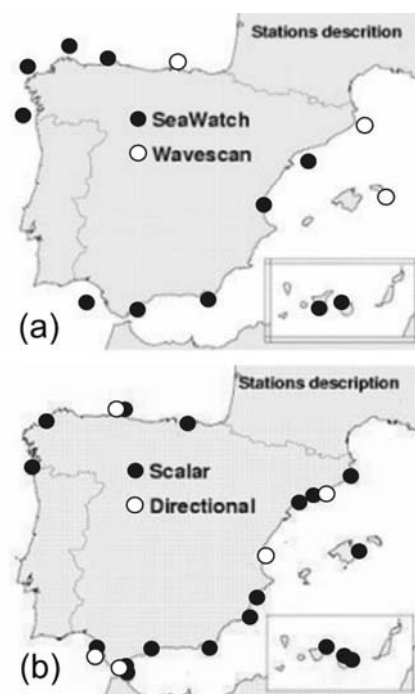


Figure 1: (a) Spanish deep sea buoy network, (b) Spanish coastal buoy network (<http://www.puertos.es>, Oceanography and Meteorology section).

The French buoy network consists of a

number of coastal and deep sea buoys, shown in Figure 2. In the Mediterranean Sea the two buoys operate owned and maintained by Meteo France: (i) Station 61001 - Nice Buoy, location: 43.40 N 7.80 E (43°23'60" N 7°47'60" E), and (ii) Station 61002 - Lion Buoy 42.10 N 4.70 E (42°6'9" N 4°42'9" E). More details about the French network can be found in the web page of MeteoFrance (<http://http://www.meteofrance.com>). Measurements of these buoys can be accessible on line through the National Data Buoy Center (NDBC, <http://www.ndbc.noaa.gov>) of the National Oceanic & Atmospheric Administration (NOAA) of U.S.

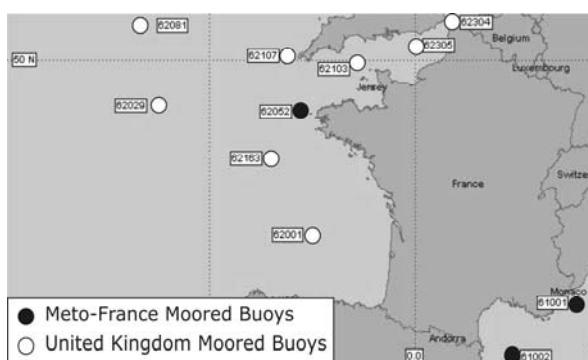


Figure 2: French buoy network (<http://www.ndbc.noaa.gov/Maps/France.shtml>).



Figure 3: Italian buoy network (<http://www.envirtech.org/ron.htm>).

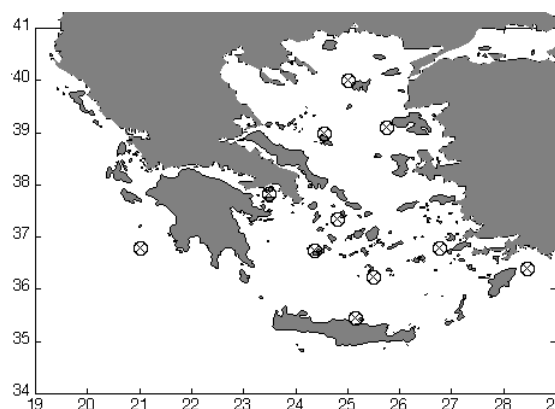


Figure 4: Greek buoy network (<http://www.poseidon.ncmr.gr>).

The Italian buoy network RON (Rete Ondametrica Nazionale) consists of a number of coastal and deep sea buoys, as shown in Figure 3. The buoy network has been appointed by the Italian Agency for Environmental Protection and Technical Services (APAT) and has been the first real-time updated Network in the Mediterranean Sea. More details about the Italian network can be found in the RON web page (<http://www.envirtech.org/ron.htm>).

The Greek buoy network is operating since 1999 in the Aegean Sea, under the supervision of Hellenic National Center for Marine Research (NCMR). The buoy positions are shown in Figure 4. The observation buoys are equipped with sensors that monitor, except of wind speed and direction and wave height, also wave period and mean wave direction, as well as other parameters (such as air-temperature, sea surface salinity and temperature, surface current speed and direction, sea surface dissolved oxygen and others). Details about the Greek buoy network in the Aegean Sea can be found in the NCMR-POSEIDON web page (<http://www.poseidon.ncmr.gr/>).

In the Mediterranean Sea the buoys represent the most accurate source of

information for wave data. The error is estimated in the order of a few percents. The error grows when we move to the highest wave heights, for the tendency of the buoys to slip around the highest crests, leading to an underestimation of the overall wave height. It is obvious that the buoy data are far from being sufficient for characterising larger areas or ship routes in the Mediterranean Sea. The buoys are mostly located very close to the coasts, and thus they are not representative of the conditions in the parts of open sea. Also, a major limitation of many of the buoy datasets is the lack of wind data. The usefulness of buoy data is that they can be used to validate satellite data, covering more extended areas; see Figure 5. Then, the latter can be used to calibrate the data from operational wind and wave models.

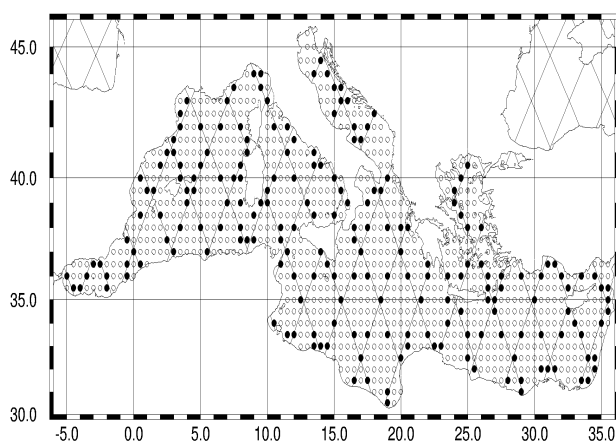


Figure 5: WAM model grid points and TOPEX tracks in the Mediterranean Sea. Filled circles are model points close to satellite tracks used for deriving calibration factors of model data vs. validated satellite data (Barstow *et al*, 2001).

In various recent projects, dealing with the derivation of wave and wind statistical information in coastal areas and in open sea, such as the EUROWAVES project (Barstow *et al*, 2001), WORLDWAVES (Barstow *et al*, 2003a, 2003b) and MEDATLAS project (Athanasoulis *et al*, 2004) the calibrated data,

as described above, have been used to derive the statistics for the geographical areas of interest. More details about the validation/calibration procedure can be found in Barstow *et al* (2001, 2003a, 2003b); see also Figure 5.

2.3 Satellite data

Satellite radar altimeters provide estimates of the significant wave height and the wind speed (at 10m above the seawater level) along the satellite track (see, e.g., Aage *et al*, 1998). Scatterometers provide the 10m wind vector on the 500km width swath by measuring the radar cross section at different incident angles. In Mediterranean Sea satellite data are available from ERS1, ERS2, TOPEX/Poseidon and ENVISAT. For waves below 1m the error of the altimeter significant wave height is quite big. Also, because of contamination of the signal by land echo, wind and wave data are not accurate close to the coast. More details about the accuracy and problems of Topex altimeter data can be found in Cotton *et al* (1997), Lefevre & Cotton (2001), for ERS data in Queffeulou (1996) and for ENVISAT in Johnsen (2005); see also Athanasoulis *et al* (2004).

2.4 Model data

Many different institutions run global atmospheric and wave models, producing daily forecast and analysis worldwide. Because of the multiscale character of the weather/wave phenomena, nested models with much higher resolution are required in order to describe with sufficient accuracy the fields in the inner basins, like the Mediterranean Sea. This is especially true for areas including fine-scale geographical features (islands etc), as for example is the case of the Aegean Sea. Nowadays most (if not all) Meteorological

Offices in Europe use the WAM wave model, Komen *et al* (1994), both for weather forecasting and hindcasting studies.

Model data is the only available data source exhibiting spatial coverage and time extent permitting the derivation of long term wind and wave statistics in the whole Mediterranean Sea. WAM model data can be provided by European Centre for Medium-Range Weather Forecasts (ECMWF, Reading, U.K.) or by the National Met Offices of European countries having association agreements with ECMWF. Two versions of the WAM model have been operational at ECMWF, one for the global ocean and one for the Mediterranean Sea. The wave model for the Mediterranean Sea became operational in July 1992. A 0.5 degree resolution was initially used in both latitude and longitude, for an overall number of about 950 points. The resolution was later increased to 0.25 degree, for an overall almost 4000 points. The original wave model for the Mediterranean Sea included the area between 6° West and 36° East in longitude, and 30° and 46° North in latitude. The area was later extended to include the Baltic Sea. In the Fall of 1998 a much more extended version was made operative.

As has been found during various research projects (e.g. EUROWAVES, MEDATLAS) WAM wave data in the Mediterranean Sea underestimate the significant wave height, in a strongly non-uniform manner. The distribution of the calibration factor, defined as the ratio of the WAM model calculated value and the (satellite) measured value, for the whole Mediterranean Sea, is shown in Figure 6, taken from EUROWAVES project (Barstow *et al*, 2001). As it can be seen in the Northern part of the Mediterranean Sea, the underestimation of H_S is significant (WAM $H_S \approx 40 - 60\%$ of measured H_S). This means that model data can be reliably used only after

proper calibration.

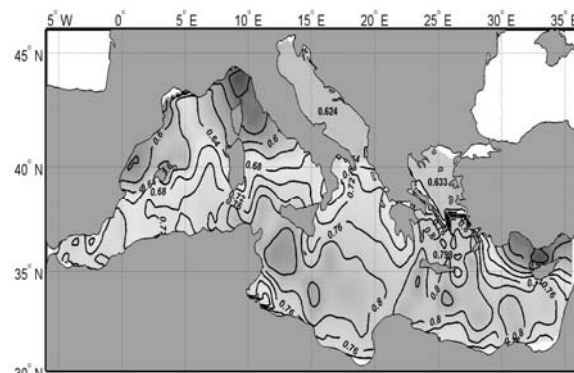


Figure 6: Geographical distribution of H_S - calibration factor in the Mediterranean.

3. DESCRIPTION OF AVAILABLE WIND AND WAVE DATA IN THE MEDITERRANEAN SEA

A 10-year database is available to NTUA from previous projects, which consists of 6-hourly time series of model wave and wind data from the European Centre for Medium-Range Weather Forecasts (ECMWF). The data are available on a 0.5° regular grid of offshore geographic locations of the Mediterranean Sea area, shown in Figure 7.

These data come from the WAM wave model run at ECMWF and have been calibrated using calibration factors in the Mediterranean Sea, available to NTUA from the EUROWAVES project (Barstow *et al*, 2001). For each geographical location, a 6-hourly timeseries is available spanning the time period from 1/7/1992 to 30/6/2002.

Each record in the time series contains the significant wave height, H_S , the energy wave period, T_{-10} , the mean wave direction, Q , for the total sea spectrum, as well as for the wind sea part and the swell part of the spectrum, and in addition contains the peak period, T_p , the wind speed (at 10 m height), $W_{10,SP}$ and the wind direction, $W_{10,dir}$. On the basis of the above data also time series of useful derived

quantities can be obtained, such as the wave slope parameter based on mean energy period ($b_{.10} = 2pH_S / gT_{.10}^2$) and the wave slope parameter based on peak period ($b_p = 2pH_S / gT_p^2$).

Using sophisticated statistical analysis tools developed at NTUA, various univariate, bivariate and directional statistical results (in the form of frequency tables or histograms or probability models fitted to the data) can be obtained from the wind and wave database. For each geographical location of the 0.5° grid, the type of statistical analysis results which are currently available are listed in detail in Tables 1 and 2. Of course, the tables can be extended to include similar type statistical results concerning the wind parameters, combinations As an example we list below various types of data that can be provided, either at specific sea areas or along ship routes in the Mediterranean Sea from the NTUA wind and wave database.

C.1 Histograms (frequency tables) of H_S vs. T_P or H_S vs. $T_{.10}$ associated with the total sea spectrum, on a monthly basis or combination of months or seasons or annually. The typical formats of NTUA (H_S vs. T_P) data, for one datapoint in the Mediterranean Sea, are shown in Table 3. It is noted here that various partitions (coarse, medium, fine) of the parameter space (significant wave height, wave period, mean wave direction etc.) are possible, in order to better model the details of the corresponding univariate and multivariate probability distributions and to better fit to the user's needs. As an example, the fine partition is shown in Table 3.

C.2 Same as in C.1, but conditionally with respect to mean wave direction (the corresponding mean wave direction bins are: $0^\circ, 15^\circ, \dots, 360^\circ$).

C.3 Histograms (frequency tables) of H_S vs. $T_{.10}$, associated with the wind-sea part of

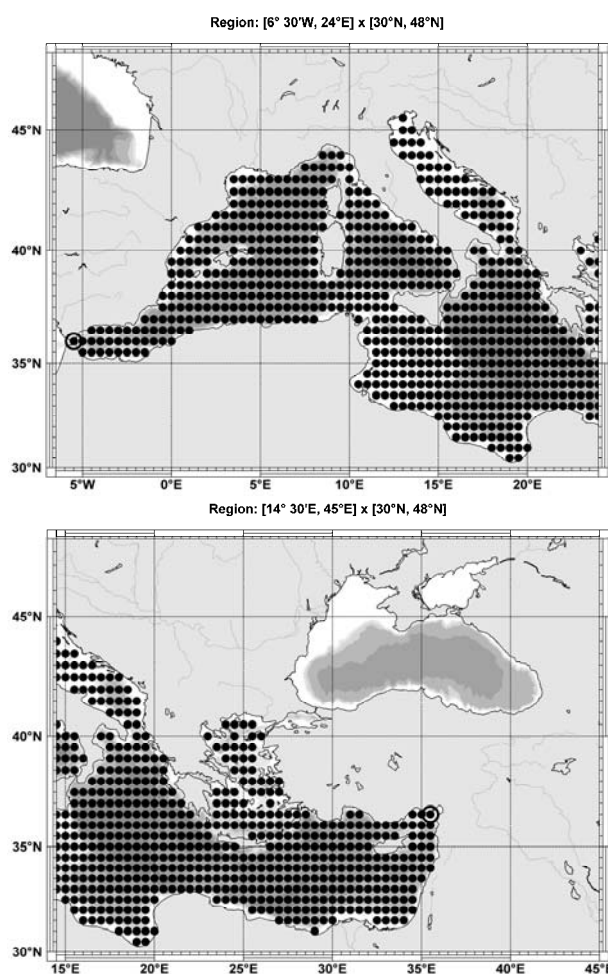


Figure 7: NTUA database: Wind and wave data points in the Mediterranean Sea. The datapoints are shown by using black bullets of wave and wind parameters as well as other derived quantities.

the spectrum, on a monthly basis or combination of months or seasons or annually, at representative points of the 0.5deg grid near the ship route.

C.4 Same as in C.3, but conditionally with respect to mean wave direction

C.5 Histograms (frequency tables) of H_S vs. $T_{.10}$, associated with the swell part of the spectrum on a monthly basis or combination of months or seasons or annually, at representative points of the 0.5deg grid near the ship route.

Table1. Univariate statistics. All the above are available on a monthly basis or combination of months or seasons or annually

Tables	Graphs
Frequency table of H_S [TS ¹ , WW, SW]	Probability density function of H_S [TS, WW, SW]
Frequency table of T_{-10} [TS, WW, SW]	Probability density function of T_{-10} [TS, WW, SW]
Frequency table of T_P [TS]	Probability density function of T_P [TS]
Frequency table of Q [TS, WW, SW]	Probability density function of Q [TS, WW, SW]
Frequency table of $DQ = Q_{WW} - Q_{SW}$	Probability density function of $DQ = Q_{WW} - Q_{SW}$
Frequency table of b_{-10} [TS, WW, SW]	Probability density function of b_{-10} [TS, WW, SW]
Frequency table of b_P [TS]	Probability density function of b_P [TS]

Table 2. Bivariate statistics. All the above are available on a monthly basis or combination of months or seasons or annually.

Tables	Graphs
Frequency table of (H_S, T_{-10}) [TS, WW, SW]	Probability density function of (H_S, T_{-10}) [TS, WW, SW]
Frequency table of (H_S, T_P) [TS]	Probability density function of (H_S, T_P) [TS]
Frequency table of (H_S, b_{-10}) [TS, WW, SW]	Probability density function of (H_S, b_{-10}) [TS, WW, SW]
Frequency table of (H_S, b_P) [TS]	Probability density function of (H_S, b_P) [TS]
Frequency table of (H_S, DQ)	Probability density function of (H_S, DQ)

Table 3. Typical format of H_S vs. T_{-10} data (Image format, fine partition) for one datapoint in the Mediterranean Sea.

Bivariate frequency table of (H_S, T_{-10}) (Sea and Swell)

T_{-10} \ H_S [m]	0	0.5	1	1.5	2	2.5	3	3.5	4	4.5	5	5.5	6	6.5	7	7.5	8	8.5	9	10	15	Total	
0.00-0.10	0	0	0	0	0	0	0	0	0	0	0	0	0	0	0	0	0	0	0	0	0	0	0
0.10-0.20	0	0	0	0	0	0	1	2	1	0	0	0	0	0	0	0	0	0	0	0	0	0	5
0.20-0.30	0	0	0	0	0	0	2	12	11	5	3	2	2	0	0	0	0	0	0	0	0	0	46
0.30-0.40	0	0	0	0	0	3	16	18	17	9	4	2	1	0	0	0	0	0	0	0	0	0	88
0.40-0.50	0	0	0	0	4	19	28	19	10	4	2	1	0	0	0	0	0	0	0	0	0	0	113
0.50-0.60	0	0	0	0	1	4	16	21	30	16	8	3	2	1	1	1	1	0	0	0	0	0	105
0.60-0.70	0	0	0	0	0	2	11	22	28	20	11	5	3	3	1	1	1	0	0	0	0	0	171
0.70-0.80	0	0	0	0	0	1	9	17	22	20	10	6	4	4	2	2	2	1	1	1	0	0	222
0.80-0.90	0	0	0	0	0	0	5	13	19	21	14	8	4	4	2	2	1	1	1	0	0	0	281
0.90-1.00	0	0	0	0	0	0	3	8	14	17	13	7	7	7	5	2	2	1	1	1	0	0	366
1.00-1.10	0	0	0	0	0	0	1	6	12	14	15	8	8	5	2	2	1	1	1	0	0	0	467
1.10-1.20	0	0	0	0	0	0	1	4	7	9	11	6	4	4	2	1	1	1	0	0	0	0	567
1.20-1.30	0	0	0	0	0	0	0	3	5	7	7	7	5	5	2	2	1	1	0	0	0	0	667
1.30-1.40	0	0	0	0	0	0	0	2	4	6	7	8	6	5	3	2	1	1	0	0	0	0	767
1.40-1.50	0	0	0	0	0	0	0	1	3	3	4	6	5	3	3	1	1	0	0	0	0	0	867
1.50-1.60	0	0	0	0	0	0	0	0	2	3	3	4	4	3	3	3	1	1	0	0	0	0	967
1.60-1.70	0	0	0	0	0	0	0	0	1	3	3	4	4	3	3	3	3	1	1	0	0	0	1067
1.70-1.80	0	0	0	0	0	0	0	0	1	2	2	2	2	2	2	2	2	1	1	0	0	0	1167
1.80-1.90	0	0	0	0	0	0	0	0	0	2	2	2	2	2	2	2	2	1	1	0	0	0	1267
1.90-2.00	0	0	0	0	0	0	0	0	0	1	2	2	2	2	2	2	2	2	1	1	0	0	1367
2.00-2.25	0	0	0	0	0	0	0	0	0	1	2	3	3	4	4	4	4	2	2	1	1	0	1467
2.25-2.50	0	0	0	0	0	0	0	0	0	0	2	3	3	4	4	4	4	3	2	1	1	0	1567
2.50-2.75	0	0	0	0	0	0	0	0	0	0	0	0	0	0	0	0	0	0	0	0	0	0	1667
2.75-3.00	0	0	0	0	0	0	0	0	0	0	0	0	0	0	0	0	0	0	0	0	0	0	1767
3.00-3.25	0	0	0	0	0	0	0	0	0	0	0	0	0	0	0	0	0	0	0	0	0	0	1867
3.25-3.50	0	0	0	0	0	0	0	0	0	0	0	0	0	0	0	0	0	0	0	0	0	0	1967
3.50-3.75	0	0	0	0	0	0	0	0	0	0	0	0	0	0	0	0	0	0	0	0	0	0	2067
3.75-4.00	0	0	0	0	0	0	0	0	0	0	0	0	0	0	0	0	0	0	0	0	0	0	2167
4.00-5.00	0	0	0	0	0	0	0	0	0	0	0	0	0	0	0	0	0	0	0	0	0	0	2267
5.00-6.00	0	0	0	0	0	0	0	0	0	0	0	0	0	0	0	0	0	0	0	0	0	0	2367
6.00-10.00	0	0	0	0	0	0	0	0	0	0	0	0	0	0	0	0	0	0	0	0	0	0	2467
Total	0	0	0	0	1	17	96	167	181	164	127	96	68	39	23	11	5	3	2	2	2	1000	

Data point(s) identification

1 MED-043 (0.5)
(35° 30' N, 32° E)
Data:1992-07-01
2002-06-30

Month(s): 1, 2, 3, 4, 5
7, 8, 9, 10,
11, 12

Num. of observ.: 14600

Empirical Statistics

	H_S [m]	T_{-10} [s]
Mean Value	0.97	4.78
Stand. Dev.	0.63	1.18
Var. Coeff.	0.63	0.25
Skewn. Coeff.	2.45	1.03
Kurt. Coeff.	11.06	2.45
Sample Min	0.13	2.24
Sample Max	3.48	15.86

C.6 Same as in C.5, but conditionally with respect to mean wave direction.

C.7 Histograms (frequency tables) of H_S vs. $W_{10,SP}$, on a monthly basis or combination of months or seasons or annually.

4. CONCLUSIONS

A description of the wind and wave data available in the Mediterranean Sea is given, and the problems and consequent limitations associated to each source of these data have been discussed as concerns their exploitation for the long-term probabilistic assessment of ship stability.

The above data can also be exploited for the short-term assessment of ship stability by reconstructing wave spectra from integrated parameters. Future work is planned towards: (i) the investigation of simple mixture-type models for modelling the directional wave spectrum along ship routes in the Mediterranean Sea, and (ii) the evaluation of the predictive capability of the model spectrum

¹ Statistics of the various parameters are available for each one of the following three categories of spectra:

- TS : Total sea spectrum,
- WW : Wind sea part of the spectrum,
- SW : Swell part of the spectrum.

as concerns critical events associated with the short-term ship stability.

5. ACKNOWLEDGMENTS

The present work has been partially supported by EU in the framework of the SAFEDOR (design, operation and regulation for safety) Integrated Project 516278, 6th framework programme of the European Commission.

6. REFERENCES

- Aage C, Allan T., Carter D., Lindgren G., Olagnon M., 1998, Oceans from Space, Editions Ifremer.
- Athanassoulis G.A., Skarsoulis, E., 1992, "Wind and Wave atlas of the North Eastern Mediterranean Sea", prepared by NTUA under the authority of Hellenic Navy General Staff, ISBN 960-254-030-3.
- Athanassoulis G.A. *et al*, 2004, "Metadlas: Wind and wave atlas of the Mediterranean Sea", WEAU (consortium: CS, NTUA, CNR /ISMAR, THETIS, Semantic, Meteo-France), ISBN 2-11-095674-7.
- Barstow S. F., Athanassoulis G.A., Cavaleri L., Mørk G, Belibassakis K.A., Stefanakos Ch.N., Gerostathis Th.P., Sclavo M., Bertotti L. and H. E. Krogstad, 2001, "EUROWAVES: A user-friendly tool for the evaluation of wave conditions at any European coastal location", Final Technical Report of project EUROWAVES (MAS3-CT97-0109).
- Barstow S., Mørk G, Lønseth L, Schjølberg P., Machado U., Athanassoulis G.A., Belibassakis K., Gerostathis T., Stefanakos Ch., Spaan G., 2003a, "WORLDWAVES: Fusion of data from many sources in a user-friendly software package for timely calculation of wave statistics in global coastal waters", Proceedings of 13th Intern. Offshore and Polar Conference and Exhibition, ISOPE2003, Honolulu, Hawaii, USA.
- Barstow S., Mørk G, Lønseth L, Schjølberg P., Machado U., Athanassoulis G.A., Belibassakis K., Gerostathis T., Stefanakos Ch., Spaan G., 2003b, "WORLDWAVES: High quality coastal and offshore wave data within minutes for any global site", Proceedings of 22nd International Conference on Offshore Mechanics and Arctic Engineering, *OMAE2003*, Cancun, Mexico.
- Cotton, D., Challenor, P.G., Carter, D., 1997, "An assessment of the accuracy and reliability of Geosat, ERS-1, ERS-2 and Topex altimeter measurements of significant wave height and wind speed", Proceedings of CEOS wind and wave validation workshop, ESTEC, Noordwijk, The Netherlands.
- Johnsen H., 2005, "ENVIWAVE: Development and Application of Validated Geophysical Ocean Products from Envisat ASAR and RA-2 Instruments", Final Technical Report of project ENVIWAVE (EVG1-CT-2001-00051).
- Komen G.J., Cavaleri L., Donelan M., Hasselmann, K., Hasselmann, S., and Janssen, P.A.E.M., 1994, "Dynamics and Modelling of Ocean Waves", Cambridge University Press.
- Lefevre, J.-M., Cotton, D., 2001, "Ocean Surface Waves" in "Fu, L.L. & Cazenave, A. (Eds): Satellite Altimeters and Earth Sciences", Academic Press, Int. Geophysics Series, Vol. 69.
- Queffeuilou P., 1996, "Significant wave height

and backscatter coefficient at ERS1/2 and Topex-Poseidon ground-track crossing points”, FDP final report ESA contract 143189, Dept. d’Oceanographie Spatial, IFREMER.

Physics and Statistics of Extreme and Freak Waves

Leonid Lopatoukhin, *St. Petersburg State University*

Alexander Boukhanovsky, *St. Petersburg State University*

ABSTRACT

Problem of estimation of high waves is not as critical as 10-20 years ago. Now it is possible to make continues hindcasting (30 and longer years duration) of directional spectra for any region and to estimate probability of high waves with n-years return period. For ship navigations, transport operations, offshore supplying etc spatiotemporal variability of wave fields may be also estimated. One of the most interesting extreme phenomena is freak (or rogue) waves. Freak wave is unusual not only by there height, but by their form. Results of hindcasting do not display any suspicion to a freak wave as this is a single wave. Classical statistical approach to analysis of time series do not allows estimating the probabilities of freak waves. Proposed approach to statistics of freak waves is based on probabilistic treatment of a wave field as random model with contaminated distribution

In order to efficiently use calculated statistics in practice it is important to focus on the measure of risk, which is taken as acceptable limit. This is very delicate balance of factors in which consequence of damage, cost of construction, and cost of mitigation of possible accident are major players.

Keywords: *wind waves, extremes, freak*

1. INTRODUCTION

Presently the main source of wave climate information is based on the results of hydrodynamic simulation (in other words hindcasting). Reanalysis data are the input to hindcasting are. The NCEP/NCAR, ERA40 and Sweden reanalysed wind fields were used in present report. For extreme wave estimation reanalysis data have to be improved by assimilation of additional ship observation and synoptic data. Regression and Kalman filtration approaches are used. (For details see, e.g. (Lopatoukhin et al, 2004)). Nested models Wave Watch (versions 1.18, 2.22) and SWAN (versions 40.11, 40.31) are applied. Barents, Caspian, Baltic, North, Okhotsk, Azov seas and Ladoga Lake used as deep and shallow water basins. Metocean fields, like ocean waves, have a complex spatial and temporal variability

(synoptic, annual, year-to-year). Traditionally, the approach for statistical formalization of such phenomena has been based on a multiscale hypothesis and modelling the total variability by means of a set of stochastic models for each temporal scale.

2. EXTREME WAVES

2.1 Extremes at a Point

There are a lot of approaches to calculations of extreme wave heights in a point. The main are IDM (Initial Distribution Method), AMS (Annual Maxima Series), POT (Peak Over Threshold) and BOLIVAR. Short resume with the example is presented at fig. 3. IDM method estimates the extreme wave height h_{\max} of certain return period as quantile h_p of wave height distribution $F(h)$ with probability p . For

log-normal long-term wave height distribution, the quantile with probability p can be computed as follows:

$$h_p = h_{0.5} \exp\left(\frac{U_p}{s}\right) \quad (1)$$

U_p is quantile of the standard normal distribution. Here quantile h_p should be understood as wave height, which is likely to be observed once (at the standard synoptic observation times) in T years. In applied studies the period T is called "return period", and the corresponding probability is defined as

$$p = \frac{\Delta t}{24 \cdot 365 \cdot T} \quad (2)$$

Where Δt is interval (in hours) between subsequent observations (say, 6 hours). Then we get $p = 0.000684/T$. For $\Delta t = 3(hr)$, we get $p = 0.000342/T$.

AMS approach defines h_{max} as the last term of the ranked independent series of wave heights h . The AMS method has the most solid theoretical background with Gumbel distribution

$$F(x) = \exp(-\exp(-a(x-b))) \quad (3)$$

Where a , b – parameters. The POT approach uses k strongest storms with the heights greater than selected threshold. Thus, the POT method estimates depend on the choice of threshold and approximations for corresponding distributions. Unlike other methods, in the POT approach the uncertainty is connected both with the wave height h_p^* and return period. BOLIVAR approach (Rozhkov et al, 1999; Lopatoukhin et al, 2000) excludes the limitations of the POT method and take into account the asymptotic characteristics of AMS. BOLIVAR approach considered n samples, consisting of heights h_{ij}^+ of the largest waves in the k the strongest storms in year number i , ($i=1, \dots, n$; $j=1, \dots, k$). The BOLIVAR method represents its further development that includes

into consideration the second, third and, potentially, other maximums in a year. Each of the considered methods has its advantages and disadvantages and has to be used accordingly (Lopatoukhin et al, 2000).

2.2 Extremes at a Field

Storm evolution in any basin may be presented as an impulse random field

$$\zeta(\vec{r}, t) = \sum_k W_k^{z(\vec{r})}(\vec{r}, t | X) \quad (4)$$

Where $W_k^{z(\vec{r})}(\bullet)$ – spatiotemporal impulse with respect level $z(\vec{r})$. At any time $W_k^{z(\vec{r})}(\bullet)$ can be presented as an elliptic cone. The size of the storm $\{r_0(t), h^+(t), S_\Omega(t)\}$ is equal to the fraction of total area of the region, where wave heights larger than z .

The behavior of the extreme wave in a single storm in a fixed point is known [Boukhanovsky et al 1998]. For spatial region this problem more complex, because unique enumeration available only for two-dimensional waves.

In the simplest case, with a narrow angular spreading of sea waves, the generalized distribution of maximal wave in a spatial storm region is

$$F_m(h) = \exp\left[2\pi \int_0^L \left(-\exp\left(-\frac{\pi}{4} \left(\frac{h}{\bar{h}(r)}\right)^2\right)\right) \frac{rdr}{\lambda(r)}\right] \quad (5)$$

Here $2L$ is the equivalent diameter of the storm, where $L = 2\sqrt{S_\Omega(t)/\pi}$, $S_\Omega(t) = \int_{\Omega(t)} d\vec{r}$. For small-amplitude waves $\lambda(r) \approx 36\bar{h}(r)$.

The storm impulse $\bar{h}(r)$ is approximated by expression $\bar{h}(r) = h^+ - (h^+ - z)(r/L)^m$, where m is the shape parameter of storm impulse ($m=1$ – cone, $m=2$ – parabolic etc).

Fig. 1 shows extreme wave heights (0.1% probability) with return period 100 years. This figure (as a lot of similar, published in different

papers, handbooks and atlases) is a result of calculation at separate points and driving isolines. Data of such figure represent the wave heights estimates that are possible at any point, *but not in all points simultaneously*. In the last case the return period of such events will be highly more, than 100 years.

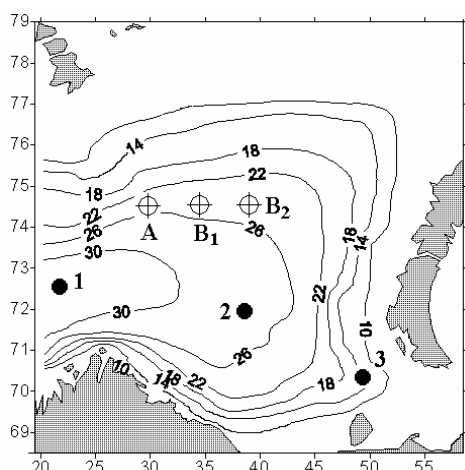


Fig. 1. Spatial estimates of waves (0.1%) with return period 100 years. Barents Sea.

This became more clear from the Fig. 2. There are shown annual maxima $h_s^{(A)}$ in the point "A" and conditional values $h_s^{(B/A)}$ in the points B₁ and B₂. They are at distance 120 and 240 km from point "A". It is seen, that in spite of significant distance between points, the values of wave heights of rare probability are dependent. This also means that the same return period may appropriate to different combinations of waves. E.g. (fig. 2), 100 years significant wave in the point "A" is 14.4m, but wave height in the point "B₁" is 13.7m (i.e. with return period 50 years). Moreover 100-year event may result from a set of events each of it is less than 100 year. E.g., 100 years case will be, when:

- in the point "A" $h_s^A = 12.1\text{m}$ (10 years return period);
- in the point "B₁" $h_s^{B_1} = 13.2\text{m}$ (30 years return period);
- in the point "B₂" $h_s^{B_2} = 13.8\text{m}$ (60 years return period).

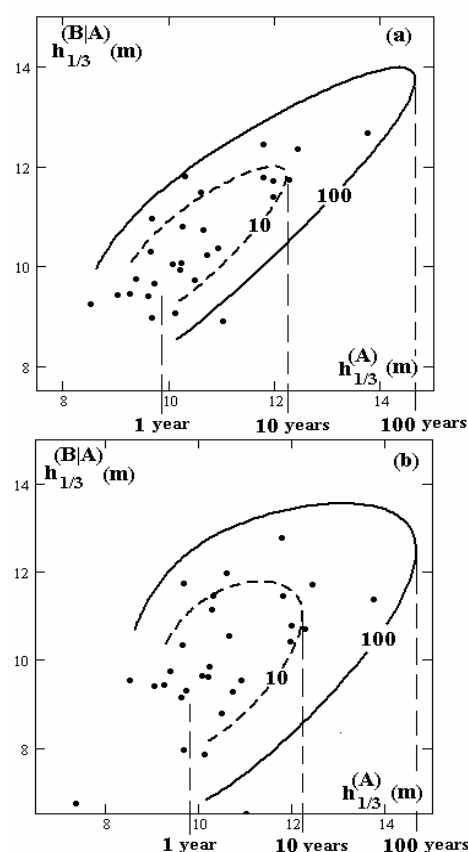


Fig. 2. Points and curves of return periods of annual maxima. Significant wave heights $h_{1/3}^A$ in the point "A" and wave heights $h_{1/3}^{B/A}$ in the points «B₁» (a) and «B₂» (b), at the same time.

3. FREAK WAVES

One of the most interesting extreme phenomena is freak waves (Mallory 1974, 1984; Provision, 1998; Proceedings, 2000, 2002; Rogue 2000, 2004), – as anomaly steep and high waves. Today a lot of hypotheses try to explain freak wave generation mechanism. All the reasons may be separated on *external* or *internal* (Lopatoukhin, Boukhanovsky, 2003, 2004, 2005). The external reasons include the opposing wave-current interaction, refraction around shoals or from inclined seabed, wave caustics from diffraction at coastlines, and crossing wave systems. The internal reasons are mainly the frequency and (or) amplitude wave modulation in a random sea, cooperative effect of four- and five-wave interactions, the

high-order nonlinearities and nonlinear focusing (Rogue, 2000, 2004; Lopatoukhin, Boukhanovsky, 2003). Some definitions of freak waves as set of parameters $\Xi = \{h, \tau, c, \dots\}$, characterizing the shape of the wave and the steps of its selection from a record are presented in the fig. 3. Really, hypotheses of freak wave generation allow their arising in any place of the Ocean, and not only in the well-known dangerous regions, such as South shore of Africa etc. **Any metocean event described by a system of nonlinear thermo hydrodynamic equations, possesses their own freaks.** Hindcasting of waves do not allow revealing freak wave (Lopatoukhin et al, 2005). Freak wave had been recorded in such “calm” region as the NE part of Black sea (Lopatoukhin et al, 2003, 2005). There were three such waves recorded during six years of measurements, i.e. three waves from more than million recorded.

3.1 Probabilistic scenarios for freak waves generation

There are two ways to formulate the conditions of freak waves generation in the Ocean. The first way considers the arising of the different external conditions, leading to possibility of freak wave generation, and computation the joint probability of these conditions (e.g. combinations the severe waves and opposite currents etc.). But the real input of this approach is not obvious, because it is hard to take into account all the driving factors. Another way considers the ensemble of all waves (their heights h , periods τ , crests c etc.) and estimate occurrence of its crucial combinations, leads to freak wave arising. This approach seems more reliable in practice, because it is based on the consideration of freak waves as the elements of the same ensemble, as all the waves. But, it requires the sophisticated statistical techniques for rare events analysis, because the extreme combinations of the waves parameters belong to the tails of its joint probability function.

The problem of freak wave occurrence, and associated scenarios, include the procedures of statistical analysis and synthesis of huge data samples, because freak wave is very rare event. Moreover, due to multiscale and spatio-temporal variability of sea waves, the numerical simulation here is very resource-consuming procedure. It requires the development of special approach for stochastic simulation, that allows investigating the freak waves occurrence efficiently and precisely.

Freak wave is unusual not only by their height, but by their form. This uncommonness specified by means:

- Set of parameters, e.g. $h > 2.4h_s$, $\text{crest} > 0.65h$, unusual steepness δ of a wave and (or) its front or back slope, deep trough, twice as greater than preceding and subsequent waves, etc. Not all of these parameters are realized simultaneously, but as a rule at least three can be achieved.
- Governed by nonlinear Schrödinger equation.
- Suddenness of arising in some point of a wave field.

One of the main objectives of investigation is a probabilistic treatment of a wave field $\zeta(\vec{r}, t)$ as probabilistic contaminated distribution.

$$\Phi_{\zeta}(\vec{x}, \vec{r}, t) = (1 - \varepsilon)F_{\Xi}(\vec{x}) + \varepsilon\hat{F}_{\Xi}(\vec{x}). \quad (6)$$

Where $F(\vec{x})$ - joint distribution of wave parameters (e.g., height, crest, steepness), $\hat{F}(\vec{x})$ - asymptotic distribution of these parameters, $\varepsilon(\vec{r}, t)$ - probability of freak wave arising in specific place at a moment t . Ξ - multidimensional system of random values (h, c, δ, \dots) .

The first term in (6) describes “background” distribution of Ξ in short-term domain. It is approximated as,

$$F_{\Xi}(X) = F_h(x_1)F_{c|h}(x_2|x_1)F_{\delta|h}(x_3|x_1) \quad (7)$$

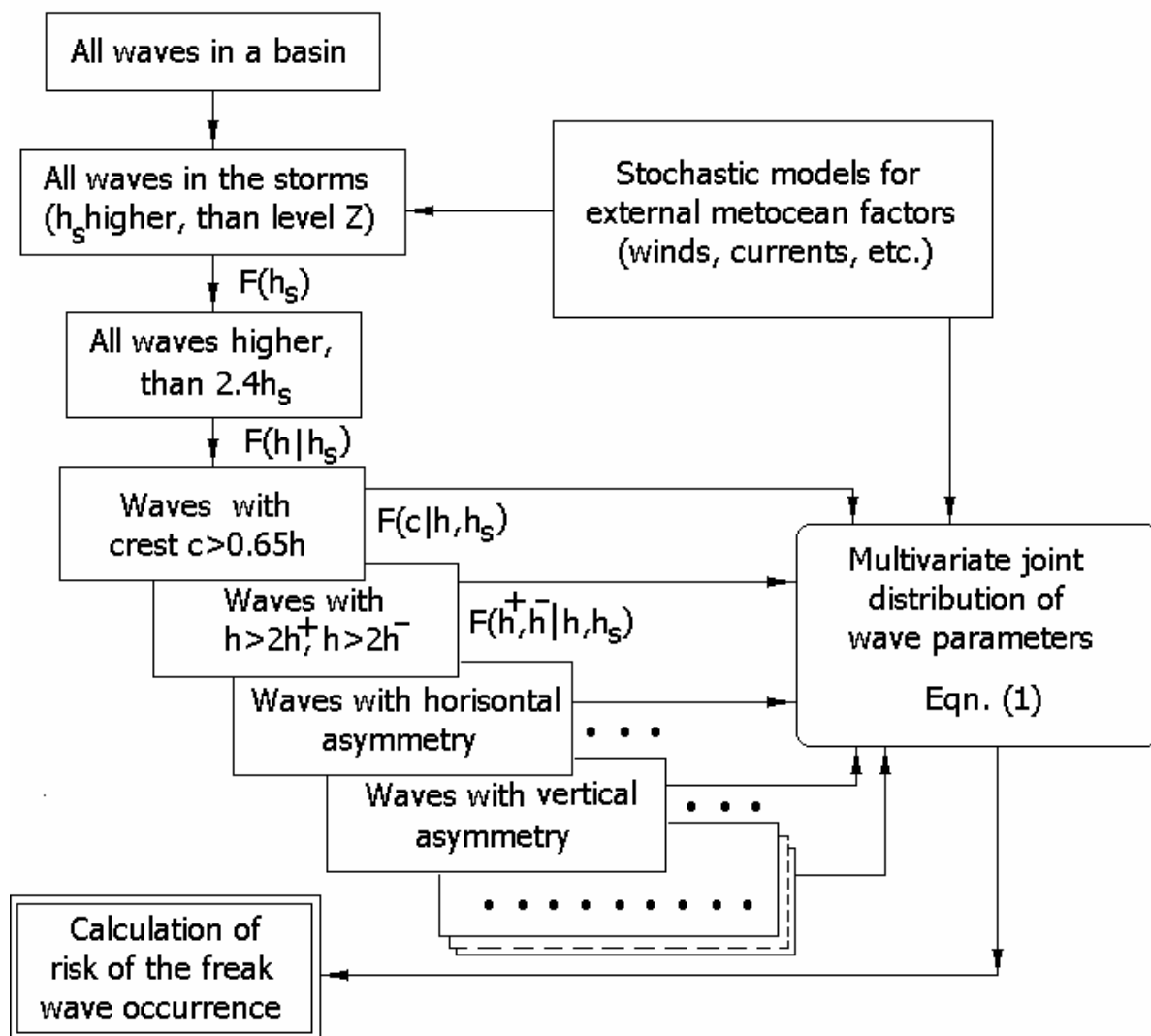


Fig. 3. General scheme of freak wave generation scenarios

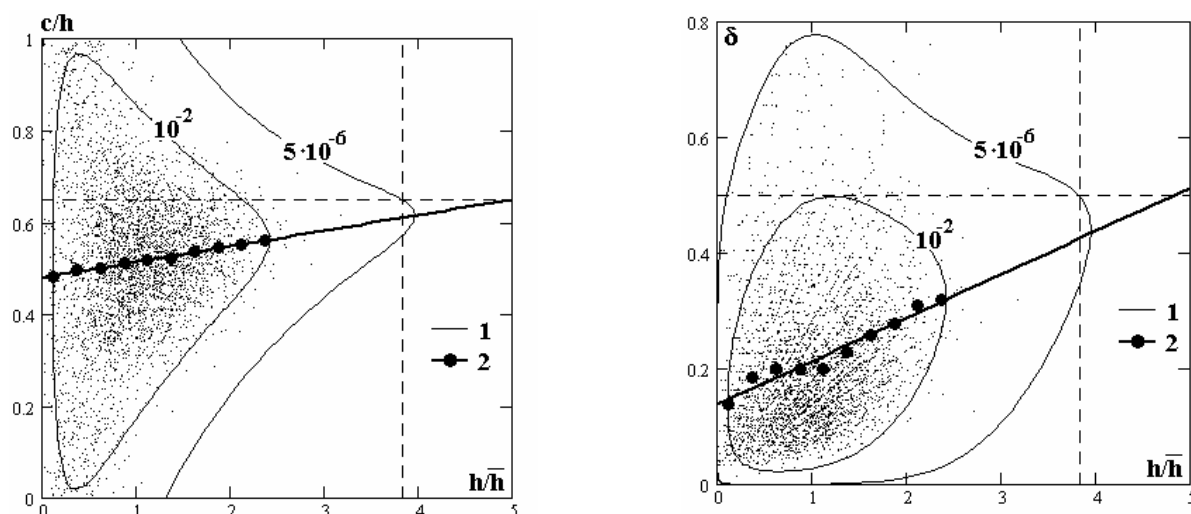


Fig. 4. Joint distribution of parameters $\{h, c/h\}$ (a) and $\{h, \delta\}$ (b). (1) – Lines of equal probability; (2) – Regression.

In short-term scale distribution (6) is a set of Weibull distributions with different shape parameters. The second term in (6) incorporate contamination (litters) of a “background” distribution by freak wave. Asymptotic distribution $F(x_1, x_2, x_3)$ may be used. Some definitions of freak waves as set of parameters $\Xi = \{h, \tau, c, \dots\}$, characterizing the shape of the wave and the steps of it selection from a record are presented in the fig. 3.

Short tem distributions (7) may be the following: Rayleigh distribution as marginal distribution $F_h(x_1)$, conditional distributions of wave crests c and steepness δ as Weibull distributions with scale parameter from 2 to 7. Joint distributions $F_h(x_1)F_{c|h}(x_2|x_1)$ and $F_h(x_1)F_{\delta|h}(x_3|x_1)$ are presented at fig. 4. This fig. is generalization of about 5000 wave records, but without freaks. The equal probability (p%) curves for values $\{h, c/h\}$ и $\{h, \delta\}$ are drawn. It is seen, that value $\{h/\bar{h} \geq 3.8, c/h \geq 0.65\}$ for any δ , or $\{h/\bar{h} \geq 3.8, \delta \geq 0.5\}$ for any c/h have the probability $5 \cdot 10^{-6}$. Probability defined from three-dimensional distribution

$P\{\delta \geq 0.5 | h/\bar{h} \geq 3.8 \cap c/h \geq 0.65\} = 0.12$ This means, that probability of three conditions simultaneously $\{h/\bar{h} \geq 3.8, c/h \geq 0.65, \delta \geq 0.5\}$, will be $5 \cdot 10^{-6} \cdot 0.12 = 6 \cdot 10^{-7}$. This means, that only one wave from 1.7 million will be with height greater, than $3.8\bar{h}$, crest greater than $0.65h$ and steepness $\delta > 0.5$. This value is the lower limit of probability ε , i.e. probability of freak wave in a specific point not greater than $6 \cdot 10^{-5}$ %.

For short term range with 1000 waves, freak wave may arise in one of 1660 time series. Relation (8) may be adopted as asymptotic distribution in (6).

$$F_{\Xi}(X) = F_h(x_1)F_{c,\delta|h}(x_2, x_3) \quad (8)$$

First limit distribution may be used.

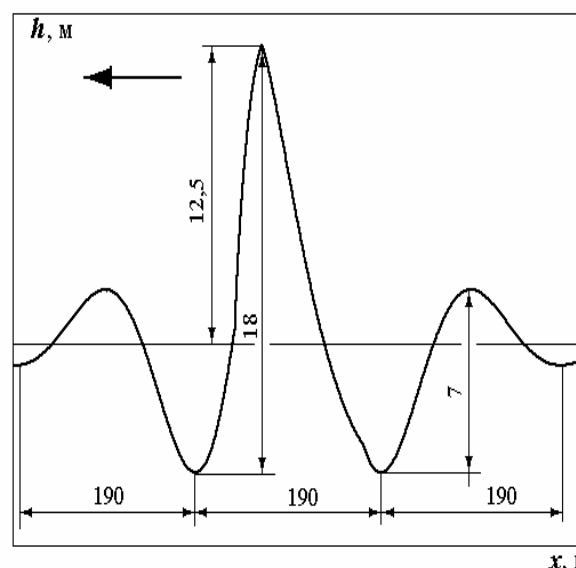


Fig. 5. Possible freak wave during loss of ship «Aurelia». February 2, 2005, N. Pacific.

Estimation of $\varepsilon = 6 \cdot 10^{-7}$ in short-term range may be increased due to specific of some meteocean situations. As an example loss of ship “Aurelia” (Class of Russian Register of shipping, 34000tonn) in February 2005 in the N. Pacific took place during passing of atmospheric front with wind waves and swell. Fig. 4 shows possible parameter of freak wave during this case.

Wave measurements shows that in Black and North seas freak waves arise during transformation of wind wave spectra to waves with swell. In this case both wave spectrum and angular distribution became more broad (Lopatoukhin et al, 2005).

4. CONCLUSION

Classical statistical analysis of time series does not allow estimating the probabilities of freak waves occurrence and associated weather conditions. Results of hindcasting for any specific time also do not display any suspicion to such a wave. Directional spectrum of wave record does not reveal existence of freak wave. Occurrences of freak wave have to be regarded as multidimensional random event. This is the main difference between extreme and freak wave. General scheme of freak wave selection

from the sample of measured waves is shown on the fig. 3. Special attention is paid to investigation of field conditions leading to freak wave generation. These include weather features, current effects and bottom bathymetry.

5. REFERENCES

- Boukhanovsky A.V., Lopatoukhin L.J., Ryabinin V.E., 1998, "Evaluation of the highest waves in a storm"/ Marine Meteorology and Related Oceanographic Activities/ World Meteorological Organization. Report N 38, WMO/TD -N 858.
- Lopatoukhin L., Boukhanovsky A., 2003, "Wind and wave climate investigations, related to offshore activity". Proceedings 10th Workshop on Ocean Models for the APEC Region (WOM-10). October 7-10, Hanoi, Vietnam.
- Lopatoukhin L., Boukhanovsky A., 2003, 2004, "Freak wave generation and their probability". Proceedings 8th International Conference on Stability of Ships and Ocean Vehicles. STAB 2003. Madrid, Spain. 2003, International Shipbuilding Progress. 2004, v.51, N 2/3, p.157-172.
- Lopatoukhin L.J., Boukhanovsky A.V., Chernysheva E.S., Ivanov S.V. 2004, "Hindcasting of wind and wave climate of seas around Russia". 8th Int. Workshop on Wave Hindcasting and Forecasting. November 14-19. North Shore, Oahu, Hawaii.
- Lopatoukhin L., Boukhanovsky A., 2005, "Approaches, methods and some results of wind wave climate investigations". Fifth International Conference: "Ocean Wave Measurements and Analysis", Madrid, Spain. 3-7 July.
- Lopatoukhin L., Boukhanovsky A., Guedes Soares C., 2005, "Hindcasting and forecasting the probability of freak wave occurrence"/ Maritime Transportation and Exploitation of Ocean and Coastal Resources, C. Guedes Soares, Y. Garbatov and N. Fonseca (eds.), Taylor & Francis Group, London, UK, pp 1075-1080.
- Lopatoukhin L.J., Rozhkov V.A., Ryabinin V.E., Swail V.R, Boukhanovsky A.V., 2000, "Estimation of extreme wind wave heights"/ World Meteorological Organisation (WMO). WMO/TD-No. 1041, JCOMM Technical Report, 71p.
- Lopatoukhin L., Rozhkov V., Boukhanovsky A., Degtyarev A., Sas'kov K., Athanassoulis G., Stefanakos C., Krogstad H., 2002. "The spectral wave climate in the Barents sea". Proceedings of 21st International Conference Offshore Mechanics and Arctic Engineering (OMAE). June 23-28, 2002. Oslo, Norway, paper 28397.
- Mallory J.K. 1974, 1984, "Abnormal waves off the South-East coast of South Africa". International Hydrographic Review, vol. LI, N 2, 1974. The Marine Observer, 1984, N 283, p.29-37.
- Proceeding of the Tenth (2000) International Offshore and Polar Engineering Conference. Seattle, USA .May 28-June 2, 2000
- Proceeding of OMAE'02. 21 International Conference on Offshore Mechanics and Arctic Engineering, June 23-38, 2002. Oslo, Norway.
- Provision and Engineering/Operational Application of Ocean Wave Spectra. Program and Abstracts of Int. Conf. UNESCO Paris 21-25 Sept. 1998.
- "Rogue waves 2000, 2004". Proceedings of a Workshops 2000, 2004 organized by Ifremer. Brest, France. 2000, 2004.

Rozhkov V.A., Boukhanovsky A.V.,
Lopatoukhin L.J., 1999. "Method for
calculation of extreme metocean events".
Proc. Int. Conf. MEDCOAST'99, Turkey.

A Potential Framework for a Performance Based Damage Stability Standard for Naval Vessels

Andrew J. Peters, *QinetiQ, Haslar Marine Technology Park, (UK)*

Philippa Harrison, *MoD, DPA, Sea Systems Group, Surface Ship Hydromechanics (UK)*

ABSTRACT

This paper investigates the possibility of moving from the current prescriptive damage stability criteria used by the UKMoD, to performance based criteria by using a ‘goal based’ approach. The current stability criteria and damage extents that U.K naval vessels have to be able to survive is defined in DEFSTAN 02-109 [2] (The defence standard). This document presents the damage lengths that different size vessels are to be able to survive anywhere along their length. This document also states the minimum acceptable intact and damaged stability standards for the vessels for which the UKMoD is responsible.

This paper describes how the goal based approach could be applied to the damage stability assessment of naval vessels. The following sections describe a framework that could be used for defining a performance based damage stability standard. This includes a description of what should be considered at each stage and some of the aspects that the authors believe should be defined in the standard.

1. INTRODUCTION

This paper investigates and presents a possible framework for moving from the current prescriptive damage stability standard, used by the UKMoD, to a performance based standard, by using a ‘goal based’ approach.

The current stability criteria and damage extents that U.K naval vessels have to be able to survive are defined in DEFSTAN 02-109 [2] (The defence standard). This document presents the damage lengths that the different size vessels are to be able to survive anywhere along their length.

This document also states the minimum acceptable intact and damaged stability standards for the vessels for which the UKMoD is responsible. The current damage lengths are defined as follows:

- Vessels of waterline length less than 30m; any single main compartment.

- Vessels of waterline length between 30m and 92m; any two adjacent main compartments. A “main compartment” is to have a minimum length of 6m.
- Vessels of waterline length greater than 92m; damage anywhere along its length, extending 15% of the waterline length, or 21m whichever is greater.

Significant subdivision is common practice in naval ship design. These internal arrangements introduce the potential for both symmetric and asymmetric flooding when damaged. The current stability criteria are based largely upon the criteria originally suggested by Sarchin and Goldberg [1] in 1962. The work by Sarchin and Goldberg was based on data gathered from WWII hull forms. This traditional damage stability analysis using quasi-static approximations cannot account for the behaviour in a seaway or for example, the head of water on a bulkhead, bounding a damaged region. For this V-line example for the Royal Navy, a dynamic allowance over and above the static damage waterline is included in order to account for

vessel motions in a seaway. It has until recently not been possible to assess the suitability of these criteria.

In 1990 the Cooperative Research Navies (CRNAV) Dynamic Stability group was established with the aim of deriving dynamic stability guidance for naval vessels. To help achieve their objectives the numerical simulation program FREDYN was developed, and continues to be applied extensively – both to intact and damaged vessels. This time-domain program is able to take account of non-linearities associated with drag forces, wave excitation forces, large-angle rigid-body dynamics and motion control devices. The latest version of FREDYN permits investigations into the dynamics of damaged vessels operating in realistic environments.

Tools like FREDYN permit investigations into the dynamics of damaged vessels in realistic environments, rather than simple pseudo-static analysis, which is the current practice. This allows all aspects of the stability performance to be evaluated for a particular vessel. This step forward in evaluation has the potential to allow stability standards to move towards a specified level of performance that is expected after damage rather than the current prescriptive criteria.

In recent times there has been a trend in many areas of the engineering industry to move away from traditional prescriptive based regulation and apply a ‘goal based’ approach to regulation instead [3][4][5][6][7]. The advantage of the ‘goal based’ approach is that there are no prescriptive ways of how to meet the goals, just the goals and requirements that must be met. This gives a greater level of flexibility to a designer, particularly for novel design where a conventional prescriptive standard may be unsuitable.

The objective of this paper is to discuss the work that is currently being conducted to assess the possibility of a performance based stability standard for Royal Navy vessels.

2. CURRENT PRESCRIPTIVE STANDARDS

Current stability standards used in many navies, including the UK, almost exclusively follow a prescriptive format, in which the stability code or standard specifies a detailed means to achieve an un-quantified level of intact and damage stability performance which is largely generic for all types of vessels.

These prescribed means include the specification of set damage lengths, list and heel angles and a list of GZ parameters.

Some existing requirements have performance elements, such as the V-lines criteria that include static levels of heave and roll allowance to account for dynamic motion behaviour after damage. Although these V-lines are used mainly for structural calculations, these standards still do not indicate clearly how they work with the other damage criteria to achieve a desired stability goal.

Most prescriptive standards both in the navies and in the commercial world, only establish minimum damage requirements.

These standards do not provide a means to quantify an actual level of performance or safety in the vessel design. This could lead to vessel designs with costly features that do not actually improve the performance or safety.

Additionally, vessel designs can incorporate features not explicitly covered by the current standards, the consequences of these novel features may be unknown.

By providing a performance-based standard, or by adding a performance-based option to the existing DEFSTAN 02-109 [2] standard, a formal measure to prove the performance is acceptable to all of the customers (i.e. the equipment capability customer and fleet) may be developed.

3. THE 'GOAL BASED' APPROACH

The 'goal based' approach can be demonstrated by using a multi-layer pyramid similar to that shown in Figure 1. In simple terms, this shows the systematic refinement into greater detail at each level of what is required to meet the overall performance goals and objectives defined at the top level.

Tier 0 details the aims of the standard in general terms.

Tier 1 details the overall goals i.e. what is to be achieved by application of the standard.

Tier 2 breaks down these goals into functional areas which detail the functions performed by application of that section of the standard.

Tier 3 is the requirements level. Requirements are presented for each functional area. In some generic diagrams showing the 'goal based' approach, the 'requirements levels' are subsumed into the verification level. For the application to naval damage stability, it is desirable to split this into two separate distinct requirements levels commensurate with the UKMoD acquisition methodology. The two levels allow for a definition of what is required in the form of User Requirements and the level of performance deemed acceptable in the form of Systems Requirements.

Tier 4, the verification layer, then becomes the processes by which the performance against the requirements is demonstrated. The Verification level is used to measure the performance of the vessel and to identify whether the vessel meets all the requirements detailed in tier 3 and hence whether it meets the overall goals.

Tier 5 is the Justification level. This is the final layer that provides the feedback to check and justify that the standard provides the necessary performance against the original goals.

4. CATEGORISING VESSELS

Currently in DEFSTAN 02-109 [2] damage criteria, vessels are categorised by ship length, which then prescriptively defines the damage length that the vessel must survive, and the static criteria values that they must meet. A new way of categorising Naval vessels has been proposed by QinetiQ [8], which introduces a way of categorising front line fighting vessels by their role, rather than just on ship length. Included in the definition of the vessels role are the characteristic weapon threats from a variety of weapon types that the vessel is expected to survive, operating in that role. The UKMoD is also in the process of defining appropriate accidental damage (collision, grounding and raking) extents to be included in future standards.

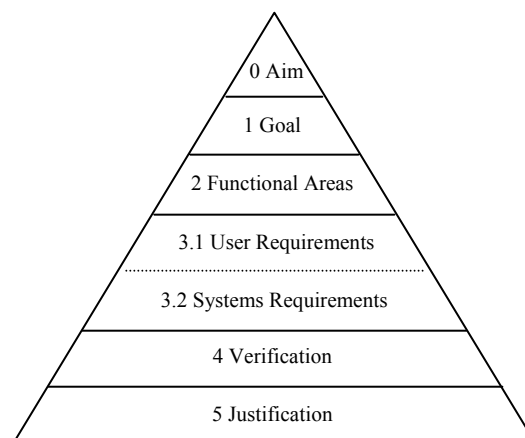


Figure 1 Goal Based Pyramid

5. THREATS TO WATERTIGHT INTEGRITY

There are many potential threats to Royal Naval vessels these may be categorised as described in the NATO Naval Ship Code [9] into Foreseeable Damage and Extreme Threat Damage. In simple terms Foreseeable Damage (in terms of damage stability assessment) is that resulting from accidental damage such as collision, grounding or raking and Extreme Threat Damage is damage caused by a hostile act.

There have been numerous studies into

accidental damage in the commercial world, such as the HARDER project [10], that have analysed the statistics from past ship collisions. This has allowed algorithms to be developed, which allow expected damage caused by collisions to be calculated. This collision damage is often based on length and displacement of vessels and relates to the statistical information gathered from previous collision incidents.

From survivability studies completed for the UKMoD, it is possible to list the weapon threats to the vessels in each of the roles.

From the list of weapon threats that a particular vessel is likely to be subject to in its specified role and expected to survive and remain operational means that realistic damage lengths can be calculated. Existing detailed information regarding the damage effect from a wide selection of weapons is contained in the UKMoD survivability library. The damage caused to the structure in the surrounding area is also detailed. These documents present the damage extent data for various weapons.

In general a range of damage extents may be applied with different criteria based on the damage extent to ensure that the effect of damage is not disproportionate to the initial damage event.

6. DEFINING THE ‘GOAL’

The goals of a performance based standard should provide a broad, qualitative expression of the overall, primary concern of the document. Goals should be stated in terms that are potentially quantifiable, even if the precise measurement scale is not specified. Goals therefore, may be stated in terms of impact on the vessel, the crew, the mission operability, the environment or any combination of these.

The goal or set of goals should encompass the overall aim for the performance and safety of the vessel. They should be generic in nature and not specific to a particular vessel role. Achieving

these goals should ensure that the vessel is sufficiently stable so that the safety of the crew and the vessel itself is commensurate with the expectations of the customers for a Royal Navy warship. These should also be grouped into overall goals, goals in hostile situations (extreme threat damage) and those caused by accidental damage (foreseeable damage), as the accepted level of risk and hence safety can vary significantly between hostile and accidental damage scenarios.

The high level goals should be clearly defined in the stability standard as a requirement for any front line naval vessel.

7. OVERALL GOALS AND OBJECTIVES

For a front line naval vessel the hostile and accidental damage overall Goal could be defined as follows:

‘The vessel should provide adequate buoyancy, freeboard, stability and subdivision to survive damage from any of the perceived hostile or accidental damage threats to the watertight integrity for a vessel in its role’

Additional Hostile Overall Goal - Mandatory
To provide safe evacuation of crew following unforeseeable damage (i.e. that in excess of design extreme threat damage).

The set of goals can be then presented in a number of broad categories, which also divide into separate accidental and hostile damage goals such as:

- (a) **Life Safety**; Accidental and Hostile Goals
- (b) **Vessel Protection**; Accidental and Hostile Goals
- (c) **Mission Continuity**; Hostile Goals

The stability standard would define these categories for the goals as they are suitable for all roles of vessel. The standard would require mandatory goals under these headings that must be included for all vessels. This may not be an extensive list and will also encourage the project team to add other goals for their vessel based on

the vessels individual survivability requirements:

7.1 Life Safety – Accidental and Hostile Goals

Goals relating to life safety are the most common and clearly the most important in damage emergency situations. The crew places trust in the vessel to maintain a level of safety and protection from adverse conditions.

The following are examples of the goals that may be defined in the Life Safety Category:

The vessel is to be able to provide a safe environment for the crew on board after an accidental or hostile damage incident.

The vessel is to remain habitable and safe for the crew either until a place of safety can be reached or the threat has receded.

The vessel should allow damage control parties to undertake damage control in a safe manner.

An additional Hostile damage Goal might be:

The vessel should allow safe evacuation of the crew following unforeseeable hostile damage (i.e. that in excess of design extreme threat damage).

7.2 Vessel Protection – Accidental and Hostile time Goals

Vessel protection considers the impact of damage on the equipment and contents in the vessel. This goal is primarily for the purpose of protecting the asset that is the vessel and ensure its availability. There is no account for this within current damage stability standards. Instead, there are ways to predict areas and volumes affected by damage (e.g., flooding). Thus, the goal of reducing the impact of flooding (maintaining watertight integrity) within the vessel would fall into the general category of vessel protection; e.g., limiting the spread of progressive flooding for example. This is commensurate with the current UKMoD damage stability guidance presented in SSP24 [3] which state that the consequences of the damage should not be disproportionate to the initial event.

The following is an example of what could be

defined in the standard as a mandatory goal for all front line naval vessels and are directly linked to requirements defined in the UKMoD subdivision standard which is still under development:

The subdivision of the vessel is to minimise the spread of floodwater and allow the ships crew to limit the extent of flooding due to damage.

7.3 Mission Continuity – Hostile Damage Goals

The goal of ‘mission continuity’ is similar to that of vessel protection. However, instead of considering the physical damage to the vessel, mission continuity is more concerned with the ability of vessel and crew to both defend herself and perform its required mission. Mission interruption is one example of a mission continuity loss and can be described as “indirect loss,” as contrasted with “direct loss” from damage to ship systems due to structural and flooding damage. Obviously, the vessel must remain afloat and stable for a required period of time for this to happen, so there is a link between vessel protection and mission continuity. However, mission continuity is intended to allow the Navy to protect themselves and continue their mission. This category of goals would not have any specified mandatory goals in the standard. The goals in this category would depend on the specific vessels survivability requirements as required by the customers.

The following is an example of what could be defined by the project team.

‘The vessel should remain operational with the ability to defend herself against further damage following all perceivable hostile damage incidents’.

The standard will state that Mission Continuity goals for hostile time goals must be defined for the vessel, but will not mandate explicitly what this would be for the vessel.

8. THE FUNCTIONAL AREAS

The functional areas of performance-based standards are intended to be more specific than goals. In the context of performance based standards, functional areas provide a greater level of detail than goals. Functional areas are stated in more specific terms than goals. Functional areas are the link between goals and requirements and therefore the required performance criteria. In general, functional areas describe a series of actions necessary to achieve the goals. They are a further expansion of the goals related to the expected performance. This breakdown is expanded until the requirements can be derived in the next level of the process.

A number of techniques can be performed to do this for the specific vessel role. For Naval vessels, the goals defined above are specified further with these functional areas and can be split into two, for both accidental and hostile damage scenarios.

The stability standard would describe the accidental and hostile damage functional requirements under the following functional areas:

Functional Area 1 – Life Safety

Functional Area 2 – Vessel Protection

Functional Area 3 – Mission Continuity

Under each of these functional areas the functional requirements will be defined. Some of which will be considered mandatory as they are safety related, others will be dependant on the survivability requirements of the platform. These additional requirements should be reasonably detailed and vessel specific. For example, the requirement should include the definition of the sea conditions in which the vessel should be able to meet the required goals.

This section of the standard will define the damage threats that the vessel in each of the roles is required to meet along with a qualitative level of acceptable performance based on the severity of the threats. The level of qualitative performance, i.e. the vessel performance against

the severity of damage would be defined in the standard as a minimum level that is acceptable. These should provide a clear link to the goals for that vessel. This level of acceptable performance will be ultimately used with the measures of performance to demonstrate satisfactory compliance with the goals during the Verification process.

The ability to realistically state the possible accidental and hostile damage threats allows the resulting damage from accidental and hostile threats to be calculated. This results in a number of damage cases that can be ranked in order of severity, often rated by how many compartments have lost watertight integrity.

8.1 Examples of Functional Requirements for the Life Safety Functional Area

An example of a functional requirement which would fall under the Life Safety functional area is:

Following significant damage from one of the accidental or hostile damage threats defined for the vessel in this role, anywhere along her length, the vessel shall:

Remain sufficiently afloat and upright so that the crew can remain safe onboard in a sea state up to that agreed with the Naval Authority (the UKMOD certifying body for stability).

For example the agreed sea state could be the maximum operational sea state when considering hostile damage.

The minimum level of performance required is “Crew Safe” and this is required for damage up to the following lengths, Table 8-1-1, for the different roles of vessel:

Table 8-1-1 – Crew Safe Level

Vessel Role	Compartments flooded (up to)
2	2
3	3
4	3
5	4

The definition of **Crew safe** is – The vessel is not operational and the weapon systems are not on line. The vessel is unable to defend herself from further attack. Through extensive damage control the flooding can be contained and the vessel will remain afloat with sufficient stability.

The vessel no longer has self-propulsion. The vessel is unlikely to sink/capsize in the next 3hrs.

Following damage from any unforeseeable hostile damage (i.e. that in excess of design extreme threat damage) for a vessel in this role, anywhere along her length, the vessel shall: -

Survive long enough to allow safe evacuation all of the crew onboard in up to a sea state defined by the Naval Authority, if the vessel cannot be prevented from sinking.

The minimum level of performance required is defined as “Sinking” and this is required for damage over the following lengths, Table 8-1-2, for the different roles of vessel:

Table 8-1-2 – Sinking Level

Vessel Role	Compartments flooded (up to)
2	3+
3	4+
4	4+
5	5+

The definition of **Sinking** is – The vessel has been damaged significantly. There is no operational capability and most systems are off line. It is unlikely the flooding can be contained and the vessel is likely to sink/capsize in the next 3 hours. Evacuation of the crew is the priority and should be achieved before the vessel sinks/capsizes. Table 8-1-2 provides the extent of damage that would be considered by the Naval Authority to allow the sinking performance level.

8.2 Examples of Functional Requirements for the Vessel Protection Functional Area

The Vessel Protection goals could be refined into the following functional areas.

Following moderate damage from one of the accidental or hostile damage threats defined for the vessel in this role, anywhere along her length, the vessel shall:

Remain sufficiently afloat and upright so that she can continue to provide the level of defence required with at least one weapon system and the ability to manoeuvre in a sea state up to that agreed with the customers.

The minimum level of performance required is “Defence” and this is required for damage up to the following length, Table 8-2, for the different roles of vessel:

Table 8-2 – Defence level

Vessel Role	Compartments flooded (up to)
2	1
3	2
4	2
5	3

The definition of **Defence** is – The vessel is not fully operational, but has some communications and has some weapon systems on line to continue to defend herself and move. Damage control is more difficult but the flooding can be contained. Moving under her own propulsion is limited or not possible. The vessel will be lower in the water with list and trim.

The stability standard would provide the functional requirements defined from the overall goals along with a minimum mandatory level of performance for each role of vessel. For example, for a small 1 compartment damage, a role 2 vessel i.e. MCM, should pass performance level ‘defence’ or better. The expect level of damage for this performance level is given in Table 8-2.

8.3 Examples of Functional Requirements for the Mission Continuity Functional Area

The Mission Continuity Goals could be refined into the following functional areas.

Following minor damage from one of the accidental or hostile damage threats given for the vessel in this role, anywhere along her length, the vessel shall:

Remain sufficiently afloat and upright so that she can continue to provide the level of "Operation" required with at least one weapon systems in a sea state up to that agreed by the customers.

The minimum level of performance required is to be "Operational" and this is required for damage up to the following lengths, Table 8-3, for the different roles of vessel:

Table 8-3 – Operational Level

Vessel Role	Compartments flooded (up to)
2	Minor slow fill to 1 compartment
3	1
4	1
5	2

The definition of **Operational** is – The vessel is still close to fully operational. The vessel has most systems still on-line including most weapon systems, communications and radar. The vessel may have reduced propulsion capability, but could move at least slowly to a safe port under her own power and control. Damage control parties can work effectively and the flooding extent will be quickly limited and controlled. The vessel maintains a substantial reserve of buoyancy without significant list or trim.

The stability standard would provide the functional requirements defined from the overall goals along with a minimum mandatory level of performance for each role of vessel. For example for a frigate, with small weapon damage causing flooding to a single compartment, should be fully operational and meet all of the performance goals. The expected level of damage for this performance level is shown in Table 8.3.

9. DEFINING THE REQUIREMENTS

The next level down from the functional areas is the requirements level. This is where the level of performance to achieve the functional requirements and hence the overall goals is defined. This layer has been again split into a URD (user requirements document) and SRD

(system requirements document) levels. The URD will describe a set of requirements relevant to the functional areas. These will then be used to define actual levels of performance required in the SRD. This set level of performance will be compared against the actual vessel performance in the verification level.

The standard would explicitly provide some of the URD requirements but will not define the SRD requirements, as these may be vessel specific and must be agreed with the customers based on the required performance. The measure of the performance level is to be stated in the standard by the Naval Authority responsible for the standard. The stability assessment will require both the URD and SRD requirements to be clearly defined in the submission report for a certificate of safety stability. It must also provide existing standards, statute requirements or policies that must be met in order to achieve any of the goals.

9.1 URD Requirements

In this level the performance requirements (limiting factors) to meet all of the functional requirements are specified. The performance requirements would be related to the physics of the flooding vessel, the onboard systems and the human factors effects relating to the crew.

9.2 SRD Requirements

In the system requirement level, the actual performance level that is deemed acceptable to meet the functional areas and overall goals is defined. This level will draw out the actual measurable terms that can be evaluated during the verification level.

Possible examples of the limiting measurable factors are:

- (a) Limiting a heel or trim angles;
- (b) Limiting vertical and lateral accelerations;
- (c) Limiting flooding levels
- (d) Limiting flooding rates
- (e) Limiting submergence

As an example of how the requirements can be drawn down following are examples of the 'Life Safety' functional area defined above:

In order to achieve the functional requirements for 'Life Safety' the URD should state:-

Minimum performance of Crew Safe requires:-

- Reserve of buoyancy – deck above water
- Reserve of stability
- Low motions and accelerations
- Watertight integrity
- Minimum performance of Sinking requires:-
- Time to sink > Time to evacuate
- Further refining the **SRD requirement** to achieve the Life Safety functional requirements requires: **(Note: numbers are for example purposes only)**
- Deck edge above the water
- Mean roll angle < 25 degs
- Mean pitch angle < 5 degs
- Peak roll motions < ± 12 degs (4 degs RMS for 1% exceedence)
- Peak Pitch motion < ± 6 degs (1 degs RMS for 1% exceedence)
- >20 degrees range of positive stability from mean list angle
- Time to sink > time to evacuate
- The **Crew Safe** performance level would require the following or the equivalence proved:-
- All motion criteria are met more than 95% of the time i.e. a probability of exceedence of motion criteria of less than 5%.
- The deck edge is not continually submerged at any point.
- The probability of sinking in the three hours is less than 4% (1/25) in any sea state up to and including the required design sea state at the worst heading.
- The **Sinking** performance level would require the following or the equivalence proved:
- The deck edge is regularly submerging.
- When the probability of sinking in the three hours is equal or greater than 4% in any sea state up to and including the design sea state at the worst heading.

- Time to sink must be 1.5 (or agreed by Naval Authority and the customers) times the time to evacuate the remaining crew.

10. THE VERIFICATION PROCESS

Since a performance-based design will involve performance requirements that do not necessarily comply with simple prescriptive requirements, it is necessary to verify that the design will produce a warship that meets the damage stability goals and objectives. A procedure to do this is defined as a "verification methodology," and the Naval Authority will need to provide guidelines on the selection and use of such methods.

In this context "verification" is to establish the accuracy of the claim that a proposed solution meets the established damage stability goals and objectives for a vessel in its role. The stability standard would state that the verification process must confirm that the vessel's ability to achieve the level of performance set in the requirements has been demonstrated by qualified people, appropriately using sound methods applied to appropriate and accurate data.

The verification method is the point where one demonstrates whether the vessel designed to the required design specifications and assumptions, and confronted with the challenges of the hostile and accidental damage scenarios, will perform in accordance with the goals and functional areas, as measured by the performance criteria. The design specifications define the role and function of the vessel, along with the characteristics, assumptions, and scenario data, are required inputs to the verification method. The outputs of verification methods are compared to the required performance from the SRD criteria in order to determine the acceptability of proposed, alternate solutions.

10.1 Methodology and Tool Selection

There are various types of tools available to use in the verification process, ranging from basic hand calculations to full computer models.

Each of the many types can be used to provide results for various, necessary pieces of information that are required to verify a design's performance. It is important to be thorough when selecting a verification method. One must carefully consider what information the verification method needs in order to show that the criteria are satisfied, and ensure that this information is included among the available input. Methodologies can range from quasi-static analysis to dynamic analysis using a tool such as FREDYN or even model tests.

10.2 Level of Acceptable Performance

Unlike many engineering scenarios that use the goal based approach, the measure of the performance against the criteria derived from the requirements and hence overall goals can be difficult to clearly evaluate.

The level of acceptable performance is expressed primarily in the criteria brought out of the SRD requirements. The criteria are quantifiable measures of the goals and objectives. In performance-based design it will be the Naval Authority in discussion with the main customers who will determine the level of acceptable performance subject to overall limits set in the performance-based standard. The standard quantifies the Navies expectations with goals for the design to meet, and the Naval Authority determine whether the criteria provide the performance and safety required by the UKMoD. The Naval Authority would have mandatory safety goals and requirements defined in the stability standard, which would have to be proved as a minimum regardless of vessel role.

Statements of goals, objectives and criteria in the submission document, will together with the qualitative level of performance, specify the naval requirement for acceptable performance. The choice of high-challenge scenarios (significant asymmetric damage for example) required by the standard, is another area where the Naval Authority could drive the acceptable performance. When selecting scenarios, it is

important to note that damage scenarios in excess of the threats assessed are effectively deemed to be acceptable losses. Considerable thought should go into drawing the line between damage scenarios which are deemed severe enough and likely enough to use in assessing a design and more severe damage case which are deemed too unlikely to use in the assessment.

The threats that were assigned to the vessel roles should ensure that most of the damage threats result in only moderate or minor damage that result in performance levels of defence or operational. However, the more significant threats are still accounted for in the crew safe and sinking performance levels.

After defining the problem, selecting appropriate scenarios, documenting the assumptions on environment and vessel conditions, and selecting an appropriate verification method, it is necessary to verify the proposed design. Whichever methods are chosen the output must be carefully analysed and compared to the criteria from the requirements levels. While the Naval Authority generally will not specify that an exact type of verification method be used, they may place restrictions on certain model or calculation types. Either way, the project team must verify that the method can reasonably predict or produce the appropriate results. The project team will have to select a verification method that generates output data that can be directly compared to the performance criteria or they will have to prove performance equivalence with an alternative method.

11. JUSTIFICATION

The approval of the Naval Authority would be the final activity in the process, and it is his/her decision to either give approval or request further verification of the proposed solution. It is not the role of the Naval Authority to judge whether or not a prescriptive method could have been done in place of the performance-based submission; only to evaluate the design he/she receives.

The justification layer is a feedback layer where the performance is traced back up the goal based pyramid layers to identify if the overall goals have been achieved. The Naval Authority will examine the verification methods in detail and the results produced to identify whether they believe that the verification method and the requirements actually complete the goals.

12. CONCLUSIONS

It has been shown that:

- Current prescriptive standard are used for damage stability in many navies including the UK. The Goal Based approach could allow a greater level of flexibility to a designer, particularly for novel design where a conventional prescriptive standard may be unsuitable.
- The ‘goal based’ approach could be applied to the damage stability for naval vessels and cover both accidental and hostile threats.
- A framework as described in this paper could be used for defining a performance based damage stability standard as an addition to the current prescriptive standard.

13. ACKNOWLEDGEMENTS

The authors would like to gratefully acknowledge the permission granted by QinetiQ and the UKMoD for publishing some of the findings from the investigation.

14. REFERENCES

Sarchin, T.H. and Goldberg, L.L., 1962 “Stability and Buoyancy Criteria for US Naval Surface Ships”, SNAME proceedings.

MoD Defence Standard 02-109 (NES 109), UK Ministry of Defence, 2000, Stability Standards for Surface Ships, Part 1,

Conventional Ships.

National Fire Protection Association. 1999, “Performance based Codes and Standards Preparation”, December.

Hamburger R.O . 1997, “A Framework for Performance-Based Earthquake Resistant Design”, EERC-CUREe Symposium, February 1997.

Hui S.C.M , 2002 “Using Performance Based Approach in Building Energy Standards and Codes”, University of Hong Kong, July.

Callan, J.L , 1998, “White paper on risk-Informed and Performance Based Regulation” U.S Nuclear Regulatory Commission” June,

Allen, Tom, 2004 , “Goal Based Standards – Strategy of IMO on Design and Safety”, 2nd International Maritime Conference on Design for Safety, October.

Wright, D.J. and Murrery, R., 2004 “Minimum Requirements for Damage Resistance for all Vulnerability Damage Mechanisms” QinetiQ report, 31 August.

NATO Naval Ship Code, Draft Edition

SLF, 2002, Paper 45/3/5, Norway and UK, Investigations and proposed formulations for factors “p””r” and “v” the probability of damage to a particular compartment or compartments, Report from Project HARDER, April.

Sea System Publication number 24, 1999, (SSP 24) Stability of Surface Ships Part 1 Conventional Ships Issue 2.

SOLAS Consolidated Edition, 2001, International Maritime Organization, London.

Ship Stability - Working with the Operator

Andrew J. Peters, *QinetiQ Haslar Marine Technology Park (UK)*

Stephen Marshall, *MoD, DPA, Sea Systems Group, Surface Ship Hydromechanics (UK)*

ABSTRACT

A strategy has been developed in the UKMoD which brings the operator and scientist closer together to further advance ship safety. It has been known for some time that the ability and experience of the ship operator has a large influence on the overall level of safety of the vessel. This paper discusses the recent interaction between the scientist and the operator which has provided a greater insight into how ships are operated in heavy weather, and has allowed the operator to gain from the latest knowledge and tools developed by the scientists.

Traditionally, guidance in how to operate ships and ship systems in extreme weather forms part of the seamanship lectures given during navigational training and through experience at sea. Additional onboard assistance is provided for ship/aircraft operations in the form of Ship Helicopter Operating Limits (SHOLs) but these have no predictive capability.

Currently, computer based tools providing guidance on how to minimise the risk to the ship and ship systems in severe seas are not in routine use by the Royal Navy. There is a very small amount of ship specific guidance provided but this tends to consist of ship manuals which have very limited use *in situ*.

1. INTRODUCTION

In 1990 the Cooperative Research Navies (CRNAV) Dynamic Stability group was established with the aim of deriving dynamic stability criteria for naval vessels. To derive such criteria, the group needed to evaluate in-service and new ship designs, in moderate to extreme seas in terms of their relative safety and probability of capsize. This would ensure that new vessels continued to be safe, while avoiding high build and life-cycle costs associated with over-engineering.

To achieve these objectives the numerical simulation program FREDYN was developed, and continues to be applied extensively – both to intact and damaged ships. This time-domain program is able to take account of

nonlinearities associated with drag forces, wave excitation forces, large-angle rigid-body dynamics and motion control devices. The current CRNAV group comprises representatives from UK MoD, Naval Sea Systems Command (NAVSEA), the Australian, Canadian, French and the Netherlands navies, as well as the U.S. Coast Guard, Defence Research & Development Canada, (DRDC), Maritime Research Institute in the Netherlands (MARIN), Naval Surface Warfare Center Carderock Division (NSWCCD) and QinetiQ.

The objective of this paper is to discuss the work that is currently being conducted for developing and implementing shore based training and active on-board operator guidance to deliver improved operational capability, increased availability, lower through life costs in normal conditions and

reduction of risks of loss in heavy weather.

2. MAINTAINING CAPABILITY

The maintenance of a maritime strategic capability demands the capability of rapid deployment to any area of conflict or humanitarian crisis. The naval operational philosophy and doctrine places major demands upon vessel and crew with respect to high risk/threat encounters, be they military or environmental. The seakeeping performance of naval shipping is a key enabler in delivering this capability. Operational requirements demand that mission effectiveness is maintained even in rough weather and the ships are able to survive extreme weather conditions. Examples of such capability and safety requirements are:

- Ship Speed
- Weapon & Sensor effectiveness
- Ability to launch & recover and handle aircraft
- Replenishment at sea
- Crew effectiveness and safety
- Structural integrity
- Intact survivability

The operational capability of a warship will be reduced due to excessive motions and related phenomena in bad weather. The seakeeping and dynamic stability characteristics of a ship are fixed early in the design process and, once in service performance is reliant upon the precepts of good seamanship in course and speed selection. Traditionally, guidance on how to operate ships in rough & extreme weather to maximise capability forms part of generalised seamanship classroom lectures given during navigational training and through feedback from experience. There is a very small amount of ship specific guidance provided but this tends to consist of only paper copies of a few graphs which have very limited use *in situ*.

With the growing complexity of equipment and the general reductions in manning levels mean a greater workload on operators to deliver capability. Furthermore, with the current trend towards having less time at sea, the experience of extreme conditions will perhaps become more infrequent. Seamanship training is classroom based as is the teaching of heavy weather doctrine as the UK simulator facilities at HMS Collingwood in Gosport, were not designed for this capability. It is believed that the training requirements to reverse the trend in the decline in heavy weather experience can be addressed through a combined approach of validating doctrine for modern naval hullforms, conducting heavy sea simulator training and implementing onboard operator guidance.

3. SIMULATOR AND COMPUTER BASED SEAMANSHIP TRAINING

Although heavy sea doctrine exists in order to safeguard operations in hazardous situations there is great benefit, prior to exposure to the real conditions, in being able to train for such eventualities in a safe environment. In general, time at sea has reduced over the last 50 years and thus experience is, in general, less amongst today's navigators & seamen. However well skilled operators are, heavy weather damage does occur leading to downtime and a loss of availability.

The CRNAV group has linked the FREDYN program to the simulator at the Royal Netherlands Navy KIM facility at Den Helder in order to assess the feasibility to assess extreme sea ship handling training in a simulator environment. CRNAV have held two workshops at the facility so far. These workshops demonstrated the feasibility of using simulators to assess current doctrine in a safe training environment. Further work however is required to improve operator cues such as deck wetness, slamming and the sea

surface definition. At the most recent workshop the active operator guidance system ORPHEUS (described later) was integrated with the simulator to test and demonstrate the benefit of such a capability.

Prior to assessing the feasibility of transferring the technology demonstrated at Den Helder to the simulator at HMS Collingwood, QinetiQ and the UKMoD have developed a user friendly version of the FREDYN programme to allow operators to quickly and easily evaluate doctrine and associated manoeuvres and operations in rough and extreme weather in different ship conditions. This capability, known as Easy-FREDYN, is a cheaper and easier solution, installed in the computer based training facility (CBT) and provides an effective way of introducing heavy weather training into the already packed RN training programme.

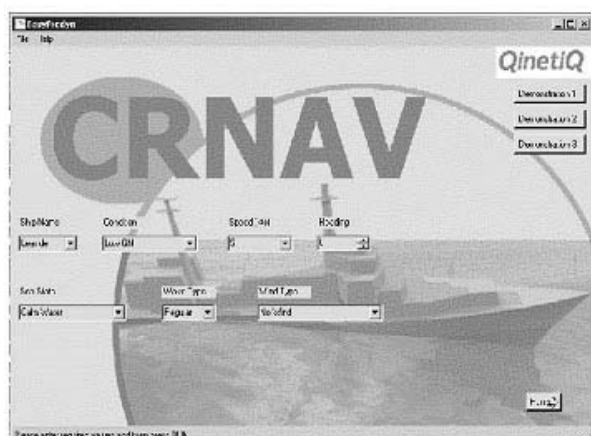


Figure 4-1 Easy FREDYN

Easy-FREDYN also has the facility for demonstrating hazardous situations through a number of “pre captured runs” to illustrate the conditions where broaching, and capsize through a loss of dynamic and static stability can occur.

Having Easy-FREDYN in the CBT facility allows the officers to get a good understanding of their vessels behaviour in heavy weather before they actually join the ship, or the ship actually enters service.

4. ACTIVE OPERATOR GUIDANCE

Advances in the accuracy of computer based modelling and simulation tools, have given rise to the opportunity to use ship specific simulations as a base for supplying information as part of an onboard decision aid tool. Such a tool would increase the operational envelope and/or improve operational safety of most shipboard tasks that are degraded by the presence of rough weather.

The UKMoD and QinetiQ have developed an understanding of how information can be provided to the operators in a clear, concise but useful manner to improve capability in rough weather and risks of damage or in the extreme loss, in extreme seas. This work resulted in a prototype demonstration system named, ORPHEUS, (Onboard Risk Performance Hazard Evaluation System) which was evaluated in 2004 on a Type 23 frigate during exercises in rough weather off the West Coast of Scotland.

ORPHEUS can provide information on course and speed selection to minimise motions for tasks often limited by ship motion, such as safe aircraft operations, helicopter removal of injured crew, towed array/towed body deployment, small boat operations and weapon firing. In non-combat scenarios the system will aid operators to maximise crew comfort and crew effectiveness. There is also the benefit of maintaining the safety of cargo stowage.

In respect of aircraft operations, the use of ORPHEUS would maximise the launch and recovery envelope of embarked aviation assets including UAVs, in all sea states and ensure the safety of both aircraft and personnel while operating on deck in adverse conditions.

ORPHEUS provides a means of displaying measured motions, predictions of motions at alternative speeds and heading

combination alongside operating limits, thus providing a decision aid tool to the officers on the bridge. The MS Windows® based system combines real-time information with a database of previously generated results which are then plotted to the screen when selected. This flexible approach allows future developments to be easily incorporated, where the pertinent ship motions can be combined to provide an overall operability plot relating to the specific ship task.

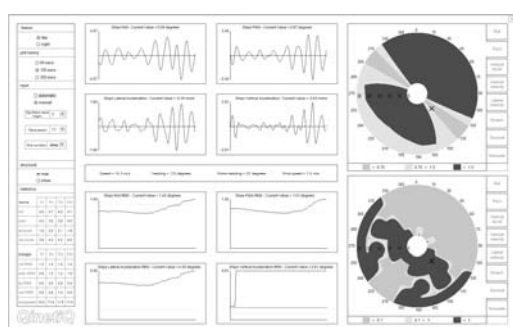


Figure 5-1 ORPHEUS day View



Figure 5-2 – ORPHEUS Low Light View

Simple to interpret polar contour plots provide a method of deciding how ship speed and course changes might affect their ability to perform their tasks interpreting the data for several speeds and headings. The important point being to provide useful and understandable information to the officers on the bridge in the form of guidance plots, for example, of helicopter operations, crew comfort & effectiveness, boat operations, slamming, deck wetness as well as hazardous situations such as broaching and capsizing.

Royal Navy feedback on the 2004 sea trial

was very positive and hence the UKMoD decided to enhance the capabilities of the system. QinetiQ have undertaken a development program to enhance the tool into a full Naval solution.

5. ORPHEUS DEVELOPMENT

The increasing complexity of ship and aircraft systems means a decision support aid that provides information giving guidance on the ability to undertake aircraft operations is of value. This information must, of course be in a form that the operator can use in a meaningful way.

A system of monitoring the current level of motions is a key part of an operator guidance system. The operators needs to be presented with reliable information on the condition of the ship and the effect the waves are having on it before they can take a decision to alter speed and or heading. Whilst the advisory part of the systems predicts the ship motions given the seaway, the motion monitoring is done using a small standalone instrumentation system developed by QinetiQ to measure and display the actual ship motions.

The ORPHEUS system provides statistical and risk based information detailing options for speed and heading changes that reduce the impact of the wind and wave environment on their ability to undertake operations. One issue that has been apparent when designing the operator guidance tool is the need to ensure that information is presented in a meaningful way and that the human machine interface (HMI) is considered from an ergonomic point of view.

The presentation of the live motion feedback, the polar plots and the long term statistical data, have been investigated in close collaboration with the operators both within the UK and the other Navies. The future enhancements will look at building on

the current usability of the system both in day and night operating modes.

The range of data that can be incorporated into the system is still evolving. A number of new operational plots are currently being reviewed and discussed with the operators such as further plots for air, boat, and weapon operations.

The ORPHEUS[®] system has been enhanced to incorporate additional operation plots as well as incorporating enhancements to the presentation of the information. Other enhancements, such as those requested by the Royal Navy following the demonstrator trial, are the inclusion of statistics, structural monitoring as well as user defined limits on the polar plots.

The wave environmental input was done by hand on the initial system. From the trial the UK Navy operators were found to be good at estimating wave height but not so accurate at estimating modal period. They could however, calculate encounter period very well, so algorithms were included to calculate the modal period from their encounter period input. Current developments include incorporating automated environmental input and Quiescent Period Prediction into the system to further enhance its capabilities.

6. ORPHEUS AT SEA

Since the 2005 development project, ORPHEUS has been installed on a number of Type 23 frigates and integrated with the existing structural strain gauging data logs. Further vessels are planned for during 2006 as well as linking it into the simulator and computer based training facility.

7. SUMMARY

A team within QinetiQ Platform Support Services Group has developed ORPHEUS, a unique navigational safety tool initially

developed for Royal Navy ships.

ORPHEUS, an acronym for Onboard Risk Performance Hazard Evaluation System, is a dedicated and flexible operator guidance tool that provides clear and concise information on how a ship will perform in a variety of weather scenarios.

The Royal Navy has a continuing need to provide ship handling training for watch keeping officers and specialist navigators. QinetiQ's development of classroom programs and ORPHEUS has already delivered improvements in hull design and understanding platform behaviour in extreme sea conditions. Harnessing the capabilities of these programmes to enhance both training and guidance at sea can only result in improvements in operational capability, increased safety and availability, lower through life costs, more competent operators and better management of risk.

ORPHEUS has now been installed on a number of frigates within the RN fleet after initial trials onboard their sister ship, HMS *Marlborough*, proved a veritable success.

The benefits of the ORPHEUS[®] system can be summarised as:

- Provide the operator with the means to minimise the risk of ship survival in extreme weather
- Provide the operator with the means to minimise the risk of damage to the ship in heavy weather.
- Increase the operational envelope and/or improve operational safety of most shipboard tasks that are degraded by ship motions caused by the presence of rough weather, such as aircraft operations, UXVs, towed array/towed body deployment, small boat operations and weapons firing.
- Aid ship operators to maximise crew comfort and crew effectiveness.

8. ACKNOWLEDGEMENTS

The authors would like to gratefully acknowledge the permission granted by QinetiQ and the UKMoD for publishing some of the findings from the project.

9. REFERENCES

Sarchin, T.H. and Goldberg, L.L., 1962, "Stability and Buoyancy Criteria for US Naval Surface Ships", Transactions SNAME.

MoD Defence Standard 02-109 (NES 109), UK Ministry of Defence, 2000, Stability Standards for Surface Ships, Part 1, Conventional Ships.

Maritime Acquisition Publication number 01024 (MAP 01024), 2006, Stability of Surface Ships Part 1 issue 1.

© British Crown Copyright and Copyright QinetiQ Ltd 2006

Published with the permission of the controller of Her Majesty's Stationery Office

Preliminary Research on Stability of Warship Models

Waldemar Mironiuk, *Naval University of Gdynia, Poland*

ABSTRACT

In the paper a description of the stability and unsinkability of the navy ships in a laboratory stand bed- designed and built in the Naval University of Gdynia- has been presented. Some scores of preliminary research of warship's model stability have been presented as well.

The range of research and training of crew can include static and dynamic stability. The presented laboratory offers a possibility not only to analyse the influence of free water surface effect in the compartments or tanks but also to analyse the influence of taking on, moving and removing loads on the initial stability of the ship. Experience acquired in the research station can lead to a better phenomenon recognition occurring in the everyday ship operations and cause increasing of sailing safety.

Keywords: *stability and unsinkability of a warship model, laboratory stand bed*

1. INTRODUCTION

A warship is a complex technical system whose reliability influences fighting ability (Mironiuk & Wróbel, 2004). However, as the literature analysis and maritime experience point out, even perfectly organised war fleets have to deal with accidents and ship failures. These can pose a threat to the health of a ship's crew and lead to death. In the complex international situation ship damages caused by enemy fighting means (rockets, mines, bombs, explosives) are more and more frequent. A good example is the ship USS STARK (FF0 — 31) which was hit by two rockets in 1987 on the waters of the Persian Gulf (35 victims). USS SAMUEL B. ROBERTS (FF0 —58) which operated on the water of the Persian Gulf in 1988 touched the mine and sustained heavy damages. Another example is a destroyer DDG 67 USS COLE which became an aim of the terrorist attack in Yemen in October 2000 (17 killed and 12 injured) (Korczewski & Wróbel, 2005).

There are plenty of examples, but the most important thing in such a situation is to make a correct assessment of the ship's state after a damage, which enables us to carry out a proper action of damage control. It is obvious that firm determination of the states of a ship after damage is impossible, all the more, a state of the sea has a great influence on an act of sinking. Therefore, a commanding officer (making decisions while fighting for unsinkability and for the survival of the ship) should assess the state of the ship after an accident, making use of his own experience and taking all the circumstances into account. The commanding officer - on the basis of the situation assessment - should determine the time when further fighting for unsinkability is senseless and should direct all the efforts to save the crew and documents (Miller, 1994).

Today, many countries start to pay more and more attention to improving the damage control elements. The action which increases the safety of both a ship and a crew (apart from construction solutions) is training in damage control exercises.

Training is carried out in well prepared training centres which are situated in the United Kingdom, Germany, Netherlands and Pakistan. These centres have ship models designed for the simulation of failure states which occur most frequently while operating a ship. Investigating the phenomenon during break-down is one of the research aims. Research results are used by creators of software, which gives assistance to a crew while making decisions in critical situations. However, there are not many ships with such programs. Thus the ship's crew must be prepared in early stages of training to face situations which threaten safety of the ship.

On the basis of the analysis of the existing Polish centres which provide training in damage control, we can draw the conclusion that there are not such specialized centres as mentioned above. The tasks in the Polish Navy are more and more complicated and demand well educated officer staff and an entire crew.

Taking didactic aims and needs into account as well as meeting expectations concerning the assessment of stability, unsinkability and sailing safety, the stability and unsinkability research on ship's models has been done. This station gives an opportunity to simulate a few failure situations for damaged and not damaged ship.

2. THE SCHEME OF STABILITY AND UNSINKABILITY OF SHIPS MODELS IN A STAND BED

Research on damage stability and unsinkability establishes the source of the knowledge according to a ship reaction in the different operating states. The big advantage of this research is a possibility of failure simulations in the laboratory

conditions using special models of real objects. Thanks to a suitable construction and new concepts applied for the station shown in Figure 2, it will be possible to research the ship

reaction even in the failure situations. This station is designed to develop the skills and habits while: (Mironiuk & Wróbel, 2004)

- assessing and restoring stability in failure situations;
- working out the procedures of moving a ship from shoal;
- determining the gravity centre and centre of buoyancy coordinates while adding, removing and shifting masses on the ship.

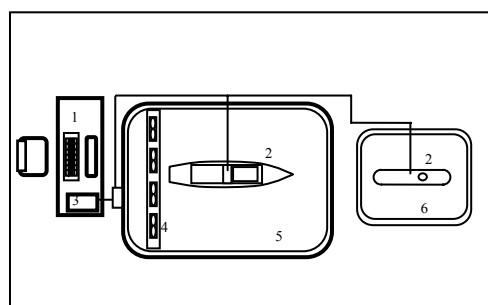


Figure 2. Scheme of damage stability and unsinkability research station for ship models.

- 1 – manager station,
- 2 – ship models,
- 3 – control computer gathering data,
- 4 – unit of fans,
- 5 – experimental tank for ship model,
- 6 – experimental tank for submarine model.

The unsinkability research on the ship's model after damaging one or more compartments will enable us to assess the time of flooding the model compartments and a whole model as well. Moreover, the station gives an opportunity to research the ship model reaction with taking into account influence of the free surface effect. The unit of fans on the experimental tank extends its possibilities for research on a dynamic stability.

3. EQUIPMENT OF THE LABORATORY STAND BED

The main parts of the damage stability and unsinkability research station, on this stage of work, are two warship models: 888 type and

660 type. The hull of each model was made in accordance with the body plan. The elements of the superstructure and the ship equipment were simplified in the model but the appropriate scale was kept (Mironiuk & Wróbel, 2004).

3.1. The Ship's Model Type 888

The ship's model type 888 is the main object of research because it is set up with specialized devices used for measurement of the position and for the analysis of the ship reaction during simulated damages. The shape of the model is shown in Figure 3.



Fig. 3. Model of the ship type 888.

The model of the ship type 888 consists of two main parts: the hull made of plastic and superstructure made of plywood protected from moisture. All elements whose area is significant during stability calculations were placed on the decks of the models. Because of the tasks carried out by warships, it is very important to create a ship model designed for simulation of holing. To accomplish this aim, chosen compartments (III, V, VII) were set up with remotely operated valves which enable the simulation of damage shown in Figure 4. These valves allow flooding the compartment to sea surface level. The electromagnetic valves are placed in the compartments with the biggest cubature

because these compartments influence unsinkability of the model the most. Another group of valves marked with numbers 4-8 in Figure 4, is designed for flooding the compartments used during the process of righting the ship when the damage is not symmetrically placed. The model of ship 888 was equipped with water system supplied by pumps located outside the model and water level indicator. These indicators mounted in compartments nr III, IV, VII measure the water level on the basis of hydrostatic pressure. An inclinometer mounted on the bow of the model is used for the measurement of the angle of the heel and the trim. The signals received from the indicators are transmitted by a wire to a computer which is equipped with two analog-digital cards and presented on the screen as simple values. Dislocation of main elements of the measurement system is shown in Figure 4.

The indicators and elements placed on the model are connected with the computer by little reduced mass conductors which display the received values on the screen. Taking advantage of a computer, we can carry out the operation of flooding and draining of the chosen compartments. These operations are controlled by a program installed on the computer. The screenshot shown in Figure 5 presents the window of the program.

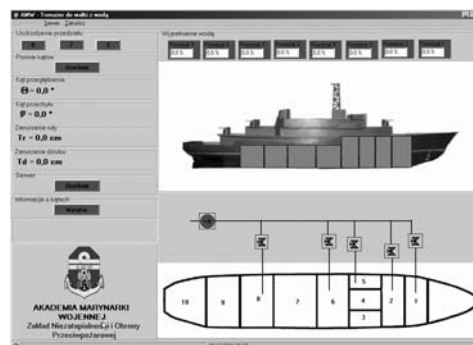


Fig.5. The window of computer program.

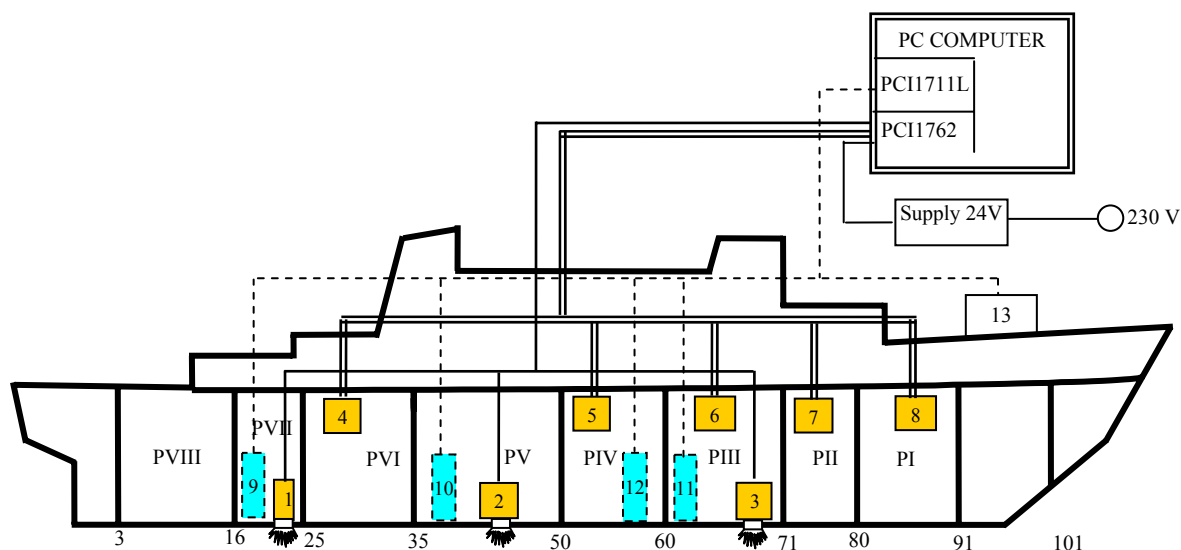


Fig.4. Disposition of elements in the model of ship type 888.

1,2 and 3: Valves for a puncture simulation in the compartment PIII, PV and PVII; 4,5,6,7 and 8: Valves for flooding the compartment PVI, PIV, PIII,PII and PI; 9,10 and 11: Water level indicators in the compartment PVII, PV and PIII; 12: Indicator of ship draught; 13: List indicator.

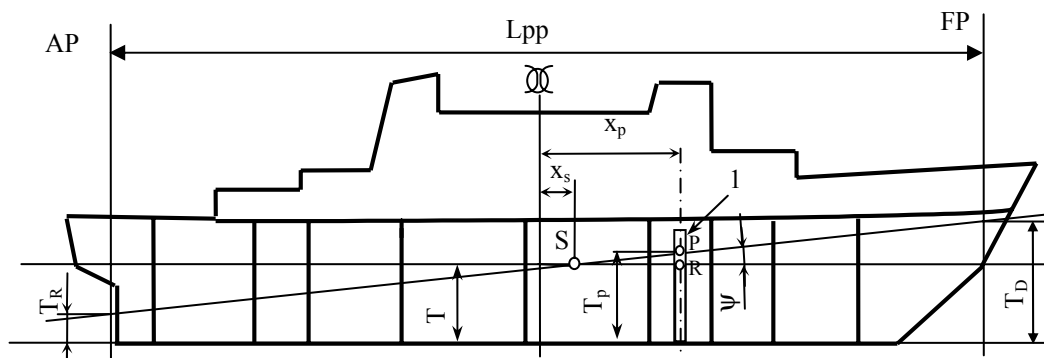


Fig.6. The scheme for calculation bow and stern draught.

1- draught indicator, AP- after perpendicular, FP- forward perpendicular, T- mean draught, Lpp- length between perpendiculars, T_R - after draught, T_D - forward draught, T_p – measured draught, ψ - angle of trim.

The amount of water in the compartment visible in the window program is presented in %. In addition, such parameters of the position as the angle of heel, the angle of trim, bow and stern draught are shown in the real time.

The parameters of bow and stern draught can be obtained in an indirect way. The

indicator of mean draught is located near the midship section. Knowing the mean draught and the angle of trim, we can calculate other parameters from mathematical formulas. We take advantage of the scheme presented in Figure 6.

Tangent of the angle trim of a model shown in Figure 6 equals:

$$\operatorname{tg} \psi = \frac{\overline{PR}}{x_p - x_s} \quad (1)$$

The mean draught of the model is found by the formula:

$$T = T_p - \overline{PR} \quad (2)$$

\overline{PR} - the vertical distance between water-plane and water level within the compartment,

x_p - the distance between draught indicator and midship section,

x_s - longitudinal centre of flotation

We can obtain bow and stern draught from the formula (1):

$$T_D = T_p + \left(\frac{L_{pp}}{2} - x_p \right) \operatorname{tg} \psi \quad (3)$$

$$T_R = T_p + \left(-\frac{L_{pp}}{2} - x_p \right) \operatorname{tg} \psi \quad (4)$$

T_p - measured draught,

L_{pp} - length between perpendiculars.

3.2. The Model of Ship Type 660

The research on stability and unsinkability includes numerous issues whose presentation on one model only is impossible. Therefore, the station was provided with a second model of the ship type 660 which is designed to conduct the research, especially from unsinkability domain. The model of this ship is shown in Figure 7.

The model is adapted to flooding the compartments in any way and to any level. On

the hull of the model the draught line and draught signs are plotted. Moreover, the position of bulkheads is marked, which helps the user to locate a damaged place.



Fig.7. Model of the ship type 660.

The model of ship type 660 was adapted to the presentation of the problem of influence a free surface effect of the liquid on the stability. In this connection a special superstructure was designed. In its higher part there is a hole used for providing water inside. The water from the high placed compartment can be moved out or moved to the lower watertight compartment. Such operations are carried out while restoring or correcting the stability. In this way it is possible to demonstrate a change of stability after changing the position of the gravity centre and to conduct research on flooding time either of damaged compartments or of the whole model.

3.3. The Model of a Rectangular Pontoon

The process of heaving the ship is very complicated. The best way to recognize this problem is to do some research on a simple object like a rectangular pontoon (Mironiuk & Wróbel, 2003). The construction of a rectangular pontoon model, presented in Figure 8, was designed by a team of workers from the Naval University in Gdynia.

It enables us to carry out the simulation of many states and critical situations which can occur on the ship. The dimensions of the construction and its mass were selected in order to use it for doing research and exercises relating to many more domains.

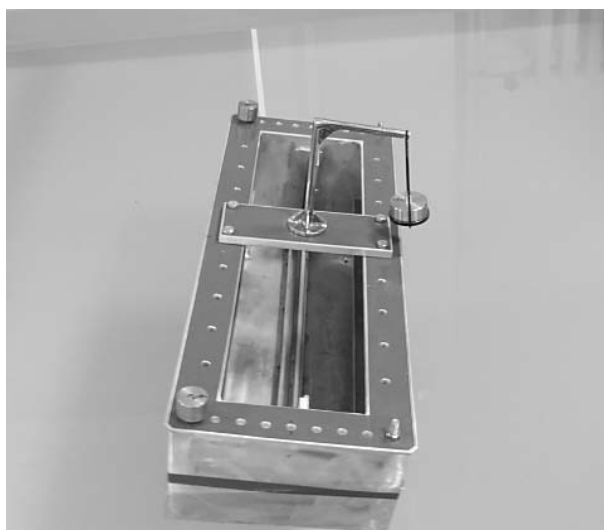


Fig.8. The construction of a rectangular pontoon model.

3.4. Submarine Stability Research Station.

The Polish Navy is equipped with a few submarines. The research on submarine stability is not as frequent as on normal ships but it is very important for our navy. A submarine stability research station is provided with an experimental tank which enables us to initiate research. In the preliminary stage of research it will be possible to present operations of emerging and immersing typical for a submarine only. A very narrow group of scientists bring up a matter of stability of a submarine so making use of new possibilities at the station is a step in a direction of research development as far as reacting of a submarine in different operating states is concerned.

4. PRELIMINARY RESEARCH ON THE POSITION OF A MODEL AFTER ITS DAMAGE

Stability research was started in a prepared laboratory stand bed for a warship type 888. Preliminary research consisted of checking operation of measuring instruments of draught, the angle of heel and the angle of trim. This research required calibrating measuring instruments and choosing the appropriate scale.

The measurement of the angle of heel and the angle of trim on a ship's model was carried out in the initial period of preliminary research when the compartment was damaged. The compartment damage simulation can be done by opening the suitable valve situated in the bottom of the model's bow. The model is trimmed on the bow after flooding the compartment. The measured parameters of values of the model's position were similar to the values of the real object for suitable weight. The difference of measured parameters of values can be affected by the position of the gravity centre of the model and the gravity centre of a real object. The scheme of ship's model with a damaged compartment is shown in the computer window in Figure 9.

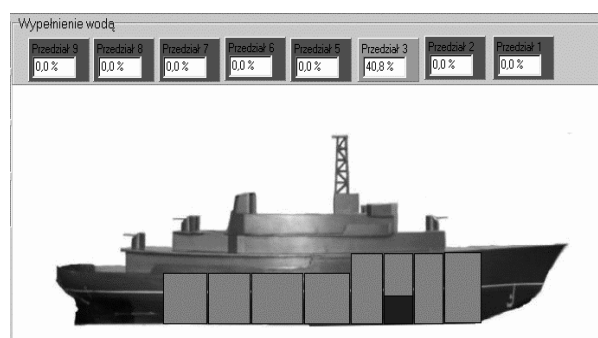


Figure 9. The scheme of ship's model with damaged compartment

During the second part of the preliminary research we tested a stand bed while simulating dynamic influence of flowing air on the warship's model. The stand bed is shown in Figure 10.



Figure 10. The stand bed for ship's dynamic stability simulation.

The initial speed of flowing air was measured directly from the unit of fans. The value of the air speed reached only 3 m/s. Since the level of air speed was too low to cause the dynamic heeling of the model, the stand bed was equipped with a coat. After this operation the air stream was concentrated and the air speed level increased to 6,5 m/s. The value of the air speed was enough to simulate dynamic heels of the model.

5. CONCLUSIONS

The research on stability and unsinkability of ship's models will be the source of knowledge to start researching of real warships.

The presented research station will allow conducting research and exercises including many stability problems, especially damage stability and unsinkability

The main emphasis was laid down on a possibility of creating different events scenario concerning every day ship operation. Students will develop habits and gather experience in the early stage of training. Running the exercises at well prepared station will allow people responsible for sailing safety to increase their qualifications and skills. This is important since the Polish Navy ships take part NATO in international exercises held in military conflict regions.

The simulation of damage states at a suitably prepared research station allows to form the habits of analysis and to produce new assessment or to make decisions to protect against critical situations.

6. REFERENCES

Jacobsen, T., 2003, "A potential of reducing the risk of ship casualties by 50%". Marine Technology V, pp171-181

Jakus, B., Korczewski, Z., Mironiuk, W., Szyszka, J., and Wróbel, R., 2001, "Obrona przeciwwawaryjna okrętu", Naval University, Gdynia.

Kobyliński, L.K., 2001, "Podstawy i filozofia bezpieczeństwa w żegludze", Summer School Safety at Sea. Technical University of Gdańsk,

Korczewski, Z., Pawłędzio, A. and Wróbel, R., 2005, "Analiza ilościowa wypadków i awarii na okrętach Marynarki Wojennej RP w latach 1985-2004", Przegład Morski nr 1. Gdynia.

Miller, D., 1994, "Damage control - an „insurance policy” International Defence Review nr 5.

Mironiuk, W., Pawłędzio, A., and Wróbel, R., 2004, "Trenażer do walki z wodą", Gdynia, pp 14-30.

Mironiuk, W., Pawłędzio, A., and Wróbel, R., 2003, "Analiza stateczności statycznej pontonu prostopadłościennego o wymiarach LxBxH", Gdynia.

Plewiński, L., 2000, "Wypadki na morzu", Szczecin.

Theoretical Prediction of Broaching in the Light of Local and Global Bifurcation Analysis

Naoya Umeda, *Osaka University*

Masatoshi Hori, *Osaka University*

Hirotsada Hashimoto, *Osaka University*

ABSTRACT

For developing design and operational criteria to be used at the International Maritime Organization (IMO), critical conditions for broaching are explored in the light of bifurcation analysis. Since surf-riding, which is prerequisite to broaching, can be regarded as a heteroclinic bifurcation, one of global bifurcations, of a surge-sway-yaw-roll model in quartering waves, the relevant bifurcation condition was mathematically formulated and then a numerical procedure for obtaining its solution was presented with successful example. This identified bifurcation condition was compared with direct numerical simulation in time domain. As a result, it was confirmed that the heteroclinic bifurcation provides a boundary between motions periodically overtaken by waves and non-periodic motions such as surf-riding, broaching and so on. Then a local bifurcation analysis was applied to the surf-riding equilibria. This results could explain a boundary between stable surf-riding and oscillatory surf-riding as a Hopf bifurcation. Furthermore, comparison with free-running model experiments shows some discrepancies and an improvement with an aid of nonlinearity in wave-induced surge force is presented.

Keywords: *broaching, surf-riding, capsizing, heteroclinic bifurcation, Hopf bifurcation, intact stability*

1. INTRODUCTION

Broaching is one of the three major capsizing scenarios that the new performance-oriented stability criteria to be added to the Intact Stability Code at the International Maritime Organization (IMO) are requested to cover. (Germany, 2005) This is a phenomenon that a ship cannot keep a constant course despite the maximum steering effort and the centrifugal force due to this uncontrollable yaw motion could result in capsizing. This phenomenon often occurs when a ship runs in following and quartering seas with relatively high forward speed, especially when a ship is surf-ridden. Thus, this phenomenon is relevant

to ships having their Froude number of 0.3 or above, such as destroyers, high-speed RoPax ferries, fishing vessels and so on.

For avoiding this phenomenon, currently the guidance to the master for avoiding danger in following and quartering seas (MSC/Circ. 707) provide an operational criterion for preventing from surf-riding, which is a prerequisite to broaching. This criterion was developed with a phase plane analysis of an uncoupled surge model in pure following seas. (Umeda, 1990) For accurately determining the surf-riding threshold, numerical simulation for obtaining a global picture of surf-riding should be systematically repeated. This is because the occurrence of surf-riding can be regarded as a heteroclinic bifurcation of a nonlinear mathematical model (Umeda, 1999).

It is important to reduce such computational efforts for developing operational or design criterion applicable to individual ships. For this purpose, Ananiev (1966) developed an approximated analytical method, Spyrou (2001) did an exact analytical method of a simplified model and Umeda et al. (2004) did a geometric method, which can identify the heteroclinic bifurcation point with the Newton method.

On the other hand, once broaching occurs, a ship has heading angle from wave direction. This means coupling with a manoeuvring motion in quartering waves is essential. Thus, a surge-sway-yaw-roll model is required to identify the threshold. For this purpose, the geometric method was applied to the manoeuvring mathematical model. So far the authors had already developed a manoeuvring model with linear wave forces and qualitatively validated it with model experiments. (Umeda & Hashimoto, 2002). The major difficulty arises here is the increase of dimensions of state vector describing this four degrees-of-freedom (DOF) model. This requires us to upgrade bifurcation analysis in a phase plane to that of a vector field. Therefore, the authors attempted to develop such a new methodology, as briefly introduced by Umeda et al. (2005). In this paper, more details are described and the numerical example here demonstrates its applicability and limitation and then an improvement is provided.

2. MATHEMATICAL MODEL

The mathematical model used in this paper is a manoeuvring model of the surge-sway-yaw-roll motion developed for prediction of broaching associated with surf-riding in following and quartering waves. (Umeda, 1999) In cases of ship runs with higher forward velocity in following and quartering waves, the encounter frequency becomes much smaller than the natural frequencies in heave and pitch. Therefore these motions were estimated by simply tracing their stable equilibrium.

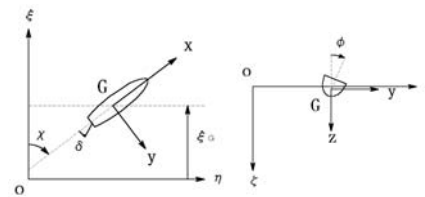


Figure 1 Coordinate systems

As can be seen in Fig.1, two coordinate systems are used: (1) a wave fixed with its origin at a wave trough, the ξ axis in the direction of wave travel; and (2) an upright body fixed with its origin at the centre of ship gravity, with the x axis pointing toward the bow, the y axis to starboard, and the z axis downward. The state vector, \mathbf{x} , and control vector, \mathbf{b} , of this system are defined as follows:

$$\mathbf{x} = (x_1, x_2, \dots, x_8)^T = \{\xi_G / \lambda, u, v, \chi, r, \phi, p, \delta\}^T \quad (1)$$

$$\mathbf{b} = \{n, \chi_c\}^T \quad (2)$$

The dynamical system can be represented by the following state equation:

$$\dot{\mathbf{x}} = \mathbf{F}(\mathbf{x}; \mathbf{b}) = \{f_1(\mathbf{x}; \mathbf{b}), f_2(\mathbf{x}; \mathbf{b}), \dots, f_8(\mathbf{x}; \mathbf{b})\}^T \quad (3)$$

where

$$f_1(\mathbf{x}; \mathbf{b}) = \{u \cos \chi - v \sin \chi - c\} / \lambda \quad (4)$$

$$f_2(\mathbf{x}; \mathbf{b}) = (T(u; n) - R(u) + X_w(\xi_G / \lambda, \chi)) / (m + m_x) \quad (5)$$

$$f_3(\mathbf{x}; \mathbf{b}) = (- (m + m_x)ur + Y_v(u; n)v + Y_r(u; n)r + Y_\phi(u)\phi + Y_\delta(u; n)\delta + Y_w(\xi_G / \lambda, u, \chi, n)) / (m + m_y) \quad (6)$$

$$f_4(\mathbf{x}; \mathbf{b}) = r \quad (7)$$

$$f_5(\mathbf{x};\mathbf{b}) = (N_v(u;n)v + N_r(u;n)r + N_\phi(u)\phi + N_\delta(u;n)\delta + N_w(\xi_G / \lambda, u, \chi; n)) / (I_{ZZ} + J_{ZZ}) \quad (8)$$

$$f_6(\mathbf{x};\mathbf{b}) = p \quad (9)$$

$$f_7(\mathbf{x};\mathbf{b}) = (m_x z_H u r + K_v(u;n)v + K_r(u;n)r + K_p(u)p + K_\phi(u)\phi + K_\delta(u;n)\delta + K_w(\xi_G / \lambda, u, \chi; n) + mgGZ(\phi)) / (I_{xx} + J_{xx}) \quad (10)$$

$$f_8(\mathbf{x};\mathbf{b}) = \{-\delta - K_R(\chi - \chi_C) - K_R T_D r\} / T_E \quad (11)$$

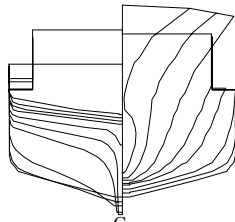


Figure 2 Body plan of the subject ship

Table.1 Principal particulars of the ship

Items	Values
length: L_{BP}	34.5 m
breadth: B	7.60 m
depth: D	3.07 m
draught at FP: d_f	2.50 m
mean draught: d_m	2.65 m
draught at AP: d_a	2.80 m
block coefficient: C_b	0.597
metacentric height: GM	1.00 m
pitch radius of gyration: κ_{yy}/L_{BP}	0.302
l.c.b. (aft)	1.31 m
rudder aspect ratio	1.84
time constant for steering gear: T_E	0.63 s
rudder gain: K_R	1.0
time constant for differential control: T_D	0.0 s

Based on the above-mentioned mathematical model, numerical calculations were carried out for a 135GT Japanese purse seiner used as a subject ship of the ITTC benchmark testing. (Umeda et al., 2001) Principal particulars and body plan are shown in Table1 and Figure 2, respectively. Hydrodynamic coefficients and other relating

coefficients can be found in the literature. (Umeda and Hashimoto., 2002)

3. HETEROCLINIC BIFURCATION

A nonlinear dynamical system described by Eq. (3) could have fixed points,

$$\bar{\mathbf{x}} = (\bar{\xi}_G / \lambda, \bar{u}, \bar{v}, \bar{\chi}, \bar{r}, \bar{\phi}, \bar{p}, \bar{\delta}) \quad (12)$$

where

$$\mathbf{F}(\bar{\mathbf{x}}; \mathbf{b}) = \mathbf{0} \quad (13)$$

These fixed points correspond to surf-riding, under which a ship runs with a regular wave train. $\mathbf{F}(\mathbf{x};\mathbf{b})$ is linearised at $\bar{\mathbf{x}}$, putting $\mathbf{x} = \bar{\mathbf{x}} + \mathbf{y}$ to obtained following equation:

$$\dot{\mathbf{y}} = \mathbf{DF}(\bar{\mathbf{x}}; \mathbf{b})\mathbf{y} \quad (14)$$

where

$$\mathbf{DF}(\mathbf{x}; \mathbf{b}) = \partial / \partial x_j f_i(\mathbf{x}; \mathbf{b}) \quad (15)$$

If an eigenvalue of $\mathbf{DF}(\bar{\mathbf{x}}; \mathbf{b})$, λ_i , which is obtained by

$$[\mathbf{DF}(\mathbf{x}; \mathbf{b}) - \lambda_i] \mathbf{y} = 0 \quad (16)$$

has a positive real part, local asymptotic behaviour at $\bar{\mathbf{x}}$ is unstable.

Hartman's theorem and the stable manifold theorem (Guckenheimer & Holmes, 1983) enable us to investigate the local topological structure of the system by Eq. (3). That is, there exist local stable and unstable manifolds, $W_{loc}^S(\bar{\mathbf{x}}; \mathbf{b})$ and $W_{loc}^U(\bar{\mathbf{x}}; \mathbf{b})$, tangent to eigenspaces, spanned by $\mathbf{DF}(\bar{\mathbf{x}}; \mathbf{b})$ at $\bar{\mathbf{x}}$. Then the global stable and unstable manifolds W^S and W^U are obtained by letting points in W_{loc}^S flow

backward in time and those in W_{loc}^U flow forward.

The numerical survey for the system described by Eq. (3) applied to the subject ship (Umeda, 1999) indicates that there is normally one fixed point having only one eigenvalue having a positive real part, λ_1 , if a fixed point exists. Thus, such fixed point has a 1-dimensional unstable invariant manifold and a 7-dimensional stable invariant manifold. A heteroclinic bifurcation requires that W^U of a fixed point is connected to W^S of other fixed point. Although calculation of W^S is not easy, W^U is easily calculated as a trajectory, which is obtained by numerically integrating Eq. (3) from the fixed point with small perturbation, δ_1 , for the direction of eigenvector as follows:

$$\mathbf{x}(t) = \varphi(t, \mathbf{x}_\alpha; b) \tag{17}$$

where

$$[\mathbf{x}_\alpha - \bar{\mathbf{x}}]^T [\mathbf{x}_\alpha - \bar{\mathbf{x}}] = \delta_1^2 \tag{18}$$

Then, if we find \mathbf{b}_0 satisfying the following relationship (Kawakami et al., 1997):

$$[DF^T(\bar{\mathbf{x}}^*; \mathbf{b}_0) - \lambda_1 \mathbf{I}]h = 0 \tag{19}$$

$$\mathbf{h}^T [\mathbf{x}_\omega^* - \bar{\mathbf{x}}^*] = 0 \tag{20}$$

$$[\mathbf{x}_\omega^* - \bar{\mathbf{x}}^*]^T [\mathbf{x}_\omega^* - \bar{\mathbf{x}}^*] - \delta_2^2 = 0 \tag{21}$$

$$\bar{\mathbf{x}}^* = \{(\bar{\xi}_G / \lambda - 1), \bar{u}, \bar{v}, \bar{\chi}, \bar{r}, \bar{\phi}, \bar{p}, \bar{\delta}\} \tag{22}$$

$$\varphi(T, \mathbf{x}_\alpha; \mathbf{b}_0) - \varphi(-T, \mathbf{x}_\omega^*; \mathbf{b}_0) = \mathbf{0} \tag{23}$$

$$\delta_2 \ll 1 \tag{24}$$

this is a heteroclinic bifurcation point.

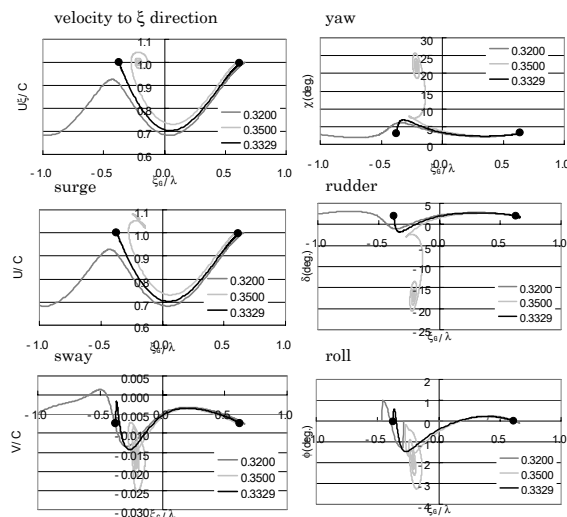


Figure 3 An example of the heteroclinic bifurcation under the wave steepness of 0.05, the wave length to ship length ratio of 1.0 and the auto pilot course of 5 degrees.

In this paper, the above equation set was numerically solved by the Newton method. A numerical example is shown in Figure 3. here the wave steepness is 0.05 and the wave length to the ship length ratio is 1.0. In this case the obtained heteroclinic bifurcation point is the nominal Froude number, Fn , of 0.3329 for the autopilot course of 5 degrees from the wave direction. Below this value the ship is overtaken by waves and above this value the ship is captured by a wave downslope.

This method was applied to different auto pilot courses and wave conditions and then the results are compared with numerical results obtained from time series based on sudden change concept as shown in Figure 4. Here the initial state for the sudden change concept is fixed with a periodic state under $Fn=0.1$ and $\chi_c=0$ degrees and its computational time is 1000 seconds. The time series were categorised into periodic motions, surf-riding, broaching

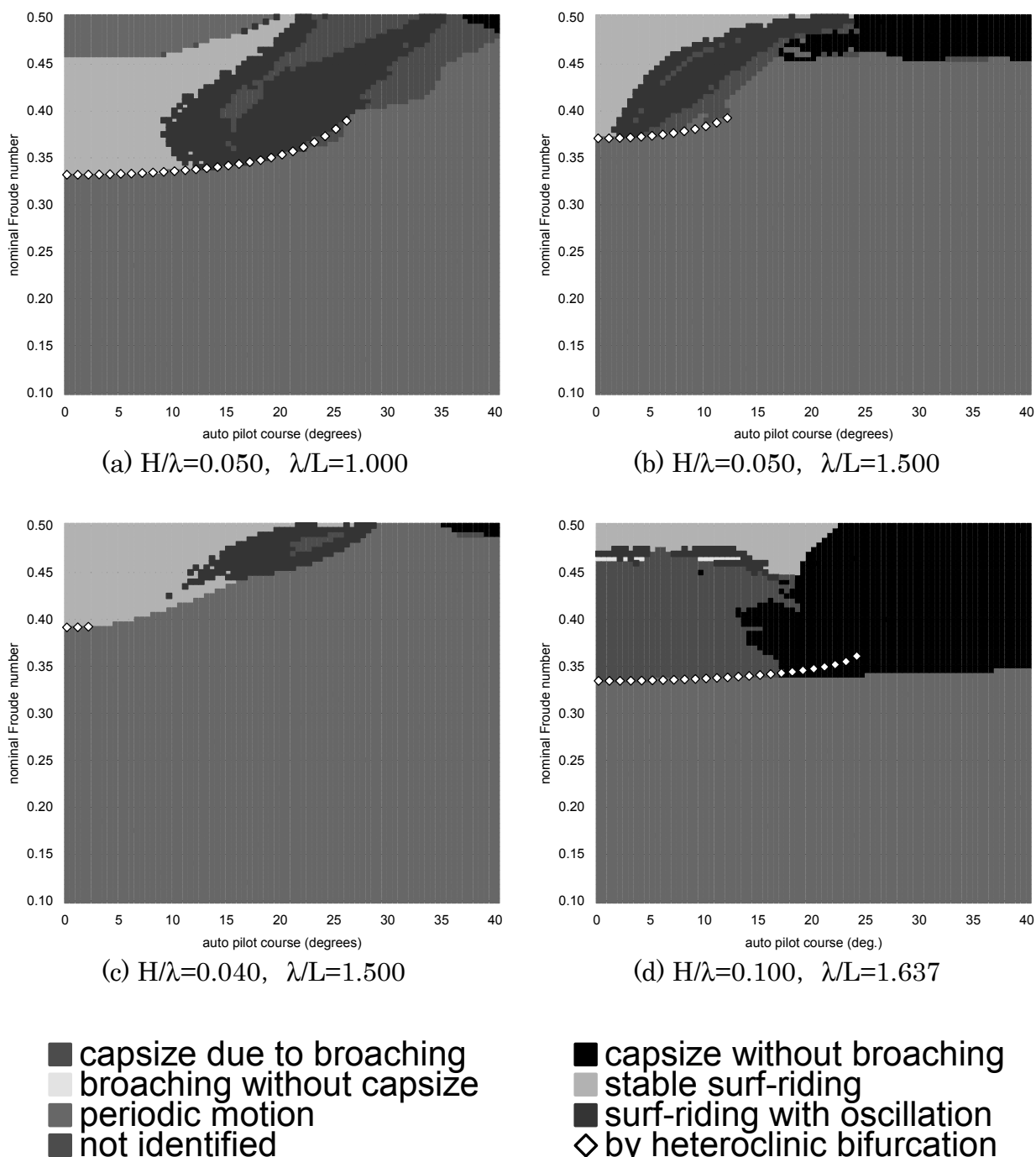


Figure 4 Numerical simulation and Hetero-clinic bifurcations

and capsizing with judging criteria (Umeda & Hashimoto, 2002). The heteroclinic bifurcation points obtained by the present method reasonably well predict the boundary between the periodic motions overtaken by waves and other motions such as surf-riding at least for

smaller auto pilot course from the wave direction. Therefore, the present method for identifying a surf-riding threshold can be used as an alternative to time-consuming numerical simulation. When the auto pilot course increases, the surf-riding threshold also

increases. This is comparable to the current MSC/Circ. 707. When the wave steepness increases, the surf-riding threshold decreases because of the increase of wave-induced surge force. For the wave steepness is 0.05 or below, stable or oscillatory surf-riding occurs above the heteroclinic bifurcation points. For much larger wave steepness, such as 0.1, broaching and/or capsizing occur. This is because broaching could occur once surf-riding happens under such wave condition. Thus, the heteroclinic bifurcation can be used as a threshold for broaching. However, it is noteworthy that the heteroclinic bifurcation does not distinguish broaching from surf-riding.

Although the sudden change concept used here for the numerical simulation is designed to minimise the initial-value dependence, small disagreement between the bifurcation and the surf-riding threshold could be explained as the initial-value dependence. (Umeda, 1999) In the case of larger wave steepness, a heteroclinic connection could occur beyond more than one wave length in a special case. And periodic broaching could occur in the very limited region. In addition, the existing range of heteroclinic bifurcation may depend on a sweeping direction for providing the initial value of the Newton method. Thus, these should be further investigated in future.

4. LOCAL BIFURCATION

To investigate the ship behaviour above the heteroclinic bifurcation, local bifurcation analysis on fixed points were carried out. Here the eigenvalues of locally-linearised system at all fixed points were calculated as shown in Figures 5-6.

For smaller wave steepness, the region where fixed points exist is slightly larger than the region above the heteroclinic bifurcation. When the auto pilot course increases, eigenvalues having non-zero imaginary part appear. This can be regarded as the Hopf bifurcation. The numerical simulation also

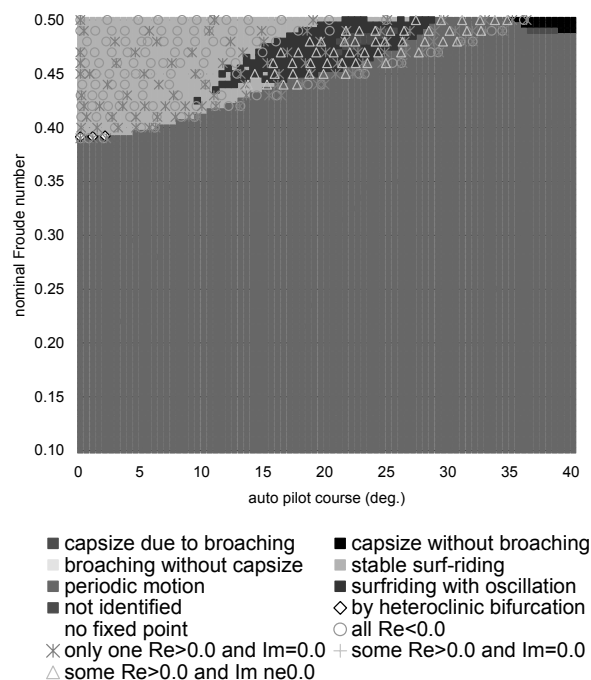


Figure 5 Numerical simulation and Eigenvalues of fixed points with $H/\lambda=0.040$, $\lambda/L=1.500$

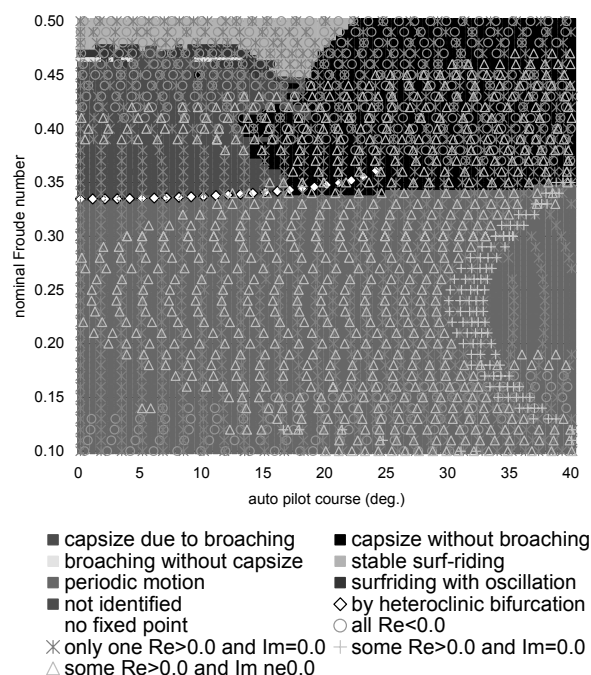


Figure 6 Numerical simulation and Eigenvalues of fixed points with $H/\lambda=0.100$, $\lambda/L=1.637$

provides the region of oscillatory surf-riding, which is almost inside the zone of the fixed points whose eigenvalues have non-zero

imaginary parts. This suggests that the Hopf bifurcation results in limit cycle around unstable surf-riding. This phenomenon was discussed by Spyrou (1995).

For larger wave steepness, the region that fixed points exist is enlarged to cover all explored region. In the region of stable surf-riding, which is identified with the numerical simulation, fixed points whose eigenvalues have no positive real parts can be found so that stable surf-riding can exist. Regarding capsizing due to broaching or capsizing without broaching, a fixed point of which an eigenvalue has a positive real part can be found for each operational condition but it is not sufficient to distinguish these phenomena. In general, the local bifurcation analysis can provide prerequisite for dangerous phenomena but can identify their sufficient conditions. This is because a trajectory does not always approach to fixed points.

5. COMPARISON WITH EXPERIMENT AND IMPROVEMENT

So far the prediction of heteroclinic bifurcation was successfully validated with numerical simulation. As a next step, the calculated heteroclinic bifurcation was compared with existing free-running model experiments for the subject ship (Umeda et al., 1999). In the experiment periodic motions, stable surf-riding, broaching and capsizing were observed. The comparisons are shown in Figure 7. Here the heteroclinic bifurcation (A) indicates that from the above mentioned method, and overestimates danger. The measured periodic motions overtaken by waves can be found even above the heteroclinic bifurcation (A). It can be presumed that this is because the accuracy of mathematical modelling of the motions is insufficient. After proposing the mathematical model described in Eq. (3), the authors have continued their effort to improve it by utilising captive model tests and hydrodynamic modelling. As a result, Hashimoto et al. (2004B) proposed an improved mathematical model for

- exp.(capsize due to broaching)
- ✱ exp.(capsize without broaching)
- ✕ exp.(broaching without capsize)
- △ exp.(near stable surf-riding)
- exp.(periodic motion)
- ◇ heteroclinic bifurcation(A)
- ◆ heteroclinic bifurcation(B)

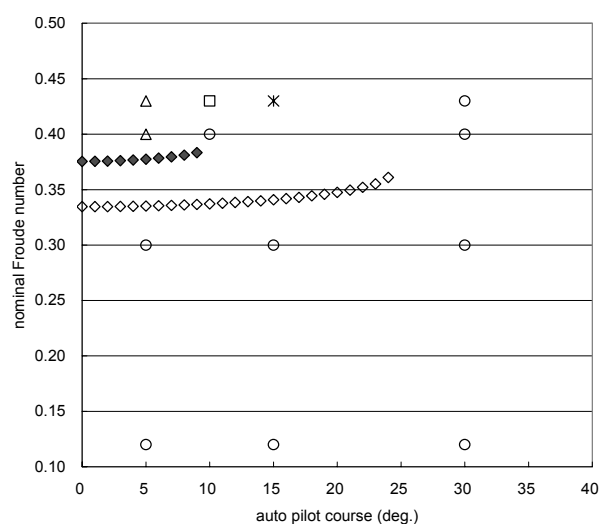


Figure 7 Comparison between the calculated heteroclinic bifurcation and free-running model experiment. Here the heteroclinic bifurcations (A) and (B) are based on Eq. (3) and an improved mathematical model, respectively.

quantitatively predicting broaching. The crucial factors are nonlinear hull manoeuvring forces, wave effect on linear manoeuvring forces, wave effect on rudder forces, wave effect on restoring moment, wave effect on propeller thrust, nonlinearity of wave-induced surge force, nonlinear coupling effect between sway and roll, heel-dependent nonlinear hydrodynamic forces in calm water. Among them, nonlinearity of wave-induced surge force is identified as the main cause of discrepancy in surf-riding threshold, which can be obtained from a captive model test in following waves. (Hashimoto et al., 2004A) Therefore, in this paper, these experimental data were incorporated into the mathematical model and then the above mentioned technique for estimating heteroclinic bifurcation was applied. The calculated results are also plotted in Figure 7 as the heteroclinic bifurcation (B). This new results improves agreement between the

experiment and calculation significantly. Because of nonlinear relationship between the wave-induced surge force and wave steepness, the wave-induced surge force becomes smaller than that from a linear theory. As a result, the nominal speed of heteroclinic bifurcation increases. Thus, it is also important to utilise accurate but still practical hydrodynamic modelling for correctly estimate broaching and capsizing. The authors (Hashimoto and Umeda, 2005) proposed a mathematical model as an candidate. It is desirable to incorporate it into the global bifurcation analysis, and is a future task.

6. CONCLUSIONS

This paper presents a numerical method for estimating the heteroclinic bifurcation of the surge-sway-yaw-roll model in quartering waves, which can be regarded as a threshold for surf-riding and/or broaching. Numerical examples are reasonably well compared with numerical simulation from some initial value sets. Hydrodynamic modelling in wave-induced surge force was improved with a captive model test data so that sufficient agreement with the free-running model experiments was realised. In addition, the existence of the Hopf bifurcation, which could result in oscillatory surf-riding, was confirmed with the bifurcation analysis on fixed points.

7. ACKNOWLEDGEMENTS

The work described here was carried out as a research activity of RR SPL project of Japan Ship Technology Research Association in the fiscal year of 2005, funded by the Nippon Foundation. The authors express their sincere gratitude to the above organisations.

8. REFERENCES

- Ananiev, D.M., 1996, "On Surf-Riding in Following Seas", Transaction of Krylov Society, Vol. 13, pp.169-176, (in Russian).
- Germany, 2005, "Report of the Intersessional Correspondence Group (part 1)", SLF48/4/1, IMO.
- Guckenheimer, J. and Holmes, P., 1983, Nonlinear Oscillations, Dynamical Systems, and Bifurcations of Vector Fields, Springer Verlag, New York, pp. 12-16.
- Hashimoto, H., Umeda, N. and Matsuda, A., 2004A, "Importance of Several Nonlinear Factors on Broaching Prediction", Journal of Marine Science of Technology, Vol. 9, pp. 80-93.
- Hashimoto, H., Umeda, N. and Matsuda, A., 2004B, Model Experiment on Heel-Induced Hydrodynamic Forces in Waves for Broaching Prediction", Proceedings of the 7th International Ship Stability Workshop, Shanghai Jiao Tong University, pp.144-155.
- Hashimoto, H. and Umeda, N., 2005, "An Investigation on Quantitative Prediction of Broaching Phenomenon", Proceedings of the Kansai Society of Naval Architects, No. 24, pp. 5-8, (in Japanese).
- Kawakami, H., Yoshinaga, T. and Ueda, T., 1997, "Methods of Computer Simulation on Dynamical Systems", Bulletin of Japan Society for Industrial and Applied Mathematics, Vol.7, No.4, pp.49-57, (in Japanese).
- Spyrou, K.J., 1995, "Surf-Riding, Yaw Instability and Large Heeling of Ships in Following/ Quartering Waves", Schiffstechnik, Vol. 42, pp. 103-112.
- Spyrou, K.J., 2001, "Exact Analytical Solutions for Asymmetric Surging and Surf-Riding", Proceedings of the 5th International Workshop on Stability and Operational Safety of Ships, University of Trieste, pp.4.4.1-3.

Umeda, N., 1990, "Probabilistic Study on Surf-riding of a Ship in Irregular Following Seas", Proceedings of the 4th International Conference on Stability of Ships and Ocean Vehicles, University Federico II of Naples, pp.336-343.

Umeda, N., 1999, "Nonlinear Dynamics on Ship Capsizing due to Broaching in Following and Quartering Seas", Journal of Marine Science of Technology, Vol.4, pp.16-26.

Umeda, N., Matsuda, A., Hamamoto, M. and Suzuki, S., 1999, "Stability Assessment for Intact Ships in the Light of Model Experiments", Journal of Marine Science of Technology, Vol.4, pp.45-57.

Umeda, N. and Renilson, M.R., 2001, "Benchmark Testing of Numerical Prediction on Capsizing of Intact Ships in Following and Quartering Seas," Proceedings of the 5th International Workshop on Stability and Operational Safety of Ships, University of Trieste, pp.6.1.1-10.

Umeda, N. and Hashimoto, 2002, "Qualitative Aspects of Nonlinear Ship Motions in Following and Quartering Seas with High Forward Velocity", Journal of Marine Science and Technology, Vol., 6, pp. 111-121.

Umeda, N., Ohkura, Y., Urano, S., Hori, M. and Hashimoto, H., 2004, "Some Remarks on Theoretical Modelling of Intact Stability", Proceedings of the 7th International Ship Stability Workshop, Shanghai Jiao Tong University, pp.85-91.

Umeda, N., Hashimoto, H., Paroka, D. and Hori, M., 2005, "Recent Developments of Theoretical Prediction on Capsizes of Intact Ships in Waves", Proceedings of the 8th International Ship Stability Workshop, Istanbul Technical University, pp.1.2.1-1.2.10.

9. NOMENCLATURE

c	wave celerity
F_n	nominal Froude number
g	gravitational acceleration
GZ	righting arm
H	wave height
I_{xx}	moment of inertia in roll
I_{zz}	moment of inertia in yaw
J_{xx}	added moment of inertia in roll
J_{zz}	added moment of inertia in yaw
K_p	derivative of roll moment with respect to roll rate
K_r	derivative of roll moment with respect to yaw rate
K_R	rudder gain
K_T	thrust coefficient of propeller
K_v	derivative of roll moment with respect to sway velocity
K_w	wave-induced roll moment
K_δ	derivative of roll moment with respect to rudder angle
K_ϕ	derivative of roll moment with respect to roll angle
L	ship length between perpendiculars
m	ship mass
m_x	added mass in surge
m_y	added mass in sway
n	propeller revolution number
N_r	derivative of yaw moment with respect to yaw rate
N_v	derivative of yaw moment with respect to sway velocity
N_w	wave-induced yaw rate
N_δ	derivative of yaw moment with respect to rudder angle
N_ϕ	derivative of yaw moment with respect to roll angle
p	roll rate
r	yaw rate
R	ship resistance
t	time
T	propeller thrust

T_D	time constant for differential control	Y_ϕ	derivative of sway force with respect to roll angle
T_E	time constant for steering gear	z_H	vertical position of centre of sway force due to lateral motions
u	surge velocity	δ	rudder angle
v	sway velocity	λ	wave length
X_w	wave-induced surge force	ξ_G	longitudinal position of centre of gravity
Y_r	derivative of sway force with respect to yaw rate	ϕ	roll angle
Y_v	derivative of sway force with respect to sway velocity	χ	heading angle from wave direction
Y_w	wave-induced sway force	χ_c	desired heading angle for auto pilot
Y_δ	derivative of sway force with respect to rudder angle		

The Transverse Stability and Rolling of a Vessel Loaded by Elastically Movable Cargo

Yuriy L. Vorobyov, *University, Ukraine*

Victor G. Sizov, *National Maritime Academy, Ukraine*

ABSTRACT

Stability and rolling of a vessel loaded with elastically movable cargo (EMC) are studied. Springing and being deformed such cargo shifts down and aside causing variations in mass moment of inertia of an oscillatory system, position of ship's gravity center and appearance of an additional heeling moment. Under assumption of small angles of inclinations the differential roll equation is analyzed for a vessel loaded with EMC which mass moment of inertia is varying harmonically with incoming waves frequency. The parametric resonance conditions are formulated.

The nonlinear differential roll equation for finite oscillations of a vessel loaded with EMC is presented and the loss of stability conditions are studied. Theoretical points are illustrated by calculation results for motor vessel "Rechitsa".

Key words: *elastically movable cargo (EMC), stability of ship in waves, capsizing conditions.*

1. INTRODUCTION

Motor vessel "Rechitsa" of the Soviet Danube shipping company, making trip from port Reni (Danube river) to port Alexandria with a cargo of a rolled wire in coves, loaded by bulk, tipped and sunk on November, 26th, 1976 at an exit to Mediterranean sea.

According to the testimony of the survived crew members during the moment of accident there were force 7 sea waves, thus the vessel was rolling with the amplitude of $10^0 - 12^0$ on both sides. Having wind heel nearby 2^0 and making a sharp turn aside for a divergence with a meeter, motor vessel "Rechitsa" at the next inclination has tilted on a port side up to $20 - 25^0$. The vessel has not returned to the vertical position and at several subsequent fluctuations the angle of inclination on a port side continued to increase. After 8 - 10 minutes the vessel has

laid down on a port side, then was turned over bottom up and has sweepingly sunk. The increase of heel angle was escorted by a hum, a gnash, perceptible hull vibration.

Onboard a vessel there was a cargo of a steel rolled wire in coves, loaded by bulk in all eight cargo compartments. The cove of a rolled wire has the form of spring ring - a torus of 1,2 m in diameter and weight of 0.8 т.

The analysis of ship documentation has shown that at the departure the vessel completely met the stability requirements of the Register of Shipping of the USSR. The rolled wire in coves had never been mentioned in any official normative document as a cargo which is dangerous for ship stability conditions. Thus no resolutions existed regarding special measures to be taken during the loading of a vessel with EMC.

The official investigation, including both

calculational analysis and special natural experiments, was performed after loss of a vessel. This investigation allowed to establish the following facts:

- the cargo of rolled wire steeped by bulk presents a continuous springing mass in which under the act of gravity and vibration appreciable elastic and residual deformations of compression and shifting are obtained,
- the deformability of this cargo was studied experimentally by keeling of a tank filled with it. It was shown that modification of a specific loading volume of that cargo varied from 1.8 - 1.9 m³/T up to 1.3 m³/T during the inclination,
- experiments with the tank have also shown that if the heel angle exceeded 18° the cargo filling tank space not completely started to shift aside, keeping its free surface close to horizontal level.

The presented special properties of a cargo could render significant effect on actual stability of a vessel (Bondar V.M., 1999; Sizov V.G., 1999). This effect has been strengthened owing to incomplete filling of cargo compartments at loading and the subsequent self-packing of cargo. So at the moment of accident more than 25% of the volume of total space in the upper part of cargo compartments was empty. Formation of voids promoted shifting of cargo after the vessel reached angle exceeding 18°.

The mentioned special properties of a cargo, manifested during oscillating of a vessel in waves, their probable role in outcome of accident with "Rechitsa", lack of precise rules on conveyance special cargoes with similar properties (rubber, wool and wooden chips in bales) if they are steeped by bulk and not shared with rigid separation, cause an imperative need of comprehensive study of dynamics of the vessel, loaded with EMC under heavy wave conditions.

Among prime follows:

- to evaluate necessity of taking into consideration fluctuations of mass moment of inertia of cargo and vessel,

- to find differential rolling equation for a vessel taking into account particular properties of EMC,
- to conduct the analysis of mentioned rolling equation for a vessel with EMC and to outline the zones with stable and unstable solutions,
- to illustrate the obtained results by predicted data for motor vessel "Rechitsa". The main characteristics of motor vessel "Rechitsa" are given in table 1.

Table 1. – The characteristics of motor vessel "Rechitsa"

Length between perpendiculars	$L_{\perp\perp}$	109.0
Breadth	B	16.6
Depth	D	8.36 m
Draft	d	6.53 m
Displacement	Δ	8420 t
Load weight	P	4032 t
Volume of cargo spaces	V	6885 m ³
Mass moment of inertia of vessel (including water added mass moment) round longitudinal axis	J_x	30325 t·sec ² /m
Height of gravity center of vessel (at the end of loading)	z_g^0	6.34 m
Height of gravity center of vessel before accident	z_g	6.06 m

Let's notice that lowering of ship's gravity centre before accident in comparison with the moment at the end of her loading is caused by compression of EMC.

2. EFFECT OF EMC MASS MOMENT OF INERTIA FLUCTUATIONS ON ROLLING OSCILATIONS OF VESSEL

Let's consider oscillations of vessel with periodically varying mass moment of inertia of EMC loaded on board (Sizov V.G., 2002).

The mass moment of inertia of vessel is represented in the form

$$J_x = I_1 + I_c, \quad (1)$$

where I_1 is a constant component of mass moment of inertia of a vessel (moment of inertia of added mass of water included); I_c mass moment of inertia of strained and displaced part of cargo.

Let's present I_c in the form

$$I_c = i_0 + mr^2, \quad (2)$$

where m is a mass of straining and displacing cargo; $r = r_0 \sin \sigma t$ is radius of inertia of mass m ; σ is frequency of encounter; i_0 - inertia moment of mass m at it's the most compact disposition relatively axis of fluctuations.

Assuming $I + i_0 = I_0$, we receive

$$J_x = I_0 + mr_0^2 \sin^2 \sigma t = I_0 (1 + \varepsilon \sin^2 \sigma t), \quad (3)$$

where $\varepsilon = \frac{mr_0^2}{I_0}$, and it is accepted $\varepsilon \ll 1$.

In a problem considered it is impossible to use the traditional equation of rolling which is fair for a constant mass moment of inertia of vessel. Using a principle of conservation of angular momentum for oscillating system, we receive in case of small inclinations

$$\frac{d}{dt} \left(J_x \ddot{\theta} \right) + N \dot{\theta} + K\theta = K\alpha_0 \sin \sigma t, \quad (4)$$

where N is drag coefficient of rolling; $K = \Delta h$ - coefficient of transverse stability; h - metacentric height; α_0 - an effective wave slop angle of incoming waves with angular frequency σ .

From (4) it is found

$$J_x \ddot{\theta} + \frac{\partial J_x}{\partial t} \dot{\theta} + N \dot{\theta} + K\theta = K\alpha_0 \sin \sigma t, \quad (5)$$

and

$$\frac{dJ_x}{dt} = \varepsilon I_0 \sigma \sin 2\sigma t, \quad (6)$$

$$\frac{1}{J_x} = \frac{1}{I_0(1 + \varepsilon \sin^2 \sigma t)} = \frac{1}{I_0} (1 - \varepsilon \sin^2 \sigma t) + O(\varepsilon^2) \quad (7)$$

Let us take a new variable

$$\chi = \theta \exp\left(\frac{1}{2} \int B(t) dt\right), \quad (8)$$

where $B(t) = N + \frac{\dot{J}_x}{J_x}$.

From the equation (5) it comes

$$\ddot{\chi} + \left(n^2 - \frac{1}{4} B^2 - \frac{1}{2} \dot{B} \right) \chi = \quad (9)$$

$$= n^2 \alpha_0 \sin \sigma t (1 - \varepsilon \sin^2 \sigma t) + O(\varepsilon^2),$$

$$B(t) = v - \varepsilon \left(\frac{v}{2} + \sigma \sin 2\sigma t + \frac{v}{2} \cos 2\sigma t \right); v = \frac{N}{I_0},$$

$$\dot{B}(t) = \frac{dB(t)}{dt} = 2\varepsilon \sigma^2 \cos 2\sigma t -$$

$$- \varepsilon v \sigma \sin 2\sigma t + O(\varepsilon^2),$$

where $n = \sqrt{K/I_0}$ - frequency of free oscillations of vessel.

The equation (9) takes a form

$$\ddot{\chi} + \left[n^2 - \frac{v^2}{4} (1 - \varepsilon) - \varepsilon \left(\sigma^2 - \frac{v^2}{4} \right) \cos 2\sigma t \right] \chi = \quad (10)$$

$$= n^2 \alpha_0 \sin \sigma t (1 - \varepsilon \sin^2 \sigma t).$$

Let's enter dimensionless time $\tau = \sigma t$, so

$$\ddot{\chi} = \frac{d^2 \chi}{dt^2} = \sigma^2 \frac{d^2 \chi}{d\tau^2} \text{ and the equation of oscillations (10) rewrite in the form}$$

$$\frac{d^2 \chi}{d\tau^2} + (a - 2q \cos 2\tau) \chi = \frac{n^2}{\sigma^2} \alpha_0 \sin \tau (1 - \varepsilon \sin^2 \tau) \quad (11)$$

$$a = \frac{n^2}{\sigma^2} - \frac{v^2}{4\sigma^2} (1 - \varepsilon), \quad q = \frac{\varepsilon}{2} \left(1 - \frac{v^2}{4\sigma^2} \right).$$

Besides forced oscillations under exciting moment action described by (11) parametric

oscillations can arise defined by the uniform equation

$$\frac{d^2\chi}{d\tau^2} + (a - 2q \cos 2\tau)\chi = 0. \quad (12)$$

The equation (12) is an initial form of Mathieu equation. Solutions of this equation have oscillatory character. Depending on values of parameters a and q these oscillations have limited or unlimited amplitude increasing by the exponential law. Borders of parameters a and q , zones corresponding to stable and unstable condition of the oscillatory system described by the equation (12) can be find on Eince - Strett diagram (Smirnov, 1968). In our case the value of q is small, and the least ε value of relative change in mass moment of inertia of a displaced cargo at which amplitude of oscillations increases infinitely can be find from inequality

$$\varepsilon > \frac{n^2 - \frac{v^2}{4}}{\sigma^2 - \frac{v^2}{2}}. \quad (13)$$

On returning from χ to roll angle θ an exponential multiplier appears

$$\begin{aligned} \exp\left[-\frac{1}{2}\int B(t)dt\right] = \\ = \exp\left[-\frac{v}{2}\left(1 - \frac{\varepsilon}{2}\right) + \frac{\varepsilon}{4}\sqrt{1 + \frac{v^2}{4\sigma^2}} \cos(2\sigma t - \delta)\right] \end{aligned} \quad (14)$$

This multiplier ensures damping action on oscillations. The solution of equation (12) can be find in the form

$$\chi = e^{\mu\tau} f_1(\tau) + e^{-\mu\tau} f_2(\tau), \quad (15)$$

where $f_1(\tau)$ and $f_2(\tau)$ - are periodic functions of τ .

It allows to write down additional condition

for excitation of parametric oscillations with increasing amplitude

$$\mu > \frac{v}{2}\left(1 - \frac{\varepsilon}{2}\right), \quad (16)$$

as soon as the average value of second component (14) for a period of oscillations is equal to zero.

It is obvious that damping action narrows area where parametric resonance exists.

The described method is applicable for an estimation of a principal opportunity of existence of a parametric resonance in rolling for vessel "Rechitsa" in her last trip. Fluctuation of cargo mass moment of inertia which has arisen in connection with elastic and residual strains of EMC has been considered only. Change of mass moment of inertia of cargo due to its transverse displacement at heel is not considered here. It is made in following section of work.

The analysis of documents concerning the loading of the vessel, results of experiment and calculations allowed to find that inertia moments in (2) have values $I_c = 11959t \cdot \text{sec}^2/m$, $i_0 = 10025t \cdot \text{sec}^2/m$, $I_0 = 28391t \cdot \text{sec}^2/m$, so that $\varepsilon = 0.068$.

The value of $\nu = N/I_0$ as function of a wave length (frequency of oscillations) was calculated according to (Remez J.V., 1983).

On the basis of (13) maximum values of metacentric height h^M were defined as function of wave length λ . If for a given loading conditions $h < h^M(\lambda)$, parametric resonance under such wave excitation is possible, but if $h > h^M(\lambda)$ the parametric resonance does not occur. Values of h^M for wave lengths λ are given in table 2. Here the minimal values of μ_{min} from (16) are also presented.

Table 2 – Values of metacentric height h^M

λ, m	45	67	95	140	160
h^M, m	0.310	0.210	0.148	0.100	0.090
μ_{min}	0.020	0.024	0.025	0.028	0.030

It is visible that the accepted scheme does not allow to find the possibility of parametric resonance appearance as soon as actual metacentric height values for motorship “Rechitsa” both on departure ($h = 0.36 \text{ m}$) and before capsizing ($h = 0.64 \text{ m}$ due EMC compression) exceeded values given in table 2.

Nevertheless, results of the analysis have proved the necessity of taking into account change of mass moment of inertia for EMC in calculations of rolling for vessel with specific cargoes of EMC type.

3. THE DIFFERENTIAL ROLL EQUATION OF A VESSEL WITH EMC AND ITS ANALYSIS

Let's find a differential roll equation of the vessel transporting EMC, taking into account its special properties related with the advent of variations in mass moment of inertia, position of ship gravity center, appearance of additional heeling moment.

Considering the form of equation (4), the differential roll equation of a vessel in regular beam sea can be presented in the form

$$J_x \ddot{\theta} + \frac{\partial J_x}{\partial t} \dot{\theta} + N \dot{\theta} + \kappa_\theta m(\theta) + M(\theta) = \kappa_\theta m(\alpha_0 \sin \sigma t). \quad (17)$$

Here in addition to (4) following symbols are introduced

$m(\theta)$ - restoring moment,

$M(\theta)$ - heeling moment called by shifting EMC aside, $M(\theta)$ and $m(\theta)$ are acting opposite,

κ_θ - reduction coefficient for exciting and

restoring moments (Remez, 1983)

Let's note, that

$$J_x = I_0 + I(\theta), \quad (18)$$

where $I(\theta)$ is a variable part of mass moment of inertia of oscillating system due to compression and shifting aside of EMC.

Considering (18), we find

$$\frac{dJ_x}{dt} = \frac{dI(\theta)}{d\theta} \frac{d\theta}{dt} = \frac{dI(\theta)}{d\theta} \dot{\theta}, \quad (19)$$

Let's introduce the dimensionless time $\tau = \sigma t$ so that $\frac{\partial}{\partial t} = \sigma \frac{\partial}{\partial \tau}$, $\dot{\theta} = \sigma \frac{d\theta}{d\tau}$, $\ddot{\theta} = \sigma^2 \frac{d^2\theta}{d\tau^2}$ and rewrite the equation (17)

$$\frac{d^2\theta}{d\tau^2} [1 - Q(\theta)] - \frac{dQ(\theta)}{d\theta} \left(\frac{d\theta}{d\tau} \right)^2 + \bar{N} \frac{d\theta}{d\tau} + \frac{\kappa_\theta \bar{m}(\theta)}{\sigma^2} + \frac{\bar{M}(\theta)}{\sigma^2} = \frac{\kappa_\theta}{\sigma^2} \bar{m}(\alpha_0 \sin \tau). \quad (20)$$

In (20) magnitudes of $Q(\theta) = \frac{I(\theta)}{J_x}$, $\bar{m}(\theta) = \frac{m(\theta)}{J_x}$, $\bar{M}(\theta) = \frac{M(\theta)}{J_x}$ are introduced.

The damping coefficient \bar{N} is determined under the supposition that the viscous damping moment is proportional to square of oscillation velocity and linearised using energy reasons (Remez, 1983), so that $N = \frac{\sigma \bar{N}}{J_x}$, and \bar{N}

depends on displacement Δ , mass moment of inertia J_x , metacentric height h , the ration B/d and hull coefficients δ and α . Thus all items in (20) are dimensionless.

The stability diagram $m(\theta)$, accepted in the subsequent calculations, corresponds to a maximum compression of EMC directly before an accident ($h = 0,64 \text{ m}$, $z_g = 6,06 \text{ m}$). The mass

moment of inertia $I(\theta)$ $\theta > 18^\circ$ is taken under supposition, that the side shifting of cargo arises when roll angles θ exceed the angle $\varphi = 18^\circ$. It is accepted that from a state of maximum vertical compression the free surface of cargo, remaining flat, is turned to tilted side on angle $\theta - \varphi$ when the vessel's heel angle equals θ . The cargo fills free volume of compartment and amount of cargo remains constant.

Functions $Q(\theta)$, $\frac{dQ(\theta)}{d\theta}$, $\bar{m}(\theta)$ and $\bar{M}(\theta)$ are

calculated using arrangement plans in the form of polynomials of heel angle θ . It has been considered, that

$$Q(-\theta) = Q(\theta), \quad \frac{dQ(\theta)}{d\theta} = -\frac{dQ(-\theta)}{d\theta},$$

$$\bar{m}(\theta) = -\bar{m}(-\theta), \quad \bar{M}(\theta) = -\bar{M}(-\theta), \quad \theta > 0.$$

Damping coefficient \bar{N} and reduction coefficient κ_θ are presented in the form of polynomials of incoming wave length λ .

The primal problem for examination of dynamics of the system governed by a differential equation (20) consists in studying the structure of phase plane $\left(\theta, \dot{\theta}\right)$ stuffing with phase trajectories. (Butenin N.V., Naimark Y.I, Fufaev N.A., 1987).

For this purpose it is enough to examine the behavior of special trajectories for the homogeneous equation corresponding to equation (20). The interior forces are counterbalanced in fixed points where $\theta = \dot{\theta} = 0$. Limit cycles are closed curves on a phase plane to which aspire eventually ($\tau \rightarrow +\infty$) certain set of phase trajectories. Separatrices separate those parts of phase plane where phase curves describe qualitatively equivalent behavior of oscillatory system.

Let's find the fixed points of equation (20) on a phase plane where $\dot{\theta} = \ddot{\theta} = 0$.

Introducing a new variable

$$K = \dot{\theta}[1 - Q(\theta)] + \bar{N}\theta, \quad (21)$$

instead of equation (20) we find system of two first order differential equations for fixed points $\dot{\theta} = 0$ and $\dot{K} = 0$

$$\begin{cases} \dot{\theta} = \frac{K - \bar{N}\theta}{1 - Q(\theta)}; \\ \dot{K} = -\frac{\bar{M}(\theta) + \kappa_\theta \bar{m}(\theta)}{\sigma^2} \end{cases} \quad (22)$$

From the first equation of system (22) it follows that $\dot{\theta} = 0$ along straight line $K = \bar{N}\theta$ on the plane (θ, K) . From the second equation of (22) it comes that $\dot{K} = 0$ in points θ_i which are zeroes of the function $\bar{M}(\theta) + \kappa_\theta \bar{m}(\theta)$. Getting from (21)

$$\dot{K} = \ddot{\theta}[1 - Q(\theta)] - \frac{\partial Q(\theta)}{\partial \theta} \left(\dot{\theta}\right)^2 + \bar{N}\dot{\theta}, \quad \text{we discover}$$

that in the fixed points $\ddot{\theta} = 0$, so function $Q(\theta)$ is continuous. Taking into consideration oddness on θ of function $\bar{m}(\theta)$ as well as the fact that $\bar{M}(\theta) \equiv 0$ for $|\theta| \leq 18^\circ$ and for $|\theta| > 18^\circ$ this function also is odd on θ , we find that system (22) and naturally the equation (20) have three fixed points: one in zero of phase plane ($\theta = \dot{\theta} = 0$) and two others with abscissas corresponding to zeroes of polynomial function $\bar{M}(\theta) + \kappa_\theta \bar{m}(\theta)$. This function is governed by properties of vessel as well as reduction coefficient κ_θ that is additionally defined by incoming wave length. The calculations fulfilled for "Rechitsa" have shown that in a range of $0 < \lambda \leq 160$ m the fixed points have abscissas $\theta_1 = 0,38$, $\theta_2 = -0,38$, $\theta_3 = 0$ which practically do not depend on wave length λ .

Topological type and stability of fixed points we can define, exploring the linearized system, gained from (22), in a neighborhood of these points. Let u_ϵ be a small vicinity of fixed points $(\theta_i, 0)_i = 1, 2$. For any point of

$(\theta_i + \varepsilon_\theta, \varepsilon_K)$ from the vicinity of u_ε it comes with an accuracy $O(\varepsilon_\theta^2 + \varepsilon_K^2)$

$$\begin{cases} \dot{\varepsilon}_\theta = \frac{\partial F_1}{\partial K} \varepsilon_K + \frac{\partial F_1}{\partial \theta} \varepsilon_\theta; \\ \dot{\varepsilon}_K = \frac{\partial F_2}{\partial K} \varepsilon_K + \frac{\partial F_2}{\partial \theta} \varepsilon_\theta, \end{cases} \quad (23)$$

where $F_1 = \frac{K - \bar{N}\theta}{1 - Q(\theta)}$, $F_2 = -\frac{\bar{M}(\theta) + \kappa_\theta \bar{m}(\theta)}{\sigma^2}$.

Roots $p_{1,2}$ of characteristic polynomial of linear system

$$\sigma^2 [1 - Q(\theta_i)] p^2 + \sigma^2 \bar{N} p + \frac{\partial}{\partial \theta} [\bar{M}(\theta_i) + \kappa_\theta \bar{m}(\theta_i)] = 0, \quad i = 1, 2 \quad (24)$$

are determined in the form

$$p_j = \frac{-\sigma^2 \bar{N} \pm \sqrt{D}}{2\sigma^2 [1 - Q(\theta_i)]} \quad (j = 1, 2). \quad (25)$$

Here D is discriminant of a characteristic polynomial (24). The topological type of the fixed points and behavior of dynamic system in their neighborhood are defined by roots (25). If roots p_j ($j = 1, 2$) are complex conjugate the corresponding fixed point is a focal point. The focal point is stable, if the real part of roots is negative and it is unstable if the real part is positive. When roots p_j ($j = 1, 2$) are real and have one sign the corresponding fixed point is a knot. If both roots are negative this is a stable knot, otherwise a knot is unstable. If roots p_j ($j = 1, 2$) are real with different signs this is saddle.

From (25) it follows, that the type of the roots p_j ($j = 1, 2$) for dynamic system is completely determined by discriminant D .

For $|\theta_i| \leq 18^\circ$ the discriminant is

$$D = \sigma^4 \bar{N}^2 - 4\sigma^2 \kappa_\theta [1 - Q(\theta_i)] \frac{\partial \bar{m}(\theta_i)}{\partial \theta}. \quad (26)$$

In this range of θ the only fixed point

$\theta_i = 0$ exists.

It is a stable focus if

$$h > \frac{J_x \sigma^2 \bar{N}^2}{4\Delta \kappa_\theta [1 - Q(0)]}. \quad (27)$$

When $|\theta_i| > 18^\circ$ the discriminant is

$$D = \sigma^4 \bar{N}^2 - 4\sigma^2 \kappa_\theta [1 - Q(\theta_i)] \frac{\partial}{\partial \theta} [\bar{M}(\theta_i) + \kappa_\theta \bar{m}(\theta_i)] \quad (28)$$

For fixed points $\theta_1 = 0.38$, $\theta_2 = -0.38$ $\frac{\partial}{\partial \theta} [\bar{M}(\theta_i) + \kappa_\theta \bar{m}(\theta_i)] < 0$. From (25) and (28) it comes that for fixed points θ_i ($i = 1, 2$) among two roots (25) one is positive and another one is negative, so both fixed points θ_i ($i = 1, 2$) are saddles.

Trajectories on phase plane (θ, K) are de-

termined from obvious equality $\frac{dK}{d\theta} = \frac{\dot{K}}{\dot{\theta}}$. Substituting into this equality corresponding expressions from system (22), we find the differential equation of trajectories in the form

$$(K - \bar{N}\theta) \frac{dK}{d\theta} + \frac{1}{\sigma^2} [\kappa_\theta \bar{m}(\theta) + \bar{M}(\theta)] [1 - Q(\theta)] = \quad (29)$$

If there is no damping $\bar{N} = 0$, this equation is easy to integrate and considering (21) to write down the equation of a set of phase trajectories

$$\left(\dot{\theta}\right)^2 + \frac{2}{\sigma^2 [1 - Q(\theta)]} \int \frac{\kappa_\theta \bar{m}(\theta) + \bar{M}(\theta)}{1 - Q(\theta)} d\theta = C \quad (30)$$

The phase trajectories corresponding to stable solutions with various values of C are closed curves. They lay inside of area limited by separatrices for which constant C in equa-

tion (30) is easy to find, having substituted in it coordinates of saddle points $\theta_{1,2}$. The position of these points do not depend on magnitude of \bar{N} , therefore the trajectories for stable solutions of system with damping $\bar{N} \neq 0$ will not go out the area limited by separatrices (30). On fig. 1 the phase portrait of the homogeneous system without damping, on fig. 2 for this system with damping and on fig. 3 phase portrait of the system with damping and exterior periodic perturbation are shown. On fig. 4 free oscillations of system without damping (1) and with damping (2) both in phase and time spaces are shown.

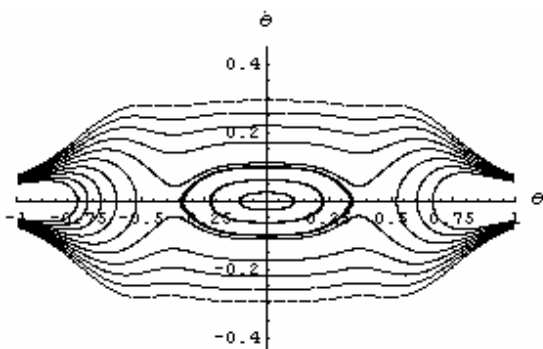


Figure 1 The plane portrait of the homogeneous system without damping ($\bar{N} = 0$)

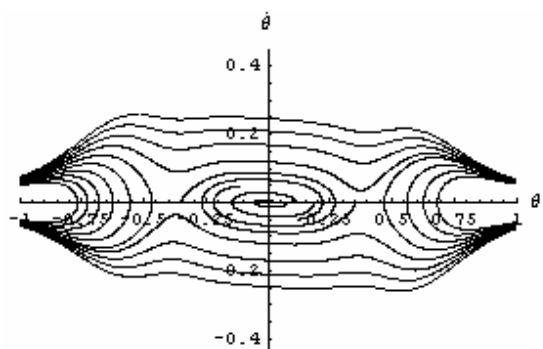


Figure 2 The plane portrait of the homogeneous system with damping ($\bar{N} \neq 0$)

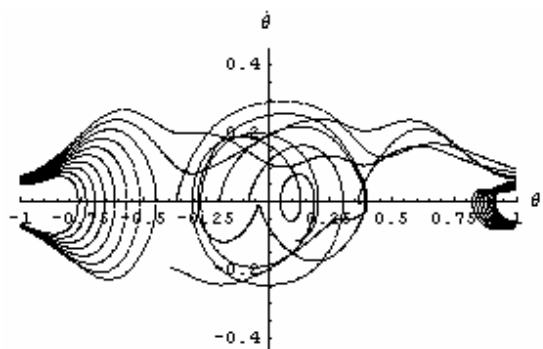


Figure 3 The plane portrait of system with damping and exterior periodic perturbation

For comparison the dynamic system is studied for rolling of the same vessel under supposition that the load is unmovable. In this case $Q(\theta) \equiv 0$, $\frac{dQ(\theta)}{d\theta} \equiv 0$, $\bar{M}(\theta) \equiv 0$ and differential roll equation looks like

$$\ddot{\theta} + \bar{N} \dot{\theta} + \frac{\kappa_{\theta}}{\sigma^2} \bar{m}(\theta) = \frac{\kappa_{\theta}}{\sigma^2} \bar{m}(\alpha_0 \sin \tau). \quad (31)$$

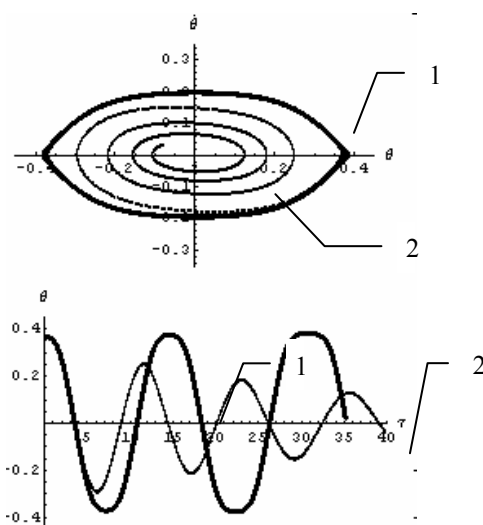


Figure 4 Free oscillations of system with and without damping in phase and time spaces

Comparing phase portraits of the homogeneous differential equations corresponding (20) and (31), it is easy to reveal qualitative differences in behavior of corresponding oscillating systems.

The differential equation $\ddot{\theta} + \bar{N} \dot{\theta} + \frac{\kappa_{\theta}}{\sigma^2} \bar{m}(\theta) = 0$ has three equilibrium points at phase plane, one of which $(\theta = \dot{\theta} = 0)$ is a focal point, and two others θ_1 and θ_2 are saddles ($\theta_1 = -\theta_2, \theta_1 > 0$). It is easy to show that θ_1 and θ_2 correspond to zeroes of function $\bar{m}(\theta)$ i. g. the angles $\pm\theta_v$ of vanishing stability on starboard and port sides. Thus, the area with stable oscillations of system appears for differ-

ential equation (31) significantly larger than analogous area for differential equation (20). It means that some situations defined for vessel with EMC by means of differential equation (31) as safe, can lead to real capsizing of a vessel if the capsizing comes from solution of equation (20).

Two rolling processes of motor vessel "Richitsa" with EMC under similar wave conditions are given in fig. 5. The process marked by 1 corresponds to supposition that loaded cargo is unmovable and equation (31) is used, the process marked by 2 corresponds to equation (20) where all special properties of EMC are taken into consideration. The result is obvious: to predict dangerous situation one has to take in mind specific qualities of EMC and use for calculation differential equation (20).

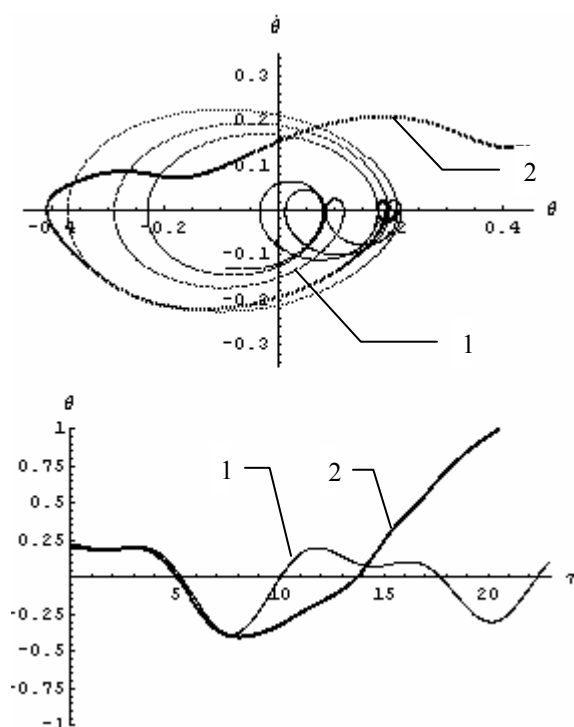


Figure 5 The comparison of rolling processes

4. CONCLUSIONS

The vessel, loaded with EMC, possesses special dynamic properties causing the unusual response to incoming waves when navigations in heavy seas.

Special properties of a cargo lead to:

- fluctuation in mass moment of inertia of a cargo that provokes a parametric resonance of a vessel rolling;
- appreciable changes on vertical position of ship's gravity centre due to condensation and deformation of a cargo;
- action of additional heeling moment due to lateral cargo motion when ship is oscillating.

These reasons have been considered when deducing differential roll equation for vessel with EMC. The specified differential equation has basic differences from a standard roll equation in connection with the account of fluctuations in mass moment of inertia and occurrence of additional heeling moment of a cargo transferred due to rolling.

Applying practice of introduction reduction coefficient to disturbing moment, authors have considered it natural to enter the same coefficient into restoring moment as the hydrodynamic nature of both moments is identical.

The situation is demonstrated that under same loading and wave conditions the solution of traditional roll equation which doesn't take into consideration specific cargo properties demonstrates a normal rolling process while specialized equation when the decision of the standard differential equation demonstrated in this report and accounting special properties of EMC shows the capsizing of vessel.

Results of this research demonstrate the vital necessity of introducing into a known line of moving cargoes (liquid, hanging, rolling, loosing) an additional one – elastically movable cargo (EMC). It is necessary to supply the navigators transporting this cargo with reliable regulating documents.

5. REFERENCES

Bondar V.M., 1999, "On a model of behavior of one variety of a movable cargo under

rolling of a vessel”, the Collection of proceedings “Offshore navigation” of the Odessa state maritime academy, Vol. 1, pp. 25-28 (in Russian).

Butenin N.V., Naimark Y.I., Fufaev N.A., 1987, “Introduction into nonlinear oscillation theory”, Nauka, Moscow, p. 382 (in Russian).

Remez J.V., 1983, “Ship motions”, Shipbuilding, Leningrad, 327 p. (in Russian).

Sizov V.G., 1999, “About effect of deformability of transported cargoes on the stability of a vessel”, Proceeding of the Odessa state maritime university, Vol. 3, pp. 59-65. (in Russian).

Sizov V.G., 2002, “About a rocking of a vessel with elastically movable cargoes”, Proceeding of the Odessa national maritime university, Vol. 9, pp. 28-33. (in Russian).

Smirnov J.N., 1968, “Lines of equal values of μ in zones of instability for Mathien equation”, Papers of the Academy of Science of the USSR, Vol. 178, pp. 546-547. (in Russian).

Real-time Identification of Behavior Leading to Capsize

Leigh McCue, *Aerospace and Ocean Engineering, Virginia Tech*

Christopher Bassler, *Aerospace and Ocean Engineering, Virginia Tech*

William Belknap, *Seakeeping Division, Naval Surface Warfare Center, Carderock Division*

ABSTRACT

In this paper the authors present a methodology to detect instabilities leading to capsize in real-time. Specifically, variations in finite-time Lyapunov exponent (FTLE) time series are identified from experimental data. As shown in prior work, FTLEs have potential, both numerically and experimentally, to indicate the onset of chaotic behavior leading to capsize through detection of idiosyncrasies in the FTLE time series. The principle objective of this work is to identify instabilities from experimental data without dependence upon time-consuming numerical simulation. A demonstration of the concept is given through application to experimental data for a notional destroyer model (DTMB model 5514).

Keywords: *capsize, chaos, finite-time Lyapunov exponent*

1. INTRODUCTION

Large amplitude vessel motions and capsize have served as hazards of the maritime community for centuries. Therefore, it is of benefit to all sectors of the marine industry to develop tools which could provide mariners with indicators of the onset of inclement ship motions. Establishing a tool to aid vessel operators in identifying the onset of threatening ship motion conditions would allow time for changes to be made, thus altering the commanded response to environmental conditions and possibly reducing exposure to devastating ship motions or capsize. For large amplitude ship motions and capsize, small variations in wave and/or position initial conditions can result in largely varying end behavior. Finite-time Lyapunov exponents (FTLEs) measure convergence or divergence of nearby trajectories thus providing a quantitative measure of a system's sensitivity to initial conditions and an indication of long-term behavior for a chaotic system. FTLEs are

feasible for use as a predictive tool to provide early warnings for vessel instabilities, or motions leading to capsize.

For a system of equations written in state-space form $\dot{\mathbf{x}} = \mathbf{u}(\mathbf{x})$, small deviations from the fiducial trajectory can be expressed by the equation $\delta\dot{\mathbf{x}}_i = (\partial u_i / \partial x_j) \delta x_j$ (Eckhardt & Yao, 1993). $\delta\mathbf{x}$ is a vector representing the deviation from the trajectory with components for each state variable of the system. From this, the equation for the finite-time Lyapunov exponent can be written as Equation 1 (Eckhardt & Yao, 1993).

$$\lambda_T(\mathbf{x}(t), \delta\mathbf{x}(0)) = \frac{1}{T} \log \frac{\|\delta\mathbf{x}(t+T)\|}{\|\delta\mathbf{x}(t)\|} \quad (1)$$

Positive FTLEs indicate exponential divergence of a nearby trajectories and conversely, negative FTLEs indicate exponential convergence. That is, if one were to envision an infinitesimal ball of points surrounding an initial point along the fiducial trajectory, FTLEs measure whether that ball stretches into an ellipsoid, contracts to a point,

or remains a ball over small increments in time. If any one principal axis of the ball grows at an exponential rate over a time increment, there will be a positive FTLE for this time increment. (Or, in the asymptotic sense, if as time approaches infinity one finds exponential growth, there is at least one positive Lyapunov exponent.)

Methods for computing Lyapunov exponents and FTLEs from equations of motion are well developed in references such as Benettin *et al.* (1980), Wolf *et al.* (1985), and Eckhardt & Yao (1993). In this work, FTLEs from experimental time series are calculated based on a modified version of the algorithm developed for Lyapunov exponents by Sano & Sawada (1985)¹. While Lyapunov exponents have been used to demonstrate chaotic behavior for numerous naval architecture applications such as Papoulias (1987), Falzarano (1990), Spyrou (1996), Murashige and collaborators (1998a; 1998b; 2000), Arnold *et al.* (2003), McCue & Troesch (2004; 2005) and McCue, Belknap, & Campbell (2005), it is only recently that FTLEs have been exploited for the purposes of anticipating ship motions. See, for example, works by McCue & Bassler (2005), McCue (2005), McCue & Troesch (2006), and McCue & Bulian (2006).

A demonstration of the concept is given through application to experimental data for a notional destroyer model (DTMB model 5514). Over 100 experimental runs were conducted in regular waves to examine the capsizing behavior of the 1/46.6th scale model (full-scale ship length is 142.04 m). Run conditions were at nominal Froude numbers from 0.1 to 0.4, wave length to ship length (λ/L) of 0.75 to 1.5, wave height to wave length (H/λ) of 1/10 to 1/20, and ship headings ranging from following to stern-quartering to beam seas. The term ‘nominal’ is used with respect to Froude number because the propeller shafts are given a

commanded voltage corresponding to an equivalent calm water speed, rather than prescribing speed specifically. Further discussion is provided in Section 2 on model test details. This paper focuses upon 37 capsizing and non-capsizing tests in stern-quartering seas, that is, 45 degrees off the stern, identified as a dangerous heading. FTLE methods are applied to model 5514 experimental data analyzed in a variety of wave conditions to illustrate the generality of the method.

2. MODEL TEST DETAILS

The model 5514 regular wave dynamic stability test was performed in the Maneuvering and Seakeeping Basin at the Carderock Division of the Naval Surface Warfare Center in November, 2004. Figure 1 shows model 5514 during a dynamic stability run in regular waves. The model was radio controlled, self-propelled, and free in all 6 degrees of freedom. A PID controller autopilot was used to maintain the desired heading, while the motor powering the two propeller shafts was given a constant voltage equal to the voltage needed to achieve the desired model speed in calm water. Because the model is self-propelled with an autopilot, forward speed and heading do oscillate with wave interaction over the course of an experimental run (McCue *et al.*, 2005). For the model runs analyzed in this study, the KG was set such that the calm water range of positive stability was approximately 70 degrees. Instruments measured roll, roll rate, pitch, pitch rate, heading, yaw rate, and ship-referenced accelerations at several points. The initial conditions of the simulation were not controlled, but rather the model was accelerated out of the corner of the basin into the wave field at essentially random points relative to the wave phase. The initial heading was nominally the desired heading.

¹ The Sano and Sawada algorithm is quite similar to that proposed by Eckmann *et al.* (1986).

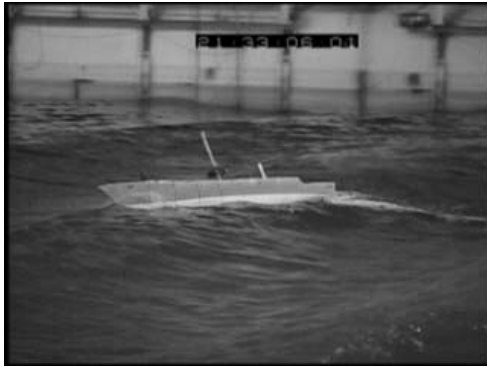


Figure 1: DTMB Model 5514 in regular seas.

3. METHODOLOGY

As in prior Stability Workshop papers (McCue & Troesch, 2004; McCue *et al.*, 2005), the basis for the algorithm used to calculate Lyapunov exponents is that detailed in Sano & Sawada (1985). Tangent space methods for Lyapunov exponent calculations were developed simultaneously by the separate research teams of Sano & Sawada (1985) and Eckmann and coauthors (1985; 1986). This approach allows for calculation of the full spectrum of Lyapunov exponents through local predictions of the Jacobian along the time series trajectory. For example, for a given trajectory $\mathbf{x}(t)$ defined by Equation 2, the tangent vector ξ is given by the linearized form of Equation 2 presented in Equation 3 where \mathbf{J} is the Jacobian matrix of \mathbf{f} , $\mathbf{J} = \partial\mathbf{f}/\partial\mathbf{x}$ (Sano & Sawada, 1985). Sano & Sawada (1985) solve Equation 3 through a least squares estimate of the time dependent linear operator A_j which approximates the map from $\xi(0)$ to $\xi(t)$.

The Lyapunov exponents are then computed using Equation 4 where τ is a flow scale time increment, n is the number of data points, and \mathbf{e} is an orthonormal basis maintained using a Gram-Schmidt renormalization process (Sano & Sawada, 1985). For details of this process refer to Sano & Sawada (1985) or the similar works of Eckmann *et al.* (1985; 1986).

$$\dot{\mathbf{x}} = \mathbf{f}(\mathbf{x}) \quad (2)$$

$$\dot{\xi} = \mathbf{J}(\mathbf{x}(t)) \cdot \xi \quad (3)$$

$$\lambda_i = \lim_{n \rightarrow \infty} \frac{1}{n\tau} \sum_{j=1}^n \ln \|A_j e_i^j\| \quad (4)$$

To overcome the difficulties associated with the brevity of the DTMB Model 5514 experimental data, time series for all runs conducted at the same target heading were treated as containing possible neighbors for all other time series at that heading. For the case of stern-quartering seas, rather than solely searching the single recorded time history of interest for neighboring points with which to approximate the Jacobian of the system, all model runs released in stern quartering seas were searched for neighboring points for each instant of interest in the analyzed time history. In order to demonstrate the generality of this method, all wave conditions were grouped for each given heading, that is to say, in searching for neighboring points it is deemed just as acceptable to search time series with differing wave heights and lengths and forward speeds because they yield as much information as to the ship's mechanism of response as those runs with identical wave conditions. In addition, this allows for added realism as typical seaways contain a spectrum of wave heights and frequencies and any method to detect instabilities must be capable of identifying stability trends in varying sea conditions.

Additionally, in this work, roll, pitch, roll rate, and pitch rate time series were used rather than embedding single variate roll time series data as done previously for Lyapunov exponent calculations (McCue *et al.*, 2005). Since multivariate data was readily available, this approach was taken to potentially improve the accuracy of the algorithm and remove the limitations inherent in embedding. This approach restricts the dimensionality of the system to 4, and therefore it is possible that higher order information about the attractor is lost. However, it is hoped that with four variables, the primary attractor dynamics are captured. Increasing the dimensionality of the system would run the risk of spurious

exponents, increased computation times, and/or numerical inaccuracies. Only rotational state variables (and their associated derivatives) were chosen to avoid dimensionality concerns associated with mixing displacements and rotations.

Table 1 compares values for the first Lyapunov exponent calculated using the previous, more simplistic approach, embedding univariate roll time history data into 5 dimensions and using the individual time series data to calculate Lyapunov exponents (Method 1), to the modified approach detailed above (Method 2)². For each analyzed run under Method 2, 37 separate time histories were scanned for ‘neighbors’ to each state space vector in time for the analyzed run.

For example, when calculating the Lyapunov exponent for Run 400, at each instant in time in Run 400, neighbors are selected from 36 additional time histories for the model in stern quartering seas, in addition to searching Run 400 for neighbors. As can be seen in Table 1 the agreement between the two methods is good given the time series length limit constraints.

Table 1: Table of largest Lyapunov exponents comparing model-scale results from embedded approach with $d=5$ (McCue *et al.*, 2005) to non-embedded approach. All cases non-capsize.

Run #	Experimental Data		Method 1, $d=5$	Method 2
	H/λ	λ/L	Lyap. Exp. (1/s)	Lyap. Exp. (1/s)
400	0.0518	1.498	0.2066	0.2712
239	0.0679	0.998	0.2020	0.1929
313	0.0671	1.248	0.1270	0.3392
312	0.0681	1.246	0.7464	0.5146
418	0.0971	0.773	1.0724	0.6131
417	0.0999	0.750	0.7401	0.4293
281	0.1020	1.002	0.6341	0.4157
329	0.1003	1.252	0.6005	0.7922

² Note, all results in this paper are presented model scale. To reconcile the values given for Method 1 with those published in McCue, Belknap, and Campbell (2005), scale by $\sqrt{(L_M / L_S)} = 1/\sqrt{46.6}$.

4. FINITE-TIME LYAPUNOV EXPONENTS

Finite-time Lyapunov exponents are calculated using the same approach discussed previously for Lyapunov exponents in which all similar time series are treated as potential sources of neighbors for each analyzed run and time series consist of roll, pitch, roll rate and pitch rate data.

A simple flow chart detailing the steps in the computation of FTLEs is presented in Figure 2. Unlike the asymptotic Lyapunov exponent which is averaged over the entire length of the time series, finite-time Lyapunov exponents are calculated over short intervals of time, reference Equation 1. Algorithmically, anytime that insufficient neighbors were found with which to approximate the Jacobian of the system, the number -1000 was stored as a flag for the FTLE time series.

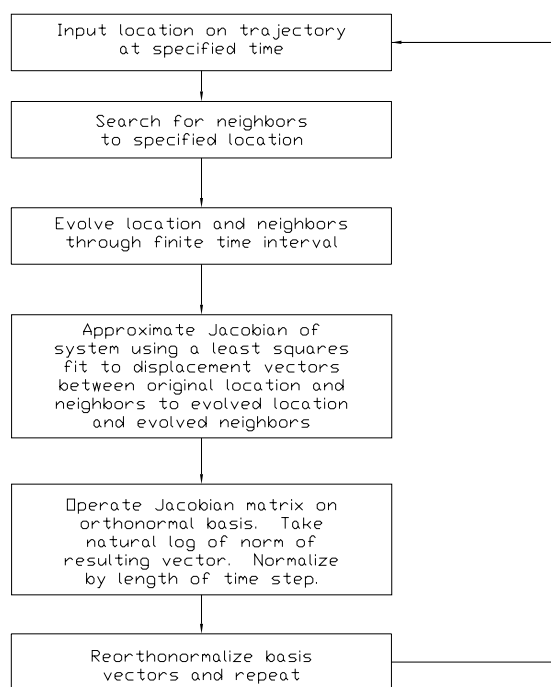


Figure 2: Flowchart for calculation of FTLEs.

Figures 3 and 4 show roll time histories, FTLE time histories, and roll/roll velocity phase space for similar capsize and non-capsize runs. In the capsize run, the point at which the trajectory leaves the stable attractor, as determined by examination of the phase

portrait, is marked with an 'x' on the phase space plot and vertical lines on the roll and FTLE time series.

For the non-capsize case run 329, large variations in the FTLE time series are observed at the onset and during large amplitude rolling. As apparent in the phase portrait, while roll conditions in excess of 70 degrees are encountered leading to complicated trajectories, capsizes does not occur.

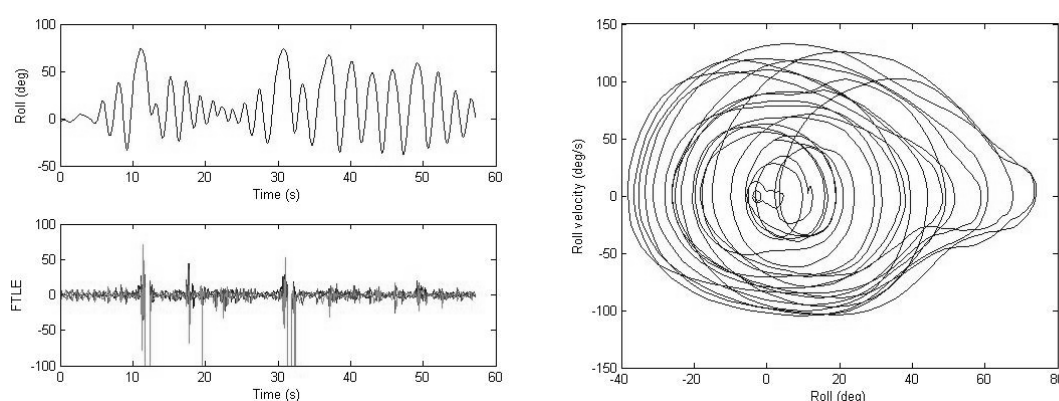


Figure 3: No Capsize Run 329: $H/\lambda=1/9.972$, $\lambda/L=1.252$, $F_n=0.40$ released in stern quartering seas.

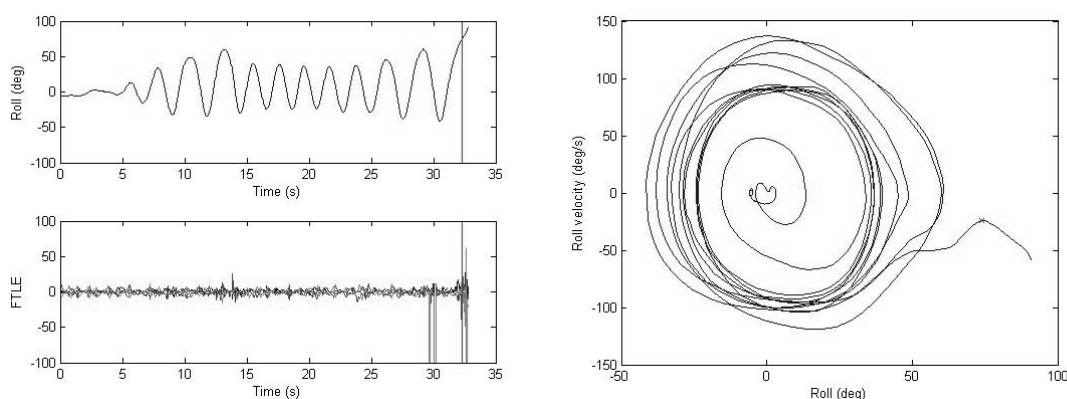


Figure 4: Capsize Run 331: $H/\lambda=1/9.48$, $\lambda/L=1.228$, $F_n=0.40$ released in stern quartering seas.

In an effort to tabulate quantifiable indicators of capsizes. The FTLE time series for each run was scanned to identify if a critical value was exceeded, chosen as 20 1/s in order to be roughly twice the max $FTLE_1$ found in typical cases for these experiments, and/or if there were periods for which insufficient neighbors were found flagged in the FTLE

Conversely, Run 331 encounters much smaller roll motions until the oscillation immediately preceding that leading to capsizes. In this case as well, large variations in the FTLE time series and/or the flag of a lack of appropriate neighbors is detected in advance of the trajectory's deviation from limit-cycle behavior.

time series with the value -1000, *i.e.* behavior not regularly detected in any other time series. Those runs in which $FTLE_1$ exceeds the critical value and/or has periods with insufficient neighbors are then marked as potential dangers. Table 2 gives a summary of the analyzed runs including their run number, whether or not they were flagged for hazardous behavior, and whether or not the vessel ultimately capsized during that run.

Table 2: Summary of 37 DTMB hull 5514 experimental runs indicating capsize/non-capsize and if hazardous periods were identified using FTLE analysis.

<i>Run#</i>	<i>H/λ</i>	<i>λ/L</i>	<i>Fn</i>	<i>Hazard</i>	<i>Capsized</i>	<i>Run#</i>	<i>H/λ</i>	<i>λ/L</i>	<i>Fn</i>	<i>Hazard</i>	<i>Capsized</i>
212	0.092	0.748	0.20	No	No Capsize	312	0.068	1.246	0.40	Flag	No Capsize
213	0.091	0.750	0.20	No	No Capsize	313	0.067	1.248	0.40	Flag	No Capsize
214	0.092	0.753	0.30	No	No Capsize	323	0.096	1.244	0.10	No	No Capsize
215	0.099	0.755	0.30	No	No Capsize	324	0.100	1.245	0.20	No	No Capsize
216	0.103	0.747	0.40	Flag	Capsize	325	0.100	1.247	0.30	Flag	No Capsize
220	0.094	0.752	0.40	Flag	Capsize	326	0.106	1.254	0.30	No	No Capsize
237	0.068	0.995	0.30	No	No Capsize	327	0.101	1.234	0.40	Flag	Capsize
238	0.069	1.000	0.30	No	No Capsize	329	0.100	1.252	0.40	Flag	No Capsize
239	0.068	0.998	0.40	No	No Capsize	331	0.105	1.228	0.40	Flag	Capsize
240	0.070	1.000	0.40	No	No Capsize	333	0.101	1.254	0.40	Flag	Capsize
276	0.106	0.998	0.20	No	No Capsize	399	0.055	1.486	0.30	No	No Capsize
277	0.102	0.998	0.20	No	No Capsize	400	0.052	1.498	0.40	No	No Capsize
278	0.103	0.993	0.30	No	No Capsize	404	0.069	1.504	0.20	No	No Capsize
280	0.101	0.996	0.40	No	No Capsize	405	0.068	1.496	0.30	No	No Capsize
281	0.102	1.002	0.40	No	No Capsize	406	0.068	1.494	0.40	No	No Capsize
305	0.055	1.250	0.30	No	No Capsize	415	0.100	0.754	0.40	Flag	No Capsize
307	0.052	1.252	0.30	No	No Capsize	417	0.100	0.750	0.40	No	No Capsize
309	0.067	1.242	0.20	No	No Capsize	418	0.097	0.773	0.40	Flag	No Capsize
311	0.070	1.256	0.30	No	No Capsize						

Table 2 shows that runs leading to capsize are consistently flagged by searching for FTLE values in excess of a critical value and/or when behavior is sufficiently anomalous in comparison to other data that insufficient neighbors are found. However, this method also appears overly conservative issuing warnings for non-capsizing runs. Figure 5 gives time histories of roll and $FTLE_1$ for runs which are flagged yet do not lead to capsize. It is apparent that the triggering aspects of the $FTLE_1$ time series occur near very large amplitude motions or even immediately after large motions for cases where roll motion rapidly decreases, as in Run 329, as a particularly striking example. Of primary note

in this figure is that many of these “false positives” occur in runs which are dangerously close to capsize, therefore, providing an operator warning would be prudent for safe operations.

Figure 6 presents the time histories of roll and $FTLE_1$ for those runs leading to capsize, all of which were flagged using this FTLE approach. In Run 327 the flag trigger occurs essentially simultaneously with the catastrophic loss of stability. However, for each of the other four cases, triggers occur prior to capsize, at times even multiple cycles prior to the capsize event.

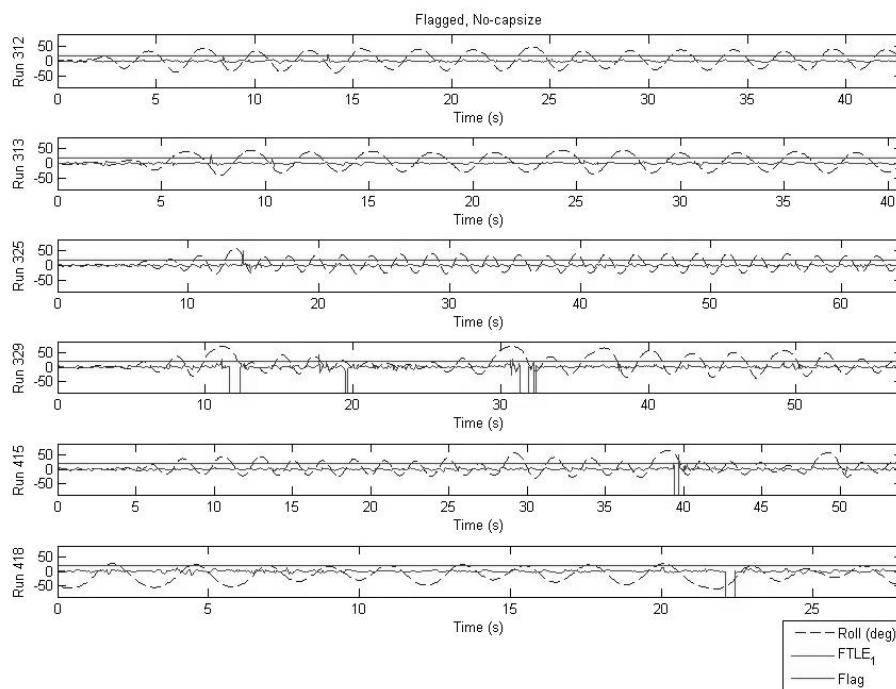


Figure 5: Roll and $FTLE_1$ time series of those runs flagged not leading to capsizing. The flag trigger is denoted with a solid horizontal red line, that is, the run is flagged if either the solid green $FTLE_1$ time series exceeds the solid red horizontal line or if there are insufficient neighbors with which to estimate the Jacobian thus causing the $FTLE$ time series to default to a value of -1000, indicated on the figure by those times when $FTLE_1$ exceeds the negative 'y'-ordinate limit of the figure.

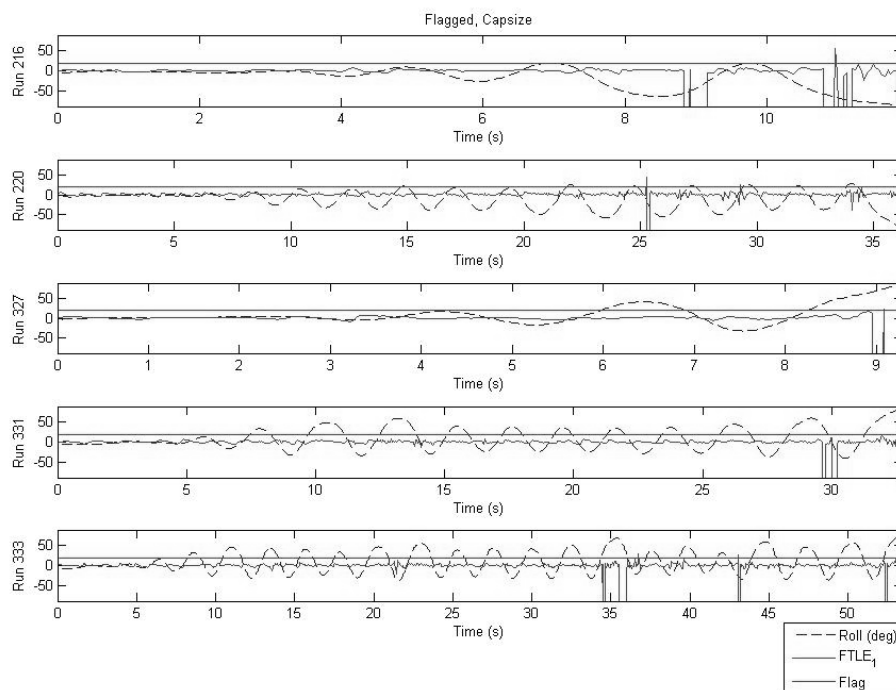


Figure 6: Roll and $FTLE_1$ time series of those runs flagged and leading to capsizing. The flag trigger is denoted with a solid horizontal red line, that is, the run is flagged if either the solid green $FTLE_1$ time series exceeds the solid red horizontal line or if there are insufficient neighbors with which to estimate the Jacobian thus causing the $FTLE$ time series to default to a value of -1000, indicated on the figure by those times when $FTLE_1$ exceeds the negative 'y'-ordinate limit of the figure.

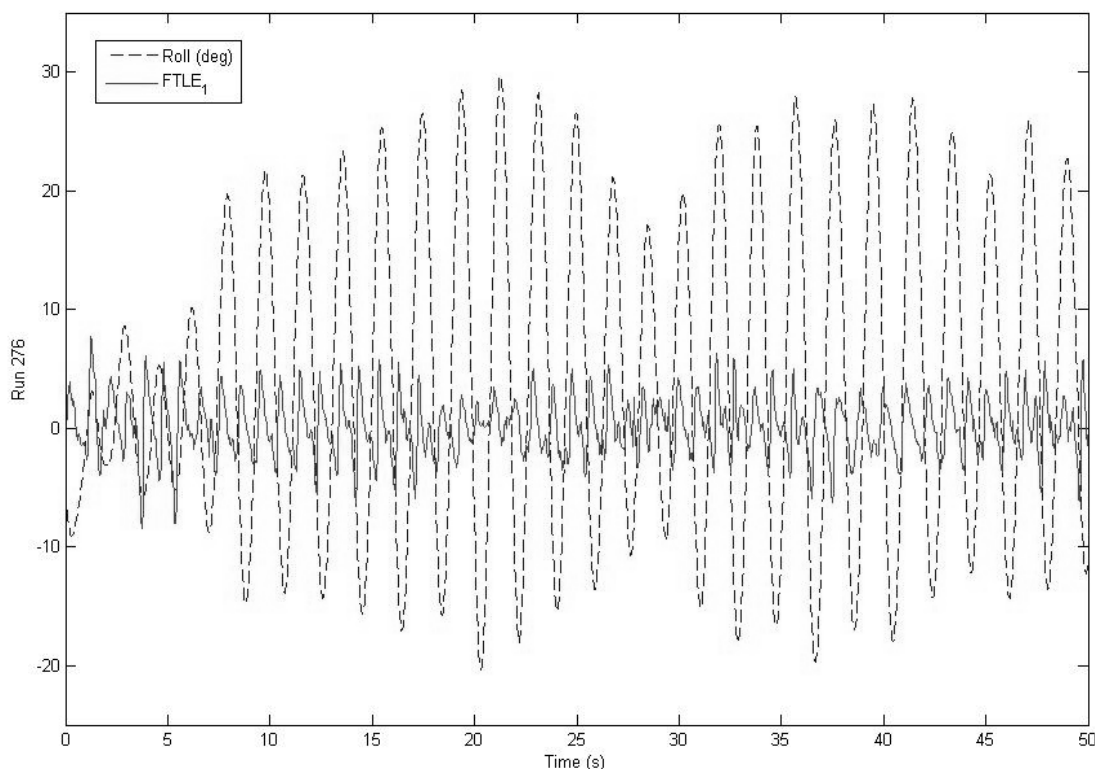


Figure 7: Roll and $FTLE_1$ time series for Run 276

As shown previously (McCue, 2005; McCue & Troesch, 2006; McCue & Bulian, 2006), qualitative changes in the FTLE time series behavior were also noted corresponding to changes in the magnitude of ship motions. For Run 276, a non-capsize, non-flagged case presented in Figure 7, it is apparent that the qualitative behavior, *i.e.* the regularity of the FTLE time series varies as roll motions increase or decrease. Quantifying this qualitative behavior could assist in reducing the number of false warnings and potentially indicate changes to yet more subtle behavior, such as the inverse problem of capsizing, that is detecting quiescence for safe at sea launch and recovery operations.

5. CONCLUSIONS

In this work, the authors demonstrate the feasibility of using FTLEs to detect chaotic behavior leading to large amplitude motions and/or capsizing as applied to experimental tests

conducted in the Maneuvering and Seakeeping Basin at the Carderock Division of the Naval Surface Warfare Center for DTMB Hull 5514. Large fluctuations in the FTLE time series and/or flagging due to insufficient neighbors with which to estimate the Jacobian of the system preceded and coincided with large amplitude motions particularly those leading to capsizing.

Future work will include testing this method using simulation-based time histories in random seas. This will allow iteration and optimization of the chosen variables, such as incorporation of yaw. Also, simulated data can provide sufficiently long time histories to allow tests of highly specified scope, *e.g.* limiting the number of conditions included in the search for neighboring points such as only looking at conditions with the same heading and speed and/or conditions with slowly varying heading, speed, and sea states in an effort to emulate realistic operating conditions.

To be useful in an onboard sense the calculation algorithms could easily be modified to search the recent past history of data for the ship as it is operating in any given sea state. As available time series grow longer, *e.g.* if this approach were to be used onboard a ship for some relatively long time period by comparison to the length of the experimental data sets, the accuracy of this method is anticipated to only improve with the precision of the Jacobian estimation. Further study is warranted to quantify qualitative behavior observed in the FTLE time series, identify appropriate bounds for flagging from the FTLE time series, and to ensure warnings are issued in sufficient time for corrective measures so as to enable use of this methodology on-board, in real time as a stand-alone package or as a companion to an intelligent systems or other dynamic motion monitoring approach.

6. ACKNOWLEDGEMENTS

The authors wish to acknowledge the support of AdvanceVT, Virginia Tech's Aerospace and Ocean Engineering Department, the ASEE-ONR Summer Faculty Research Program, and the Hydromechanics Department of the Carderock Division of the Naval Surface Warfare Center. Additionally, the authors thank Dan Hayden for his work in reducing and documenting the DTMB Model 5514 experimental data.

7. REFERENCES

- Arnold, L., Chueshov, I., & Ochs, G. 2003. "Stability and capsizing of ships in random sea-a survey." Tech. rept. 464. Universität Bremen Institut für Dynamicsche Systeme.
- Benettin, G., Galgani, L., Giorgilli, A., & Strelcyn, J.-M. 1980. "Lyapunov characteristic exponents for smooth dynamical systems and for Hamiltonian systems; a method for computing all of them." *Meccanica*, 9–20.
- Eckhardt, B., & Yao, D. 1993. "Local Lyapunov exponents in chaotic systems." *Physica "D"*, **65**, 100–108.
- Eckmann, J.-P., & Ruelle, D. 1985. "Ergodic theory of chaos and strange attractors." *Reviews of Modern Physics*, **57**(3), 617–656.
- Eckmann, J.-P., Oliffson Kamphorst, S., Ruelle, D., & Ciliberto, S. 1986. "Liapunov exponents from time series." *Physical Review A*, **34**(6).
- Falzarano, J. M. 1990. "Predicting complicated dynamics leading to vessel capsizing." Ph.D. thesis, Department of Naval Architecture and Marine Engineering, University of Michigan, Ann Arbor, MI.
- McCue, L. S. 2005 (October). "Applications of finite-time Lyapunov exponents to the study of capsize in beam seas." *In: 8th International Ship Stability Workshop*. Istanbul Technical University, Turkey.
- McCue, L. S., & Bassler, C. 2005 (November). "An alternative quiescence detection method for sea-based aviation operations." *In: ASNE's Launch and Recovery of Manned and Unmanned Vehicles from Surface Platforms: Current and Future Trends Symposium*. presentation only.
- McCue, L. S., & Bulian, G. 2006 (June). "A numerical feasibility study of a parametric roll advance warning system." *In: 25th International Conference on Offshore Mechanics and Arctic Engineering (OMAE2006)*. ASME, Hamburg, Germany.
- McCue, L. S., & Troesch, A. W. 2004 (November). "Use of Lyapunov exponents to predict chaotic vessel motions." *In: 7th International Ship Stability Workshop*. Shanghai Jiao Tong University, China.
- McCue, L. S., & Troesch, A. W. 2005 (September). "Identification of nonlinear

- and chaotic behavior in model-scale liquefied natural gas (LNG) carrier experimental data." *In: 2005 International Design Engineering Technical Conferences & Computers and Information in Engineering Conference*. ASME, Long Beach, California.
- McCue, L. S., & Troesch, A. W. 2006. "A combined numerical-empirical method to calculate finite time Lyapunov exponents from experimental time series with application to vessel capsizing." *Ocean Engineering*. In press.
- McCue, L. S., Belknap, W., & Campbell, B. 2005 (October). "Reconciling experimental and numerical data: techniques of nonlinear seakeeping code validation." *In: 8th International Ship Stability Workshop*. Istanbul Technical University, Turkey.
- Murashige, S., & Aihara, K. 1998a. "Coexistence of periodic roll motion and chaotic one in a forced flooded ship." *International Journal of Bifurcation and Chaos*, **8**(3), 619–626.
- Murashige, S., & Aihara, K. 1998b. "Experimental study on chaotic motion of a flooded ship in waves." *Proceedings of the Royal Society of London A*, **454**, 2537–2553.
- Murashige, S., Yamada, T., & Aihara, K. 2000. "Nonlinear analyses of roll motion of a flooded ship in waves." *Philosophical Transactions of the Royal Society of London A*, **358**, 1793–1812.
- Papoulias, F. A. 1987. "Dynamic analysis of mooring systems." Ph.D. thesis, Department of Naval Architecture and Marine Engineering, University of Michigan, Ann Arbor, MI.
- Sano, M., & Sawada, Y. 1985. "Measurement of Lyapunov Spectrum from a Chaotic Time Series." *Physical Review Letters*, **55**(10).
- Spyrou, K. J. 1996. "Homoclinic connections and period doublings of a ship advancing in quartering waves." *Chaos*, **6**(2).
- Wolf, A., Swift, J., Swinney, H., & Vastano, J. 1985. "Determining Lyapunov exponents from a time series." *Physica D*, **16**, 285–317.

On Manoeuvrability of Semi-Displacement Craft in Astern Seas

Evren Armaoğlu, *Department Universities of Strathclyde and Glasgow*

Zafer Ayaz, *Universities of Strathclyde and Glasgow*

Dracos Vassalos, *Universities of Strathclyde and Glasgow*

Toru Katayama, *Osaka Prefecture University*

ABSTRACT

The motions of semi-displacement ships travelling in astern seas are investigated. The focus is on the vertical dynamic forces which should not be neglected at this speed range. A database of dynamic forces acting on the ship depending on the running attitude and speed of the ship is measured from fully captive model experiments and used to characterize their effect on numerical simulations. A manoeuvring mathematical model using horizontal body axis, which allows for a combination of seakeeping and manoeuvring models, taking into account high-amplitude motions and memory effects, is used and the forces and motions are evaluated in six degrees of freedom in time domain. The results are validated with semi-captive model experiments in waves for regular following seas in three degrees of freedom. The effect of speed on transverse stability is discussed.

Keywords: *Semi-displacement, Astern seas, Manoeuvring*

1. INTRODUCTION

Over the last forty years, the number of High-Speed Craft (HSC) has increased exponentially. The increasing demand for speed in marine surface vehicles, combined with the technological advances have resulted in the development of large HSC, capable of carrying large number of passengers and cargo (Ritter & Templeman, 1998). Due to economical interests the general type of research for these kind of ships are mainly focused on propulsion, machinery, lightweight materials and hydrodynamically efficient hull forms. However if safety is of prime importance when designing, building and operating HSC, the dynamic behaviour in a seaway must be assessed properly.

There is an increased awareness of safety in marine community and the types of

dangerous situations a ship may be subject to are well defined. Anecdotal evidence of the way in which HSC behave in conditions such as surf-riding, broaching and bow-diving has given cause for concern in relation to passenger safety (BMT, 2003). For astern seas, benchmarks are set by ITTC based on experiments with a fishing vessel and a container both displacement ships (ITTC, 2002). Focus of these experiments were unstable phenomena like parametric-roll, surf-riding and broaching. The critical speed was defined as approximately Froude number 0.4 in pure following seas where the wave is travelling with the ship. It is reasonable to think that this is the most dangerous situation for a ship especially if travelling on a wave crest where transverse stability is greatly reduced. What has not been included by many is the effect of dynamic forces as the speed increases.

While the dynamic stability for displacement ships are concentrated on horizontal motions, for high speed craft the initial interest

was for planing craft and vertical motions. This is because the interest in high speed sea craft has started with the seaplanes that can land to sea with very high speed. The impact force applied to the seaplane floats during landing was a concern first as a structural problem (Von Karman, 1921). Later the problem turned to deal with the porpoising phenomenon, which is a coupled pitch and heave motion that can be seen in high speed at sea (Martin, 1978). As the problem turned to ship motions as propulsion mechanisms allowed ships to travel in those speed regions, additional problems such as corkscrew were seen (Katayama, 2002).

Because of navy's demand for high speed displacement ships, couple of series research were performed in different countries and the well known Series 64 and NPL series were born (Yeh., 1965, Bailey., 1976). It was with the NPL series that the speed induced instability non-zero heel was reported and interest in roll-induced instability for high speed craft began (Marwood & Bailey., 1968).

Baba, Asai & Toki (1982) used a sway-yaw-roll coupled motion model to investigate roll-induced instabilities of high-speed semi-displacement crafts and compared simulations with experiments. They found that GM/U rather than the hull forms has a major effect on the roll-induced instability at high speeds.

Codega & Lewis (1987)'s case study of a planing hull that goes unstable at high speed unlocked many of the reasons why many unstable phenomena happen at high speeds. They referred to Yegorov et al. (1981) and stated that until a high-speed boat reaches a purely planing region the stability of the hull will decrease from the static case. This is because the static hydrodynamic forces have decreased but the planing pressures have not been developed at the bottom. Codega has underlined a very good point that although the studies for high-speed hulls are made for prismatic hulls only, which have constant deadrise angle, this is not the case for a practical boat. Although the bottom pressures for prismatic craft are well defined, the bottom pressures for craft with varying deadrise angle

are unknown. They performed systematic experiments in full-scale to measure these pressures. In the end they recommended that a naval architect should avoid a high-speed, round bilge boat with any appreciable amount of deadrise because it will become transversely unstable if driven fast enough.

The concentration of the major studies being for head sea calculations is a very convenient one because as the speed increases to the planing range the encounter frequency in following waves become negative and the ship starts overtaking the waves. This however happens generally after Froude number 0.7 where the craft has already developed a running attitude due to speed. The effect of the running attitude on transverse stability for this speed region and heading in waves is, to the author's knowledge, uninvestigated.

The aim of this paper is to probe deeper to the already known following seas instabilities by focusing on the effects of vertical motions and speed on the transverse characteristics of the hull. An existing numerical program is further developed to include the effect of dynamic forces. Experiments are performed following Ikeda et. al. (1993) to obtain a database of hydrodynamic forces by fully captive model experiments. Vertical motions in regular waves are also measured by semi-captive tests to validate the numerical results.

2. MATHEMATICAL MODEL

The equations of motion are presented with respect to horizontal body axes. External forces are described with respect to this axis system in the right hand side of the equations of motion. The ship is assumed as a rigid body having six degrees of freedom with no restriction on motion amplitudes.

The relationships between coordinate systems are shown in Fig. 1. It is seen that in deriving the basic equations of motion, we make use of three different coordinate systems. First is an earth fixed system $O-\xi\eta\zeta$. The

second is the general body axes which is fixed in the ship and the origin G located at the center of gravity of the ship defined by $G-xyz$. The third is the horizontal body axes fixed in the ship with origin at G defined by $G-x'y'z'$.

In Fig. 1, x, y, z represent kinematics; u, v, w are linear velocities; p, q, r are angular velocities; and φ, θ, ψ are Euler angles of rotations. Newton's second law describes the equation of motion for a ship having six degrees of freedom and under the action of certain external forces. The representation of equations of motion in horizontal body axes are derived in previous studies (Hamamoto & Kim, 1993 and Ayaz, 2003).

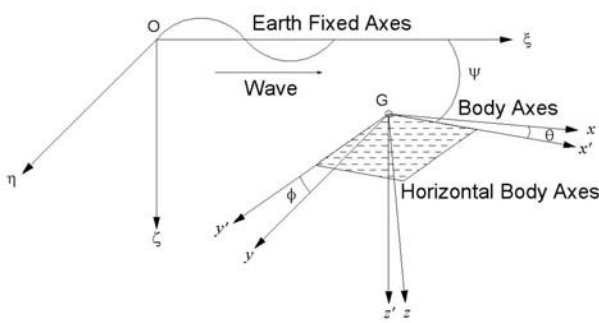


Figure 1. Systems of Coordinates

The generalized form of equations of motion is as follows:

$$\begin{aligned} m(\dot{V}_G + \omega \times V_G) &= F \\ H_G + \omega \times H_G &= G \end{aligned} \quad (1)$$

where m is the mass of the ship, H_G is the momentum about the center of gravity, ω angular velocity, V_G linear velocity and F and G are the sum of all forces and moments acting on the ship respectively. The resultant equations are as follows considering force and moment components:

$$\begin{aligned} m(\dot{U} - VR) &= X' \\ m(\dot{V} + UR) &= Y' \\ m\dot{W} &= Z' + mg \end{aligned} \quad (2)$$

$$\begin{aligned} (I_{yy} - I_{xx}) \left[\sin 2\theta \left(QP + \frac{1}{2} \dot{R} \right) + \cos 2\theta QR \right] \\ + (I_{xx} \cos^2 \theta + I_{yy} \sin^2 \theta) \dot{P} - I_{yy} RQ &= K' \\ (I_{yy} - I_{xx}) \left[\sin 2\theta \left(\frac{1}{2} R^2 \right) \right] \\ + (I_{xx} \cos^2 \theta + I_{yy} \sin^2 \theta) RP + I_{yy} \dot{Q} &= M' \\ (I_{xx} - I_{zz}) \left[\sin 2\theta \left(QR - \frac{1}{2} \dot{P} \right) - \cos 2\theta QP \right] \\ + (I_{xx} \sin^2 \theta + I_{zz} \cos^2 \theta) \dot{R} &= N' \end{aligned} \quad (3)$$

where, X', Y', Z', K', M' and N' are surge, sway, heave, roll, pitch and yaw external forces and moments composed of forces due to waves, speed and control systems. U, V, W are surge, sway and heave linear velocities; Q, P, R are roll, pitch and yaw angular velocities in the horizontal body axes system; I_{xx}, I_{yy}, I_{zz} are roll, pitch and yaw moment of inertias respectively. The external forces and moments in equations of motion are represented as follows:

$$\begin{aligned} X' &= -\iint_S p \mathbf{n}_x dS + X_H + X_P + X_S \\ Y' &= -\iint_S p \mathbf{n}_y dS + \rho U \int_{\Gamma_x} \Phi_D \mathbf{n}_y dS + Y_H + Y_S \\ Z' &= -\iint_S p \mathbf{n}_z dS + \rho U \int_{\Gamma_x} \Phi_D \mathbf{n}_z dS + Z_H + Z_D \\ K' &= -\iint_S p (\mathbf{r} \times \mathbf{n}_{yz}) dS + \rho U \int_{\Gamma_x} \Phi_D (\mathbf{r} \times \mathbf{n}_{yz}) dS \\ &+ K_H + K_S \\ M' &= -\iint_S p (\mathbf{r} \times \mathbf{n}_{zx}) dS + \rho U \int_{\Gamma_x} \Phi_D (\mathbf{r} \times \mathbf{n}_{zx}) dS \\ &+ M_H + M_D \\ N' &= -\iint_S p (\mathbf{r} \times \mathbf{n}_{xy}) dS + \rho U \int_{\Gamma_x} \Phi_D (\mathbf{r} \times \mathbf{n}_{xy}) dS \\ &+ N_H + N_S \end{aligned} \quad (4)$$

Here the first terms on the right hand side of the equations represents the incident wave forces and moments, including hydrostatic forces, where p is the pressure evaluated at the instantaneous hull surface, \mathbf{n} is the normal vector and $\mathbf{r} \times \mathbf{n}$ is the vector fixed with respect

to the center of gravity (Hamamoto & Kim, 1993). The second terms are diffraction forces which are obtained as disturbance forces using Ohkusu (1986)'s low encounter frequency slender body theory, where Φ_D is the disturbance due to waves and Γ_x denotes integration over section contour to the still water surface. Diffraction force in surge is ignored because the incident wave force is dominant. For the rest of the forces, subscript H indicates manoeuvring (hull) forces, P indicates forces due to propulsion mechanism, S indicates forces due to steering mechanism and D indicates dynamic forces due to speed.

The implementation of dynamic forces can be done by either direct calculation methods or from a database containing the necessary force and moment components obtained from either experiments or a calculation procedure such as a CFD methodology. The method of calculation for propulsion and steering system varies depending on the system being a propeller-rudder combination, azimuthing pod drive or a waterjet. For convenience MMG model is used in the calculations. Wind forces and ride control systems can also be added but are left out for the initial study.

The detailed descriptions of the mathematical model in whole were given in numerous previous studies (Ayaz et. al., 2002, Ayaz., 2003, Ayaz, Vassalos, Turan, 2006). The only addition here is the dynamic forces due to speed. The non-linear equations (2) and (3) can be expressed in matrix form representing displacements, velocities and accelerations in the following form;

$$(M + A)\ddot{X}(t) + B\dot{X}(t) + CX(t) = F(\zeta_w, X(t), \dot{X}(t), \ddot{X}(t)) \quad (5)$$

where X is the solution vector to the equations of motion, M is the inertia matrix, A is the added mass matrix, B is the damping matrix, C is the restoring coefficient matrix and F is the external force matrix where ζ_w is the wave profile which can be represented as regular or long crested irregular seas.

According to previous studies the most dangerous situations the ship is going to be in are in regular waves, followed by long crested irregular waves. Short crested waves are the least likely for unstable behaviour leading to capsize (ITTC, 1999).

The equations (5) are solved in time domain via Fourth Order Runge-Kutta algorithm. In order to evaluate the frequency dependence of the hydrodynamic coefficients impulse response functions are implemented in the numerical model. Since the computations are done in time domain they are represented by convolution integrals. Following Cummins (1962)'s work, radiation forces in time domain is represented as :

$$F_{ij} = -a_{ij}(\infty)\dot{V}_j - \int_0^{\infty} K_{ij}(t)V_j(t-\tau)d\tau \quad (6)$$

$i, j = 1, 2, 3, 4, 5, 6$

where the first term is the infinite frequency added mass and the second term is the impulse response function. Kernel function $K_{ij}(t)$ is represented as the frequency domain damping function in the following form:

$$K_{ij}(t) = \frac{2}{\pi} \int_0^{\infty} B_{ij}(\omega) \cos \omega t d\omega \quad (7)$$

$i, j = 1, 2, 3, 4, 5, 6$

Calculation of the damping terms are done according to the methodology of Kang (TBP) which is a 3-D unsteady potential theory method using a green function representing a translating pulsating source therefore taking speed effects into account.

3. EXPERIMENTAL STUDIES

3.1 Steady Force Measurements with Fully Constrained Model.

Implementation of the dynamic forces will be through a database obtained from experiments. In a low-encounter frequency

environment the problem is very close to steady problem therefore it can be assumed that the dynamic forces the craft is going to be subject to will also act like steady. Experiments to systematically measure the steady forces acting on the hull of a semi-displacement craft (Figure 2) were carried out¹. The model was attached to a 6 degrees of freedom load-cell and constrained in predefined positions to measure the forces acting on the hull. The test matrix is given in Table 1 where the sign convention is the same as the numerical model.

Table1 Test Matrix

Fn	0.4	0.5	0.6	0.7	0.8
Trim (degrees)	+2	+1	0	-2	-4
Sinkage (mm)	+20	+10	0	-10	-20

The forces measured are F_z , which is the force component in vertical direction, F_x , which is the force component in the direction of the carriage movement and M_y , which is the moment around the center of gravity in vertical direction. The load-cell is calibrated to measure the forces around the center of gravity and the model setup is set in such a way that the rotations are around center of gravity and the sway, roll and yaw motions are restrained completely and the sinkage and trim can be set manually. The resultant forces due to carriage speed are only dynamic components as the load-cell is set to zero before each run.

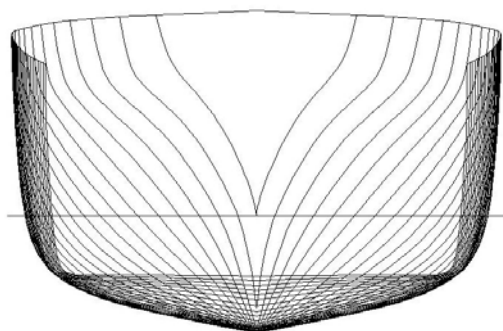


Figure 2. TC-60 Lines Plan

Table 2. TC-60 Principal Particulars

L_{OA} (m)	1.000
L_{WL} (m)	0.950
B (m)	0.166
T (m)	0.044
C_B	0.542
C_M	0.734
C_P	0.738
Wetted Surface (m^2)	0.159
Δ (N)	34.923

Because of spray limitations especially at bow-down trim angles with high sinkage values, some tests are immeasurable, hence the total number of tests performed are 98 instead of the proposed 125 cases. The results of the tests are summarized in Figures 3 to 8. The effect of change of sinkage and speed for constant trim angle are shown for Dynamic Lift Force, which is defined as the force component acting normal to keel, and Trim Moment around the center of gravity.

The results are open to discussion since there was no time to run consistency tests. The force changes almost linearly as the sinkage is decreased from negative to positive for a single speed and trim is increased bow-up. As speed increases significant trim moment occurs after Froude number 0.4. A certain relationship between sinkage and bow-down trim with force and moment could not be established because spray generated at higher speeds made it difficult to get a healthy measurement. The results seem to generally agree with each other and are consistent with Ikeda et. al. (1993) and Ikeda, Katayama and Okumura (2000).

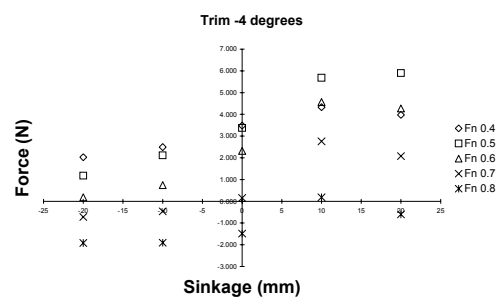


Figure 3. Change of Lift (-4 degrees trim)

¹ Test were performed at
The Center for Marine Hydrodynamics
Acre Road, Glasgow, UK, G20 OTL

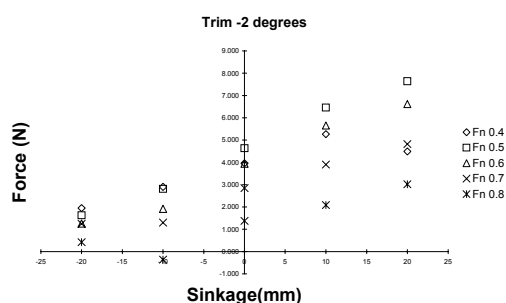


Figure 4. Change of Lift (-2 degrees trim)

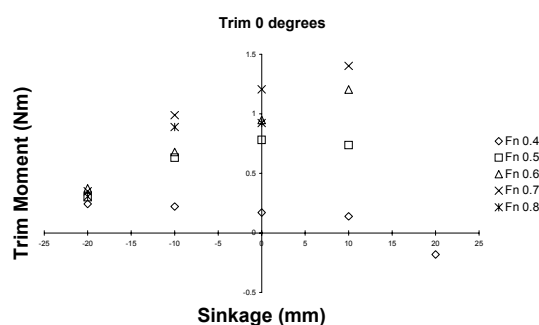


Figure 8. Change of Moment (0 degrees trim)

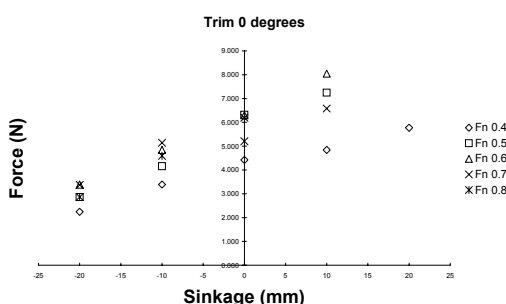


Figure 5. Change of Lift (0 degrees trim)

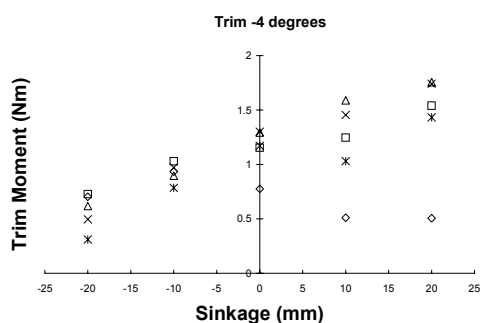


Figure 6. Change of Moment (-4 degrees trim)

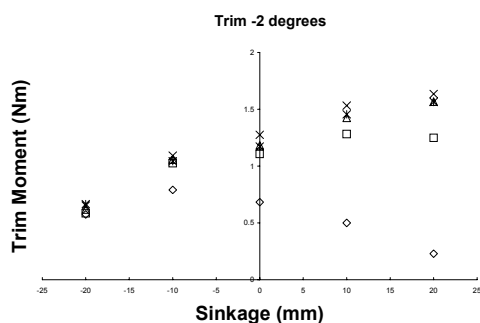


Figure 7. Change of Moment (-2 degrees trim)

3.2 Seakeeping Experiments with Semi-captive Model Tests.

Motion response of the craft for regular waves at following seas was tested for differing wave conditions and hull speeds in order to validate the applicability of the numerical tool. The model was attached to the carriage and was free to heave and pitch motions only. This setup by definition ignores surge coupling and therefore numerical simulations were performed considering this effect. Table 2 presents the tested wave frequencies and Froude numbers.

Table3. Cases for Seakeeping Experiments

ω Fn	3.502	4.530	5.548	6.410	7.835
0.4	X	X	X	X	X
0.6	X	X	X	-	-
0.7	-	-	X	X	X
0.8	X	X	X	-	-

Experimental results are compared to numerical results using the database approach initially. It was observed that results obtained using this method gives insufficient results in both motions even for low speeds as seen in Figures 9 and 10.

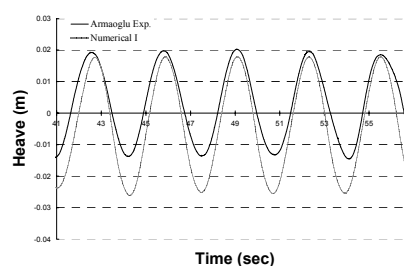


Figure 9. Heave Motion $\omega=3.502$ $Fn=0.4$

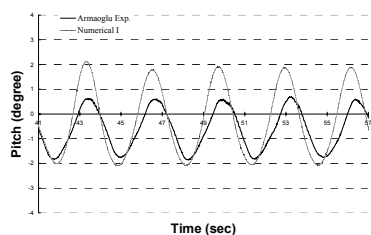


Figure 10. Pitch Motion $\omega=3.502$ $F_n=0.4$

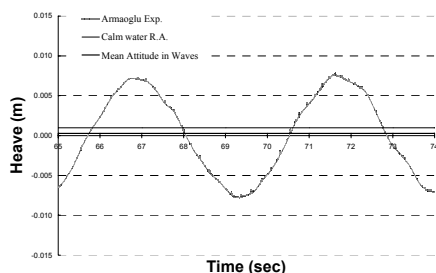


Figure 11. Mean Attitude in Heave $\omega=5.548$ $F_n=0.7$

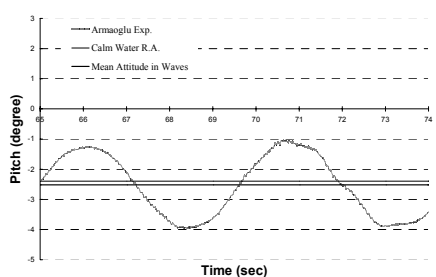


Figure 12. Mean Attitude in Pitch $\omega=5.548$ $F_n=0.7$

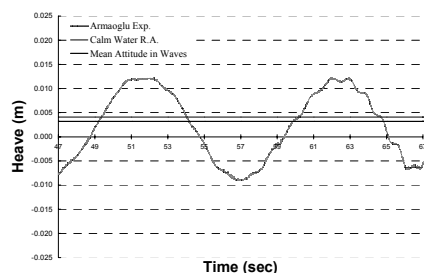


Figure 13. Mean Attitude in Heave $\omega=4.530$ $F_n=0.6$

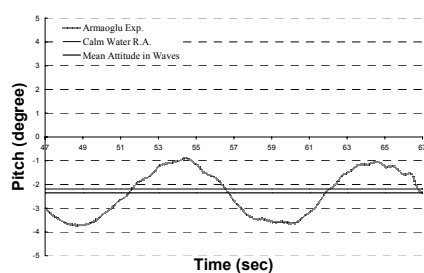


Figure 14. Mean Attitude in Pitch $\omega=4.530$ $F_n=0.6$

In due process of analysing the seakeeping results it is seen that the mean attitude of the motions is very close to the running attitude in calm water regardless of the wave frequency. This might be because the planing pressures are not developed sufficiently and the static forces are still dominant. This is better seen in Figures 11 to 14. From these figures it is observed that the pitch moment in Figure 10 is not sufficiently high enough to bring the craft to the running attitude.

3.3 Roll Decay Tests

Roll decay tests were performed for four speed conditions including zero speed. The results and the comparison with numerical simulations are presented in the following figures. For higher speeds a deviation from the zero roll angle is seen at the model tests. This may be caused by the shifting of the weights used to properly ballast the model as the initial roll angle is quite big and the model beam is very small.

Roll damping is increased because of speed and the effect can be seen from the reduced roll period in $F_n 0.4$. Roll period of $F_n 0.6$ is slightly

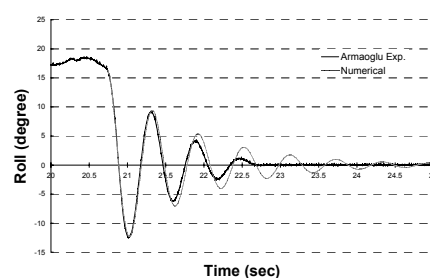


Figure 15. Roll Decay at Zero Speed

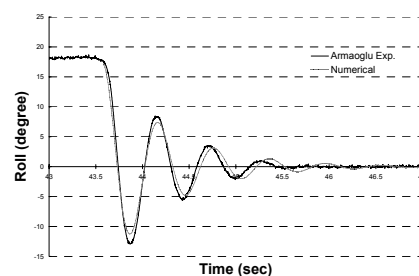
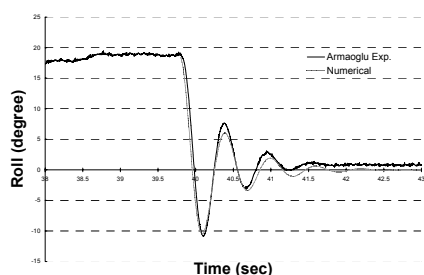
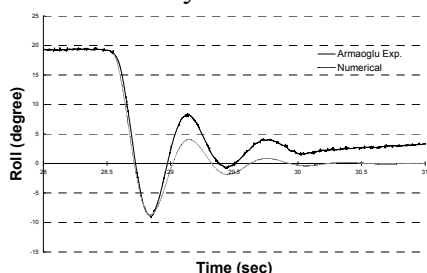


Figure 16. Roll Decay at $F_n=0.4$

Figure 17. Roll Decay at $F_n=0.6$ Figure 18. Roll Decay at $F_n=0.8$

higher than $F_n 0.4$. A possible reason for this is the running attitude's effect on roll restoring moment or a tendency for unstable roll motion at this speed. In $F_n 0.8$, the roll period and the number of oscillations and the amplitude of a cycle are reduced. The roll period reduction clearly shows the increase of roll damping due to speed meanwhile the reduction of the number of roll oscillations and amplitude of a cycle shows the increased roll restoring moment because of the dynamic lift. The change in roll period is shown in Table 4.

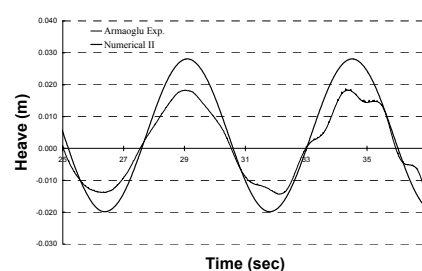
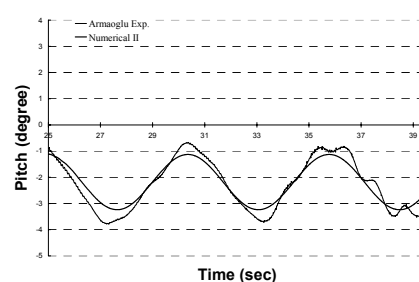
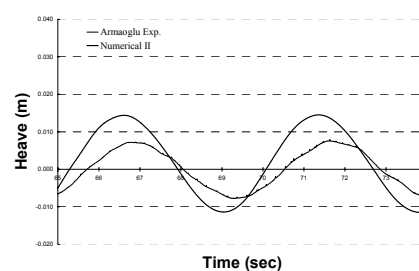
Table 4 Change of Roll Period with Speed

<i>Froude Number</i>	<i>Roll Period (sec)</i>
0.0	0.909
0.4	0.550
0.6	0.625
0.8	0.267

4. VALIDATION OF THE NUMERICAL RESULTS

From the observations of seakeeping experiments as mentioned in 3.2 a different approach will be implemented to include the effect of dynamic forces to the model. This will be the assumption that the calm water running attitude is equal to the mean running attitude in waves for this speed range. This assumption

although very simple, is applicable to initial design stage and is very fast, omitting the overcomplicated (thus prone to error) database approach. The results are presented in Figures 19-23. In Figures 19 and 20 heave amplitude is slightly overestimated and pitch amplitude slightly underestimated. This shows the importance of using correct damping coefficients taking speed effects into account. The effect of running attitude is reflected correctly with the mean attitude assumption. Figures 21 and 22 shows even better agreement with the experiments with higher speeds for different modes of motion. It is seen that our assumption is valid in this speed range and numerical results are well within engineering limits however calculation of hydrodynamic coefficients must be handled properly.

Figure 19. Heave Motion $\omega=3.502 F_n=0.6$ Figure 20. Pitch Motion $\omega=3.502 F_n=0.6$ Figure 21. Heave Motion $\omega=3.502 F_n=0.8$

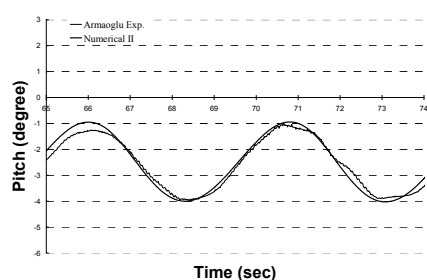


Figure 22. Pitch Motion $\omega=5.548$ $F_n=0.7$

5. EFFECT OF RUNNING ATTITUDE ON TRANSVERSE STABILITY

In general practice GZ curve is used to assess the intact transverse stability of a HSC. Calculations in IMO HSC Code are performed at the design waterline which corresponds to the maximum operational weight of the craft with no lift or propulsion machinery active. Roll and pitch stability is qualitatively assessed during safety trials and operational restrictions may be imposed according to the results. This however tells very little in initial design stage of how the actual stability is affected because of speed. If it is assumed that the running attitude of the craft is the actual balance condition of the craft for a given speed, then GZ curve calculations can be performed in this balance condition for relatively small roll angles assuming that the speed loss due to roll angle is negligible. In Figure 23 it is clearly seen that running attitude alone reduces the transverse stability of the craft by reducing the lever arm even for small angles of roll.

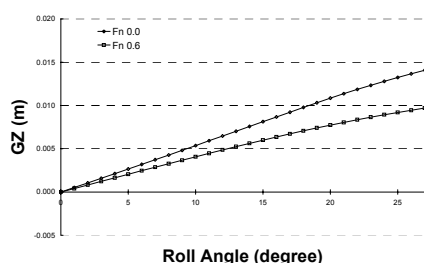


Figure 23. Effect of Speed on GZ Curve

Further reduction to this effect will be imposed in waves and also because of weather conditions. Although the roll damping characteristics are increased because of speed, if the

righting arm lever is negative for a given roll angle, this will not prevent the craft from capsizing. This also shows that evaluating intact stability of HSC on static design criteria is insufficient. Therefore, applying performance based criteria would be the way forward for robust and accurate transverse-stability analysis of semi-displacement craft. A detailed effort applying this approach is currently being carried out following validation analysis presented herein.

6. CONCLUSIONS

Several aspects of the effect of speed on semi-displacement ships are investigated. Experiments were performed to verify the results produced by the numerical tool. Following conclusions were obtained:

For low encounter frequencies the dynamic forces can be assumed to act steady.

Database approach to evaluate the dynamic forces is over-engineered and prone to error in this speed range. The assumption that the mean running attitude in waves is equal to the calm water running attitude is valid.

The effect of roll motion on vertical dynamic forces is not taken into account however roll-pitch coupling is achieved via non-linear restoring calculation in mathematical model.

Running attitude alone causes reduction in transverse stability. Combined with further reduction in waves and wind this might lead to dangerous situations.

Even the small analysis of the effect of speed on transverse stability herein indicate that the static criteria might be insufficient to evaluate High Speed Craft characteristics. Performance based criteria imposed on early design stage could be a good way forward to assess stability thoroughly and safety based design.

7. REFERENCES

- Ayaz, Z., 2003, "Manoeuvring Behaviour of Ships in Extreme Astern Seas." PhD Thesis, University of Strathclyde, Glasgow, UK
- Ayaz, Z., Vassalos, D., Spyrou, K.J., & Matsuda, A., 2002, "Towards a Six Degrees of Freedom Manoeuvring Mathematical Model in Random Seas." In: Proceedings of the Sixth International Workshop on Stability and Operational Safety of Ships, Webb Institute, New York, USA.
- Ayaz, Z., Vassalos, D., & Turan, O., 2006, "Parametric Studies of a new numerical model for controlled ship motions in extreme astern seas" *Journal of Marine Science and Technology*, Vol. 11, No. 1, pp.19-38.
- Baba, E., Asai, S., & Toki, N., 1982, "A Simulation Study on Sway-Roll-Yaw Coupled Instability of Semi-Displacement Type High Speed Craft." In: Proceedings of the Second International Conference on Stability of Ships and Ocean Vehicles., pp. 79-90.
- Bailey, D., 1976, "The NPL High Speed Round Bilge Displacement Hull Series." *Maritime Technology Monograph*, No. 4.
- Codega, L., & Lewis, J., 1987, "A Case Study of Dynamic Instability in a Planing Hull." *Marine Technology*, Vol. 24 (2), pp. 143-163.
- Cummins, W. E., 1962, "The Impulse-Response Function and Ship Motions." *Schiffstechnik*, Vol. 47, pp.101-109.
- De Kat, J.O., & Paulling, J.R., 1989, "The Simulation of Ship Motions and Capsizing in Severe Seas." *Transactions of the Society of Naval Architects and Marine Engineers*, Vol. 97, pp.139-168.
- Hamamoto, M., & Kim, Y., 1993, "A New Coordinate System and the Equations Describing Manoeuvring Motion of a Ship in Waves." *Journal of the Society of Naval Architectures of Japan*, Vol. 173, pp. 209-220.
- Ikeda, Y., Katayama, T., & Okumura, H., 2000, "Characteristics of Hydrodynamic Derivatives in Manoeuvring Equations for Super High Speed Planing Hulls." In: Proceedings of the 10th International Offshore and Polar Engineering Conference, Vol. 4, pp. 434-444. Seattle, USA.
- Ikeda, Y., Yokomizo, K., Hamasaki, J., Umeda, N., & Katayama, T., 1993, "Simulation of Running Attitude and Resistance of a High-Speed Craft Using a Database of Hydrodynamic Forces Obtained by Fully Captive Model Experiments." In: The 7th International Conference on Fast Sea Transportation., pp. 583-594.
- IMO, 2000, *International Code of Safety for High-Speed Craft*, Publisher: International Maritime Organization, London, UK.
- ITTC, 1999, "The Specialist Committee on Stability." Final Report and Recommendations to the 22nd ITTC. In: Proceedings of the 22nd ITTC, Seoul and Shanghai. Retrieved May , 23, 2006. from: <http://itcc.sname.org/proceedings.htm>
- ITTC, 2002, "The Specialist Committee on Prediction of Extreme Ship Motions and Capsizing." Final Report and Recommendations to the 23rd ITTC. In: Proceedings of the 23rd ITTC, Vol 2, Venice, Italy., pp. 611-657.
- Katayama, T., 2002, "Experimental Techniques to Assess Dynamic Instability of High-Speed Craft - Non-zero Heel, Bow-Diving, Porpoising and Transverse Porpoising." In: Proceedings of the Sixth International Ship Stability Workshop. Glen Cove, New York, USA.

- Kang, J., (To Be Published), "Time Domain Mathematical Model for Manoeuvring Simulation in a Wave", PhD Thesis, University of Strathclyde, Glasgow, UK.
- Martin, M., 1978, "Theoretical Determination of Porpoising Instability of High-Speed Planing Boats." *Journal of Ship Research*, Vol. 22 (1), pp. 32-53.
- Marwood, W.J., & Bailey, D., 1968, "Transverse Stability of Round-Bottomed High Speed Craft Underway." National Physics Laboratory, Ship Report N^o. 98.
- BMT SeaTech Limited, 2003, "High Speed Craft in Following and Stern Quartering Seas: Report on Phase 1 of MCA Research Study 502", Project No: C3423.
Retrieved May , 22, 2006. from:
http://www.mcga.gov.uk/c4mca/research_report_502_phase_1.pdf
- Ohkusu, M, 1986, "Prediction of Wave Forces on a Ship Running in Following Waves with Very Low Encountered Frequency." *Journal of Society of Naval Architects of Japan*, Vol. 159, pp. 129-138.
- Ritter, O.K & Templeman M.T., 1998, "High-Speed Sealift Technology" Total Ship Systems Engineering Directorate Technology Projection Report, Carderock Division Naval Surface Warfare Center, USA. Retrieved March , 19, 2004. from:
http://www.ccdott.org/hss_volume2/01_hss_workshop_tech.pdf
- Von Karman, T., 1929, "The Impact of Seaplane Floats During Landing." NACA TN N^o.321.
- Yegorov, I., Bun'Kov, M., & Sadovnikov, Y. M., 1981, "Propulsive Performance and Seaworthiness of Planing Vessels." NAVSEA Translation N^o. 1965. Washington D.C., USA.
- Yeh, H. Y. H., 1965, "Series 64 Resistance Experiments on High-Speed Displacement Forms." *Marine Technology*, Vol. 2, pp. 248-272.

Numerical Study of Ship Rolling in Turning Manoeuvres

Serge Sutulo, *Unit of Marine Technology and Engineering, Technical University of Lisbon*

Instituto Superior Técnico

C. Guedes Soares, *Unit of Marine Technology and Engineering, Technical University of Lisbon*

Instituto Superior Técnico

ABSTRACT

A unified mathematical model describing both manoeuvring and seakeeping motions of surface displacement ships is used for numerical investigation of the ship motions in turning manoeuvres under action of regular waves. The 6DOF model combines a semi-empiric model for the still-water manoeuvring forces with a model for the seakeeping forces built as a generalization of the ordinary strip method. Comparative simulations included unrestrained and restrained straight runs in beam seas, and turning manoeuvres in still water and under action of waves, and are demonstrating that the attained instantaneous roll angles can be higher in turning than in the straight run.

Keywords: turning manoeuvre, rolling, regular waves, simulation.

1. INTRODUCTION

Historically, the ship rolling was the first kind of ship motions in waves studied theoretically and it remained the most important one from the viewpoint of the ship safety. While the first studies were dealing with a ship at zero speed and subject to the action of regular beam seas, further developments of the theory accounted for the speed of advance and already at arbitrary wave encounter angles.

Instead of simpler mathematical models based on an isolated roll equation, effects of coupling were accounted for leading to sophisticated 6DOF time-domain simulation codes. Also, consideration of the irregular waves, and/or nonlinear phenomena, such as the parametric and sub-harmonic resonance etc. was done.

At the same time, one basic assumption, which can be considered as traditional for the seakeeping in general, was kept unchanged: the reference motion of the ship was assumed to be a

rectilinear motion with constant speed and zero mean drift angle. In fact, the problem statement involving this assumption not only is the simplest possible but is also reasonable and rather well based. First of all, running in straight path is the predominant regime for most seagoing vessels. Another typical situation is stationing, i.e. free drifting or positioning, at zero speed but this is just a particular case of the previous situation. Any sort of manoeuvring takes only a small fraction of many ships' operational time.

Also, from certain viewpoints, the straight run can occur to be one of the most dangerous options: in the case of an unfavourable combination of the parameters of the incident waves and of the ship's speed and heading, any possible resonance will benefit from a long and steady exposure and will be able to develop up to a possible critical situation.

On the other hand, however, it is known from the maritime practice that manoeuvres in stormy weather can become dangerous and are to be avoided completely or should be performed in a gentle and careful way as otherwise the combined effect of the manoeuvre-induced roll

and of the wave action can result in fatal consequences. But there are many situations when hard manoeuvring in extremely rough sea cannot be avoided: rescue and salvage operations, weapon- or collision-avoidance manoeuvres etc. This indicates that rolling of a ship moving along a curvilinear trajectory deserves special study and, probably, such a statement should be considered as standard in the future.

Unfortunately, so far, too few studies, if any, related to this situation are known. This is caused not only by a possible underestimation of the problem but also by the lack of suitable mathematical models. Most of such models (Ottozon & Bystrom, 1991, Bailey & Price, 1997, Ayaz & Vassalos, 2003) were models devised primarily for studying manoeuvring motion in waves and with the roll considered as a secondary effect.

A certain exception happened to be a study by Remez (1985) who studied rolling in the steady turn from the viewpoint of the seakeeping safety. However, his mathematical model was deficient in the sense that no manoeuvring-originated forces participated in the roll equation. As result, Remez came to the then obvious conclusion that the maximum attainable absolute values of the roll angle during the turn were always inferior to those reached in the most unfavourable corresponding straight run which is, however, contradicting the common sense and the practice of the ship operations.

Moreover, even in still-water manoeuvring, some ships show quite significant instantaneous heel angle absolute values: over 25deg according to Trägårdh (2003). No doubt, this value can be tangibly amplified when the incident wave's action is added. In addition, it was found that such a large dynamic heel correlated with the dynamic trim. This indicates that the usual 4DOF manoeuvring model is not always able to predict this phenomenon correctly.

On the other hand, a number of 6DOF time-domain seakeeping models appeared (Pawlowski

& Bass, 1991, Belenky et al., 2003) which contain certain manoeuvrability elements, such as the rudder and propeller forces and are often complemented with a numerical representation of a simple automatic controller to maintain the straight course, i.e. the canonical seakeeping regime, in the presence of wave disturbances. However, typically such codes miss appropriate description of the hull manoeuvring forces and do not fairly reproduce the ship's behaviour in manoeuvring.

It is rather difficult, anyway, to build a mathematical model equally suitable for manoeuvring and seakeeping studies as the quasi-steady viscous forces are highly essential in the first case while the substantially unsteady potential forces, including the hydrostatic part, dominate in seakeeping. An appropriate direct CFD modelling based on the (still Reynolds-Averaged) Navier–Stokes equations could, in principle, provide adequate description of all physics. But this approach is still highly numerically inefficient even when an exquisite hardware is used. Another problem is connected to difficulties in arranging an appropriate turbulence model which is especially difficult in the highly challenging case of curvilinear motion of a surface displacement ship as the flow around the ship's hull is then rich in separations, re-attachments, vortex formation, let alone substantial interaction with the rudder and propeller. That is why, all practical manoeuvring models are based on empiric data combined with various more or less justified assumptions. As the experimentally determined forces contain also inseparable potential parts, their correct superposition with the seakeeping loads is not trivial.

The present study is based on a newly developed approximate manoeuvring-and-seakeeping mathematical model suitable for slender displacement ships. Some elements of this model are described in (Sutulo & Guedes Soares, 2005). The model is used in this study to model the ship rolling in turning manoeuvres by means of the time-domain simulation of the manoeuvring motion in regular sea of moderate

height and weak steepness. As the used model is nonlinear, and accounts for most coupling effects, it can potentially reveal the parametric resonance, describe the broaching phenomenon in astern sea and the capsizing situations. However, envisaging corresponding studies in the future, this particular contribution does only deal with the situation close to the main roll resonance with the main purpose of comparing the roll's severity in straight runs and in relatively tight manoeuvres. Only full-helm turning manoeuvres are considered here as they can be considered a priori as being of the most dangerous ones, especially at the initial phase which also is similar to the initial phase of many other manoeuvres, like fast course changes, fast lane changes etc.

2. SHIP MATHEMATICAL MODEL

2.1. Frames of Reference

The following right-hand Cartesian frames of reference are used:

The Earth-fixed frame $O_0\xi_0\eta_0\zeta_0$ with the origin O_0 and the ξ_0 -axis lying on the undisturbed free surface (some appropriate direction of this axis can be chosen arbitrarily). The ζ_0 -axis is directed vertically downwards.

The body axes $Cxyz$ linked to the ship treated as a rigid body. The x -axis lies in the centre-plane of the ship and is directed to the bow. It is supposed that at some initial time moment $t=0$ and at the ship's equilibrium position this frame coincides with the Earth frame i.e. the z -axis is directed from top to bottom and the y -axis—to the starboard. The body frame's position and orientation with respect to the Earth frame is described by the origin's advance ξ_C , transfer η_C , sinkage (or heave) ζ_C , and by the three Euler angles defined as usual: the heading angle ψ , pitch angle θ and roll angle φ .

The body semi-fixed axes $O\xi\eta\zeta$ differing from the body-fixed axes $Cxyz$ by not being involved into the heave, pitch and roll.

During the evaluation, one more system of co-ordinates $O_1\xi_1\eta_1\zeta_1$ was used which differed from the frame $O\xi\eta\zeta$ by its non-involvement into the wave-induced yawing. These axes are usually called the seakeeping axes in the orthodox linear consideration.

2.2. Basic Equations of Motion

The ship is assumed to be rigid. The Euler equations of motion in the non-central body axes are written as:

$$\begin{aligned}
 (m + \mu_{11})\dot{u} + (mz_G + \mu_{15})\dot{q} - mvr \\
 - mx_G r^2 + mz_G pr + mwq - mx_G q^2 = X, \\
 (m + \mu_{22})\dot{v} - (mz_G + \mu_{24})\dot{p} + (mx_G + \mu_{26})\dot{r} \\
 + mur - mur - mwp + mx_G pq + mz_G qr = Y, \\
 (m + \mu_{33})\dot{w} - (mx_G + \mu_{35})\dot{q} - muq \\
 - mz_G q^2 + mvp + mx_G pr - mz_G p^2 = Z, \\
 -(mz_G + \mu_{24})\dot{v} + (I_{xx} + \mu_{44})\dot{p} - (I_{xz} + \mu_{46})\dot{r} \\
 + mz_G wp + (I_{zz} - I_{yy})qr - mz_G ur - I_{xz} pq = K, \\
 (mz_G + \mu_{15})\dot{u} - (mx_G + \mu_{35})\dot{w} + (I_{yy} + \mu_{55})\dot{q} \\
 + mx_G uq + mz_G wq + (I_{xx} - I_{zz})pr \\
 + I_{xz}(p^2 - r^2) - mz_G vr - mx_G vp = M, \\
 (mx_G + \mu_{26})\dot{v} - (I_{xz} + \mu_{46})\dot{p} + (I_{zz} + \mu_{66})\dot{r} \\
 + mx_G ur - mx_G wp + (I_{yy} - I_{xx})pq + I_{xz}qr = N,
 \end{aligned} \tag{1}$$

where m is the ship's mass, x_G and z_G are the 'centre-of-mass' co-ordinates; X, Y, Z, K, M, N are the total forces and moments for the surge, sway, heave, roll, pitch, and yaw respectively, and u, v, w, p, q, r are the (quasi)-velocities of surge, sway, heave, roll, pitch and yaw respectively.

The dynamic equations are also complemented with the standard kinematic

differential equations linking the generalized ship co-ordinates with the quasi-velocities.

For each force or moment component $F = X, Y, \dots, N$, the following decomposition takes place:

$$F = F_g + F_{sk} + F_m - F_{sk0}, \quad (2)$$

where the subscripts have the following meaning: g stands for the gravitational forces; sk —seakeeping forces; m —manoeuvring forces; $sk0$ corresponds to the seakeeping forces which are computed at the zero wave amplitude and are subtracted to eliminate double account of potential components present in both the seakeeping and manoeuvring loads. In the slender-body theory, the last component is defined by the zero-frequency added mass longitudinal distribution. When integrated along the reduced ship length to account for viscous effects, as done in the present study, this distribution results in the horizontal plane in the slender-body estimate of the manoeuvring forces which are introduced here independently.

2.3. Seakeeping Forces

Assumptions. The ship is assumed to be slender so that the strip method is applicable and the oncoming waves are regular, with constant parameters. The flow is supposed to be potential and described with the absolute fluid velocity potential $\phi(\xi_0, \eta_0, \zeta_0)$ satisfying the Laplace equation within the fluid domain and all the usual boundary conditions. The free-surface boundary condition is supposed to be linear and satisfied on the undisturbed free surface.

Representation of the Velocity Potential. As usual, the velocity potential can be decomposed as follows:

$$\phi = \phi_r + \phi_w + \phi_d, \quad (3)$$

where ϕ_r is the potential caused by the ship motions, ϕ_w is the incident wave potential, and ϕ_d is the diffraction potential.

The potential ϕ_r satisfies the usual body boundary condition on the instantaneous submerged hull surface S_B and the incident wave potential is taken as

$$\phi_w = \text{Re} \left[\frac{iga_w}{\omega} e^{-k\zeta_0 - i(k_1\xi_0 + k_2\eta_0)} e^{i\omega t} \right], \quad (4)$$

where $k_1 = k \cos \chi_{w0}$, $k_2 = k \sin \chi_{w0}$, $k = \omega^2 / g$ is the wave number, ω is the wave frequency, and χ_{w0} is the wave propagation angle with respect to the axis $O_0\xi_0$.

Decomposition of Seakeeping Forces. the ship velocity \mathbf{V}_C is supposed to be constituted of two parts: the steady velocity of advance \mathbf{V}_{C0} and the seakeeping part per se \mathbf{V}_{C1} . A similar decomposition can be made in a more general seakeeping-and-manoevring formulation. For the total velocity of any point fixed in the moving frame $\mathbf{V}(x, y, z)$ it can be written:

$$\mathbf{V}(x, y, z, t) = \mathbf{V}_0(x, y, z, t) + \mathbf{V}_1(x, y, z, t), \quad (5)$$

where the subscript 0 corresponds to the base manoeuvring motion which is assumed to be time-dependent but changing slowly: time derivatives of any variables related to that motion are neglected. The variables with the subscript 1 correspond to the wave-induced motion and their derivatives are not neglectable. The velocity potential can be represented similarly i.e. $\phi = \phi_0 + \phi_1$, where ϕ_0 is the slowly-varying potential associated with the base manoeuvring motion and ϕ_1 is the potential originating from the incident waves' action.

Using the usual Bernoulli pressure equation written in the semi-fixed axes $O\xi\eta\zeta$ and applying the subdivision of the velocity and of the potential into the slow and fast parts the

following representation of the pressure is obtained:

$$p = p_{hs} + p_0 + p_{01} + p_1 + p_2, \quad (6)$$

where $p_{hs} = \rho g \zeta$ is the hydrostatic pressure; $p_0 = \rho \mathbf{V}_0 \cdot \nabla \phi_0 - \frac{1}{2} \rho (\nabla \phi_0)^2$ is the usual quasi-steady contribution whose second term is dropped in linear theories; $p_{01} = \rho \mathbf{V}_1 \cdot \nabla \phi_0 - \rho \nabla \phi_0 \cdot \nabla \phi_1$ is the quasi-steady-unsteady interaction part; $p_1 = -\rho (\partial \phi_1 / \partial t) + \rho \mathbf{V}_0 \cdot \nabla \phi_1$ is the usual first-order seakeeping contribution, and $p_2 = -\frac{1}{2} \rho (\nabla \phi_1)^2 + \rho \mathbf{V}_1 \cdot \nabla \phi_1$ is the pressure creating a part of the second-order seakeeping force, while another second-order contribution stems from the variability of the wetted hull surface over which the total pressure is integrated.

As the total hydrodynamic force \mathbf{F} and moment \mathbf{M} are linear functionals of the pressure distribution, they can be decomposed similarly to the pressure itself. The contribution of p_0 will not be considered further as it relates to the manoeuvring part of the forces accounted for outside the potential theory. Similarly, dropped is the part associated with the interaction pressure p_{01} as this part is neglected in most seakeeping theories and can only be important for fast vessels. The part related to p_2 can be essential in manoeuvring problems but is currently dropped for simplification purposes as it constitutes just a part of the second-order force.

The scalar product in the second term in the equation for p_1 can be represented as

$$\mathbf{V}_0 \cdot \nabla \phi_1 = V_{0\xi} \frac{\partial \phi_1}{\partial \xi} + (V_{0\eta} + \xi r_0) \frac{\partial \phi_1}{\partial \eta}, \quad (7)$$

where $V_{0\xi, \eta}$ are the ship velocities' projections in the semi-fixed axes.

The first term is present in normal seakeeping theories while the second term appears due to the more general character of the base motion. At present, there are reasons to neglect it as its contribution can only be expected to be

comparable to that by the first term at large local drift angles which can only happen in the low-speed manoeuvring when the term containing the local derivative $\partial \phi_1 / \partial t$ will dominate anyway. In addition, on a slender ship this contribution will be mainly compensated by the term $-\rho \nabla \phi_0 \cdot \nabla \phi_1$.

As $\phi_1 = \phi_r + \phi_w + \phi_d$, the force can be decomposed similarly and the radiation force is

$$F_r = \rho \int_S \frac{\partial \phi_r}{\partial t} n_F dS - \rho V_{0\xi} \int_S \frac{\partial \phi_r}{\partial \xi} n_F dS, \quad (8)$$

where n_F is the generalized projection of the normal \mathbf{n} .

Connection Between the Frequency Domain and the Time Domain. Considered is the Fourier image $\hat{\phi}(\omega)$ of the unsteady radiation potential $\phi(t)$ (all the spatial arguments are dropped). As a radiation force component $X_{ri}(t)$, $i=1, \dots, 6$ is represented as

$$X_{ri} = \rho \int_S \left(\frac{\partial}{\partial t} - V_{0\xi} \frac{\partial}{\partial \xi} \right) \phi_r n_i dS, \quad (9)$$

its Fourier image is

$$\hat{X}_{ri}(\omega) = i\omega \rho \int_S \hat{\phi}_r n_i dS - \rho V_{0\xi} \int_S \frac{\partial \hat{\phi}_r}{\partial \xi} n_i dS, \quad (10)$$

where the wetted surface S is supposed to be invariant or depending on the time parametrically so that this could be ignored in evaluating the Fourier transform.

Further, the Fourier transform of the radiation potential is expressed through the radiation functions $\hat{\phi}_1, \dots, \hat{\phi}_6$ and the complex amplitudes of the generalized velocities $\hat{U}_1, \dots, \hat{U}_6$ as $\hat{\phi}_r = \sum_{i=1}^6 \hat{\phi}_i \hat{U}_i$, where $\hat{U}_j = i\omega \hat{\xi}_j$, $j=1, 4, 5, 6$, $\hat{U}_2 = i\omega \hat{\xi}_2 - V_{0\xi} \hat{\xi}_6$, $\hat{U}_3 = i\omega \hat{\xi}_3 + V_{0\xi} \hat{\xi}_5$, and where $\hat{\xi}_j$ are the displacements' complex amplitudes.

Representation of the first-order force on a slender ship. According to the strip method, the radiation forces in the frequency domain are represented as

$$\begin{aligned}\hat{X}_{r5} &= -\int_{L'} \xi \hat{R}_3(\xi) d\xi, \\ \hat{X}_{r6} &= \int_{L'} \xi \hat{R}_2(\xi) d\xi,\end{aligned}\quad (11)$$

where the integration interval L' is the part of the ship's length depending on the force component and subcomponent in concern, and the transverse loading is:

$$\begin{aligned}\hat{R}_k &= -i\omega \sum_{\ell=2}^4 \hat{\mu}_{k\ell}(\xi) \hat{u}_\ell(\xi) \\ &+ V_{0\xi} \sum_{\ell=2}^4 \frac{\partial}{\partial \xi} [\hat{\mu}_{k\ell}(\xi) \hat{u}_\ell(\xi)], \quad k = 2, 3, 4.\end{aligned}\quad (12)$$

and where the sectional complex added masses are defined as usual through the complex potential distribution and the sectional generalized velocities are:

$$\begin{aligned}\hat{u}_2(\xi) &= \hat{U}_2 + \xi \hat{U}_6 - \frac{V_{0\xi}}{i\omega} \hat{U}_6, \\ \hat{u}_3(\xi) &= \hat{U}_3 - \xi \hat{U}_5 + \frac{V_{0\xi}}{i\omega} \hat{U}_5, \quad \hat{u}_4(\xi) \equiv \hat{U}_4.\end{aligned}\quad (13)$$

Then, the final relations for the radiation forces on a slender hull in the frequency domain will be

$$\hat{X}_{rj}(\omega) = \sum_{k=2}^6 \hat{A}_{jk}(\omega) \hat{U}_k(\omega), \quad j = 2, 3, \dots, 6, \quad (14)$$

where the complex amplitude functions are:

$$\begin{aligned}\hat{A}_{jk} &= -i\omega \hat{\mu}_{jk} + V_{0\xi} \hat{\bar{\mu}}_{jk}, \quad k = 2, 3, 4; \\ \hat{A}_{j5} &= -i\omega \hat{\mu}_{j5} + V_{0\xi} \hat{\bar{\mu}}_{j5} - 2V_{0\xi} \hat{\mu}_{j3} + \frac{V_{0\xi}^2}{i\omega} \hat{\bar{\mu}}_{j3}, \\ \hat{A}_{j6} &= -i\omega \hat{\mu}_{j6} + V_{0\xi} \hat{\bar{\mu}}_{j6} + 2V_{0\xi} \hat{\mu}_{j2} - \frac{V_{0\xi}^2}{i\omega} \hat{\bar{\mu}}_{j2},\end{aligned}\quad (15)$$

Here, the ship complex added masses $\hat{\mu}_{jk}(\omega)$ are obtained through appropriate weighted integration of the sectional complex added masses $\hat{\mu}_{r\ell}(\xi, \omega)$ over the entire ship length L while the quantities $\hat{\bar{\mu}}_{jk}(\omega)$ are obtained similarly but integrated are the derivatives $\partial \hat{\mu}_{r\ell} / \partial \xi$ along the reduced length L' .

These forces are transformed into the time domain by using the method of auxiliary state variables described by Sutulo & Guedes Soares (2005). The resulting model is still a set of ordinary differential equations though of a much higher order (over 200 in the present implementation).

Hydrostatic and Froude–Krylov forces. These forces can be easily computed with the only assumption of the absence of the water surface' deformation due to presence of the ship. In the current implementation, also the longitudinal curvature of the hull surface is neglected. As this force must be estimated with account for the actual wetted surface, the latter is found as the intersection of the entire hull positioned with actual instantaneous values of the heave, pitch and roll with the instantaneous water surface which is described as

$$\zeta_w = -a_w e^{i[\omega t + \Phi(t)]} e^{-ik[\xi \cos(\chi_{w0} - \psi) + \eta \sin(\chi_{w0} - \psi)]}, \quad (16)$$

where $\Phi = -k(\xi_{C0} \cos \chi_{w0} + \eta_{C0} \sin \chi_{w0})$ is the total wave phase and the real part is supposed to be taken. The wave profile at any ship section can be easily determined and this defines approximately the wetted surface at any given instant. The hydrostatic and Froude–Krylov forces $X_{hsk} + X_{wk}$ are then computed as follows:

$$\begin{aligned}X_{hsk} + X_{wk} &= -\rho g \int_S \zeta dS - \rho g a_w e^{i[\omega t + \Phi(t)]} \\ &\times \int_S e^{-k\xi - ik[\xi \cos(\chi_{w0} - \psi) + \eta \sin(\chi_{w0} - \psi)]} n_k dS.\end{aligned}\quad (17)$$

Diffraction forces. This part of the excitation forces is also evaluated under the assumption that

the wetted surface doesn't participate in the wave-induced motion although in the final formulae this assumption can be lifted. Then, in the frequency domain, the primary diffraction force representation is quite similar to that for the radiation potential.

After using the second Green identity, the boundary condition $(\partial\hat{\phi}_d/\partial n) = -(\partial\hat{\phi}_w/\partial n)$ on S for the diffraction potential, and the Tuck transformation (Salvesen et al., 1970), the following formulae for the Fourier images of the diffraction forces on a slender hull:

$$\begin{aligned}\hat{X}_{dk} &= \int_L f_{dk}^{(1)}(\xi) d\xi + f_{dk}^{(2)}(\xi_m), \quad i = 2, 3, 4; \\ \hat{X}_{d5} &= -\int_L f_{d3}^{(1)}(\xi) \xi d\xi - \int_{L'} f_{d3}^{(2)}(\xi) \xi d\xi \\ &\quad - \xi_m f_{d3}^{(2)}(\xi_m), \\ \hat{X}_{d5} &= \int_L f_{d2}^{(1)}(\xi) \xi d\xi + \int_{L'} f_{d2}^{(2)}(\xi) \xi d\xi \\ &\quad + \xi_m f_{d2}^{(2)}(\xi_m),\end{aligned}\quad (18)$$

where ξ_m is the last section corresponding to the end of the length L' , $f_{dk}^{(1)} = i\omega f_{dk}$, $f_{dk}^{(2)} = V_{0\xi} f_{dk}$, and

$$f_{dk} = -\rho\omega a_w e^{i\Phi} e^{-ik\xi \cos(\chi_w - \psi)} \cdot \int_C [n_2 \sin(\chi_w - \psi) - in_3] e^{-k\xi - ik\eta \sin(\chi_w - \psi)} \hat{\phi}_k dC, \quad (19)$$

where $\hat{\phi}_k$ are the two-dimensional radiation functions for each contour C . As within the linear theory at slowly varying base motion parameters, the diffraction force will vary in time almost harmonically i.e. with some slowly varying encounter frequency ω_e , the time domain representation of the diffraction forces will be

$$X_{dk}(t) = \hat{X}_{dk} e^{i\omega_e t} \quad (20)$$

The instantaneous encounter frequency is then estimated as

$$\omega_e = \omega - k(V_{0\xi} \cos \chi_w + V_{0\eta} \sin \chi_w). \quad (21)$$

2.4 Still-Water Manoeuvring Forces

Any suitable still-water manoeuvring mathematical model could be used as the base model for describing the ‘‘manoeuvring’’ contribution F_m . In this particular study, the well-known 4DOF model developed by Inoue et al. (1981) was preferred but the implementation of this model in the wave manoeuvring code had certain peculiarities.

Although the original model is 4DOF, all the hydrodynamic forces depend also on the ship's draught and trim. These two parameters can be assumed to be varying in course of the simulation and this transforms the model into an effectively 6DOF one.

Although the experiment-based yawing moment is dependent on the roll angle, this dependence is only valid for the roll angles not exceeding (or slightly exceeding) 10deg in absolute value. As extension of this range requires additional captive-model tests, in this implementation the regressions were simply extrapolated as constant limiting values.

The angle of attack of the rudder is computed with account for the wave-induced velocities.

3 NUMERICAL RESULTS

3.1 Ship Description

One of the well-known benchmark ships, namely the container ship S-175 was chosen for simulations. The ship's length between the perpendiculars is 175m, breadth 25.4m, draught 9.5m, mass (as estimated) 24571.25 tonnes. The centre of mass' elevation $KG = 9.52\text{m}$, the estimated transverse metacentric height $GM = 1.02\text{m}$, and the natural roll period is 18s. The body plan of the ship as described in the program's input is shown on Figure 1, with all the input vertices present. More details about the

vessel's particulars can be found in (ITTC, 1983).

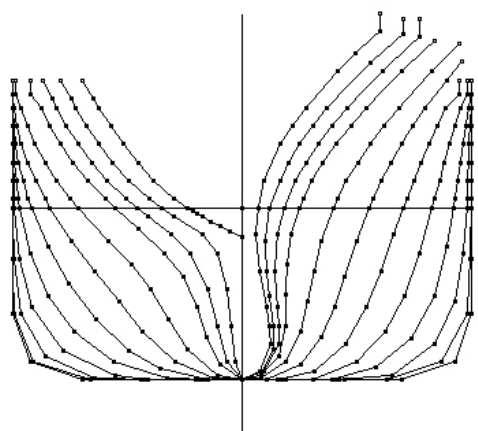


Figure 1 Ship body plan

The ship is directionally stable in still water though the stability margin is rather low. All the simulations were carried out with the approach speed of 15 knots although the design speed for this ship is equal to 22kn. The roll damping coefficient was assumed as recommended by (ITTC, 1983). The simulated decay curve is shown on Figure 2.

3.2 Results of Simulation

Sea Conditions. All simulations, except those in still water, were performed on regular beam seas (at least, at the approach phase) with the steepness $1/80$ and with three frequencies:

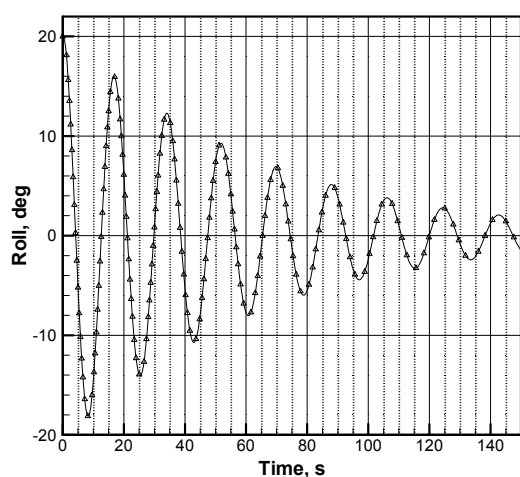


Figure 2 Roll decay curve

$0.35s^{-1}$ corresponding to the ship's natural frequency in roll, $0.292s^{-1}$ and $0.403s^{-1}$.

Constrained Straight Runs. Strictly straight runs were simulated to validate the code against the results available for this ship. Instead of using an autopilot, the ship was artificially constrained in heading and in the rate of yaw. Additional constraints were also tried for all the degrees of freedom except for the roll and surge but that did not change the roll output substantially. Truncated time histories for the three mentioned wave frequencies are presented on Figures 3 through 5. Further simulations did not reveal changes in the ship's behaviour. A good or reasonable agreement with the published amplitude data was found for roll (demonstrated below) as well as for other motions.

Free Straight Runs. Free runs with the rudder fixed in neutral position were simulated as well. In still water such simulation do not lead to interesting results as the ship keeps on the straight path for long, and are mainly used for checking purposes.

The situation changes dramatically in a seaway as an uncontrolled ship in still water and in absence of wind is never directionally asymptotically stable and can change her heading. In most cases, these changes are performed at a relatively low rate (except for the case of broaching not considered here) but under continuous action of the wave excitation forces the resulting trajectory becomes substantially curvilinear and periodic with the lowest harmonic's frequency much inferior to the instantaneous wave encounter frequency.

The time histories for the resonance case and the simulation time 50 minutes are presented on Figures 6 and a stretched 200s interval of the same process—on Figure 7. It is clearly seen that the wave-induced oscillations are modulated with a much lower frequency corresponding to the ship's spontaneous course performing a sequence of turns and a similar picture was observed with

the waves below and above resonance. However, all these cases correspond to significant although low-slope regular waves with the height varying from 4.7 to 9 meters and such behaviour doesn't seem impossible for a beam sea directed initially to the starboard.

Several simulations on lower-height waves resulted in trajectories without intersections i.e. the ship was meandering. However, in all the cases of spiralling or meandering, the ship in the mean was displacing straight, along some oblique virtual path.

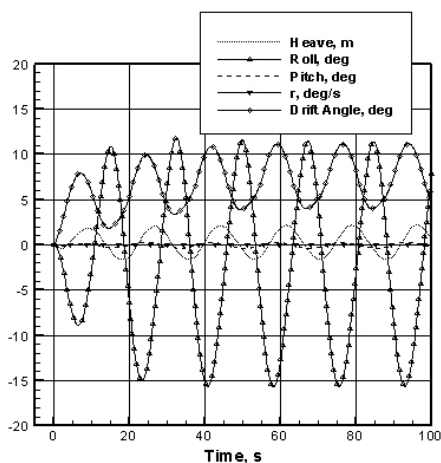


Figure 3 Constrained straight run time histories at the resonance wave frequency $\omega = 0.35$

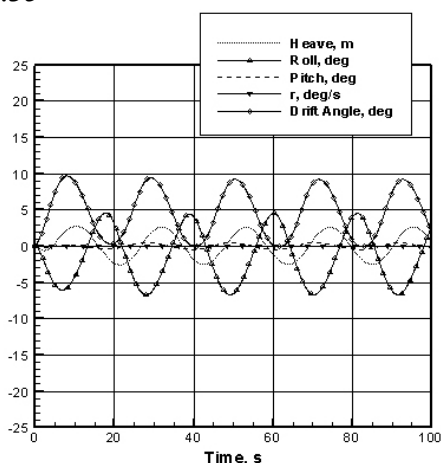


Figure 4 Constrained straight run time histories at $\omega = 0.292$

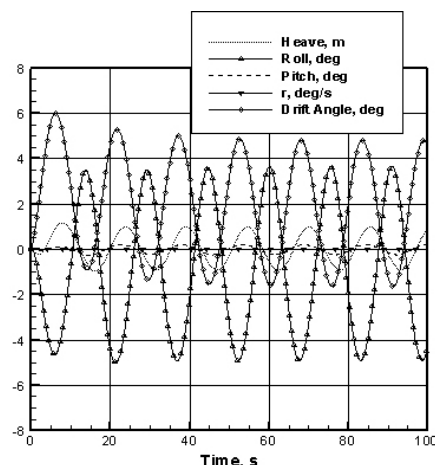


Figure 5 Constrained straight run time histories at $\omega = 0.403$

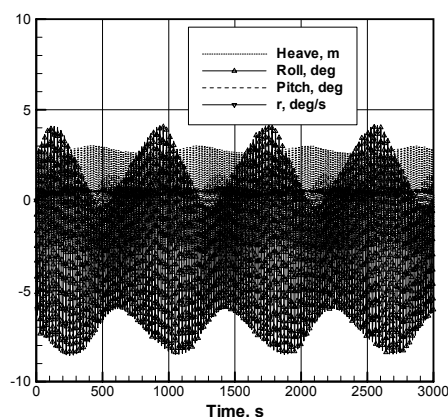


Figure 6 Free straight run time histories at $\omega = 0.35$

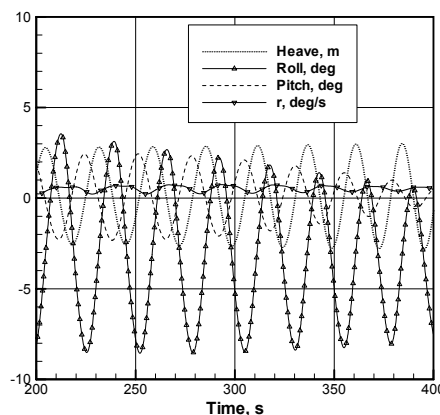


Figure 7 Free straight run: time histories at $\omega = 0.35$ (stretched)

In other words, the ship becomes in a certain sense directionally asymptotically stable in the

average while this can never happen in still water and in absence of wind. A somewhat similar result was obtained by Ananyev & Gorbachova (1993) through analysis of stability of the motion described by a linear equation of yaw with periodically varying coefficients. However, as the mathematical models are very different, it still cannot be stated with certainty that in the both cases the same phenomenon was traced.

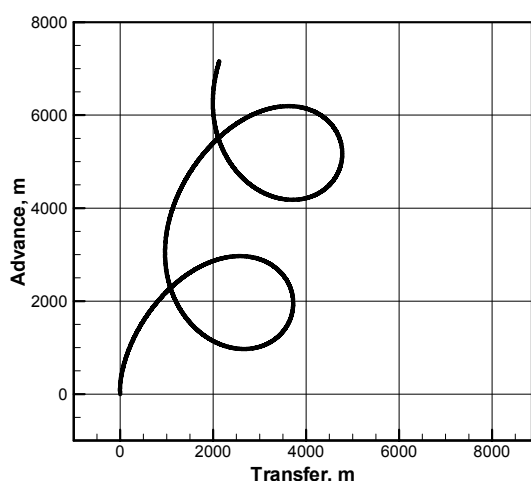


Figure 8 Free straight run trajectory at $\omega = 0.35$

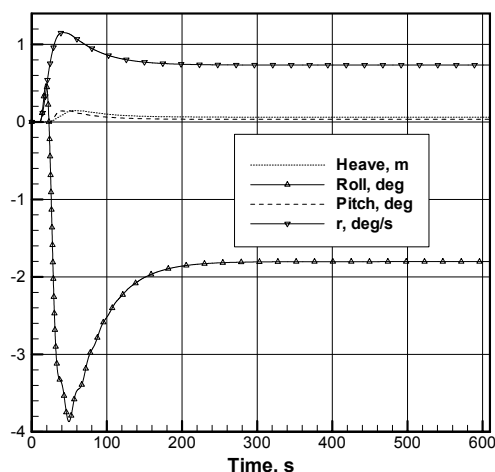


Figure 9 Turning manoeuvre: time histories in still water

Turning Manoeuvres. First, the turn with the 35 degrees helm was simulated in still water to reveal the roll triggered by the manoeuvre per se. Time histories for several kinematic parameters are shown on Figure 9. As usual, after a small yank inwards, the ship rolls outside the turn

reaching dynamically 4 degrees in this case but the steady turn for this relatively stable ship and low approach speed is less than two degrees.

Then, simulations of the same turn but on the roll-resonant regular waves were performed with different values of the manoeuvre delay time which is the time interval between the beginning of simulation and the start of the rudder's deflection. The minimum delay time was assumed to be 24s as judging from the straight run simulations, the rolling is practically developed by this time. Then the delay was varied with the 4.5s increment which was one quarter of the roll period.

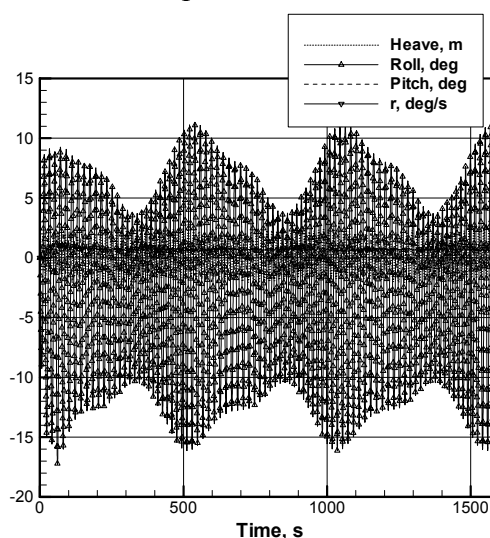


Figure 10 Turning manoeuvre: time histories at $\omega = 0.35$

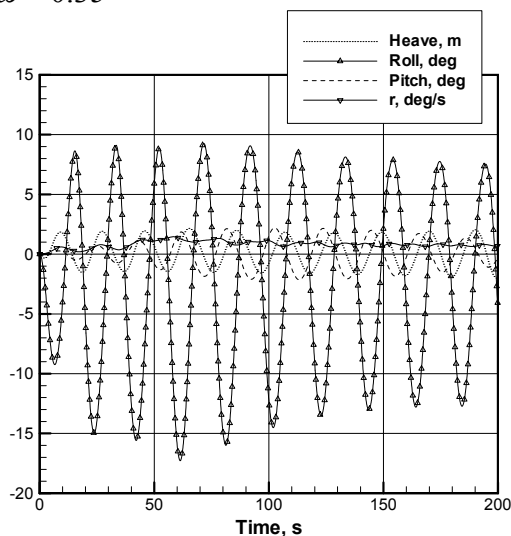


Figure 11 Turning manoeuvre: time histories at $\omega = 0.35$ (stretched).

As the largest observed absolute values of the instantaneous roll angle corresponded to the 33s delay, all the displayed results refer to this case.

The full time histories are shown on Figure 10 and their stretched cut-off—on Figure 11. Qualitatively, the general view of the time histories did not differ too much from the free straight runs case but the period is different and they show more asymmetry with respect to the zero-roll line. This is explained by tighter turns with the rudder's assistance (Figure 12).

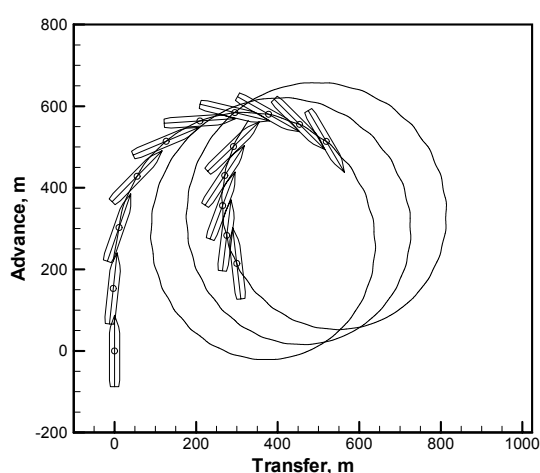


Figure 12 Turning manoeuvre: trajectory at $\omega = 0.35$; ship images are only shown for the initial and final phases of the simulation

3.3 Discussion of Results

As one of the main objectives of the present study was to check whether manoeuvring in waves is indeed a more dangerous regime than the straight run in beam seas, various numerical measures of the roll were extracted from the simulation outputs. These values are given in Table 1 together with the values of the roll amplitude obtained by different towing tanks and published by ITTC (1983).

The values of the amplitudes obtained with the present code in the constrained-run simulations agree well with the values obtained by other programs in the same conditions and this indicates credibility of further results referring to less typical situations.

It is seen from the table data that both the amplitudes and the maximum values are smaller in free straight runs than in the constrained runs representing the canonical seakeeping situation. This is likely due to a relatively short period of time when the ship is exposed to the least favourable conditions: the beam sea and the resonance (or close to resonance) effective encounter frequency. However, in 35deg turns the situation was different: the maximum reached roll angles and even amplitudes were higher than in the strictly straight run. This result, however, was not unexpected and is explained by the combined action of the seakeeping and manoeuvring moments.

Table 1: Numerical Measures of Roll

Measure	Conditions	Wave frequency, rad/s		
		0.292	0.35	0.40
(Maximum) Roll Amplitude	constrained straight run	5.75	12.5	5.0
	free straight run		6.5	
	ITTC data	4.5–6.3	10.8–14.6	3.4–6.1
	35deg helm turn		14.1	
Maximum Reached Values of Roll Angle	constrained straight run	6.0	15.5	4.4
	free straight run		8.5	
	35deg helm turn		17.2	

These results are considered as primary and still no search was made for the situation when the synergetic effect will be more pronounced. For instance, increase of the approach speed and reduction of the metacentric height will by all means lead to a much stronger effect of the tuning motion in rolling assessments. Using a turning manoeuvre instead of the straight run could have another advantage: this manoeuvre can be effectively executed without any artificial constraints, on the one hand but also without any automatic controller in the loop whose parameters can influence the resulting estimates.

4. CONCLUSIONS

Primary simulations of the roll motion of a displacement ship have been carried out with a manoeuvring-and-seakeeping code newly developed by the authors. Although these results are primary and the chosen simulation conditions were not the most characteristics in all the respects, certain conclusions can already be drawn. These are:

The roll motion in a turning manoeuvre in regular waves is modulated by some low frequency corresponding to the completion of the ship's full turn.

Qualitatively, the same behaviour is observed in the so-called free straight runs in waves i.e. when the rudder is fixed in the neutral position: the ship is in fact turning with some low rate approximately in the direction of the propagation of the waves.

The roll amplitudes did not differ much for all the three studied manoeuvres (constrained straight run, free straight run, turning manoeuvre).

Due to some roll asymmetry caused partly by the nonlinearity of the used model, and partly by the manoeuvring-originated forces, the attained absolute values of the roll angle are greater than the amplitude values.

The largest instantaneous absolute values of the roll were observed in the initial phase of the turning manoeuvre due to a synergy of the wave action and of roll moment due to manoeuvring.

Tight turns have certain advantages over the straight free runs as reference motion for the roll analysis with time-domain mathematical models.

5. ACKNOWLEDGMENTS

The first author was partly financed by The Portuguese Science and Technology Foundation

(Fundação da Ciência e Tecnologia), under the grant SFRH/BPD/8557/2002.

6. REFERENCES

- Ananyev, D.M. and Gorbachova, L.M., 1993, "Applied Problems of Ship Manoeuvring in Waves", Technical University for Fishing Publ., Kaliningrad, 151p. (in Russian).
- Ayaz, Z. and Vassalos, D., 2003, "Towards an Improved Mathematical Model for Ship Manoeuvring in Astern Seas", Proceedings of MARSIM'03, Kanazawa, Japan, August 25-28, pp. RC-14-1-RC-14-10.
- Belenky, V.L., Weems, K.,M., Liut, D., Shin, Y.S., 2003, "Nonlinear Roll with Water-on-Deck: Numerical Approach", Proc. of STAB'03: 8th International Conference on Stability of Ships and Ocean Vehicles, Madrid, Spain, pp. 59-79.
- Bailey, P.A., Price, W.G., Temarel, P., 1997, "A Unified Mathematical Model Describing the Manoeuvring of a Ship Travelling in a Seaway", Trans. RINA, pp. 131-149.
- ITTC, 1983, "Summary of Results Obtained with Computer Programs to Predict Ship Motions in Six Degree of Freedom and Related Responses", Report on 15th and 16th ITTC Seakeeping Committee Comparative Study on Ship Motion Program (1976-1981), 53p.
- Ottosson P. and Bystrom L., 1991, "Simulation of the Dynamics of a Ship Manoeuvring in Waves", SNAME Transactions, Vol. 99, pp. 281-298.
- Pawlowski, J. and Bass, D.W., 1991, "A Theoretical and Numerical Model of Ship Motions in Heavy Seas", SNAME Transactions, Vol. 99, pp. 319-352.
- Remez, V., 1985, "Dynamics of Curvilinear Motion of a Ship in Regular Seas", 5th National Congress on Theoretical and

Applied Mechanics and 14th Scientific and Methodological Seminar on Ship Hydrodynamics, Varna, Bulgaria, 23-29 September 1985, Proceedings, Vol. 1, pp. 2-1-2-7.

Salvesen, N., Tuck, E.O., Faltinsen, O.M., 1970, "Ship Motions and Sea Loads", SNAME Transactions, Vol. 78, pp. 250-287.

Sutulo, S., Guedes Soares, 2005, C. "An Implementation of the Method of Auxiliary State Variables for Solving Seakeeping Problems", International Shipbuilding Progress, Vol. 52, No. 4, pp. 363-390.

Trägårdh, P., 2003, "Roll Motion of Manoeuvring Ships", Proceedings of MARSIM'03, Kanazawa, Japan, August 25-28, pp. RC-9-1–RC-9-5.

Ships Dynamic on Wave-Breaking Condition

Yu.Nechaev, *State Marine Technical University, St.Petersburg, Russia*

A.Degtyarev, *Institute of High Performance computing and Information Systems,
St.-Petersburg, Russia*

O.Anischenko, *Institute of High Performance computing and Information Systems,
St.-Petersburg, Russia*

ABSTRACT

Features of ship stability modeling in wave-breaking conditions are discussed. Analysis includes comparison of modeling results based on two various hypotheses. S.N.Blagoveschensky and A.N.Kholodilin offered the first one. It considers dynamic process as a sudden ship inclination as a result of breaking wave impact. N.B.Sevastianov formulated the second hypothesis on the basis of physical modeling results obtained in various towing tanks. In this case dynamics is represented as a result of vessel heel appearance under action of hydrodynamic moment during development of impetuous drift from breaking wave impact. The modeling was carried out for the identical initial conditions.

Keywords: *competition principle, stability, breaking waves, on-board intelligent system*

1. INTRODUCTION

Great volume of calculations is carried out in onboard intelligent systems designed for ship's seaworthiness monitoring. They include processing and analysis of measuring information coming from measuring system, construction and analysis of mathematical models, estimation and forecast of considered situations, imitating modeling of vessel-environment interaction. The hierarchy of mathematical models is expressed with the help of the various interpretation graphs describing standard and extreme situations arising in practice. As one of such examples situations tree for description of dynamics interaction of vessel with environment in storm conditions is shown on fig.1. The diagram assumes construction of models structure describing loss of oscillation stability (capsizing) depending on wind and waves features and vessel orientation (see references).

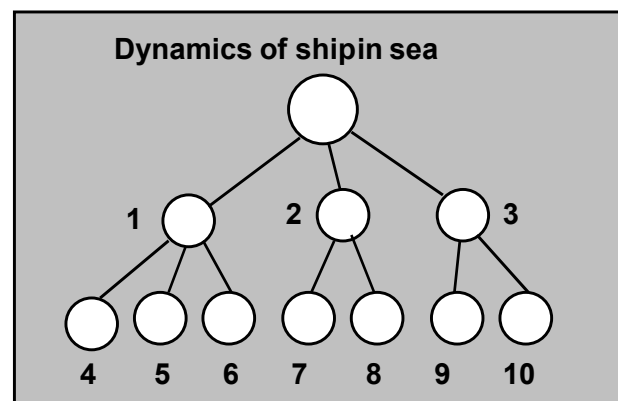


Figure 1. Decomposition tree of the system characterizing waves peculiarities and extreme situations of ship-environment interaction: 1 – random sea; 2 – breaking sea; 3 – extreme waves; 4 – pure loss of stability; 5 – resonance regimes; 6 – broaching; 7 – breaking waves in deep sea; 8 – breaking waves on shallow water; 9 – extreme wind waves; 10 – freak waves.

Methods of imitating modeling, statistical and fuzzy models (Nechaev, 2002, Intelligent systems, 2001) are applied for estimation and

forecasting of extreme situations development. With the help of such models estimation of environment parameters and vessel characteristics is conducted. The problem of filtration and forecast arises at processing of measured information in problems of prediction of dynamic characteristics and time intervals evolution determining critical conditions based on ship's safety. The classification problem (images recognition) is related with estimation of situation danger and also at realization of applied control problems and decision-making (analysis of alternatives, recognition of extreme situations, etc.). Realization of specified computing technology for seaworthiness estimation is carried out on the basis of competition principle (Nechaev, 2002) providing the comparative analysis of alternatives and a choice of the preferable decision, resulting by the shortest and more reliable way to estimation of safety of considered extreme situation

2. PROBLEM TO SOLVE

The built-in procedure based on comparison (within the framework of competition principle) of modeling results based on two various hypotheses is put in a basis of analysis of ship dynamics in breaking waves in onboard intelligent system (IS):

- hypothesis of S.N.Blagoveschensky and A.N.Kholodilin (Kholodilin, Shmyrev, 1976) considers dynamic process as sudden inclination of ship as a result of breaking wave action;
- hypothesis N.B.Sevastianov (Nechaev, 1989) is formulated on the basis of results of physical modeling of situations carried out in different towing tanks. It considers ship dynamics as a result of development of very fast drift from the kick off the breaking wave.

Initial conditions and acting forces in both cases are identical. However due to use of various models results of modeling appear various. In alternatives analysis the preference is always given to the model providing better

accuracy within the framework of accepted assumptions. Thus the mistake to dangerous side is not supposed, as modeling results are related with estimation of the major seakeeping qualities determining safety.

Mathematical description of situation in according with N.B.Sevastianov's hypothesis is given on the basis of differential equations system describing rolling and swaying (Nechaev, 1989), whereas within the framework of Blagoveshchensky-Kholodilin's hypothesis the only rolling differential equation (Kholodilin, Shmyrev, 1976) is used. Calculation of breaking waves elements is carried out on the basis of technique developed by B.V.Mirokhin (Kholodilin, Shmyrev, 1976).

Character of ship's inclination on breaking waves on shallow water and deep sea is practically identical. Difference is consist of only the following. Occurrence of extreme waves (which vertical sizes is more than height of vessel) of huge destructive force (freak wave) can appear in a deep sea. Getting in such sea zone with sharply changed form of a wave surface and complex hydrodynamic structure, the vessel is completely covered by the wave, involved in very fast drift and capsizes, exposing heeling loadings considerably exceeding external forces in usual operation conditions (Nechaev, 1989).

It is necessary to note, that small vessels are usually operated in a coastal zone. Waves formed on shallow water are commensurable with the vertical dimensions of such ships and sometimes surpass them. Breaking waves in a coastal zone represent terrible danger for navigation also because in this zone there can be a breakdown of large waves (for example, waves of tsunami).

3. PROPOSED ALGORITHM

3.1 Environment and considered object

Small fishing vessel is considered as the

object of investigation. It is known (Kholodilin, Shmyrev, 1976) that this ship was capsized by breaking wave.

Initial data for modeling:

- Average values of waves: height - $\bar{h}_w = 1,65m$; period - $\bar{\tau}_w = 6s$; length - $\bar{\lambda}_w = 56m$; average wave steepness - $\bar{\delta}^* = 0,03$.
- Ship characteristics (Table 1): main dimensions (length, beam, depth, draught in meters); displacement, GM, metacentric radius, z-coordinate of center of gravity, waterplane area coefficient, lateral area coefficient.
- Righting arm curve (fig.2).

Table 1: Ship Characteristics

Ship characteristics		
Max length of ship	19,4	(m)
Length between	18	(m)
Ship's beam	4,4	(m)
Depth	2,56	(m)
draught	1,57	(m)
Displacement	45,8	(t)
GM	0,86	(m)
Metacentric radius	4,68	(m)
Z-coordinate of center of	1,5	(m)
Waterplane area coefficient	0,8	
Lateral area coefficient	0,9	

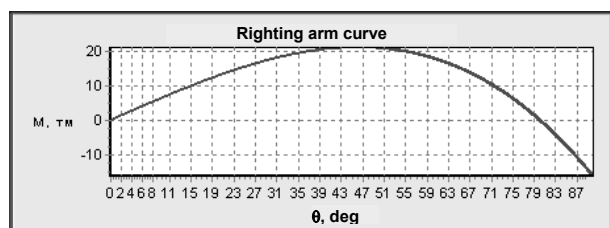


Figure 2. Form for initial data input (left) and righting arm curve (GM-curve) (right). Screenshot.

3.2 Forced impact of breaking waves

Power of breaking wave impact is

$$P_{\eta} = 1,2\lambda_{22}F_{1\max}. \quad (1)$$

where λ_{22} – added mass calculated by the following way:

$$\lambda_{22} = \lambda_{22mid}L \frac{2\beta_0^2}{1 + \beta_0},$$

β – lateral area coefficient; $\lambda_{22mid} = 0.5\pi\rho T^2$ – added mass of middle frame; $F_{1\max}$ – maximal value of acceleration in single wave (in accordance with diagram in work (Kholodilin, Shmyrev, 1976)).

Time of power impact action

$$t_y = \psi_1 \sqrt{H_c}, \quad (2)$$

where $\psi_1 = 0,76$ at relative wave height $\gamma = 0,8$ (with respect to depth), H_c – depth of sea under wave base.

Impact impulse

$$I_y = 0.5P_{\eta}t_y$$

Z-coordinate of wave impact center

$$z_y = 0.5\psi_2(T+h) \quad (3)$$

where h is minimal value of wave height or protected freeboard, $\psi_2 = 1,14$ at $\gamma = 0,8$.

Z-coordinate of ship's gravity center taking into account wave added masses:

$$z_{G1} = \frac{\frac{D}{g}z_G + \lambda_{22}z_{\lambda}}{\frac{D}{g} + \lambda_{22}}; \quad z_{\lambda} = T - \frac{\lambda_{24}}{\lambda_{22}}. \quad (4)$$

Value λ_{24} is determined in accordance with the following expression

$$\lambda_{24} = \lambda_{24mid}L \frac{1}{1-s^2} \left(\frac{2\alpha^2}{1+\alpha} - s^2 \right);$$

$$\lambda_{24mid} = \frac{\rho T^3}{2} \lambda_{yz};$$

where $s = 2T/B$; α – waterplane area coefficient; λ_{24mid} – static moment of added mass for

midship section.

For elliptic station

$$\lambda_{yz} = 1 - \frac{8}{3} \frac{p}{1+p}, \text{ where } p = T - 0.18.$$

Initial conditions and force impact in calculations of ship dynamics on breaking waves are considered as identical in comparative analysis.

3.3 Procedure based on Blagoveshchensky-Kholodilin approach

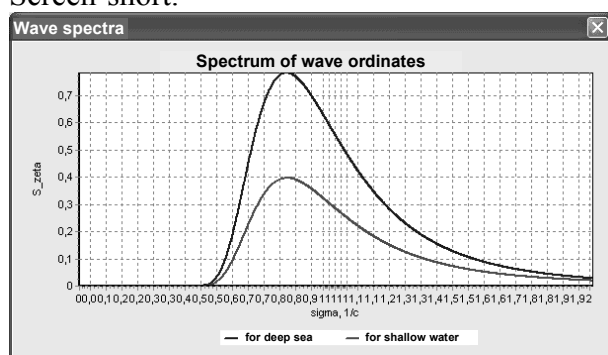
Wind waves parameters.

Deep water. Energy wave spectrum (fig.3):

$$S_{\zeta}(\sigma) = 1,78 \frac{D_{\zeta}}{\bar{\sigma}} \left(\frac{\sigma}{\bar{\sigma}} \right)^{-5} \exp \left[-0,44 \left(\frac{\sigma}{\bar{\sigma}} \right)^4 \right] \quad (5)$$

where $\bar{\sigma} = 2\pi/\bar{\tau}$ is average frequency, $D_{\zeta} = \bar{h}^2/6.25$ - variation

Fig. 3. Spectrum of wave ordinates for deep sea (blue (upper) line) and for shallow water in breaking waves zone (green (lower) line). Screen-short.



Shallow water (breaking waves zone). Clearly that it is hard problem to describe breaking waves and to develop model of such phenomenon. It is possible to propose description of energy spectra in zone from deep water to breaking waves region. There are some well-known approximations one of which is TMA spectrum. In procedure proposed by

S.N.Blagoveshchensky and A.N.Kholodilin spectrum of Yu.M.Krylov was used. He proposed to obtain energy spectrum for shallow water with the help of transfer function Π from ordinary spectrum for deep water (Krylov, 1966):

$$S_{\zeta_{sw}}(\sigma) = \Pi \left(\frac{\bar{\tau}_w}{\tau}, \frac{H}{\lambda_w}, \alpha \right) S_{\zeta}(\sigma)$$

$$\Pi \left(\frac{\bar{\tau}_w}{\tau}, \frac{H}{\lambda_w}, \alpha \right) = \frac{\int_{\alpha-\pi/2}^{\pi/2} \cos^2(\theta-\alpha) K_h^2 \left[\frac{H}{\lambda_w}, \frac{\bar{\tau}_w}{\tau}, \theta \right] d\theta}{\int_{\alpha-\pi/2}^{\pi/2} \cos^2(\theta-\alpha) d\theta} \quad (6)$$

$$K_h^2 = \frac{\cos \theta}{\sqrt{1 - \left(\frac{c}{c_0} \right)^2 \sin^2 \theta}} \left\{ \frac{c}{c_0} \left[1 + \left(\frac{4\pi H}{\lambda_0} / \frac{c}{c_0} \right) \sinh^{-1} \left(\frac{4\pi H}{\lambda_0} / \frac{c}{c_0} \right) \right] \right\}^{-1}$$

$$\frac{c}{c_0} = \tanh \left(\frac{2\pi H}{\lambda_0} / \frac{c}{c_0} \right); \quad \frac{H}{\lambda_0} = \frac{H}{\lambda_w} \left(\frac{\bar{\tau}_w}{\tau} \right)^2$$

where h_0 , c_0 , λ_0 are height, phase velocity and length of spectral component on deep water; h , c are the same for shallow water; H – depth, θ – the angle between wave crest and rectilinear isobaths, α – the angle between average direction of wave crests and rectilinear isobaths.

Transfer function. Calculation rolling transfer function is performed by the following way:

$$|\Phi_{s\theta}| = \frac{\sigma^2 \chi_{\theta} n_{\theta}^2}{g \sqrt{(n_{\theta}^2 - \sigma^2)^2 + 4\nu_{\theta}^2 \sigma^2}}, \quad (7)$$

where $\chi_{\theta} = 1 - \frac{2\pi\Gamma}{\lambda_{\theta}} \frac{r}{h}$ – reduction coefficient

taking into account finiteness of ship dimensions (calculated in accordance with Gerasimov's formula), $n_{\theta} = 2\pi/T_{\theta}$ – natural frequency of rolling, $\nu_{\theta} = 0,3(\omega_0)^{1/2}$ – linear coefficient of rolling damping, ω_0 – quadratic damping coefficient, λ_{θ} – wave length, r – metacentric radius, h – GM.

Natural rolling period is obtained by the formula $T_{\theta} = cB/\sqrt{h_0}$, where coefficient c is accepted as 0,80 — for deep water and 0,84 — for shallow water. Hence $\bar{\tau}_{\theta\kappa}/T_{\theta} \approx 1,8$. It

corresponds to negative impact phase of breaking wave.

Spectral density of rolling amplitudes and velocities (fig.4) are determined by the following way:

$$S_{\theta} = |\Phi_{\varepsilon\theta}|^2 S_{\varepsilon}; \quad S_{\dot{\theta}} = \sigma^2 S_{\theta}. \quad (8)$$

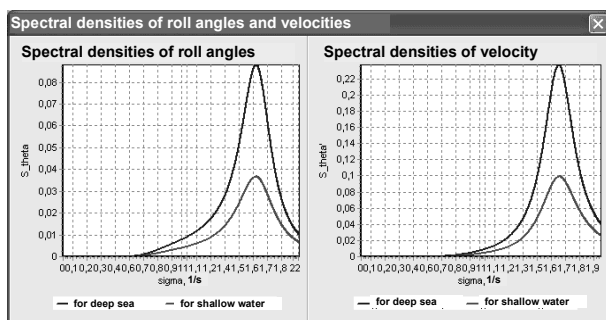


Fig.4. Spectral densities of roll angles and velocities for deep water (blue (upper) line) and shallow water (green (lower) line). Screenshot.

Ship motion. Variances D_{θ} and $D_{\dot{\theta}}$ are determined by the way of S_{θ} and $S_{\dot{\theta}}$ integration, rolling amplitude with 0.1% provision for deep and shallow water is

$$\theta_{0,1\%} = p\sqrt{D_{\theta}}, \quad (9)$$

where $p=3,7$ for 0.1%.

Calculated value of roll rate in the moment of breaking wave crest impact (taking into account roll decay):

$$\dot{\theta}_k = \dot{\theta}_{0,1\%} \exp(-n\nu T_{\theta}),$$

where n – the number of periods (for $\tau/T_{\theta} \approx 1,8$ $n=1$, for $\tau/T_{\theta} \approx 2,8$ $n=2$, etc.); T_{θ} – natural rolling period taking into account shallow water; ν – damping coefficient on shallow water.

Angular rolling velocity acquired in result of breaking wave action is,

$$\dot{\theta}_y = \frac{(z_y - z_{G1})I_y}{I_{1MB}}, \quad (10)$$

where $I_{1MB} = c^2 B^2 D / (4\pi^2)$ — moment of inertia of ship's mass relatively longitudinal axis.

Kinetic energy. Kinetic energy of rolling ship in wave impact moment is

$$K = \frac{(\dot{\theta}_k + \dot{\theta}_y)I_{1MB}}{2}. \quad (11)$$

Comparing kinetic energy with the storage of potential energy T_d , determined with the help of dynamic stability curve it is possible to determine whether ship stands simultaneous action of rolling and breaking wave impact.

3.4 Procedure based on approach of N.B.Sevastianov

The procedure consists of roll and sway differential equations integration (Belenky, Sevastianov, 2003; Nechaev, 1978; Nechaev, 1989):

$$(D/g + \mu_{\eta\eta})\eta'' + \lambda_{\eta\eta} \eta' + \lambda_{\eta\eta}^{**} (\eta')^2 = P(t); \quad (12)$$

$$(J_x + \mu_{\theta\theta})\theta'' + M_R(\theta') + M(\theta) = M_x(t) \quad (13)$$

where $D/g + \mu_{\eta\eta}$ – ship's mass with added mass; $J_x + \mu_{\theta\theta}$ – ship's inertia moment with added moment relative to longitudinal axes; $\lambda_{\eta\eta}^*$ and $\lambda_{\eta\eta}^{**}$ – coefficients of drift resistance for linear and quadratic terms; $M_R(\theta')$ – moment of damping forces; $M(\theta)$ – restoring moment; $M_x(t)$ – excitation moment inclusive of hydrodynamic forces of noninertial nature caused by drift.

Moment $M_x(t)$ acting on ship in drift conditions is characterized by expression

$$M_x(t) = [-P(t)z_p + Q_\eta z_q] \cos\theta - \mu_{\eta\theta}\eta, \quad (14)$$

where z_p – z-coordinate of origin of force caused by impact of breaking wave;

$$Q_\eta = (a_1 v + a_2 \eta) 0,5 \rho S_o \eta \quad (15)$$

is transverse horizontal noninertial force (a_1 and a_2 – coefficients determined by the experimental way, S_o – waterplane area.; z_q – z-coordinate of origin of force Q_η (for considered hull shape the value z_q significantly depends for roll angle and determined in accordance formula (Nechaev, 1989)); $\mu_{\eta\theta}$ – added static moment for the case of steady drift.

4. RESULTS OF MODELING

Results of modeling are shown on the fig.5-7 for three different situations describing interaction of ship with breaking wave. On these pictures characteristics obtained by using of Blagoveshchensky-Kholodilin procedure are shown at the left side, the same for Sevastianov's procedure are at the right side. In all cases the impact power is 25,47 tons. However the action time is different: for the first case (fig.5) it is equal to 2,3 s, for the second case (fig.6) it is equal to 1,24 s, and for the third (fig.7) – 1,19s.

Variation of impact time resulted in different characteristics of ship's dynamics. In particular variances of rolling are 0,0397; 0,0328; 0,0286 (rad²) – for deep water and 0,0196; 0,0158; 0,0135 (rad²) – for shallow water; variances of roll velocity 0,1057; 0,874; 0,761 (rad²/s²) – for deep water and 0,055; 0,0442; 0,0378 (rad²/s²) – for shallow water. Corresponding values of $\theta_{0,1\%}$ are 42,2°; 38,4°; 35,8° – for deep water and 29,7°; 26,6°; 24,7° –

for shallow water; $\dot{\theta}_{0,1\%}$ are 1,203; 1,094; 1,021 (rad/s) – for deep water and 0,868; 0,778; 0,719 (rad/s) – for shallow water.

Characteristics determining impact load of breaking wave are also changed:

- impact impulse 16,51; 15,74; 15,20 t·s;
- z-coordinate of center of gravity in the impact moment 2,44; 2,30; 2,21 m;
- ang. vel. after impact 1,31; 1,11; 0,98 s⁻¹.

Kinetic energy of oscillating ship at the moment of impact are equal correspondingly 23,75; 17,52; 14,03 t m, potential energy determining in accordance with dynamic stability curve in all cases is equal to 19,19 t m.

Comparative analysis of modeling results permits to propose the following conclusions:

- different interpretations of dynamics of “ship – breaking wave” interaction at the same initial conditions result in different stability parameters in such critical situation;
- taking into account drift influence originating at impact of breaking wave (hypothesis of N.B.Sevastianov) sometimes is more dangerous than dynamic inclination of ship in situation describing in frameworks of hypothesis of S.N.Blagoveshchensky and A.N.Kholodilin (see fig.6);
- detailed analysis of situation based on competitive principle is required for choosing of preferable computational technology for assessment of capsizing dangerous in breaking waves conditions. It permits to evenly assess stability and to increase efficiency of on-board decision support system providing navigation safety.

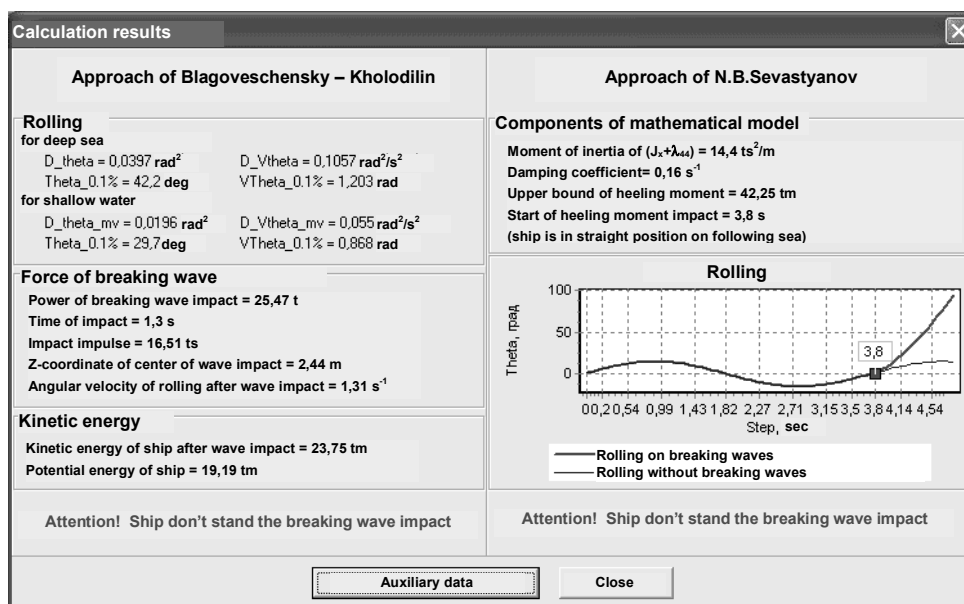


Fig.5. Modeling results. Impact time 1,3 s. Screen-short: results of approach of S.N.Blagoveshchensky and A.N.Kholodilin (left side) and approach of N.B.Sevastianov (right side).

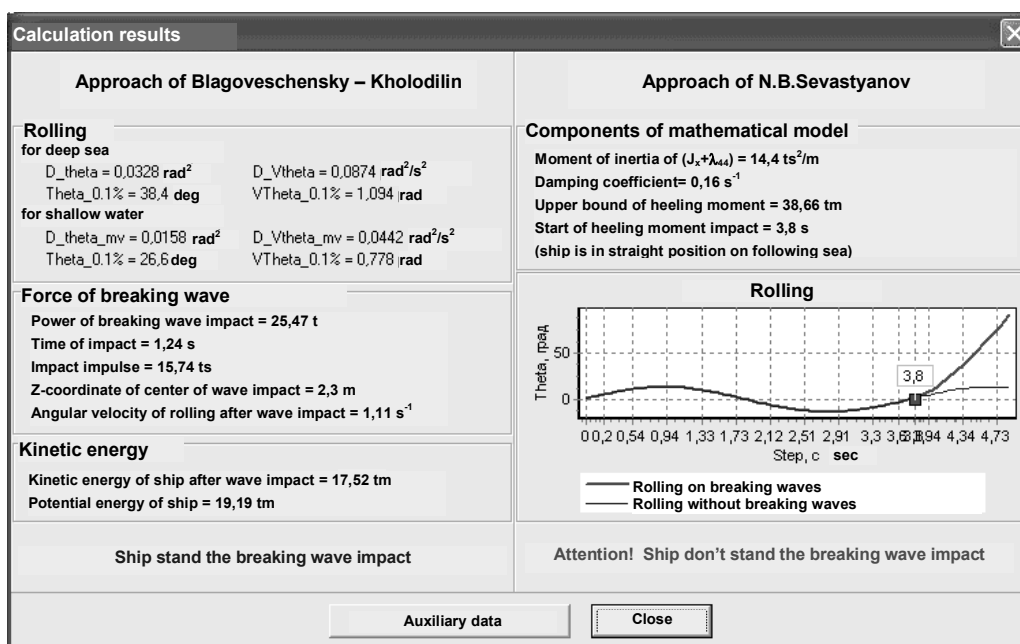


Fig.6. Modeling results. Impact time 1,24 s. Screen-short: results of approach of S.N.Blagoveshchensky and A.N.Kholodilin from the left side and approach of N.B.Sevastianov from the right side.

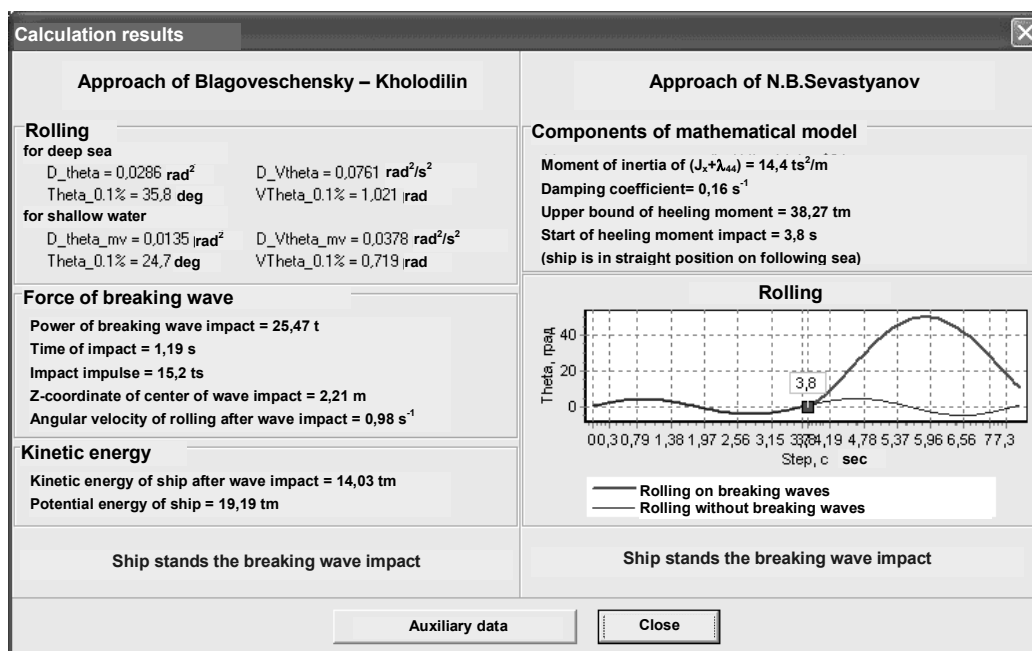


Fig.7. Modeling results. Impact time 1,19 s. Screen-short: results of approach of S.N.Blagoveshchensky and A.N.Kholodilin from the left side and approach of N.B.Sevastianov from the right side.

5. CONCLUSION

Results of carried out research show importance of competitive principle using for complicated situations analysis. Comparative analysis of different approaches, methods and models of “ship-environment” interaction in frameworks of competitive principle permits to determine more preferable computational technology that permits to obtain more reliable result. It is especially important in such situations when we have not strict theoretical models and construction of situations interpretation algorithms are based on different hypotheses. The problem of ship’s dynamics in breaking waves conditions has such characteristics in full measure. As it has seen from the analysis results attraction of physical mechanisms for algorithms construction permits to expand possibilities of the method and to carry out complete investigation of “ship-environment” interaction.

Considered approach has important sense for stability control at the board of the ship in operational conditions. It is possible “to play” different scenarios of situation development

and to present to navigator all necessary information for valid decision adoption on ship control in complex hydrometeorological situation with the help of on-board intelligent system.

6. REFERENCES

- Boroday I.K., Netsvetaev Yu.A., 1982. “Ship’s seaworthiness.” – Leningrad. Sudostroyenie. (in Russian)
- Belenky V.L., Sevastianov N.B., 2003. “Stability and safety of ships. Vol.II: Risk of Capsizing.” Elsevier Ocean Engineering Book Series, vol.10, Amsterdam
- Kholodilin A.N., Shmyrev A.N., 1976. “Seaworthiness and stabilization of ships on waves.” – Lenindrad. Sudostroyenie. (in Russian)
- Kobylynski L., Kastner S., 2003. “Stability and Safety of Ships. Vol. I: Regulation and Operation.” Elsevier Ocean Engineering Book Series, vol.9, Amsterdam
- Nechaev Yu.I., 1978. “Ship stability on

following waves.” – Leningrad.
Sudostroyeniye. (in Russian)

Nechaev Yu.I., 1989. “Modeling of ship stability on seaway. Modern tendencies”. – Leningrad. Sudostroyeniye. (in Russian)

Nechaev Yu.I., 2002. “Principle of competition at neural network technologies realization in on-board real-time intelligence systems” //Proc. of First international congress on mechanical and electrical engineering and technology «MEET-2002» and Fourth international conference on marine industry «MARIND-2002».Vol.3. Varna. Bulgaria, p.p.51-57.

“Intelligence systems in marine research and technologies,” 2001. //Ed. by Yu.I.Nechaev. SMTU. (in Russian)

Pauling J., Kastner S., Schaffran S., 1973. “Experimental studies of capsizing of intact ships in heavy seas” // IMO. STAB-7, p.54.

Krylov Yu.M., 1966. “Spectral methods for research and wind waves calculation.” Leningrad, Hydrometizdat (in Russian)

Beam Seas Tests of Two Different Ship Models in Large Amplitude Regular Waves

Angelo Olivieri, *INSEAN (Italian ship model basin), Via di Vallerano 139, 00128 Roma, Italy*

Emilio F. Campana, *INSEAN (Italian ship model basin), Via di Vallerano 139, 00128 Roma, Italy*

Alberto Francescutto, *University of Trieste, Trieste, Italy*

Fred Stern, *IIHR Hydroscience & Engineering, The University of Iowa, Iowa City, IA, 52242, USA*

ABSTRACT

The purpose of the paper is the study of the extreme ship motions through properly designed experiments aimed at both fundamental physical understanding and at collecting high-quality data for CFD codes validation. Two different ship models have been tested in regular beam waves to obtain repeatable data for time histories of measured motions, forces and moments. The tested models are geosyms of the DTMB model 5415 (INSEAN model 2385) and of the ONR Tumblehome (INSEAN model 2498), which are preliminary designs of surface combatants ca. 1980 and present time. The same scale has been adopted for both models ($\lambda = 46.6$). Models have been both equipped with bilge keels. The adopted test conditions are free heave and roll, whereas the other degrees of freedom are constrained. Forces and moments have been acquired for the restrained motions. Two series of five repeated tests have been carried out, with medium and large wave amplitudes at the resonant frequency for both models. The precision limit (PI) for all variables has been evaluated.

Keywords: *semicaptive tests, repeated tests, certified experimental data.*

1. INTRODUCTION

The problem of the certification of the safety of a ship is nowadays the more important aim to be achieved in the ship design. The prediction of the unsafe conditions for a ship in rough seas is still committed to hydrostatic calculations and the stability criteria present lack of clarity and sometimes logic in regulation systems throughout the world (Rojas and Belenky, 2003).

More recent works on capsizing have been conducted mainly on fishing vessels, cargo and container ships using potential hydrodynamics with the development of nonlinear seakeeping simulation codes such as, FREDYN, DINMA,

SIMBEL, MD2004 (24th ITTC, 2005). Nevertheless, the adopted mathematical models for the capsizing description vary very much between different research groups and the prediction of extreme motions just in few cases and only qualitatively matches the experimental results. Moreover, the mathematical models for capsizing involve a number of factors without clear guidance in place on which of these should be taken into account.

At present, there is still a lack in the understanding of physical phenomena involved in capsizing and, even more important, there is a regulation system that is often not clear in settling universal stability criteria.

On the experimental side, the free running tests reproduce, at least qualitatively, the real scenario, but the obtained results are affected by many factors and often they are not repeatable. Oppositely, the captive tests can give repeatable and certifiable experimental results, but they provide information only for forces and moments, being all the ship motions restrained.

The recent improvements of the unsteady RANS codes for the pitch and heave and for the roll motion predictions (Wilson, Carrica and Stern, 2006) allow us to nominate these solvers as good candidates in order to approach the ships capsizing problem, but for this purpose, they have to be validated by comparison with experimental results obtained by properly designed experiments.

As underlined, the free running tests cannot be used to build a database of certified experimental results provided with uncertainty assessment, whereas the captive tests do not give information on the ship motions. Hence, properly designed experiments have to be performed in order to give reliable information for testing the numerical codes.

Objective of the present work is to perform a series of repeatable experiments in semicaptive conditions (2 DoF) in order to collect an experimental database to be used as benchmark for unsteady RANS codes or other numerical solvers. The semicaptive conditions have been chosen in order to obtain repeatable tests and, at the same time, verify the capability of the numerical solvers in predicting large amplitude motions. Furthermore, the tests have been carried out for two different hull forms, which are geosyms of the DTMB model 5415 (INSEAN model 2385) and of the ONR Tumblehome (INSEAN model 2498) and the results have been compared, showing interesting differences between them.

The tests have been performed in the same conditions and the model scales are the same ($\lambda_{2385} = \lambda_{2498} = 46.6$). The tests have been done

in regular large amplitude beam waves. The allowed motions are roll and heave, while for the constrained DoF, forces and moments have been acquired. The results presented here represent a part of a wider project sponsored by ONR. The whole project includes head seas and following seas test, which are currently in progress.

2. MODELS AND TESTS DESCRIPTION

The two tested hull forms are geosyms of the DTMB model 5415 (INSEAN model 2385) and of the ONR Tumblehome (INSEAN model 2498). The two models are in the same scale ($\lambda = \lambda_{2385} = \lambda_{2498} = 46.6$) and are both equipped with bilge keels. They have been tested in the INSEAN basin n. 2 (220 m long, 9 m wide and 3.5 m deep), which is equipped with a flap wave maker at the basin end. The tests on the two models have been carried out using the same experimental apparatus. Beam seas tests have been performed at the resonant frequency, which has been determined exciting the models with small amplitude waves. During the tests the models have been disposed normally to the generated wave front, in the center of the basin in length and width. The models were free to roll and heave, with the other DoF restrained. For the restrained motions the forces and moments at the constraint have been measured. Three different wave slopes have been adopted, corresponding to small amplitude ($ak \approx 0.035$), medium amplitude ($ak = 0.073$) and large amplitude waves ($ak = 0.156$), in order to evaluate the rising and development of the nonlinearities in the allowed motions and in the measured forces and moments. The wave height has been measured by a servomechanic probe (Kenek SH) mounted 1 model length upstream the tested model. The lines of the two tested models are shown in figures 1 and 2, while the main model parameters are given in tables 1 and 2. The bilge keels profiles and locations are shown in figures 3, 4 and 5. The DTMB model 5415 (INSEAN 2385, fig. 6) is 3.048 m long, while the ONR Tumblehome (INSEAN 2498, fig. 7) is 3.305 m (L_{pp}).

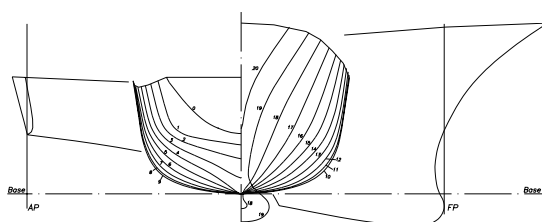


Figure 1: DTMB 5415 lines, bow and stern profiles

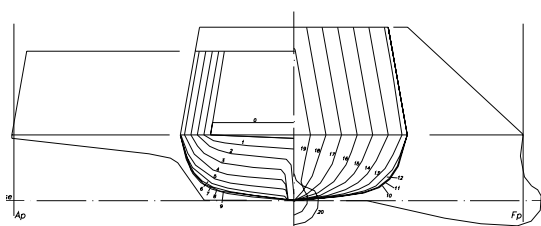


Figure 2: ONR Tumblehome lines, bow and stern profiles

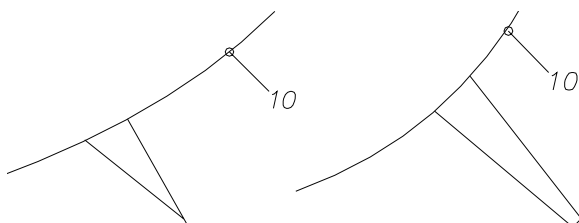


Figure 3: DTMB 5415 (left) and ONR Tumblehome (right) bilge keels profiles at midship

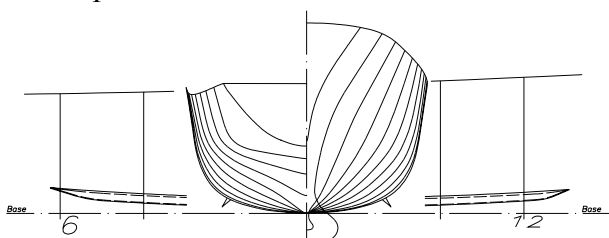


Figure 4: DTMB 5415 bilge keels: longitudinal extent and position

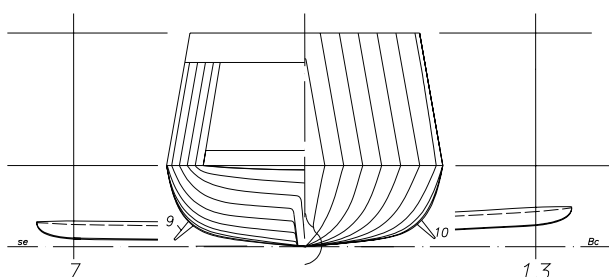


Figure 5: ONR Tumblehome bilge keels: longitudinal extent and position

The heave and roll motions have been measured by means of optical motion tracker

(Krypton), while the sway and surge forces have been measured by load cells which have been lodged inside a joint (figure 8) fixed to the model in correspondence of the center of gravity (CG). The pitch moment has been measured by a load cell mounted 100 mm upstream the CG, while the yaw moment has been measured by a torque cell. The torque cell connects the joint to a vertical bar, which is free to slide into a cylindrical guide fixed to the carriage. The yaw motion is inhibited by an additional guide that moves parallel to the vertical bar and rigidly fixed to it. The additional guide is mounted with 200 mm arm with respect to a vertical line passing through the CG. The same set of load cells and the same torque cell have been used for both models.

Table 1: main parameters of the DTMB 5415 (INSEAN model 2385)

DTMB 5415 ($\lambda = 46.6$)	
L_{pp}	3.048 m
Draft (T)	0.132 m
Beam (BWL)	0.406 m
Displ. (V)	0.083 m ³
LC_G	1.550 m (Aft of FP)
KG	0.162 m
GM_T	0.044 m
K_{XX}	0.162 m (40% BWL)
$K_{YY} = K_{ZZ}$	0.762 m (25% LPP)
Bilge Keels	c = 19.55 mm L = 1015 mm

Table 2: main parameters of the ONR Tumblehome (INSEAN model 2498)

ONR Tumblehome ($\lambda = 46.6$)	
L_{pp}	3.305 m
Draft (T)	0.118 m
Beam (BWL)	0.403 m
Displ. (V)	0.087 m ³
LC_G	1.708 m (Aft of FP)
KG	0.165 m
GM_T	0.043 m
K_{XX}	0.153 m (38% BWL)
$K_{YY} = K_{ZZ}$	0.826 m (25% LPP)
Bilge Keels	c = 33.55 mm L = 1098 mm

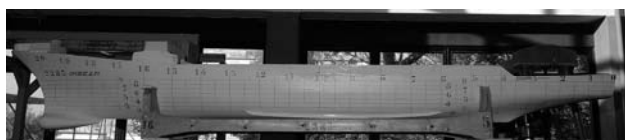


Figure 6: INSEAN model 2385, geosym of the DTMB 5415



Figure 7: INSEAN model 2498, geosym of the ONR Tumblehome

The smallest adopted wave slope was $ak = 0.036$ for the 2385 and $ak = 0.034$ for the 2498, while the medium and the highest wave slopes were $ak = 0.073$ and $ak = 0.156$ for both models. The medium and high wave slope tests have been repeated five times and the precision limit has been determined.

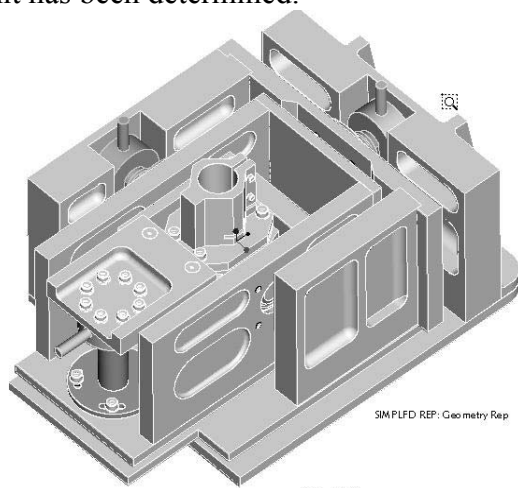


Figure 8: Illustration of the joint; the torque cell has been mounted on the top.

3. RESULTS

As a first step, the resonant frequency for small amplitude waves has been determined for both models, exciting them by a series of regular wavetrains with different frequencies. The obtained resonant frequency for the 2385 is $f_{2385} = 0.675$ Hz, while for the 2498 is $f_{2498} = 0.650$ Hz. Curiously, for both models this corresponds to a ratio between wavelength of the exciting waves and model length $\lambda/L_{PP} = 1.12$.

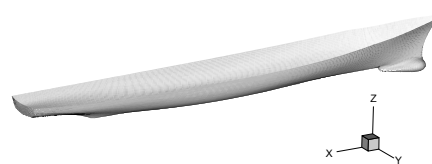


Figure 9: DTMB 5415 coordinate system with origin on the center of gravity; the same coordinates are used for the ONR Tumblehome

From every set of five repeated tests the phase locked average has been determined for all the measured variables. The results are presented in terms of averaged time histories, Fourier transform, combined plots and phase diagrams. The amplitude of the motions and forces and moment, determined as half a difference between minimum and maximum has been plotted as function of the wave slope.

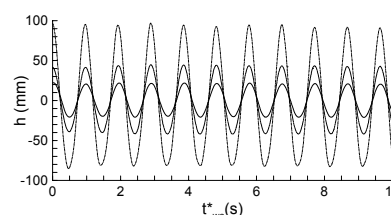


Figure 10: Wave height time histories for the three cases analyzed for the DTMB 5415; the time is normalized by the resonant frequency $f = 0.675$ Hz

Figure 9 shows the adopted coordinate system, which has the origin at the center of gravity for both models. In figure 10 the wave height time histories for the three adopted wave slopes are shown for the DTMB 5415.

In the present paper, only the main points of the experimental campaign are described, while the complete set of figures with time histories, Fourier analysis, combined plots and phase diagrams of all variables is shown in (Olivieri, Campana, Francescutto and Stern, 2006).

3.1 DTMB model 5415 results (INSEAN model 2385)

The heave motion follows almost perfectly the wave height for all three cases and the roll motion shows no evidence of nonlinearities

(figures 11 and 12). In figure 13 the heave amplitude $\|Z_G\|$ is shown as a function of the wave height amplitude $\|h\|$ together with the roll amplitude $\|\phi^\circ\|$ versus the nominal wave slope ak . For a general variable x :

$$\|x\| = \frac{x_{\max} - x_{\min}}{2} \tag{1}$$

The heave amplitude is proportional to the wave height, while the roll motion saturates for the highest wave slope.

Nonlinear behavior is shown by the axial force R_X and pitch moment M_Y , whereas the yaw moment M_Z shows no evidence of nonlinearities. The side force R_Y manifests a peculiar shape of the time history, but does not show any evidence of nonlinearities as confirmed by the Fourier analysis (figure 21).

The time histories for R_X , R_Y and M_Y for the three cases are shown in figures 14, 15 and 16 respectively.

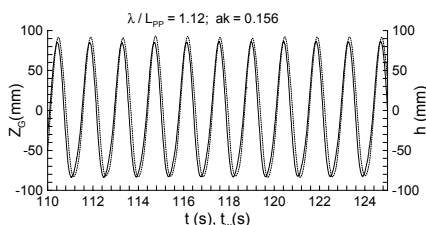


Figure 11: Heave motion (solid line) and wave height (dashed line) time histories for the DTMB 5415, $ak = 0.156$; the wave height is shifted in time the using the linear approximation for the wave celerity.

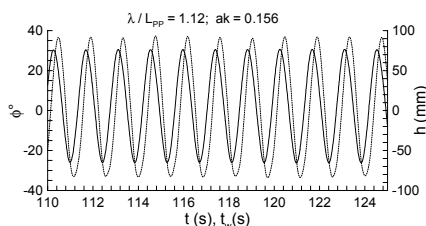


Figure 12: Roll motion (solid line) and wave height (dashed line) time histories for the DTMB 5415, $ak = 0.156$; the wave height is shifted in time the using the linear approximation for the wave celerity.

The period of the R_X time history is 1/4 of the wave period even for small amplitude waves, while the time history of the side force R_Y presents a complex shape without a presence of 2nd or higher harmonics. The pitch moment time histories show the rising of the second harmonic for all three cases.

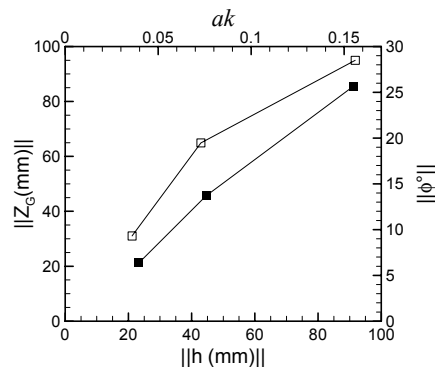


Figure 13: Heave amplitude $\|Z_G\|$ vs. wave height amplitude $\|h\|$ (filled symbols) and roll amplitude $\|\phi^\circ\|$ (open symbols) vs. the nominal wave slope ak .

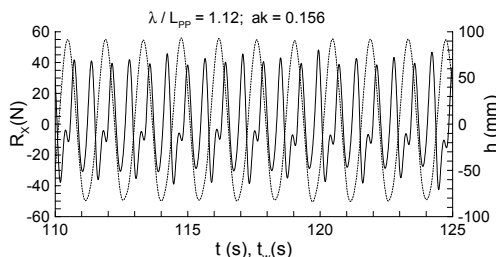
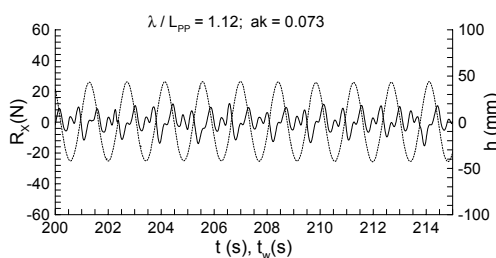
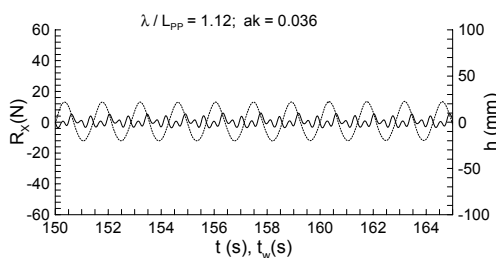


Figure 14: Time histories of the axial force R_X for small, medium and large amplitude waves (solid lines) superimposed to the time histories of the wave elevation (dashed lines)

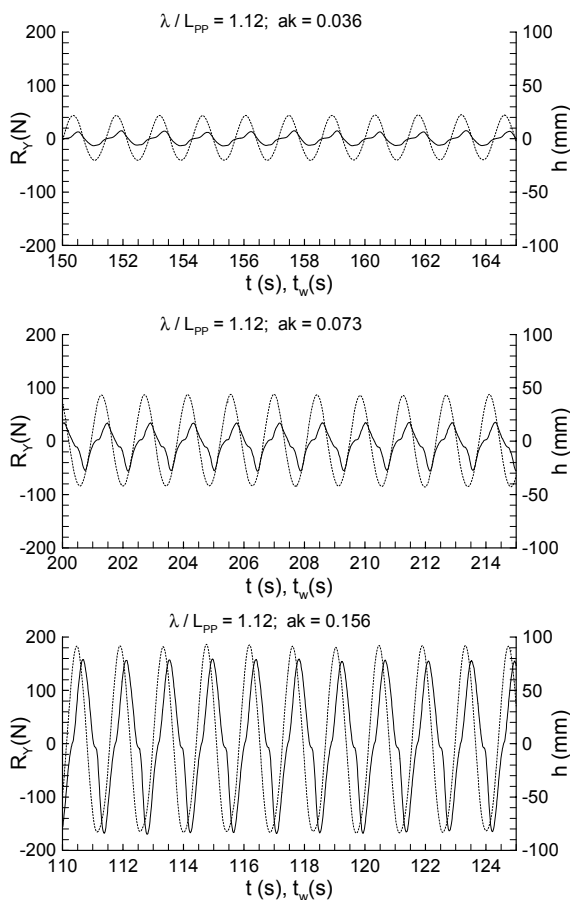


Figure 15: Time histories of the side force R_Y for small, medium and large amplitude waves (solid lines) superimposed to the time histories of the wave elevation (dashed lines)

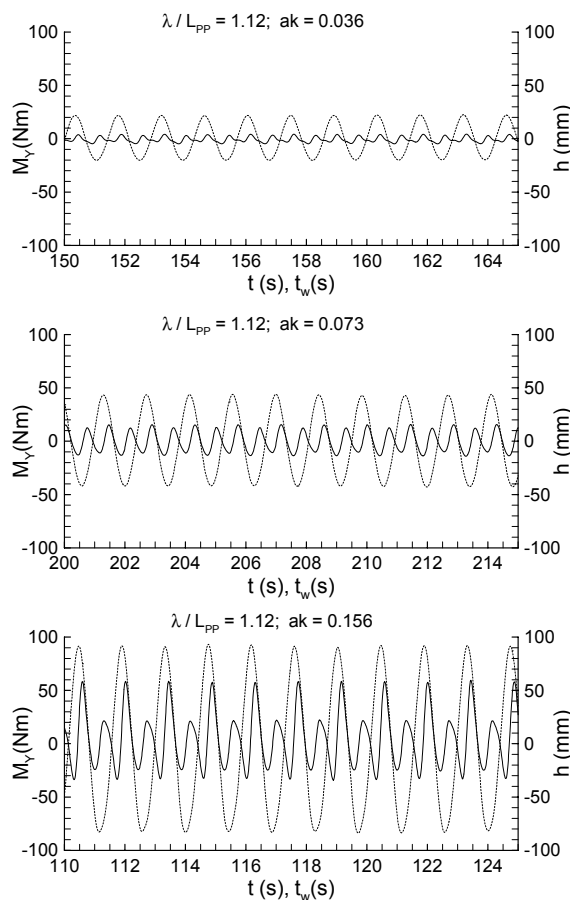


Figure 16: Time histories of the pitch moment M_Y for small, medium and large amplitude waves (solid lines) superimposed to the time histories of the wave elevation (dashed lines)

The amplitude functions of the wave height and heave motion show the presence of a very small superharmonic (figures 17 and 18), while the roll motion does not show any presence of superharmonics (figure 19). The amplitude function of the axial force is shown in figure 20 for all three wave slopes. It is noticeable that for the small wave slope the fourth harmonic dominates, while increasing the wave amplitude the second harmonic becomes leading. The side force and the pitch moment show the same trends of the amplitude function for all tested wave slopes; the results related to $ak = 0.156$ are reported in figures 21 and 22. It is evident that the side force is dominated by the fundamental frequency ($f_{2385} = 0.675$ Hz), while the pitch moment is dominated by the 2nd harmonic, although the fundamental and the 3rd harmonic are not negligible.

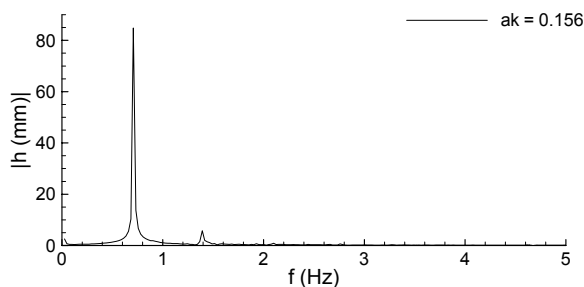


Figure 17: Amplitude function of the wave height h ($ak = 0.156$).

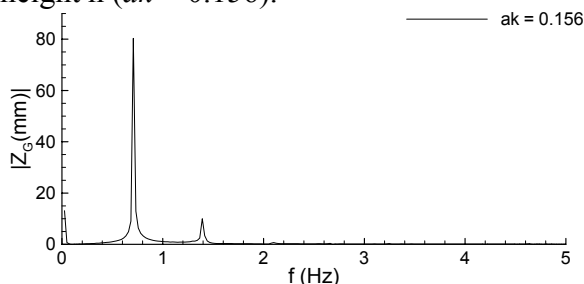


Figure 18: Amplitude function of the heave motion Z_G ($ak = 0.156$).

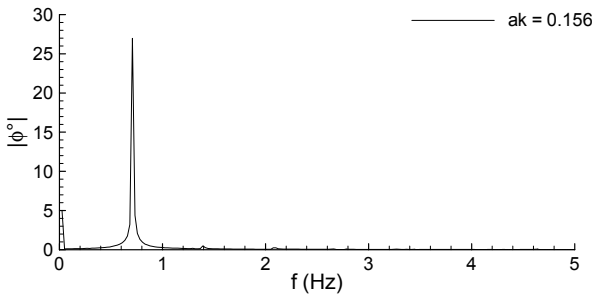


Figure 19: Amplitude function of the roll motion ϕ ($ak = 0.156$).

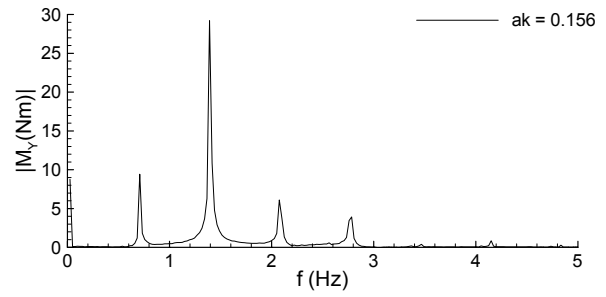


Figure 22: Amplitude function of the pitch moment M_Y for the large amplitude waves.

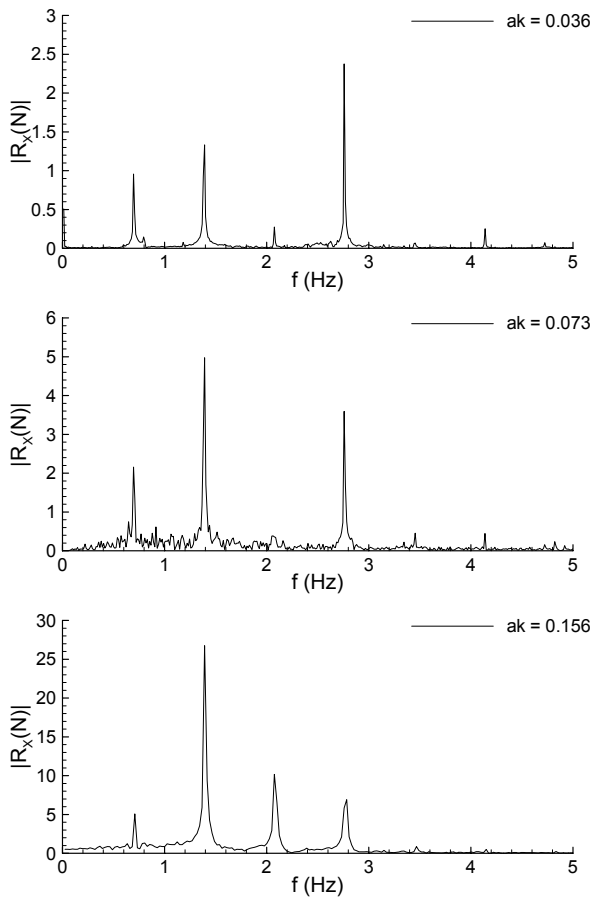


Figure 20: Amplitude function of the axial force R_X for small, medium and large amplitude waves.

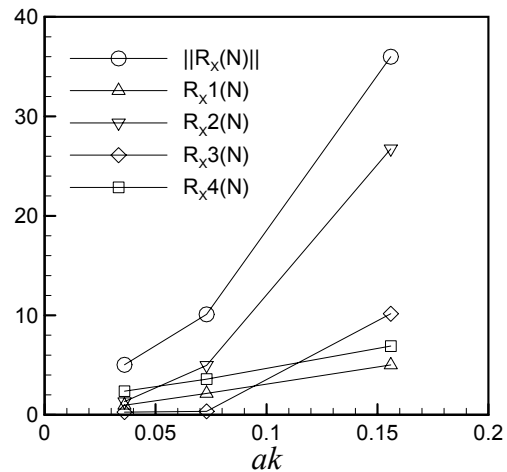


Figure 23 a: Amplitude of the axial force R_X versus the wave slope: total and first four harmonics.

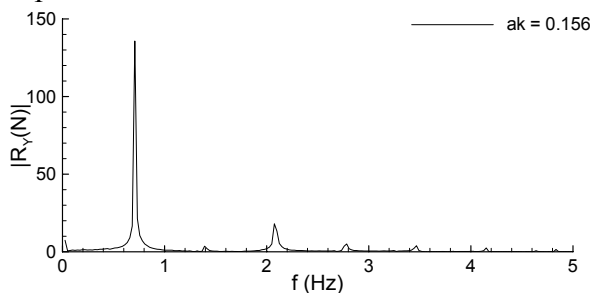


Figure 21: Amplitude function of the side force R_Y for the large amplitude waves.

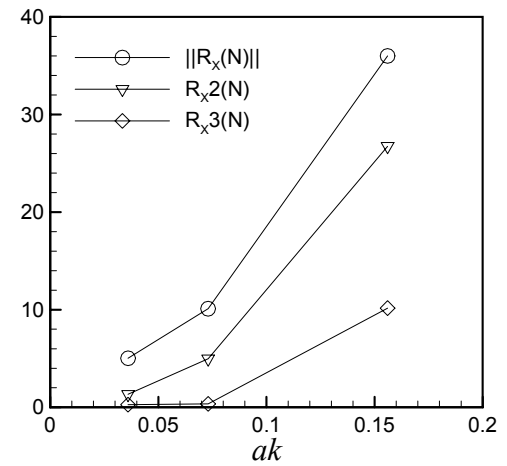


Figure 23 b: Amplitude of the axial force R_X versus the wave slope: total and 2nd and 3rd harmonic.

In figures 23 (a, b, c) the amplitude of the axial force $\|R_X\|$ defined by (1) is plotted together with the amplitudes of its first four harmonics (R_{X1} , R_{X2} , R_{X3} , R_{X4}) versus the wave slope. It is interesting to notice that the trend of the total amplitude is determined by the 2nd and 3rd harmonic, while the 4th

harmonic, which is dominant for the small amplitude waves, do not increase significantly with ak . Other remarkable feature is the linear increase of the fundamental R_{X1} with the wave slope, as shown in figure 23 c.

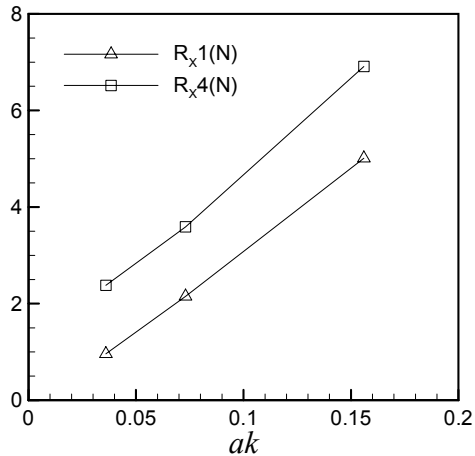


Figure 23 c: Amplitude of the axial force RX versus the wave slope: 1st and 4th harmonics.

In figure 24 the amplitude of the pitch moment $\|M_Y\|$ defined by (1) is plotted together with the amplitudes of its first three harmonics (M_{Y1}, M_{Y2}, M_{Y3}) versus the wave slope, while in figure 25 the amplitudes of the side force $\|R_Y\|$ and yaw moment $\|M_Z\|$ are plotted as a function of the wave slope. The yaw moment show a linear trend up to $ak = 0.073$, whereas it saturates for $ak = 0.156$. The three points related to the side force amplitude, seems to be aligned each other, but the line passing through them does not cross the origin, so that the trend with ak is nonlinear.

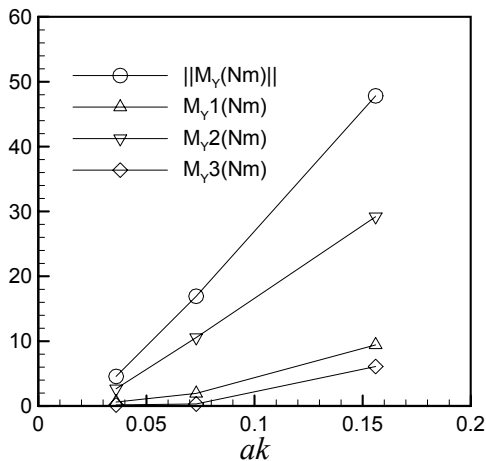


Figure 24: Amplitude of the pitch moment MY versus the wave slope: total and first three harmonics.

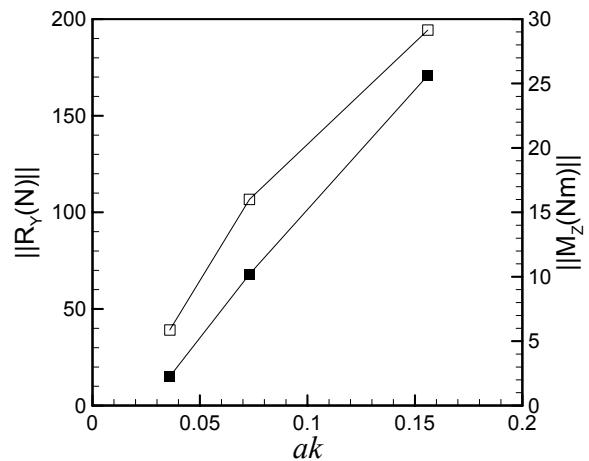


Figure 25: Amplitude of the side force RY (filled symbols) and yaw moment MZ (open symbols) versus the wave slope.

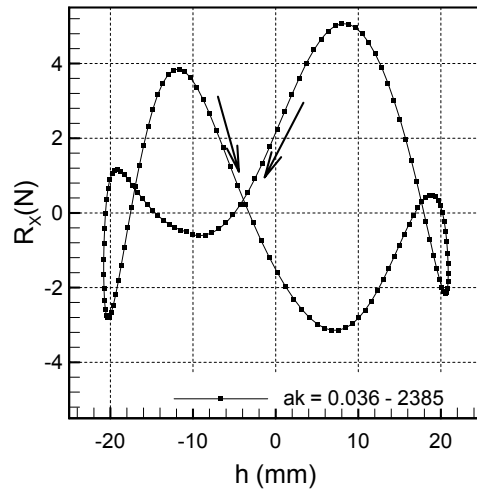


Figure 26: Combined plot of the axial force R_X versus the wave height (small amplitude waves).

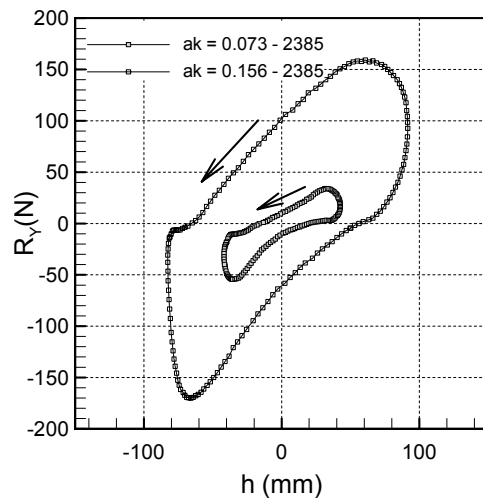


Figure 27: Combined plot of the side force RY versus the wave height.

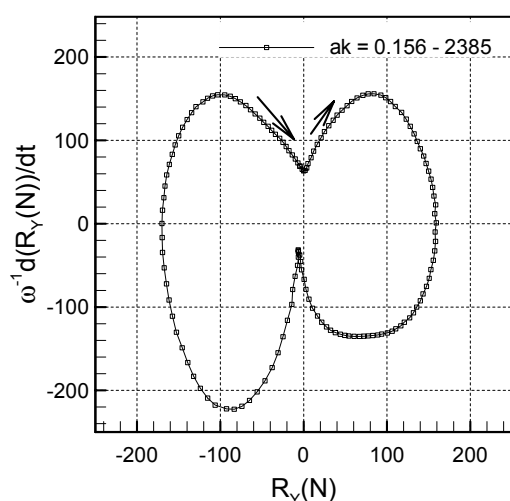


Figure 28: Phase diagram of the side force R_Y for the high amplitude waves.

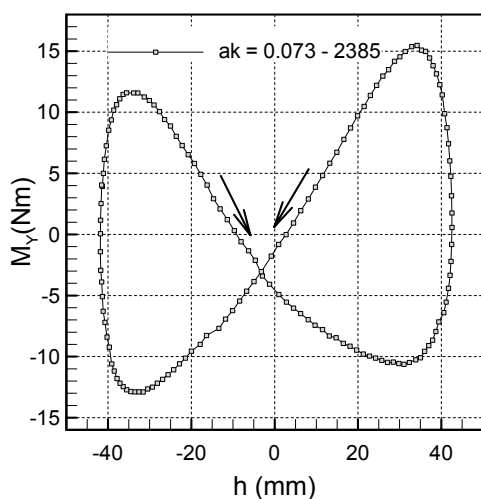


Figure 29: Combined plot of the pitch moment M_Y versus the wave height.

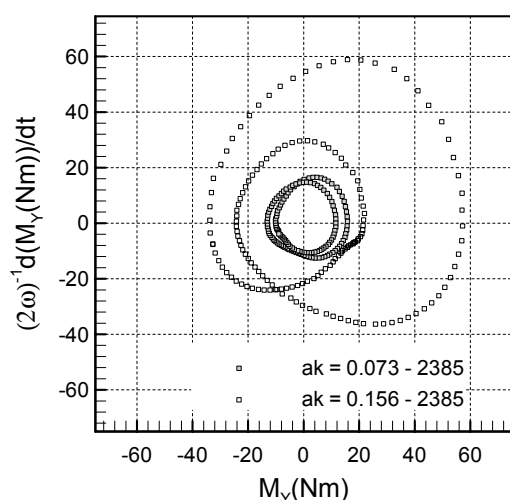


Figure 30: Phase diagram of the pitch moment M_Y for the high and medium amplitude waves.

The plot in figure 26 shows the four cycles of the axial force during one cycle of the wave height, while the plot in figure 27 confirms that the side force undergoes just one cycle each wave height cycle. On the other hand, the side force phase diagram in figure 28 shows a very peculiar trend, being close to the formation of a second cycle, which would indicate the presence of the 2nd harmonic. Different trend is shown by the pitch moment. The plot in figure 29 shows the presence of a “8-shaped” cycle each wave height cycle, as previously indicated by the preeminence of the 2nd harmonic in the amplitude function in figure 22 and confirmed by the phase diagram in figure 30.

Both axial force and pitch moment are almost zero for $h = 0$, while the side force cross the zero line close to the maximum and the minimum of the exciting wave.

3.2 ONR Tumblehome results (INSEAN model 2498)

As for the DTMB 5415, the heave motion well follows the wave height for all three cases and the roll motion shows no evidence of nonlinearities. In figure 31 the heave amplitude $\|Z_G\|$ is shown as a function of the wave height amplitude $\|h\|$ together with the roll amplitude $\|\phi^\circ\|$ versus the nominal wave slope ak . Both the heave amplitude and the roll motion show a linear growth with wave height and wave slope respectively.

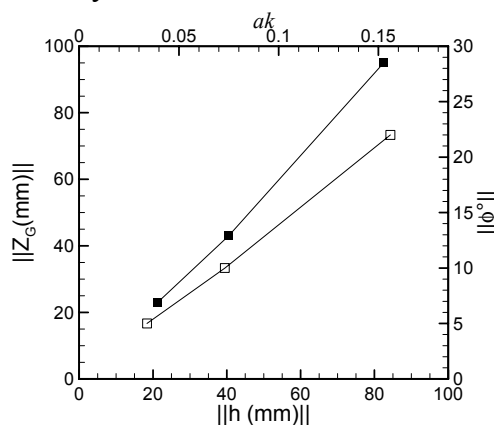


Figure 31: Heave amplitude $\|Z_G\|$ vs. wave height amplitude $\|h\|$ (filled symbols) and roll amplitude $\|\phi^\circ\|$ (open symbols) vs. nominal wave slope ak .

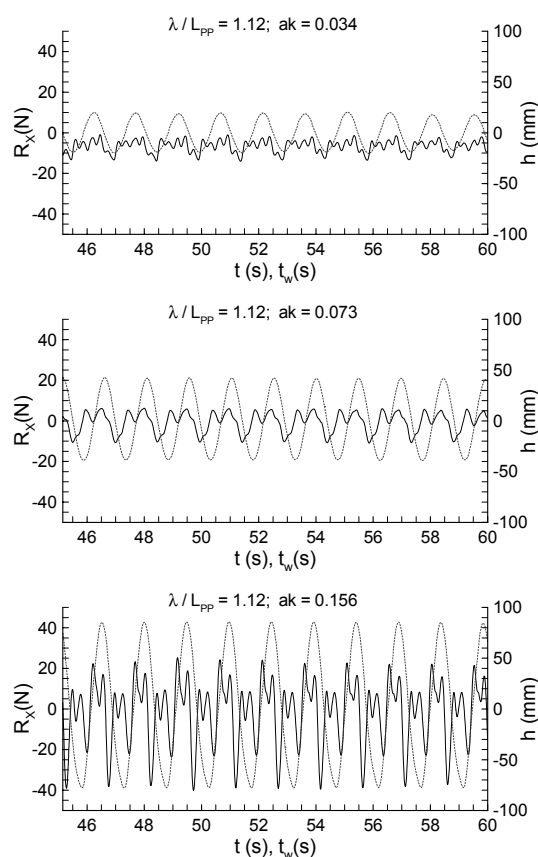


Figure 32: Time histories of the axial force R_X (solid lines) superimposed to the time histories of the wave height (dashed lines)

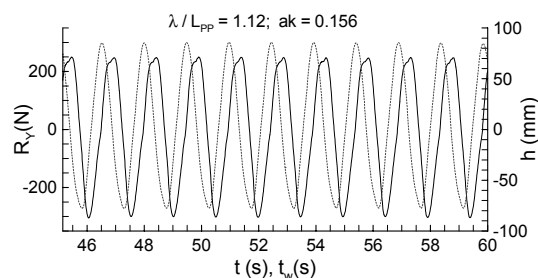


Figure 33: Time histories of the side force R_Y for large amplitude waves (solid line) superimposed to the time histories of the wave height (dashed line)

As for the DTMB 5415, nonlinear behavior is shown by the axial force R_X and pitch moment M_Y . Differently, the yaw moment M_Z shows a peculiar shape in the time history, especially for the highest wave slope, while the side force R_Y does not exhibit a particular behavior. As shown by figure 32, the time history of the axial force shows the presence of the 5th harmonic for the lowest ak ,

whereas for the higher wave slopes the 2nd harmonic starts to dominate ($ak = 0.073$). For the large wave amplitude case ($ak = 0.156$) the 5th harmonic is not visible by the time history, while the 4th harmonic becomes dominant. This behavior is confirmed by the Fourier analysis in figure 36.

The side force R_Y (figure 33) does not exhibit presence of higher harmonics as confirmed by the amplitude function in figure 37.

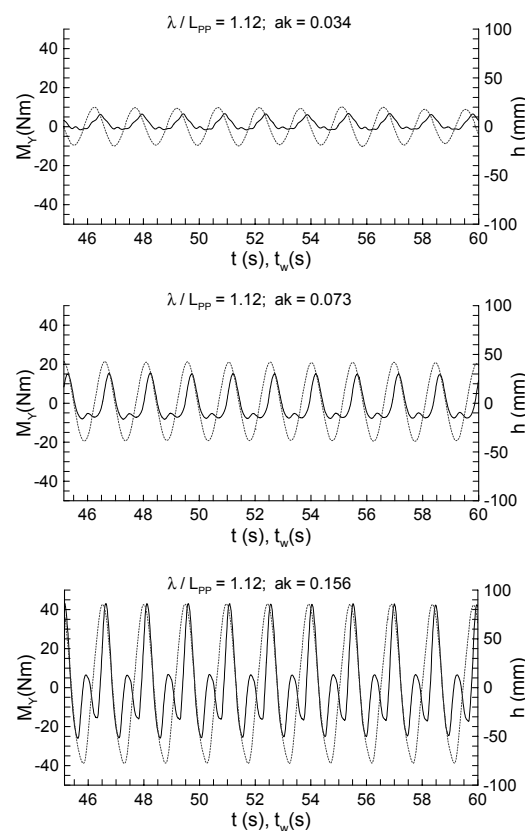


Figure 34: Time history of the pitch moment M_Y (solid lines) superimposed to the time histories of the wave elevation (dashed lines)

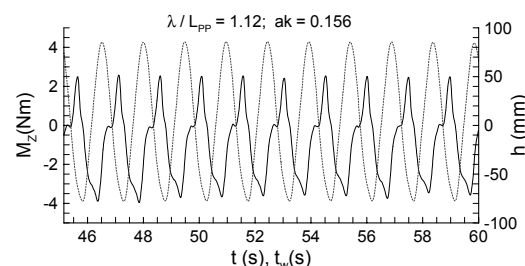


Figure 35: Time history of the yaw moment M_Z for large amplitude waves (solid line) superimposed to the time histories of the wave elevation (dashed line)

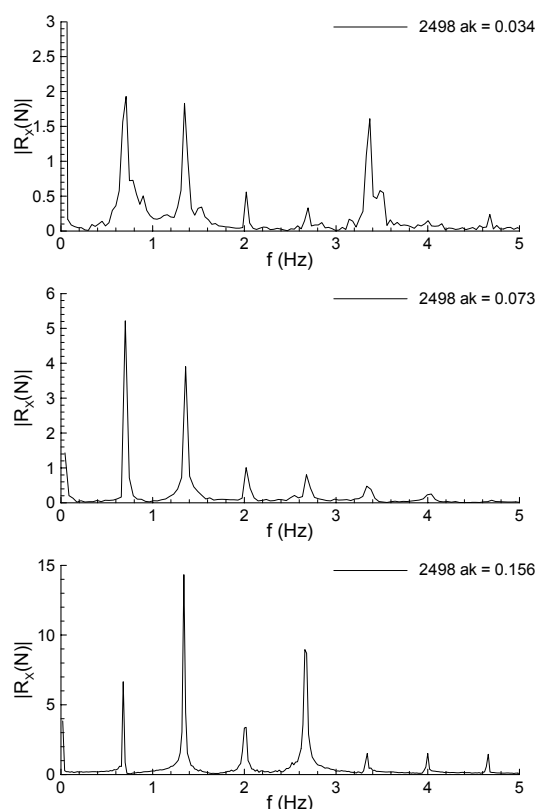


Figure 36: Amplitude function of the axial force R_X for small, medium and large amplitude waves.

The pitch moment M_Y shows the presence of the 2nd harmonic even for the small wave amplitude case, although the preeminence of the fundamental is evident for the low and medium wave slopes. On the opposite, the 2nd harmonics dominates for $ak = 0.156$, as shown by figure 38, where the amplitude function for the three cases is represented.

The time history and the amplitude function of the yaw moment M_Z are shown in figures 35 and 39 for the large amplitude waves. Here, the 3rd harmonic is clearly visible, although it is much smaller than the fundamental component.

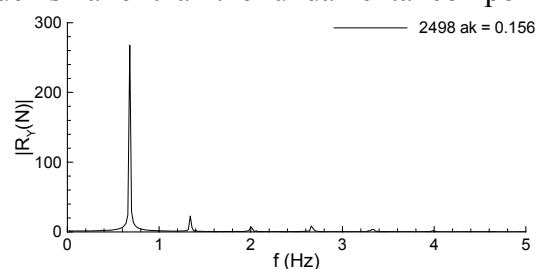


Figure 37: Amplitude function of the side force R_Y for the large amplitude waves.

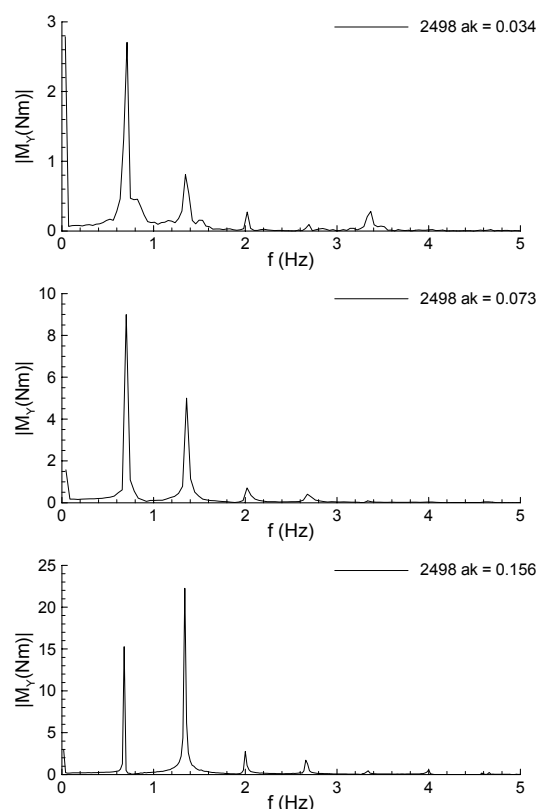


Figure 38: Amplitude function of the pitch moment M_Y for small, medium and large amplitude waves.

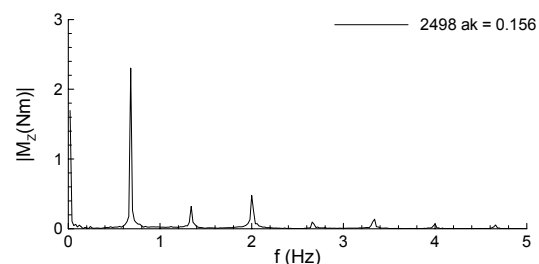


Figure 39: Amplitude function of the yaw moment M_Z for the large amplitude waves.

The amplitude of the axial force and pitch moment is shown in figures 40 and 41 together with the amplitudes of their first four harmonics.

The side force amplitude grows linearly with the wave slope as shown in figure 42, where the yaw moment amplitude is also represented.

In figures 43 and 44 the combined plot of the pitch moment with the wave height and the phase diagrams of the pitch moment are shown

for the medium and large amplitude wave cases, showing respectively a “8-shaped” cycle and a double cycle, which confirm the development of the 2nd harmonic.

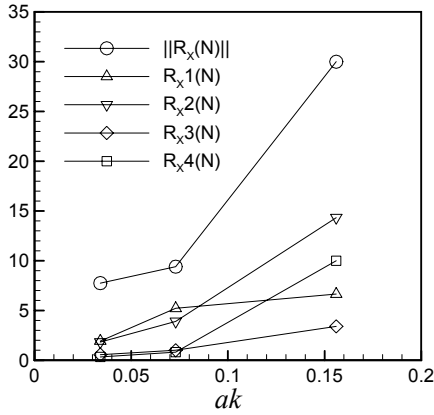


Figure 40: Amplitude of the axial force RX versus the wave slope: total and first four harmonics.

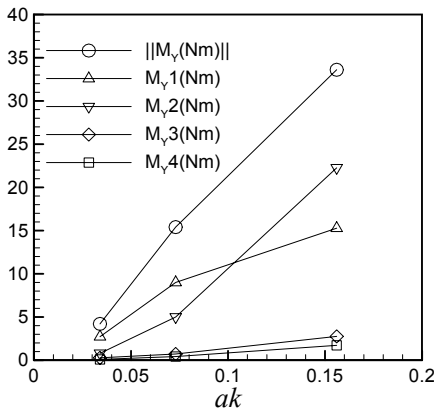


Figure 41: Amplitude of the pitch moment MY versus the wave slope: total and first four harmonics.

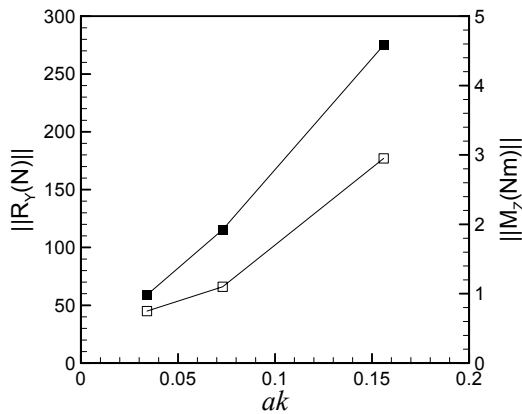


Figure 42: Amplitude of the side force RY (filled symbols) and yaw moment MZ (open symbols) versus the wave slope.

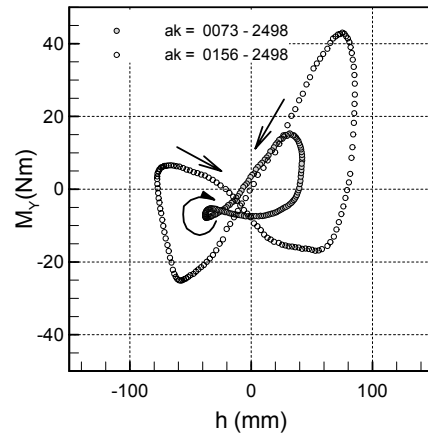


Figure 43: Combined plot of the pitch moment MY versus the wave height (medium and large amplitude waves).

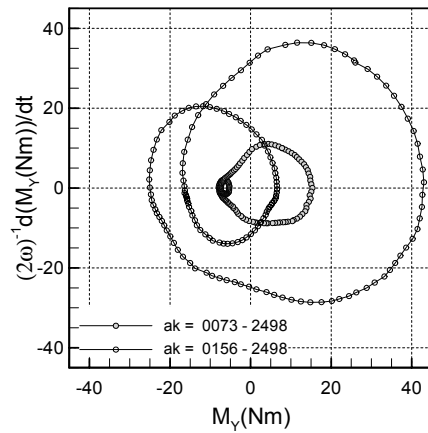


Figure 44: Phase diagram of the pitch moment MY for the high and medium amplitude waves.

3.3 Comparison of the results for DTMB 5415 and ONR Tumblehome

In order to correctly compare the results, they have been plotted using the measured wave slope (ak_M). In fact, we observed small variations on the wave height of the generated waves between the first tests on the DTMB 5415 and the second experimental campaign with the ONR Tumblehome. This could be ascribed to small differences on the water level in the basin or to small differences on the diffracted waves by the two models.

$$ak_M = \frac{2\pi \|h\|}{\lambda} \tag{2}$$

In figure 45 the heave motion amplitude is represented as a function of the measured wave height amplitude. Both models show a linear trend with comparable amplitudes, although the 2385 saturates for the large amplitude wave case. Figure 46 shows the roll motion as a function of the measured wave slope. As for the heave, the tumblehome shows a very linear trend, while the 5415 saturates for the highest wave slope. Moreover, the roll motion of the tumblehome is quite smaller, probably due to the larger span of its bilge keels (Tables 1 and 2 and figures 3, 4 and 5).

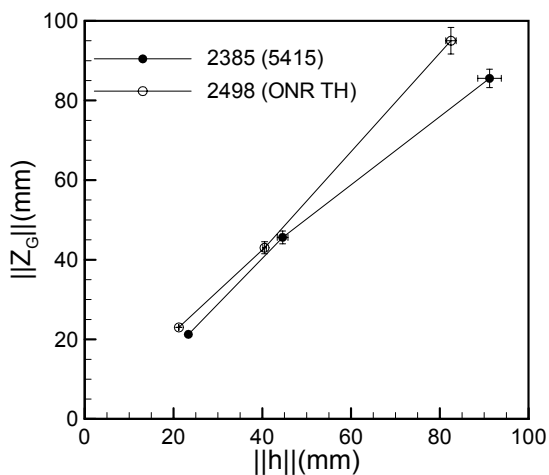


Figure 45: Heave motion amplitude versus the wave slope for both models with related PI bars.

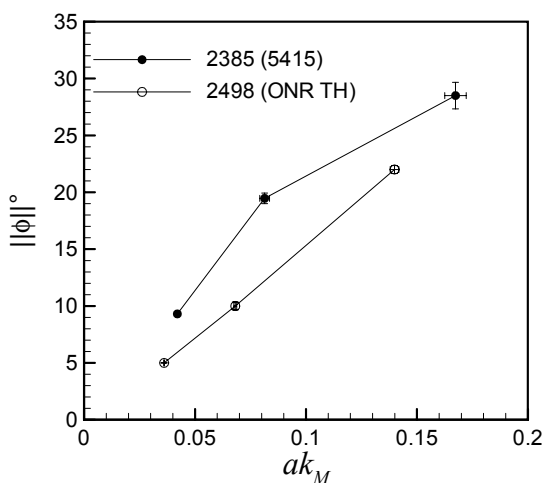


Figure 46: Roll motion amplitude versus the wave slope for both models with related PI bars.

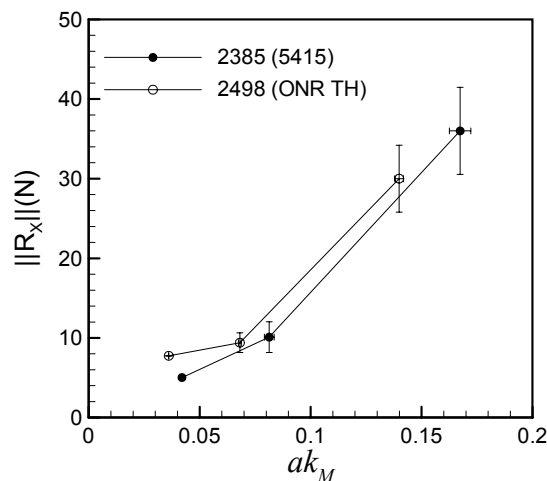


Figure 47: Axial force amplitude versus the wave slope for both models with related PI bars.

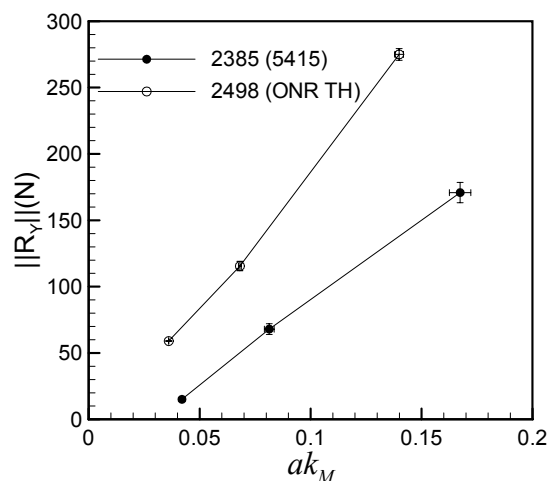


Figure 48: Side force amplitude versus the wave slope for both models with related PI bars.

The trends of the axial force are almost coincident with a small scatter for the small amplitude waves, probably due to a large measurement uncertainty (figure 47). In fact, for the small amplitude waves the reported values have been carried out based on a single test.

The side force amplitudes show large differences between the two models. The ONR Tumblehome experienced higher side forces with linear trend with respect to the wave

slope, while the DTMB 5415 undergoes lower side forces with non linear trend (figure 48).

The pitch moment is almost coincident, while the 5415 undergoes very high yaw moment, compared with the Tumblehome (figures 49 and 50). This can be related to the peculiar shape of the tumblehome, which does not present remarkable asymmetry between the aft body and fore body, with respect to the flare shaped 5415.

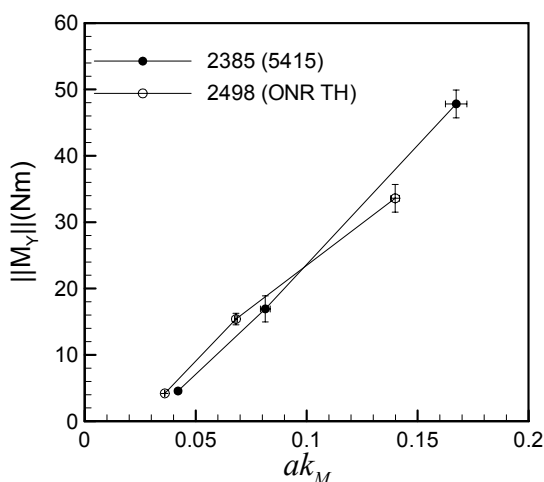


Figure 49: Pitch moment amplitude versus the wave slope for both models with related PI bars.

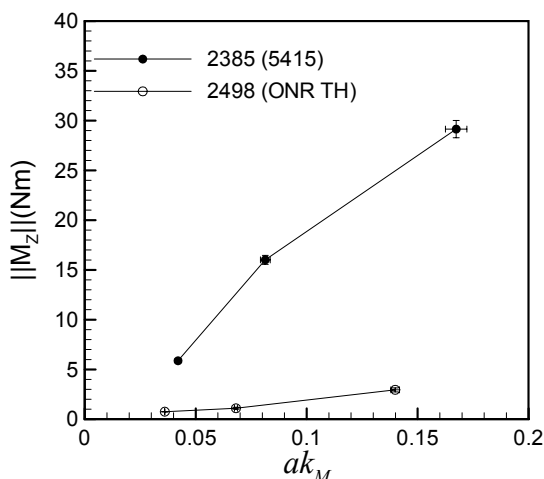


Figure 50: Yaw moment amplitude versus the wave slope for both models with related PI bars.

4. UNCERTAINTY ASSESSMENT

A detailed uncertainty assessment is still in progress. Here are presented the precision limit results (precision indexes), obtained by the repeated tests following the ITTC standards:

$$PI(x) = t_N \frac{\sigma(x)}{\sqrt{N}} \quad (3)$$

where x is the considered variable, σ is its standard deviation around the average on N repeated tests and t_N is the Student coefficient related to the 95% probability (Coleman and Steele, 1995).

The results are presented for the medium amplitude wave case (table 3) and the large amplitude wave case (table 4).

Table 3: precision index for DTMB 5415 (2385) and ONR Tumblehome ($ak = 0.073$)

Motion	DTMB 5415		ONR Tumblehome	
	Amplitude	P1	Amplitude	P1
Heave (Z_G)	45.6 mm	3.5%	44.5 mm	3.4%
Roll (ϕ)	19.5°	2.4%	10.4°	1.0%
Surge (R_X)	10.1 N	19.2%	9.4 N	13.1%
Sway (R_Y)	68.0 N	5.9%	115.5 N	3.1%
Pitch (M_Y)	16.9 Nm	11.6%	15.4 Nm	5.7%
Yaw (M_Z)	16.0 Nm	2.8%	1.1 Nm	9.1%

Table 4: precision index for DTMB 5415 (2385) and ONR Tumblehome ($ak = 0.156$)

Motion	DTMB 5415		ONR Tumblehome	
	Amplitude	P1	Amplitude	P1
Heave (Z_G)	85.6 mm	2.7%	91.0 mm	1.6%
Roll (ϕ)	28.5°	4.1%	21.5°	1.4%
Surge (R_X)	36.0 N	15.2%	30.0 N	14.0%
Sway (R_Y)	170.8 N	4.5%	275.0 N	1.6%
Pitch (M_Y)	47.8 Nm	4.4%	336.3 Nm	6.2%
Yaw (M_Z)	29.1 Nm	3.0%	3.0 Nm	6.8%

5. CONCLUDING REMARKS

Two different models of preliminary designs of surface combatants ca. 1980 (DTMB 5415) and present time (ONR Tumblehome) have been tested in regular beam seas in semicaptive conditions. The same scale has been adopted and the same facility and measurement systems have been used. The comparison of the results shows remarkable differences, especially for the roll amplitude, side forces and yaw moments. The use of captive tests instead of free running ones was dictated by the need of collecting results which can be used for validation of CFD codes. As a consequence, the results are not so realistic to allow ultimate conclusions in the frame of the comparison of dynamic stability of the two different ship forms. The roll motion amplitudes reported in figure 46, for example, don't describe the peak amplitude since they are obtained at constant frequency – nominally the small amplitude resonance frequency. This means they don't account for the different bending of the roll response curves as a consequence of the different righting arm curves. In addition, the restriction of sway introduces a non negligible disturbance in roll motion and yaw moment. It is also expected that the surge (axial) force can be influenced by the reflection of radiated waves from the walls. A detailed database for validation of theoretical and numerical models has been collected. The results are given in terms of time histories, Fourier analysis, combined plots and phase diagrams. In particular, the analysis of the results in terms of Fourier components can be very helpful for testing numerical codes. For all the presented results the precision limit has been determined on the basis of five repeated tests.

6. ACKNOWLEDGEMENTS

This work is sponsored by the Office of Naval Research contract N00014-04-1-0288 under the administration of Dr. Patrick Purtell.

Special thanks to F. Pistani, B. Jacob, M. Palini, R. Basti, F. Carta, R. Zagaglia, A. Ugolini, M. Sellini, L. Benedetti, M. Guerra, L. Brunacci for the fruitful discussion and their help in the preparation of the experimental set-ups and during the tests.

7. REFERENCES

- Rojas P. L., Belenky V. L., 2005, "A Review of the 8th International Conference on the Stability of Ship and Ocean Vehicles (STAB 2003)" *Marine Tech*, Vol. 42, No. 1, January, pp. 21-30.
- The Specialist Committee on Stability in Waves, 2005, "Final Report and Recommendations to the 24th ITTC" *Proceedings of the 24th ITTC - Volume II*, pp 369-408, Edinburgh, September
- Wilson, R.V., Carrica, P.M., and Stern, F., 2006, "Unsteady RANS Method for Ship Motions with Application to Roll for a Surface Combatant," *Computers & Fluids*, Vol. 35, Issue 5, June, pp. 501-524.
- Olivieri A., Campana, E.F., Francescutto A., and Stern F., *Capsize Project Report: Part 1*, IIHR Report (in preparation).
- Coleman, H.W., Steele, 1888-1895, W.G. 1995 *Engineering Application of Experimental Uncertainty Analysis*. *AIAA Journal*, 33, 10..

Strategy of Ship Control Under Intensive Icing Conditions

Yu.Nechaev, *State Marine Technical University, St.-Petersburg, Russia*

Yury Makov, *State Technical University, Kaliningrad, Russia*

ABSTRACT

The problem of making decisions on ship control under conditions of intensive icing has been discussed. A mathematical model of icing dynamics and criterion basis which provides ship's safety in this critical situation have been developed. The problem of making decisions on controlling ship stability in fuzzy environment has been set. Mathematical simulation of dynamics of ship's interaction with the environment in conditions changes in ice load and stability characteristics has been performed. Analyzing the results of the simulation has enabled to estimate risks under the considered conditions.

Keywords: *dynamic of ship, intensive icing, fuzzy environment, mathematical simulation*

1. INTRODUCTION

Risk estimation is one of complicated procedures in decision-making problems [Bogdanov, Degtyarev, Nechaev, 2001], [Nechaev, 2002]. Presently different approaches to risk estimation are used. The approach based on the probability theory and the catastrophe theory within the systems with a final set of discrete states is most popular. It involves application of theory and methods for analyzing risk situations scenarios. Investigation of very small probability risk scenarios, which are characterized by great damages, is the mostly developed approach in solving the problems of safe seafaring. Among the methods for judging risks in providing stability of ships the approach suggested in [Belenky, Sevastyanov, 2003], [Kobylinski, Kastner, 2003], [Kobylinski, 2003], [Ryrfeldt, 2003] should be singled out. Within the framework of this approach a set of operating situations is reduced to an ultimate

set of estimated situations. The vector of estimated situations, where each element is a set of both ship parameters and environment parameters, is found. The characteristic polynomial is designated by the level of methods applied for investigated estimated situations. It is common practice in the problems dealing with safety of seafaring to consider only extreme situations applying fairly simple approximations of spectral density of waves. It is only recently that lengths of stormy and good weather waves are taken into account for estimation of risks characteristics storms. Information on weather characteristics, in particular on alternating storms with favorable weather, as well as complicated spectral composition of waves have been realized first in the paper [Boukhanovsky at all, 2000]. The concept of climate spectrum enabled the authors to get new data of some situations which a ship can encounter in a particular voyage. The present paper contains an analysis of an extreme situation caused by dramatic decrease in stability under conditions of intensive icing on the basis of methods and

models [Nechaev, 1989], [Nechaev, Makov, 2002]. Risk estimation in this situation is performed with application of a radically new (from the point of view of estimating stability) approach dealing with making decisions in fuzzy conditions [Bellman, Zadeh, 1976]. According to the authors, this approach is mostly justified in analyzing alternatives and in selecting preferable solutions in fuzzy conditions, i.e. when information about ship's dynamics and its environment under operating conditions is limited.

2. MAKING DECISIONS IN FUZZY ENVIRONMENT

Decision making in conditions of risk can be stated as follows: there is a set of variants of solving problems (alternatives). Realization of each alternative brings to solutions. Alternatives are characterized by analyzing and estimating outcomes by indexes of efficiency. On the basis of simulating, a model of selecting alternatives enabling to solve the problem is to be built.

Formal statement of the problem is as follows. Let us assume that there is some fuzzy information characterizing a area of making decisions. This information can be presented as a cortege [Nechaev, 2002]]:

$$\langle A, E, S, T \rangle, \quad (1)$$

where A – a set of alternatives, E – area of decision making task, S – decision support system of a decision maker (DM), T – action on the alternative set A .

In the course of analyzing the set A in the environment E it is required to find the most preferable alternative which satisfies limitations C and is a way of achieving the aim G .

Solution of the problem (1) is found as a certain (specified) subset Ω of a set of alternatives A :

$$\Omega \subset 2^A \times K^A, \quad (2)$$

where 2^A – a set of all subsets of alternatives; K^A – a set of all corteges from 2 to $|A|$ in length.

Decision rule is expressed by intersection of fuzzy aims G_i and limitations C_j :

$$\Omega = G_1 \cap \dots \cap G_i \cap C_1 \cap \dots \cap C_j \dots \quad (3)$$

or with allowance made for their relative importance:

$$\Omega = \sum_i k_i G_i + \sum_j k_j^* C_j; \quad (4)$$

$$\sum_i k_i + \sum_j k_j^* = 1,$$

where k, k^* – great importance coefficient.

Modification of decision rule (3) with regard to comparing fuzzy aims by importance will look like:

$$\Omega = G_1^{k_1} \cap G_2^{k_2} \cap \dots \cap G_i^{k_i} \cap \dots; \quad (5)$$

$$\Omega = G_1/k_1 \cap G_2/k_2 \cap \dots \cap G_i/k_i \cap \dots$$

Let us specify the statement of the problem (1),(2) as applicable to analyzing alternatives when selecting a safe ship course and velocity on the basis of Bellman-Zadeh approach [Bellman, Zadeh, 1976]. We assume that X – is a universal set of alternatives. We will consider mapping $\varphi: X \rightarrow Y$. The elements of Y set are values of the mapping. This mapping is understood as reaction of the system on input fluctuations $x \in X$ or as some estimations of selection of corresponding alternatives. The fuzzy aim G is pre-assigned as a fuzzy sub-set of reactions Y , i.e. as a membership function $\mu_G: Y \rightarrow [0, 1]$.

The problem is solved to achieve the aim with specified fuzzy limitations. Let a certain alternative x enables achieving the aim with the power $\mu_G(x)$ and complies limitations with the power $\mu_C(x)$.

Then the degree of membership alternative x equals the minimum of these numbers with a membership function:

$$\mu_G(x) = \min \{ \mu_G(x), \mu_C(x) \}. \quad (6)$$

With several aims and limitations the fuzzy decision is:

$$\mu_G(x) = \min \{ \mu_{G1}(x), \dots, \mu_{Gn}(x), \mu_{C1}(x), \dots, \mu_{Cn}(x) \}. \quad (7)$$

With regard to importance of aims k_i and limitations k_j^* the result of solution is presented as

$$\mu_G(x) = \min \{ k_1 \mu_{G1}(x), \dots, k_n \mu_{Gn}(x), k_1^* \mu_{C1}(x), \dots, k_n^* \mu_{Cn}(x) \}. \quad (8)$$

Thus solution can be approached as a fuzzily formulated rule. Complying with the rule enables reaching of a fuzzily set aim. Choice of an alternative with a maximum degree of fuzzy decision membership (maximizing solution) is dictated by the condition:

$$\max_{x \in X} \mu_G(x) = \max_{x \in X} \min \{ \mu_G(x), \mu_C(x) \}. \quad (9)$$

3. MATHEMATICAL MODEL

The mathematical model is built on the basis of handling data of full scale observations. Allowances are made for basic data of real load condition and stability of the ship at the moment of estimation and the forecast of development of the situation in intensive icing. The condition of the ship at the initial moment is specified by the displacement, the centre of gravity coordinates ($M_0, X_{go}, Y_{go}, Z_{go}$) as well as by stability indexes. The principal dimensions of the ship, the hydrostatic curves,

the centre of effort (of sails) elevation of the centre of effort of sails, free board height (including bulwark) on the fore perpendicular as well as the ship's speed on calm water have been used in the course of calculations.

While the mathematical model was being developed the authors hold the traditional ship orientation as related to wind and oncoming sea. Fig. 1 shows a triangle which represents speeds and course angle. The compass bearing wave track is CB_{WT} and the wave height is $h_{3\%}$. Steady wind is characterized by the course bearing of true wind CB_{TW} and the speed U_{TW} .

The conditions, icing is developing under, feature air temperature ta and water temperature tw . If the system is used aboard a ship the aforementioned characteristics are the results of measurements, in other cases they are the results of analyzing wind and seas occurrences in the specified area of navigation.

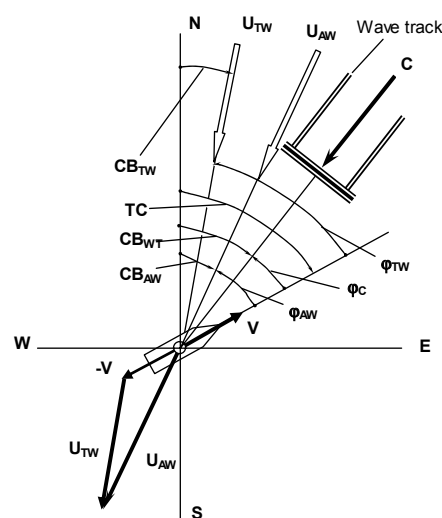


Fig.1 The triangle of speeds and course angles: V – speed of the ship, TC – true ship course, CB_{WT} – compass bearing of the wave track, CB_{AW} – compass bearing of apparent wind, CB_{TW} – compass bearing of true wind, U_{AW} – velocity of apparent wind, U_{TW} – velocity of true wind, φ_C – course angle of the ship relative to waves, φ_{TW} – course angle of true wind, φ_{AW} – course angle of apparent wind.

3.1. Rate of Ice Growing

The model of icing process depending on the course angle takes account of growing of ice in three points: 1 – on the fore perpendicular on the upper deck level, 2 – on the upper deck amid ship close aboard and 3 – on the upper deck on the after perpendicular.

The rate of ice growing in t/hr can be presented by

$$\begin{bmatrix} V_{m1} \\ V_{m2} \\ V_{m3} \end{bmatrix} = \begin{bmatrix} A_1 \\ A_2 \\ A_3 \end{bmatrix} \cdot \begin{bmatrix} \Sigma_{NAV1} \\ \Sigma_{NAV2} \\ \Sigma_{NAV3} \end{bmatrix} \quad (10)$$

where

$$\begin{bmatrix} A_1 \\ A_2 \\ A_3 \end{bmatrix} = \begin{bmatrix} F_1(\varphi_{AW}) \\ F_2(\varphi_{AW}) \\ F_3(\varphi_{AW}) \end{bmatrix} \cdot F \begin{bmatrix} h_{3\%}(h_{3\%}(0), t), f_1 \\ h_{3\%}(h_{3\%}(0), t), f_2 \\ h_{3\%}(h_{3\%}(0), t), f_3 \end{bmatrix} \cdot F(L)$$

Here $F_i(\varphi_{AW})$ are functions where influence of angle between apparent wind and longitudinal plane are taken into account:

$$F_1(\varphi_{AW}) = d_1 + d_1 \cdot \text{Cos}(d_{11}\varphi_{AW}) + kd_1 \cdot \text{Cos}(d_{12}\varphi_{AW})$$

$$F_2(\varphi_{AW}) = d_2 + d_2 \cdot \text{Cos}(d_{21}\varphi_{AW} - \pi)$$

$$F_3(\varphi_{AW}) = d_3 + d_3 \cdot \text{Cos}(d_{31}\varphi_{AW}).$$

The general view of the function $F_i(\varphi_{AW})$ is shown in Fig. 2.

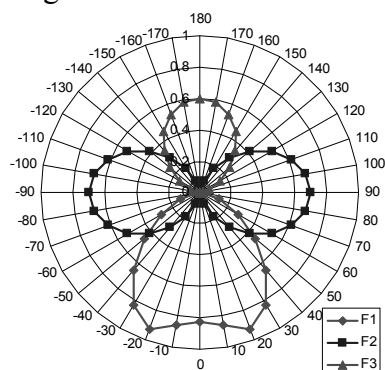


Fig.2. Functions F_1, F_2, F_3

F are functions where influence of wave height (which can be changed with time), freeboard height at points 1, 2 or 3 and ships length are taken into account:

$$F \begin{bmatrix} h_{3\%}(h_{3\%}(0), t), f_1 \\ h_{3\%}(h_{3\%}(0), t), f_2 \\ h_{3\%}(h_{3\%}(0), t), f_3 \end{bmatrix} = 1 + \frac{0.1h_{3\%}(h_{3\%}(0), t) + 0.1}{0.1 \begin{bmatrix} f_1 \\ f_2 \\ f_3 \end{bmatrix} + 0.2},$$

$$F(L) = \left(1 + \frac{L - 35}{93}\right)^3$$

The height of the design wave $h_{3\%}(0)$ at the moment of taking decision by the master was calculated as a function of the ship length from the formula

$$h_{3\%}(0) = 0.05 \left(1 + \frac{160 - L}{135}\right) L \quad (11)$$

but it may be prescribed arbitrarily.

If the storm strengthens, the increase in wave height is found from the formulae (Fig.3)

$$h_{3\%} = h_{3\%}(0) + 0,07t, \text{ m (t - hour)}$$

Σ_{NAV} are functions where influence of water and air temperatures, apparent wind velocity, sail area and ship's velocity with regard for its decreasing on rough seas are taken into account:

$$\begin{bmatrix} \Sigma_{NAV1} \\ \Sigma_{NAV2} \\ \Sigma_{NAV3} \end{bmatrix} = \begin{bmatrix} b_{11} \\ b_{21} \\ b_{31} \end{bmatrix} N^* + \begin{bmatrix} b_{12} \\ b_{22} \\ b_{32} \end{bmatrix} N^* A_v^* + \begin{bmatrix} b_{13} \\ b_{23} \\ b_{33} \end{bmatrix} V_s^*$$

$$N^* = U_{AW}(|ta| + |tw|); A^* = Av/225;$$

$$V_s^* = (Vs/Vs_{CW}) - 0,5.$$

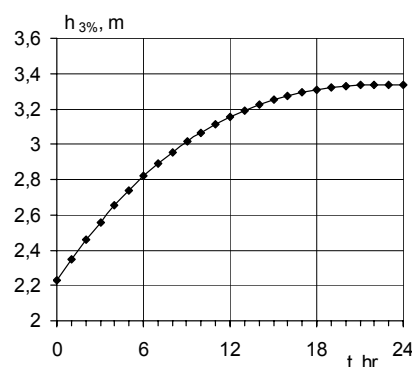


Fig. 3 Increasing of wave height shows the process of storm development

In the aforementioned formulae the following symbols are used: U_{AW} – velocity of apparent wind; ta and tw – air and water temperatures; Av – sail area; L – ship length; f_{123} – heights of freeboard on the fore perpendicular, amidships on the longitudinal centre plane and on the after perpendicular; V_s – ship velocity with regard to wind and waves; $V_{s_{CW}}$ – ship velocity on calm water; a_i, b_{ij}, d_i, d_{ij} – coefficients which values are assigned in the course of statistical handling of full scale measurements.

Ice mass grooving within δt hr interval is found from the formulas:

$$\begin{bmatrix} m_1 \\ m_2 \\ m_3 \end{bmatrix} = \begin{bmatrix} V_{m1} \\ V_{m2} \\ V_{m3} \end{bmatrix} \delta t, \quad t.$$

$$m = m_1 + m_2 + m_3.$$

The rate of ice growing (in t/hr) depends greatly on course angle and direction of wind and wave vectors.

3.2. The Rate of Changing Coordinates of the Centre of Growing Ice Masses

The rate of changing the coordinates of the center of growing ice masses (in m/hr) is found by the formula:

$$\begin{bmatrix} V_{Xm1} \\ V_{Xm2} \\ V_{Xm3} \end{bmatrix} = \begin{bmatrix} A_1 L_1^* c_{x1} m^* \\ 0 \\ A_3 L_3^* c_{x3} m^* \end{bmatrix}, \quad \begin{bmatrix} V_{Ym1} \\ V_{Ym2} \\ V_{Ym3} \end{bmatrix} = \begin{bmatrix} 0 \\ A_2 B^* c_{y2} m^* \\ 0 \end{bmatrix}, \quad (12)$$

$$\begin{bmatrix} V_{Zm1} \\ V_{Zm2} \\ V_{Zm3} \end{bmatrix} = \begin{bmatrix} A_1 H_1^* c_{z1} m^* \\ A_2 H_2^* c_{z2} m^* \\ A_3 H_3^* c_{z3} m^* \end{bmatrix}, \quad m^* = \frac{m}{M_0}.$$

Here c – coefficients, which values were found (assigned) in the course of handling the results of full scale measurements. The coordinates of ice masses center are found by the formulae:

$$\begin{bmatrix} X_{m1} \\ X_{m2} \\ X_{m3} \end{bmatrix} = \frac{L}{2} - \begin{bmatrix} V_{Xm1} \\ 0 \\ V_{Xm3} \end{bmatrix} \delta t, \quad \begin{bmatrix} Y_{m1} \\ Y_{m2} \\ Y_{m3} \end{bmatrix} = \frac{B}{2} - \begin{bmatrix} 0 \\ V_{Ym2} \\ 0 \end{bmatrix} \delta t, \quad (13)$$

$$\begin{bmatrix} Z_{m1} \\ Z_{m2} \\ Z_{m3} \end{bmatrix} = \begin{bmatrix} H_1 \\ H_2 \\ H_3 \end{bmatrix} + \begin{bmatrix} V_{Zm1} \\ V_{Zm2} \\ V_{Zm3} \end{bmatrix} \delta t,$$

$$\begin{bmatrix} L_1^* \\ B^* \\ L_3^* \end{bmatrix} = \begin{bmatrix} 0.96 + f_1 / L \\ 0.80 + f_2 / B \\ 0.96 + f_3 / L \end{bmatrix}, \quad \begin{bmatrix} H_1^* \\ H_2^* \\ H_3^* \end{bmatrix} = 0.60 + \begin{bmatrix} f_1 / H_1 \\ f_2 / H_2 \\ f_3 / H_3 \end{bmatrix}. \quad (14)$$

Here H_1, H_2, H_3 – the height of freeboard depth afore, amidships and astern. General coordinates of the centre office masses are found from the equations:

$$X_m = \frac{m_1 X_{m1} + m_3 X_{m3}}{m},$$

$$Y_m = \frac{m_2 Y_{m2}}{m}, \quad (15)$$

$$Z_m = \frac{m_1 Z_{m1} + m_2 Z_{m2} + m_3 Z_{m3}}{m},$$

And the coordinates of the centre of the ship masses are found from the equations:

$$M = M_0 + m,$$

$$X_g = \frac{M_0 X_{g0} + m X_m}{M},$$

$$Y_g = \frac{M_0 Y_{g0} + m Y_m}{M}, \quad (16)$$

$$Z_g = \frac{M_0 Z_{g0} + m Z_m}{M}$$

The calculations are made at every stage at a specified interval δt hour.

3.3. Additional Resistance Due to Wind and Rough Seas and Decrease in Velocity

Resistance of ship in rough seas is calculated from the formula [Nechaev, Makov, 2002]:

$$R = \kappa_m \psi R_{cw} + \kappa_\varphi R_{aw0} + R_a, \quad (17)$$

where R_{cw} – resistance on calm water at the moment of taking decision, $\kappa_m \psi$ – coefficient where allowances are made for influence of changes in displacement of the ship (due to ice growing) and changes in angle of trim

$$\kappa_m \psi = \kappa_m \kappa_\psi,$$

where

$$\begin{aligned}\kappa_m &= 1 + 0.52 m^* + 0.63 m^{*2} - 0.89 m^{*3}, \\ \kappa_\psi &= 1 + 0.013 \psi + 0.007 \psi^2.\end{aligned}$$

Increase in resistance in irregular seas is found from

$$R_{aw} = \kappa_\varphi R_{aw0}.$$

Here R_{aw0} – is resistance in head irregular sea

$$R_{aw0} = 2,48 L^{4,8} B^2 h_{3\%}^{-3,8} Fr^{3,16} \times \exp(-3,5Fr - 3,23 Fr^{0,143} (L/h_{3\%})^{0,5}). \quad (18)$$

In coefficient κ_φ account in taken of the course angle influence

$$\kappa_\varphi = F(\varphi, \kappa_R, \alpha).$$

$$\kappa_R = (1.2 - 0.1\sqrt{\alpha}) - (2.9\sqrt{\alpha} - 1.9)Fr,$$

Here α – waterline fullness coefficient and « α » parameter is found from the formula:

$$a = q_b \frac{10h_{3\%}}{L}.$$

q_b – coefficient depends on the rate of developing rough seas (0.75).

Additional resistance due to wind is calculated as follows:

$$R_a = C_x \frac{\rho_a U_{AW}^2}{2} A_F$$

Here: ρ_a – air density; A_F – projection of the sail area on midship section plane; $C_x(\varphi_{AW})$ – coefficient of resistance, taken as resulted from flowing of air towards above water part of ship model in a tunnel or taken as approximated estimates; U_{AW} – apparent wind velocity. Apparent wind velocity is calculated from the formula:

$$U_{AW} = \sqrt{U_{TW}^2 + V_s^2 - 2U_{TW}V_s \cdot \cos(\varphi_{TW})} \quad (19)$$

True wind velocity (m/sec) is found from the formula:

$$\text{when } h_{3\%} > 1 \text{ m } U_{TW} = 6,7 + 2,13(h_{3\%} - 1);$$

$$h_{3\%} < 1 \text{ m } U_{TW} = 16,7h_{3\%}^2 - 10h_{3\%}^3.$$

The curve of ahead pull T_e is approximated by a straight line between a point on the curve R , obtained on calm water and the point of maximum permissible bollard pull. For the ship with fixed pitch propeller the formula for T_e (kN) is presented as:

$$T_e = R_0 \left(1.35 - 0.35 \frac{V_s}{V_{sCW}} \right) \quad (20)$$

The formulae make possible to estimate the decrease in velocity and to estimate the time period required for the ship to enter a shelter port. Fig. 4 and Fig 5 shows the general character of relationship which define (govern, control) the decrease in velocity and its absolute value.

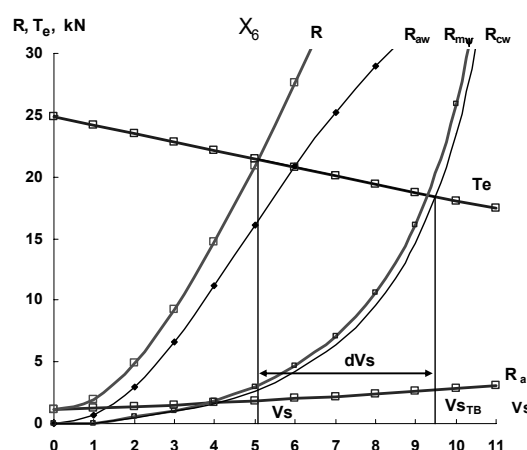


Fig. 4 Additional resistance and decrease of speed on rough seas

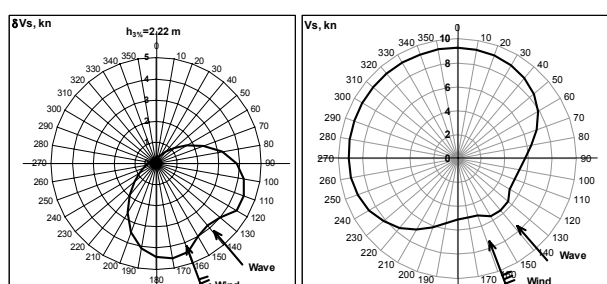


Fig.5. Character of changes of δV_s and V_s values for different course angles

4. CRITERIA BASIS

While developing criterion basis for estimating stability under conditions of icing it was assumed that intensive icing is not less dangerous than flooding a compartment. Therefore stability criteria and standards under heavy icing are determined by the following system of inequalities:

- initial metacentric height $h_0 \geq 0,05$, m;
- angle of statical heel $\theta_0 \leq 20$, deg;
- maximum righting arm $l_m \geq 0,1$, m;
- length of positive part of the diagram $\theta_p \geq 20$, deg;
- limiting value of freeboard height: afore $f_1 \geq 0,3$ m, amidships $f_2 \geq 0,3$ m, amidships side $f_{2S} \geq 0$, astern $f_3 \geq 0,3$, m.

The period of navigation before any standard was broken was assumed as critical.

The critical time interval t_{CR} which is decisive for breaking the requirements to ship safety under icing conditions is described as the minimum time interval calculated throughout all the criteria.

Simulation of ship behavior was carried out on the basis of formulae (16)–(21) and t_{CR} was found in accordance with the specified criteria:

$$t_{CR} = \min [t(h_0), t(\theta_0), t(l_m), t(\theta_p), t(f_1), t(f_2), t(f_{2S}), t(f_3)] \quad (21)$$

t_{CR} was correlated with time of proceeding to a refuge harbor t_S which was presented with re-

gard to decrease in velocity in irregular sea. Safety condition was expressed as:

$$t_{CR} \geq t_S. \quad (22)$$

When the condition (22) is broken the logical system gives practical recommendations on icing control.

5. SCENARIOS OF SHIP MOVEMENT

When simulating ship dynamics under icing conditions some scenarios of extreme situations have been developed and “performed”. The concept of a logical system enabling to create different scenarios of emerging and developing extreme situations. Analysis and forecast of sequences of development extreme situations is performed by some methods of mathematical simulating on the basis of formulae (10) – (22). Formulation of scenarios is performed using the data of dynamic measurements of the ship and the environment parameters.

Along with traditional strategies which define the space for searching on the basis of single scenarios, more complicated strategies of “generation-check” type have been used. It is convenient to use this approach when the space for searching (rational trajectory of ship motion is not clearly specified. To realize searching in these conditions it is compulsory to generate the next in turn solution (strategy of management) with follow up checking of the results. Practical realization of the strategy “generation-check” involves distribution of functions between the operator (ship master) who chooses particular strategy (course and velocity) and the algorithm of checking which enables analysis of real values of stability in the current situation on the basis of (10) – (22).

Modification of the method “generation-check” may be realized by transition to the strategy “hierarchical generation-checking”. When the latter is used the operator at first develops a partial solution which covers only a

part of the problem. In accordance with the results of the solution it is judged how effective the assumed trajectory of the ship's movement is. In case it is effective, at the following step the operator develops a complete solution and the algorithm of checking estimates effectiveness of its realization.

In the example under consideration six different scenarios have been chosen. They define strategies of ship's motion to refuge harbors **A**, **B**, **C** (fig.6).

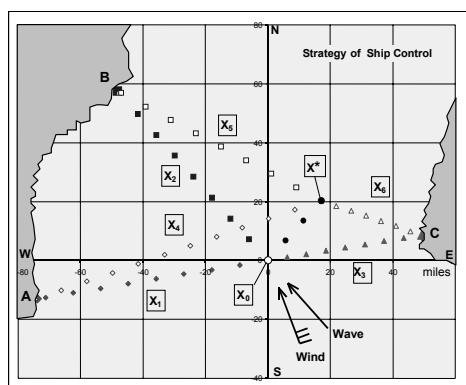


Fig. 6. The situation at the moment of decision making: disposition of the ship in X_0 and X^* and **A**, **B**, **C** refuge harbors

The first three scenarios X_1 , X_2 , X_3 characterize ship's movement from initial position X_0 . Other scenarios X_4 , X_5 , X_6 presuppose application of one of the variants of the strategy "generation-check". In compliance with the strategy the ship first makes a maneuver (generation of an immediate possible solution) and moves to some other initial point X^* . This is the initial point for realization X_4 , X_5 , X_6 strategies of management and checking the results should follow up.

Fig. 6 shows diagram containing information about ship's position in the initial point X_0 (origin), displacement of the ship to the point X^* (dark circle) and trajectories of ship movement to **A**, **B**, **C** refuge harbors. Trajectories from X_0 are marked by light diamonds, squares and triangles. Trajectories from X^* are marked by dark diamonds, squares and triangles. Distances from the initial point in miles are laid off along axes.

6. RESULTS OF SIMULATION

The results of simulating situations for the $X_1 - X_6$ scenarios under consideration are represented in Tab. 1. The first column contains data referring to initial situation X_0 . The column marked by X^* characterized the other initial point. The ship moves to this point from X_0 for realization the strategy "generation-check".

Developing the scenario "generation-check" made possible simulating three additional X_4 , X_5 , X_6 strategies of ship movement from X^* to **A**, **B**, **C** ports. The results of simulating the situation "generation-check" permit of significant increasing opportunities to analyze alternatives and make decisions.

We can see from Tab.1 that the most unfavorable situation associated with dramatic decrease in stability occurs when the ship is making to **A** (scenario X_1). It follows from the data that failing to meet requirements to ship safety in this situation is due to two criteria: substantial angle of heel θ_0 sometimes as great as $28,7^\circ$ and drastic decrease in maximum of righting arms $l_m=0,06$ m. The situation only becomes worse if the strategy "generation-check" is used. The results of simulating shows in the column for X_5 scenario prove it.

Table 1. Comparative characteristics of basic indexes of loading, stability and propulsion for the investigated scenarios

Parameter	X_0	X_1	X_2	X_3	X^*	X_4	X_5	X_6
TC, deg		260	320	80	40,0	249,9	299,7	109,8
S, miles		75	75	50	26,5	96,8	75,1	34,3
CB _{wr} , deg	140	140	140	140	140	140	140	140
CB _{TW} , deg	160	160	160	160	160	160	160	160
m, t	0,0	22,9	14,9	19,5	6,8	39,6	20,8	19,9
M, t	160,0	182,9	174,9	179,5	166,8	206,4	187,6	186,7
Xg, m	-0,50	-0,31	-0,90	-0,19	-0,48	-0,08	-0,64	0,12
Yg, m	0,00	-0,31	-0,10	0,22	0,12	-0,34	-0,13	0,23
Zg, m	2,50	2,64	2,59	2,65	2,54	2,77	2,64	2,78
Tf, m	1,86	2,21	1,74	2,25	1,94	2,63	2,02	2,55
Ta, m	2,55	2,67	2,88	2,58	2,60	2,70	2,87	2,45
Tm, m	2,21	2,44	2,31	2,42	2,27	2,67	2,45	2,50
Vs, kn	9,50	8,94	9,18	6,34	8,74	8,68	9,18	5,22
h _{3%} , m	2,22	3,01	3,01	3,01	2,65	3,69	3,54	3,47
t _A ^o + t _w ^o , deg	17,00	17,00	17,00	17,00	17,00	17,00	17,00	17,00
ho, m	0,83	0,67	0,88	0,63	0,79	0,53	0,78	0,46
θ ₀ , deg	0,00	27,64	6,22	18,12	7,98	42,61	9,25	30,88
lm, m	0,39	0,06	0,23	0,11	0,27	0,00	0,15	0,03
θ _p , deg	99,47	51,85	78,05	63,40	88,03	0,00	70,01	30,93
f ₁ , m	3,79	3,44	3,91	3,40	3,71	3,02	3,63	3,10
f ₂ , m	1,09	0,86	0,99	0,88	1,03	0,63	0,85	0,80
f _{2s} , m	1,09	-0,92	0,62	-0,23	0,55	-2,50	0,30	-1,23
f ₃ , m	1,12	1,00	0,79	1,09	1,07	0,97	0,80	1,22
t(ho), hr								
t(θ ₀), hr		6,97				7,52	7,09	5,37
t(lm), hr		6,96				6,91	7,80	5,03
t(θ _p), hr						8,79		
t(f ₁), hr								
t(f ₂), hr								
t(f _{2s}), hr		5,43		6,79		6,22	7,28	3,66
t(f ₃), hr								
t _s , hr		8,30	8,10	7,92		10,94	8,11	6,69
t _{CR} , hr		5,43	0,00	6,79	0,00	6,22	7,09	3,66

Let's analyze results of accounts on an example of the scenarios X_1 .

The critical time is tabulated in Tab. 2.

Table 2. Critical interval

Criterion	t(ho)	t(θ ₀)	t(lm)	t(θ _p)	t(f ₁)	t(f ₂)	t(f _{2s})	t(f ₃)	t _s	t _{CR}
Time, hr	0	6,97	6,96	0	0	0	5,43	0	8,30	5,43

Zero in Tab.2 show that critical time has not been reached. It follows from Tab. 2 that in 6,97 hours the angle of heel due to asymmetrical growing of ice can reach 20 deg. Even earlier in 5,43 hours the deck will immerse. In 6,96 hours the maximum righting arm will equal 0,1 m. In 8,3 hr the ship will reach a refuge harbor. The general outline of changes of analyzed loading, stability and velocity characteristics for the most unfavorable situation X_1 is given in Fig.7.

The data presented visualize very complicated transformations of information in the course of intensive icing. Information dealing with changes in stability indexes in the analyzed scenarios and its correlation with criteria of the adopted system of standardization are of

particular importance. Asymmetric icing in the investigated situations has resulted in catastrophic decrease in stability and in a dangerous angle of heel. Maneuvering of ship and passing to situation X_4 (see Tab.1) don't bring to improving stability indexes, and the ship's movement to a refuge harbor A remains threatening.

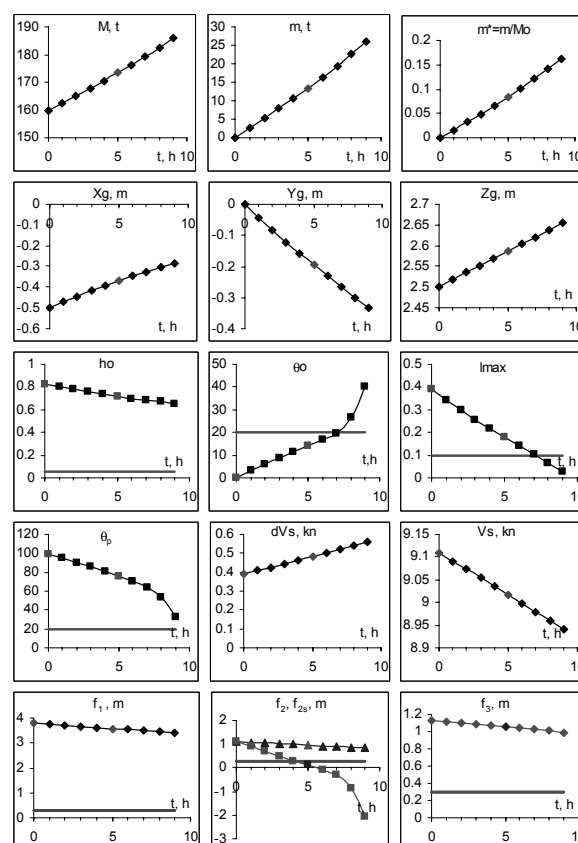


Fig. 7. Changes in ship's characteristics for most unfavorable situation appropriate to ship movement to port A

7. RISK ESTIMATION AND MAKING DECISIONS

Let's perform a more detailed expert analysis of the data given in Tab. 1. The ship dimensionless parameter $G = t_{CR}/t_s$ is considered to be a criterion of safety. This parameter characterizes relationship between critical interval of time t_{CR} and interval t_s of time of a ship proceeding to a refuge harbor. If for the specified strategy no infringements of the accepted criteria of safety are observed, $G=1$ is accepted. In

other cases we have $G < 1$. Restrictions on stability C_1 and restrictions on buoyancy C_2 are considered to be imposed restrictions. Requirements to stability diagram $h_0, \theta_0, l_m, \theta_P$ are restrictions on stability, and requirement to freeboard height f_1, f_2, f_{2S}, f_3 are restrictions on buoyancy. To each of these requirements in the specified strategy there corresponds its inherent critical time, i.e.:

$$\begin{aligned} C_1 \in [t(h_0), t(\theta_0), t(l_m), t(\theta_P)] \text{ u} \\ C_2 \in [t(f_1), t(f_2), t(f_{2S}), t(f_3)]. \end{aligned} \quad (23)$$

Using this information, we shall write down restrictions C_1 and C_2 in the dimensionless form - in relation to a critical interval of time:

$$C_1 \in [t(h_0)/t_{CR}, t(\theta_0)/t_{CR}, t(l_m)/t_{CR}, t(\theta_P)/t_{CR}], \quad (24)$$

$$C_2 \in [t(f_1)/t_{CR}, t(f_2)/t_{CR}, t(f_{2S})/t_{CR}, t(f_3)/t_{CR}]. \quad (25)$$

It is obvious, that the role of restrictions when estimating ship safety on the basis of requirements to stability and buoyancy is not equivalent. Therefore at the stage of expertise it is expedient to introduce factors of importance k_i and k_i^* ($i = 1, \dots, 4$). It is possible to use the following values as such factors:

$$\begin{aligned} k_1 = k(h_0) = 0,7, k_2 = k(\theta_0) = 0,9, \\ k_3 = k(l_m) = 1,0, k_4 = k(\theta_P) = 0,5; \end{aligned} \quad (26)$$

$$\begin{aligned} k_1^* = k^*(f_1) = 0,9, k_2^* = k^*(f_2) = 0,4, \\ k_3^* = k^*(f_{2S}) = 0,8, k_4^* = k^*(f_3) = 0,6. \end{aligned} \quad (27)$$

The received data allow to write down final expressions for restrictions $C_1(x)$ and $C_2(x)$:

$$C_1(x) \in [k_1 t(h_0)/t_{CR}, k_2 t(\theta_0)/t_{CR}, k_3 t(l_m)/t_{CR}, k_4 t(\theta_P)/t_{CR}]; \quad (28)$$

$$C_2(x) \in [k_1^* t(f_1)/t_{CR}, k_2^* t(f_2)/t_{CR}, k_3^* t(f_{2S})/t_{CR}, k_4^* t(f_3)/t_{CR}]. \quad (29)$$

Thus, on the basis of the given Tab. 1 and formulas (24) – (30) it is possible to construct an expert matrix M_E for realization of the

Bellman – Zadeh approach. The algorithm of constructing this matrix consists of the following steps.

Step 1. The criterion of safety $\mu_G(x)$ is allocated and its relative values $G_i(x) = (t_{CR}/t_S)_i$ for the considered strategy (set of alternative) $X_i, i = 1, \dots, n$ are calculated.

Step 2. The restrictions $C_1(x)$ and $C_2(x)$ on stability and buoyancy are formulated on the basis of accepted criteria ratios. These restrictions are represented as relative values (in relation to a critical interval of time t_{CR} for a specified criterion).

Step 3. The expert information in the form of factors k_i and k_i^* of importance of restrictions $C_1(x)$ and $C_2(x)$ is entered. The account of these factors makes recalculation of relative values of restrictions for use in an expert matrix possible. If the received ratio exceeds unity the restriction by the appropriate criterion is accepted as equal to unity.

Step 4. The expert matrix determining the initial information for the analysis of alternatives on the basis of the Bellman – Zadeh ap

proach is under construction. In the course of realization of a M_E matrix it is necessary to be guided by the following rules. For each strategy to the lines of restrictions $C_1(x)$ and $C_2(x)$ only the values of criteria ratio are brought which correspond to their least relative values, i.e. for each restriction the worst relative values of criterion $\mu_{C_1}(x) = \min C_1(x)$ and $\mu_{C_2}(x) = \min C_2(x)$ in view of factors of importance are chosen.

The expert matrix derived in this way is submitted in Tab. 3

Table 3. Expert M_E matrix

X_i	X_1	X_2	X_3	X_4	X_5	X_6
$\mu_G(x)$	0,65	1	0,86	0,57	0,87	0,55
$\mu_{C_1}(x)$	1	1	1	0,71	0,90	1
$\mu_{C_2}(x)$	0,80	1	0,80	0,80	0,80	0,80

Note: the strategy X_4 here is not considered, as it assumes short-term transition from an initial point 0 (light point) to point X^* (dark point) in a Fig. 7.

Using the operation of capture of the minimum for the decision of the considered task we receive (Tab. 4).

Table 4. Results of the analysis of expert matrix data

X	X_1	X_2	X_3	X_4	X_5	X_6
$\mu_G(x)$	0,65	1	0.80	0.57	0.80	0.55

Applying the operation of capture of the maximum to Tab. 4, we receive, that in the considered task the strategy X_2 (movement of a ship to port B) is optimum, therefore manoeuvre of a ship in the course of transition to point X^* will not result in increase of ship safety under the conditions of icing.

8. CONCLUSION

The offered approach to modeling of ships dynamics an intensive icing is based on a combination of methods of classical mathematics and models of fuzzy logic. This approach has the great importance to construction of algorithms of acceptance of the decisions in conditions of uncertainty and incompleteness of the initial information.

The developed computing technology takes into account features:

- the form of the case, loading and surface of a ship architecture;
- dynamics of development of an icing;
- change of external conditions (temperature of air and water, scenarios of storm development, hydro– aerodynamic resistance on waves);

The results of research can be used:

1. In onboard intelligence systems of a safety of navigation.

2. In research designing – in accounts of ship dynamics at an icing.

3. At an estimation of risk of the accepted decisions - at the comparative analysis of extreme situations.

9. REFERENCES

- Belenky V.L., N.B. Sevastianov N.B., 2003. "Stability and Safety of Ships. Vol.II: Risk of Capsizing." Elsevier Ocean Engineering Book Series, vol. 10.
- Bellman R, Zadeh L., 1976, "Acceptance of the decisions in fuzzy conditions." – Moscow, Science.
- Bogdanov A., Degtiarev A., Nechaev Yu. 2001, "Fuzzy logic basis in high performance decision support systems" // Proc. of International conference «Computational Science-ICCS 2001». San-Francisco. CA.USA. Part.1.Springer.2001, p.p.965-975.
- Boukhanovsky A., Degtyarev A., Lopatoukhin L., Rozhkov V. "Stable states of wave climate: applications for risk estimation." Proceedings of the International Conference STAB'2000, Launceston, Tasmania, Australia, February, 2000, vol.2, pp.831-846.
- Kobylinski L.,K., Kastner S. 2003 "Stability and Safety of Ships. Vol.I: Regulation and Operation." Elsevier Ocean Engineering Book Series, vol. 9.
- Kobylinski L. 2003 Capsizing scenarios and hazard identification // Stability of ships and ocean vehicles. Proceedings of 8th International conference STAB-2003. Madrid. Spain. p.p.777-785.11.
- Nechaev Yu.I., 1989, "Modeling of ship stability," Leningrad. Sudostroyenie.
- Nechaev Yu.I., 2002. "Artificial intelligence conception and application," State Marine

Technical University, St.-Petersburg.

Nechaev Yu.I., Makov Yu.L. 2002 “Software for analyzing and interpreting information on ships dynamics under conditions of intensive icing” // Proc. of third international conference ISC-2002. St.Petersburg. 2002. Sec. B. p.p.251-258.

Ryrfeldt A. 2003, “Probabilistic Assessment of the Risk of Cargo Shifting Onboard Ships in Waves.” Department of Naval Architecture and Ocean Engineering, Chalmers University of Technology, Goteborg, Sweeden.

Considerations on the Weather Criterion Applicability for the Stability Assessment of Large Vessels

Jerzy Matusiak, *Helsinki University of Technology*

Karl Hamberg, *Aker Finnyards Inc.*

ABSTRACT

The applicability of the *IMO*'s weather criterion for a large passenger ship is studied. Two very different mathematical models describing the physical scenario behind the weather criterion are employed. The results yielded by the simple model of the International Maritime Organization (abbrev. *IMO*) are compared to the computations conducted using the sophisticated time domain six-degrees-of-freedom non-linear model. Good agreement of the results obtained by the two methods is noted. The study reveals important assumptions behind the weather criterion. The weather criterion is discussed and a modification to it is proposed. The effect of this modification on the dynamic heel of a large ship is discussed.

Keywords: *weather criterion, dynamic heeling, stability*

1. INTRODUCTION

The purpose of this study is to investigate the applicability of the *IMO*'s weather criterion for a large passenger ship. This is done by using a simple mathematical model given by the legislator and by applying a sophisticated time domain six-degrees-of-freedom non-linear model called *LAIDYN* (Matusiak; 2000, 2001, 2002 and 2003) to the physical scenario behind the weather criterion. Application of two quite different models results in similar results in terms of maximum heel angle developed by a steadily rolling ship subjected to the action of gusty side wind.

Sophisticated numerical simulations of ship's behaviour in random waves and in unsteady wind were conducted by Vassalos, Jasionowski and Cichowicz (2003). Their study also deals with the problem of applicability of the weather criterion to a modern passenger ship. In particular they address the important problem of the likelihood of occurrence of the

elements making up the criterion.

The present study is mainly concerned with the model of ship dynamics used in the criterion. The environmental conditions used in the criterion are not concerned. They are taken for granted as given by the legislator. This assumption makes it possible to conduct a deterministic analysis of the criterion. Despite these simplifications the study reveals serious assumptions behind the weather criterion. The recent developments of the weather criterion done by the Intact Stability Correspondence Group are aimed, amongst the others, at updating the weather criterion and making it more suitable for large passenger vessels. However, the basic assumptions are not considered yet. These assumptions are discussed in this paper.

2. MAIN DATA OF THE SHIP AND IT'S DISCRETISED REPRESENTATION

The investigation is conducted for a cruise vessel. The main particulars of the ship are

given in Table 1 below.

Table1. Main data of the ship

Length b. p.; L_{pp}	250 [m]
Breadth, dwt; B	32.2 [m]
Draft; T	7.9 [m]
Volumetric displacement	40065 [m ³]
Vertical centre of gravity; KG	15.87 [m]
Wetted surface	9280 [m ²]
Metacentric height, GM_0	1.7 [m]
Natural roll period, T_\square	23 [s]
Windage area	9598 [m ²]
Vertical distance from the baseline to the centre of the windage area; Z_A	25.67 [m]
Vertical distance of the windage area centre from the centre of the underwater lateral area; Z	21.73 [m]
Radius of the roll moment of gyration, k_{xx}	14.55 [m]

The righting lever curve is shown in Figure 1 below.

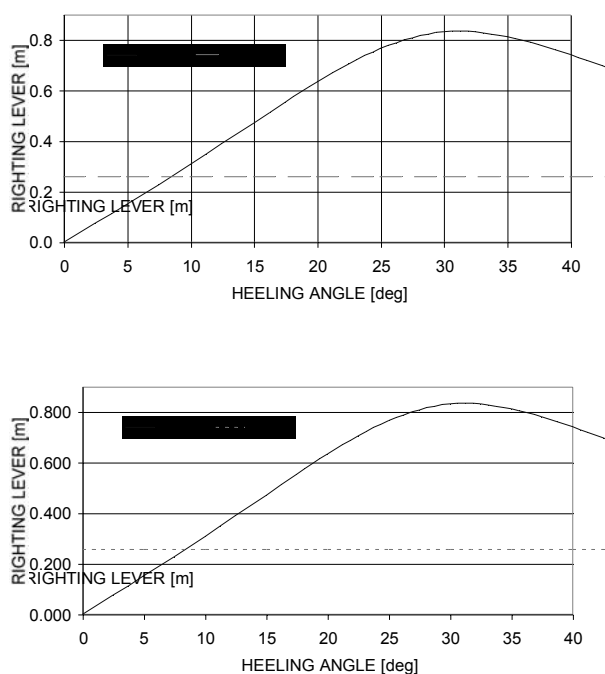


Figure 1 Righting lever curve of the ship.

This is calculated using the panel representation of the hull. The entire ship is represented by 25960 triangular panels. The ad

hoc constructed panel model extends on the ship sides to a height of 25.43 [m]. Moreover, there is no weather deck in the discretized model. However, these shortcomings of the panel model do not affect the results because the maximum values of the heel angle do not exceed 35°. The control points of the panels are shown in Figure 2.

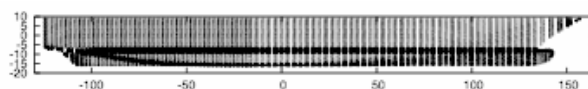


Figure 2 Side view of the discretized hull. Origin of the co-ordinate system is located at the centre of gravity. Control points of the panels are marked.

The dashed line of Figure 1 represents the static wind loading of the weather criterion.

3. SIMULATION OF THE ROLL DECAY TEST

The roll decay test was simulated first. The purpose of the simulation was to evaluate viscous roll damping to be used in the simulations so that the total damping would correspond to the result of the model test. Moreover, simulation yields the roll moment of gyration resulting in the observed value of the natural roll period of the ship ($T_\phi=23[s]$). The result of the simulation is presented in Figure 3, below.

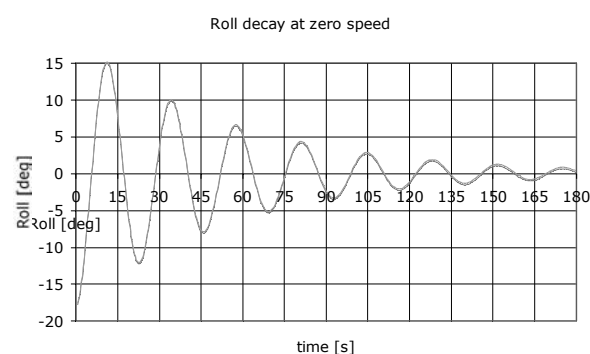


Figure 3 Simulated roll decay test. The initial heel is as in the model test. Total critical damping ratio $\zeta=0.07$.

The total critical damping ratio compares well to the corresponding value obtained in the

model tests at large roll amplitudes. This agreement was achieved adjusting the viscous part of roll damping to 0.025. The desired natural roll period was obtained with the radius of the roll moment of gyration in air being $k_{xx}=14.55$ [m].

The linearity assumption of the roll damping is believed to be sufficient in this case because of several reasons. Firstly roll damping and wave excitation roughly cancel each other at the resonance. Secondly the peak value of a transient response does not depend much on damping. Thirdly there is no scrupulous non-linear model of roll damping available that can be used in the time domain simulations.

4. ROLL AMPLITUDE AT RESONANCE FOR THE SHIP IN BEAM WAVES

4.1 Critical wave length

The natural roll period rules the length of the critical regular wave. For a deep sea condition and for the beam waves the relation between the wave length λ and the wave period T_w is

$$\lambda = \frac{gT_w^2}{2\pi} \quad (1)$$

yielding the critical wave length $\lambda=826$ [m]. The height of this wave can be evaluated using the so-called steepness factor as proposed in SLF 45/14 of 2nd of August 2002 (see also SLF 48/4/3). Thus the wave height to be used in the weather criterion check is $H=0.026 \cdot 826=21.5$ [m].

4.2 Roll amplitude at resonance

Computed roll and heave of the ship in the beam critical regular waves are presented in Figure 4.

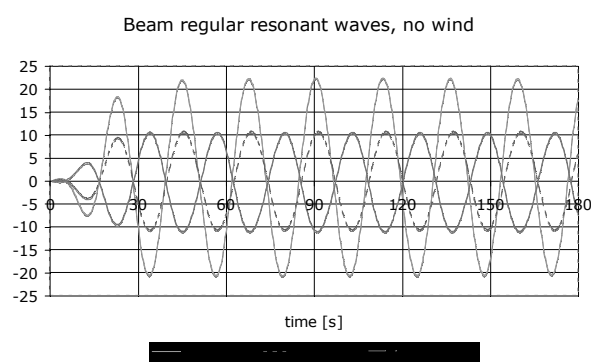


Figure 4 Steady motion of the ship in the critical beam waves.

The amplitude of roll is $\phi_A=21^\circ$. This can be identified as the steady roll amplitude θ_r of the ANNEX of the document SLF 47/6/19. The following sign definition is used:

Roll is positive when ship is heeled to the starboard.

Wave elevation means positive values.

Heave is positive for the downward motion of the ship's COG.

The effective roll-back angle is obtained by reducing the amplitude of roll at resonance as defined in the 'Guidelines for alternative assessment of weather criterion' of SLF 48/4/3. A reduction factor 0.7 accounts for the difference between resonant roll amplitudes in regular waves and irregular seas.

The summary of roll amplitudes evaluated by different approaches is presented in Table 2 below.

Table 2. Summary of the critical roll amplitudes.

ϕ_1 , DnV, rules for Ships, January 2004	Roll amplitude obtained by simulations; ϕ_A	The "effective" roll-back angle $\phi_1 = 0.7\phi_A$
15 ^o	21 ^o	15 ^o

5. SIMULTANEOUS ACTION OF REGULAR WAVES AND GUSTY WIND

According to the weather criterion the ship is subjected to a steady wind heeling the ship with a moment

$$M_{w1} = PAZ = \Delta I_{w1} \quad (2)$$

where $P=504$ [N/m²] (wind speed of 26 [m/s]), A projected lateral area of the portion of the ship above the waterline, Z vertical distance from the centre of A to the centre of the underwater lateral area. The static wind loading heels the ship by 8.5° (see Figure 1). In addition to the static wind loading, the ship is steadily rolling in the critical i.e. resonant condition. There are two possibilities to implement in the numerical simulations the scenario behind the weather criterion. The first one is as follows. The ship rolls in critical regular waves of maximum height. When the instantaneous roll angle is 70% of the amplitude value (the “effective” roll-back angle is achieved) and the ship is heeled towards the wind, the heeling moment due to wind is increased by 50%. A sudden increase of the wind moment is meant to simulate a wind gust that starts to affect the ship when she is heeled by approximately $-15^\circ + 8.5^\circ = -6.5^\circ$. The action of waves continues. The result of the motion simulation for this situation is presented in Figure 5 below.

Beam regular resonant waves ($H=21.5\text{m}$), gusty wind

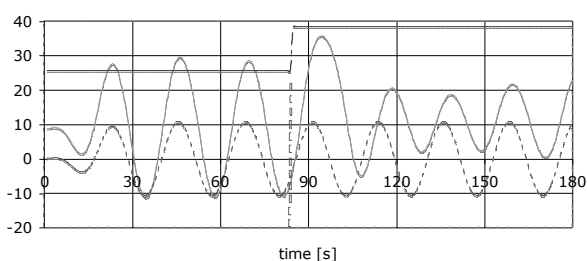


Figure 5. Steadily rolling in critical waves ship is subjected to gusty wind when roll angle is 70% of the minimum roll angle.

In this situation the ultimate value of roll as peak-to-peak value is 32° . A clear increase of heel up to 35° is noted. The ship withstands the combined action of waves and gusty wind. It is interesting to note that static heel decreases roll amplitude at the developed resonance. This may be caused by a small shift in a natural frequency or by a decrease of wave loading for a statically heeled ship. In Figure 5 gust started to act when ship was returning to the up-right position. If gust is activated for the same roll angle but with increasing heel towards the wind, the transient maximum roll reaches the value of 30° only.

Another situation, which is closer to the assumptions of the weather criterion but assumes the linearity of the roll response, is considered below. The wave height is only 70% of the previously considered value, that is it is 15 [m], but the action of a wind gust starts at the instant the vessel is heeled at the maximum towards the wind. In other words there is no kinetic energy of the roll motion at the instant of wind loading increase. The result of the simulation is presented in Figure 6, below. In this case the ultimate value of roll as peak-to-peak value is 25° .

Beam regular resonant waves ($H=15\text{m}$), gusty wind

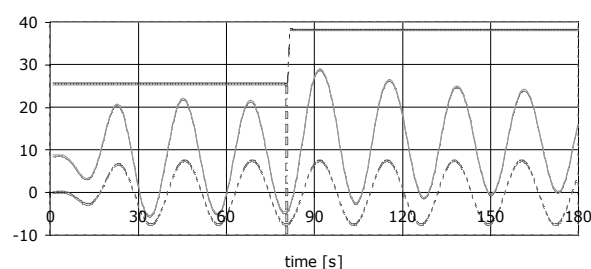


Figure 6. Steadily rolling in critical waves ship is subjected to gusty wind at the maximum roll angle towards the wind.

As we can see, the maximum roll angle is significantly lower in this case. This can be mainly attributed to the decreased wave amplitude and to the fact that there is no kinetic energy in roll motion at the instant of gust loading. Although both considered situations include two important elements of the criterion,

i.e. resonant rolling and gusty wind, the simulated situations are somewhat artificial and they may be in disagreement with the weather criterion. In the weather criterion, ship resonant roll motion is used to evaluate the initial condition for the dynamic heel analysis. The wave loading, as such, is not concerned at all. Although, as it was stated before, it may be argued that the wave loading and the roll damping compensate themselves at the resonance. This means that if we want to simulate in the time domain situation covered by the weather criterion, we can calculate or measure in model scale the ship response caused by the gusty wind loading only for the initial condition set by the resonant roll motion. This is analysed in the following with an aid of numerical simulations.

6. TRANSIENT ROLL RESPONSE COMPLYING WITH THE WEATHER CRITERION

In this Chapter the dynamic response of the ship due to gusty wind and with the initial condition set by the steady wind component and the resonant roll motion in beam waves is considered. The considered model complies with the weather criterion.

The result of the transient roll response caused by a suddenly applied wind load for the ship initially heeled to -5° by the combined action of a steady wind and resonant waves is shown in Figure 7, below. The initial heel of -5° is taken from the Figure 6.

Transient roll motion due to a gusty wind and initial heel

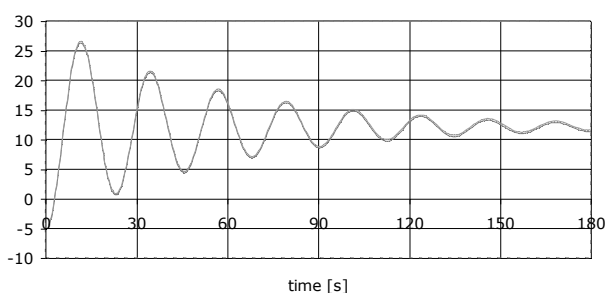


Figure 7. Ship transient rolling caused by the gusty wind and initial heel due to steady wave

and resonant roll. Gust loading is taken according to the weather criterion.

The maximum heel angle of Figure 7 is very close to the maximum heel obtained with action of beam waves being included (Fig. 6). A small, approximately 1° , difference may be attributed to the damping which decreases the maximum roll angle of the transient response. In Figure 8, the dynamical levers are used to evaluate the maximum heel of ship subjected to the action of gusty wind. The continuous line (e-curve) is the integral over the GZ -curve while the dashed line l_d corresponds to the heeling work done by the wind.

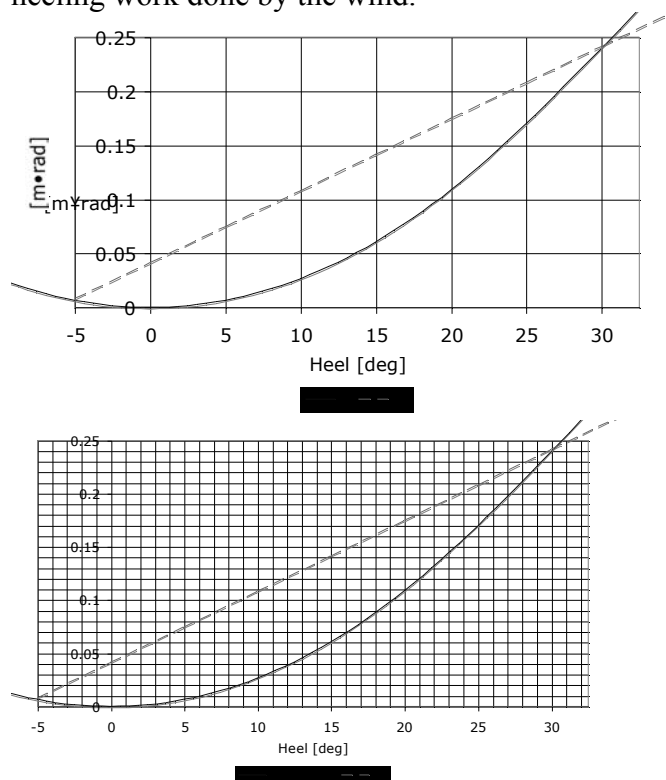


Figure 8. Ship dynamic heeling according to the weather criterion.

The lack of damping and disregarding other modes of ship motions yield a still somewhat higher maximum roll angle evaluated with the aid of dynamical levers.

7. THE PROPOSED MODIFICATION TO THE WEATHER CRITERION

7.1 Justification

A single heeling moment is a very rough approximation to a complex gusty wind loading. In the following it is shown that it is an appropriate approximation for a steady wind loading, only. A single force vector seems to be a better representation of the loading caused by wind gust for a more sophisticated model of ship dynamics. The first approximation is a force acting at the centre of gravity of the lateral area A and fixed in the body, i.e. moving with the ship, co-ordinate system. In the following we discuss this matter using a simple representation of the ship subjected to wind loading. In Figure 9 a steady wind load $F_{W,y}$ and hydrodynamic steady reaction $F_{H,y}$ are presented.

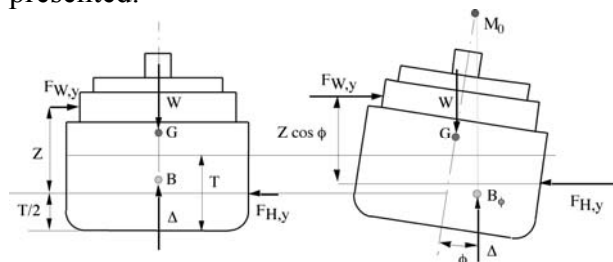


Figure 9. Steady wind loading.

For a stationary vessel or a vessel moving with a constant speed, these forces are the only ones acting athwartships and thus obviously they form a couple heeling the ship with a moment

$$M_w = F_{W,y} Z \cos \phi \tag{3}$$

For small heel angles formula (3) reduces to the expression (2), which is the wind moment of the weather criterion. The hydrodynamic steady reaction $F_{H,y}$ can be interpreted as the hull resistance opposing the steady sway motion.

In Figure 10 the forces acting on a ship

subjected to the additional gust loading $dF_{W,y}$ are presented.

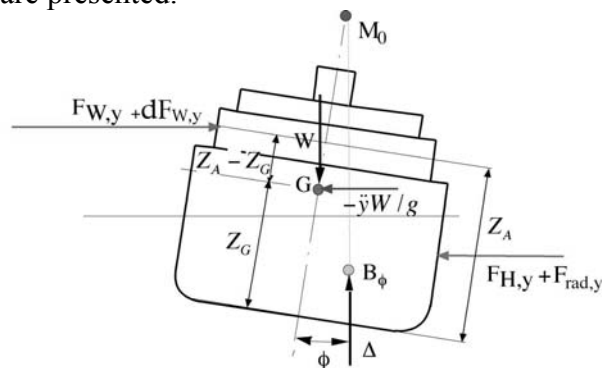


Figure 10. Ship dynamic heeling according to the weather criterion.

The steady balance of ship is perturbed by the action of wind gust. With the assumption of 50% increase of air pressure due to the wind gust the force corresponding to the gust can be evaluated as

$$dF_{W,y} = 0.5 \cdot PA, \tag{4}$$

which results in the heeling moment external loading

$$dM_{w1} = dF_{W,y} (Z_A - Z_G) \tag{5}$$

where Z_A is the vertical distance from the baseline to the centre of the lateral area A . The term $\cos \phi$ was disregarded using the small heel angles assumption.

During the transient heeling, the vector depicting the inertia force of the ship's mass appears. This vector acts at the ship's centre of gravity G and thus it does not contribute to the ship's heeling. Moreover, an unsteady component of the hydrodynamic reaction appears. This is a radiation force component $F_{rad,y}$ that primarily depends on the sway acceleration. These forces are disregarded by the weather criterion. In principle both new force components can be evaluated by a method like LAIDYN. Already from what was discussed above the following can be

concluded:

- The weather criterion seems to model properly a steady wind action if the concerned heel angles are not too big. For high heel angles, the assumption of constant valued lever Z can be questioned (see Fig. 9).
- The action of wind gust is to heel the ship dynamically. In general, the effective lever of the heeling moment is smaller than in the steady case because the inertia force of the sway motion component compensates a part of the external loading. Thus it is obvious that the weather criterion in its present form may overestimate the dynamic heel values for the considered scenario.

7.2 Transient roll response according to the proposed modification of the weather criterion

The transient roll response of this modified sea weather model (called in the following the Y-force model) is shown in Figure 11.

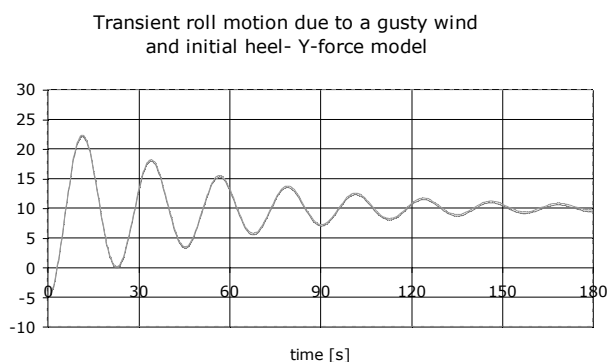


Figure 11. Ship dynamic heeling according to the modified weather criterion.

Comparing the transient roll responses given by two variations of the weather criterion (Figs. 7&11), a decrease of maximum roll angle of 4° is noted when using the proposed modification. The maximum heel angle given by considering the dynamic levers in the context of the weather criterion (refer to Figure 8) is approximately 8 degrees higher than the

one obtained by the numerical simulations using the Y-force model. The drawback of the Y-force model is the fact that it cannot be used as easily as the original weather criterion. It requires either the numerical model of ship dynamics, which allows for sway motion, or the model tests. The model tests would be similar to the roll decay tests with the model free to roll and sway. The new elements in these tests would be an a priori evaluated initial roll angle and an application of the gusty wind loading as given by formulas (3) and (5).

Finally the result of roll simulation using both the weather criterion loading represented by the Y-force model and by the action of the resonant beam waves is presented in Figure 12, below. A reasonable agreement of maximum heel angle for this case when compared to a pure transient response (given in Figure 11) is noted. Again the maximum heel angle is about 4° smaller than the one obtained with the pure heeling moment (refer to Fig. 6 for the comparison) and it is approximately 5° smaller than the one obtained by the weather criterion.

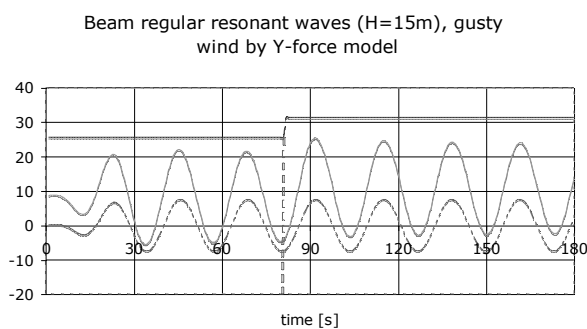


Figure 12. Steadily rolling in critical waves ship is subjected to gusty wind at the maximum roll angle towards the wind. The wind loading is represented by the Y-force model.

8. CONCLUSIONS AND RECOMMENDATIONS

The weather criterion, which is a simple check of the ship's intact stability, describes qualitatively well the transient behaviour of a ship subjected to the combined loads of gusty wind and waves. However, the criterion's

simplicity may result in higher values of the maximum heel angles than the ones produced by the more sophisticated numerical tools. The assumed scenario is simplified by disregarding the sway motion. Thus the criterion can be too conservative, especially for large passenger vessels, (as well as other ship types with dimensions beyond the statistical base of the criterion).

In the current proposal for a revised Intact Stability Code, a procedure for alternative assessment, based on model testing is included, but a numerical simulation is not accounted for. Numerical methods usually offer advantages in schedule and cost.

For this reason, we recommend that the Intersessional Correspondence Group on Intact Stability (ISCG) recommends to the Sub-Committee On Stability And Load Lines And On Fishing Vessels Safety (SLF) of IMO to make an allowance for a numerical simulation of ship transient motion as subjected by the loading of the weather criterion. The validated and benchmark tested numerical methods should at least include, in addition to a non-linear roll model also, a proper modelling of sway motion.

Moreover, a possibility for conducting dedicated model tests simulating physically the transient heel behaviour of the ship should be investigated further with an aim of allowing for it in the Intact Stability Rules. This would be in agreement with the latest suggestions of the ISCG making an allowance for the model tests when evaluating the roll-back angle.

9. REFERENCES

- DNV, 2004, "Rules for Ships", Pt. 3, Ch. 3, Sc. 9.
- Matusiak, J., 2000, "Two-stage approach to determination of non-linear motions of ship in waves". 4th Osaka Colloquium on Seakeeping Performance of Ships, Osaka, Japan.
- Matusiak, J., 2001, "Importance of memory effect for capsizing prediction". 5th International workshop University of Trieste. Università di Trieste, 6.3.1 (6 pages).
- Matusiak, J., 2002, "Two-stage Approach to Determination of Large Amplitude Motions of a Rigid Ship in Waves". 15th Nordic Seminar on Computational Mechanics, Aalborg, Denmark, Institute of Mechanical Engineering, Aalborg University, pp. 1-10.
- Matusiak, J., 2003, "On the effects of wave amplitude, damping and initial conditions on the parametric roll resonance". Proceedings of the 8th International Conference on Stability of Ships and Ocean Vehicles, Madrid, Spain, pp. 341-348.
- SLF 45/14, 2002, "Report to the Maritime Safety Committee".
- SLF 47/6/9, 2004, "Review of the Intact Stability Code"
- SLF 47/6/19, 2004, "Proposal of Guidelines for model tests to determine the roll angle for the weather criterion".
- SLF 47/17, 2004, "Report to the Maritime Safety Committee".
- SLF 48/4/3, 2005, "ANNEX: Guidelines for Alternative Assessment of Weather Criterion".
- Vassalos, D., Jasionowski, A., Cichowicz, J., "Weather Criterion - Questions and Answers", Proceedings of STAB2003, pp. 695-705

Experimental and Theoretical Study on Critical Condition of Bow-Diving

Akihiko Matsuda, *National Research Institute of Fisheries Engineering*

Hirotsada Hashimoto, *Osaka University*

Naoya Umeda, *Osaka University*

ABSTRACT

Recent model experiments by the authors indicated that bow-diving is one of the crucial capsizing modes for a high-speed vessels travelling in following and quartering seas. Bow-diving is a phenomenon that the bow plows into the water, and initiated from the situation of surf-riding without broaching-to and finally she could capsize with large negative pitch angle. In our previous paper, we discussed the relationship between occurrence of bow-diving and water level at bow under the assumption that heave and pitch motions can be approximated by tracing their static equilibrium, and compared the numerical results with free running capsizing model experiments for several fishing vessels. In this research, model experiments with various ship speeds were conducted to examine the speed-dependence of bow-diving, and show that the model could suffer broaching-to when she is running at relatively lower speed, she could capsize due to bow-diving at intermediate speed and she could be stably surf-riding at higher speed. Moreover we attempted to improve theoretical prediction method by taking nonlinear Froude-Krylov calculation and speed-dependent ship running attitude into account.

Keywords: *bow-diving, capsizing, surf-riding, free running model experiment*

1. INTRODUCTION

Even now small ships, such as fishing vessels, occasionally capsize when they run in heavy following and quartering seas with high speed. To prevent capsizing phenomena, we conducted free running capsizing model experiments in following and quartering seas for different types of 11 models in the Marine Dynamics Basin at National Research Institute of Fisheries Engineering (NRIFE). These experiments showed that the main causes of capsizing in following and quartering seas are pure-loss of stability, broaching-to, parametric resonance and bow-diving. Nowadays pure loss of stability, broaching-to and parametric resonance could be theoretically well explained

(e.g. Umeda et al., 2000, Hashimoto et al., 2004, Bulian et al., 2003), however few attempts have been done on bow-diving (e.g. Jullumstroe, 1990, Renilson et al., 2000, Taguchi et al., 2000) because it is newly recognized phenomenon from experimental research.

In the previous work (Matsuda et al., 2004), the authors conducted free running model experiments for 3 types of fishing vessels to understand mechanism of bow-diving, and discussed the possibility of theoretical prediction of bow-diving occurrence by calculating relative water height to the bulwark top at bow under the assumption that heave and pitch motions could be calculated by Froude-Krylov assumption with the running attitude for the certain ship forward velocity

corresponding to the wave celerity. As a result, the simple calculation of relative height between wave surface and height of bulwark top at bow could roughly estimate occurrence of bow-diving.

In this work, we have conducted free running model experiments for a latest 135 gross tonnage Japanese purse seiner with several Froude numbers. The model capsized due to bow-diving in severe following waves with intermediate propelling power, but experienced stable surf-riding with higher propelling power and did broaching with lower power. This means that a threshold exists for avoiding bow-diving even in surf-riding condition but the previous calculation method cannot predict it. We firstly show the results of free running model experiments of the purse seiner running in following seas. Secondly, we discuss the threshold of bow-diving and theoretical calculation with experimentally obtained ship running attitude as a function of Froude number in calm water and displacement of heave and pitch in waves with the nonlinear Froude-Krylov calculation. Moreover we apply this new calculation method to existing free running model experiments conducted with three fishing vessels.

2. EXPERIMENTAL OBSERVATION

Free running model experiments of the latest 135 gross tonnage Japanese purse seiner were carried out in the Marine Dynamics Basin of NRIFE (Fig.1). The body plan of this ship is shown in Fig.2 and its principal particulars are also done in Table 1. The ship model was propelled with an electromotor, whose power was supplied by onboard batteries. The propeller revolution number was controlled by a feed back control. They were steered by an autopilot system whose rudder gain is 1.0. The maximum rudder angle was 35 degrees. Roll, pitch and yaw angle was measured by an optical gyroscope. These measured signals were restored in the onboard computer in a digital form, and the measured yaw angle was used for the auto pilot control.

Wave parameters used in the model test were wave length to ship length ratio, λ/L , of 1.392 and wave height to wave length, H/λ , of 0.107.

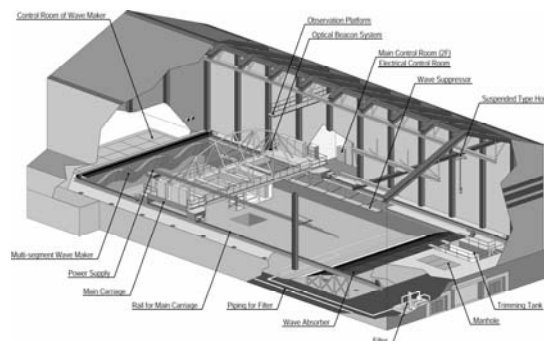


Figure 1 Marine dynamics basin of NRIFE

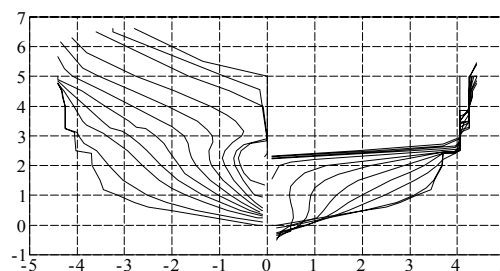


Figure 2 Body plan of the subject ship

Table 1 Principal particulars of the ship

	ship	model
Length between perpendiculars: L_{pp}	38.5m	2.14m
Breadth: B	8.10m	0.45m
Depth: D	3.30m	0.18m
Mean draught: d_m	2.85m	0.16m
Block coefficient: C_b	0.511	0.511
GM	1.79m	0.10m
Model scale		1/18

3. EXPERIMENTAL RESULTS

Experimental results are shown in Table.2. Bow-diving was observed when model speed is between $F_n=0.445$ to 0.454 , while stable surf-riding appeared over $F_n=0.464$.

The relationship between F_n and trim angle obtained from the resistance test with free heave and pitch is shown in Fig.3. The trim

angle is dramatically increasing where F_n is over than 0.37. Ship-generated waves due to high forward speed induce significant trim by stern and then the bow top is difficult to plow into water. Therefore the model experienced stable surf-riding instead of bow-diving.

Table 2 Experimental results

Propeller revolution(rps)	F_n	Results
40.00	0.492	Stable surf-riding
38.75	0.482	Stable surf-riding
37.50	0.471	Stable surf-riding
36.25	0.464	Stable surf-riding
35.00	0.454	Bow-diving
33.75	0.445	Bow-diving
32.50	0.435	Stable surf-riding
31.25	0.425	Broaching-to
30.00	0.415	Broaching-to
28.75	0.405	Periodic

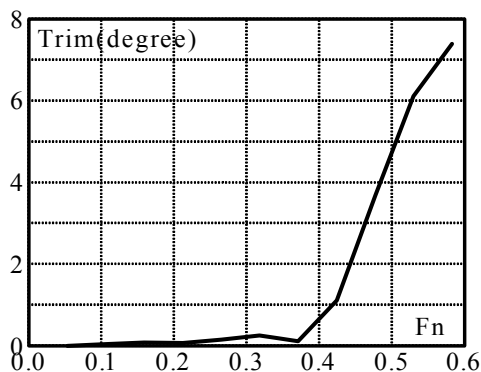


Figure 3 Relationship between ship speed and trim angle in calm water

4. THEORETICAL PREDICTION

From the experimental results, bow-diving occurs when the bulwark top at bow dived into water during transient surf-riding under intermediate propelling power. On the other hand, the bulwark top in higher propelling power did not submerge. Since the encounter frequency of a ship in surf-riding to waves was almost zero, heave and pitch motions can be approximated by tracing a static balance. Therefore, we can calculate a relative vertical distance between bulwark top at bow end and water surface using the static balance

calculation to determine whether the bow bulwark top submerges or not.

In the previous paper, we calculated heave and pitch motions in waves from the static balance calculated by the linear Froude-Krylov assumption with running attitude for the ship forward velocity corresponding to the wave celerity. However the model experiments mentioned above for several Froude numbers show that occurrence of bow-diving depend on the propeller revolution. Here ship speed itself was increased by waves from that in still water, however it is difficult to estimate ship speed and attitude during bow-diving accurately. In the experiment, bow-diving occurred before settling down into a steady state of running attitude because ship speed is drastically increased and the bow plows into a wave up-slope immediately. Therefore, in the calculation, we use the experimentally obtained ship attitude at the ordered propeller revolution in calm water. In addition, the nonlinear Froude-Krylov calculation that the wave pressure is integrated up to the wave surface with free heave and pitch is used because wave elevation changes significantly in steep waves where bow-diving could occur. The coordinate systems used in the calculation are shown in Fig.4.

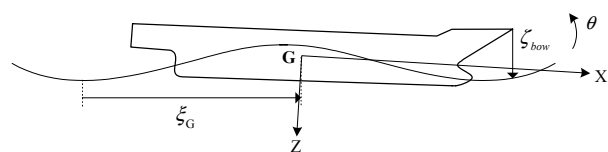


Figure 4 Coordinate Systems

The relative vertical distance between the bulwark top at bow end and the wave surface, ζ_r , can be calculated as follows: (Matsuda et al., 2004)

$$\zeta_r = \zeta_G - x_{bow} \sin \theta - \zeta_{W_{bow}} \quad (1)$$

$$\zeta_{W_{bow}} = \zeta_a \cos k(x_{bow} \cos \theta + \xi_G) - \frac{1}{2} k \zeta_a^2 \cos 2k(x_{bow} \cos \theta + \xi_G) \quad (2)$$

Here ζ_G is heave including the sinkage due to running, $\zeta_{W_{bow}}$ is the wave height at the bow edge, ζ_a is the wave amplitude, x_{bow} is the horizontal distance between the bow edge and the centre of ship gravity, θ is the pitch angle including the trim due to running, k is the wave number and ξ_G is the longitudinal position of centre of gravity from a wave trough. If ζ_r is larger than bow work top height to the still water surface, ζ_{still} , bow submergence is occurred. Therefore the relative water level of the bulwark top, ζ_{bow} , is calculated as follows:

$$\zeta_{bow} = \zeta_r - \zeta_{still} \quad (3)$$

If ζ_{bow} is less than zero, the bulwark top is below the wave surface, which means bow-diving occurs.

ζ_{bow} at $Fn=0.454$ is shown in Fig.5. Minimum ζ_{bow} is just zero around ξ_G/λ of 0.9. On the other hand, minimum ζ_{bow} at $Fn=0.464$ is positive. This result agrees with the experimental results shown in Table.2. All results of calculation are shown in Table.3. The results agree well with the experimental results. By the way, at the lower propelling power area, experimental results were broaching-to. It might be because that the lower propelling power could not make enough rudder force against yaw moment acting on the hull, then she could not keep her course.

Table 3 Comparison between experimental and calculated results

Fn	Experiments	Calculations
0.492	Stable surf-riding	Stable surf-riding
0.482	Stable surf-riding	Stable surf-riding
0.471	Stable surf-riding	Stable surf-riding
0.464	Stable surf-riding	Stable surf-riding
0.454	Bow-diving	Bow-diving
0.445	Bow-diving	Bow-diving
0.435	Stable surf-riding	Bow-diving
0.425	Broaching-to	Bow-diving
0.415	Broaching-to	Bow-diving
0.405	Periodic	Bow-diving

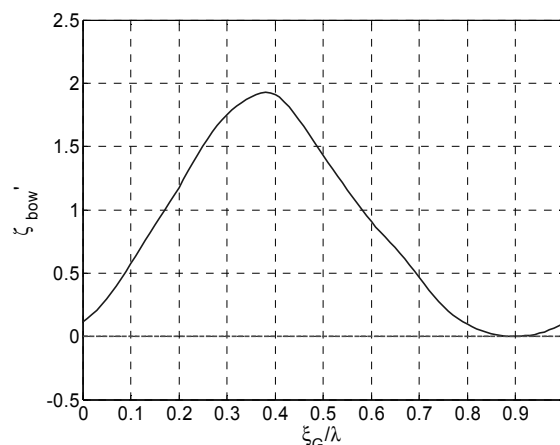


Figure 5 Relative height between bulwark top at bow end and wave surface at $Fn=0.454$, $\lambda/L=1.392$ and $H/\lambda=0.107$

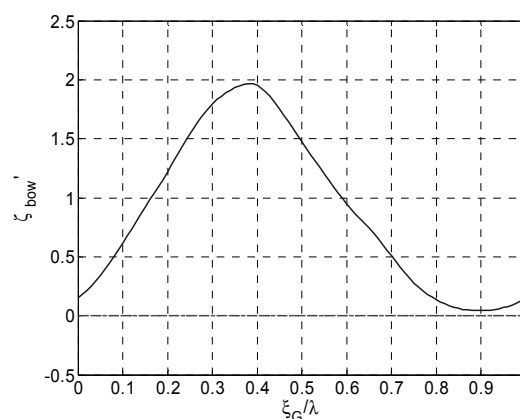


Figure 6 Relative height between bulwark top at bow end and wave surface at $Fn=0.464$, $\lambda/L=1.392$ and $H/\lambda=0.107$

5. INVESTIGATION FOR OTHER TYPES OF FISHING VESSELS

We attempt to apply the new calculation method using the speed-dependent ship attitude to the other three types of fishing vessels which are a 80 gross tonnage Japanese purse seiner (Ship A), a North European purse seiner (Ship B) and a fishing vessel for set nets (Ship C). The general arrangements of these ships are shown in Figs.7-9. Principal particulars of these ships are shown in Table 4. Ship A is one of the typical Japanese purse seiners, which experienced some capsizing accidents in recent

years. Ship B is an European purse seiner having much larger freeboard. Ship C is a semi-planing boat having large beam to depth ratio.

Free running model experiments had been conducted by the authors before for the three ships. From the experiment results, Ship A and Ship C suffered bow-diving and capsizing, but Ship B had not suffered bow-diving but stable surf-riding in similar wave condition as the 135GT Japanese purse seiner. The detail of these experimental results including time series can be found in the literature. (Matsuda et al., 2004) We carry out the comparison between free running model experiments for these three additional ships and theoretical calculations based on the new theoretical method mentioned in this paper.

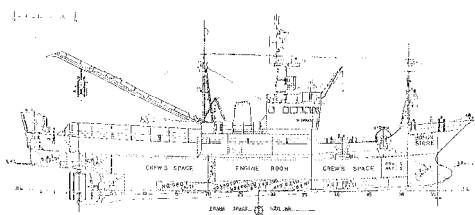


Figure 7 General arrangement of Ship A

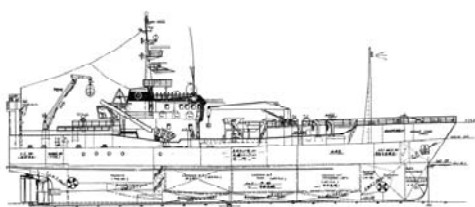


Figure 8 General arrangement of Ship B

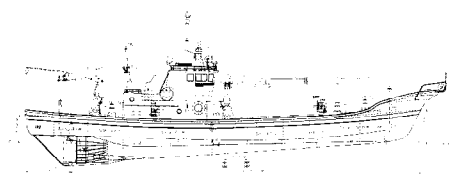


Figure 9 General arrangement of Ship C

From these results, we can conclude that the new theoretical prediction method reasonably explains the speed-dependence of the bow-diving observed in the free running model experiment for the Japanese 135GT

purse seiner, and can predict the bow-diving occurrence for the displacement type of 80GT Japanese purse seiner and European purse seiner, but cannot predict for the semi-planing vessel which is not categorized into the ordinary displacement type ship.

Table 4. Principal particulars of the ships

Ship	A	B	C
Length between perpendiculars: L_{pp}	29.0m	55.0m	21.2m
Breadth: B	6.80m	12.0m	4.82m
Depth: D	2.60m	7.60m	1.26m
Mean draught: d_m	2.30m	5.25m	0.99m
Block coefficient: C_b	0.577	0.657	0.657
Model scale	1/12.6	1/25	1/8

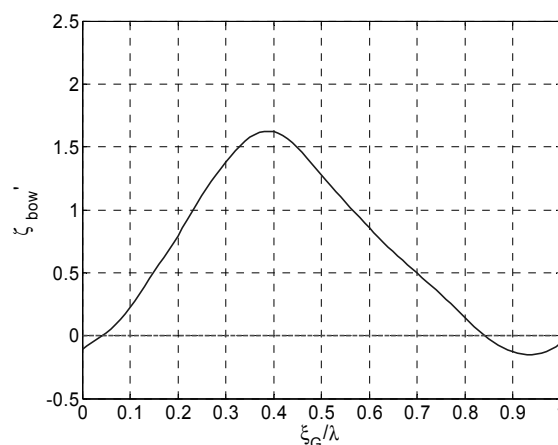


Fig.10 Relative height between bulwark top to wave surface at bow (Ship A) with $H/\lambda=0.111$ and $\lambda/L=1.41$

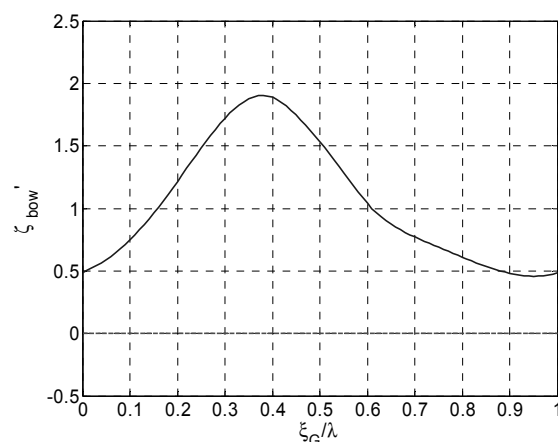


Fig.11 Relative height between bulwark top to wave surface at bow (Ship B) with $H/\lambda=0.106$ and $\lambda/L=1.39$

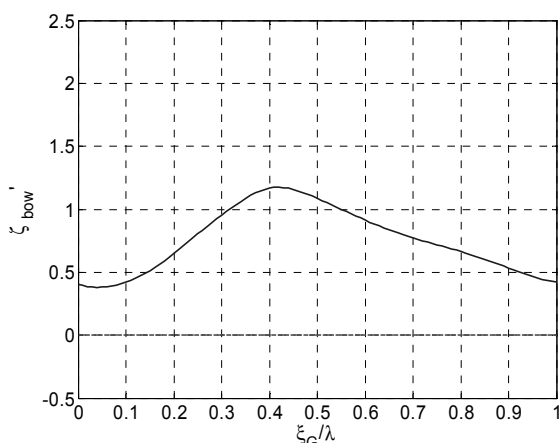


Fig.12 Relative height between bulwark top to wave surface at bow (Ship C) with $H/\lambda=0.11$ and $\lambda/L=1.38$

6. CONCLUSIONS

Following conclusions are obtained from this experimental and theoretical research on new capsizing mode of bow-diving:

1) Free running model experiment for a 135 gross tonnage Japanese purse seiner demonstrates that bow-diving occurred with intermediate propeller power, i.e. 0.44~0.46 of the Froude number.

2) The calculation of relative height between bulwark top at bow and wave surface with the experimentally obtained speed-dependent running attitude in calm water could reasonably estimate the threshold of bow-diving for the 135 gross tonnage Japanese purse seiner.

3) The calculations based on the proposed theoretical prediction method agree also well with free running model experiments for the 80 gross tonnage Japanese purse seiner and European purse seiner.

4) The proposed theoretical prediction method for bow-diving could be applicable for displacement type vessels but not for non-displacement type ones.

7. ACKNOWLEDGMENTS

The experiments described here were supported by the Fishing Boat Association of Japan. These model experiments were carried out with help of following persons;

Prof. M. Hamamoto from Fukui University of Technology, Dr. M.R. Renilson from QiInetiQ, Prof. W. Sera from Kobe University of Mercantile Marine, Messers. Y. Matsuda, T. Ooshima and N. Nakamura from Hiroshima University, Mr. Y. Uchiyama from Tokyo University of Fisheries M. Shibata from Hokkaido University and Messers. S. Urano, M. Suehisa, K. Okoh A. Maki, S. Nakamura, G. Sakamoto and M. Shuto from Osaka University.

8. REFERENCES

- Bulian, G., Francescutto, A. and Lugni, C., 2003, "On the Nonlinear Modeling of Parametric Rolling In Regular and Irregular Waves", Proceedings of the 8th International Conference on the Stability of Ships and Ocean Vehicles, pp. 305-323.
- Hashimoto, H., Umeda, N. and Matsuda, A., 2004, "Importance of Several Nonlinear Factors on Broaching Prediction", Journal of Marine Science of Technology, Vol. 9, pp. 80-93.
- Jullumstroe, E., 1990, "Stability of High Speed Vessel", Proceedings of the 4th International Conference on Stability of Ships and Ocean Vehicles, Naples, pp.322-327.
- Matsuda, A., Hashimoto, H. and Umeda, N., 2004, "Capsizing due to Bow-diving in Following Waves", International Shipbuilding Progress, Marine Technology Quarterly, Volume 51, Number 2/3, pp. 121-133.
- Renilson, M.R., Hannon, M., Duncan, B., 2000, "The Effect of Cross Deck Structure Design on Deck Diving of High Speed Catamarans

in Following Seas”, Fourth Osaka Colloquium on Seakeeping Performance of Ships, pp.89-94.

Taguchi, H., Ishida, S., 2000, “Bow Submergence Phenomenon During Surf-riding”, Fourth Osaka Colloquium on Seakeeping Performance of Ships, pp.357-361.

Umeda, N. and M. Hamamoto, 2000, “Capsize of Ship Models in Following/ Quartering Waves –Physical Experiments and Nonlinear Dynamics-”, Philosophical Transactions of the Royal Society of London, Series A, Vol. 358, pp.1883-1904.